

VOLUME 39

MARCH 1961

NUMBER 3

Canadian Journal of Chemistry

Editor: LÉO MARION

Associate Editors:

E. BAER, *University of Toronto*
D. H. EVERETT, *University of Bristol*
R. U. LEMIEUX, *University of Ottawa*
D. J. LE ROY, *University of Toronto*
C. A. MCDOWELL, *University of British Columbia*
E. W. R. STEACIE, *National Research Council of Canada*
R. W. TAFT, Jr., *The Pennsylvania State University*
H. G. THODE, *McMaster University*
A. E. VAN ARKEL, *University of Leiden*

Published by THE NATIONAL RESEARCH COUNCIL

OTTAWA

CANADA

Canadian Journal of Chemistry

Under the authority of the Chairman of the Committee of the Privy Council on Scientific and Industrial Research, the National Research Council issues THE CANADIAN JOURNAL OF CHEMISTRY and five other journals devoted to the publication, in English or French, of the results of original scientific research. Matters of general policy concerning these journals are the responsibility of a joint Editorial Board consisting of: members representing the National Research Council of Canada; the Editors of the Journals, and members representing the Royal Society of Canada and four other scientific societies.

The Chemical Institute of Canada has chosen the Canadian Journal of Chemistry as its medium of publication for scientific papers.

EDITORIAL BOARD

Representatives of the National Research Council

I. McT. Cowan (Chairman), *University of British Columbia* H. G. Thode, *McMaster University*
Léo Marion, *National Research Council* D. L. Thomson, *McGill University*

Editors of the Journals

D. L. Bailey, *University of Toronto* Léo Marion, *National Research Council*
T. W. M. Cameron, *Macdonald College* J. F. Morgan, *Department of National Health and Welfare, Ottawa*
F. E. Chase, *Ontario Agricultural College* J. A. F. Stevenson, *University of Western Ontario*
H. E. Duckworth, *McMaster University*

Representatives of Societies

D. L. Bailey, *University of Toronto* D. J. Le Roy, *University of Toronto*
Royal Society of Canada Royal Society of Canada
T. W. M. Cameron, *Macdonald College* J. F. Morgan, *Department of National Health and Welfare, Ottawa*
Royal Society of Canada Canadian Biochemical Society
H. E. Duckworth, *McMaster University* R. G. E. Murray, *University of Western Ontario*
Royal Society of Canada Canadian Society of Microbiologists
Canadian Association of Physicists J. A. F. Stevenson, *University of Western Ontario*
P. R. Gendron, *University of Ottawa* Canadian Physiological Society
Chemical Institute of Canada

Ex officio

Léo Marion (Editor-in-Chief), *National Research Council*
J. B. Marshall (Administration and Awards), *National Research Council*

Manuscripts for publication should be submitted to Dr. Léo Marion, Editor-in-Chief, Canadian Journal of Chemistry, National Research Council, Ottawa 2, Canada.

(For instructions on preparation of copy, see *Notes to Contributors* (inside back cover).)

Proof, correspondence concerning proof, and orders for reprints should be sent to the Manager, Editorial Office (Research Journals), Division of Administration and Awards, National Research Council, Ottawa 2, Canada.

Subscriptions, renewals, requests for single or back numbers, and all remittances should be sent to Division of Administration and Awards, National Research Council, Ottawa 2, Canada. Remittances should be made payable to the Receiver General of Canada, credit National Research Council.

The journals published, frequency of publication, and subscription prices are:

Canadian Journal of Biochemistry and Physiology	Monthly	\$9.00 a year
Canadian Journal of Botany	Bimonthly	\$6.00 a year
Canadian Journal of Chemistry	Monthly	\$12.00 a year
Canadian Journal of Microbiology	Bimonthly	\$6.00 a year
Canadian Journal of Physics	Monthly	\$9.00 a year
Canadian Journal of Zoology	Bimonthly	\$5.00 a year

The price of regular single numbers of all journals is \$2.00.

CORRECTIONS

Volume 38, 1960

Page 632. In the first paragraph a line of type has been misplaced. The line "hydrogenation. Liberti and Cartoni (4) used silicone and tricresyl phosphate as liquid" now appearing as line 10 should be inserted between lines 3 and 4.

Page 1181. The first sentence should read "On the other hand this table shows that for naphthalene in benzene a significant orientation polarization remains after deduction either of the observed distortion polarization (40.5 cc) or of the Eisenlohr MR_D (41.6 cc) from the observed total polarization."

Canadian Journal of Chemistry

Issued by THE NATIONAL RESEARCH COUNCIL OF CANADA

VOLUME 39

MARCH 1961

NUMBER 3

EXCHANGE REACTIONS BETWEEN ZINC AND ITS IONS¹

J. E. SANDOR²

ABSTRACT

The exchange reaction between zinc metal and zinc ions in solution has been studied by means of radioactive zinc-65. Polycrystalline zinc and bicrystals of zinc were used under conditions where the radioactive material was incorporated either in the solid or the liquid phase. Strain-free clean surfaces were obtained and autoradiographs taken.

The results of the experiments using bicrystals were interpreted on the basis that a local cell action sets up an electrochemical potential between liquid and solid at the beginning of the reaction. Exchange was found to take place in both directions, but the reaction did not follow a simple logarithmic law.

INTRODUCTION

The extensive use of radioisotopes has made possible the study of many exchange reactions. In 1915, Hevesy (1) showed that in the system $\text{Pb}^{++}/\text{Pb}(\text{NO}_3)_2$ a deep exchange takes place in a very short period of time, i.e. more than one monolayer exchanges, and this was found later to happen in other metals, too. Various mechanisms have been suggested for such exchange reactions, but no conclusive explanation has yet been put forward. In the general case one expects more or less rapid exchange in the surface layer, followed by slow penetration to the interior of the metal at a speed controlled by the diffusion coefficient and orientation of the crystals.

The heterogeneous exchange reaction between zinc and its ions has been studied by Rollin (2) in zinc dust, by Gaudin and Vincent (3), Haenney and Mivelaz (4), Matsura (5), and King and Evans (6), in both zinc dust and zinc foil; and Bushmanov and Vozdvizhenky (7) in zinc single crystals. There are considerable variations in the results obtained by the different authors in this field, due to the fact that some factors, such as surface preparation, oxidation, corrosion, are not always fully considered.

In this investigation, zinc metal was dipped in different solutions of zinc salt to show that the exchange reaction $\text{Zn}^0_{\text{metal}} \rightleftharpoons \text{Zn}^{++}_{\text{sol}}$ takes place in both directions. This was done by labeling either the metal or the zinc solution with radioactive zinc-65, and following the change in activity for different times of immersion. The influence of oxide or hydroxide on the exchange was also investigated. Finally, the exchange reaction between zinc bicrystals and carrier-free solutions of Zn^{65} was studied.

The following factors were considered of importance in this study: (1) preparing undistorted zinc surfaces; (2) working in an oxygen-free atmosphere; (3) minimizing of corrosion and adsorption. It is known that zinc is a soft metal, easily worked, and that the depth of distorted metal after mechanical polishing may commonly extend to at

¹Manuscript received May 13, 1960.

Contribution from the Mineral Sciences Division, Mines Branch, Department of Mines and Technical Surveys, Ottawa, Canada.

²National Research Council Postdoctorate Fellow, Mineral Sciences Division, Mines Branch, Department of Mines and Technical Surveys, Ottawa, Canada; now with Semiconductor Products Department, General Electric Co., Syracuse, N.Y.

least 20 times the penetration of the deepest scratch (8). For silver, Tingley, Henderson, and Coffin (9) have shown definitely that the exchange reaction is notably different with different surface preparation techniques.

Zinc is a chemically reactive metal, easily oxidized, and considerable corrosion can take place in solution in the presence of oxygen as a result of electrochemical action.

EXPERIMENTAL DETAILS

Materials

Zinc metal.—Zinc metal, 99.999% purity, was cast in an argon atmosphere in rods of 1.56-cm diameter. Disks of 0.62-cm thickness and 1.56-cm diameter were cut by means of a lathe, annealed 12 hours at 350° C and mounted in Lucite in such a way that only one face was used in the experiments.

Active metal.—From the same 99.999% Zn rods as before, a number of disks of 1.56-cm diameter were cold-rolled to 0.78-mm thickness, cut in strips of 2.5-cm length, annealed for 24 hours at 350° C, and sent to Chalk River, Ont., for irradiation. The specific activity after irradiation was 5.1 mc/g. These samples were checked for purity with a 100-channel pulse height analyzer, to see if there was any unwanted activity not resulting from Zn⁶⁵.

Carrier-free zinc.—Carrier-free zinc was used in some experiments. Obtained from Nuclear Science and Engineering Corporation (Pittsburgh), it had an activity of 0.8 mc and a specific concentration of 1.1 mc/ml.

Preparation of Samples

The polycrystalline samples were mechanically polished with emery papers, and on microcloth laps using Al₂O₃ suspensions. They were finally etched with a cold solution of equal parts of HNO₃, C₂H₅OH, and H₂O₂. When the underlying structure of the zinc became visible under a microscope and no twins appeared (10), it was considered that an undistorted surface was obtained.

To avoid oxidation of the samples after etching and rinsing, the samples were immediately immersed in the exchange solution. Solutions of active and inactive deaerated Zn(NO₃)₂ were used. The molarities were 10⁻¹ and 10⁻² and the pH varied between 5.2 and 6.2. The active solutions had a specific activity of 0.4 mc/g. The solutions were thoroughly deaerated.

After polishing the polycrystalline metal samples, they were introduced into a dry box, in which the etching and exchange were carried out in an inert atmosphere of argon. The apparatus was set up so that the exchange process of six samples could be observed simultaneously in the same solution. This solution was kept in a thermostat at 25° ± 0.5° C. The periods of immersion were varied between 1 hour and 1 week.

Bicrystals were grown from seeds provided by Dr. F. Weinberg; the bicrystals were annealed, strongly etched to remove the worked and recrystallized material, and, finally electropolished by using an orthophosphoric acid-ethanol solution (1:1). Carrier-free deaerated zinc solutions of pH 6 were used. Argon was bubbled continuously and the samples were immersed for short periods of time, ranging from a few seconds to a few minutes. The samples were then rinsed with water, washed with alcohol, and dried, and an autoradiograph was taken with No-Screen X-ray film. Different exposure times—depending on the activity of the samples—were tried, ranging from 8 to 64 hours.

For the purpose of studying the influence of oxidation on the exchange, one sample was pretreated for 24 hours in an air-free 10⁻² M Zn(NO₃)₂ solution; this led to formation of a Zn(OH)₂ film. Then half of the sample was etched and the other half was left with

the hydroxide. Again, care was taken, during the rinsing of the samples, to avoid activities resulting from contamination only and not from exchange itself.

Some 99.999% Zn irradiated samples were immersed for short periods in a glass immersion cell, which had argon bubbling continuously through the solutions. The volume of solution was 100 ml, and fresh portions were used for each immersion period. Aliquots were taken out and counted for 30 minutes in a well-type scintillation counter.

To ensure radiochemical purity, solution samples were checked for possible contamination with the gamma-ray spectrometer. Samples had to be rinsed carefully, in order to remove all traces of the etching solution prior to the exchange experiment.

Activity measurements.—The activity measurements were done with a 3-in. well-type NaI(Tl) scintillation counter, mounted on a 6655 RCA photomultiplier. For measuring the metal activity, the samples were mounted in 1-in. diameter Lucite mounts which fitted exactly the well of the counter.

RESULTS

1. Active Solution - Inactive Metal

It has been shown by MacKay (11), and others, that any homogeneous exchange reaction can be described by the following type of equation:

$$[1] \quad -\log(1 - F) = kt,$$

where F is the fraction exchanged, k is a constant, and t is the exchange time. For a heterogeneous reaction, this type of equation holds only as long as the reacting mixture remains chemically unchanged, and if the isotopic distribution is uniform in each phase during the course of the reaction.

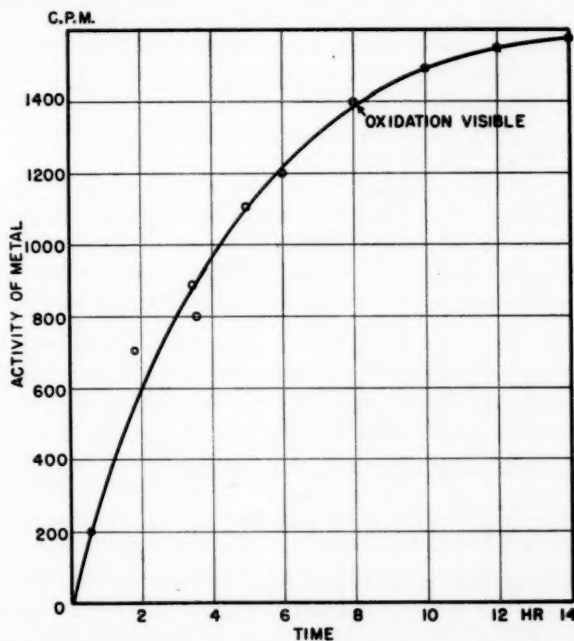


FIG. 1. Exchange between inactive metal and active $10^{-1} M \text{Zn}(\text{NO}_3)_2$ solution.

The results of the experiments done so far indicate that the activity increase (or exchanged fraction) varies exponentially with time (Figs. 1 and 2), but not in accordance

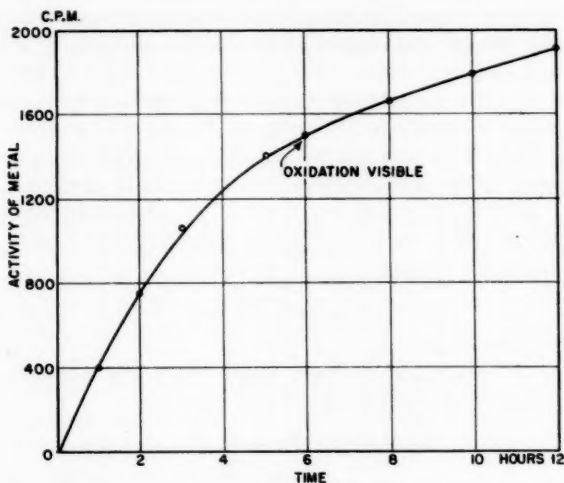


FIG. 2. Exchange between inactive metal and active $10^{-2} M \text{Zn}(\text{NO}_3)_2$ solution.

with equation [1]. In Figs. 3 and 4 the logarithm of the exchanged fraction F is plotted as a function of time of immersion and it is seen that the slope is not constant.* At the

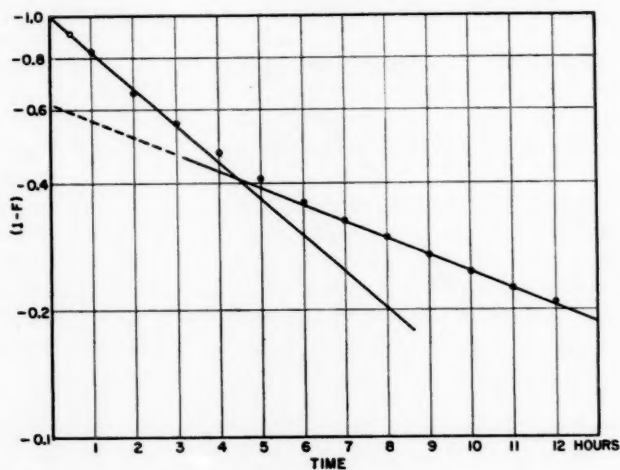


FIG. 3. Fraction exchanged as function of time. Plotted from results of Fig. 1.

same time it was observed that some visible film, presumably $\text{Zn}(\text{OH})_2$, was formed during the second stage of the reaction marked in Figs. 1 and 2. The onset of this film

* $F = A_t/A_\infty$, where A_t is activity of sample at time t and A_∞ is activity when apparent equilibrium is approached.

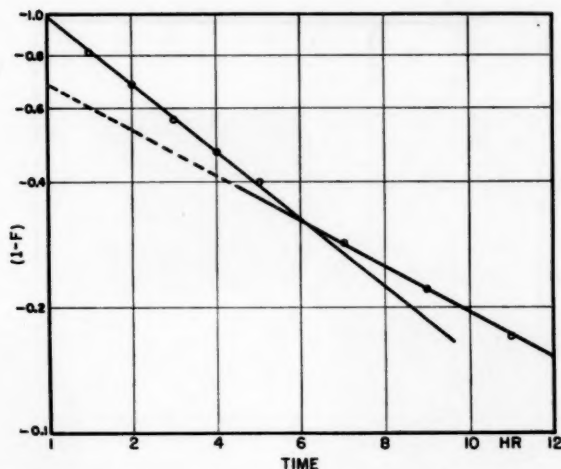


FIG. 4. Fraction exchanged as function of time. Plotted from results of Fig. 2.

formation can not be accurately determined. It was found that apparent exchange equilibrium was approached after 48 hours. Experiments with one week of immersion showed considerable scatter of results.

2. Active Metal - Inactive Solution

When the metal was immersed in acidulated water at pH 4.8, continuous dissolution was observed. No continuous increase in activity took place at pH 5.2 and 6.2; the aliquots taken had an activity slightly higher than the background. The same happened when a sample was pretreated for 24 hours in $10^{-2} M$ $Zn(NO_3)_2$ solution. When the exchange was done for 1 to 6 seconds, wide scattering was obtained giving unreliable results.

During the last set of experiments, when the exchange time was 1 to 6 minutes, it was found that a rapid exchange takes place: in 6 minutes, 20 apparent layers of atoms took part in the exchange. The samples were etched before each immersion. The curve presented in Fig. 5 was obtained when the samples were etched only at the beginning. No difference was observed between tests at pH 5.2 and tests at pH 6.2.

3. Bicrystal Experiments

The autoradiographs of three bicrystal samples shown in Fig. 6 showed a preferential exchange in one of their crystal faces. At the same time it was observed that the difference in activity acquired by each crystal soon disappeared and that after 30 seconds an even distribution of activity was obtained. (Figure 6a corresponds to 10-second, 6b to 20-second, and 6c to 30-second immersion.)

Preferential exchange was shown also by a bicrystal that was markedly twinned (Fig. 7). A sample pretreated for 24 hours and half-etched showed much higher activity in the oxide layer than in the etched layer, but in this latter area a clear difference could be seen in comparing the exchange between each grain (Fig. 8). Other autoradiographs showed that there is a difference in activity between worked and unworked areas, as had been reported for silver and other metals (9).

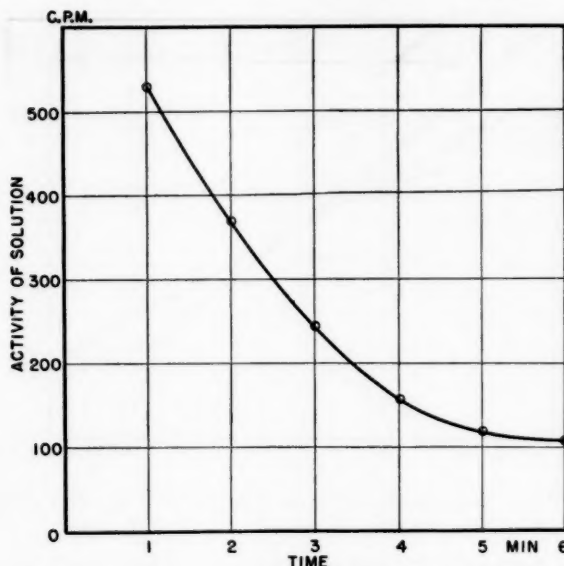


FIG. 5. Exchange between active metal and inactive $\text{Zn}(\text{NO}_3)_2$ solution.

DISCUSSION AND CONCLUSIONS

Heterogeneous exchange between atoms from a work-free zinc surface and atoms from a zinc solution was observed under conditions that minimized adsorption, corrosion, and oxidation. It could not be fully ascertained that an oxide-free surface was obtained, even if the immersion followed immediately after the etching or if the work was done under argon. (The etchants used are generally oxidizing agents.) It was observed that hydroxide formation took place even in the absence of O_2 .

According to the definition of an exchange reaction (12), for a given system the rate of the reaction is independent of the nature of the compound tagged by the indicator;

so, if $\text{A}^* \xrightarrow{k_1} \text{B}$ and $\text{B}^* \xrightarrow{k_2} \text{A}$; then $k_1 = k_2$. The results of these experiments show that an exchange takes place with deaerated 10^{-1} or 10^{-2} M $\text{Zn}(\text{NO}_3)_2$ solution at pH 5.2 or 6.2 in both directions. It could not be proved that $k_1 = k_2$, because in these experiments the rate of transfer of active zinc of one phase to the other is measured and not the exchange rate alone.

It has also been seen that the results of the $\text{Zn}_{\text{sol}}^* \rightarrow \text{Zn}_{\text{metal}}$ reactions do not fit a simple equation of the form $-\log(1-F) = kt$, because the reaction is controlled by either a recrystallization or a self-diffusion process. It would fit an exponential function of two terms, as Matsura (5) found, of the general form:

$$[2] \quad F = 1 - [A_r \exp(-k_r t) + A_s \exp(-k_s t)],$$

where F = fraction exchanged, A_r , A_s , k_r , k_s = constants.

It is concluded, from the experimental results available so far, that the exchange of zinc cannot be presented simply as a diffusion process or a recrystallization-controlled process, in spite of the fact that fast exchange has been obtained in the $\text{Zn}_{\text{metal}}^* \rightarrow \text{Zn}_{\text{sol}}$ reaction. More information is needed about the adsorption properties of zinc ions on

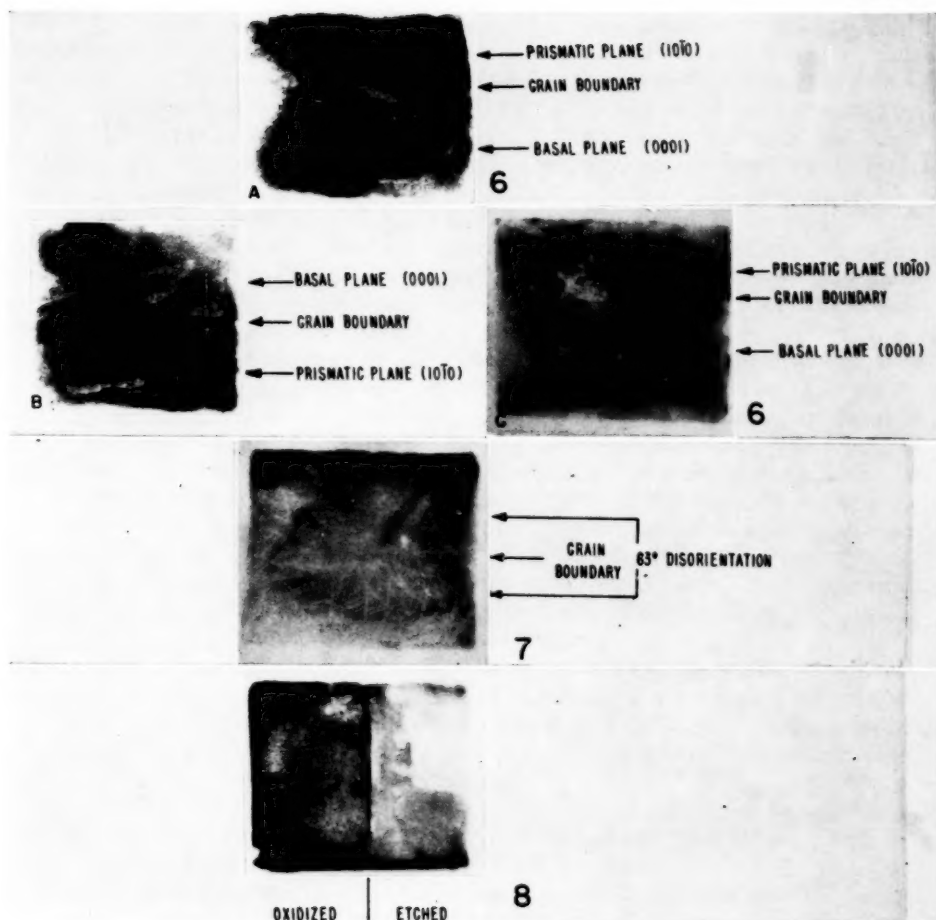


FIG. 6. Autoradiographs of zinc bicrystals.

FIG. 7. Autoradiograph of twinned zinc bicrystal.

FIG. 8. Autoradiograph of a preferentially oxidized zinc bicrystal.

zinc metal. Some work has been done by Matsura with zinc dust, but he did not take into consideration either the surface oxidation or the preparation of the samples.

In the present work a deep exchange has been found between the active metal and the inactive solution in a relatively short period of time. The same effect has been found in silver (13) and it has been explained as caused by a disordered layer of atoms close to the surface giving rise to a very fast diffusion process near the surface of the solid. The surface reaction is not a simple one. In addition to exchange with surface atoms, there always takes place an exchange resulting from local cell action, as postulated by Hevesy (1). It is the author's suggestion that the rapid exchange noticed at the beginning of the experiments is due mainly to this type of mechanism, i.e., one crystal face behaves as an anodic area and the other as a cathodic.

It has been known for some time that the different crystallographic faces of a metal have different electrochemical and physical properties, and hence different electrode potentials, dissolution and oxidation rates, and adsorption. Preferential adsorption may take place, but is relatively unimportant here, since the solutions were very dilute and the immersion periods were very short.

The experiment performed with a half-oxidized and half-etched sample showed that the oxide layer picked up much more activity than did the etched one. This would indicate that the preferential exchange could be caused by preferential oxidation (possibly by the same electrochemical corrosion mechanism as mentioned before). The fact that the activities were soon evened out in the samples indicated that a very small "exchange current" flowed between the two "electrodes". In support of this idea, the recent work of Bushmanov and Vozdvizhenky (7) shows that different crystal faces of zinc single crystals that are connected together act as a galvanocouple. They also found that the different faces exchange at different rates. Alternatively the difference in exchange and adsorption can be ascribed to the difference in surface free energy associated with the different atom densities along the lattice planes involved.

It should be pointed out that in the carrier-free solutions the concentration of the tracer is so low that the products formed may not be the same as those formed at ordinary concentrations, because of rate effects, equilibrium shifts, etc. In some respects this is an advantage, because with so low a concentration no spurious precipitations can happen, since the solubility product cannot be exceeded.

While there is strong evidence that an exchange reaction is involved as a first step in the pickup of activity, this reaction is likely accompanied by other processes, e.g. corrosion and oxidation.

There are considerable variations in the exchange processes described in the literature, mainly because of difficulties in obtaining reproducible, clean metallic surfaces that correspond in composition and structure to the bulk of the metal. It is believed that the surfaces used in this work were of a cleanness comparable with or better than those used in published experiments, but the difference in surface conditions obtained make direct comparisons of results difficult. Even in the case where an oxide-free surface is obtained it is always covered by a thin layer of gases and vapors. Holm and Meissner (14) in their work on platinum had to heat platinum wires for hours at 1100° C in a perpetually evacuated glass vessel, the walls of which were cooled with liquid hydrogen, to obtain a thoroughly degassed surface.

Another problem that has to be solved is to obtain an exact knowledge of the "true" area of the sample, as compared with the geometric area, because in exchange experiments the results are generally expressed in "number of exchanged atom layers". Several methods

are available to determine the surface roughness of metals and some general information is available about the average height of the "hills" and "valleys" in a metallic surface (15); this magnitude is of the following order:

in steel, lapped or polished	—	2 to 25×10^{-6} cm,
die-cast	—	40 to 400×10^{-6} cm,
ground	—	50 to 250×10^{-6} cm,
turned, shaped	—	300 to 600×10^{-6} cm.

There are no similar figures for zinc, but since it is a very soft metal and flows very easily during the polishing operations, comparable figures may differ from those for steel by as much as a factor of 10.

The results can be summarized as follows:

1. The zinc exchange reaction takes place with work-free surfaces in deaerated 10^{-1} and 10^{-2} M $\text{Zn}(\text{NO}_3)_2$ solutions at pH 5.2. to 6.2 and it takes place in both directions.
2. The reaction $\text{Zn}^{++}_{\text{sol}} \rightarrow \text{Zn}^0_{\text{metal}}$ can be described by a relation of the form

$$F = 1 - [A_r \exp(-k_r t) + A_s \exp(-k_s t)],$$

rather than by a single exponential function.

3. Fast exchange has been found in the reaction $\text{Zn}^0_{\text{metal}} \rightarrow \text{Zn}^{++}_{\text{sol}}$, indicating that adsorption was low compared with exchange under the conditions of the experiments.

4. ZnO and $\text{Zn}(\text{OH})_2$ are formed in the metallic samples, preventing the exchange from continuing. $\text{Zn}(\text{OH})_2$ is formed even in the absence of air.

5. Preferential exchange on certain crystal faces has been found to take place in zinc bicrystals.

6. It is suggested that the deep-exchange mechanism involved in the short periods is a local cell action, one crystal behaving as an anode and the other as a cathode.

ACKNOWLEDGMENTS

The author wishes to express his appreciation to Dr. G. G. Eichholz for his help during all this work, to Dr. F. Weinberg and Mr. I. I. Tingley for many helpful discussions, to J. R. Barkley for some experimental help, and to many members of the Physics and Radiotracer Section of the Mineral Sciences Division, Mines Branch, for their advice and assistance. This work was done during the tenure of a National Research Council of Canada postdoctorate fellowship at the Mines Branch of the Department of Mines and Technical Surveys, Ottawa. This paper is published by permission of the Director of the Mines Branch, Department of Mines and Technical Surveys.

REFERENCES

1. G. v. HEVESY. *Physik. Z.* **16**, 52 (1915).
2. B. V. ROLLIN. *J. Am. Chem. Soc.* **62**, 86 (1940).
3. A. M. GAUDIN and K. VINCENT. *Trans. Am. Inst. Mining Met. Engrs.* **169**, 340 (1946).
4. C. HAENNEY and P. MIVELAZ. *Helv. Chim. Acta*, **31**, 633 (1948).
5. NIRO MATSURA. *Sci. Papers Coll. Gen. Educ., Univ. Tokyo*, **5**, 97 (1955).
6. C. V. KING and S. EVANS. *J. Phys. Chem.* **63**, 1816 (1959).
7. B. N. BUSHMANOV and G. S. VOZDVIZHENKY. *Doklady Akad. Nauk S.S.S.R.* **114**, 1046 (1957).
8. G. L. KEHL. *The principles of metallographic laboratory practice*. McGraw-Hill Book Company, New York, 1943.
9. I. I. TINGLEY, I. H. S. HENDERSON, and C. C. COFFIN. *Can. J. Chem.* **34**, 14 (1956).
10. F. WEINBERG. Private communication. Mines Branch, Ottawa, 1959.
11. H. MACKAY. *Nature*, **142**, 997 (1938).
12. M. HAUSSINSKY. *J. chim. phys.* **47**, 957 (1950).
13. J. E. SANDOR. Exchange reactions between silver and its ions. Mines Branch Research Report R 62. Department of Mines and Technical Surveys, Ottawa, 1960.
14. R. HOLM and W. MEISSNER. *Z. Physik*, **74**, 715 (1932).
15. J. J. BIKERMAN. *Surface chemistry*. Academic Press, New York, 1958.

PROTONATION OF THE AMIDE GROUP

II. DICYCLOHEXYLUREA-O¹⁸

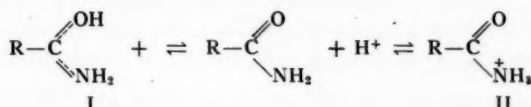
ROSS STEWART AND L. J. MUENSTER

ABSTRACT

Dicyclohexylurea-O¹⁸ containing 78% oxygen-18 has been prepared. The amide I and II bands in this molecule are located at 1611 and 1575 cm⁻¹ respectively compared to 1628 and 1575 cm⁻¹ in ordinary dicyclohexylurea (KBr disk). Thus the amide I band (carbonyl stretching) undergoes the expected shift to lower frequency on isotopic substitution. The *p*-toluenesulphonate salt of dicyclohexylurea has been prepared and been found to have a band at 1669 cm⁻¹ commonly attributed to carbonyl stretching in amide salts. This band, however, undergoes no isotopic shift and is clearly not due to a carbonyl stretching motion. This result casts doubt on the infrared evidence supporting N-protonation of amides.

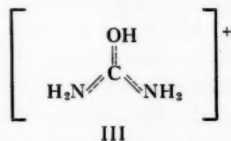
INTRODUCTION

In the previous paper in this series the evidence both for N-protonation and for O-protonation of amides was reviewed (1). In that paper we reported the basicity of a series of benzamides and pointed out that this evidence lent some support to the charge-localized structure II (N-protonated form) for the amide conjugate acid rather than the resonance-stabilized structure I (O-protonated form).

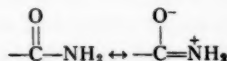


This situation is in contrast to that of the carboxyl group where the resonance-stabilized form appears almost certainly to be the more stable (2).

The principal evidence favoring O-protonation is provided by N.M.R. spectroscopy (2a, 2b). The principal evidence favoring N-protonation is provided by infrared spectroscopy, viz., the observed shift of the carbonyl stretching band to higher frequencies when amides are converted to their salts (3, 4, 5, 6). Thus the carbonyl stretching frequency in propionamide at 1660 cm⁻¹ is replaced by a band at 1710 cm⁻¹ in the hydrobromide (6). Urea, more than ordinary amides, would be expected to undergo O-protonation because of the very favorable resonance possibilities in the conjugate acid, III. Urea salts, however, in particular the well-known urea nitrate, are reported to



have infrared spectra which include a carbonyl stretching band (3, 4). This band is at higher frequency in agreement with the idea that N-protonation would produce more double bond character in the carbonyl group by eliminating resonance of the following type.



¹Manuscript received October 6, 1960.

Contribution from the Department of Chemistry, University of British Columbia, Vancouver, B.C.

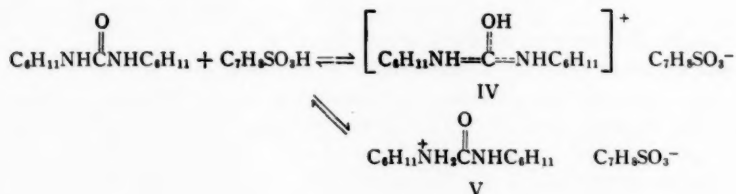
This evidence in favor of N-protonation is difficult to controvert if it can be proved that the bands in question are, in fact, due to carbonyl stretching motions. The purpose of this research was to check the identity of this band in an amide salt by the use of oxygen-18. Halmann and Pinchas have studied the infrared spectra of benzophenone labelled with oxygen-18 (76%) in the carbonyl group (7). They found the only significant difference in the spectra of benzophenone and benzophenone-O¹⁸ was in the carbonyl stretching region; benzophenone absorbs at 1664 cm⁻¹, benzophenone-O¹⁸ at 1635 cm⁻¹ in carbon tetrachloride. This shift of 29 cm⁻¹ to shorter frequency on isotopic substitution is similar to that observed by Braude and Turner (8) for the shift (30 cm⁻¹) of the carbonyl band in cinnamyl *p*-nitrobenzoate on isotopic substitution. More recently Pinchas, Samuel, and Weiss-Brodsky have prepared benzamide-O¹⁸ and have made a thorough study of its infrared spectrum (9). They found that the carbonyl band, amide I, shifts by 24 cm⁻¹ (in carbon tetrachloride), the N—H bonding, amide II, by 10 cm⁻¹ (in chloroform).

We attempted to prepare urea labelled in the carbonyl group but had little success with controlled hydration of cyanamide using stoichiometric amounts of water. We have turned therefore, to dicyclohexylurea, which can be readily prepared by the hydration of dicyclohexylcarbodiimide. This proved to be a very satisfactory alternative.

Dicyclohexylurea-O¹⁸ was prepared from dicyclohexylcarbodiimide according to the following equations.



The para toluenesulphonate salt can have either structure IV or V.



EXPERIMENTAL

Apparatus and Reagents

Infrared spectra were recorded with a Perkin-Elmer Model 21 instrument equipped with sodium chloride optics using potassium bromide pellets. Since it is known that the latter can sometimes give spurious results (10) the spectra of dicyclohexylurea-O¹⁶ and -O¹⁸ and their *p*-toluenesulphonate salts were also recorded in Nujol mulls. The spectra were virtually identical in the two media. The mass spectrometric work was done on a Metropolitan-Vickers mass spectrometer, type 45/1.

The D₂O¹⁸ (91% O¹⁸, 1.1% O¹⁷) was obtained from The Weizmann Institute of Science, Israel.

N,N'-Dicyclohexylurea-O¹⁸

To 15 ml of dioxane (purified and dried with sodium metal) contained in a 50-ml beaker was added 2.34 g (0.0114 mole) of dicyclohexylcarbodiimide. The beaker was placed in an ice-water bath and 0.25 g (0.0114 mole) of D₂O¹⁸ was pipetted into the solution. Dry hydrochloric acid gas was bubbled through the mixture via a capillary

for 1½ minutes. The resulting white precipitate was filtered at the pump, washed with a little dioxane, and dried in a vacuum desiccator. The crude product weighed 1.66 g or 64% of the theoretical yield.

To obtain a deuterium-free sample, 300 mg of the crude product was dissolved in 5 ml of boiling absolute ethanol. On cooling of the solution to room temperature, colorless, broad needles separated out which melted at 237–238° (uncorr.).

The percentage of O¹⁸ contained in the compound was determined according to the method by Rittenberg and Ponticorvo (11). The oxygen-18 content of the carbon dioxide was measured by scanning the masses from 44 to 48. The average value obtained from five determinations was 78.3% O¹⁸, though the precision was rather low (standard deviation of the mean: ±2.3%).

N,N'-Dicyclohexylurea-O¹⁸ *p*-Toluenesulphonate

N,N'-Dicyclohexylurea-O¹⁸ (0.50 g, 0.0021 mole) and *p*-toluenesulphonic acid (0.38 g, 0.0021 mole) were added to 2 ml of dry dioxane and refluxed for 10 minutes. On cooling to room temperature colorless, small needles separated out. After several recrystallizations from thiophene-free dry benzene 0.33 g (39% of the theory) of the *p*-toluenesulphonate was obtained which melted at 154–155° (corr.). Calc. for C₂₀H₃₂N₂SO₃O¹⁸: C, 60.24; H, 8.10; N, 7.03; O, 16.56; S, 8.04. Found: C, 60.33; H, 8.02; N, 6.91; O, 16.23; S, 8.02.

When this salt was crystallized from absolute ethanol it reverted to dicyclohexylurea with no loss of isotopic oxygen. This was shown to be so by a comparison of infrared spectra.

Urea p-Toluenesulphonate

Urea (3.0 g, 0.05 mole), *p*-toluenesulphonic acid (10.7 g, 0.06 mole), and 100 ml of dry dioxane were heated to boiling. The voluminous white precipitate which formed was filtered and washed with ice-cold water and ether. After one recrystallization from water the yield was 8.9 g (77%). During three subsequent recrystallizations from water the melting point remained constant at 181–183° (corr.). Calc. for C₈H₁₂N₂O₄S: C, 41.37; H, 5.21; N, 12.05; S, 13.80%. Found: C, 41.36; H, 5.14; N, 12.02; S, 13.61%.

The melting point of this compound is near that reported for the covalent compound, *p*-toluenesulphonylurea (m.p., 191–2° (12)) and its resistance to hydrolysis during crystallization from water is also compatible with the latter structure. The analytical data together with the following facts show the compound to be the salt: (a) titration with standard base gives the correct neutral equivalent, (b) passage of a solution of the compound through a strongly acid cation-exchange column (Nalco HCR-W) produces *p*-toluenesulphuric acid.

RESULTS AND DISCUSSION

The infrared spectra of dicyclohexylurea, dicyclohexylurea-*d*-O¹⁸, and dicyclohexylurea-O¹⁸ are shown in Fig. 1. The spectra of the *p*-toluenesulphonates of dicyclohexylurea and dicyclohexylurea-O¹⁸ are shown in Fig. 2.

Dicyclohexylurea

The infrared spectrum of this compound (Fig. 1) is similar to those of other substituted ureas and to that of urea itself (13, 14, 15, 16). The amide I band (carbonyl stretching) is at 1628 cm⁻¹ and the amide II band (17, 18) is at 1575 cm⁻¹. In addition a third band is present in dicyclohexylurea at 1539 cm⁻¹ which is also present (1550 cm⁻¹) in monocyclohexylurea (14). The "amide band" locations are listed in Table I.

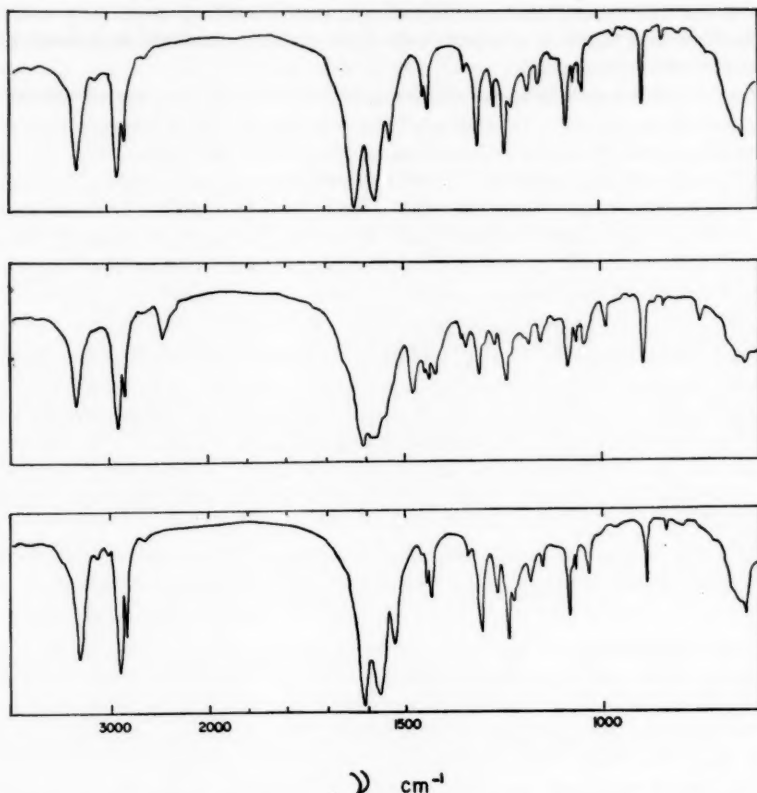


FIG. 1. The infrared spectra of dicyclohexylurea (upper), dicyclohexylurea- $d\text{-O}^{18}$ (middle), and dicyclohexylurea- O^{18} (lower).

TABLE I
"Amide bands",* cm^{-1}

	I	II	(†)
Dicyclohexylurea	1628	1575	1539
Dicyclohexylurea- O^{18}	1611		
Dicyclohexylurea- O^{18}	1611	1575	1533
Dicyclohexylurea <i>p</i> -toluenesulphonate	1669	1620	
Dicyclohexylurea- O^{18} <i>p</i> -toluenesulphonate	1668	1618	

*The first two bands in both the amides and amide salts are designated here as amide I and II bands.
†The third band in this region.

Dicyclohexylurea-d-O¹⁸

The percentage deuterium in this compound is unknown. However, the considerably greater intensity of the N—H stretching band at 3343 cm^{-1} than the N—D stretching band at about 2480 cm^{-1} indicates that there is probably more protium than deuterium present. The amide II band at 1575 cm^{-1} is broadened and five new peaks at 2480, 1480, 1425, 988, and 795 cm^{-1} appear in the spectrum of the partly deuterated compound.

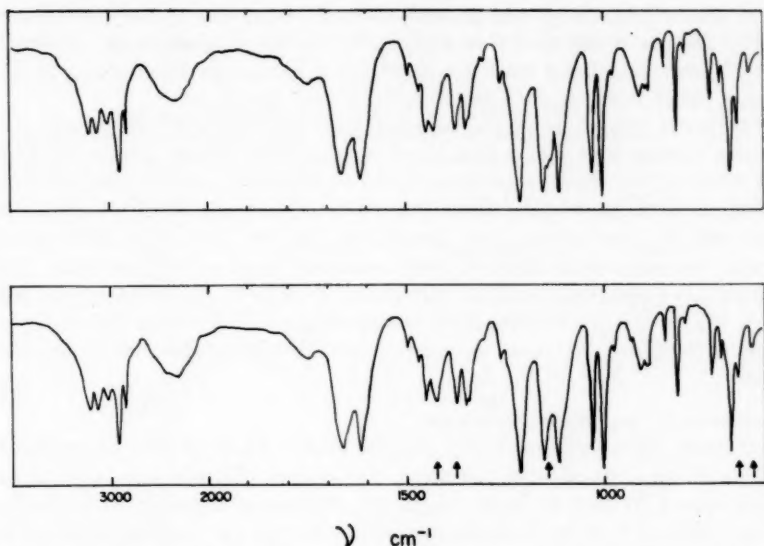


FIG. 2. The infrared spectra of dicyclohexylurea *p*-toluenesulphonate (upper) and dicyclohexylurea- O^{18} *p*-toluenesulphonate (lower).

Dicyclohexylurea- O^{18}

The principal feature of interest in this system is the shift of the amide I band on isotopic substitution. This band, which is generally attributed to carbonyl stretching, shows the isotopic shift to lower frequency expected for such a band. The shift of 17 cm^{-1} (1628 to 1611 cm^{-1} in KBr) is smaller than the corresponding shift observed for benzophenone (29 cm^{-1} in CCl_4) (7), and for benzamide (24 cm^{-1} in CCl_4) (9). (The magnitude of the isotopic shift appears to depend on the medium since Pinchas *et al.* (9) observed that it was considerably less in chloroform than in carbon tetrachloride.) The smaller shift in the present case may be due to a contribution from the C—N stretching vibration to the amide I band as suggested by Myazawa *et al.* (18). (See, however, ref. 9.)

The amide II band at 1575 cm^{-1} undergoes no isotopic shift at all. The third band in this region, the one at 1539 cm^{-1} in ordinary dicyclohexylurea undergoes a small isotopic shift and appears at 1533 cm^{-1} in the oxygen-18 compound. Table II lists the bands in the amide which undergo oxygen isotopic shifts of 3 cm^{-1} or more.

TABLE II
Isotopic shifts,* cm^{-1}

Dicyclohexylurea	1628	1539	1160	1047	643
Dicyclohexylurea- O^{18}	1611	1532	1157	1038	640
Dicyclohexylurea <i>p</i> -toluenesulphonate	1437	1378	1135	666	635
Dicyclohexylurea- O^{18} <i>p</i> -toluenesulphonate	1427	1375	1129	661	629

* 3 cm^{-1} or more.

Dicyclohexylurea *p*-Toluenesulphonate

Above 1600 cm^{-1} the spectrum of this compound resembles that of urea nitrate. The N—H stretching bands are broadened and shifted to lower frequency in both compounds

resulting in a set of moderately sharp bands above 3000 cm^{-1} and a very broad absorption in the $2400\text{--}2600\text{ cm}^{-1}$ region. These changes in the N—H absorption and the absence of an O—H stretching band contributed to the rejection by Davies and Hopkins (3) and Spinner (4) of the idea of O-protonation in urea nitrate.

In the carbonyl stretching region between 1600 and 1700 cm^{-1} there are two bands in both urea nitrate and dicyclohexylurea *p*-toluenesulphonate. These are located at 1705 and 1675 cm^{-1} in the former (Davies and Hopkins (3) report 1708 and 1670 cm^{-1}) and at 1669 and 1620 cm^{-1} in the latter. The 1670 cm^{-1} band in urea nitrate has been assigned by Davies and Hopkins to carbonyl absorption and the shift from 1610 cm^{-1} in urea attributed to the increase in carbonyl bond order as a result of N-protonation (3). Other investigators have assigned carbonyl stretching in urea to the band in the 1680 cm^{-1} region (15, 16). If one of these bands in the spectrum of the salt of dicyclohexylurea is in fact due to carbonyl stretching an isotopic shift should be observed in the oxygen-18 compound.

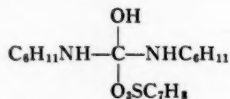
Dicyclohexylurea-O¹⁸ p-Toluenesulphonate

Figure 2 shows the spectrum of this compound and Table II lists those peaks which undergo an isotopic shift of 3 cm^{-1} or more. The largest of these is the shift of the 1437 cm^{-1} peak which moves 10 cm^{-1} to lower frequency. Particularly significant is the fact that the peak at 1669 cm^{-1} is in virtually the same place in the oxygen-18 compound. An average of several runs gave the peak locations as 1669 and 1668 cm^{-1} in the isotopically unsubstituted and substituted compounds respectively. One can therefore conclude that this band in dicyclohexylurea *p*-toluenesulphonate is not, in fact, caused by a carbonyl stretching motion and its location at higher frequency than the amide I band in dicyclohexylurea *does not* constitute support for the idea of N-protonation of amides.

The infrared evidence, in fact, supports the idea of O-protonation of urea-type compounds. (It is true that an O—H stretching band cannot be detected in the infrared (14) but this band may be shifted and masked by the broad N—H absorption. Furthermore, hydrogen stretching bands are sometimes of very low intensity in organic cations (19).) The isotopic shift in dicyclohexylurea *p*-toluenesulphonate (Table II) from 1437 cm^{-1} to 1427 cm^{-1} probably corresponds to O—H bending (20) and the isotopic shift from 1135 cm^{-1} to 1129 cm^{-1} can also be explained on the basis of O-protonation since C—OH stretching vibrations are usually found in this region. The first band in the carbonyl region of the urea and dicyclohexylurea *p*-toluenesulphonates may be due to N—H bending increased in frequency by strong inner hydrogen bonding with the tosylate oxygen atoms. (We are grateful to Dr. S. Pinchas for drawing our attention to some of these points.)

Ionic Character

We have considered the possibility that the *p*-toluenesulphonate of dicyclohexylurea might be a covalent compound of some such structure as the following.



Although this is unlikely in view of the high stability of the *p*-toluenesulphonate ion we attempted to prepare other salts of this compound. Our attempts to prepare the perchlorate, hydrochloride, and nitrate were unsuccessful, however.

We turned then to a comparison of the infrared spectra of other *p*-toluenesulphonates, both covalent and ionic, with that of the compound in question. Table III lists the

TABLE III
p-Toluenesulphonate infrared bands below 1200 cm⁻¹

Dicyclohexylurea compound (cm ⁻¹)	Sodium salt (cm ⁻¹)	Potassium salt (cm ⁻¹)	Ammonium salt (cm ⁻¹)	Methyl ester (cm ⁻¹)	Urea compound (cm ⁻¹)
1218	1222				1201
	1188	1185-1205	1155-1200	1190	
1156	1179			1179	1153
1118	1130	1127	1127		1129
				1095	
1031	1045	1038	1036		1038
1007	1014	1013	1011	1020	1013
				990	
888					871
849	854	846	845		
					818
817	816	813	815	817	814
				765	
730					
710	711	709	708	705	710
683	688	687	686	687	690
	678				
				662	

principal absorption bands below 1200 cm⁻¹ of the following *p*-toluenesulphonates:

- the dicyclohexylurea compound,
- the sodium, potassium, and ammonium salts (ionic),
- the methyl ester (covalent).

A comparison of the absorption bands shows a very close correspondence between the bands in the ionic sulphonates (except for the band at 1156 cm⁻¹) and those in the dicyclohexylurea compound whereas the bands in the covalent methyl ester are missing in the latter. We conclude that dicyclohexylurea *p*-toluenesulphonate is an ionic compound.

The similarity between dicyclohexylurea *p*-toluenesulphonate and urea nitrate can be seen by a comparison of the infrared spectra of these compounds and those of other salts of urea. We have prepared the *p*-toluenesulphonates and perchlorates of urea and it can be seen from the absorption data in Table IV that the peaks of these compounds

TABLE IV
Infrared bands in urea and its compounds in the range, 1500-2500 cm⁻¹

Urea	Urea nitrate	Urea <i>p</i> -toluenesulphonate	Urea perchlorate*
1680	1705	1709	1700
1615	1675	1670	1650
	1570	1564	1558

*Hygroscopic, poor spectrum.

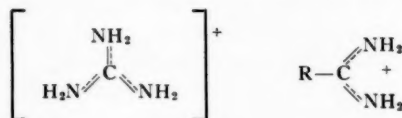
in the carbonyl stretching region correspond closely to those of the well-studied salt, urea nitrate, indicating that the character (presumably ionic) of these two compounds is the same. If one then examines the spectrum of one of these, urea *p*-toluenesulphonate,

in the region below 1250 cm^{-1} where the tosylate group absorption occurs, one can see (Table III) that the peaks correspond fairly closely to those of dicyclohexylurea *p*-toluenesulphonate and sodium, potassium, and ammonium *p*-toluenesulphonates.

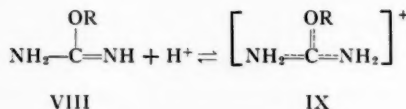
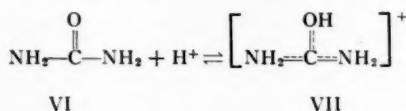
Thus both urea nitrate and dicyclohexylurea *p*-toluenesulphonate appear to be ionic compounds. Both show an amide I band at higher frequency than in the neutral compounds. This evidence does not support N-protonation, however, since this band, at least in the one case, does not correspond to carbonyl stretching. One cannot, of course, conclude that the band assigned to carbonyl stretching in the salts of ordinary amides is misassigned but the present work shows that caution should be used in making the assignment. We intend to conduct a similar investigation to the present one using ordinary amides.

Amidine Protonation

It should be made clear that the uncertainty with regard to the structure of the amide cation does not apply to the guanidinium ion, or amidinium ions in general, where the following resonance-stabilized structures are unquestionably the stable ones.



It seems clear, however, that the high basicity of amidines is due as much to decreased resonance in the neutral molecules (compared to urea and ordinary amides) as it is to increased resonance in the ions. Indeed, the fact that O-alkyl ureas are about 10^{10} times as basic as urea (21, 22) must be attributed almost entirely to the difference in resonance energies of the neutral molecules VI and VIII, since it is highly improbable that ions VII and IX have very different resonance energies. (The equilibrium between N- and O-protonated forms of urea does not affect this argument.)



ACKNOWLEDGMENT

We thank Dr. D. C. Frost for the mass spectrometric analysis and the National Research Council for its financial support. The helpful comments of Drs. S. Pinchas and D. Samuels are gratefully acknowledged.

REFERENCES

1. J. T. EDWARD, H. S. CHANG, K. YATES, and R. STEWART. *Can. J. Chem.* **38**, 1518 (1960).
2. R. STEWART and K. YATES. *J. Am. Chem. Soc.* **82**, 4059 (1960).
- 2a. A. BERGER, A. LOEWENSTEIN, and S. MEIBOOM. *J. Am. Chem. Soc.* **81**, 62 (1959).

- 2b. G. FRAENKEL and C. FRANCONI. *J. Am. Chem. Soc.* **82**, 4478 (1960).
3. M. DAVIES and L. HOPKINS. *Trans. Faraday Soc.* **53**, 1563 (1957).
4. E. SPINNER. *Spectrochim. Acta*, **2**, 95 (1959).
5. E. H. WHITE. *J. Am. Chem. Soc.* **77**, 6215 (1955).
6. K. YATES. Ph.D. Thesis. University of British Columbia, Vancouver, B.C. 1959.
7. M. HALMANN and S. PINCHAS. *J. Chem. Soc.* 1703 (1958).
8. E. A. BRAUDE and D. W. TURNER. *Chem. & Ind. (London)*, 1223 (1955).
9. S. PINCHAS, D. SAMUEL, and M. WEISS-BRODAY. Personal communication.
10. C. C. WATSON. *Chem. & Ind. (London)*, 964 (1960) and references therein.
11. D. RITTENBERG and L. PONTICORVO. *Intern. J. Appl. Radiation and Isotopes*, **1**, 208 (1956).
12. F. KURZEN and J. R. POWELL. *J. Chem. Soc.* 1497 (1955).
13. P. A. BOIVIN, W. BRIDGEO, and J. L. BOIVIN. *Can. J. Chem.* **32**, 242 (1954).
14. J. L. BOIVIN and P. A. BOIVIN. *Can. J. Chem.* **32**, 561 (1954).
15. J. E. STEWART. *J. Chem. Phys.* **26**, 248 (1957).
16. R. B. PENLAND, S. MIZUSHIMA, C. CURRAN, and J. V. QUAGLIANO. *J. Am. Chem. Soc.* **79**, 1575 (1957).
17. R. N. JONES and C. SANDORFY. *In* *Technique of organic chemistry*. Vol. IX. Edited by A. Weissberger. Interscience Publishers, New York. 1956. p. 521.
18. T. MIYAZAWA, T. SHIMANOCHI, and S. MIZUSHIMA. *J. Chem. Phys.* **24**, 408 (1956).
19. R. STEWART, M. MOCEK, and R. B. MOODIE. To be published.
20. R. N. JONES and C. SANDORFY. *In* *Technique of organic chemistry*. Vol. IX. Edited by A. Weissberger. Interscience Publishers, New York. 1956. pp. 431-434.
21. M. ZIEF and J. T. EDSALL. *J. Am. Chem. Soc.* **59**, 2245 (1937).
22. C. R. NOLLER. *Chemistry of organic compounds*. 2nd ed. W. B. Saunders Co., Philadelphia. 1957. p. 319.

STEROIDS

V. PYRIDINIUM BETAINES OF 2- α -BROMOCHOLESTAN-3-ONE^{1,2}

G. FRANGATOS³ AND A. TAURINS

ABSTRACT

2- α -Bromocholestan-3-one reacts with pyridine, and 3- and 4-methylpyridines to give the 1-[2-(3-oxocholestanyl)]pyridinium bromides which, on dehydrobromination with bases, form the betaines of 1-[2-(3-oxocholestanyl)]pyridinium hydroxides.

DISCUSSION

The treatment of α -bromo ketones with pyridine and its homologues leads to the elimination of hydrogen bromide from the α -bromo ketone and to the formation of a double bond in α,β -position to the carbonyl group. On several occasions it has been observed that intermediate adducts are formed in the reaction of steroidal α -bromo ketones and pyridine bases. In some instances differences in opinion exist regarding the structure of the intermediates. Thus two entirely different structural formulae II and III have been proposed by Ruzicka (1), and Inhoffen (2), respectively, for the product of the reaction between 2- α -bromocholestan-3-one (I) (3) and pyridine.

In an attempt to establish which of the structures was correct, the present work was undertaken. If the formula set forth by Ruzicka is correct, then elimination of a molecule of hydrogen bromide from II (a pyridinium bromide) should result in the formation of a pyridinium enol betaine (IV) (4,5). Elimination of hydrogen bromide from III (a hydrobromide of a 4-substituted pyridine), on the other hand, should produce a 4-substituted pyridine base. With this in mind, hydrogen bromide was eliminated from the reaction product of pyridine and 2- α -bromocholestan-3-one (I), and isolation of the reaction product attempted. When a solution of the product in chloroform was treated with solid anhydrous potassium carbonate, a deep-red oil was isolated which resisted all attempts of crystallization and exhibited a pronounced tendency to form thin films. It was sensitive to heat and decomposed gradually on exposure to light. Elementary analysis indicated the presence of nitrogen but not of bromine. Upon treatment with hydrogen bromide, the product afforded the starting material. When an aqueous solution of perchloric acid was added to the oil, the corresponding colorless perchlorate was formed readily.

These experimental facts supported the assumption that the reaction product of pyridine and the bromo ketone (I) was the pyridinium salt (II) which formed the betaine of 1-[2-(3-hydroxy-2-cholestanyl)]pyridinium hydroxide (IV) upon elimination of a molecule of hydrogen bromide.

In other attempts to obtain the betaine (IV), the pyridinium bromide (II) was suspended in water or ethanol and treated with aqueous solutions of inorganic bases. Piperidine, morpholine, and guanidine carbonate reacted similarly, and in all cases hydrogen bromide was eliminated. However, the betaine (IV) was always obtained as an amorphous material. Finally, the betaine of 1-[2-(3-hydroxy-2-cholestanyl)] pyridinium hydroxide (IV) was obtained in crystalline form, when the dehydrobromination of the

¹Manuscript received October 28, 1960.

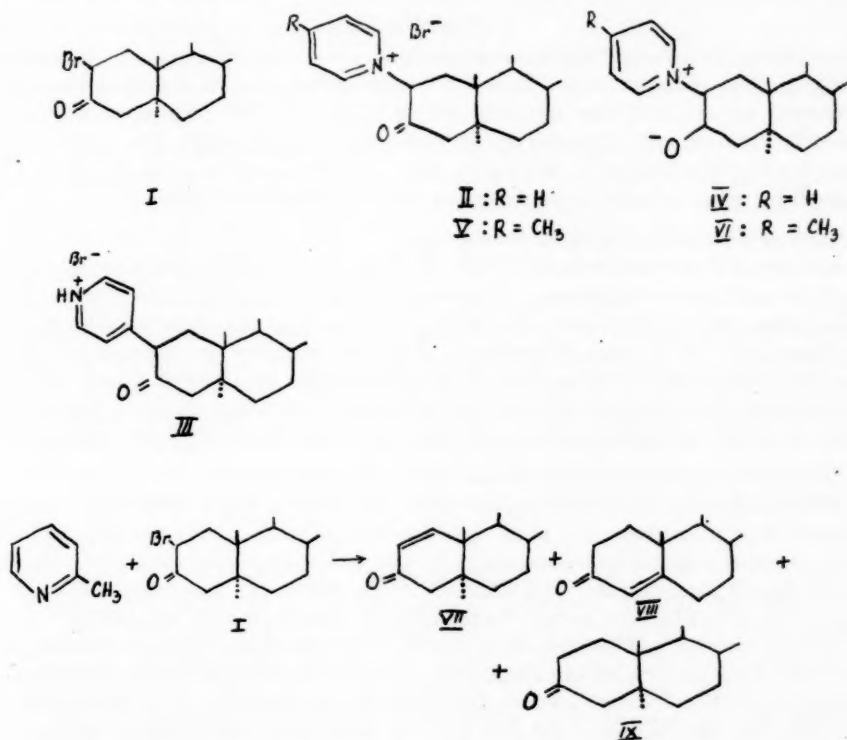
Contribution from the Department of Chemistry, McGill University, Montreal, Quebec, with financial assistance from the National Research Council, Ottawa, Canada.

²Steroids. IV. T. H. Waid and A. Taurins. *Can. J. Chem.* 38, 1983 (1960).

³Holder of a Canadian Industries (1954) Limited Fellowship, 1954-55, and of a National Research Council Studentship, 1955-1956.

pyridinium bromide (II) was carried out in the three-component system ethanol-water - dimethylamine. The ultraviolet spectrum of the betaine showed three absorption maxima at 245, 304, and 430 μ . The similarity in pattern of the spectrum of IV and of the betaines obtained from methylpyridines and 2-bromo-1,3-indandione by Frangatos and Taurins (5) provided further proof that IV was a typical pyridinium betaine.

On the basis of the assumptions made by Inhoffen (2), the addition product of pyridine and 2- α -bromocholestan-3-one (I) should be a 4-substituted pyridine hydrobromide. If this is correct, then 4-methylpyridine should not react with the bromo ketone (I). It was found, however, that the reaction of 4-methylpyridine with I proceeded smoothly to give the salt, 1-[2-(3-oxocholestanyl)]4-methylpyridinium bromide (V). The dehydrobromination of V was achieved in chloroform solution using anhydrous potassium carbonate. The product, the betaine of 1-[2-(3-hydroxy-2-cholestanyl)]4-methylpyridinium hydroxide (VI), was an amorphous, dark-red solid. In sunlight, it gradually decomposed, and on



treatment with acids, colorless solids, the pyridinium salts, were formed. Elementary analysis and the ultraviolet absorption spectrum of VI were in agreement with the assignment of a betaine structure to this compound. 3-Methylpyridine reacted similarly and the betaine of 1-[2-(3-hydroxy-2-cholestanyl)]3-methylpyridinium hydroxide was obtained as a dark-red powder which could not be crystallized.

The reaction of the bromo ketone (I) with 2-methylpyridine did not afford the corresponding pyridinium bromide. Instead 2-methylpyridine hydrobromide was isolated from

the reaction mixture indicating that dehydrobromination of the bromo ketone (I) had occurred. Dehydrobromination could proceed directly or through the formation of the intermediate salt, 1-[2-(3-oxocholestanyl)]2-methylpyridinium bromide. However, by analogy with the reactions of pyridine, and 3- and 4-methylpyridines and the bromo ketone (I), the formation of the salt would seem improbable since it would interfere with the elimination of hydrogen bromide. This assumption was confirmed experimentally by taking samples from the reaction mixture at different times, and treating them with alkali. No change in color was observed. If 1-[2-(3-oxocholestanyl)]2-methylpyridinium bromide had been present in the reaction mixture, it should have undergone a dehydrobromination and formed the corresponding betaine. This process would have been accompanied by a change in color. It was presumed that dehydrobromination of the bromo ketone (I) yielded a mixture of compounds (VII, VIII, IX), similar to those isolated by Jacobsen (6) from the reaction of I with 2,4,6-trimethylpyridine.

EXPERIMENTAL

The melting points below 225° were determined in a Thiele-Dennis melting-point tube containing sulphuric acid. Those above 225° were determined in a melting-point block constructed according to the specifications of Fieser (7). All melting points are uncorrected. Pyridine and methylpyridines were dried and purified. The analyses were carried out by Schwarzkopf in Woodside, N.Y. The ultraviolet absorption spectra were measured by means of a Beckman recording spectrophotometer Model DK1.

1-[2-(3-Oxocholestanyl)]pyridinium Bromide (II)

A solution of 2- α -bromocholestan-3-one (I) (7 g, 0.015 mole) in pyridine (34 ml) was heated, in a nitrogen atmosphere, to the reflux temperature. After 10 minutes, a solid material separated rapidly. When the reaction mixture had been refluxed for 2 hours, it was allowed to cool to room temperature. The solid material was filtered off, washed thoroughly with three 25-ml portions of petroleum ether (b.p. 60–90°), and dried. Recrystallization from ethanol provided 1-[2-(3-oxocholestanyl)]pyridinium bromide (II) (6.2 g), m.p. 310° (decomposed); lit. (1) m.p. 310° (decomp.); $\lambda_{\text{max}}^{\text{EtOH}}$ 261 m μ (log ϵ 3.5).

1-[2-(3-Hydroxy-2-cholestanyl)]pyridinium Hydroxide, Betaine (IV)

1-[2-(3-Oxocholestanyl)]pyridinium bromide (II) (0.54 g, 0.001 mole) was suspended in alcohol (3 ml), and stirred in a nitrogen atmosphere at the reflux temperature, while a 25% aqueous solution of dimethylamine was added dropwise. Gradually the solid material passed into solution. The addition of dimethylamine was continued until the yellow solution had become turbid. As the reaction mixture cooled very slowly to room temperature, fine yellow needles separated from the solution. Recrystallization from alcohol and aqueous 25% dimethylamine in a nitrogen atmosphere gave the betaine of 1-[2-(3-hydroxy-2-cholestanyl)]pyridinium hydroxide (IV) (0.029 g), m.p. 169° (decomp.); $\lambda_{\text{max}}^{\text{EtOH}}$ 245, 304, 430 m μ (log ϵ 3.8, 3.0, 3.7). An analytical sample was dried *in vacuo* over phosphorus pentoxide at 34° for 72 hours in the dark. Anal. Calcd. for C₃₂H₄₉NO: N, 3.02. Found: N, 3.19%.

1-[2-(3-Oxocholestanyl)]4-methylpyridinium Bromide (V)

A solution of 2- α -bromocholestan-3-one (I) (4.65 g, 0.01 mole) in 4-methylpyridine (15 ml) was refluxed for 4 hours; the reaction mixture was allowed to cool to room temperature. The solid precipitate was collected, washed with petroleum ether, and dried. Recrystallization from hot acetic acid gave 1-[2-(3-oxocholestanyl)]4-methylpyridinium

bromide (V) (3.7 g) in shining colorless prisms, m.p. 316° (decomp.); $\lambda_{\text{max}}^{\text{EtOH}}$ 225, 257.5 μ (log ϵ 4.0, 3.6). Anal. Calcd. for $\text{C}_{33}\text{H}_{51}\text{BrNO}$: C, 70.95; H, 9.36; N, 2.5. Found: C, 71.35; H, 9.57; N, 2.75%.

1-[2-(3-Hydroxy-2-cholestanyl)]4-methylpyridinium Hydroxide, Betaine (VI)

The pyridinium bromide (V) (0.28 g, 0.005 mole) was added to a stirred suspension of anhydrous potassium carbonate (1 g) in chloroform (10 ml). The mixture became orange immediately, and deepened in color as the reaction proceeded. The reaction mixture was refluxed gently for 5 minutes in a nitrogen stream. Then it was cooled to 0°, filtered, and washed with two 5-ml portions of chloroform. The washings and filtrate were combined and evaporated to dryness. The residue was dried *in vacuo* at 34° for 72 hours, and in this way the betaine (VI) (0.19 g) was obtained. The substance softened above 100° but had an indefinite melting point. $\lambda_{\text{max}}^{\text{EtOH}}$ 248, 308, 431 μ . Anal. Calcd. for $\text{C}_{33}\text{H}_{51}\text{NO}$: N, 2.93. Found: N, 2.92%.

1-[2-(3-Oxcholestanyl)]3-methylpyridinium Bromide

This substance was prepared in a manner analogous to that used for the preparation of compounds (II) and (IV). Colorless plates (from a 2:3 acetic acid - water mixture), m.p. 314° (decomp.).

1-[2-(3-Hydroxy-2-cholestanyl)]3-methylpyridinium Hydroxide, Betaine

This betaine was obtained in a manner analogous to that employed for the preparation of compounds (IV) and (VI). Yellow needles (from chloroform); the substance softened at 128°, but did not melt at a definite temperature. $\lambda_{\text{max}}^{\text{EtOH}}$ 255, 314, 432 μ (log ϵ 3.2, 3.2, 3.0). Anal. Calcd. for $\text{C}_{33}\text{H}_{51}\text{NO}$: N, 2.93; Found: N, 2.74%.

Reaction of 2- α -Bromocholestan-3-one (I) with 2-Methylpyridine

A mixture of 2-methylpyridine (10 ml) and I (2.33 g, 0.005 mole) was refluxed, in a nitrogen atmosphere, for 5 hours. No precipitate was formed at any time during the reflux period. Several samples were taken by means of a micropipette at different times; no pronounced change in color was observed when those samples were added to dilute alkaline solutions. The excess 2-methylpyridine was removed from the reaction mixture in a stream of nitrogen under reduced pressure. A white substance, sublimed from the residue at 125–130° under 2 mm pressure, was characterized as 2-methylpyridine hydrobromide.

REFERENCES

1. L. RUZICKA, P. A. PLATTNER, and R. AESCHBACHER. *Helv. Chim. Acta*, **21**, 866 (1938).
2. H. H. INHOFFEN, G. ZUHLSDORFF, and HUANG-MINLON. *Ber. deut. chem. Ges.* **73**, 451 (1940).
3. A. BUTENANDT and A. WOLFF. *Ber. deut. chem. Ges.* **68**, 2091 (1935).
4. F. KRÖHNKE. *Ber. deut. chem. Ges.* **68**, 1177 (1935).
5. G. FRANGATOS and A. TAURINS. *Can. J. Chem.* **37**, 835 (1959).
6. R. P. JACOBSEN. *J. Am. Chem. Soc.* **62**, 1620 (1940).
7. L. F. FIESER. *Experiments in organic chemistry*. 2nd ed. D. C. Heath & Co., New York. 1941. p. 329.

INFRARED SPECTRA-STRUCTURE CORRELATIONS OF N-SUBSTITUTED TRIFLUOROACETAMIDINES¹

JOHN C. GRIVAS² AND ALFRED TAURINS

ABSTRACT

A correlation between the infrared spectra and the structure of some N-mono- and N-di-substituted trifluoroacetamidines is presented. It was found that there was a considerable similarity between the infrared spectra of trifluoroacetamidines and those of the corresponding trichloroacetamidines. Additional information of the existence of these amidines in the imino form, $\text{CF}_3\text{-C(=NH)NHR}$, was provided by the infrared study of N,N-dideuterioamidines.

INTRODUCTION

In a previous communication (1) the evidence for the existence of N-alkyl- and N-aryl-trichloroacetamidines in the form I was presented.



Prevorsek (2) in a study of the infrared spectra of N-substituted benzamidines (IIa and IIb) concluded that when R' was an alkyl group (ethyl) the benzamidines existed in the form IIa, but when R' was an aryl group (phenyl) the amidine had the structure IIb.

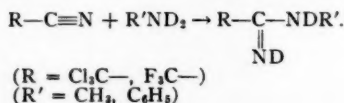


The infrared spectrum of alkyl-substituted amidines IIa showed a very strong "amidine II" band at 1560 cm^{-1} which was displaced in solution. In the spectra of deuterated amidines (IIa) this band was not present but a new band appeared at 1400 cm^{-1} . There was no "amidine II" band for the aryl-substituted benzamidines (IIb) between $1580\text{--}1500 \text{ cm}^{-1}$ since such displacement of the band observed did not occur on deuteration and was not also sensitive to the breaking of hydrogen bonds on dilution. Therefore the structure IIb of aryl-substituted benzamidines was accepted. Prevorsek (2) also found that the observed $\nu_{\text{sym}}(\text{NH})$ vibrations were in good agreement with those calculated by the Bellamy equation (3):

$$\nu_{\text{sym}}(\text{NH}) = 345.5 + 0.876\nu_{\text{asym}}$$

EXPERIMENTAL

The trifluoroacetamidines used in this infrared study were prepared by known methods (4) or by procedures outlined in the previous paper (6). The deuterioamidines were synthesized from nitriles and N,N-deuterioamines according to the following reaction scheme:



¹Manuscript received November 10, 1960.

Contribution from the Department of Chemistry, McGill University, Montreal, Quebec, with financial assistance from the National Research Council of Canada, Ottawa.

²Holder of the National Research Council Studentship, 1954-1958, and 1958-1959.

The infrared spectra were recorded on a Perkin-Elmer Model 21 spectrometer equipped with a sodium chloride prism. The solid substances were investigated in potassium bromide pellets or in Nujol mulls. Liquid substances were examined in a thin layer between two sodium chloride plates. Amidines were also studied by infrared in tetrachloroethylene solutions (10 mg in 1 ml of the solvent), and sodium chloride cells 1 mm thick were used.

N-Methyl- α,α,α -trifluoroacetamidine- d_2

Trifluoroacetonitrile (0.04 mole) was condensed in a Pyrex tube (20×700 mm) previously flushed with nitrogen. The lower part of the tube, 30 cm in length, was immersed in a dry ice-acetone mixture. Methylamine- d_2 (2 ml) was then allowed to condense through a long glass tube leading to about 5 cm above the bottom of the Pyrex tube. The top of the last tube was closed with a well-fitting rubber stopper carrying two short tubes, 4 and 0.5 mm in diameter. The two tubes allowed the slow circulation of dry nitrogen through the upper part of the Pyrex tube during the whole operation, thus preventing the condensation of atmospheric moisture in the reaction mixture. Finally the stream of nitrogen was stopped, and the tube was quickly sealed and left at room temperature for 4 hours. The mixture was then transferred quickly to a semimicro distillation apparatus and distilled at reduced pressure in a nitrogen atmosphere to give a colorless amidine, b.p. 39–40°/15 mm (yield 80%).

N-Methyl- α,α,α -trichloroacetamidine- d_2

For the synthesis of this compound the same method was used. Equimolar amounts of trichloroacetonitrile and methylamine- d_2 were allowed to react in a sealed tube and were then distilled at reduced pressure in nitrogen atmosphere. B.p. 50–52°/15 mm.

N-Phenyl- α,α,α -trichloroacetamidine- d_2

Aniline- d_2 (1 g) and an excess of trichloroacetonitrile were mixed and left in a tightly closed sublimation apparatus at room temperature for 5 days. The excess of the nitrile was then eliminated in vacuum and the remainder sublimed at 1 mm pressure. The first portion was discarded and the sublimation continued until pure amidine- d_2 was collected. All the operations were conducted in a dry nitrogen atmosphere.

RESULTS AND DISCUSSION

Table I summarizes the positions of absorption maxima (cm^{-1}) in the infrared spectra of N-substituted trifluoroacetamidines. As was expected, the infrared spectra of these compounds showed a considerable similarity to those of the corresponding N-substituted trichloroacetamidines, except the bands produced by C—F and C—Cl respectively.

I. Region 4000–1800 cm^{-1}

The spectra of trifluoroacetamidine, $\text{CF}_3\text{—C(=NH)NH}_2$ (III), and trichloroacetamidine, $\text{CCl}_3\text{—C(=NH)NH}_2$ (IV) showed three absorption peaks in dilute tetrachloroethylene solutions. These peaks corresponded to the asymmetric and symmetric stretching vibrations of the primary amino group ($\nu(\text{NH}_2)$) and the stretching vibration of the imino group ($\nu(\text{=N—H})$). They were in agreement with the spectrum of perfluorobutyramidine, $\text{C}_2\text{F}_7\text{C(=NH)NH}_2$ (5).

This proves that the $\nu(\text{NH}_2)_{\text{sym}}$ and $\nu(\text{=NH})$ absorption bands do not overlap in the spectrogram and this circumstance may be used in deciding which of the two tautomeric forms of the N-substituted trifluoroacetamidines is present.

Assuming that the validity of the Bellamy equation holds in N-substituted trifluoroacetamidines having the structure (Vb), the difference, $\Delta\nu = \nu_{\text{sym calc}} - \nu_{\text{sym obs}}$, was calculated. Although these values were obtained using a NaCl prism possessing a low

TABLE I
Positions of absorption maxima (cm^{-1}) in the infrared spectra of N-substituted trifluoroacetamides

No.	Trifluoro- acetamide	State ¹	$\nu(\text{N}-\text{H})$	$\nu(=\text{N}-\text{H})$	Hydrogen-bonded $\nu(\text{N}-\text{H})$	$\nu(\text{C}=\text{N})$	$\delta(\text{NH})$ "amide II"	$\nu(\text{C}_\alpha-\text{N})$	$\nu(\text{C}_{\text{alk}}-\text{N})$
1	N-Methyl-	L Sol	3515m 3515m	3380w	3350sh, 3300sh, 3220s None	1655vs 1660vs	1555m 1530m		
2	N-Ethyl-	L Sol	3475s 3475s	3355m	3250vs, ² 3090vs None	1645vs 1655vs	1545s 1530m		
3	N-n-Butyl-	L Sol	3460m	3300s ² 3340w	3500w, 3100m None	1650vs 1653vs	1455s 1527m		
4	N-Benzyl	S Sol (1.3 M)	3485m 3475m 3465m	3340 3360	3300m, 3280m, 3150s ² 3270s, 3200s None	1650vs 1650vs 1655vs	absent ⁴ 1530s 1517s		
5	N-Phenyl-	S Sol	3465s 3535s	3425m	3270s, 3140s ² None	1670vs 1690vs	1607vs 1582vs ⁴	1410vs	
6	N,N-Dimethyl-	L Sol		3375m ³ 3355m	3330sh None	1615vs 1620vs		1090vs 1090vs	
7	N,N-Diethyl-	L Sol		3365s ³ 3375m	3360sh None	1625vs 1625vs		1070vs 1070vs	

¹S = solid, L = liquid, Sol = solution.

²Broad band with inflections.

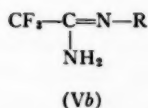
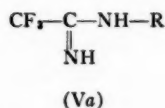
³Sharp bands.

⁴The "amide II" bands disappear in the solid state.

⁵Together with the C=C aromatic mode.

$\text{CF}_3\text{—C—NH}_2$ NH	$\text{CCl}_3\text{—C—NH}_2$ NH	Assignment
3580 s	3530 s	$\nu(\text{NH}_2)_{\text{asym}}$
3480 w	3425 m	$\nu(\text{NH}_2)_{\text{sym}}$
3410 m	3370 m	$\nu(=\text{N—H})$
3290 m	3350 w	{Hydrogen-bonded N—H groups
3120 s	3150 s	

resolving power in the high-frequency region and so cannot be considered very accurate, they were in the range of $17\text{--}35\text{ cm}^{-1}$, much larger than the standard deviation of 4.8 cm^{-1} reported for 64 primary amines examined. Such evidence favored the structure (Va) for both the N-alkyl and N-aryl series of trifluoroacetamidines, although the value of the deviation decreased in passing from the first to the second series. N-substituted trichloroacetamidines behaved in a similar way.



N-substituted trifluoroacetamidines, $\text{CF}_3\text{—C}(=\text{NH})\text{NHR}$, showed strong association in the liquid and solid phase except the N-dialkyl compounds, which presented only one inflection on the sharp $\nu(=\text{NH})$ band in the condensed phase. Thus, in the spectra of the solid and liquid amidines, more than two bands were found, and in some cases it was difficult to distinguish between the free and bonded NH stretching frequencies. Dilution in tetrachloroethylene resulted in two sharp peaks only. For example, four strong bands were present in the spectrum of N-benzyl- α,α,α -trifluoroacetamidine and were still persistent near 3475 , 3340 , 3270 , and 3200 cm^{-1} at 1.3 M concentration in tetrachloroethylene. Upon further dilution they were replaced by a sharp band, $\nu(>\text{NH})$, of medium intensity at 3465 cm^{-1} and a weak one, $\nu(=\text{NH})$, at 3360 cm^{-1} .

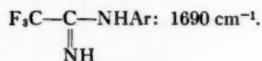
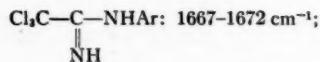
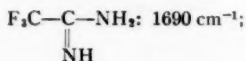
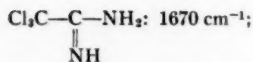
In N-monosubstituted amidines (Va) there are two hydrogen atoms which might be involved in hydrogen bonding. Theoretical considerations demonstrate that amino hydrogen bears a partial positive charge owing to resonance and is more acidic than the imino hydrogen ($=\text{N—H}$).

II. Region $1800\text{--}1000\text{ cm}^{-1}$

(a) The $\nu(\text{C=N})$ Absorption

This easily recognizable frequency appeared as a very strong band at $1615\text{--}1690\text{ cm}^{-1}$ in all the spectra examined. Upon dilution it was slightly displaced to the higher frequencies as was expected for a $\nu(\text{C=N})$ vibration. The $\nu(\text{C=N})$ absorption bands in the N-aryl-, N-alkyl-, and N-dialkyl-trifluoroacetamidines followed exactly the same pattern as those of the trichloroamidines (1) and provided evidence for the existence of the N-substituted trihaloacetamidines in the imino form (Va).

A comparison of the $\nu(\text{C=N})$ vibration of the following amidines in dilute tetrachloroethylene solutions showed the occurrence of this mode at the same frequency:



This behavior may not be a pure coincidence but may indicate that the presence of the aryl groups does not influence the resonance within the amidine system, whereas substitution by one or two alkyl radicals in the amino group does increase the contribution of the ionic structures of the resonance hybrid. This results in the progressive displacement of the C=N stretching vibration towards the lower frequencies which has its lowest value in the case of N-dialkyl-substituted amidines.

(b) *The "Amidine II" Band, $\delta(\text{N}-\text{H})$*

This infrared absorption appeared as a medium to strong band in the spectra of four N-alkyltrifluoroacetamidines (see Table I). It was absent from the spectra of the N-dialkyl compounds and was displaced to the higher frequencies (10–20 cm^{-1}) when association occurred. Nevertheless, it was not found in the spectrum of the solid N-benzyl- α,α,α -trifluoroacetamide but appeared as usual (at 1530–1517 cm^{-1}) when solutions of this substance were studied. The $\delta(\text{N}-\text{H})$ band was also identified when the spectrum of the melted N-benzyl- α,α,α -trifluoroacetamide was taken but vanished when the melt was left to resolidify, this being done several times with the same result. Since the melting point of the compound was low (51°), decomposition by heating was not likely to occur and the spectrum of the solidified melt was exactly the same as that of the original substance in Nujol mull or in potassium bromide pellet. This behavior, which presents an example unique in the literature, could only be attributed to changes in the crystal lattice.

A strong absorption band with two well-separated peaks at 1607 and 1582 cm^{-1} appeared in the spectrum of the solid N-phenyl- α,α,α -trifluoroacetamide but was replaced by only one very strong band at 1582 cm^{-1} upon dilution. The 1607 cm^{-1} band was taken as evidence for the "amidine II" vibration which had been displaced and therefore coincided with the aromatic ring absorption.

The assignment of the "amidine II" band to the 1570–1590 cm^{-1} absorption in N-aryl-trifluoro- and -trichloro-acetamidines was supported by the study of the infrared spectrum of the deuterated N-phenyl- α,α,α -trichloroacetamide, $\text{Cl}_3\text{C}-\text{C}(=\text{ND})\text{NHC}_6\text{H}_5$. The 1580 cm^{-1} band of the ordinary N-phenyl- α,α,α -trichloroacetamide could not be observed in the deuterated analogue. A similar phenomenon was also noted with the deuterated N-methyl- α,α,α -trifluoro- and N-methyl- α,α,α -trichloro-acetamide. In this case, changes in the infrared spectra occurred in the low-frequency region, indicating that coupled (mixed) rather than pure vibrations were present in this type of molecule.

(c) *The $\nu(\text{C}-\text{N})$ Frequencies*

The very strong absorption bands of the F_3C -group varying in number from two to five even for the simplest molecules occurred in the same region (1100 to 1250 cm^{-1}) as the $\nu(\text{C}-\text{N})$ vibrations and produced complicated infrared spectra. However, the $\nu(\text{C}_{\text{ar}}-\text{N})$ frequency could be related to a very strong absorption at 1407 cm^{-1} in the N-phenyl- α,α,α -trifluoroacetamide. This was clearly understood, since it was the only strong band between 1125 and 1480 cm^{-1} , and it was not present in the spectrum of trifluoroacetamide and did not change on deuteration. The existence of a strong

absorption near 1080 cm^{-1} in the spectra of N-dialkyl amidines could be attributed to a $\nu(\text{C}_{\text{alk}}-\text{N})$ mode in these N-dialkyl compounds, since this band was absent in the case of the N-monoalkyl compounds.

REFERENCES

1. J. C. GRIVAS and A. TAURINS. *Can. J. Chem.* **37**, 795 (1959).
2. D. PREVORŠEK. *J. chim. phys.* **55**, 840 (1958).
3. L. J. BELLAMY and R. L. WILLIAMS. *Spectrochim. Acta*, **9**, 341 (1957).
4. W. L. REILLY and H. C. BROWN. *J. Am. Chem. Soc.* **78**, 6032 (1956).
5. D. HUSTED. U.S. Patent No. 2,676,985 (April 27, 1954); *Chem. Abstr.* **49**, 5511 (1955).
6. J. C. GRIVAS and A. TAURINS. In press.

THE REACTION OF ALKYL IODIDES WITH IODO-ARSINES IN THE PRESENCE OF MERCURY¹

M. M. BAIG AND W. R. CULLEN

ABSTRACT

The reaction of alkyl iodides with iodo-arsines in the presence of mercury generally gives arsonium derivatives of triiodomercury (II). Thus tetramethylarsonium triiodomercury (II) is obtained from the reactions of methyl iodide with the compounds $(CH_3)_{3-n}AsI_n$ ($n = 1, 2, 3$). Phenyl-iodo-arsines give the new compounds $C_6H_5AsR_2HgI_3$ and $(C_6H_5)_2AsR_2HgI_3$ ($R = CH_3$ or C_2H_5) from similar reactions. However, the reaction of iododimethylarsine with ethyl iodide gives the 1:1 arsine complex $(CH_3)_2AsC_2H_5 \cdot HgI_2$. The compounds $(C_2H_5)_4AsI$ and $(C_2H_5)_4AsHgI_3$ were reinvestigated, and used to prepare the compound $((C_2H_5)_4As)_2HgI_4$.

DISCUSSION AND RESULTS

The reaction of alkyl- and aryl- iodo-arsines with perfluoroalkyl iodides in the presence of excess mercury has been found to yield alkyl- or aryl- perfluoroalkyl-arsines (1, 2). In the present investigation the reactions of alkyl iodides with iodo-arsines in the presence of mercury have been studied. Apart from one reaction, the main products are compounds which in the past have been named as arsonium derivatives of triiodomercury (II) (3, 4). Similar derivatives are known for other elements which form -onium compounds and there is good evidence that some of these mercuri-iodides are ionic in solution and that one of the ions is HgI_3^- (4, 5). However, solid state structural studies are clearly necessary.

The reactions involving alkyl iodides, mercury, and iodo-arsines, which were investigated, are shown in Table I and the new compounds prepared in this way are listed in Table II.

TABLE I

Reactants	Time of reaction	Products	Yields*
$AsI_3 + Hg + CH_3I$	10 days	$(CH_3)_4AsHgI_3$	32%
$MeAsI_2 + Hg + CH_3I$	10 days	$(CH_3)_4AsHgI_3$	98%
$Me_2AsI + Hg + CH_3I$	5 days	$(CH_3)_4AsHgI_3$	87%
$C_6H_5AsI_2 + Hg + CH_3I$	18 days	$C_6H_5As(CH_3)_2HgI_3$ and CH_3HgI	44% 38 g
$C_6H_5AsI_2 + Hg + C_2H_5I$	18 days	$C_6H_5As(C_2H_5)_2HgI_3$ and C_2H_5HgI	33% 14 g
$(C_6H_5)_2AsI + Hg + CH_3I$	21 days	$(C_6H_5)_2As(CH_3)_2HgI_3$	91%
$(C_6H_5)_2AsI + Hg + C_2H_5I$	21 days	$(C_6H_5)_2As(C_2H_5)_2HgI_3$ and C_2H_5HgI	>90%† 4 g
$(CH_3)_2AsI + Hg + C_2H_5I$	5 days	$(CH_3)_2AsC_2H_5 \cdot HgI_2$	37%

*Yields are based on the iodo-arsine added (ca. 10 g).

†Estimated because of difficulty in separating the two compounds.

Like the other arsonium mercuri-iodides the new compounds are low-melting yellow solids, easily soluble in hot acetone and alcohol. The reaction between ethyl iodide, mercury, and iododimethylarsine, however, gives as a main product the 1:1 complex of mercuric iodide and ethyldimethylarsine. The molecular weight of this substance in camphor indicates that it is predominantly in the form of a monomer instead of the

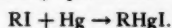
¹Manuscript received November 16, 1960.

Contribution from the Chemistry Department, University of British Columbia, Vancouver, B.C.

TABLE II

Compound	m.p.	Analysis											
		C	Found %		I	Mol. wt.	C	Calculated %		I	Mol. wt.		
			H	Hg				H	Hg				
$C_6H_5As(CH_3)_3HgI_3$	128°	12.9	1.80	24.4	48.0	822	13.7	1.80	25.8	48.8	779		
$C_6H_5As(C_2H_5)_3HgI_3$	129°	17.8	2.44	24.1	46.7	847	17.5	2.44	24.5	46.4	821		
$(C_6H_5)_2As(CH_3)_2HgI_3$	131°	19.9	1.60	23.6	45.4	814	19.9	1.90	23.9	45.3	841		
$(C_6H_5)_2As(C_2H_5)_2HgI_3$	86°	22.3	3.03	23.3	44.0	918	22.1	2.30	23.2	43.8	869		
$(CH_3)_2AsC_2H_5HgI_3$	111°	8.15	1.94	34.1	43.0	615	8.15	1.87	34.1	43.2	589		

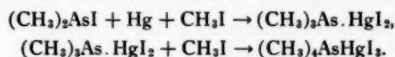
expected halogen-bridged dimer (6), and consequently could contain 3-co-ordinate mercury. A similar situation is found in certain 1:1 tertiary phosphine mercuric iodide complexes (7). The arsine complex seems to decompose slowly and cannot be repurified by fractional crystallization. The alkyl-mercury iodides isolated from the reactions involving aryl-iodo-arsines are probably produced by the side reaction



Such reactions are well known for alkyl iodides and would be catalyzed by any free iodine present in the iodo-arsines (8).

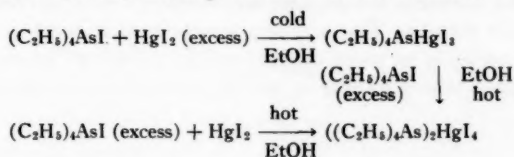
The rate of reaction of alkyl iodides with the aryl-iodo-arsines in the presence of mercury seems to be slower when there are two iodine atoms on the arsenic. Similar behavior is found when these arsines are reacted in the same way with trifluoroiodomethane (2). The reaction of methyl iodide with arsenic triiodide and mercury is slower than with the substituted iodo-arsines, though it appears that methyl iodide reacts more easily in such reactions than does trifluoroiodomethane (1, 2). The latter compound does not react with arsenic triiodide and mercury (9). Antimony triiodide also reacts with methyl iodide in the presence of mercury but not with trifluoroiodomethane (10).

The most probable mechanism for the formation of the arsonium mercuri-iodides appears to be firstly, the formation of an arsine mercuric iodide complex (most likely 1:1), followed by the addition of alkyl iodide to give the final product: for example



This route is supported by the isolation in one instance of the 1:1 arsine mercuric iodide complex, by the result that 2:1 arsine mercuric iodide complexes add on alkyl halides to give arsonium derivatives of tetraiodomercury (II) (7), and by the result that only aryl- and alkyl-perfluoroalkyl-arsines are isolated when perfluoroalkyl iodides are used in similar reactions (1, 2). Unfortunately the reactions so far studied give little indication as to which of the many possible mechanisms is the operative one in the formation of the perfluoroalkyl-arsine or the arsine mercuric iodide complex.

Two other arsonium mercuri-iodides have been studied in the present investigation, these are tetraethylarsonium triiodomercury (II) and bis(tetraethylarsonium) tetraiodomercury (II). The latter, a new compound, is a pale yellow crystalline substance, m.p. 238°. The triiodomercury (II) derivative is the usual low-melting yellow solid (m.p. 117°). Their preparation and relationship can be shown as follows.



The anomalously low melting point of tetraethylarsonium iodide (160° (decomp.) (11)) is now found to be incorrect. The compound prepared and characterized in this investigation decomposed at 307° , a more reasonable figure in view of the value of 326° (decomp.) for tetramethylarsonium iodide (12). The low melting points of other tetraalkylarsonium compounds are probably also incorrect.

The infrared spectra of these arsonium derivatives have been measured. These are in the main complex and further work is in progress in an attempt to correlate these spectra with those of other arsenic compounds.

EXPERIMENTAL

Preparation of the Arsonium Derivatives of Triiodomercury (II)

The alkyl- and aryl- iodo-arsones were prepared as previously described (1, 2), the arsenic triiodide was prepared using the procedure in *Inorganic syntheses* (13).

The reactions shown in Table I were carried out at room temperature in sealed tubes (250-ml capacity) in the absence of air and light. The reaction mixtures were shaken continuously to ensure the exposure of a clean mercury surface to the solution of the iodo-arsones in the alkyl iodide. A large excess of mercury (ca. 200 g) and alkyl iodide (ca. 60 g) was used: the amount of iodo-arsones was 10 g. The reaction mixture was worked up by extracting the contents of the tubes with acetone and separating the soluble components by fractional crystallization from this solvent. Final purification was achieved by repeated crystallization from alcohol. The by-products of alkyl-mercury halides produced in the reactions of the aryl-iodo-arsones were identified in each case by analysis. Anal.: Methylmercury iodide: found: C, 3.52; H, 0.93; Hg, 57.9; I, 36.8%; mol. wt. 319; m.p. 147° . CH_3HgI requires: C, 3.50; H, 0.87; Hg, 58.6; I, 37.0%; mol. wt. 343; m.p. 152° (8). Ethylmercury iodide: found: C, 6.83; H, 1.41; Hg, 55.5; I, 35.7%; mol. wt. 340; m.p. 187° . $\text{C}_2\text{H}_5\text{HgI}$ requires: C, 6.72; H, 1.40; Hg, 56.3; I, 35.6%; mol. wt. 357; m.p. 186° (8).

In the reaction producing dimethyldiphenylarsonium triiodomercury (II) a small fraction was isolated which contained an impurity melting at 122° . Infrared spectra and X-ray powder photographs were used in order to establish the impurity as methylmercury iodide or the complex $(\text{C}_6\text{H}_5)_2\text{AsCH}_3 \cdot \text{HgI}_2$ which was prepared for the purpose of comparison (m.p.: found, 117° ; lit. value, 116° (14)). However, no definite conclusions could be reached from either the spectra or the powder photographs. The tetramethylarsonium compound was identified by its melting point, found: m.p. 189° ; lit. value, 185° (11), and by the identity of its infrared spectrum with that of a sample produced from tetramethylarsonium iodide and mercuric iodide (11).

No unchanged iodo-arsones was recovered from these reactions.

Reaction of Iododimethylarsine with Ethyl Iodide in the Presence of Mercury

The iodo-arsones (7.1 g), ethyl iodide (50 g), and mercury (200 g) in a sealed tube (250 ml) which was not evacuated, were shaken at room temperature for 5 days. The contents of the tube were extracted with acetone. The solution was diluted by an equal volume of alcohol and a yellow precipitate appeared. This was soluble on warming, and on cooling 6 g of the mercuric iodide complex of ethyldimethylarsine were obtained (see Table II for analysis results). The complex was recrystallized from the mixed solvent, m.p. 111° . On the addition of more ethanol to the combined mother liquors a pale red liquid separated which was insoluble in boiling ethanol but crystallized on standing to

pale yellow needles. This solid phase seemed to contain more than one compound and was not further characterized.

The arsine mercuric iodide complex was unstable as after 2 months the melting point changed from 111° to 100–110° and repurification could not be achieved by fractional crystallization. One of the larger fractions, m.p. 105–108°, analyzed as follows: found: Hg, 30.9; I, 41.1%. Calc. for $C_4H_{11}AsHgI_2$: Hg, 34.1; I, 43.2%.

Preparation of Tetraethylarsonium Iodide

Triethylarsine was prepared by a Grignard reaction using arsenic trichloride and ethyl bromide: the product distilled at 138–139° in a nitrogen atmosphere (15). When excess ethyl iodide was added to the arsine at room temperature a colorless solution was obtained which slowly deposited a white solid. After 2 days the solid was filtered off and purified by dissolving it in ethanol and reprecipitating by adding a large volume of ether. The product was identified as tetraethylarsonium iodide. Anal.: found: C, 30.3; H, 6.44; I, 39.3%. $C_8H_{20}AsI$ requires: C, 30.2; H, 6.39; I, 39.9%. The compound decomposed at 307° without melting (lit. value, 160° (decomp.) (11)).

Preparation of Tetraethylarsonium Triiodomercury (II) and Bis(tetraethylarsonium) Tetraiodomercury (II)

When a solution of tetraethylarsonium iodide in ethanol was added to a stirred solution of excess mercuric iodide in ethanol at room temperature, a yellow precipitate was obtained. This solid was washed with ethanol and was identified as tetraethylarsonium triiodomercury (II). Anal.: found: C, 12.4; H, 2.78; Hg, 25.8; I, 48.9%; mol. wt. 731; m.p. 117°. $C_8H_{20}AsHgI_3$ requires: C, 12.4; H, 2.59; Hg, 26.0; I, 49.3%; mol. wt. 773; m.p. 112° (11). When hot arsonium iodide and excess mercuric iodide solutions were mixed a yellow precipitate was obtained, m.p. 87–90°, containing two phases which could not be separated by fractional crystallization. However, the infrared spectrum of this mixture indicated that it was mainly the arsonium triiodomercury (II) derivative. When a hot solution of excess tetraethylarsonium iodide in ethanol was added to a hot solution of mercuric iodide in ethanol, a pale yellow precipitate was obtained. This was filtered, washed with alcohol, recrystallized, and identified as bis(tetraethylarsonium) tetraiodomercury (II). Anal.: found: C, 18.0; H, 3.66; Hg, 18.2; I, 46.2%; m.p. 238°. Calc. for $C_{16}H_{40}As_2HgI_4$: C, 17.5; H, 3.66; Hg, 18.4; I, 46.4%. The same compound was produced when a solution of tetraethylarsonium triiodomercury (II) (0.5 g) in a minimum volume of hot ethanol was added to a solution of excess tetraethylarsonium iodide (1 g) in hot ethanol (5 ml). The bis(tetraethylarsonium) tetraiodomercury (II) which was precipitated was identified by its melting point of 236–238° and by its infrared absorption spectrum.

ACKNOWLEDGMENTS

The authors wish to acknowledge financial assistance from the National Research Council. One of us (M.M.B.) expresses thanks for a scholarship received under the auspices of the Colombo Plan. Microanalyses were carried out by Dr. Alfred Bernhardt.

REFERENCES

1. W. R. CULLEN. *Can. J. Chem.* **38**, 439 (1960).
2. W. R. CULLEN. *Can. J. Chem.* **38**, 445 (1960).
3. W. J. JONES, W. J. C. DYKE, G. DAVIES, D. C. GRIFFITHS, and J. H. E. WEBB. *J. Chem. Soc.* 2284 (1932).

4. N. V. SIDGWICK. The chemical elements and their compounds. Oxford University Press, London. 1950.
5. H. J. CAVELL and S. SUGDEN. J. Chem. Soc. 2572 (1930).
6. R. C. EVANS, F. G. MANN, H. S. PEISER, and P. PURDIE. J. Chem. Soc. 1209 (1940).
7. R. C. CASS, G. E. COATES, and R. G. HAYTER. J. Chem. Soc. 4007 (1955).
8. E. KRAUSE and A. VON GROSSE. Die Chemie der Metal-organischen Verbindungen. Borntraeger, Berlin. 1937.
9. W. R. CULLEN. To be published.
10. M. M. BAIG and W. R. CULLEN. To be published.
11. E. MANNHEIM. Ann. **341**, 182 (1905).
12. W. STEINKOPF and G. SCHWENN. Ber. **54**, 1437 (1921).
13. W. C. FERNELIUS. Inorganic syntheses. Vol. I. McGraw-Hill Book Co. Inc., New York. 1946.
14. J. J. ANDERSON and G. J. BURROWS. J. Proc. Roy. Soc. N.S. Wales, **70**, 63 (1936).
15. W. J. C. DYKE and W. J. JONES. J. Chem. Soc. 2426 (1930).

THE COMPLEX DIELECTRIC CONSTANT AT LOW MICROWAVE FREQUENCIES OF ETHYL CHLORIDE ADSORBED ON POROUS VYCOR GLASS¹

J. D. McCOWAN² AND R. MCINTOSH

ABSTRACT

The complex dielectric constant of the system Vycor glass-ethyl chloride has been measured at three temperatures in the range $+11^{\circ}\text{C}$ to -33°C and in the frequency range between 500 Mc sec^{-1} and 4000 Mc sec^{-1} by the use of a coaxial line. The real and imaginary parts of the dielectric constant of the adsorbate have also been evaluated. Appreciable loss in the adsorbed matter is found for small quantities adsorbed, and loss is again detected at the highest frequencies and lowest temperatures for the matter held in multilayers or condensed in capillaries. The frequency range and accuracy of measurement were not sufficient to classify the type of loss curve, but other evidence suggests that the loss for the first quantities adsorbed will turn out to be that for rotational oscillators. In general earlier observations of this system are confirmed and extended.

INTRODUCTION

In a series of papers from this and other laboratories, the apparent dielectric constants have been reported of polar and non-polar substances adsorbed on porous adsorbents. There is agreement among several of the investigators (1, 2, 3, 4, 5, 6, 7) that there are at least two linear sections of the primary data of either dielectric constant or capacitance change as a function of quantity adsorbed. Channen and McIntosh (5) have stressed the need to understand the experimental observation that the second linear region has a lower slope than the first, even for non-polar butane. As this is found only with porous adsorbents, Petrie and McIntosh (7) suggested that the internal field in which the matter is located changes suddenly at some critical quantity of adsorbate, and that this change is due to the location of the molecules in relation to the internal structure of the solid. In the case of polar adsorbates it is possible that explanations in terms of the value of the orientational polarization might be possible. Thus, molecules adsorbed initially with large apparent polarization, might, in the later stages of adsorption, be followed by molecules which are rotational oscillators with a lesser average dipole moment in the field. Although such concepts are unable to provide an explanation of the behavior of normal butane, nevertheless, since it is possible that adsorbates show specific differences of properties, any evidence concerning the dipolar character of adsorbates would be of value. To this end techniques have been developed to permit examination of adsorbates from 20°C to -183°C over a frequency range $3000\text{ cycles sec}^{-1}$ to 4 Mc sec^{-1} and from 10°C to -40°C in the frequency range 500 Mc sec^{-1} to 4000 Mc sec^{-1} . A description of the devices used for the high frequency experiments and the results found for ethyl chloride on porous Vycor glass are given in this paper. The reproducibility of results has proved excellent although the variation from one frequency to another has caused disappointment, and seems to be due to the coaxial line itself. Before describing the experimental assembly and reporting the results, it is useful to state what experimental findings can be (at least qualitatively) interpreted in elucidating the nature of the adsorbed phase.

¹Manuscript received October 24, 1960.

Contribution from the Department of Chemistry based upon a thesis submitted by J. D. McCowan as partial fulfillment of the requirements for the Ph.D. degree.

²Graduate Student and holder of National Research Council Studentship 1958-59. University of Toronto Open Fellowship 1959-60. Present address: Christ's College, Cambridge, England.

(1) A negative temperature coefficient of dielectric constant, from experience gained with bulk matter, signifies an assembly of molecules free to align themselves in the field, or of dipolar molecules with several possible orientations relative to the field, as discussed by Frohlich (8). Such systems, if of normal liquid density, would be expected to possess a fairly large value of the dielectric constant, approximately that of the liquid state.

(2) Alternatively, experiment might reveal a negligible temperature coefficient of the dielectric constant of the adsorbate. This as Kurbatov (9), and Benson, Channen, and McIntosh (10) have stated, suggests that the adsorbate consists of an assembly of rotational oscillators. For these the orientational polarization, and hence the dielectric constant of the assembly, might be small.

(3) If the adsorbate exists in thick liquid-like layers, dispersion might be expected in the frequency and temperature ranges normal to the liquid state.

(4) Lastly, in the first adsorbed layer, dispersion of rotational oscillators, which would presumably be the nature of the adsorbed molecules, might not be found until very high frequencies. An estimate of the frequency was attempted by Benson, Channen, and McIntosh (10) for a simple molecule like hydrogen chloride adsorbed on a sodium chloride surface. The frequency at which dispersion occurs would depend, of course, upon the molecular structure of the adsorbate and the surface.

In the results given below, the real and imaginary parts of the dielectric constant of the total system, and of the adsorbate, are given. The tedious calculations necessary to obtain the adsorbate properties were based upon the extended Böttcher treatment which has been discussed in earlier papers (5, 7), and allowance had to be made for the lossy character of the substrate itself. The omission of the values of the real part of the dielectric constant for the total system and the fact that the properties of the adsorbate were not computed by Waldman (11) has much reduced the significance of that work. The findings of the present investigation may be briefly summarized as follows:

1. The measurement of the real and imaginary parts of the dielectric of both the adsorbent and a polar adsorbate has been successfully achieved over a temperature range $+11^{\circ}$ to -33° C and a frequency range 500 Mc sec^{-1} to 4000 Mc sec^{-1} by means of a coaxial line system. The reproducibility of any given measurement was finally established as better than $\pm 0.2\%$ over the 40 degree temperature range studied, but random variations with frequency amounted to $\pm 2\%$. This variation appears to be inherent in the line used, not in the method employed, nor in the procedures of amplification.

2. The existence of losses in the adsorbed dielectric has been established for the first time in this temperature range. Moreover, the losses of the adsorbate alone have been evaluated, and, as might be anticipated from the knowledge that the measurable loss of the total dielectric is caused by a comparatively small amount of adsorbate, the loss in the adsorbate is substantial.

3. The pronounced losses are found for the adsorbate in equilibrium with low relative pressures, and little loss is to be observed for the adsorbate in the multilayer or capillary condensed material, although a slight loss is observed at the lowest temperature and highest frequencies.

4. The existence of loss permits the occurrence of a positive temperature coefficient of the real part of the dielectric constant. Earlier work with the same adsorbent-adsorbate system (7) has shown a negligible temperature coefficient of the dielectric constant when measuring frequencies that were too low to create losses were employed. Since a

negligible temperature coefficient suggests rotational oscillators, the loss detected appears to be for an oscillatory or resonant type of motion.

5. No evidence of hysteresis in the dielectric constant was obtained, as found by Thorp (12) for several systems, and more recently by Fiat (13). The lack of hysteresis confirms the statement by Petrie and McIntosh (7) published without supporting evidence. A graph of their results, which were obtained with greater precision than the present data, is included below.

EXPERIMENTAL

The equipment used for the preparation of the materials and to obtain adsorption data was relatively simple and described in detail elsewhere (14, 15, 16). Hoke type 413 metal valves were used throughout the measuring system to ensure that no mercury or stopcock grease could distill into the cell.

Small equilibrium pressures were measured by condensing the gas from a large known volume to a small volume in which the pressure was measured. From a knowledge of all the volumes in the system, equilibrium pressures and amount adsorbed were calculated.

The dielectric measurements were carried out by setting up a standing electromagnetic wave for which the node positions and voltage standing wave ratio were dependent on the complex dielectric constant of the adsorbate-adsorbent system.

The cell is shown in Fig. 1. The two coaxial cylinders which channel the microwave were of 0.007-inch wall German silver tubing. Their dimensions, and those of the tapers leading to the UG30C/U adapter, were chosen to present an impedance of 50.0 ohms to the microwave. The adapter formed a vacuum seal and, together with the gasketed plate behind the shorting plate, permitted evacuation of the sample chamber and the admission of known quantities of gas. The evacuation and admission were accomplished through a copper tube leading to the small chamber behind the short and through a pinhole in the outer conductor.

Around this whole structure, a brass cylinder was attached which could be sealed by a gasket at its open end. The Genitron 21, used to control the temperature of the sample, was circulated through this chamber. Details of the temperature control may be found elsewhere (17).

Temperature was measured by calibrated copper-constantan thermocouples inserted in the wells shown in the diagram. They showed a temperature gradient of 0.3°C and fluctuation of $\pm 0.2^{\circ}\text{C}$ for a temperature of $+11^{\circ}\text{C}$ and a gradient of 1.5°C and long term fluctuations of $\pm 1^{\circ}\text{C}$ at -33°C .

The porous Vycor glass, brand number 7930, was ground to make a sliding fit with both conductors. In the final assembly, care was taken to have it adjacent to the short. Both ends were planar and orthogonal to the axis.

Preparation of the Vycor involved gentle heating, first in a succession of 30% nitric acid solutions and then in distilled-water baths. It was then sealed in the final assembly and the water pumped off gently over 2 days. The glass was then heated to 65°C and pumping continued for 1 day more. An ultimate vacuum of 10^{-6} mm Hg was obtained.

Three signal generators, covering a range from 200 to 4000 Mc sec^{-1} , could be connected, in turn, to two General Radio LBA slotted lines in series. Connections between a generator and the first line, called the reference line, and between the reference line and the second or signal line, were made by RG21/U attenuating cable. This reduced reflection into the generator. The signal line was attached directly to the cell. In this slotted line, the standing wave pattern was studied by means of a travelling carriage

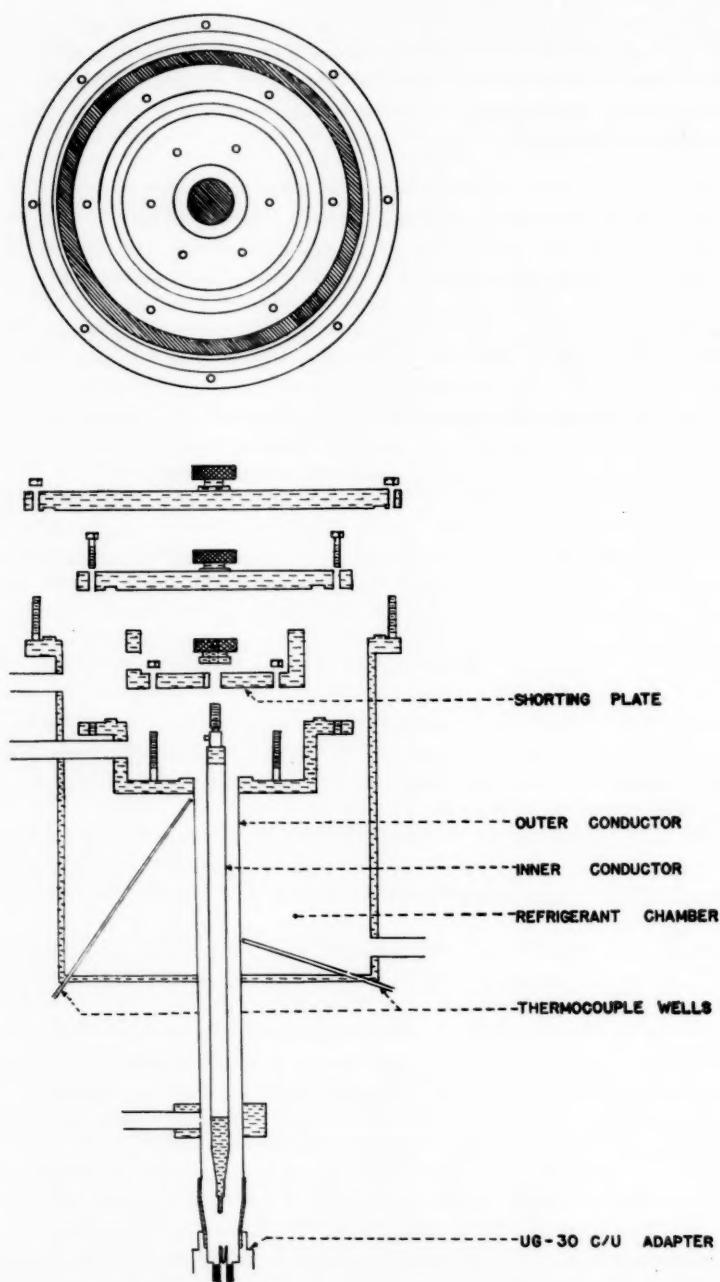


FIG. 1. Side cross-sectional and end views of coaxial cell assembly.

containing a probe and a 1N21B crystal diode. The output of this diode showed no detectable departure from square law response in the voltage range studied. The carriage was moved by the rotation of a threaded bar running the length of the slotted section. Motion of the carriage could be estimated to 0.002 cm.

The line nearer the signal source was not fitted with the worm drive device and was used to produce a reference voltage.

The d-c. outputs of the crystal diodes were fed into two identical d-c. amplifiers each with amplifications of 10^2 , 3×10^2 , and 10^3 . The amplifiers were of a negative feedback type employing the action of a light beam reflected from a galvanometer on two photo-cells in series. Separate power supplies must be used for the two amplifiers. Oscillations in the output occur if several resistors are not kept within fairly narrow tolerances (15).

Precautions were taken to ensure that ground potential was the same throughout the d-c. system. Small contact potentials were eliminated from input switches by the use of Leeds and Northrup type 31-3 switches but it was found impossible to eliminate them from the spring type General Radio connectors of the slotted lines.

The output of the reference amplifier was applied to the input of a General Radio decade voltage divider. The divided output was fed, through a switch, to one terminal of a galvanometer. The output of the signal amplifier was applied to the other terminal. For a null reading of the galvanometer, the voltage divider box read the exact ratio of the signal amplifier output to the reference amplifier output. A block diagram is shown in Fig. 2. The signal was measured as a ratio, rather than in absolute terms, to eliminate

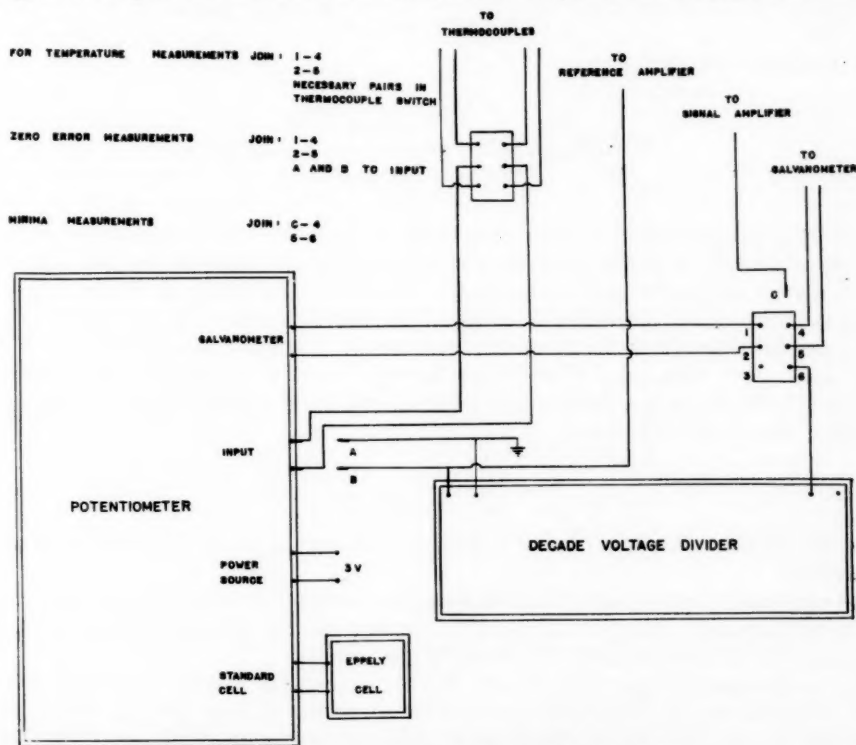


FIG. 2. Block diagram showing all external d-c. circuits.

the effects of both the short and comparatively long term variations in the source voltage from the signal generator.

In practice, this ratio, K , differed from the ratio of the crystal voltages, k , by about 1% due to the zero errors arising from the spring contacts. These small voltages of less than 3 microvolts were measured for every minimum as was the total output of the reference amplifier, V . If x and y are the residual voltages of the signal and reference amplifiers respectively for no microwave signal, then

$$k = \frac{A_s S + x}{A_r R + y}$$

and

$$K = \frac{S}{R} = \frac{A_r}{A_s} \left[k + \frac{ky}{V-y} - \frac{x}{V-y} \right]$$

where A_s and A_r are the amplifications, and S and R the magnitudes of the crystal voltages for the signal and reference lines respectively.

The probe carriage had a range of travel of about 45 cm and, for each determination, the two minima furthest apart within this range were studied. Voltage readings were recorded every 0.025 cm or, in the case of broad minima, every 0.050 or 0.100 cm, in the region of the minimum. Care was taken to extend these readings beyond the points of twice minimal voltage.

CALCULATIONS

Von Hippel (18) shows that

$$\frac{\tanh \gamma_2 d}{\gamma_2 d} = \frac{-j\lambda_1 \frac{E_{\min}}{E_{\max}} - j \tan \frac{2\pi X_0}{\lambda_1}}{2\pi d \left(1 - j \frac{E_{\min}}{E_{\max}} \tan \frac{2\pi X_0}{\lambda_1} \right)} \equiv C e^{j\zeta}$$

where γ_2 is the propagation factor of medium 2, the adsorbate-adsorbent system; d is the sample length; λ_1 is the wavelength of the radiation in the slotted section; E_{\min}/E_{\max} is the inverse voltage-standing wave ratio; and X_0 is the position of the first minimum from the surface of the sample. X is defined as positive in the direction of the incident wave and has its origin at the interface of the sample. The short, then, occurs at $x = d$.

If $\gamma_2 d = T e^{j\tau}$, then, once C and ζ are known, T and τ can be evaluated either by charts (19, 20, 21) as was done in the present work or by a series approximation of the function $\tanh T e^{j\tau}/T e^{j\tau}$. Hence

$$\frac{\epsilon^*}{\epsilon_s} = \frac{\gamma_2^2}{\gamma_s^2} = \frac{\lambda_1^2}{(2\pi d)^2} (T e^{j\tau})^2.$$

ϵ^* is the complex dielectric constant of medium 2, and ϵ_s is the dielectric constant of free space.

An examination of the above formulae shows that, depending entirely on the magnitudes of the primary data, great variations in the accuracy of the calculated values can occur. This fact has its source in two stages of the calculation.

One is the nature of equation for $C e^{j\zeta}$. It will be seen that, if X_0 is very small or very near $-(\lambda_1/2)$, the term $\tan(2\pi X_0/\lambda_1)$, cannot be evaluated with great accuracy, even although the precision and accuracy of the primary data remain unchanged. Similarly,

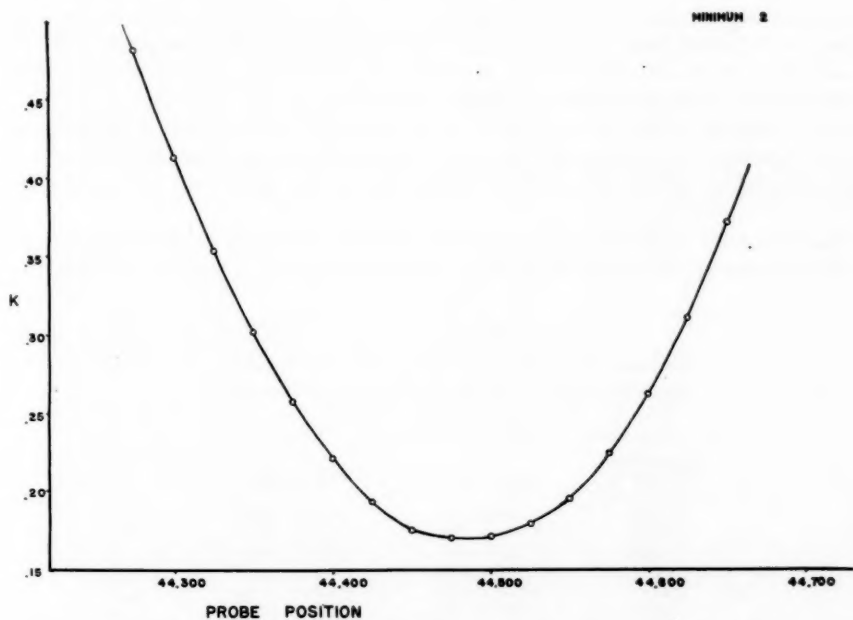
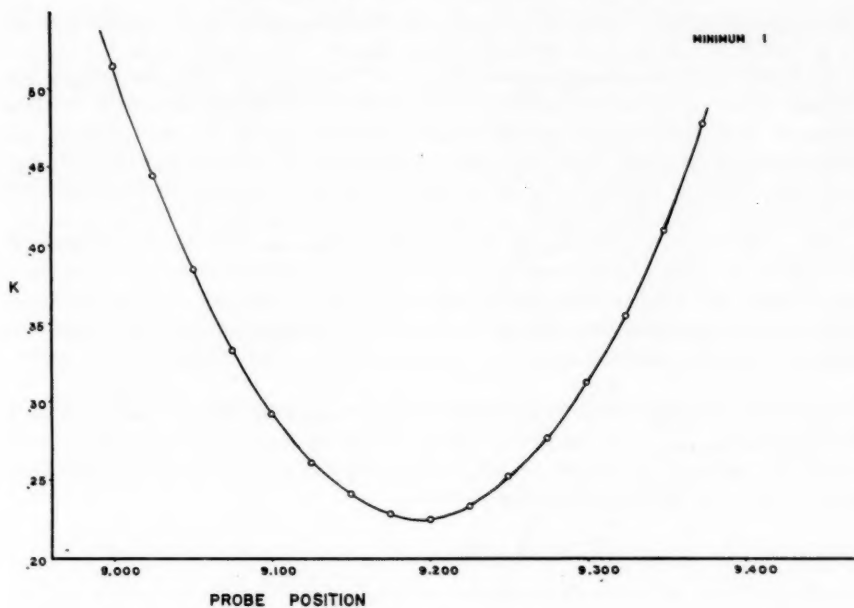


FIG. 3. Plots of K against probe position for measurements of 1280 Mc sec^{-1} , 339.8 cc of ethyl chloride adsorbed, and -33.2°C .

when X_0 is approximately equal to $-(\lambda_1/4)$, $\tan 2\pi X_0/\lambda_1$ varies very rapidly with X_0 and the accuracy of $Ce^{i\delta}$ becomes much less than that of the primary data.

It is the nature of these measurements that, as ϵ' increases, all else remaining equal, X_0 decreases from $-\lambda_1/2$ to 0 in cycles. Hence it was inevitable in the course of these measurements that, for a fixed sample length, certain regions of interest were not capable of accurate analysis. This was true, for example, at 1600 megacycles for comparatively low dielectric values and at 1280 megacycles for comparatively high dielectric values, despite the fine primary data, an example of which is shown in Fig. 3.

The other source of variation in the magnitude of the error is the $T-\tau$ chart. In each $T-\tau$ chart are areas of curvature and skew which make linear interpolation between the plotted lines very approximate. Other areas are nearly Cartesian in their regularity and can be read to four significant figures with ease. It is suggested that the programming of a computer to solve equation for γ_2 by a series approximation would be an improvement.

Care was taken to apply corrections to ΔX for attenuation in the line and its fittings (22), for asymmetry (22), and for deviations of the wave form, at low standing wave ratios, from the assumed form (18, 19, 20, 23) by which E_{\min}/E_{\max} was evaluated from the width of the curve at twice minimal voltage.

RESULTS

For small admission of gas, a fixed amount of gas was put in the cell system and the temperature varied. For large admissions, the temperature was kept constant while known amounts of gas were admitted to the system. This procedure was adopted in the multilayer since it was one of the purposes of this research to determine if hysteresis existed in the dielectric data corresponding to the hysteresis in the adsorption data. The latter method proved very satisfactory, although slightly slower, and is recommended. Isotherms for the three temperatures studied are shown in Fig. 4.

For each isotherm, dielectric constants were obtained at from six to nine chosen frequencies for eight or nine adsorptions. A disappointing error between frequencies was observed, which hindered accurate assessment of the dependence of ϵ' or ϵ'' on frequency.

For glass alone, no variations of ϵ' or ϵ'' with temperature could be observed. Average values of the dielectric constants, with their average deviations, are shown in Table I.

TABLE I
Dielectric constants of Vycor glass. Average, for each frequency, of data obtained at three temperatures at which isotherms were studied

Frequency (Mc sec ⁻¹)	$\epsilon' \pm \text{av. dev.}$	$\epsilon'' \pm \text{av. dev.}$
530	3.304 \pm .015	.0674 \pm .0032
640	3.246 \pm .006	.0739 \pm .0017
820	3.113 \pm .006	.0797 \pm .0040
1020	3.116 \pm .003	.0859 \pm .0024
1280	3.120 \pm .015	.0720 \pm .0044
1600	2.935 \pm .004	.0890 \pm .0032
2000	3.000 \pm .008	.0763 \pm .0020
2550	3.071 \pm .002	.0853 \pm .0084
3200	3.186 \pm .021	.0956 \pm .0060

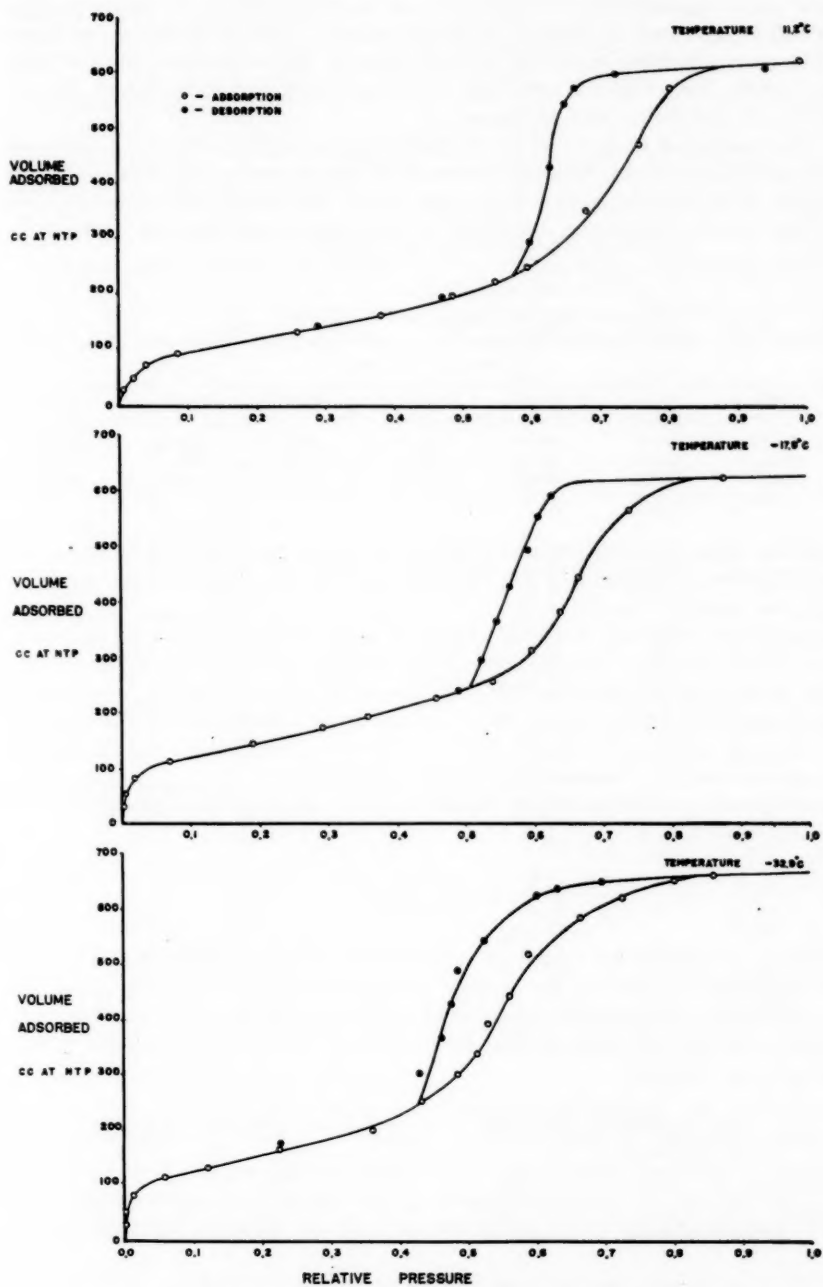


FIG. 4. The variation of volume adsorbed with relative pressure for the three temperatures studied.

Plots of ϵ' and ϵ'' against volume adsorbed were made. Examples are shown in Figs. 5 and 6. It will be seen that the plots of ϵ' against volume adsorbed consist of two linear portions. The second section, beginning between 100 and 150 cc adsorbed, always has a lower slope than the first. This is in agreement with results obtained by McIntosh, Rideal, and Snelgrove (3) and Petrie and McIntosh (7).

Straight lines are fitted to the data by the least-squares method, different lines being fitted above and below 125 cc. Since the values of ϵ_0' for glass were the means of three determinations, the additional constraint was put on the first section that it pass through this point. The values of the slopes, calculated by this method are shown in Table II.

TABLE II
Slopes of plots of ϵ' against volume adsorbed

Temperature (°C)	Frequency (Mc sec ⁻¹)					
	530	640	1020	1280	1600	3200
+11.2	.00464	.00445	.00541	.00437	.00552	.00420
-17.9	.00464	.00408	.00482	.00414	.00480	.00392
-32.9	.00438	.00386	.00469	.00394	.00446	.00357

Values of the dielectric constant of the adsorbed phase were calculated using the extension of Böttcher's treatment (3, 5). This was done for two representative points in each straight line portion. (See below.)

In calculating the adsorbate dielectric constant, the volume fraction of pore space was taken as 0.370 (24). The density of the ethyl chloride was taken to be that of the liquid at the appropriate temperature (25). Calculated values are shown in Table III.

Since the expressions arising in the extended Böttcher treatment are complicated when both the solid adsorbent and adsorbate exhibit loss, a statement concerning the method of solution and the necessary equations will be given.

The usual expression of the extended treatment, when the dielectric constant of the gas phase is taken as 1.0, is

$$[1] \quad \frac{\epsilon+2}{3} - \frac{3\epsilon}{2\epsilon+1} \delta_3 = \frac{\epsilon_0-1}{4\pi C_1} + \frac{\epsilon-\epsilon_0}{4\pi C_2};$$

ϵ is the dielectric constant of the composite system, ϵ_0 of the porous glass, δ_3 the volume fraction of free space, C_1 and C_2 the volume average polarizability of the glass and adsorbate, respectively. It must be remembered in the general case that ϵ , ϵ_0 , C_1 , and C_2 are complex quantities. On making these terms complex and equating real and imaginary quantities, one obtains

$$[2] \quad \frac{\epsilon'+2}{3} - 3\delta_3 \left[\frac{2(\epsilon')^2 + \epsilon' + 2\epsilon''^2}{(2\epsilon'+1)^2 + (2\epsilon'')^2} \right] = \frac{\epsilon_0' C_1' - C_1' + \epsilon_0'' C_1''}{4\pi(C_1'^2 + C_1''^2)} + \frac{(\epsilon_1' - \epsilon_0') C_2' + (\epsilon_1'' - \epsilon_0'') C_2''}{4\pi(C_2'^2 + C_2''^2)}$$

$$[3] \quad -\frac{\epsilon''}{3} + 3\delta_3 \left[\frac{\epsilon''}{(2\epsilon'+1)^2 + (2\epsilon'')^2} \right] = \frac{C_1''(\epsilon_0'-1) - C_1' \epsilon_0''}{4\pi(C_1'^2 + C_1''^2)} + \frac{(\epsilon_1' - \epsilon_0') C_2'' + (\epsilon_0'' - \epsilon_1'') C_2'}{4\pi(C_2'^2 + C_2''^2)}.$$

Calling the left-hand sides of equations [2] and [3] L_1 and L_2 , respectively, and the first term of the right-hand side of each of equations [2] and [3], A_1 and A_2 , respectively, it

follows that

$$[4] \quad \frac{L_1 - A_1}{L_2 - A_2} = \frac{C_2'(\epsilon' - \epsilon_0') + C_2''(\epsilon'' - \epsilon_0'')}{C_2''(\epsilon' - \epsilon_0') + C_2'(\epsilon_0'' - \epsilon'')}$$

and therefore that

$$[5] \quad C_2'' = \frac{(\epsilon_0'' - \epsilon'')(L_1 - A_1) - (\epsilon' - \epsilon_0')(L_2 - A_2)}{(\epsilon'' - \epsilon_0'')(L_2 - A_2) - (\epsilon' - \epsilon_0')(L_1 - A_1)} C_2' = X C_2'.$$

TABLE III
Dielectric constants of adsorbed phase

Temp. (°C)	Frequency (Mc sec ⁻¹)					
	530	640	1020	1280	1600	3200
40 cc adsorbed ϵ_2'						
11.2	10.22	9.68	12.29	9.45	12.50	8.93
-17.9	10.09	9.28	11.26	9.24	11.23	8.06
-32.9	9.76	8.77	11.18	8.89	10.22	7.16
40 cc adsorbed ϵ_2''						
11.2	1.20	.56	.51	.88	1.10	.89
-17.9	1.71	1.42	1.68	1.77	2.35	1.93
-32.9	2.56	2.04	2.27	2.62	3.67	2.42
100 cc adsorbed ϵ_2'						
11.2	10.31	9.66	12.31	9.49	12.55	8.96
-17.9	10.28	9.41	11.33	9.39	11.49	8.20
-32.9	10.17	9.02	11.27	9.24	10.91	7.43
100 cc adsorbed ϵ_2''						
11.2	.53	.24	.22	.62	.68	.65
-17.9	.78	.76	1.36	1.21	1.46	1.50
-32.9	1.41	1.23	2.00	1.77	2.29	1.87
250 cc adsorbed ϵ_2'						
11.2	5.63			5.83		5.86
-17.9	5.62			5.85	6.59	5.85
-32.9	5.62			5.84	6.55	5.81
250 cc adsorbed ϵ_2''						
11.2	.10			.14	.33	.24
-17.9	.17			.30	.57	.43
-32.9	.29			.39	.70	.68
500 cc adsorbed ϵ_2'						
11.2	5.63			5.86	6.60	5.86
-17.9	5.63			5.80	6.59	5.86
-32.9	5.62			5.85	6.58	5.85
500 cc adsorbed ϵ_2''						
11.2	.08			.13	.26	.24
-17.9	.13			.21	.34	.28
-32.9	.23			.24	.49	.41

Substitution in [2] for C_2'' yields

$$L_1 = A_1 + \frac{1}{4\pi C_2'} \frac{(\epsilon' - \epsilon_0') + (\epsilon'' - \epsilon_0'')X}{1 + X^2}.$$

A plot of L_1 versus the coefficient of $1/(4\pi C_2')$ gives the value of C_2' , C_2'' follows from equation [5]. Once these two quantities are known the values of ϵ_2' and ϵ_2'' may be obtained by equating the real and imaginary parts of the equation

$$[6] \quad \frac{4}{3} \pi (C_2' - jC_2'') = \frac{\epsilon_2' - 1 - j\epsilon_2''}{\epsilon_2' + 2 - j\epsilon_2''}$$

and solving for ϵ_2' and ϵ_2'' .

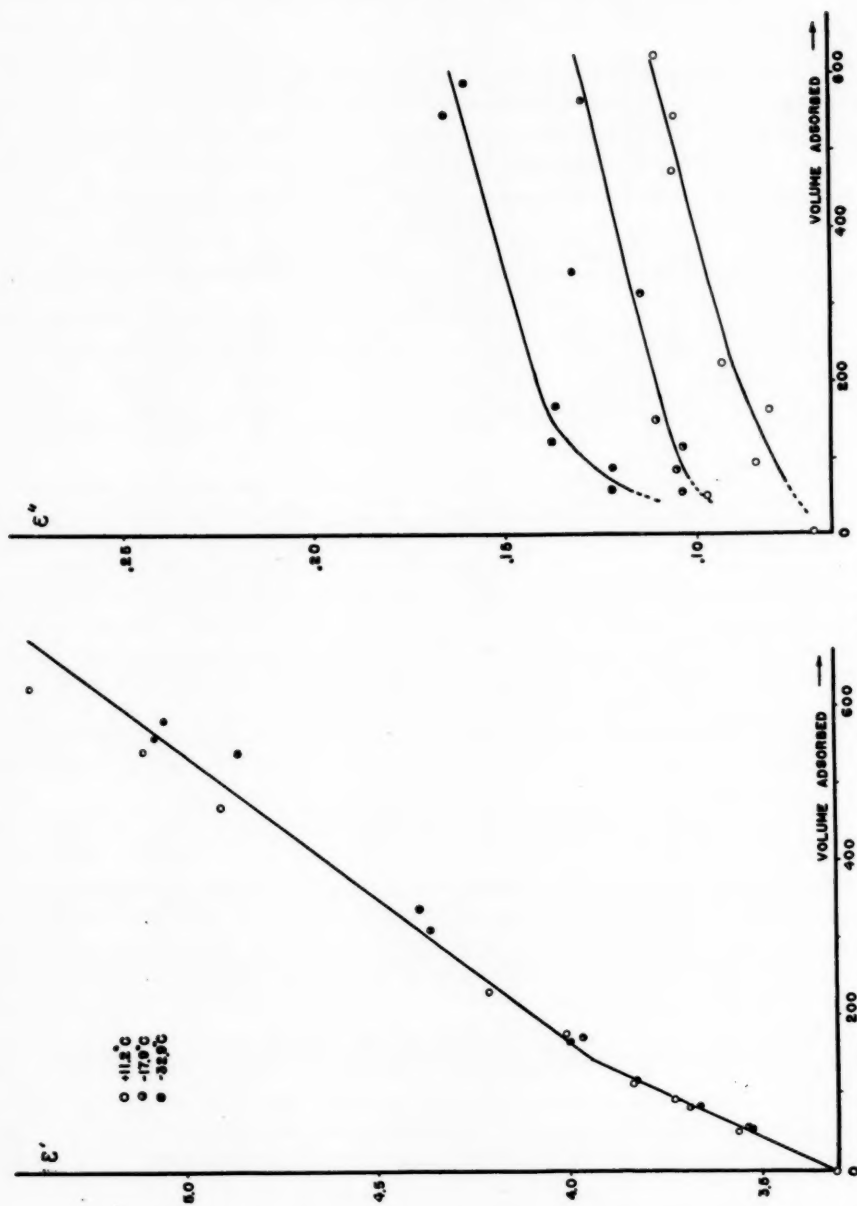


Fig. 5a.

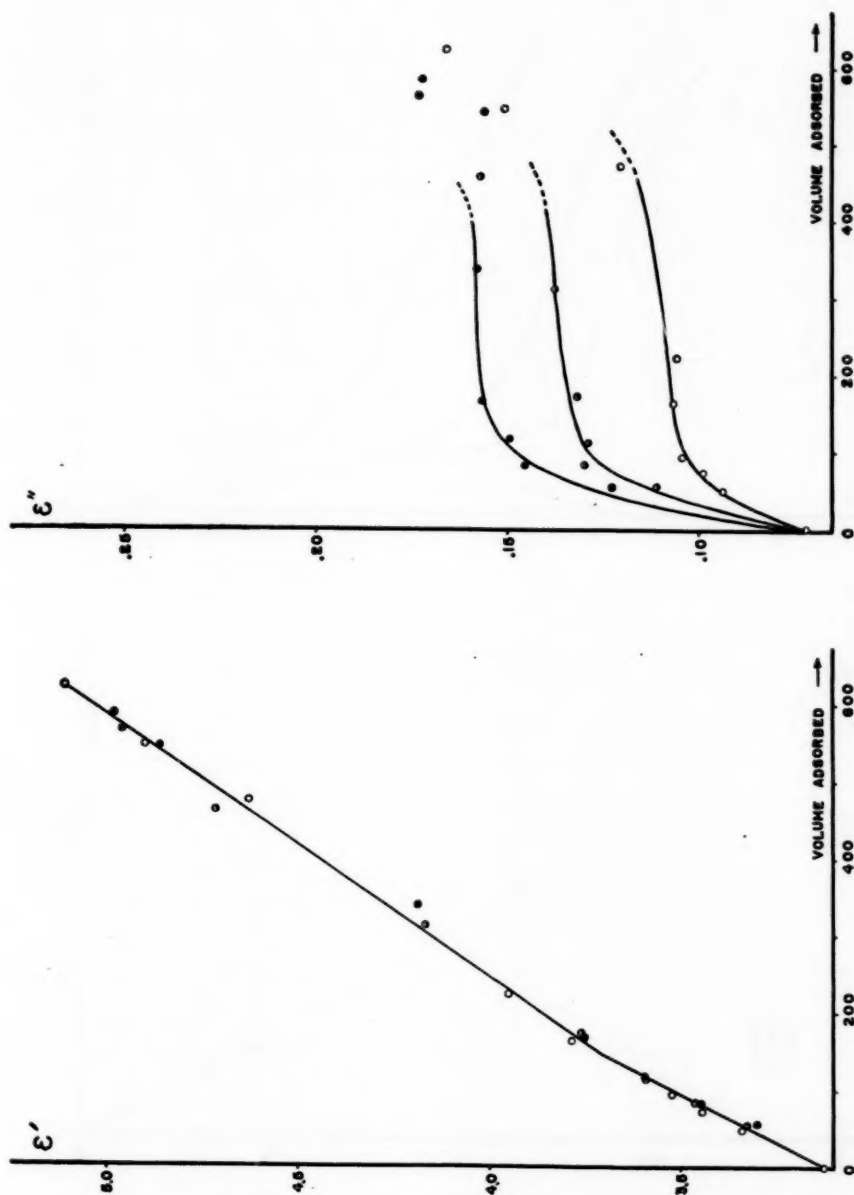


Fig. 5b.

Fig. 5. Variation of dielectric constant with volume adsorbed at (a) 530 Mc sec⁻¹, (b) 1280 Mc sec⁻¹ for 10.241 g of Vycor glass.

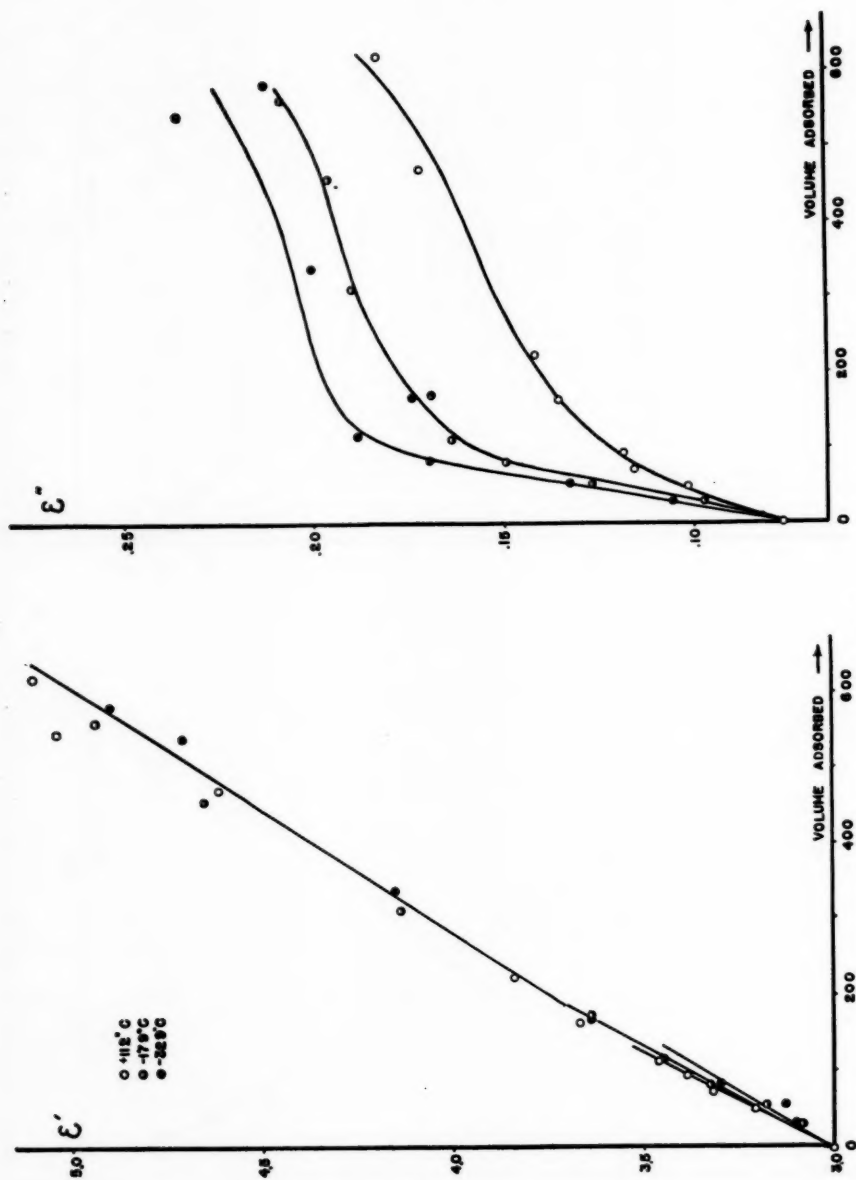


Fig. 6a.

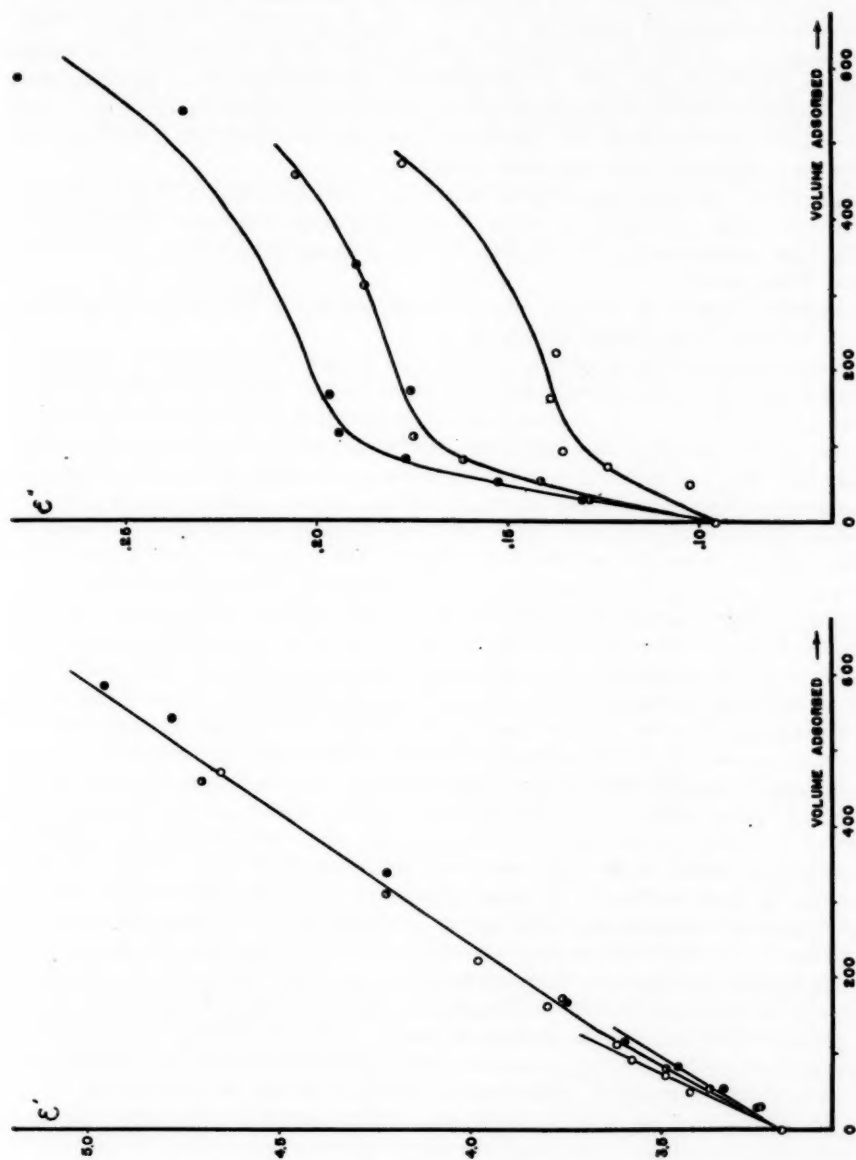


FIG. 6b.

FIG. 6. Variation of dielectric constant with volume adsorbed at (a) 2000 Mc sec⁻¹, (b) 3200 Mc sec⁻¹ for 10.241 g of Vycor glass.

DISCUSSION

In spite of the scatter of results as a function of frequency, the reality of certain findings appears definite. Thus, for quantities of gas adsorbed below about 140 cc, a slight positive temperature coefficient of ϵ_2' and large values of ϵ_2'' are found. These facts are sufficient to establish the existence of dispersion in the adsorbate for coverages which suggest the formation and the filling of the first layer. Since, as was suggested in the introduction, a zero or negligible temperature coefficient implies rotational oscillators it is not improbable that when the loss curve is adequately established, it will turn out to have a form associated with resonance absorption.

The values of ϵ_2'' are much higher for 40 cc adsorbed than for 100 cc adsorbed although ϵ' for the total system is higher at 100 cc. This indicates that the new material in the adsorbed phase contributes less to the loss. The same observation is even more marked for higher adsorptions.

The absolute values of ϵ_2' and ϵ_2'' are, of course, subject to the uncertainties which have been pointed out in earlier papers (5).

In the present instance the value of ϵ_2' is quite close to that of bulk liquid for adsorption below 140 cc, and this must mean that the amplitude of the oscillations of the adsorbed molecules is large. This, in turn, implies that the frequency of rotational oscillations need not be very great. Assuming, then, that the adsorbed molecules do behave as rotational oscillators and that the evidence of a loss maximum at a frequency in the order of a few thousand megacycles per second may be accepted, the two findings are not mutually inconsistent. Where estimates have been attempted to ascertain the natural frequency of such a mode of motion for an adsorbed molecule (10), a much simpler molecule and surface were assumed, and the frequency was much higher than observed here.

According to Figs. 5 and 6 the value of ϵ' of the total system and that of ϵ'' change in a different manner with volume adsorbed once about 140 cc of gas has been adsorbed. The anomaly of low values of ϵ_2' which results from these primary data even when there is no evidence of dispersion has already been emphasized in earlier publications (5). As the calculated value of ϵ_2' is appreciably greater than could be accounted for by distortion polarization alone, a situation which is not found in the case of normal butane, it is again possible that rotational oscillations of smaller amplitude than for the first adsorbed matter could account for the result. In the present instance, however, the variation of ϵ_2'' with amount adsorbed is much less than for the initially adsorbed matter. Moreover, the effect of temperature on the loss, as the plots of ϵ'' show, is much less than for the first section of the data. The matter does not behave, however, as bulk liquid, since the temperature coefficient of ϵ_2' is negligible. Moreover, the beginning of absorption in the multilayer region is evident only at the highest frequencies used and for the highest adsorptions where the material might be expected to approximate most closely to the liquid structure. Calculations for the absorption peak for liquid ethyl chloride (26) based on the equation of Debye (27) and Powles (28) show that the peak for the liquid should occur between 7000 and 10,000 Mc sec⁻¹ at -30° C. Between 140 and 400 cc adsorbed, there is little evidence of loss. It would seem, then, that the adsorbate, particularly at the beginning of the multilayer region, does not have liquid properties. It is thus shown that the lower absolute value of ϵ_2' is not wholly caused by whatever factor brings about the low value of dielectric constant in butane.

Although it is true that absolute values of ϵ_2' differ to some extent from values reported by Petrie, Channen, and McIntosh (16) for rutile as the substrate, and by Petrie and

McIntosh (7) for powdered Vycor glass and silica gel as the adsorbent, the general measure of agreement is good. All work has shown higher dielectric constants for the first matter adsorbed than for the second on porous adsorbents, and the temperature coefficients are small or zero, except for the situation described here of a positive temperature coefficient in a region where dispersion is clearly apparent.

Comment upon the existence of hysteresis in the dielectric curves as claimed by Thorp (12) and more recently by Fiat (13) is difficult. No evidence in support of their claims appears in this work or in that done by Petrie (see Fig. 7). Thorp's claim to relate

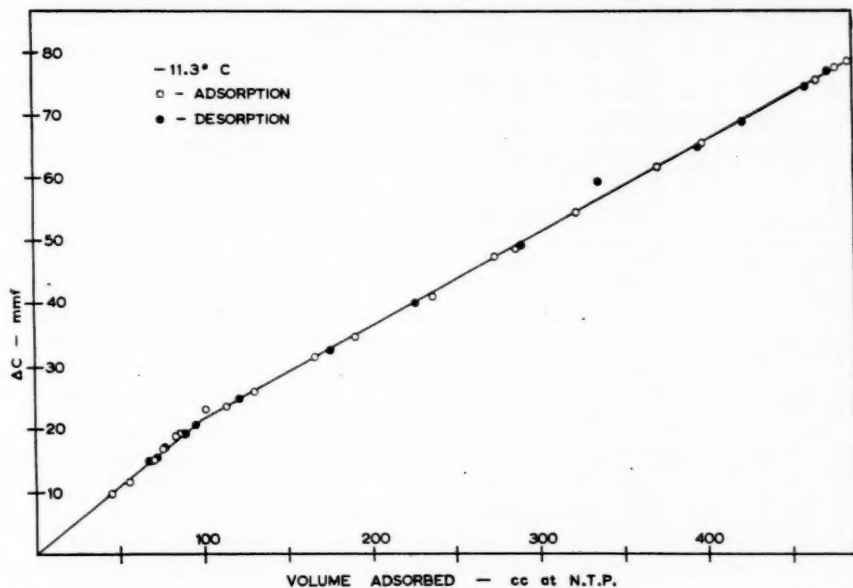


FIG. 7. Variation of capacity with volume adsorbed at -11.3°C , 3.70 Mc sec^{-1} , and 7.053 g of Vycor glass granules.

the variations of type of hysteresis to pore-size distribution appears unwarranted in view of the doubt that pore-size distributions may be assessed even qualitatively from the shape of isotherms and the Kelvin theory (29). On the other hand, gel systems like Vycor glass, activated carbon, etc. are known to shrink and swell due to the presence of adsorbate (24, 30, 31), and such movement may cause changes of packing in powders. Additionally, very long time lags occur before the establishment of apparent equilibrium, and possibly these are involved. In any event, some difference of experimental procedure of the several investigators seems to be the cause of the discordant results, because the gel systems employed appear very similar in terms of the type of adsorption isotherm which they exhibit.

ACKNOWLEDGMENTS

Grateful acknowledgment is made to the National Research Council and to the Advisory Committee on Research of the University of Toronto for financial support

of this work. It is also a pleasure to acknowledge once again our indebtedness to Professor J. M. Anderson of the Department of Physics for his aid in connection with the amplifiers and his advice on all aspects of the electrical measurements.

REFERENCES

1. R. L. McINTOSH, H. S. JOHNSON, N. HOLLIES, and L. McLEOD. *Can. J. Research, B*, **25**, 566 (1947).
2. I. HIGUTI. *Sci. Repts., Tohoku Univ.* **33**, 99, 174, 231 (1949).
3. R. McINTOSH, E. K. RIDEAL, and J. A. SNELGROVE. *Proc. Roy. Soc. (London), A*, **208**, 292 (1951).
4. S. KUROSAKI. *J. Phys. Chem.* **58**, 320 (1954).
5. E. W. CHANNEN and R. L. McINTOSH. *Can. J. Chem.* **33**, 172 (1955).
6. M. H. WALDMAN, J. A. SNELGROVE, and R. L. McINTOSH. *Can. J. Chem.* **33**, 268 (1955).
7. S. E. PETRIE and R. L. McINTOSH. *Can. J. Chem.* **35**, 183 (1957).
8. H. FROHLICH. *Theory of dielectrics*. Oxford. 1949.
9. L. N. KURBATOV. *J. Phys. Chem. (U.S.S.R.)* **24**, 899 (1950).
10. G. C. BENSON, E. W. CHANNEN, and R. L. McINTOSH. *J. Colloid Sci.* **11**, 593 (1956).
11. M. H. WALDMAN. *J. phys., radium*, **17**, 426 (1956).
12. J. M. THORP. *Trans. Faraday Soc.* **55**, 442 (1958).
13. FIAT. Private communication. 1960.
14. S. E. PETRIE. Ph.D. Thesis, University of Toronto, Toronto, Ont. 1957.
15. J. D. McCOWAN. Ph.D. Thesis, University of Toronto, Toronto, Ont. 1960.
16. S. E. PETRIE, R. McINTOSH, and E. W. CHANNEN. *Can. J. Chem.* **35**, 1534 (1957).
17. M. H. WALDMAN and R. McINTOSH. *Can. J. Chem.* **33**, 268 (1955).
18. A. R. VON HIPPEL. *Dielectrics and waves*. Wiley, New York. 1954.
19. S. ROBERTS and A. VON HIPPEL. *Phys. Rev.* **57**, 1056 (1940).
20. S. ROBERTS and A. VON HIPPEL. *J. Appl. Phys.* **17**, 610 (1946).
21. A. R. VON HIPPEL. *Dielectric materials and applications*. Wiley, New York. 1954.
22. E. M. PURCELL. *Techniques of microwave measurements*. Edited by C. G. Montgomery. New York. 1947.
23. A. VON HIPPEL, D. G. JELATIS, and W. B. WESTPHAL. *The measurement of dielectric constant and loss with standing waves in coaxial wave guides*. Massachusetts Institute of Technology, Cambridge, Mass. 1943.
24. C. H. AMBERG and R. McINTOSH. *Can. J. Chem.* **30**, 1012 (1952).
25. J. D. NICKERSON and R. McINTOSH. *Can. J. Chem.* **35**, 1325 (1957).
26. I. D. CHAPMAN. Private communication.
27. P. DEBYE. *Polar molecules*. Chemical Catalogue, New York. 1929.
28. J. G. POWLES. *J. Chem. Phys.* **21**, 633 (1953).
29. H. W. QUINN and R. McINTOSH. *Proceedings of Second International Congress of Surface Activity*. Butterworth Scientific Publications. 1957.
30. R. S. HAINES and R. McINTOSH. *J. Chem. Phys.* **15**, 28 (1947).
31. E. A. FLOOD and R. D. HEYDING. *Can. J. Chem.* **32**, 660 (1954).

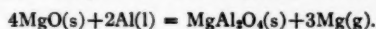
THE ALUMINUM REDUCTION OF MAGNESIUM OXIDE

I. THE VAPOR PRESSURE OF MAGNESIUM OVER THE SYSTEM Al-MgO¹

K. GRJOTHEIM, O. HERSTAD, AND J. M. TOGURI

ABSTRACT

The equilibrium vapor pressure of magnesium over the reaction between magnesium oxide and aluminum was measured by means of the transportation method. In the temperature range 850–1150° C the results can be expressed by the equation $\log P_{\text{mm of Hg}} = -9617/T + 8.93$. From X-ray diffraction analysis this reaction proceeds according to the equilibrium



INTRODUCTION

Very little information exists in the literature on the reaction between solid magnesium oxide and metallic aluminum. On the assumption that this reaction proceeds according to equation [I],



Treadwell (1) has calculated the equilibrium vapor pressure of magnesium over this reaction. His calculations showed that at 1470° C the equilibrium pressure of magnesium is 7.6 mm of Hg.

Later Beljajew (2) has reported that the equilibrium pressure of magnesium over reaction [I] is 1 atm at 1300° C.

From the available thermodynamic data (3) the present authors have calculated the pressure of magnesium over reaction [I] to be 98 mm of Hg at 1300° C.

Since this discrepancy exists, it was the purpose of the present investigation to examine the reaction between solid magnesium oxide and metallic aluminum. The logical approach to the study of reactions of this type, involving components in the vapor, is the measurement of the equilibrium vapor pressure associated with the reaction, and to identify the end products of the reaction in order to establish the reaction scheme.

EXPERIMENTAL

The experimental method adopted to measure the equilibrium vapor pressure of magnesium was the transportation method, since the expected vapor pressure range was 10^{-2} – 10^2 mm of Hg over the desired temperature range. This method of measuring vapor pressure has proved to be successful for a number of similar reactions (4, 5). It is a dynamic method, in which the magnesium vapor in equilibrium with the solid components is carried away by a stream of inert gas flowing at a constant velocity. The amount of magnesium vapor transported is determined by condensing the vapor in a suitable condenser. The vapor pressure is then proportional to the mass of entrained vapor divided by the total volume of gas leaving the equilibration zone.

The important feature of the transportation method is the geometry of the apparatus. It must be designed to insure saturation of the carrier gas over a range of flow rates where the diffusion errors are negligible, and where the measured pressure is independent of flow rate.

¹Manuscript received October 3, 1960.

Contribution from the Institute of Inorganic Chemistry, The Technical University of Norway, Trondheim, Norway.

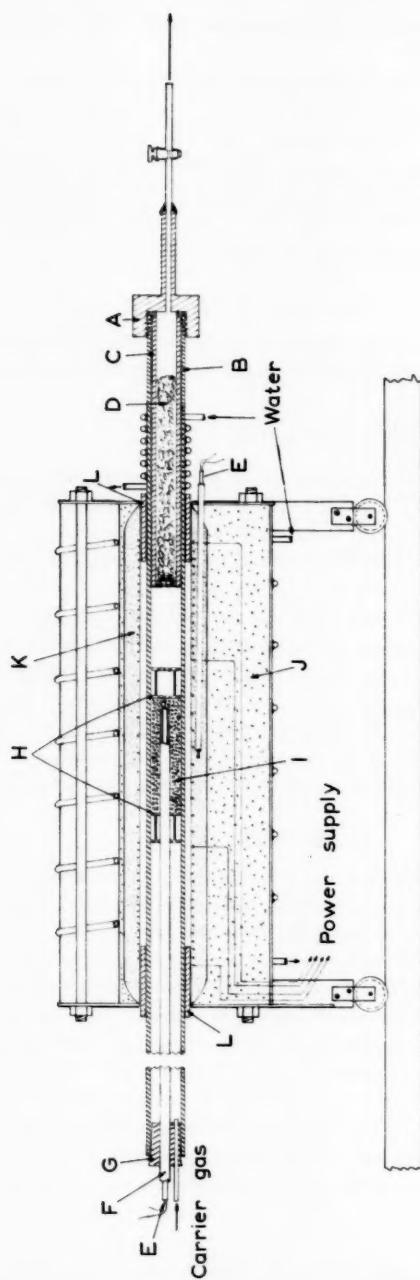


FIG. 1. Diagram of furnace showing position of sample.

- | | |
|-------------------------------------|-------------------------------------|
| A. Muffle | G. Rubber stopper |
| B. Retort tube | H. Perforated spacers |
| C. Condenser | I. Reaction material |
| D. Steel wool | J. Silica gel (insulating material) |
| E. Thermocouple (Pt-Pt 10% Rh) | K. Heating element |
| F. Protecting tube for thermocouple | L. Pythagoras tube |

The furnace utilized for this purpose is shown in Fig. 1. It is a Kanthal A wire-wound electrical furnace similar to that described in detail by Motzfeldt (6). With this furnace an uniform temperature zone was obtained readily to within $\pm 1.5^\circ\text{C}$, along the middle 15 cm of the furnace for temperatures of 800–1200°C.

An inconel tube (76% Ni, 15% Cr, and 9% Fe) of 3.2-cm I.D. was used as the reaction tube, since it was found to be chemically inert against the reactants and products of the reaction concerned, below 1150°C.

The charge is placed between two inconel perforated spacers, as shown in Fig. 1. These spacers not only keep the charge in place but also aid in packing the charge together, thus contributing towards the saturation of the carrier gas.

A steel condenser filled with washed steel wool is placed near the outlet of the reaction tube. This serves to condense and collect completely the evolved magnesium gas.

The carrier gas utilized throughout this investigation was S-argon gas obtained from Norsk Hydro, the analysis given was 99.94%. The impurities CO_2 and H_2O were removed by passing the argon through an Ascarite and a Dehydrite tower respectively. The hydrogen was obtained from Norsk Surstoff og Vandstoffabrik A/S (99.7%) and was similarly purified.

The gas flow rate was measured using a calibrated rotameter and the total volume was determined by means of a calibrated gas meter.

A Pt-Pt 10% Rh thermocouple was placed into the charge, as shown in Fig. 1, to measure the temperature in conjunction with a precision Tinsley potentiometer with a mirror Lange-galvanometer.

PREPARATION OF CHARGE

The magnesium oxide and aluminum powder used throughout this investigation was obtained from Merck, Germany. The magnesium oxide was of pro analysis grade and the analysis of the aluminum was 99.9%.

Before use, the MgO was dried at 1000°C for 12 hours. The MgO and aluminum was then mixed and ground in a ball mill. The powdered mixture was pressed into briquettes at 500 kg/cm². The size of the briquettes were 2.0 cm in diameter by 1.5 cm in height.

These briquettes were broken into pieces of approximately 5 mm and packed into the reaction tube. Approximately 120 g of charge was used. The reactants prepared in this manner gave rise to a large sample surface area to reaction tube volume ratio and thus a condition which is favorable for insuring saturation of the carrier gas.

The experiment was started by moving the furnace, which is 100°C higher than the required temperature, along the reaction tube to a position such that the sample was located in the uniform temperature zone. During this period a stream of argon was passed from the opposite end until the required temperature was obtained, a period of approximately 5 to 10 minutes. When the temperature was reached the flow of argon was reversed and zero time was observed.

RESULTS AND DISCUSSION

(A) *Effect of Flow Rate on the Apparent Vapor Pressure*

A number of experiments were carried out to determine the effect of the flow rate of the carrier gas on the measured vapor pressure. In Fig. 2 results are shown for such experiments carried out at 998°C. In the case of argon as the carrier gas, the flow rate

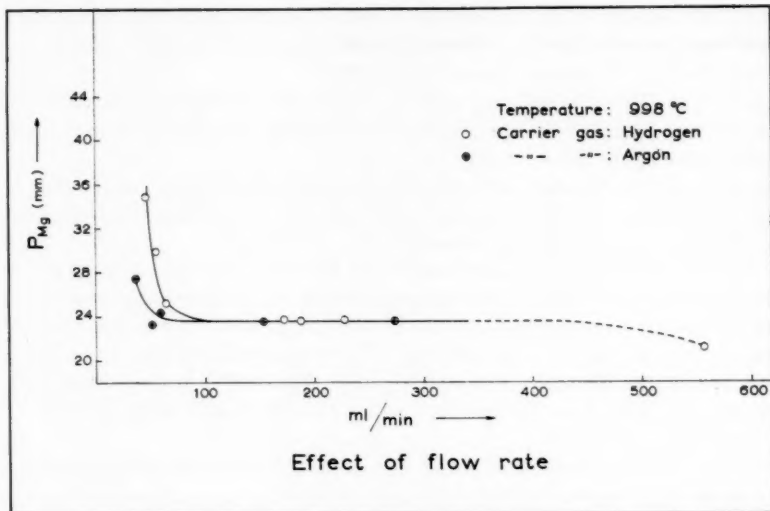


FIG. 2. Effect of flow rate using hydrogen and argon as carrier gas.

was varied from 37 to 274 ml/minute. For flow rates exceeding 100 ml/minute, there appears a plateau where the vapor pressure is independent of the flow rate. At lower flow rates, the resulting pressure, that is the mass of magnesium collected per unit volume, is much higher. This indicates that in addition to the equilibrium concentration of the vapor in the carrier gas, there is movement of vapor due to thermal diffusion and self-diffusion. This feature has been analyzed by Lepore and Van Wazer (7).

The existence of a relatively large region where the pressure is independent of the flow rate insured saturation of the carrier gas as well as a satisfactory design of the apparatus.

(B) Effect of Carrier Gas on the Vapor Pressure

To insure that the pressure measurements were independent of the nature of the carrier gas, hydrogen was also utilized as the entrainment gas. The results are shown in Fig. 2, at a temperature of 998°C. The flow rate was varied from 43 to 557 ml/minute. In the range from 100–350 ml/minute the vapor pressure is independent of the flow rate and is identical to that observed with argon. However, as expected the pressure increases very rapidly at low flow rates. At 43 ml/minute a 50% increase in pressure was observed.

These experiments showed that the measured pressure is independent of the nature of the carrier gas in the region of the plateau.

(C) Vapor Pressure Measurements over the Reaction

Measurements of the equilibrium vapor pressures of magnesium were carried out over the temperature range 870 to 1141°C. The results are shown in Fig. 3 and tabulated in Table I.

TABLE I
Experimental vapor pressure of
magnesium

Temp. (° C)	Pressure (mm of Hg)
870	3.55
921	7.56
959	13.3
998	23.6
1072	56.0
1106	89.0
1115	100.1
1117	102.5
1141	143.2

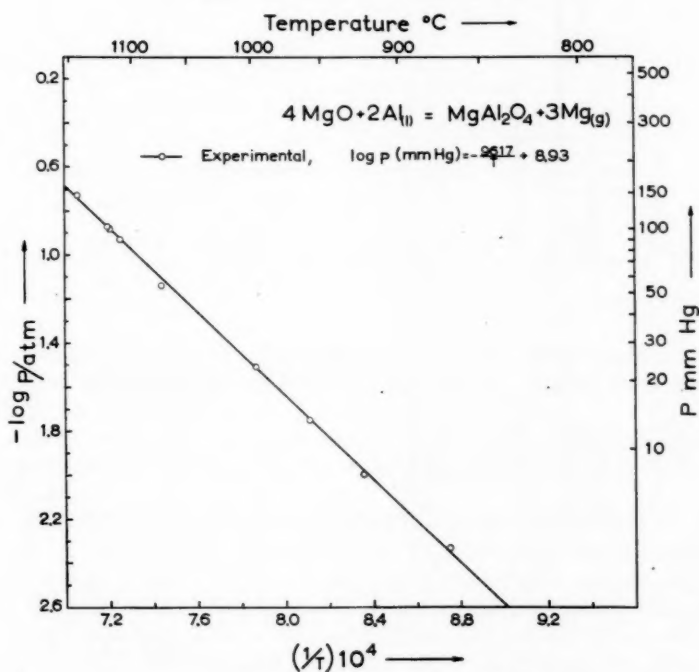


FIG. 3. Log P_{atm} of Mg versus $1/T^\circ \text{K}$.

In the temperature range investigated the data may be represented as a straight line and fitted to the equation,

$$\log P_{\text{mm of Hg}} = -(9617/T) + 8.93,$$

where P is pressure in mm of Hg and T the absolute temperature.

(D) Analysis of the Reaction Product

The observed vapor pressure of magnesium in this investigation is in the same order of magnitude as that given by Beljajew (2) for reaction [I]. However, because the

measured and calculated vapor pressure is so vastly different for this reaction, the reaction product was determined by X-ray diffraction analysis.

It was found that the product is not Al_2O_3 but consisted of the spinel MgAl_2O_4 as shown in Fig. 4, and as compared to the ASTM Index (8). When the unreacted MgO and Al were removed by washing the reaction product in 0.5 M HCl acid, the resulting X-ray analysis showed only the spinel MgAl_2O_4 . Chemical analysis of the product also confirmed the formation of the spinel.

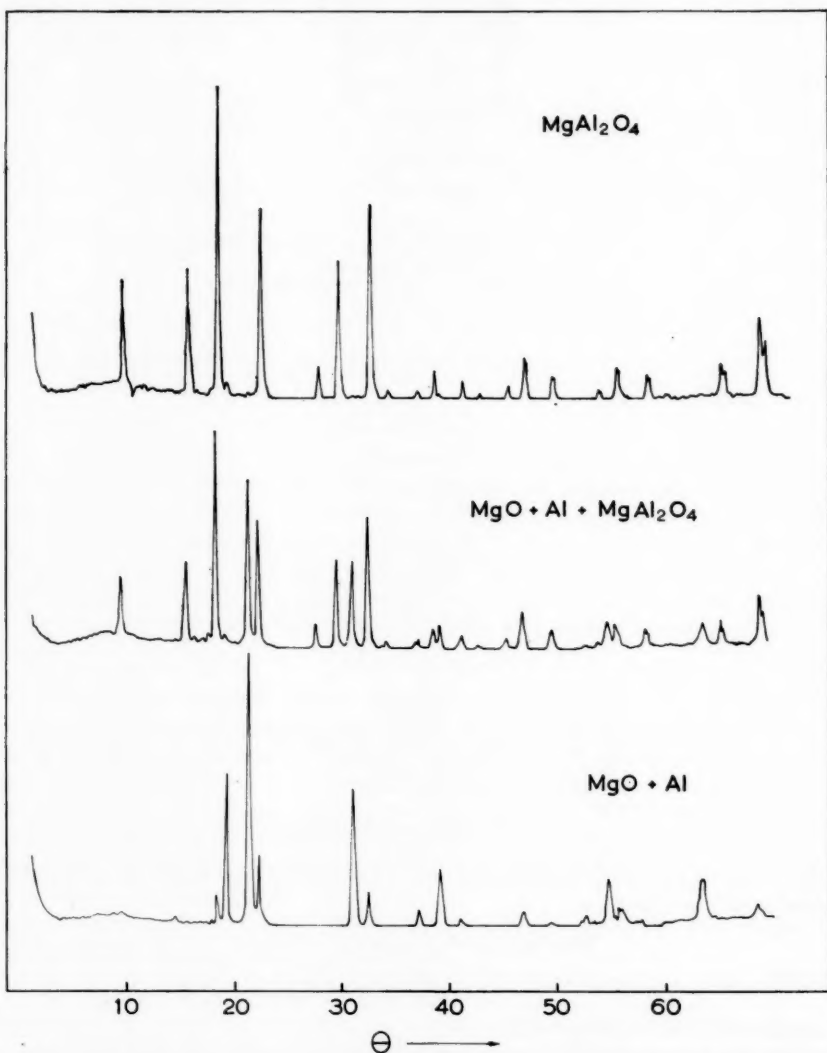
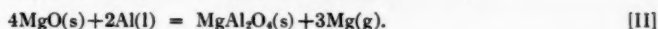


FIG. 4. X-Ray diffraction patterns obtained on using Cu target and Ni filter. The bottom shows the diffraction pattern of the reactants, the middle the residue. The top figure shows the pattern obtained after washing the residue with 0.5 M HCl acid, and indicates only MgAl_2O_4 .

The reaction can therefore be represented by the equation



Upon altering the ratio of MgO/Al from 2/1 to 3/2 the measured vapor pressures were found to be identical.

(E) Thermodynamic Considerations

In the reaction concerned, aluminum appears as a liquid, and thus some solution of magnesium would be expected. For this reason the unreacted aluminum balls were collected from the reaction products and analyzed. In a few experiments small beads of aluminum were placed between the charge and condenser, in the uniform temperature zone, and these were also analyzed. The results at four temperatures are shown in Table II.

TABLE II
Analysis of magnesium in aluminum

Temp. (°C)	Mole% of Mg in aluminum	Activity of magnesium	
		From analysis of aluminum	From pressure measurements
870	3.7 ± 5%	0.037	0.048
921	5.9 ± 5%	0.059	0.056
959	6.0 ± 5%	0.060	0.066
998	10.4 ± 5%	0.104	0.079

Assuming ideality, the activity of magnesium has been calculated from the analysis. This is found to be in good agreement with the activity derived from the measured pressure, as shown in Table II.

Thus it was assumed that within the limits of the error of the analysis, aluminum formed an ideal solution with magnesium at the temperature at which the investigation was carried out.

In order to derive the thermodynamic functions of the spinel MgAl_2O_4 , the equilibrium constant of the reaction was calculated for each temperature investigated, on the assumption that aluminum formed an ideal solution with magnesium. The phase diagram for the system $\text{MgO-MgAl}_2\text{O}_4$ (9) shows no solid solubility thus the activity of the oxides are assumed to equal unity. A "Σ-plot" has been carried out using the specific heat functions recommended by Kelley (10). The derived functions are shown in Table III for the over-all reaction.

TABLE III
Thermodynamic functions for the reaction $4\text{MgO(s)} + 2\text{Al(l)} = \text{MgAl}_2\text{O}_4\text{(s)} + 3\text{Mg(g)}$
where $a_{\text{Al}} = 1$ (in the temperature range 932–1423°K)

$\Delta C_p = -3.01 - 0.56 \times 10^{-3}T - 3.86 \times 10^6 T^{-2}$
$\Delta H^\circ_T = 137,400 - 3.01T - 0.28 \times 10^{-3}T^2 + 3.86 \times 10^6 T^{-1}$
$\Delta G^\circ_T = 137,400 + 6.93T \log T + 0.28 \times 10^{-3}T^2 + 1.93 \times 10^6 T^{-1} - 109.74T$
$\Delta H^\circ_{1280^\circ\text{K}} = 133,400 \text{ cal}$
$\Delta G^\circ_{1280^\circ\text{K}} = 25,100 \text{ cal}$
$\Delta S^\circ_{1280^\circ\text{K}} = 84.61 \text{ e.u.}$

NOTE: It must be emphasized that these functions are also subjected to the inaccuracies of the C_p values obtained from the literature.

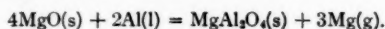
Combining the experimental data with the data on MgO and Al_2O_3 given by Kubaschewski and Evans (3), one obtains for reaction [III]



the following data, $\Delta H_{298}^0 \text{ K} = +1.1 \text{ kcal}$, $\Delta G_{298}^0 \text{ K} = -1.9 \text{ kcal}$, and $\Delta S_{298}^0 \text{ K} = 10.1 \text{ e.u.}$ The positive heat and the unreasonable large value of the entropy can be accounted for by the assumptions made with respect to the solubility of MgO in MgAl_2O_4 and the ideality of the Al-Mg system as well as the uncertainty of the existing literature data which is accumulated in the above type of calculation.

CONCLUSIONS

The reaction between solid magnesium oxide and metallic aluminum was found to proceed according to the equation



The solid reaction product is the spinel MgAl_2O_4 and not Al_2O_3 as reported by previous investigators.

The equilibrium pressure of magnesium over this reaction, in the temperature range $850\text{--}1150^\circ \text{C}$, can be represented by the equation,

$$\log P_{\text{mm of Hg}} = -(9617/T) + 8.93$$

as determined by means of the transportation method.

ACKNOWLEDGMENTS

This investigation, one of the series on the reduction of magnesium compounds, has been carried out under a research grant from ELEKTROKEMISKS FORSKNINGSFOND, for which the authors are grateful. One of the authors (J.M.T.) is indebted to the National Research Council of Canada for financial support in a form of a Postdoctorate Overseas Fellowship.

REFERENCES

1. W. D. TREADWELL. *Helv. Chim. Acta*, **19**, 126 (1936).
2. A. I. BELJAJEW. *Metallurgie des Aluminiums*. Vol. II. VEB Verlag Technik, Berlin. 1956. p. 281.
3. O. KUBASCHEWSKI and E. EVANS. *Metallurgical thermochemistry*. Pergamon Press Ltd., London. 1958.
4. L. M. PIDGEON and J. A. KING. *Discussions Faraday Soc.* **4**, 197 (1948).
5. T. ROSENQVIST and B. ELLINGSAETER. *J. Metals*, **212**, 1111 (1956).
6. K. MOTZFELDT. *Physico-chemical measurements at high temperature*. Butterworths Scientific Pub., London. 1959. p. 51.
7. J. V. LEPORE and J. R. VAN WAZER. U. S. Atomic Energy Commission, MDDC 1188. 1948.
8. ASTM X-RAY POWDER DATA. File 5-0672.
9. E. LEVIN, H. McMURDIE, and F. HALL. *Phase diagram for ceramists*. Am. Ceram. Soc. 1956.
10. K. K. KELLEY. U.S. Bureau of Mines Bulletin 584. 1960.

THE CRYSTAL SPECTRUM OF PERYLENE¹

ROBIN M. HOCHSTRASSER

ABSTRACT

The electronic absorption spectrum of crystalline perylene has been examined in the spectral region 3000–4700 Å. The lowest energy electronic state of perylene has a large oscillator strength and the crystal spectrum deviates considerably from that calculated from a weak coupling (Davydov) model.

The sublimation flakes were examined at room temperature and at the temperature of boiling nitrogen. The lowest energy crystal state was polarized along the crystallographic *a*-axis (B_u) and the factor group splitting of lowest vibrational envelope of the electronic band was 800 cm⁻¹. The whole spectrum was more intense along the *a*- than along the *b*-axis of the crystal. These results are consistent with the notion that the crystal spectrum is derived from dipole-induced dipole interactions between molecular B_{2u} levels of perylene and neighboring unexcited molecules. This assignment of the lowest excited level of perylene is in agreement with theory.

The molecular vibrational structure is severely altered in the crystal and the observed crystal shift is much smaller than that predicted by the Davydov theory.

INTRODUCTION

It is now well established that the Davydov theory of the energy states of molecular crystals (1) can predict to a fair degree of accuracy the main features of the electronic absorption spectra of crystals. The theory has been most often applied to crystals of aromatic hydrocarbons such as naphthalene (2), anthracene (3), and phenanthrene (4).

With the exception of the 2500 Å system of anthracene the Davydov splittings that have been measured are usually from 10 cm⁻¹ to 500 cm⁻¹, the actual value depending on the oscillator strength of the transition involved. In the intense short wavelength system of anthracene the splitting is much greater than this (ca. 15,400 cm⁻¹) (5) although in this case detailed examination of the structure is difficult because of the awkward spectral location of the bands.

Perylene has an intense absorption in the visible region and it is the purpose of this paper to present measurements of the polarized absorption spectra of single crystals of perylene and to compare these with the above-mentioned theory.

THE CRYSTAL STRUCTURE OF PERYLENE

Perylene is monoclinic prismatic (6). There are 4 molecules per unit cell occupying the general positions in the space group $C_{2h}^8(P2_1/a)$. The unit cell dimensions are as follows: $a = 11.35$, $b = 10.87$, $c = 10.31$ Å, $\beta = 100.8^\circ$.

The angles which the molecular axes *L* (long) and *M* (short) make with the crystal axes *a* and *b* are denoted by χ and ψ . The calculated values of these angles along with the oriented gas ratios for absorption intensity along the *a* and *b* crystallographic axes for light incident perpendicular to the *ab* (001) face of the crystal are given in Table I.

TABLE I
The orientation of the molecules in the crystal and the oriented gas ratios

Molecular axis	χ	ψ	D_a/D_b
L	83.3°	89.2°	73:1
M	55.4°	35.0°	1:2.08

¹Manuscript received November 14, 1960.

Contribution from the Chemistry Department, University of British Columbia, Vancouver, B.C. Work supported by the National Research Council, Ottawa, Canada.

THE ENERGY LEVELS OF THE CRYSTAL

It is assumed that the allowed $^1(\pi\pi^*)$ electronic states of perylene are polarized in the molecular plane. In this event the lowest energy molecular singlet level will have the symmetry B_{2u} (short axis polarized) or B_{3u} (long axis polarized). The site symmetry in the crystal is lower than the D_{2h} symmetry of the molecule and each of the molecular levels will split into two allowed crystal states. The polarizations and relative energies of these states—the A_u and B_u representations in the space group C_{2h}^b —can be calculated if the oscillator strength of the molecular transition and the dipole interaction integral summations are known (5). Table II gives the intermolecular interaction integrals within the dipole-dipole approximation. Only the sums over non-translationally equivalent molecules are given; p runs over molecules related by the operation C_2^b (twofold screw along the b -axis) and q runs over molecules related by σ^{ac} (glide reflection in the ac -plane). The geometry factors used were calculated to convergence by Craig and Walmsley (7).

Figure 1 illustrates the type of splitting expected for B_{2u} and B_{3u} molecular levels. In the former case the splitting is $196\text{ cm}^{-1}(\text{\AA})^{-2}$ with the B_u (a axis polarized) crystal state at lowest energy. For B_{3u} levels the lowest crystal state is also B_u and the splitting is $2592\text{ cm}^{-1}(\text{\AA})^{-2}$. The shift of the crystal spectrum relative to that in solution was calculated from the data of Craig and Walmsley (7) and the results are included in Fig. 1. The B_{2u} and B_{3u} molecular levels are thus predicted to show widely different properties when these crystal interactions are taken into account.

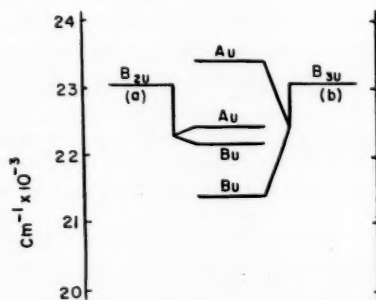


FIG. 1. The predicted arrangement of absorption bands of the perylene crystal for transitions to B_{2u} and B_{3u} molecular levels. Calculated for a dipole length of 1 Å.

EXPERIMENTAL

The perylene was purified further by recrystallization followed by sublimation *in vacuo*. Large rectangular plates were obtained when perylene was sublimed just below its melting point in an atmosphere of carbon dioxide. This was the only method whereby very thin crystals of this substance could be grown. Recrystallization from solution or the melt, sublimation *in vacuo*, and recrystallization between quartz disks all proved unsuccessful techniques in this case. The pure crystals were golden yellow. The thin crystals were pleochroic and exhibited symmetrical extinction under the polarizing microscope. A detailed examination of the isogyre patterns and the order of the interference colors indicated that the plates were basal sections with 001 as the most fully developed face. The b -axis was found to run parallel to the bisector of the slightly obtuse corner of the approximate rectangle. The optic plane of the crystal, containing the

a-axis, was normal to the exposed surface and bisected the acute-angled edge. Visual observations of the pleochroism indicated that the crystal absorbed most strongly when the electric vector of the light was made to vibrate parallel to the *a*-crystallographic axis.

The light source was a voltage-stabilized, air-cooled tungsten lamp. The spectrometer has been described previously. For the measurements at 77° K a metal cell was constructed with a copper holder in the nitrogen-free optical path. This cell has been described previously (8). The crystals were mounted over a pinhole by employing their own adhesive properties to metal or quartz. The analyzer was a Wollaston prism. In the low temperature experiments the polarized absorption spectra were obtained by spectrographic examination of each of the beams from the prism. For the experiments at room temperature the crystal was rotated relative to the prism and the optical system was not otherwise disturbed.

The *f*-number used in this work was determined by integration of the absorption spectrum of perylene in ethanol solution. A value of 5.4 ± 0.3 was obtained. The *f*-numbers of the vibronic components of the spectrum were obtained from the estimated areas of the individual vibronic bands of the spectrum in ethanol.

The Absorption Spectra

Figure 2 shows the absorption spectrum of a perylene crystal at room temperature. The relative intensities and exact spectral location of the bands were extremely sensitive to the crystal orientation. Figure 3 shows the spectrum of a thicker crystal at room temperature. The bands were much sharper at 77° K but even at this temperature (see Figs. 4 and 5) the details of the spectra were considerably altered by rotating the crystal through only fractions of a degree. This was understandable if the long axis of the molecule was active. This axis makes angles of 83.3° and 89.2° with the *a*- and *b*-crystallographic axes and very slight misorientations of the crystal would result in drastic changes of the expected oriented gas ratio of absorption intensities.

Table III shows the band positions measured in both crystal polarizations. The *b*-

TABLE II
Intermolecular interaction integrals (7)

Summations	Integral sums [cm ⁻¹ (Å) ⁻²]	
	<i>B</i> _{2u} ← <i>A</i> _g	<i>B</i> _{2u} ← <i>A</i> _g
$\sum_q I_{iq}/M^2$	-531	-774
$\sum_r I_{ir}/M^2$	-765	+876
Splitting	2592	204

polarized spectra were particularly difficult to interpret owing to the extreme weakness of some of the ill-resolved bands. The values which are quoted on Table III were seldom all observed with one crystal. It is for this reason that four representative spectra are shown.

Only a very broad, weak fluorescence emission was detected and the present experimental technique was not sensitive enough to enable a detailed study to be made. In this regard perylene resembles pyrene (9), a molecule that has also a similar crystal structure (6).

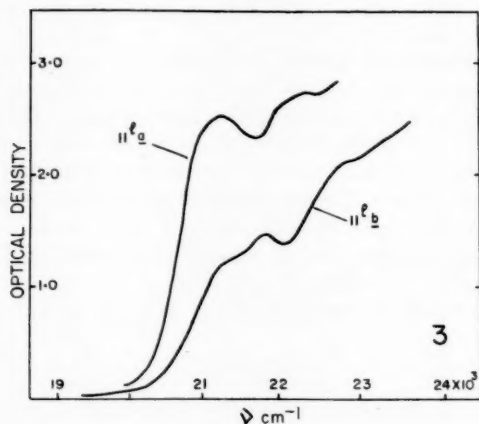
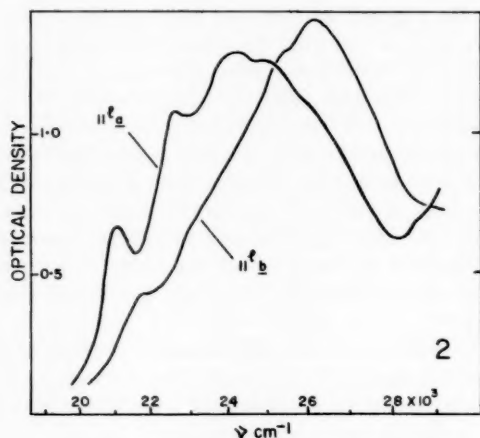
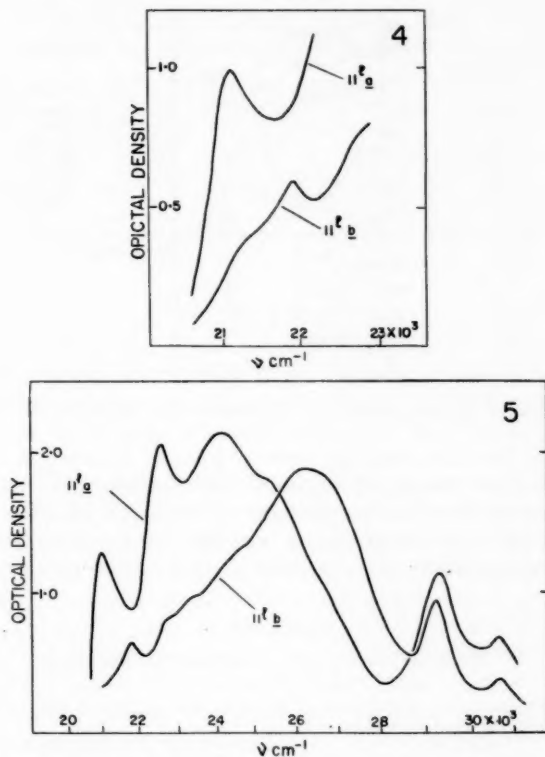


FIG. 2. Polarized absorption spectrum of perylene at room temperature.

FIG. 3. Polarized absorption spectrum of a thick perylene sublimation flake at room temperature.

DISCUSSION

The electronic levels of perylene have not yet received much theoretical attention. Platt (10) has predicted the polarizations of the transitions in this molecule using the simple free electron box model. The three lowest energy singlet states were calculated to have the same polarization properties; namely, they were all long axis polarized states thus belonging to the representation B_{2u} of the D_{2h} point group. A straightforward L.C.A.O.-A.S.M.O. calculation using Hückel orbitals yields the result that the lowest two excited molecular levels should have different symmetry. These two levels are predicted to lie at 19.8 kK (B_{2u}), and 28.4 kK (B_{3u}) respectively (1 kK \equiv 1000 cm^{-1}). A further intense level is expected at 42.4 kK with B_{3u} symmetry. These results are in fair agreement with the solution spectrum (11), which exhibits four separable absorptions in this spectral region. These were assigned on the basis of analogy, band structure, and intensity by Clar (11) as follows: 22.75 kK (p , B_{2u}); 29.60 kK (α , B_{3u}); 34.32 kK (β , B_{2u}); 39.86 (β , B_{3u}).



FIGS. 4 and 5. Polarized absorption spectrum of the perylene crystal at 77° K.

These predictions were substantiated by the results of Williams (11), who has shown that the lowest molecular level of perylene is polarized at right angles to the level at 39.86 kK.

In summary, it may be expected that absorption to the lowest excited singlet state of perylene will be intense and that the next lowest excited level will be active along the short molecular axis of the molecule (B_{3u}).

Figure 6 shows the observed energy scheme for the perylene crystal. A comparison with Fig. 1 clearly indicates that it is the B_{2u} molecular level from which the crystal spectrum is derived. The observed splittings are one order of magnitude too small to be accounted for by interactions between dipoles directed along the short molecular axes.

The over-all intensity of absorption in the a -polarized spectrum is greater than in the b -spectrum. This observation is in agreement with the predictions in Table I. The polarization ratios, however, were not expected to correlate with the oriented gas ratios in view of the large splitting. The poor agreement between theory and experiment in regard to polarization ratio is probably concerned with the near coincidence of the long molecular axis with the C' -crystallographic axis thus making it difficult to measure this quantity. In any case, the measured quantity in this work was the optical density ratio. This ratio may only be equal to the polarization ratio if the bands have similar shapes and have

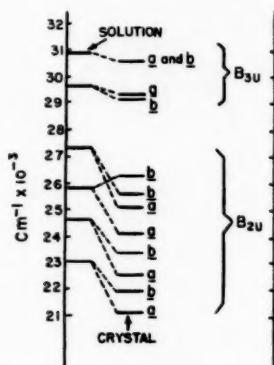


FIG. 6. Comparison of the observed data for perylene in solution and in the crystalline state.

nearly equal frequencies of maximum absorption. Clearly these conditions are not satisfied.

The absorption spectra show four bands in the region 20,000–28,000 cm^{-1} . The relationship between the *a*- and *b*-polarized spectra is apparent for the two lowest energy bands in each polarization (see Table III) but there may be some ambiguity regarding the

TABLE III
The band maxima in the absorption spectrum of the perylene crystal

Energy of band maximum $\pm 40 \text{ cm}^{-1}$	Polarization	Assignment
21,160	<i>a</i>	B_u
21,930	<i>b</i>	A_u
22,510	<i>a</i>	$B_u \times a_g$
23,400	<i>b</i>	$A_u \times a_g$
24,110	<i>a</i>	$B_u \times (a_g)^2$
25,100	<i>a</i>	$B_u \times (a_g)^2$
25,575	<i>b</i>	$A_u \times (a_g)^2$
26,300	<i>b</i>	$A_u \times (a_g)^2$
29,130	<i>b</i>	Different crystal state; molecular ${}^1B_{3u}$ level?
29,300	<i>a</i>	
30,160	<i>a</i>	
30,160	<i>b</i>	

remaining bands. The frequency intervals other than that between the two lowest energy maxima do not correspond to a regularly spaced vibrational structure. Nor do the wave numbers between the centers of gravity of the pairs of A_u and B_u states follow any regular pattern. It is expected from the Davydov theory that in the crystal each molecular vibronic state will be split by an amount which depends on the strength of that separate oscillator. Accordingly Table IV gives the experimental *f*-numbers for the four principal vibronic levels of the perylene molecule. The *f*-numbers for the crystal vibronic levels could not be calculated as neither the crystal thickness nor the reflection corrections were known accurately.

TABLE IV
 Comparison of crystal and solution data

Solution absorption maximum ν cm^{-1}	$(\nu_{\text{cryst}} + 1500 \text{ cm}^{-1})^*$ (cm^{-1})	f_{mol}	Splitting (cm^{-1})	
			Calc.	Expt.
23,050	23,050	1.4	1098	780
24,650	24,490	2.4	1764	820
25,850	26,340	1.2	844	1490
27,330	27,200	0.4	281	1200

*The values in this column refer to the centers of gravity of the pairs of *a*- and *b*-polarized bands which are shown in Fig. 6.

THE COUPLING PROCESS

The coupling energy of the molecular vibronic forces in the perylene crystal by resonance force interaction is extremely large. The magnitude of the splitting is determined by the crystal geometry and the dipole strength of the crystal under study. It is therefore of interest to examine the applicability of the Davydov model, which was intended to treat only weakly coupled systems. Simpson and Peterson (13) have defined criteria in the form of inequalities which should distinguish one type of coupling from another. Clearly perylene falls into the class of strong to intermediate coupling as the band widths and interaction energies are of the same order of magnitude. The zeroth level splitting of 780 cm^{-1} was in fair agreement with the calculated value of 1098 cm^{-1} . This appears to imply that the Davydov theory is useful even in strongly coupled situations. On the other hand the higher vibronic levels, with the vibrational quantum number of the upper state greater than one, appear to split apart much more than is predicted by the Davydov theory. This suggests that it is the introduction of strong vibrational-electronic coupling which causes the deviations from the simple picture.

If the oscillator strength for a single vibronic transition is f_v then the total oscillator strength of the electronic transition is given by $\sum f_v$. The energy of interaction (splitting) between vibronic states with electronic symmetry B_{2u} is given by θm_v^2 where θ is the appropriate geometry factor and m_v is the dipole length corresponding to f_v . Thus the total interaction energy ΔE is

$$\Delta E = e^2 \theta \sum m_v^2 = e^2 \sum (\theta m_v^2).$$

The calculated value of ΔE , which is the sum of the splittings in the second last column of Table IV, was found to be 3987 cm^{-1} . Experimentally observed was a total interaction energy of 4290 cm^{-1} , which is in excellent agreement with that calculated within the dipole-dipole approximation.

Thus it is safe to conclude that the lack of agreement between theory and experiment for the individual vibronic transitions did not arise because of the use of a dipole-dipole approximation. Instead it appeared that a drastic redistribution of intensity compared to that in solution had occurred.

THE SPECTRUM AT HIGHER ENERGIES

Above $28,000 \text{ cm}^{-1}$ there appears to commence a new electronic transition. This transition is weaker than the first transition and virtually no splitting was observed. In solution there is a weak band at $29,600 \text{ cm}^{-1}$, which Clar assigned as the α' -band. The

absorption in this region is then expected to be due to the excitation of a state belonging to the ${}^1B_{3u}$ representation of the D_{2h} point group. This band appears to be much stronger in the crystal than in solution. Neither the small splitting nor the polarization ratio would fit with the assignment of the bands as absorption to a short axis polarized level. This region of the crystal spectrum was experimentally difficult to study and some reflection data is needed before the intensity may be measured more accurately.

A more complete account of the absorption spectrum of perylene sublimation flakes, including calculations of the band intensities and the emission spectrum at liquid helium temperature is in preparation.

REFERENCES

1. A. S. DAVYDOV. *Zhur. Eksptl. i Teoret. Fiz.* **18**, 210 (1948).
2. D. S. McCLURE and O. SCHNEPP. *J. Chem. Phys.* **23**, 1575 (1955).
3. D. P. CRAIG and P. C. HOBBS. *J. Chem. Soc.* 2309 (1955).
4. D. S. McCLURE. *J. Chem. Phys.* **25**, 481 (1956).
5. D. P. CRAIG and P. C. HOBBS. *J. Chem. Soc.* 539 (1955).
6. D. M. DONALDSON, J. M. ROBERTSON, and J. G. WHITE. *Proc. Roy. Soc. (London), A*, **220**, 311 (1952).
7. D. P. CRAIG and S. H. WALMSLEY. In course of publication; private communication.
8. R. M. HOCHSTRASSER. *Spectrochim. Acta*. In press.
9. J. FERGUSON. *J. Chem. Phys.* **28**, 765 (1958).
10. J. R. PLATT. *J. Chem. Phys.* **22**, 1448 (1954).
11. E. CLAR. *Aromatische Kohlenwasserstoffe*. Springer-Verlag, Berlin, 1952. p. 284.
12. R. WILLIAMS. *J. Chem. Phys.* **26**, 1186 (1956).
13. W. T. SIMPSON and D. L. PETERSON. *J. Chem. Phys.* **26**, 588 (1957).

THE EFFECT OF INTRAMOLECULAR TWISTING ON THE EMISSION SPECTRA OF HINDERED AROMATIC MOLECULES

PART I. 1,1'-BINAPHTHYL¹

ROBIN M. HOCHSTRASSER

ABSTRACT

The fluorescence spectrum of 1,1'-binaphthyl has been examined in solution, in rigid glass, and in the crystal. It is found that in rigid media the spectral location of the emission is very sensitive to temperature. At 300° K the band is broad and structureless with a maximum at 26,700 cm^{-1} and a zero-zero band at about 30,200 cm^{-1} with very low intensity. The same is true at 273° K and 195° K. At temperatures below 157° K structure starts to appear until at 77° K the center of gravity of the emission is around 29,000 cm^{-1} and the 0-0 band at 31,270 cm^{-1} is quite clear and strong. Even at 77° K there is apparent a broad, but now weak band at 27,260 cm^{-1} . In the crystal the spectrum is broad and structureless at 300° K with a maximum emission intensity at 26,300 cm^{-1} . On lowering the temperature to about 142° K the intensity is built up on the high energy side of this band until eventually a new peak at 27,850 cm^{-1} becomes apparent at 77° K.

These results are interpreted on the basis of unsymmetrical potential energy variations with angle of twist which permit two origins for the fluorescence spectra of double molecules of this type.

INTRODUCTION

Aromatic molecules which consist of two identical planar aromatic systems joined through a single carbon-carbon bond may exhibit ultraviolet spectra which are either very different from or virtually identical with the known spectrum of one half of the molecule. If the rings are coplanar then resonance interaction is strong and the spectrum of the double molecule is vastly different from that of the isolated chromophores. If the molecular planes are perpendicular, the systems are essentially non-interacting, within a π -electron approximation, and the double-molecule spectrum does not appear different from that of one ring of the system. Perhaps the most extensively studied group of compounds in this regard are the biphenyls (1).

The binaphthyls were studied by Friedel and Orchin (2) and the ultraviolet spectra in solution at room temperature indicated that resonance interaction was at a minimum for 1,1'-binaphthyl whose spectrum was quite similar to that of naphthalene. 2,2'-Binaphthyl on the other hand exhibited a spectrum which extended much further to the red than did that of naphthalene, and in this case the steric inhibition of resonance was presumed to be at a minimum.

Unfortunately the spectra of these materials at room temperature are characteristically broad, and exact spectral comparisons are out of the question. The same is true of the luminescence spectra (phosphorescence and fluorescence) so that from such spectra little can be explained of the exact spectral shifts or of the true degree of interaction between the ring systems.

In this work a detailed study has been made of the low temperature absorption spectrum of 1,1'-binaphthyl and of the fluorescence and phosphorescence spectra of this compound at a variety of temperatures and in various rigid media.

¹Manuscript received November 14, 1960.

Contribution from the Chemistry Department, University of British Columbia, Vancouver, B.C. Research supported by a grant from the National Research Council of Canada.

EXPERIMENTAL

The low temperature absorption spectra were taken on a Cary 14 recording spectrophotometer. The low temperature cell has been previously described (3). Extinction coefficients were calculated after corrections for contraction on cooling from 300° K to 77° K.

The fluorescence and phosphorescence spectra were excited by one of the mercury 3131 Å group of lines from a G.E. AH6 arc. A good monochromatic source was obtained by using a high aperture Bausch and Lomb grating monochromator with the entrance and exit slits at 1 mm in conjunction with the mercury arc. The parallel beam from the monochromator was directed onto the sample, which was contained in a quartz test tube, itself immersed in an unsilvered quartz Dewar flask. When the coolant was transparent to 3130 Å an immersed region of the solution was irradiated, otherwise the region just above the coolant surface was used.

The emission was focused on the slit of a medium Hilger quartz spectrograph. In order to obtain comparative fluorescence and phosphorescence spectra the emission was recorded automatically. The travelling photomultiplier (R.C.A. 1P28) photocurrent was amplified by a Keithley (200B) vacuum tube micromicroammeter.

The solvents used were E.P.A. (ether, 5 parts; isopentane, 5 parts; ethyl alcohol, 2 parts); ethyl alcohol, which forms a slightly strained but nevertheless useful rigid glass at liquid nitrogen temperature; *n*-heptane, which when freshly distilled forms transparent crystals at 77° K; glycerol, which is virtually transparent to 3131-Å radiation ($\log I_0/I$ 0.12 in 1-cm path) and forms a rigid glass over the range 273° K–150° K. Dextrose and *n*-hexadecane were also used as solvents.

The following were employed as coolants: boiling nitrogen (77° K); *n*-pentane (142° K); diethyl ether (157° K); solid carbon dioxide (195° K); and melting ice (273° K).

RESULTS

Figure 1 shows the absorption spectrum of 1,1'-binaphthyl in ethyl alcohol at 300° K and in E.P.A. at 77° K. Only the long wavelength region is shown in the figure. Figure 2 shows the total emission spectra of naphthalene and 1,1'-binaphthyl in alcohol at 77° K. These spectra emphasize the similarity of vibrational structure in each tracing. The intensity scale in Fig. 2 was chosen such that the area under each of the fluorescence curves was comparable.

Figure 3 shows the fluorescence spectra of 1,1'-binaphthyl in glycerol at 273° K and 142° K; the fluorescence of 1,1'-binaphthyl in alcohol at 77° K is also shown in Fig. 3. Again, the curves were adjusted until they had similar areas on the drawn scale.

The 0-0 band of the lowest energy transition was measured at room temperature in ethyl alcohol and in the same solvent at 77° K. The crossing point of the broad high temperature absorption and emission curves was taken as the 0-0 band energy in this case. At low temperatures the mirror relationship between the long wavelength absorption and the fluorescence permitted accurate measurement of the 0-0 band energy. Table I

TABLE I

Substance	Temperature (°K)	Solvent	0-0 energy (cm ⁻¹)	Emission maximum (cm ⁻¹)
Naphthalene	77	Alcohol	31,730	30,000 ± 100
1,1'-Binaphthyl	300	Glycerol	30,200 ± 150	26,700 ± 20
1,1'-Binaphthyl	77	Alcohol	31,270 ± 20	29,100 ± 100
1,1'-Binaphthyl	77	<i>n</i> -Heptane	31,230 ± 20	29,000 ± 100

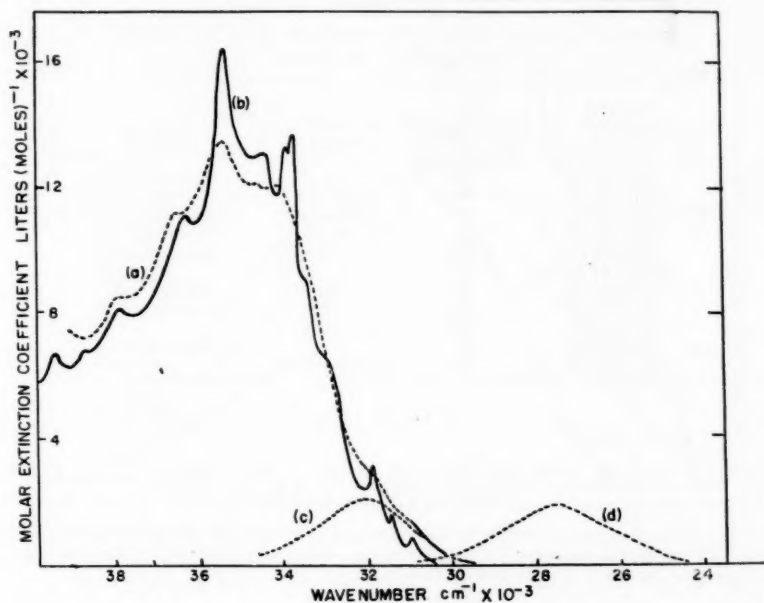


FIG. 1. The absorption spectra of 1,1'-binaphthyl. (a) In E.P.A. at 300° K. (b) In E.P.A. at 77° K. (c) The absorption to the lowest energy state after subtracting the long-wavelength tail of the first strong band. (d) The fluorescence spectrum at 300° K drawn in arbitrary units as the mirror image of curve (c).

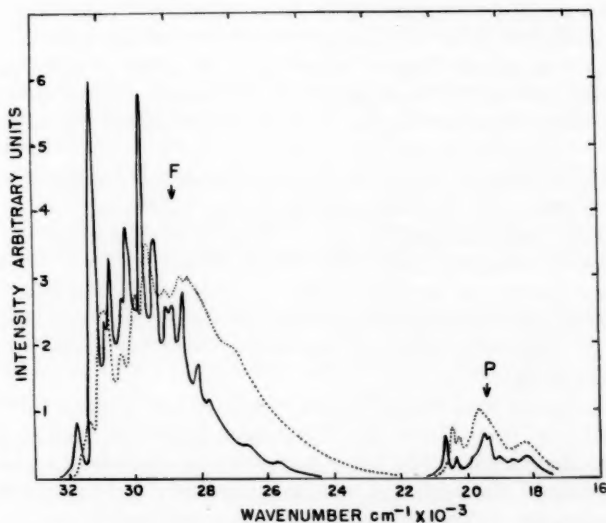


FIG. 2. The total emission spectra of naphthalene and 1,1'-binaphthyl in ethyl alcohol at 77° K. 1,1'-Binaphthyl. — Naphthalene. F = Fluorescence region. P = Phosphorescence region.

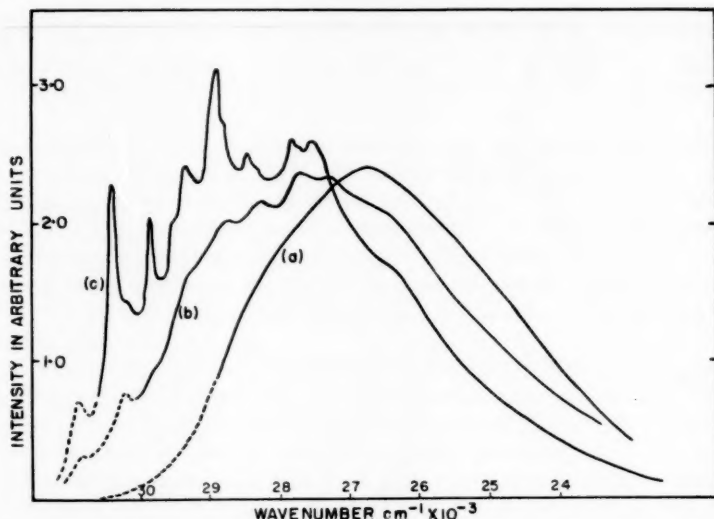


FIG. 3. The effect of temperature on the fluorescence spectrum of 1,1'-binaphthyl. (a) Glycerol, 273° K. (b) Glycerol, 142° K. (c) Ethyl alcohol, 77° K. The regions where very slight corrections for reabsorption of fluorescence may be necessary are covered by dashed curves.

summarizes these measurements. In all the experiments described so far the concentration of 1,1'-binaphthyl (10^{-4} M) and the optical arrangement, as far as possible, were uniformly maintained. When necessary, proper corrections were made for reabsorption of the fluorescence emission. The spectral response of the photomultiplier was not linear over the whole spectral range of phosphorescence plus fluorescence. However, the naphthalene spectra were so similar to those of the double molecule that accurate comparisons could be made without a complete spectral response curve. The phosphorescence emission spectra of naphthalene and 1,1'-binaphthyl were similarly located in the spectrum so that they also could be compared without a detailed knowledge of the spectral response curve.

The following is a summary of the experimental results including a few observations which may not be clear from the foregoing figures and description.

(1) The 0-0 band position was different at 300° K to that at 77° K. However, the error on the former measurement was large (see Table I).

(2) The center of gravity of the fluorescence band lay at $27,370 \pm 80$ cm^{-1} at 300° K, 273° K, or 194.7° K; the band was then broad and devoid of vibrational structure. At 77° K and 142° K vibrational structure was evident and the center of gravity of the spectrum was around 29,000 cm^{-1} .

(3) No radical changes were effected in the spectra at any temperature by altering the medium. This is clear from Table II. There were, however, marked changes in the phosphorescence - fluorescence yield ratios which will be discussed in a later paper.

(4) The 0-0 band of 1,1'-binaphthyl in alcohol was found to lie only 460 cm^{-1} to lower energies than that of the corresponding transition in naphthalene.

(5) Apart from the more subtle changes in the relative intensities of some vibrational bands in the low temperature fluorescence spectra, there was a shoulder at 27,260 cm^{-1}

TABLE II
The effect of solvent and temperature on the energy of maximum emission of 1,1'-binaphthyl

Solvent	Structure of the solvent	Temperature (°K)	Emission maximum (cm ⁻¹)
Crystal lattice		300	26,300±20
Dextrose	Rigid glass	300	27,000±150
Ethyl alcohol	Strained glass	77	27,260±100 ^a
<i>n</i> -Heptane	Crystalline	77	27,260±100 ^a
Hexadecane	Rigid	273	27,340±20
Glycerol	Rigid	273	27,340±20
Ethyl alcohol	Viscous	142	27,460±20
Ethyl alcohol	Liquid	300	27,380±20
Nujol	Very viscous	273	27,500±20
Crystal lattice		77	27,850±20
Glycerol	Strained glass	142	28,170±20 ^b

^aShoulder.

^bTo be compared to the 28,540 cm⁻¹ band at 77° K.

in all of the liquid nitrogen temperature spectra. There is no such shoulder in the naphthalene spectrum. The emission in this region was thus at about the same energy as the emission maximum of the higher temperature spectra.

(6) A similar set of phenomena have been observed for 1-phenylnaphthalene and to a lesser extent for biphenyl and 2,2'-binaphthyl. These results are being prepared for publication.

The Fluorescence Spectrum of the Crystal

The crystal emission was broad and structureless at 300° K with a peak at 26,300 cm⁻¹. At 77° K a little structure appeared at the high energy side of the band but the band maximum was shifted to 27,850 cm⁻¹. This blue shift amounted to 1550 cm⁻¹ and was comparable to the shift of the center of gravity of the rigid glass fluorescence over the same temperature range. These spectra, which are shown in Fig. 4, were from randomly oriented crystals and they were not corrected for reabsorption of fluorescence. The spectra were taken under conditions which would minimize the reabsorption, i.e. front face illumination, and this correction probably becomes important at about 29,000 cm⁻¹. The third spectrum of Fig. 4 is of the crystal fluorescence at 194.7° K and the fourth was taken with the crystals at 157° K. From these spectra it was apparent that the 26,300 cm⁻¹ band was not actually shifting to the blue with decreasing temperature but rather the intensity of the emission in this region was dropping as the intensity in the 27,850 cm⁻¹ region was increasing.

The crystal spectra, solution spectra, and the fluorescence spectra in rigid glasses and their variations with temperature strongly indicate that emission is arising from two origins in the molecule of 1,1'-binaphthyl and that the lower energy level is favored at room temperature.

Vibrational Analysis of the Fluorescence in Alcohol

Table III compares the spectra of naphthalene and 1,1'-binaphthyl. It is quite clear from this analysis that the naphthalene state from which the emission occurs and the ground state at this same instant are not much affected by the presence of another α -naphthyl group. Thus at low temperatures the molecule behaves like two virtually non-interacting naphthalene molecules. Clearly there is no naphthalene analogue for the

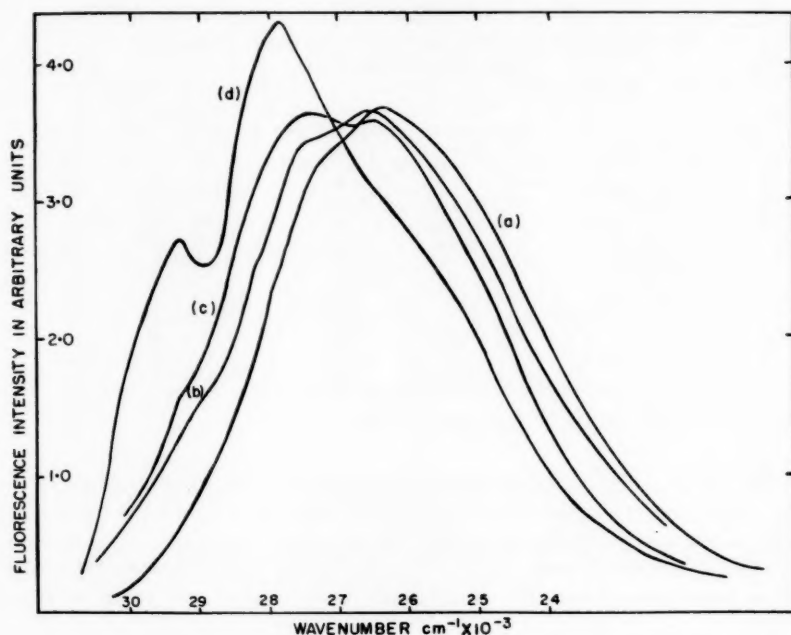


FIG. 4. The fluorescence of crystalline 1,1'-binaphthyl. (a) 300° K. (b) 195° K. (c) 157° K. (d) 77° K. No correction was applied to take into account the reabsorption of fluorescence.

TABLE III
Comparison of the vibrational structure of the fluorescence of
naphthalene and 1,1'-binaphthyl

Naphthalene* (cm ⁻¹)	1,1'-Binaphthyl (cm ⁻¹)	$\Delta\nu$ (cm ⁻¹)	Analysis Naphthalene; * 1,1'-Binaphthyl
31,731 (w)	31,270 (w)	460	0-0
31,236 (vs)	30,910 (vs)	326	495 ; 360 b_{1g}
30,804 (s)	30,440 (s)	364	927 ; 830 b_{1g}
30,464 (s)	29,900 (s)	560	495+772 ; 360+(1010)
29,850 (s)	29,540 (vs)	310	495+1386 ; 360+1370
29,419 (s)	29,080 (s)	339	927+1386 ; 830+1360
28,824 (s)	28,540 (w)	284	Ill-resolved doublet
28,465 (s)	28,310 (w)	150	495+2×1386 ; 360+2×1300
	27,260 broad		

Only very weak bands

*See reference 4; the emission spectrum of naphthalene in π -pentane at 77° K.

shoulder of medium intensity which appeared at 27,260 cm⁻¹. The analysis is based on the more complete findings of Bolotnikova (4), who studied naphthalene in pentane at 77° K.

Of the more subtle differences between the spectrum of 1,1'-binaphthyl and naphthalene is the large change in the frequency of the b_{1g} vibration (495 cm⁻¹ in naphthalene ground state), which is lowered to 360 ± 20 cm⁻¹ in 1,1'-binaphthyl. It has been suggested that this vibration is one of those responsible for the appearance of short axis polarized

absorption in the spectrum of the lowest energy $B_{2u} \leftarrow A_{1g}$ (long axis polarized) transition in naphthalene (4). If this in fact is the case, vibrations of this symmetry would be more modified in the double molecule than the totally symmetric ones because at interplanar angles around 90° the dipole-dipole interaction - vibronic coupling between the rings can only be significant for short axis polarized levels. In future experiments at higher resolution these discrepancies may be cleared up.

DISCUSSION

Firstly it is of interest to discuss the results in terms of known models. Jaffé and Orchin (5) have recently proposed a model to explain the wavelength shifts and intensity variations in hindered stilbenes. In this model the potential energy curves for the upper and lower states have double minima. These arise after the superimposition of a rotation barrier on the usual resonance potential versus angle of twist curve. The barrier is assumed small compared to the resonance stabilization at zero twist, and because the resonance interaction is not the same in both states it follows that the equilibrium angle of twist is not the same in the upper and lower states. The $1,1'$ bond is most likely shorter in the upper state so the ground and excited state rotation barriers may not be identical.

If such a model is accepted for $1,1'$ -binaphthyl then the fluorescence spectrum would not be expected to alter markedly with temperature. Certainly the center of gravity of the emission would remain at the same energy at all temperatures in view of the Franck-Condon principle. Besides this, the experiments show that the spectral location of the bulk of the emission intensity red shifts as the temperature is raised, which would imply that the ground state potential curves were steeper than those of the upper state. This is contradictory to an increase of resonance interaction in the upper state. Even the postulate that emission may occur from highly excited twisting modes does not explain the observed phenomena on this model.

The Probable Configuration of 1,1'-Binaphthyl

In the trans planar configuration the $2-8'$ and $8-2'$ repulsions must be very great. In this configuration (see Fig. 5(a)) the molecule could be likened to 3,4-benzphenanthrene, which is known to be distorted from the planar configuration (6). In the cis planar configuration the interactions are akin to those in biphenyl (for the $2-2'$ positions) and

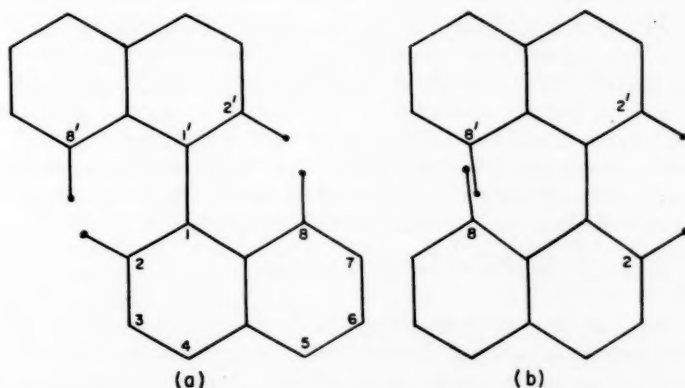


FIG. 5. $1,1'$ -Binaphthyl: (a) Trans-planar, (b) Cis-planar. C—H bands were drawn to terminate at the hydrogen nucleus in each case.

3,4-5,6-dibenzphenanthrene (for the 8-8' positions). Certainly in the latter there is a large repulsion as dibenzphenanthrene is non-planar (7). The repulsions in 1,1'-binaphthyl will be smaller than those of the above analogies as the 1-1' bond is presumably longer than for the condensed hydrocarbons.

Calculation has shown that when the H—H and C—C repulsions are minimized, i.e. the molecule is rotated about 1-1' until each H—H and C—C distance is maximized and as near as possible equalized, then the most stable configuration on this basis is with the rings inclined to cis with an angle of 78° between the ring planes. Trotter (8) has recently determined the configuration from X-ray data at room temperature; the cis configuration was confirmed and the angle was 72°. The angle of twist was measured from 0° at the cis planar configuration.

It was also clear, both from the above discussion of the polynuclear hydrocarbon analogues and from geometrical calculations, that the energy required to reduce the angle by any given amount from 78° is much greater than the energy required to increase the angle by the same amount. This implies that the repulsion energy versus angle of twist curve will be *much steeper on the low angle (or cis) side of the equilibrium situation* than on the high angle (or trans) side.

The 1,1'-binaphthyl-5,5'-dicarboxylic acid has been resolved into optically active isomers at room temperature (9). This indicates that the rotation barrier is extremely large both at the trans and cis planar configurations.

The Resonance Energy of Interaction between Rings

There is some confusion regarding the resonance interaction between the two naphthalene units. On the one hand Magnus and Becker (10) have found an experimental resonance energy of 174.4 kcal for 1,1'-binaphthyl. From this they concluded that the molecule was planar. This result is at variance with conclusions from the optical activity of the 5,5'-dicarboxylic acid and the X-ray data, both of which indicate a severely twisted molecule. The ultraviolet absorption spectrum does not differ considerably from that of naphthalene, nor does the low temperature fluorescence spectrum; these results indicate that neither in the ground nor the excited state are the two rings strongly interacting. The broadness of the absorption spectrum in solution is most likely caused by librations about the equilibrium angle rather than by a permanent, strong, resonance force interaction.

The assumption will be held here that the resonance stabilization energy in the ground state is small in comparison to the van der Waals repulsive energy in either of the planar situations. In biphenyl the experimental resonance interaction energy is about 6 kcal/mole (2080 cm⁻¹) in the gas phase where the interplanar angle is probably near 45°. Thus the planar form should be stabilized by at least 12 kcal/mole.

After electronic excitation it is likely that the 1-1' bond will be shortened because of the redistribution of charge at the 1 and 1' carbon atoms. The resonance interactions in the excited state will therefore be greater than in the ground state.

The Potential Curves for the Ground and Excited States

Figure 6 shows the approximate variation of van der Waals repulsion energy with the interplanar angle. The curve is drawn steeper to the cis side in accordance with the above discussion. The dotted curve in Fig. 6 indicates the variation of the resonance interaction energy with interplanar angle and the extent of this variation is assumed to be larger in the excited state.

The van der Waals repulsive curves are drawn approximately in order that the ground

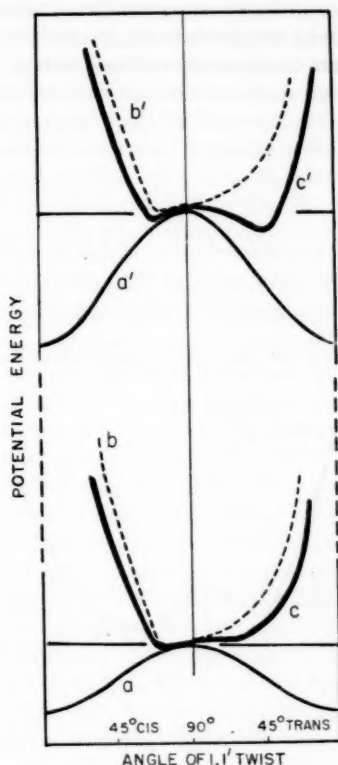


FIG. 6. The potential curves of the ground and excited states of a sterically hindered double molecule. Dashed curve: the non-uniform van der Waals repulsive energy. Thin line curve: resonance interaction. Thick line curve: resultant variation of potential with angle of twist.

NOTE: The resonance interaction potential may not, in the general case, be symmetric about $\theta = 90^\circ$. However, this is probably the case for molecules such as biphenyl, 1-phenylnaphthalene, and 2,2'-binaphthyl for which comparable experimental data has been collected. Therefore the particular case of 1,1'-binaphthyl, where the resonance interaction is greatest in the trans planar configuration and non-zero when the interplanar angle is 90° is avoided in this more general diagram. The curves on Fig. 7, on the other hand, refer specifically to 1,1'-binaphthyl. The resonance interaction energy discussed above is taken to be the potential energy of interaction of two dipoles (dipole-induced dipole) each of which is directed along the long axis and in the plane of one half of the molecule.

state minimum occurs when there is about 72° between the ring planes. The same curves have been drawn in the upper state although in fact the repulsive forces in the upper state may be considerably altered. The equilibrium angle may also be different in the excited state but in the absence of detailed information on this point the minimum at 72° is drawn for both the ground and excited states. It is not thought that these assumptions will seriously affect the ensuing discussion.

In Fig. 6 the curve of the upper state has two potential minima while the ground state curve has only one. The trans-side minimum in the upper curve is probably lower than the cis-side minimum and it is certainly broader. This implies that molecules in this configuration are flapping with greater amplitude than molecules with the same thermal energy in the cis configuration.

It should be emphasized that potential energy curves of this type will arise even if the molecule under consideration does not have the trans and cis planar configurations. All that is required is that the equilibrium configuration is different from 90° . This condition may also be satisfied in phenylnaphthalene. For this molecule the 2 and 6 phenyl positions are subject to different repulsion energies at the planar position. Phenylnaphthalene would therefore be at least less planar than biphenyl on the basis of atom - atom repulsion energy.

The Fluorescence Spectra

It is proposed that there are two fluorescence origins in double molecules of this type. The origins arise because of the asymmetry of the potential in relation to angle of twist. Figure 7 shows one arrangement of ground and excited state potential curves

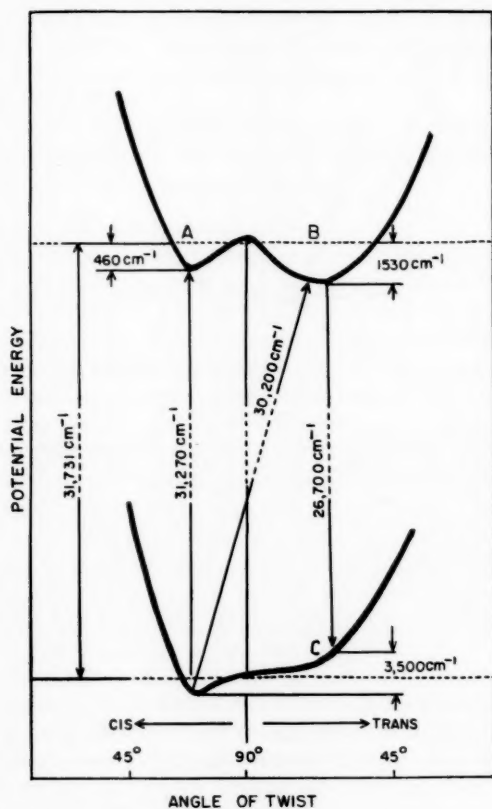


FIG. 7. The potential energy versus angle of twist relationships for 1,1'-binaphthyl: a model which accounts for the emission spectrum.

which may account for all the observed features of the fluorescence spectra of 1,1'-binaphthyl. It has been shown in the foregoing that curves of this type can arise from a combination of van der Waals and resonance forces which have slightly dissimilar angular variations in the ground and excited electronic states.

The difference in energy between the zero-point vibrational levels in the minima A and B is given by the difference in 0-0 band frequencies at 77° K and 300° K, that is 1050 cm^{-1} . This is necessarily approximate due to the uncertainty in the measurement at 300° K. The upper limit to the depth of minimum A is given to a first approximation by the difference in 0-0 band energies of naphthalene and 1,1'-binaphthyl at 77° K, that is 480 cm^{-1} . Thus the depth of the potential minimum B is approximately the sum of these two derived quantities (1050 + 480) cm^{-1} yielding 1530 cm^{-1} . The energy difference between the configuration represented by C in Fig. 7 and the zeroth vibrational level in the ground state is then 3500 cm^{-1} assuming vertical transitions (31,730-26,700-1,530 cm^{-1}).

At temperatures below room temperature virtually all molecules have a cis-inclined configuration and this configuration must be maintained immediately after light absorption in accordance with the Franck-Condon principle. Thus newly formed excited molecules have A-type configurations with an excess of vibrational energy. Within an extremely short time after this, the excited molecule will be vibrationally deactivated while retaining the cis configuration. This will arise because the twisting frequency should be small and hence the twisting time large (10^{-11} - 10^{-12} seconds) in comparison to the time of vibrational deactivation (10^{-13} seconds). At a short time after light absorption the excited molecules will be in thermal equilibrium with the surrounding medium and the configuration A will be preferred. The potential barrier between A and B then determines the number of excited molecules which will remain in state A.

The height of this potential barrier is, however, not the only factor which will determine the relative yields of emission from state A and state B. It is unlikely that the rates of fluorescence emission will be the same in each of these states. Although the natural radiative lifetimes between the excited states and the ground state may be about equal in each configuration, any difference in the form of the potential minima, which describe the amplitude of any particular twisting mode, will alter the actual lifetimes of emission from these levels. Due to the different ring orientations in each minimum the internal conversion processes which bring about non-radiative transitions to the ground electronic state will not necessarily be identical for type A and B situations.

The following situations are envisaged after light absorption: (a) At 300° K—the thermal energy ($kT \doteq 200 \text{ cm}^{-1}$) is comparable to the barrier height ($< 480 \text{ cm}^{-1}$) and the rate of emission from state A is considerably slower than from state B. Thus nearly all the radiatively lost energy originates from state B where the barrier height (1530 cm^{-1}) is large in comparison to kT . (b) At 77° K—the thermal energy ($kT \doteq 48 \text{ cm}^{-1}$) is now small in comparison with the barrier height. Thus only about 5% of the emission will originate from state B (for a barrier of 480 cm^{-1}). (c) At intermediate temperatures both states will emit to some degree. The critical temperature appeared to be about 130° K ($2kT \doteq 140 \text{ cm}^{-1}$), which may mean that the barrier height was overestimated by spectral measurements.

On the basis of the model presented here the experimental value of the zero-zero band energy at 300° K must lose significance. Instead the measured value is an upper limit of the actual value of the difference in energy between the zeroth level of the ground state and the zero-point vibrational level of the type B potential energy situation of Fig. 7. This stipulation is necessary because of the impossibility of knowing the exact form of the absorption to state B at the higher temperatures. The curve (c) in Fig. 1 is almost certainly composed of absorption to both A and B. In this event the zero (ground state) to zero (state B) energy can only be at lower energy than the measured value.

In conclusion, and in conjecture, it may be possible to say which of the potential curves has the greatest amplitude for the low frequency twist. The configuration which occupies the greatest volume (i.e. the trans) would probably exchange vibrational energy most rapidly with the surrounding medium. Thus the internal conversion from this to the ground level might be greater than for the cis configuration. This would imply that the curves A and B should be interchanged such that A is at lowest energy while B becomes shallow and flat-bottomed. The phosphorescence results do indicate that intersystem crossing is more favorable from the emitting level in 1,1'-binaphthyl than from the lowest singlet state of naphthalene (see Fig. 2). This problem will be treated more fully in Part II of this series.

CONCLUSIONS

Still many questions remain to be answered in regard to the effect of intramolecular twisting on the spectra of molecules of this type. Similar studies to the above on biphenyl, stilbene, 1-phenylnaphthalene, and 2,2'-binaphthyl and on the phosphorescence spectra of these materials are in preparation for publication. It is believed that much detailed information, some of this previously unforeseen, may be extracted from a study of the luminescence of such compounds.

It is not inconceivable that two emission origins A and B could arise for some other reason than has been presented here. The upper state of naphthalene would certainly be split into two double-molecule states of different polarization and radiative lifetime (11). It is also conceivable that one of these states is preferred over the other only at certain interplanar angles. Polarized fluorescence measurements will help to clear up these points. Preliminary calculations within a dipole-dipole approximation have, however, strengthened the present interpretation. The resonance interactions between the rings in the excited state at the cis, 90°, and trans configurations are in the respective ratios 0:1:5. These calculations indicate that the resonance interaction potential also varies in a non-uniform manner with angle of twist. The inclusion of this refinement in Fig. 7 would pull the minimum B down even further below A.

REFERENCES

1. STERIC EFFECTS IN CONJUGATED SYSTEMS. Chemical Society Symposium, Hull, 1958. Edited by G. W. GRAY. Butterworth Scientific Publications, London, 1958.
2. R. A. FRIEDEL, M. ORCHIN, and L. REGGEL. *J. Am. Chem. Soc.* **70**, 199 (1948).
3. R. M. HOCHSTRASSER. In press.
4. T. N. BOLOTNIKOVA. *Optics and Spectroscopy*, **7**, 24 (1959).
5. H. H. JAFFÉ and M. ORCHIN. *J. Chem. Soc.* 1078 (1960).
6. F. H. HERBSTSTEIN and G. M. J. SCHMIDT. *J. Chem. Soc.* 3302 (1954).
7. A. D. MCINTOSH, J. M. ROBERTSON, and V. VAND. *J. Chem. Soc.* 1661 (1954); *Nature*, **169**, 322 (1952).
8. J. TROTTER. Private communication.
9. F. BELL, W. H. D. MORGAN, and J. F. B. SMYTH. *Chem. & Ind. (London)*, 634 (1951); F. BELL and W. H. D. MORGAN. *J. Chem. Soc.* 1716 (1954).
10. A. MAGNUS and F. BECKER. *Erdöl u Kohle*, **4**, 115 (1951).
11. D. S. MCCLURE. *Can. J. Chem.* **36**, 59 (1958).

THE INFRARED FREQUENCIES AND INTENSITIES OF THE HYDROXYL BAND IN ORTHO-SUBSTITUTED PHENOLS¹

K. U. INGOLD AND D. R. TAYLOR²

ABSTRACT

The infrared frequencies, intensities, and half-band widths of the fundamental stretching vibration of the hydroxyl group have been measured for a large number of ortho-alkyl phenols. It has been found that phenols containing a single ortho-alkyl substituent exist as *cis* and *trans* isomers in unequal amounts, the *trans* isomer being the more abundant. The difference in free energy between the two isomers in dilute solution in carbon tetrachloride at 24° C has been measured for ortho-cresol, 2,3-dimethyl phenol, and several ortho-*tert*-alkyl phenols.

INTRODUCTION

The fundamental frequencies of the hydroxyl group in *o*-alkyl-substituted phenols have been reported for a rather limited range of alkyl substituents by a number of workers (1, 2, 3, 4), but, with the exception of 2,6-di-*t*-butyl-4-substituted phenols (5), there has been no systematic study of the effect of these substituents on band intensities. The present work describes a comprehensive examination of both the frequencies and the intensities over a large range of *o*-alkyl substituents.

The O—H vibrational frequency, in carbon tetrachloride solution, of 2,6-di-*t*-butyl phenol is 36 cm⁻¹ higher than phenol (5) and since the O—H band is coplanar with the ring in both cases (5) it should therefore be possible to observe two bands in the spectra of *o*-*t*-butyl phenol, and perhaps in other *o*-*t*-alkyl phenols as well. The two bands would correspond to geometrical isomers i.e. *cis* and *trans* structures in which the O—H group points towards the alkyl substituent and away from it, respectively. These two bands were, in fact, observed in all *o*-*t*-alkyl phenols, and while this work was being prepared for publication Goddu (6) reported finding two bands in *o*-*t*-butyl phenols and in 2-*t*-butyl-6-methyl phenols.

The possibility of detecting geometrical isomerism in non-tertiary-alkyl-*o*-substituted phenols was also examined.

EXPERIMENTAL

A Beckman I. R. 4 spectrophotometer with lithium fluoride optics was used to measure the O—H bands, the frequencies being calibrated by the standard absorption lines of water vapor. The effective slit width was about 4 cm⁻¹. Carbon tetrachloride was employed as the solvent and solution concentrations (*C*) were in the range 0.01 to 0.002 molar. Three cells of thickness (*l*), 1, 5, and 10 mm were used. Throughout this paper the term "intensity" (*A*) refers to the ratio, for the substituted phenol to phenol, of the apparent integrated absorption intensities, i.e. the band areas, and numerical values of *A* are given relative to the intensity of phenol. The band areas were obtained from the product of the half-band width ($\Delta\nu_{\frac{1}{2}}$) and the molecular extinction coefficient ($E_{\max} = (1/C) \log_{10} (I_0/I)_{\nu_{\max}}$) (7).

Many of the phenols employed were commercial products which were purified by recrystallization or distillation before use. The purity of the liquid samples was checked

¹Manuscript received November 1, 1960.

Contribution from the Division of Applied Chemistry, National Research Council, Ottawa, Canada.

Issued as N.R.C. No. 6145.

²National Research Council Summer Student, 1960. Present address: College of Science and Technology, Manchester, England.

by gas chromatography and some of the phenols were purified on a preparatory column. The phenols 2-*t*-amyl-4-methyl; 2,6-di-*t*-amyl-4-methyl (8); 2-*t*-octyl-4-methyl (m.p. 50–51.2°) (9);* 2,6-di-*t*-octyl-4-methyl (m.p. 53.2–54.2°) (9); 2-triethylmethyl-4-methyl (m.p. 43–44°); and 2,6-di-triethylmethyl-4-methyl (m.p. 44°) were obtained by alkylation of *p*-cresol with the appropriate olefin by the method of Stillson, Sawyer, and Hunt (8). The hindered (2,6-substituted) and partially hindered (2-substituted) *p*-cresols were separated by adsorption chromatography on alumina. The yield of the last two hindered phenols was only 5 or 10%. 2-*t*-Butyl-5,6-dimethyl phenol (m.p. 52–53°) was obtained by alkylation of 2,3-dimethyl phenol with the theoretical amount of isobutylene. 2,6-Di-*t*-octyl-4-formyl phenol (white needles, m.p. 157–158°) was prepared in 25% yield from the 4-methyl derivative by oxidation with bromine (10). The main product of this reaction is a yellow crystalline material m.p. 124° C, the infrared spectrum of which suggests a para-quinolide structure (11). Since it appears to contain an equimolar quantity of HBr the analysis suggests it is 4-bromo-4-methyl-2,6-di-*t*-octyl-cyclohexadiene-2,5-one-1, hydrobromide. Analysis: Found C, 56.4; H, 8.15; Br, 32.6. Calculated for $C_{23}H_{40}OBr_2$: C, 56.1; H, 8.19; Br, 32.4.

2-*t*-Octyl-4-methyl-6-*t*-butyl phenol (m.p. 33–34°) was prepared by butylating 2-*t*-octyl-4-methyl phenol.

We are indebted to the Eastman Kodak Co. for gifts of the following phenols: 2,4,6-tri-*sec*-butyl; 2,4-di-*n*-amyl; 2,4,6-tri-*n*-amyl; 2-*n*-decyl-4-methyl; and 2-*sec*-dodecyl-4-methyl.

RESULTS

It has been shown previously (5) that the frequencies of the O—H band maxima (ν_m) for 4-substituted phenols and for 4-substituted-2,6-di-*t*-butyl phenols can be correlated by a Hammett $\rho\sigma$ relation. Two parallel straight lines were obtained whose slopes (ρ) were both -13.7 cm^{-1} . The intensities of the two groups of substituted phenols relative to phenol and to 2,6-di-*t*-butyl phenol respectively can be represented on a Hammett plot by a single straight line whose slope equals 0.37 (5). The measured values of ν_m and of the intensity relative to phenol (A) for the phenols studied here have therefore been compared with the values calculated from the Hammett equation to show up any departures from the predicted values. $\Delta\nu_m$ represents the difference between the measured and calculated values of ν_m and ΔA represents the difference between the measured and calculated values of A . It has been assumed in the calculations that the σ constant for an ortho substituent is the same as that for a para substituent (12). The σ values for the *t*-octyl and triethylmethyl groups have been assumed to be -0.19 and -0.18 respectively for structural reasons. All results are averages of at least two experiments.

The frequencies of single bands and of the main band in those phenols which show a double band are probably relatively correct to within 1 cm^{-1} .† Relative intensities should be correct to within about ± 0.05 . The absolute intensity of phenol obtained by graphical integration over the absorption band using $\log_{10} (I_0/I)$ and applying Ramsey's correction for the wing absorption (7) has been redetermined to be $5.30 (1 \times 10^4 \text{ mole}^{-1} \text{ liter cm}^{-2})$. If the band is measured only to the flat wings of the curve (13) the intensity is 4.35 in the same units. These values are in good agreement with other recent estimates (13).

The results obtained with those phenols which were substituted with at least one *t*-alkyl group in an ortho position are given in Table I. The symmetrically substituted

*The *t*-octyl group is $(CH_3)_3CCH_2(CH_2)_5C-$.

†Frequencies given in reference 5 were low by 2 or 3 cm^{-1} owing to an error in the spectrometer calibration.

phenols show only a single band but the asymmetrically substituted compounds show a complex band which consists of a main band at approximately the same frequency as phenol and a smaller, incompletely resolved band at a frequency approximately that of the 2,6-di-*t*-alkyl phenol. The value of ν_m for the side band is probably correct only to 2 or 3 cm^{-1} , owing to the difficulty of separating the contribution from the main band. Typical spectra are shown in Fig. 1. Table I also includes the ratio of the intensities of the two bands (denoted by $A(\text{trans})/A(\text{cis})$).

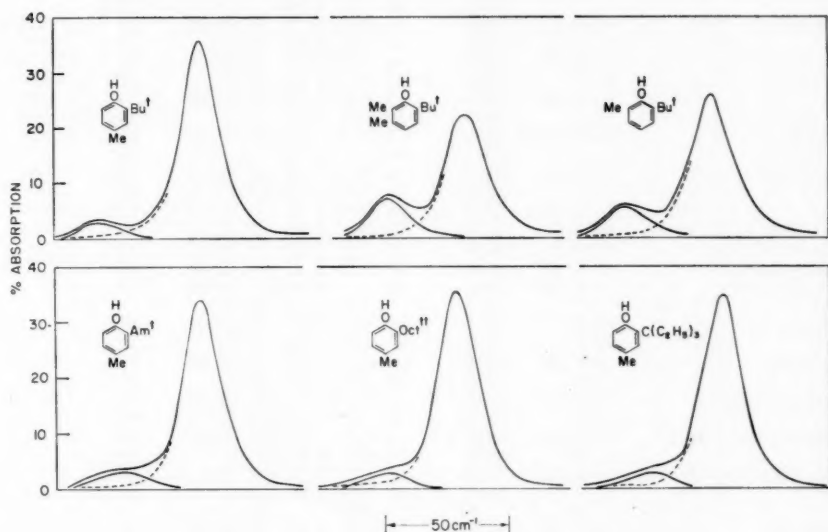


FIG. 1. The fundamental O—H vibration bands of ortho-*tert*-alkyl phenols.

The results obtained with phenols which do not contain an ortho-*t*-alkyl substituent are given in Table II.

DISCUSSION

The increases in frequency observed with 2,6-di-*t*-alkyl phenols compared with phenol are too large to be explained by the polar contributions of the *t*-alkyl groups. It has been shown previously (5) that the increase associated with 2,6-di-*t*-butyl phenols cannot be attributed to the twisting of the O—H bond out of the plane of the benzene ring. Similar evidence that the O—H bond is coplanar with the ring, or at least is nearly coplanar, has now been extended to 2,6-di-*t*-octyl phenols.

The fundamental stretching frequency of the C=O group in substituted benzaldehydes has been shown to follow a Hammett $\rho\sigma$ relation (14). If the O—H group is coplanar in 2,6-di-*t*-alkyl-4-formyl phenols the effective σ will be the sum of $\sigma_{\text{para}}(\text{OH}) = -0.36$ plus σ_{meta} for two *t*-alkyl groups = 2×-0.12 , i.e. -0.60 . The shift in C=O frequency from benzaldehyde to *p*-hydroxybenzaldehyde and to 2,6-di-*t*-alkyl-4-formyl phenol should therefore be in the ratio 0.36:0.60, i.e., 3:5. If, however, the O—H bond is twisted away from the plane by the *t*-alkyl groups its effective σ will be increased i.e. become more

TABLE I
Frequencies and intensities of *t*-alkyl phenols

Substituents	$\Sigma\sigma$	ν_m cm ⁻¹	$\Delta\nu_m$ cm ⁻¹	<i>A</i>	ΔA	$\Delta\nu_1$ cm ⁻¹	$\frac{A(\text{trans})}{A(\text{cis})}$
Phenol	0	3612 _s	—	1.00	—	18 _s	—
2-Bu ^t	-0.20	3607 _s	-8	0.92	0.07	18	11.0
		3647 _s	32	0.08 ₄		18 _s	
2-Bu ^t -4-Me	-0.37	3610	-7 _s	0.85	0.06	17 _s	12.3
		3649 _s	32	0.06 ₉		17 _s	
2-Bu ^t -4-MeO	-0.47	3614	-5	0.79	0.02	17	13.9
		3653	34	0.05 ₇		16 _s	
2-Bu ^t -5-Me	-0.27	3608	-8	0.86	0.04	17 _s	9.5
		3648	32	0.09 ₀		18	
2,4-Bu ₂ ^t	-0.39	3610	-8	0.86	0.09	18	11.5
		3648	30	0.07 _s		19	
2-Bu ^t -4-OH	-0.52 av.	3616 _s	-3	1.62/2	0.06	19	26.8/2
		3651	31 _s	0.06 ₀		19	=13.4
2,5-Bu ₂ ^t -4-OH	-0.67	3614	-8	1.50/2	0.11	16 _s	13.7
		3652	30	0.10 ₉ /2		16	
2,6-Bu ₂ ^t	-0.39	3648	30	1.02	0.17	17 _s	
2,6-Bu ₂ ^t -4-Me	-0.56	3650	29 _s	0.95	0.16	19	
2,6-Bu ₂ ^t -4-CHO	+0.73	3633	30 _s	1.43	0.16	17 _s	
4,4'-bis(2,6-Bu ₂ ^t)	-0.30*	3645	28 _s	2.40/2	0.31	17	
4,4'-CH ₃ bis(2,6-Bu ₂ ^t)	-0.47*	3649	30	2.06/2	0.20	19	
2-Bu ^t -6-Me	-0.37	3617	-1	0.67	-0.05	17 _s	4.8 _s
		3649 _s	31 _s	0.13 _s		18	
2,4-Bu ₂ ^t -6-Me	-0.56	3618	-2 _s	0.63	-0.03	17 _s	4.8 _s
		3652 _s	32	0.13		17 _s	
4,4'-bis(2-Bu ^t -6-Me)	-0.28*	3616	0	1.54/2	-0.04	18	5.0
		3650	33 _s	0.31/2		17	
4,4'-CH ₃ bis(2-Bu ^t -6-Me)	-0.45*	3618 _s	0	1.38/2	0.01	20	5.1
		3653	34 _s	0.27/2		19 _s	
4,4'-Thio bis(2-Bu ^t -6-Me)	-0.26*	3615	-1	1.62/2	0.1	19 _s	4.5
		3648	32	0.36/2		19	
2-Bu ^t -5,6-Me ₂	-0.44	3621	2	0.56	-0.09	18 _s	3.0
		3652	33	0.18 ₇		18	
2-Am ^t	-0.19	3608	-7	0.92	0.06	20	12.4
		3643	28	0.07 ₄		21	
2,4-Am ₂ ^t	-0.38	3609	-9	0.86	0.07	17	12.3
		3645	27	0.07 ₀		18 _s	
2-Am ^t -4-Me	-0.36	3609 _s	-8	0.83	0.03	17	12.4 _s
		3644 _s	27	0.06 ₇		18	
2,6-Am ₂ ^t -4-Me	-0.55	3642 _s	22 _s	1.15	0.35	19 _s	
2,4,6-Am ₃ ^t	-0.57	3642	21 _s	1.13	0.34	20	
2-Oct ^t -4-Me	-0.36	3608 _s	-9	0.86	0.06	18	13.0
		3639 _s	22	0.06 _s		19 _s	
2,6-Oct ₂ ^t -4-Me	-0.55	3635 _s	15 _s	1.18	0.38	19	
2,6-Oct ₂ ^t -4-CHO	+0.75	3617	14 _s	1.70	0.42	20 _s	
2-(C ₂ H ₅) ₃ C-4-Me	-0.35	3608	-9 _s	0.86	0.06	17 _s	13.2
		3638 _s	21	0.06 _s		18	
2,6-((C ₂ H ₅) ₃ C) ₂ -4-Me	-0.52	3635	15	1.21	0.40	18	
2-Oct ^t -4-Me-6-Bu ^t	-0.56	3647	27	1.22	0.43	25 _s	See text
		(max) 3642	22				
		(center)					

* $\Sigma\sigma$ assigned on basis of ν_m and *A*.

positive (12, 15). The observed C=O frequencies were benzaldehyde 1710 cm⁻¹, *p*-hydroxybenzaldehyde 1701 cm⁻¹, 2,6-di-*t*-butyl-4-formyl phenol 1695 cm⁻¹ (5), and 2,6-di-*t*-octyl-4-formyl phenol 1695 cm⁻¹; the frequency differences are in the ratio 9:15 in agreement with the ratio predicted for a coplanar hydroxyl group.

TABLE II
 Frequencies and intensities of non-tertiary alkyl phenols

Substituents	$\Sigma\sigma$	ν_m cm ⁻¹	$\Delta\nu_m$ cm ⁻¹	<i>A</i>	ΔA	$\Delta\nu_1$ cm ⁻¹
Phenol	0	3612. _s		1.00		18. _s
3-Me	-0.07	3613. _s	0	0.99	0.02	18 _s
4-Me	-0.17	3615	0	0.94	0	17
3,4,5-Me ₃	-0.31	3617	0	0.90	0.01	17. _s
2-Me	-0.17	3615	0	0.95	0.01	19. _s
2,4-Me ₂	-0.34	3617	0	0.92	0.05	19. _s
2-Me-4-Cl	+0.06	3612	0	1.08	0.06	20. _s
2,4,5-Me ₃	-0.41	3618	0	0.89	0.04	19. _s
2,6-Me ₂	-0.34	3622. _s	5. _s	0.76	-0.11	18. _s
2,6-Me ₂ -4-Cl	-0.11	3618	4	0.93	-0.03	21
2,4,6-Me ₃	-0.51	3624. _s	4. _s	0.72	-0.09	18
2,3-Me ₂	-0.24	3616	0	0.94	0.03	19
2,3,5-Me ₃	-0.31	3617	0	0.90	0.02	19
2,3,6-Me ₃	-0.41	3623	5	0.75	-0.10	18
2,3,4,6-Me ₄	-0.58	3625. _s	5	0.69	-0.10	18
2,3,5,6-Me ₄	-0.48	3626	7	0.68	-0.14	18. _s
2,3,4,5,6-Me ₅	-0.65	3630	8. _s	0.61	-0.15	20. _s
2-Et	-0.15	3614. _s	-0. _s	0.97	0.03	19. _s
2,6-Et ₂	-0.30	3623	6	0.84	-0.05	18
2-Pr ^a	-0.13	3614. _s	0	0.99	0.04	19. _s
2-Pr ^a -4-Me	-0.30	3616. _s	-0. _s	0.90	0.01	19
2,6-Pr ^a ₂	-0.25	3621	5	0.82	-0.09	18. _s
2-Pr ^a -6-Me	-0.30	3623	6	0.78	-0.11	19
2-Pr ⁱ	-0.15	3614. _s	-0. _s	0.91	-0.03	19. _s
2-Pr ⁱ -4-Me	-0.32	3616. _s	-0. _s	0.88	0	19
2,6-Pr ⁱ ₂	-0.30	3623	6	0.72	-0.17	19
2-Bu ^a	-0.12	3614	0	0.89	-0.06	18. _s
2,4-Bu ^a ₂	-0.25	3616	0	0.87	-0.04	18. _s
2,4,6-Bu ^a ₃	-0.37	3622	5	0.71	-0.15	18
2,4-Am ^a ₂	-0.32	3616. _s	-0. _s	0.88	0	18
2,4,6-Am ^a ₃	-0.48	3622	3	0.67	-0.15	18
2-Am ⁱ	-0.23	3615. _s	-0. _s	0.86	-0.06	18
2,4-Am ^a ₂	-0.25	3615. _s	-0. _s	0.89	-0.02	19. _s
2- <i>n</i> -decyl-4-Me	-0.33	3616	-1	0.88	0	19
2- <i>sec</i> -dodecyl-4-Me	-0.29	3615. _s	-1. _s	0.79	-0.10	18

Although the OH group is coplanar in the presence of strong electron-attracting groups such as CHO this does not necessarily imply that it is also coplanar when the 4-substituent is electron releasing (e.g. CH₃). However, the differences in frequency between the hydroxyl groups of the 4-methyl and 4-formyl derivatives of phenol, 2,6-di-*t*-butyl phenol, and 2,6-di-*t*-octyl phenol are 16.5 (5), 17, and 18.5 cm⁻¹ respectively compared with a calculated difference of 17.5 cm⁻¹.^{*} That is, within the limits of experimental error the plots of ν_m against σ for these three classes of phenols are parallel (5) and therefore the OH group has the same orientation, independent of the 4-substituent, in all cases.

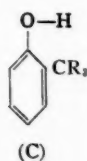
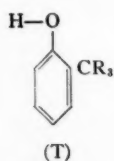
The intensities of the hindered phenols give further confirmation that they are true phenols and not "pseudo" phenols containing a non-planar hydroxyl group. The intensity of phenol is two or three times as great as the intensities of alcohols (13, 16), and, therefore, since the hindered phenols have even higher intensities than phenol, they must be true phenols. Moreover, the ratio of the intensities of the 4-formyl to 4-methyl derivatives of phenol; 2,6-di-*t*-butyl phenol; and 2,6-di-*t*-octyl phenol are 1.66 (5), 1.51, and 1.44

^{*} An interesting difference between the OH bands of 2,6-di-*t*-butyl and 2,6-di-*t*-octyl phenols is that their half-band widths appear to change in opposite directions with a change in σ (Table I) (5).

respectively, compared with a calculated ratio of 1.48, again suggesting that the structure of the phenols is independent of the 4-substituent.

Although the results quoted above strongly suggest that the OH group is coplanar with the ring, the accuracy of the experiments does not preclude the possibility that it is slightly twisted away from the plane. Both the resonance energy and the charge density at the carbon atom para to the resonance-inhibited group vary approximately as $\cos^2\theta$ (15, 17, 18) where θ is the angle of twist. That is, the resonance energy and charge density fall off rather slowly for small values of θ and therefore we could not detect small angles of twist in our experiments.

The conclusion that the OH group is in the plane, or at least close to it, makes the interpretation of the results obtained with single ortho-*t*-alkyl substituents comparatively straightforward. The results given in Table I and Fig. 1 clearly demonstrate the presence of two forms of *o*-*t*-alkyl phenols, as was predicted. Since the frequencies of the two bands are fairly close the one to the frequency of phenol, and the other to that of the corresponding 2,6-di-*t*-alkyl phenol, it is logical to suppose that the two forms represent geometrical isomers. The more intense band at the lower frequency will correspond to the trans isomer (T) and the less intense band at the higher frequency to the cis isomer (C).



Geometrical isomerism has been reported previously (19, 20) for *o*-substituted phenols in which the substituent can form an intramolecular hydrogen bond with the phenolic hydrogen (e.g. *o*-chlorophenol). This isomerism, which was deduced from infrared spectra, arises from the attraction of the phenolic hydrogen towards the *o*-substituent since the main band occurs at a much lower frequency than in phenol and the minor band occurs near the phenol frequency. In other words, the cis form is the most stable, whereas in *o*-*t*-alkyl phenols it is the trans form that is more stable. This suggests the presence of a steric repulsion between the phenolic hydrogen and the *t*-alkyl group, as might be expected.

Substitution of a methyl group in the 6-position increases the proportion of the isomer cis to the *t*-alkyl group. Substitution of a second methyl at the 5-position increases the proportion of the cis isomer even further, presumably because of its "buttressing" action on the methyl in the 6-position.

It should be pointed out that the occurrence of two bands does not necessarily imply that they correspond to geometrical isomers, since the low intensity band could conceivably be due to Fermi resonance (21) as has been postulated for hydroxy compounds containing the $-\text{CH}_2\text{OH}$ group (13). This possibility can, however, be discarded since the intensity of the subsidiary (cis) band decreases slightly as the two bands get closer together on going from *o*-*t*-butyl to *o*-*t*-amyl phenol, which is contrary to what would be expected from Fermi resonance. The results obtained with 2-*t*-butyl-6-methyl phenols and with 2-*t*-butyl-5,6-dimethyl phenol would also be difficult to explain on this basis. Furthermore, the spectra of structurally similar phenols e.g. *p*-*t*-butyl phenol, 2,6-diethyl phenol, 2,6-di-isopropyl phenol, etc. do not show any subsidiary bands.

The difference in free energy (ΔG) between the two isomers can be calculated from the

ratio of the intensities of the trans to cis bands in an *o-t*-alkyl phenol. This energy difference should be independent of the presence or absence of a 4-substituent, since any change in resonance energy produced by a 4-substituent will presumably alter the depths of the two coplanar potential minima by the same amount. However, the measured ratio of the intensities should be corrected for the fact that when the O—H group is cis to the *t*-alkyl group, as it must be in 2,6-di-*t*-alkyl phenols, the intensity is higher than phenol, whereas when it is trans to the substituent the intensity probably approximately follows the Hammett equation (5) and will be lower than phenol. For example, the average calculated cis intensity for 2-*t*-butyl phenol (1.09) is obtained from the intensities of 2,6-di-*t*-butyl phenol (1.02), and 2,6-di-*t*-butyl-4-methyl phenol (0.95) by applying corrections for the polar effects of an *o-t*-butyl group ($-(-0.20 \times 0.37)$) and for the effect of an *o-t*-butyl group and a *p*-methyl group ($-(-0.20 - 0.17) \times 0.37$). The calculated trans intensity is based on phenol (1.00) less the effect of an *o-t*-butyl group i.e. 0.93. For 2-*t*-butyl-6-methyl phenol the calculated intensity cis to the *t*-butyl group is based on the calculated cis intensity of *o-t*-butyl phenol corrected for the polar effect of the 6-methyl group, and the calculated trans intensity is based in the same way on the measured intensities of 2,6-dimethyl and 2,4,6-trimethyl phenol. The measured trans to cis intensity ratio must be multiplied by the calculated cis to trans intensity ratio in order to obtain the true relative amounts of the two isomers. Table III gives the steps in the calculations

TABLE III
Cis-trans isomerism of *o*-alkyl phenols

<i>o</i> -Substituents	Av. calc. cis intensity	Av. calc. trans intensity	Calc. $A(\text{cis})$ $A(\text{trans})$	Measured $A(\text{trans})$ $A(\text{cis})$	$\frac{[\text{trans}]}{[\text{cis}]}$	ΔG kcal/ mole	% trans isomer	% cis isomer
2-Bu ^t	1.09	0.93	1.17	12.3	14.39	1.5 ₇	93.5	6.5
2-Am ^t	1.27 ₈	0.93	1.37	12.4 ₈	17.06	1.6 ₇	94.5	5.5
2-Oct ^{tt}	1.31	0.93	1.41	13.0	18.30	1.7 ₁	94.8	5.2
2-(C ₂ H ₅) ₂ C	1.34	0.93	1.44	13.2	19.01	1.7 ₄	95.0	5.0
2-Bu ^t -6-Me	1.03	0.83	1.24	4.8 ₅	6.01	1.0 ₆	85.7	14.3
2-Bu ^t -5,6-Me ₂	1.00	0.76 ₃	1.31	3.00	3.92	0.8 ₉	79.7	20.3
2-CH ₃						0.5 ₁	70.5	29.5
2,3-(CH ₃) ₂						0.7 ₇	78.6	21.4

of the percentage of cis and trans isomers and the difference in free energy (ΔG) in kcal/mole between the two isomers in dilute solution in carbon tetrachloride at 24° C. ΔG is obtained in calories from the relation

$$\log_{10} \frac{[\text{trans}]}{[\text{cis}]} = \frac{\Delta G}{2.3RT}$$

The measured trans/cis ratio for 2-*t*-butyl and 2-*t*-amyl have been taken from the values found for their 4-methyl derivatives; and for 2-*t*-butyl-6-methyl the ratio obtained with this phenol has been used. This was done since these compounds were known to be very pure and since the measurements were repeated at least six times, including once on a high-resolution Perkin-Elmer prism-grating spectrometer, model 112 G. Average values of the ratio for the other phenols of these types are in quite good agreement with the values chosen. The measured trans/cis ratio for 2-*t*-butyl and 2-*t*-butyl-6-methyl phenols are in good agreement with the values of Goddu (6), although our frequencies are from 3 to 8 cm⁻¹ higher than the values he reported, the differences being most pronounced for 2,6-di-*t*-butyl phenols and for the cis isomers of various *o-t*-butyl phenols.

The percentages of the *cis* isomers given in Table III show, as would be expected, that the *cis* isomer decreases as the size of the *t*-alkyl substituent is increased, but is increased by substitution of a methyl at the 6-position or by two methyls at the 5- and 6-positions.

The values of ΔG obtained for 2-*t*-butyl-6-methyl phenol and for 2-*t*-butyl-5,6-dimethyl phenol can be combined with the value for 2-*t*-butyl phenol to give the differences in free energy between the *cis* and *trans* isomers of *o*-cresol and 2,3-dimethyl phenol. These values are also included in Table III. It was also possible to obtain a rough estimate of ΔG for the two forms of 2-*t*-octyl-4-methyl-6-*t*-butyl phenol. The OH band of this compound is asymmetric and from the degree of asymmetry observed on the prism-grating instrument ΔG was estimated to be 0.17 kcal/mole. The intensity of the band was also compared with the intensity of the combined band of mixtures of different proportions of 2,6-di-*t*-octyl-4-methyl phenol and 2,6-di-*t*-butyl-4-methyl phenol. A value of ΔG of 0.30 kcal/mole was obtained in this way. These values are in reasonably good agreement with the value of 0.14 kcal/mole obtained by difference from 2-*t*-octyl and 2-*t*-butyl phenol.

The ratio of the intensities of the *cis* to *trans* isomers of *o*-chlorophenol is about 50:1 in carbon tetrachloride at room temperature (22, 23), corresponding to $\Delta G \sim 2.3$ kcal/mole. We have found that for 2-chloro-6-methyl phenol this ratio increases to $\geq 100:1$ ($\Delta G \geq 2.7$ kcal/mole). The two values of ΔG can be combined to obtain ΔG for *o*-cresol ≥ 0.4 kcal/mole, in reasonable agreement with the value given in Table III.

The results given in Table II show that a single non-tertiary alkyl group substituted in the ortho position gives a measured increase in frequency and decrease in intensity in good agreement with the values calculated from the Hammett equation (5). However, the results given in Table III show that these phenols must exist as *cis-trans* isomers in unequal amounts. The only direct evidence for this is that the half-band widths ($\Delta\nu_{1/2}$) are definitely greater for these *o*-alkyl phenols than for phenol or for the corresponding 2,6-dialkyl phenols. This suggests the presence of two unresolved bands, particularly since the half-band widths would be expected to decrease below the value for phenol with alkyl substitution (5) (see also results for 3-methyl, 4-methyl, and 3,4,5-trimethyl phenol in Table II). Failure to resolve these bands is not surprising since the band maxima would appear to be less than 10 cm^{-1} apart in general and even the prism-grating spectrometer would not resolve the two bands of 2-*t*-octyl-4-methyl-6-*t*-butyl phenol where a separation of about 15 cm^{-1} is expected.

The positive values of $\Delta\nu_m$ observed with the 2,6-dialkyl phenols in Table II (and which are also encountered with 2,6-di-*t*-alkyl phenols) suggest a steric interaction between these non-tertiary alkyl groups and the hydroxyl group. On the other hand, the values of ΔA are negative for these phenols, whereas positive values were obtained with the 2,6-di-*t*-alkyl phenols. This shows that the intensities cannot be simply related to the extent of steric interference by the alkyl groups. However, for the phenols listed in Table II the values of $\Delta\nu_m$ and ΔA both tend to increase with the expected increase in steric interaction (see 2,6-dimethyl; 2,3,6-trimethyl; 2,3,4,6-tetramethyl; 2,3,5,6-tetramethyl; and penta-methyl phenol). This result cannot be due to any saturation of the electronic effects produced by the increasing number of substituents (5) since this would cause both $\Delta\nu_m$ and ΔA to decrease. The magnitude of these differences may, however, have been reduced because of saturation effects; somewhat larger values would smooth out the curves in Fig. 2 (see below).

In Fig. 2 values of $\Delta\nu_m$ and ΔA for 2,6-dialkyl phenols have been plotted against the values of ΔG obtained from the *o*-alkyl phenols. There is no direct justification for this

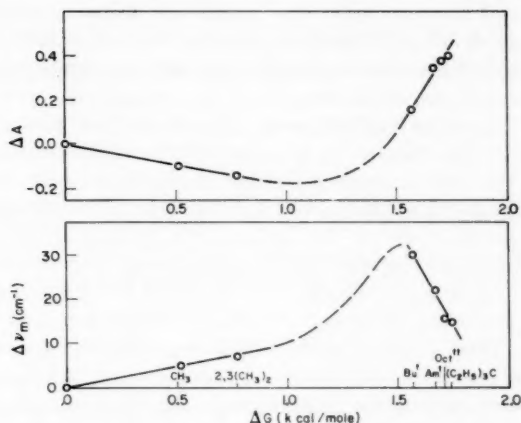


FIG. 2. Differences between measured and calculated frequencies, and intensities, of 2,6-dialkyl phenols plotted against ΔG .

procedure, but it is obvious that the values of ν_m and A for these phenols must be related in some way to the steric interaction of the alkyl groups with the hydroxyl group, and that this is measured approximately by ΔG . Both plots apparently show a discontinuity between the methyl phenols and the *t*-alkyl phenols, the curves going through a maximum or minimum. This shows that ortho-alkyl groups have two different effects on the hydroxyl, the magnitude of the two effects varying with the size of the alkyl groups.

A possible explanation of these results is that mild steric interaction between the alkyl and hydroxyl groups narrows the potential-energy well of the stretching mode of the O—H bond; this will increase the vibration frequency and decrease its amplitude and hence decrease the intensity. Stronger steric repulsions will begin to separate the proton from the electrons of the O—H bond since the repulsion is exerted primarily on the electrons of the phenolic hydrogen and only through them on the proton itself. This will tend to polarize the bond (i.e. $\overset{+}{\text{O}}-\overset{-}{\text{H}}$) and increase the intensity, and at the same time will weaken the internal force constant and so decrease the frequency. Incidentally the values of ΔG do not increase with the size of the *t*-alkyl substituent as rapidly as might be expected, which may be because the energy is minimized by an increase in the $\text{C}-\overset{\wedge}{\text{O}}-\text{H}$ angle. This forcing of the phenolic hydrogen away from its equilibrium position, as the substituents become larger than *t*-butyl, would also tend to decrease the O—H bond strength and hence ν_m .

The frequencies of the trans isomers of *o-t*-alkyl phenols, which are appreciably below their calculated values, are obviously much more readily influenced by the alkyl substituent than are the intensities (cf. small values of ΔA for these phenols in Table I); i.e. the intensities, but not the frequencies, follow the usual Hammett $\rho\sigma$ relations. The low frequencies observed must mean that an *o-t*-alkyl substituent has an effect on the hydroxyl group even when the latter is pointing away from it. This effect might be due to a more rigid geometry in the trans isomer compared to phenol (5). An alternative explanation that appears to be more consistent with the results is that *t*-alkyl groups exert van der Waals attraction on the lone pairs of electrons on the oxygen. This withdrawal of electrons from the oxygen would be transmitted to the O—H bond, the

frequency of which would be decreased. This suggestion helps to explain why $\Delta\nu_m$ is higher for the cis isomer of *o*-*t*-alkyl phenols than for the corresponding 2,6-di-*t*-alkyl phenol. In the cis isomer the only effect on the hydroxyl is one of steric repulsion, whereas in di-*t*-alkyl phenols there is also the attraction of the oxygen's electrons by the second *t*-alkyl group, which will decrease the frequency. The same effect may also be operating in ortho halophenols since the frequency, in carbon tetrachloride solution, of the trans isomer decreases by 5 cm⁻¹ on increasing the size of the substituent from bromine to iodine, whereas the corresponding decrease for these two para-substituted phenols is only 1 cm⁻¹ (22, 23).

An *o*-methyl or 2,3-dimethyl group has no effect, other than the calculated polar effect, on the frequency of the trans isomer (Table II). Therefore in 2-*t*-butyl-6-methyl and in 2-*t*-butyl-5,6-dimethyl phenol $\Delta\nu_m$ for the cis (to *t*-butyl) isomer has about the same value as for 2-*t*-butyl phenols (Table I). On the other hand, $\Delta\nu_m$ values for the trans (to *t*-butyl) isomers of these phenols are below $\Delta\nu_m$ values for 2,6-dimethyl and 2,3,5,6-tetramethyl phenol because of the influence of the *t*-butyl group. Non-tertiary alkyl groups in the ortho position apparently, therefore, only affect the hydroxyl group when it points towards them.

The barrier to rotation of the hydroxyl group in 2,4,6-tri-*t*-butyl phenol has been estimated from dielectric measurements to be 2.8 kcal/mole (24). The rotational barrier in this compound will be lower than in phenol owing to steric repulsion by the *t*-butyl groups (~1.6 kcal/mole) and also, perhaps, to a decrease in the resonance interaction between the hydroxyl and the ring because of the polar effects of the alkyl substituents. The barrier in phenol is, therefore, ≥ 4.4 kcal/mole.

ACKNOWLEDGMENTS

The authors are indebted to Dr. R. N. Jones for the spectra on the prism-grating spectrometer, and to Dr. D. Davidson and Dr. I. E. Puddington for several helpful discussions.

REFERENCES

1. P. J. KRUEGER and H. W. THOMPSON. Proc. Roy. Soc. (London), A, **250**, 22 (1959).
2. W. C. SEARS and L. J. KITCHEN. J. Am. Chem. Soc. **71**, 4110 (1949).
3. L. J. BELLAMY and R. L. WILLIAMS. Proc. Roy. Soc. (London), A, **254**, 119 (1960).
4. N. A. PUTTNAM. J. Chem. Soc. 486 (1960).
5. K. U. INGOLD. Can. J. Chem. **38**, 1092 (1960).
6. R. F. GODDU. J. Am. Chem. Soc. **82**, 4533 (1960).
7. D. A. RAMSAY. J. Am. Chem. Soc. **74**, 72 (1952).
8. G. H. STILLSON, D. W. SAWYER, and C. K. HUNT. J. Am. Chem. Soc. **67**, 303 (1945).
9. L. J. KITCHEN. J. Am. Chem. Soc. **70**, 1290 (1948).
10. L. A. COHEN. J. Org. Chem. **22**, 1333 (1957).
11. E. MÜLLER and K. LEY. Chem. Ber. **88**, 601 (1955).
12. R. W. TAFT. Steric effects in organic chemistry. John Wiley & Sons, Inc., New York, 1956. Chap. 13.
13. T. D. FLYNN, R. L. WERNER, and B. M. GRAHAM. Australian J. Chem. **12**, 575 (1959).
14. H. W. THOMPSON, R. W. NEEDHAM, and D. JAMESON. Spectrochim. Acta, **9**, 208 (1957).
15. R. W. TAFT and H. D. EVANS. J. Chem. Phys. **27**, 1427 (1957).
16. R. MOCCIA and H. W. THOMPSON. Proc. Roy. Soc. (London), A, **243**, 154 (1957).
17. C. A. COULSON. Conference on quantum mechanical methods in valence theory. U.S. Govt. Printing Office, 1951. p. 47.
18. E. G. McRAE and L. GOODMAN. J. Mol. Spectroscopy, **2**, 464 (1958).
19. O. R. WULF, U. LIDDEL, and S. B. HENDRICKS. J. Am. Chem. Soc. **58**, 2287 (1936).
20. L. PAULING. J. Am. Chem. Soc. **58**, 94 (1936).
21. E. FERMI. Z. Physik, **71**, 250 (1931).
22. G. ROSSMY, W. LÜTTKE, and R. MECKE. J. Chem. Phys. **21**, 1606 (1953).
23. A. W. BAKER. J. Am. Chem. Soc. **80**, 3598 (1958).
24. M. DAVIES and R. J. MEAKINS. J. Chem. Phys. **26**, 1584 (1957).

THE EFFECT OF SOLVENT AND TEMPERATURE ON THE CIS-TRANS ISOMERISM OF ORTHO-*tert*-ALKYL PHENOLS¹

K. U. INGOLD AND D. R. TAYLOR²

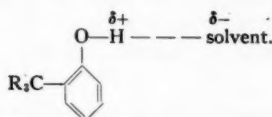
ABSTRACT

The effects of different solvents and of a change of temperature on the infrared band due to the fundamental hydroxyl stretching vibration in several 2,6-di-*t*-alkyl phenols and in the corresponding ortho-*t*-alkyl phenols have been examined. The conclusion that the two bands observed in ortho-*t*-alkyl phenols represent cis and trans isomers has been confirmed. The differences in enthalpy and entropy between the two isomers have been measured for six different phenols.

INTRODUCTION

The conclusions reached in the previous paper (1) as to the nature of the two hydroxyl stretching bands observed in *o*-*t*-alkyl phenols has been confirmed by an examination of the effects of different solvents and of changes in temperature on the ratios of the intensities of the two bands.

It was predicted, on the basis that the two bands represent cis and trans isomers, that an increase in the polarity or polarizability of the solvent would decrease the percentage of the cis isomer owing to the increased stability of structures of the type



It was also predicted that the trans/cis intensity ratio should decrease with increasing temperature. Both the predictions have been experimentally verified.

EXPERIMENTAL

The spectrometer and slit conditions have been described previously (1). The high-temperature cell consisted simply of a 5-mm cavity cell enclosed by an electrically heated glass tube, the ends of which were sealed by NaCl windows. Hexachloro-1,3-butadiene (HXB) was used as the solvent because of its high boiling point and because frequencies and intensities in this solvent are closely similar to their values in carbon tetrachloride. The concentration of the solute phenol was 0.005 *M*.

RESULTS

Bellamy and Williams (2) have shown that the effect of various solvents on the frequency of the O—H band (ν_m) of 2,6-di-*t*-butyl-4-methyl phenol is quite different from the solvent effect on phenol and on 2,6-dialkyl phenols in which the substituents are not tertiary alkyl groups. Their results have been confirmed with a limited number of solvents for phenol and 2,6-di-*t*-butyl-4-methyl phenol and the measurements have been extended to other 2,6-di-*t*-alkyl-4-methyl phenols. Pentamethyl phenol was also

¹Manuscript received November 1, 1960.

Contribution from the Division of Applied Chemistry, National Research Council, Ottawa, Canada.

Issued as N.R.C. No. 6148.

²National Research Council Summer Student, 1960. Present address: College of Science and Technology, Manchester, England.

examined in order to discover whether this phenol behaved like the 2,6-di-tertiary or non-tertiary alkyl phenols. The frequencies (ν_m cm⁻¹) are given in Table I, which also includes intensities relative to phenol in carbon tetrachloride (A) and half-band widths ($\Delta\nu_{1/2}$ cm⁻¹). Intensities were obtained from the product of $\Delta\nu_{1/2}$ and the molecular extinction coefficient (I), they are probably not very accurate as they are based only on a single measurement in each case. Results are also included in Table I for the effect of solvent on the cis and trans bands of 2-*t*-butyl-4-methyl phenol.

TABLE I
Effect of solvent on O—H band of alkyl-substituted phenols

Substituent		Hexane	CCl ₄	HXB	CS ₂	1,2-Dichloro-ethane	Nitro-methane
None (phenol)	ν_m	3622.5	3612.5	3609	3593.5	3565	3511
	A	0.90	1.00	1.02	0.97	1.47	4.27
	$\Delta\nu_{1/2}$	15	18.5	23	29	58	133
(Me) ₃	ν_m	3637.5	3630	—	3618.5	3596.5	3582
	A	0.55	0.61	—	0.60	0.73	~2.12
	$\Delta\nu_{1/2}$	16.5	20.5	—	26	42	54
2,6-Bu ₂ ^t -4-Me	ν_m	3656	3650	3648.5	3645	3637.5	3629.5
	A	0.91	0.95	0.93	0.96	1.13	1.86
	$\Delta\nu_{1/2}$	16	19	22	19.5	28	42
2,6-Am ₂ ^t -4-Me	ν_m	3647	3642.5	3643	3636	3631	3624.5
	A	0.93	1.15	1.05	1.00	1.04	1.50
	$\Delta\nu_{1/2}$	17	19.5	19.5	18.5	30	40
2,6-Oct ₂ ^t -4-Me	ν_m	3639	3635.5	3637.5	3633	3627	3622.5
	A	1.08	1.18	1.12	1.01	1.20	1.60
	$\Delta\nu_{1/2}$	18.5	19	21	19.5	31	39
2,6-((C ₂ H ₅) ₃ C) ₂ -4-Me	ν_m	3638.5	3635	3636	3631.5	3625.5	3621
	A	1.18	1.21	1.14	0.96	1.35	1.76
	$\Delta\nu_{1/2}$	17.5	18	20.5	18.5	32.5	37
2-Bu ^t -4-Me							
Trans	ν_m	3619.5	3610	3607.5	3591	3567	3506
	A	0.58	0.85	0.89	0.90	1.44	3.58
	$\Delta\nu_{1/2}$	16	17.5	19.5	27.5	50	118
Cis	ν_m	3658.5	3649.5	3649	3643.5	~3634	?
	A	0.06 ₀	0.06 ₉	0.07 ₂	0.06 ₂	0.05 ₉	<0.04
	$\Delta\nu_{1/2}$	17	17.5	20.5	20	~30	40*
$A(\text{trans})$ $A(\text{cis})$		9.6	12.3	12.3	14.5	25	>85
$\frac{[\text{trans}]}{[\text{cis}]}$		11.5	14.4	14.3	17	23	>45

*See text.

For the work at different temperatures it was necessary to examine not only the *o*-*t*-alkyl phenols, but also the corresponding dialkyl phenols and an unhindered phenol in order to find out whether the correction for the intrinsic differences in intensity between cis and trans isomers varied with temperature. 4-*t*-Butyl phenol was used in place of phenol because of its lower volatility—the presence of a para-substituent would not be expected to affect the results.

The intensities of symmetrically substituted phenols in HXB relative to phenol in HXB at room temperature (i.e. A_{HXB}) decrease linearly with increasing temperature within the accuracy of the measurements (Fig. 1). The points plotted in this figure have not been corrected for expansion of the solvent nor for changes in the path length. Over

the temperature range studied the former effect will cause values of A_{HXB} to decrease by about 10%. The percentage absorptions ($\log(I_0/I)_{\text{max}}$) of the bands decreased (3, 4) and their half-band widths increased as the temperature was raised. In contrast to a previous report (3) ν_m was found to increase regularly with temperature. The values of ν_m and $\Delta\nu_3$ at room temperature are given in Table I except for 4-*t*-butyl phenol ($\nu_m = 3610.5 \text{ cm}^{-1}$, $A = 0.94$, $\Delta\nu_3 = 22.5 \text{ cm}^{-1}$) and 2,3,5,6-tetramethyl phenol ($\nu_m = 3626 \text{ cm}^{-1}$, $A = 0.64$, $\Delta\nu_3 = 21.5 \text{ cm}^{-1}$). The increases in ν_m and $\Delta\nu_3$ in cm^{-1} on raising the temperature from 24° to 150° C are respectively: 4-*t*-butyl 7.5 and 3; 2,3,5,6-tetramethyl 4 and 2; 2,6-di-*t*-butyl-4-methyl 2.5 and 5.5; 2,6-di-*t*-amyl-4-methyl 2 and 4; 2,6-di-*t*-octyl-4-methyl 1.5 and 3; 2,6-di-triethylmethyl-4-methyl phenol 1.5 and 3.5.

Table II shows the effect of temperature on *o*-*t*-alkyl phenols. The temperatures are only approximately ($\pm 5^\circ \text{C}$) those at which the measurements were made, in order to simplify the Table. ν_m values for *cis* isomers are less accurate than for the *trans* isomers (1). The increases in ν_m and $\Delta\nu_3$ appear to follow the same relations as were observed with the symmetrically substituted phenols, i.e. ν_m and $\Delta\nu_3$ increase by about 6 cm^{-1} and 3 cm^{-1} respectively in the range 24° to 150° C for the *trans* band and by about 2.5 cm^{-1} and 3 cm^{-1} respectively for the *cis* band. However, the plots of A_{HXB} against temperature for *trans* isomers have much steeper slopes than are observed with the symmetrically substituted phenols, presumably because of the relative increase in the amount of *cis* isomers as the temperature rises. These plots appear, in general, to be slightly convex towards the temperature axis. As the temperature is raised it becomes increasingly difficult to separate the *cis* band since not only are both bands smeared out owing to the increase in $\Delta\nu_3$, but also the two band maxima move slightly closer together.

The parallel straight lines shown in Fig. 1 for symmetrically substituted phenols indicate that the correction factors for the intrinsic differences in intensity between *cis* and *trans* isomers are independent of temperature. The intensities of substituted phenols relative to phenol when plotted against Hammett σ constants are independent of solvent for a small range of solvent types (5). This means that ρ is independent of solvent and therefore the correction factors in HXB can be readily obtained (1). These factors are

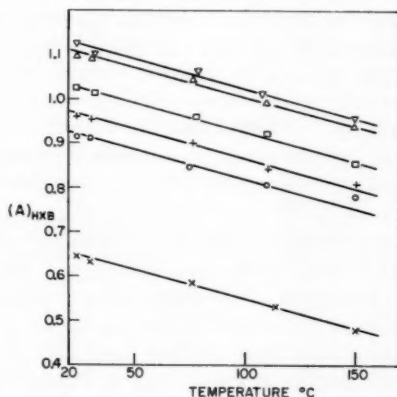


FIG. 1. Effect of temperature on the relative intensities of symmetrically substituted phenols. Key: 2,3,5,6-tetramethyl X; 2,6-di-*t*-butyl-4-methyl O; 4-*t*-butyl +; 2,6-di-*t*-amyl-4-methyl □; 2,6-di-*t*-octyl-4-methyl Δ; 2,6-di-triethylmethyl-4-methyl phenol ∇.

TABLE II
Effect of temperature on *o*-*t*-alkyl phenols in hexachlorobutadiene

Phenol		Approximate temperature (°C)							
		24°		75°		110°		150°	
		Trans	Cis	Trans	Cis	Trans	Cis	Trans	Cis
2-Bu ^t -4-Me	ν_m	3607.5	3649	3611	3649.5	3612.5	3651	3615	3652
	A	0.88	0.07 ₂	0.79	0.09 ₀	0.72	0.10 ₂	0.67	0.113
	$\Delta\nu_1$	19.5	20.5	20.5	23	21.5	24	23	24
2-Bu ^t -6-Me	ν_m	3615.5	3649	3618	3650	3619	3651	3620.5	3652
	A	0.65	0.12 ₈	0.58	0.14 ₉	0.53	0.16 ₁	0.48	0.15 ₉
	$\Delta\nu_1$	22	21	23	22	24	23	25	24
2-Bu ^t -5,6-Me ₂	ν_m	3622	3652	3623.5	3652	3625	3653	3626	3654
	A	0.54	0.17 ₇	0.48	0.19 ₂	0.42	0.18 ₇	0.37	0.18 ₃
	$\Delta\nu_1$	21.5	21	22	22	22.5	23	23	24
2-Am ^t -4-Me	ν_m	3607	3645.5	3609	3646	3611	3646.5	3613	3647
	A	0.88	0.07 ₀	0.80	0.09 ₄	0.69	0.09 ₉	0.63	0.10 ₅
	$\Delta\nu_1$	19	18.5	20.5	22.5	22	24.5	23	25
2-Oct ^u -4-Me	ν_m	3607	3637	3609	3638	3610	3638	3612	3638
	A	0.92	0.06 ₅	0.82	0.09 ₀	0.77	0.10 ₄	0.70	0.11 ₅
	$\Delta\nu_1$	18.5	20.5	19.5	22	21.5	23	22.5	25
2-(C ₂ H ₅) ₃ C-4-Me	ν_m	3606	3637	3607.5	3638	3609	3638.5	3610.5	3639
	A	0.89	0.06 ₆	0.78	0.09 ₁	0.71	0.10 ₁	0.64	0.10 ₅
	$\Delta\nu_1$	19.5	20.5	20.5	22	21.5	23	22.5	24.5

given in Table III; they are only slightly different from the values calculated in carbon tetrachloride (1). The measured ratios $A(\text{trans})/A(\text{cis})$, which will, of course, be independent of solvent expansion etc., were multiplied by these factors to give the true concentration ratios of the two isomers at each temperature. The logarithms of the true concentration ratios have been plotted against $1/T$ (°K) in Fig. 2, since the relation

$$\log_{10} \frac{[\text{trans}]}{[\text{cis}]} = \frac{\Delta G}{2.3 RT} = \frac{\Delta H}{2.3 RT} - \frac{\Delta S}{2.3 R}$$

should be obeyed. That is, the slopes of the lines in Fig. 2 give ΔH , the enthalpy difference between the cis and trans isomers, and the intercepts give ΔS , the entropy difference. These results, as well as values of ΔG obtained at room temperatures in carbon tetrachloride (1) are given in Table III.

TABLE III
Enthalpy difference between cis and trans isomers of *o*-*t*-alkyl phenols

Phenol	Correction factor in HXB	ΔS e.u. (HXB)	ΔH kcal/mole (HXB)	ΔG kcal/mole (CCl ₄) (1)
2-Bu ^t -4-Me	1.16	-0.2	1.5 ₅	1.5 ₇
2-Am ^t -4-Me	1.24	-0.2	1.5 ₃	1.6 ₇
2-Oct ^u -4-Me	1.32	-0.2	1.6 ₅	1.7 ₁
2-(C ₂ H ₅) ₃ C-4-Me	1.35	-0.2	1.6 ₅	1.7 ₄
2-Bu ^t -6-Me	1.23	-0.1	1.0 ₅	1.0 ₆
2-Bu ^t -5,6-Me	1.28	0	0.8 ₀	0.8 ₀

Owing to the increased difficulty of separating the two bands with increasing temperature the accuracy of the results was such that there is no real difference between the

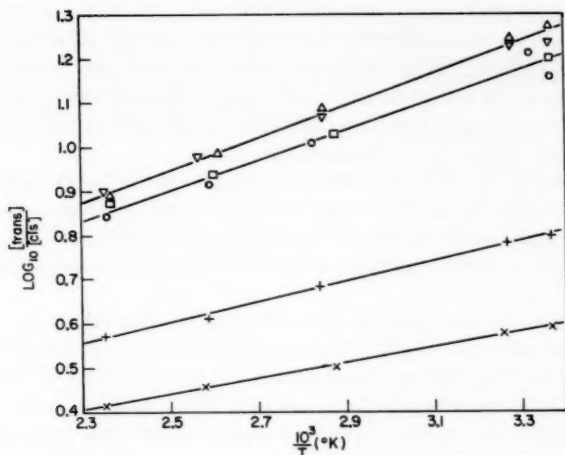


FIG. 2. Effect of temperature on $\log_{10}[\text{trans}]/[\text{cis}]$ for ortho-alkyl phenols. Key: 2-*t*-butyl-5,6-dimethyl \times ; 2-*t*-butyl-6-methyl $+$; 2-*t*-butyl-4-methyl \circ ; 2-*t*-amyl-4-methyl \square ; 2-*t*-octyl-4-methyl Δ ; 2-triethylmethyl-4-methyl phenol ∇ .

plots of 2-*t*-butyl-4-methyl and 2-*t*-amyl-4-methyl phenol and between 2-*t*-octyl-4-methyl and 2-triethylmethyl-4-methyl phenol, a single line has therefore been drawn through each pair.

Although a small positive intercept is obtained in each case, it may well be due to an overestimation of the correction factors. Moreover, the intercepts are sufficiently small that the data for each phenol could be fitted almost equally well by straight lines passing through the origin. That is, ΔS is certainly small in each case and is very probably zero.

DISCUSSION

Bellamy and Williams (2) have shown that the changes in ν_m for phenol and 2,6-dialkyl phenols on passing from one solvent to another are due to local association effects, which occur even in non-polar solvents. By comparing ν_m for 2,6-dimethyl, -diethyl, and -diisopropyl phenol in different solvents with ν_m for phenol, these workers concluded that there is no significant steric hindrance to solvent effects in these phenols, the small effects observed being ascribed to the polar effects of the alkyl substituents. The results given in the previous paper (1) suggest that two *o*-methyl groups backed up by *m*-methyl groups may exert a greater effect on the hydroxyl group than is exerted by, for example, two *o*-isopropyl groups. For this reason it was considered of interest to study the effect of solvents on ν_m for pentamethyl phenol to see whether any steric hindrance to solvent effects could be observed. The results obtained (Table I) are not significantly different from the results reported for dialkyl phenols (2), the small differences that are observed are very likely due to the increased polar effect of five methyl substituents. Therefore, on the basis of Bellamy and Williams' work it could be concluded that steric hindrance to solvent effects does not occur in pentamethyl phenol. However, the changes in $\Delta\nu_3$ (which were not reported by Bellamy and Williams) of pentamethyl phenol compared to phenol do suggest some small steric effects are present, and therefore small effects may also have been operating in the dialkyl phenols they studied.

For 2,6-di-*t*-butyl-4-methyl phenol, however, Bellamy and Williams have shown that there is a very noticeable steric hindrance to the approach of solvent molecules. Our results confirm this, and also show that this hindrance increases with increasing size of the alkyl substituents, as would be expected. The comparatively small changes in A and $\Delta\nu_3$ for 2,6-di-*t*-alkyl phenols compared with phenol or pentamethyl phenol can also be ascribed to a steric hindrance of solvent effects.

The results obtained with 2-*t*-butyl-4-methyl phenol are in agreement with theory. That is, in terms of changes in ν_m , A , and $\Delta\nu_3$ the trans band behaves similarly to phenol and the cis band similarly to 2,6-di-*t*-butyl-4-methyl phenol, although the cis band does not appear to be quite as highly protected from solvent effects as is the band in the di-*t*-butyl phenol.

As the polarizability or polarity of the solvent increases the two band maxima move further apart, but the resolution of the two bands becomes more difficult owing to the increase in half-band widths. The values obtained for $A(\text{trans})/A(\text{cis})$ with 2-*t*-butyl-4-methyl phenol in the different solvents are given in Table I. In nitromethane no separate cis band was observed. A maximum value was estimated for this band from the value of $\Delta\nu_3$ for 2,6-di-*t*-butyl-4-methyl phenol and the maximum contribution to $\log(I_0/I)$ at the expected ν_m that could be due to the cis band. The trend in the ratio of $A(\text{trans})/A(\text{cis})$ overemphasizes the true increase in the percentage of the trans isomer since the solvent effect on this isomer will be greater than on the cis isomer, (cf. effect of solvent on A for phenol and 2,6-di-*t*-butyl-4-methyl phenol in Table I). However, even after this effect is approximately allowed for (i.e. $[\text{trans}]/[\text{cis}]$ in Table I), the results still show the predicted increase in the concentration of the trans isomer with increasing solvent interaction. The results also show that even in carbon tetrachloride the percentage of trans isomer is greater than would be present in the vapor phase at the same temperature. A similar result has been observed with the isomers of *o*-halophenols by Rossmly, Lüttke, and Mecke (6). These workers, found, for example, that the trans isomer of *o*-iodophenol is stabilized by solvent interaction in carbon tetrachloride by about 1.4 kcal/mole with respect to the gaseous state. The values of ΔG and ΔH recorded in Table III must, therefore, be larger than they would be in the vapor state.

The increase in ν_m with temperature is probably related to the decreasing density of the solvent. That is, as the temperature is raised the solvent molecules are, on average, further removed from the solute molecules and therefore their influence will decrease and ν_m will increase. The smaller effect of temperature on ν_m for di-*t*-alkyl phenols compared with non-hindered phenols is to be expected since the effect of the solvent even at room temperature is greatly reduced by the shielding afforded to the OH group by the *t*-alkyl substituents.

As was mentioned above, ΔS values given in Table III are zero within the limits of experimental error, which suggests equal, a priori, probability for the two isomers and supports isomerization of the cis-trans type with the OH group coplanar in both isomers. If the O—H bond were twisted out of the plane in 2,6-di-*t*-alkyl phenols and also, therefore, in the cis isomer of *o*-*t*-alkyl phenols there would be two equivalent cis isomers and the a priori probability for this isomer would be twice that of the trans. Since ΔS is close to zero there is good agreement between ΔH and ΔG for the different phenols.

All the results obtained in this work support our original interpretation that the two infrared OH bands observed in *o*-*t*-alkyl phenols represent cis and trans isomers, the latter being thermodynamically more stable.

REFERENCES

1. K. U. INGOLD and D. R. TAYLOR. *Can. J. Chem.* This issue.
2. L. J. BELLAMY and R. L. WILLIAMS. *Proc. Roy. Soc. (London), A*, **254**, 119 (1960).
3. R. H. HUGHES, R. J. MARTIN, and N. D. COGGESHALL. *J. Chem. Phys.* **24**, 489 (1956).
4. T. L. BROWN. *J. Chem. Phys.* **24**, 1281 (1956).
5. K. U. INGOLD. *Can. J. Chem.* **38**, 1092 (1960).
6. G. ROSSMY, W. LÜTTKE, and R. MECKE. *J. Chem. Phys.* **21**, 1606 (1953).

PHOTOCHEMICAL SYNTHESSES

I. THE REACTION OF ALDEHYDES AND KETONES WITH CYCLOALKENES¹

P. DE MAYO,² J. B. STOTHERS,² AND W. TEMPLETON

ABSTRACT

The irradiation of dialkyl ketones in cyclohexene leads to the formation of cyclohexenyl-dialkylcarbinols. The use of aldehydes leads to the formation of the corresponding secondary alcohols, but the reaction is more complex because of concomitant Kharasch addition which can, however, be suppressed. The mechanism of the alcohol formation has been elucidated by the use of an optically active substrate, carvomenthene, and has been shown to involve the intermediacy of a cyclohexenyl radical. The structure and genesis of a biscarbinol by-product is discussed.

It was first observed by Bowen and Horton (1) that the irradiation of acetone in cyclohexane gave, in poor yield, an alcohol which was presumed to be cyclohexyldimethylcarbinol. More recent investigations (2) confirmed this, but the yield (12%) was not such as to render the reaction preparatively a very useful one.

It seemed probable that if the reaction proceeded by initial hydrogen atom abstraction by the photoactivated carbonyl compound, then any functional group designed to stabilize that radical should render the reaction more facile; and indeed there were indications in the literature (see, for instance, refs. 3, 4, 5) that in related transformations this was so.

A simple function that would fulfill the requirements was the ethylenic linkage and to this end the symmetrical hydrocarbon cyclohexene was selected. Irradiation at room temperature of a solution of acetone in this hydrocarbon until no carbonyl band could be detected in the infrared gave, after removal of excess hydrocarbon and distillation from a polymeric residue, a colorless oil. This could be separated by gas-liquid chromatography into an alcohol, shown to be the desired carbinol, and 3,3'-bicyclohexenyl. The latter was characterized as the known two tetrabromides (6).

The alcohol showed bands in the infrared at 3322 (hydroxyl), 1378 and 1368 (geminal dimethyl), and 733 cm^{-1} (cis disubstituted ethylene) in accordance with structure (I, $R = R' = \text{Me}$), and had the required analysis. It was characterized as the 3,5-dinitrobenzoate, and an authentic specimen of the alcohol was synthesized from cyclohexene-3-carboxylic acid by esterification (diazomethane) and Grignard reaction with methyl magnesium iodide. The alcohol so obtained and the derived 3,5-dinitrobenzoate were identical in every respect with the corresponding photoproducts.

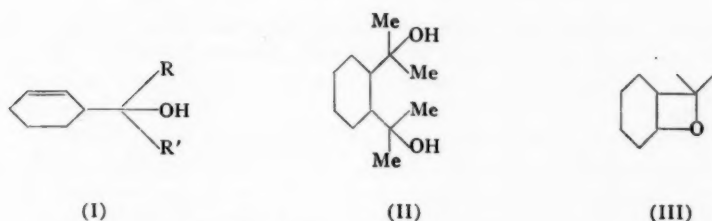
Under similar conditions the carbinols (I, $R = R' = \text{Et}$) and (I, $R = R' = \text{Pr}$) were obtained employing diethyl and dipropyl ketone respectively.

When the cyclohexene-acetone irradiation was performed at reflux temperature there was isolated in poor yield an additional substance, a saturated alcohol, which was readily characterized as a crystalline 3,5-dinitrobenzoate. The analysis indicated the condensation of two molecules of acetone with one of cyclohexene. The absence of unsaturation suggested structure (II) and comparison with an authentic specimen (see Experimental) confirmed this.

¹Manuscript received November 8, 1960.

Contribution from the Departments of Chemistry, Imperial College, London, S.W.7, England, and the University of Western Ontario, London, Ontario. Part of the contents of this paper were contained in a preliminary communication (26).

²Present address: Department of Chemistry, University of Western Ontario, London, Ontario.

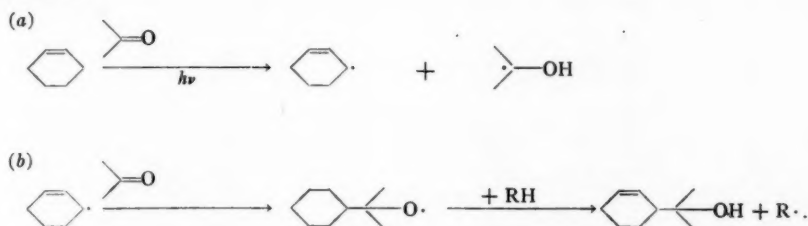


The formation of this interesting substance appears to be without photochemical parallel. Its genesis would not appear to involve, as expected, cyclohexenyl or, more probably, substituted cyclohexyl radicals, because when no attempt was made to exclude oxygen in the irradiation the formation of (I) was *totally suppressed*, all the cyclohexenyl radicals being trapped by the excess oxygen as cyclohexene hydroperoxide. The latter was characterized by conversion to cyclohexenone 2,4-dinitrophenylhydrazone. The yield of (II) remained, however, unaffected.

If such radicals are to be excluded a 'molecular' reaction must be presumed: one such reaction, known to occur with more-substituted ethylenes, is oxetane formation (7, 8). In the present case the oxide (III), not, however, isolated, would be the product. Bimolecular homolytic substitution at the cyclohexyl terminus of the oxide ring could then lead to (II). Radical displacements on carbon are rare, but are known to occur (cf. ref. 9). This possibility is being further investigated.

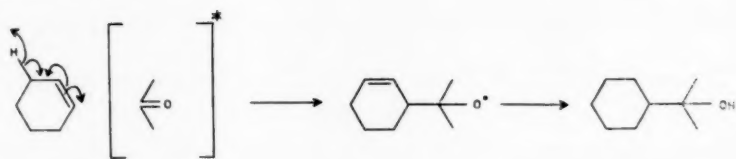
It has been the tacit assumption that the alcohols of type I were produced by the following steps:

Mechanism A

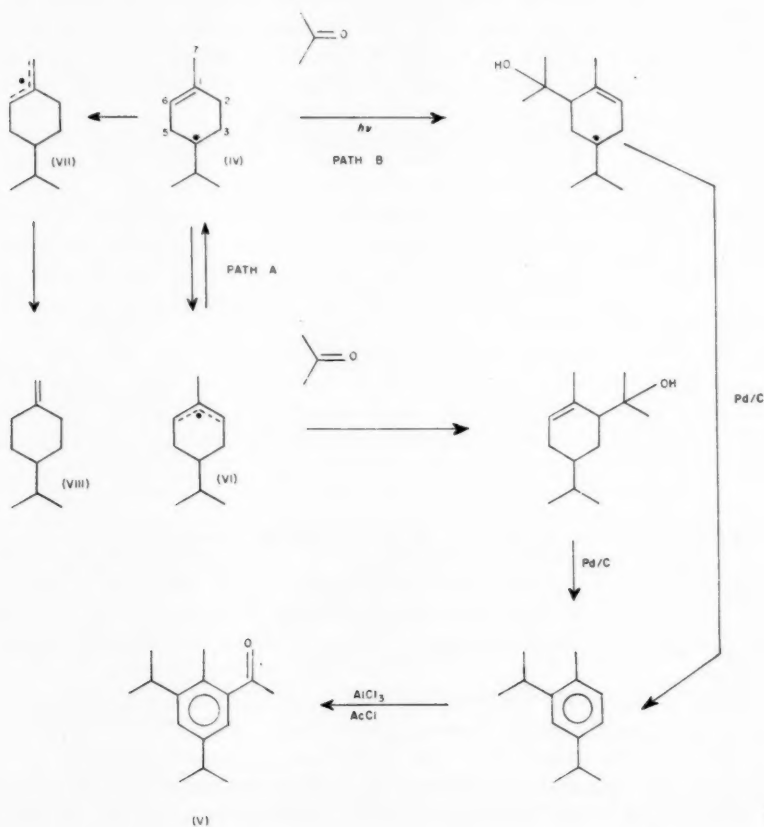


Evidence for step (a) lies in the formation of cyclohexene hydroperoxide in the presence of air, and in the formation of 3,3'-bicyclohexenyl as an important by-product. Although it is possible that in step (b) the cyclohexenyl radical may react with some other species than acetone in the ground state the assumption appears unnecessary since it is known (10) that chemically generated cyclohexyl radicals will add to carbonyl compounds in such a manner.

Nevertheless, although the evidence for step (a) is good it did not follow that the alcohol (I) was necessarily derived from a species produced in it. An alternative process, involving attack on the π -electrons of the cycloalkene appeared admissible, and such a mechanism has been proposed in radical substitutions in dienes and trienes (see, for instance, refs. 11, 12). This mechanism, in the present case, may be represented as follows:

Mechanism B

A distinction between these two mechanisms was arrived at in the following manner. (+)-Carvomenthene (IV), prepared by the hydrogenation of limonene, was irradiated in admixture with acetone. The alcoholic fraction, a mixture of stereoisomers, was completely racemized. The gross structure of the product was established by dehydrogenation and acylation to (V) characterized as the known 2,4-dinitrophenylhydrazone. The racemization of the active center during the photoreaction implies the intermediacy of the symmetrical allylic radical (VI), and supported mechanism A.



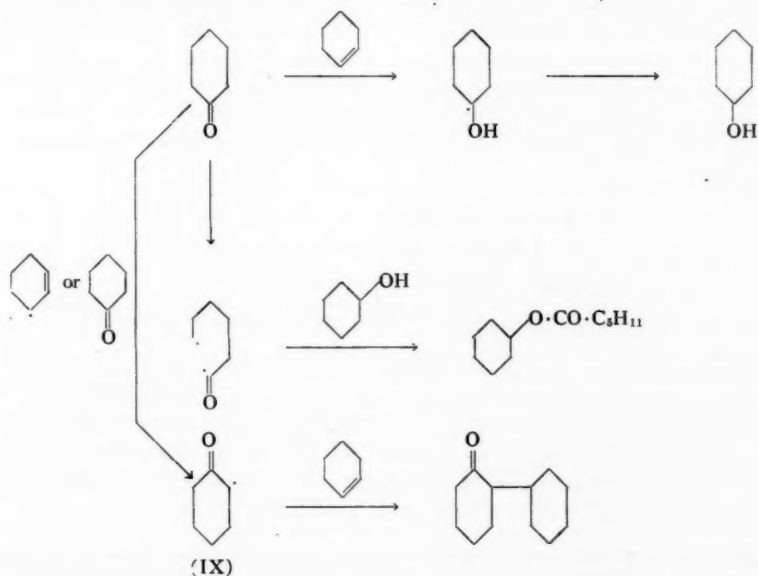
A possible criticism of the foregoing conclusions might rest on the fact that the zero rotation may have been a fortuitous combination of positive and negative rotations in stereoisomers. Since the separation of these isomers appeared difficult an alternative approach was sought.

It appeared possible that the radical (VI) might compete with the photoactivated ketone for allylic hydrogen abstraction in (IV), thus regenerating (inactive) carvomenthene on one hand and a new, equivalent, radical on the other. If this occurred, racemization could precede (apparent) reaction. In the event, interruption of the reaction before completion and recovery of carvomenthene by gas-liquid chromatography gave material which was approximately 30% racemized thus providing compelling evidence for the intermediacy of (VI). Carvomenthene, in the absence of acetone, was unaffected under the irradiation conditions.

By gas-liquid chromatography, also, a small amount of *p*-menth-1,7-ene (VIII) (13) was also isolated during the same experiment. This hydrocarbon is evidently formed by allylic hydrogen abstraction at the (alternative) primary (C_7) position, and provides further general support for the present thesis.

The irradiation of cyclohexanone in cyclohexene led to entirely different results. No alcohol of the required type was isolated, but instead, in addition to the 3,3'-bicyclohexenyl, two further liquid substances were obtained by chromatography of the total volatile product on alumina.

The first of these was readily identified as cyclohexyl *n*-caproate by hydrolysis to its components, each being characterized by a solid derivative. Evidently the cyclohexanol (or equivalent) derives from the hydrogen-abstraction step, but the cyclohexene is, however, apparently too bulky a molecule to allow of backside attack of the cyclohexenyl radical on the cyclohexanone carbonyl. Such reaction is presumably controlled by the 1,3-axial hydrogen interactions in the transition state. Under these circumstances, and



in the presence of cyclohexanol, the slower solvolytic fission may then take place. Such fission in cyclic ketones is unexceptional (14).

The resistance of the cyclohexanone carbonyl to attack by the cyclohexenyl radical is also demonstrated by the nature of the second product. This substance showed a single carbonyl band in the infrared at 1715 cm^{-1} , whilst the empirical formula indicated it to be a 1:1 adduct of cyclohexanone and cyclohexene. The presumption that it was cyclohexyl cyclohexanone was justified by comparison of the ketone and its 2,4-dinitrophenylhydrazone with authentic specimens. The cyclohexenyl radical or, perhaps, activated ketone has, therefore, abstracted an α -hydrogen atom to give (IX), which has then added to a further molecule of cyclohexene. These observations parallel those of Kharasch, Kuderna, and Nudenberg, who noted the addition of cyclohexanone to oct-1-ene (15).

The irradiation of cyclohexene with aldehydes led to similar results. Propionaldehyde for instance gave (I, $R = \text{Et}$, $R' = \text{H}$), characterized as the 3,5-dinitrobenzoate, and identified by comparison with an authentic specimen.³ The latter was prepared by reaction of cyclohexene-3-carbonyl chloride with dimethyl cadmium followed by lithium aluminum hydride reduction. The expected product of Kharasch addition (16) was also obtained.

In the case of acetaldehyde it was found, because of the volatility of the substance, more convenient to work in a closed system. Here, again, the desired alcohol (I, $R = \text{Me}$, $R' = \text{H}$) was obtained, together with the Kharasch addition product methylcyclohexyl ketone.

The 60 Mc N.M.R. spectra of the alcohol and its 3,5-dinitrobenzoate were obtained in CCl_4 solution (ca. 15%). The characteristic peaks observed (in p.p.m. from tetramethylsilane)⁴ were as follows: alcohol: CH_3 group, 1.14 (doublet, $J = 6\text{ c.p.s.}$); OH, 2.9 (concentration-dependent); H on carbon bonded to oxygen, a multiplet centered at 3.6, and olefinic Hs, 5.7 (a multiplet); the 3,5-dinitrobenzoate: CH_3 group, 1.5 (doublet, $J = 7\text{ c.p.s.}$); H on carbon bonded to oxygen, 5.3 (center of multiplet); olefinic Hs, 5.8 (center of multiplet), and aromatic Hs, 9.1–9.4. The areas of the last three bands were in the ratio 1:2:3. These assignments are entirely compatible with the proposed structure. This is most clearly demonstrated in the paramagnetic shift of the methine hydrogen on carbon bonded to oxygen from 3.6 to 5.3 on esterification.

Since the Kharasch addition is a chain reaction (24) involving most probably the following steps:

- (i) $R \cdot \text{CHO} \rightarrow \dot{R} + \dot{\text{C}}\text{HO}$,
- (ii) $R \cdot + \text{RCHO} \rightarrow \text{RH} + \text{R}\dot{\text{C}}\text{O}$,
- (iii) $\text{R}\dot{\text{C}}\text{O} + \text{R}_2\text{C}=\text{CR}_2 \rightarrow \text{RCOR}_2\text{C}-\dot{\text{C}}\text{R}_2$,
- (iv) $\text{RCOR}_2\text{C}-\dot{\text{C}}\text{R}_2 + \text{RCHO} \rightarrow \text{RCOR}_2\text{C}-\text{CHR}_2 + \text{R}\dot{\text{C}}\text{O}$ etc.;

its perpetuation ((step ii)+(step iv)) should be favored by a high ratio of aldehyde to cyclohexene. On the other hand the process leading to the alcohol should require that the concentration of hydrocarbon be high so that hydrogen atom abstraction by the photo-activated aldehyde may compete with homolysis (step i). In the event, when the concentration (w/v) of acetaldehyde in cyclohexene was decreased from 20% to 2% the ratio of ketone to alcohol changed from about 1:1 to 1:9.

³The alcohols from the aldehydes may possibly be mixtures of diastereoisomers. These did not resolve on the silicone column used. The synthetic specimens, also possibly diastereoisomers, were indistinguishable from these in chromatographic behavior as in other respects.

⁴For τ values (25) these figures should be subtracted from 10.

EXPERIMENTAL

Materials were reagent grade and were dried over magnesium sulphate and distilled before use. Cyclohexene was purified by shaking with aqueous ferrous sulphate, dried, and distilled. Before use it was filtered through a short column of alumina. Gas-liquid chromatography was conducted on a silicone-celite column at 175°. Unless otherwise specified irradiations were carried out under dry oxygen-free nitrogen in a quartz immersion apparatus (8b), the light source being a 125-watt Compton mercury arc lamp or a Hanovia 85-watt AH-8, both of which had the outer envelope removed. The yields recorded are based on carbonyl compound employed (*not* that consumed) and are in no way optimum values. Light petroleum was b.p. 60–80°.

*Irradiations**Acetone-Cyclohexene (i)*

A solution of acetone (50 g) in cyclohexene (275 ml) was irradiated at approximately 20° for 100 hours. After evaporation of the solvents the residue was distilled *in vacuo* to give a colorless oil (70 g). Gas-liquid chromatography of a portion (0.65 g) gave two fractions. The first cyclohex-2-enyl dimethylcarbinol (0.34 g; 30%) had b.p. 82°/30° mm, n_D^{21} 1.4740. Calc. for $C_9H_{16}O$: C, 77.0; H, 11.50%. Found: C, 77.02; H, 11.82%. The 3,5-dinitrobenzoate crystallized from chloroform-methanol, and had m.p. 121–124°. Calc. for $C_{16}H_{18}O_6N_2$, 0.5 CH_3OH : C, 56.55; H, 5.75; N, 8.00. Found: C, 56.94; H, 5.38; N, 8.07%. The substance was identical in every respect with an authentic synthetic specimen (see below).

The second fraction 3,3'-bicyclohexenyl (0.28 g) had b.p. 167–170/130 mm, n_D^{24} 1.5050, λ_{max} 190 m μ (ϵ 14,300) expected for two cis disubstituted ethylenes,⁵ ν_{max} 701 cm^{-1} . Bromination in carbon tetrachloride gave a crystalline mixture of bromides from which, by fractional crystallization from chloroform, the two tetrabromides of 3,3'-bicyclohexenyl, m.p. 158–160° and 191.5–192.5°, were obtained. These were identical in every respect with specimens of the same melting point prepared by the method of Farmer and Michael (6).

Acetone-Cyclohexene (ii)

Irradiation at reflux temperature, in a quartz vessel over a 500-watt Hanovia lamp, of a solution of acetone (25 g) in cyclohexene (225 ml) for 38 hours gave, after evaporation of the solvent and distillation, an oil (27 g). Gas-liquid chromatography revealed the presence of a further substance in addition to the 3,3'-bicyclohexenyl and the alcohol (I, R = R' = Me). This component was obtained as a concentrate by fractional distillation (b.p. 133–138°/150 mm) and was converted into the 3,5-dinitrobenzoate, m.p. (from methanol) 112–115°. Calc. for $C_{26}H_{28}O_{12}N_4$: C, 53.06; H, 4.80; N, 9.52%. Found: C, 53.26; H, 4.45; N, 9.95%. It was identical in every respect with an authentic synthetic specimen of *trans*-1,2-di(2'-hydroxy-2'-propyl) cyclohexane prepared as described below. The corresponding alcohols had identical retention times on the silicone column.

Acetone-Cyclohexene (iii)

A solution of acetone (16 g) in cyclohexene (200 ml) was irradiated at room temperature for 40 hours in the presence of excess oxygen. By fractional distillation an oil (2.5 g) b.p. 119–130°/140 mm was isolated. Gas-liquid chromatography showed the presence of two substances in approximately equal amounts. One was identified as *trans*-1,2-di(2'-hydroxy-2'-propyl) cyclohexane by retention time and conversion to the 3,5-dinitrobenzoate, m.p. and mixed m.p. 111–113°. The second substance cyclohex-2-ene

⁵We are indebted to Dr. D. Turner (Imperial College) for the determination of this spectrum between 170 and 200 m μ .

hydroperoxide was isolated by chromatography of the distillate (2 g) on silica gel (100 g). Elution with benzene-ether (1:1) gave a fraction (600 mg) which was optically transparent in the ultraviolet, gave a strong starch-iodide reaction, and had ν_{\max} 3365 and 702 cm^{-1} . On treatment with 6 *N* sulphuric acid a maximum appeared in the ultraviolet at 228 $\text{m}\mu$ and rose to ϵ 8000. To convert the hydroperoxide into the α,β -unsaturated ketone 2,4-dinitrophenylhydrazone it was mixed with reagent hydrochloride at room temperature in dioxan-water and left to stand overnight; its melting point and mixed m.p. 163° were identical with those of an authentic specimen of cyclohexenone 2,4-dinitrophenylhydrazone.

Acetone - Diethyl Ketone

A solution of diethyl ketone (40.8 g) in cyclohexene (300 ml) was irradiated at room temperature for 138 hours. Fractional distillation of the product then gave a colorless oil (28 g). Chromatography of a portion (5 g) on alumina (Brockman Grade 3, 200 g) gave (eluted with light petroleum) 3,3'-bicyclohexenyl (3.5 g) identified by retention time and infrared spectrum. Elution with 4:1 benzene-ether then gave 3-cyclohex-2'-enylpentan-3-ol, b.p. 140°/50 mm, n_D^{25} 1.4823. Calc. for $\text{C}_{11}\text{H}_{20}\text{O}$: C, 78.51; H, 11.98%. Found: C, 78.25; H, 11.76%. The retention time and infrared spectrum were identical with those of an authentic specimen (see below).

Acetone - Dipropyl Ketone

A solution of di-*n*-propyl ketone (40 g) in cyclohexene (300 ml) was irradiated at room temperature for 72 hours. Fractional distillation yielded an oil (67 g) a sample of which (5 g) was chromatographed on alumina (Brockman Grade 3, 200 g). Elution with light petroleum gave 3,3'-bicyclohexenyl (4.0 g) identified as previously. Elution with ether-benzene (1:9) gave a mixture from which, by gas-liquid chromatography, the required alcohol could be isolated. It had n_D^{25} 1.4790. Calc. for $\text{C}_{13}\text{H}_{24}\text{O}$: C, 79.53; H, 12.32%. Found: C, 78.77; H, 12.27%. It was identical in infrared spectrum, retention time, and refractive index with a specimen prepared by an unambiguous route as described below.

Acetone - (+)-Carvomenthene (i)

A solution of acetone (80 g) in carvomenthene (270 g) ($[\alpha]_D +76^\circ$) (17) was irradiated at room temperature for 290 hours. Fractional distillation gave a crude product (41 g) which on gas-liquid chromatography gave an oil, $[\alpha]_D \pm 0^\circ$, ν_{\max} 3434. Calc. for $\text{C}_{13}\text{H}_{24}\text{O}$: C, 79.53; H, 12.32%. Found: C, 79.43; H, 12.17%.

The crude alcohol (1.7 g) was refluxed with palladized charcoal (10%, 0.4 g) for 4 hours. The hydrocarbon (100 mg) was then acetylated in the manner described by Pines (23), and converted to the known 2,4-dinitrophenylhydrazone in the usual manner. The product, crystallized from chloroform-ethanol, had m.p. 161-165° undepressed on admixture with an authentic specimen of the same melting point (23).

Acetone - (+)-Carvomenthene (ii)

A solution of carvomenthene ($[\alpha]_D +105^\circ$; 3.1 g) in acetone (60 ml) was irradiated at room temperature for 45 hours during which time the rotation of the solution fell from 102° to 43°. Distillation gave an oil b.p. 65-115°/14 mm. Gas-liquid chromatography then afforded carvomenthene ($[\alpha]_D +74^\circ$ (c, 0.43)) identical in all respects except rotation with the starting material. A substance with lower retention time than carvomenthene was isolated and shown to be *p*-menth-1,7-ene. It had maxima in the infrared at 6.08 (s), 9.35, 9.62, 9.85, 10.07, 10.22, 11.07, and 11.26 (s) μ , and n_D^{25} 1.4578. The literature records (13) maxima in the infrared at 6.08 (s), 9.37, 9.62, 9.85, 10.07, 10.22, 11.07, 11.26 (s) μ and n_D^{25} 1.4575.

Carvomenthene was unaffected under the irradiation conditions in the absence of acetone.

Cyclohexanone-Cyclohexene

A solution of cyclohexanone (25 g) in cyclohexene (100 ml) was irradiated at reflux temperature over a 500-watt Hanovia lamp for 40 hours. Distillation then gave a colorless oil (15 g) b.p. 72–197°/25 mm. A portion (5 g) of the oil was chromatographed on alumina (Brockman Grade 5, 200 g). Three fractions were obtained. Fraction (i) (1 g) eluted with light petroleum had b.p. 108–109°/18 mm, n_D^{24} 1.5062, and was identical in every respect with 3,3'-bicyclohexenyl. Fraction (ii) (1.3 g) also eluted with light petroleum had b.p. 125°/7 mm, n_D^{24} 1.4513. Calc. for $C_{12}H_{22}O_2$: C, 72.68; H, 11.18%. Found: C, 72.68; H, 10.98%. The substance was identified as cyclohexyl *n*-caproate by hydrolysis, the caproic acid being characterized as the *p*-bromophenacyl ester (m.p. and mixed m.p. 70–71°) and the cyclohexanol as the 3,5-dinitrobenzoate (m.p. and mixed m.p. 109–111°). Fraction (iii) (1.5 g) eluted with benzene–light petroleum (1:4) had b.p. 145–146°/20 mm, n_D^{23} 1.4970, ν_{\max} 1715 cm^{-1} . It gave an orange 2,4-dinitrophenylhydrazone, m.p. 172–5° from ethanol–chloroform. Calc. for $C_{13}H_{24}O_4N_4$: N, 15.55%. Found: N, 15.56%. It was undepressed in melting point on admixture with the 2,4-dinitrophenylhydrazone of cyclohexyl cyclohexanone prepared by the method of Hückel *et al.* (18), and the infrared spectra in chloroform solution were superposable.

The same substances were produced by irradiation at room temperature in similar yields.

Propionaldehyde-Cyclohexene

A solution of propionaldehyde (40 g) in cyclohexene (200 ml) was irradiated at reflux temperature over a 500-watt Hanovia lamp for 24 hours. Distillation gave a colorless oil (25 g). A portion of the oil (5 g) was chromatographed on alumina (Brockman Grade 5, 175 g) to give three fractions. Fraction (i) (650 mg), eluted with light petroleum, was identified, as previously, as 3,3'-bicyclohexenyl. Fraction (ii), also eluted with light petroleum, had b.p. 71–73°/15 mm, n_D^{25} 1.4547, ν_{\max} 1709 cm^{-1} . It gave a 2,4-dinitrophenylhydrazone, m.p. 149–151° (from benzene). Calc. for $C_{15}H_{26}O_4N_4$: C, 56.24; H, 6.29; N, 17.49%. Found: C, 56.46; H, 6.40; N, 17.43%. This, and its derivative, were identical in every respect with a specimen of ethylcyclohexyl ketone and its 2,4-dinitrophenylhydrazone prepared by the method of Morris and Lusth (19). Fraction (iii) (1.05 g), eluted with benzene–ether (19:1) had b.p. 87–88°/11 mm, n_D^{25} 1.4772. It gave a 3,5-dinitrobenzoate, m.p. 74–8°. Calc. for $C_{16}H_{16}O_6N_2$: C, 57.48; H, 5.43; N, 8.38%. Found: C, 57.65; H, 5.50; N, 8.22%. It was identical with the derivative of 1-cyclohex-2'-enylpropan-1-ol from the alcohol prepared by an unambiguous route prepared as described below.

The same products, with a somewhat lower yield of ketone, were obtained by irradiation at room temperature.

Acetaldehyde-Cyclohexene

A solution of acetaldehyde (10.2 g) in cyclohexene (50 ml) in a sealed quartz tube was irradiated for 65 hours with an AH-8 lamp, the tube being cooled in a current of air. The crude oil, b.p. 60–120°/14 mm (4.9 g), on gas-liquid chromatography gave three main components. The last (retention time 110 minutes) was shown, as in previous cases, to be 3,3'-bicyclohexenyl. The first (retention time 32 minutes) had n_D^{25} 1.4498 and gave a semicarbazone m.p. 172.5–173.5° undepressed on admixture with the semicarbazone of methylcyclohexyl ketone of the same melting point. The infrared spectrum of the first component and that of a methylcyclohexyl ketone were superposable.

The second component (retention time 45 minutes) was most readily isolated in larger amounts by heating, under reflux, of the crude distillate (2.4 g) with Girards 'T' reagent

(3.3 g) in 95% ethanol (15 ml) containing acetic acid (0.5 ml) for 12 hours. Isolation of the non-ketonic material (1.6 g) followed by chromatography on alumina (Brockman Grade 1, 50 g) gave, on elution with benzene-ether (3:1) 1-cyclohex-2'-enylethan-1-ol, n_D^{21} 1.4798, b.p. 88–90°/13 mm. Calc. for $C_8H_{14}O$: C, 76.14; H, 11.18%. Found: C, 75.21; H, 11.59%. The substance was identical in infrared spectrum with that of the alcohol prepared by an unambiguous route described below. The substance gave a 3,5-dinitrobenzoate, m.p. 75.5–76.5° (from light petroleum). Calc. for $C_{18}H_{16}O_6N_2$: C, 56.25; H, 5.04; N, 8.75%. Found: C, 55.76; H, 5.07; N, 8.59%.

Under these conditions the yields of alcohol and ketone were approximately 6%. A similar irradiation employing a more dilute solution of acetaldehyde (1.2 g) in cyclohexene (55 ml) gave the same products, but whereas the yield of ketone was essentially unchanged, the yield of alcohol was now 38%.

2-Cyclohex-2'-enylpropan-2-ol, 3,5-Dinitrobenzoate

Cyclohexene-3-carboxylic acid (20) (2 g) was esterified with excess diazomethane. After evaporation of the excess diazomethane the ester in ether (50 ml) was added to a solution of methyl magnesium iodide (from methyl iodide (5 g) and magnesium (0.8 g)) and the mixture stirred for 1 hour. Isolation of the neutral material gave 2-cyclohex-2-enylpropan-2-ol (2 g) (identical in retention time with the photochemical product), which was converted directly into the 3,5-dinitrobenzoate. Crystallized from chloroform-light petroleum this had m.p. 122–125°.

trans-1,2-Di(2'-hydroxy-2'-propyl)cyclohexane, 3,5-Dinitrobenzoate

trans-Cyclohexan-1,2-dicarboxylic acid (21) (3 g) was esterified with excess diazomethane, the excess diazomethane reagent removed by evaporation, and the ester in ether (50 ml) added to methyl magnesium iodide prepared from methyl iodide (213 g) and magnesium (45 g) in ether (11.) and the mixture refluxed for 150 hours. Isolation of the neutral material in the usual way gave an oil (2 g). A portion (1.5 g) of the oil was converted into the 3,5-dinitrobenzoate by the method of Brewster and Ciotti (22). Chromatography of the product on silica gel (100 g) gave on elution with benzene-ether (9:1) and crystallization from methanol and from ethyl acetate-light petroleum the bis 3,5-dinitrobenzoate, m.p. 110–112.5°, undepressed on admixture with the 3,5-dinitrobenzoate of the product obtained by irradiation.

4-Cyclohex-2'-enylheptan-4-ol and 3-Cyclohex-2'-enylpentan-3-ol

Methyl cyclohexene-3-carboxylate (2.15 g) was added to the Grignard reagent prepared from *n*-propyl iodide (18.5 g) and magnesium (2.4 g) in dry ether (100 ml). After 1-hour stirring the neutral material was isolated in the usual way, and purified by gas-liquid chromatography. Its retention time on the silicone column, its refractive index, and its infrared spectrum were identical with those of the photochemical product.

3-Cyclohex-2'-enylpentan-3-ol, n_D^{23} 1.4800, was prepared in a similar manner. It was identical in retention time and infrared spectrum with the photochemical product.

1-Cyclohex-2'-enylpropan-1-ol

A solution of cyclohexene-3-carboxylic acid (2 g) and oxalyl chloride (3 g) in dry benzene (15 ml) was allowed to stand at room temperature for 2 days after which solvent and excess oxalyl chloride were removed *in vacuo*. The acid chloride was added to cadmium diethyl (from anhydrous cadmium chloride (6.25 g), ethyl bromide (15 g), and magnesium (1.75 g)) at 10° and the mixture stirred for 2 hours and allowed to stand at room temperature for 16 hours. Decomposition of the complex with water, and isolation of the

neutral material gave an oil which was filtered through a column of silica gel in light petroleum - benzene (4:1) to remove alcoholic impurities. The crude unconjugated ($\epsilon_{220} < 600$) ketone (1.8 g) in ether (50 ml) was then added to a solution of lithium aluminum hydride in ether (100 ml) at 0°. After 1 hour the mixture was decomposed with ethyl acetate and the neutral material isolated in the usual way. The alcohol had the same retention time as the photochemical product on the silicone column, and gave a 3,5-dinitrobenzoate m.p. 65–78° undepressed on admixture with the derivative of the photochemical product and having identical infrared spectrum. However, although the column used in the gas-liquid chromatography showed a single peak it is probable in view of the diffuse melting point of the derivative that the product is a mixture of diastereoisomers.

1-Cyclohex-2-enylethan-1-ol was prepared in a precisely analogous fashion. The product had ν_{\max} in the infrared at 3580, 3380, and 722 cm^{-1} and n_D^{25} 1.4806. It was identical in retention time with the photochemical product.

ACKNOWLEDGMENTS

The authors wish to thank the British Petroleum Company for support (for W. T.) and the Imperial Oil Ltd., of Canada for generous financial support. The authors are indebted to Professor D. H. R. Barton for his interest and for many discussions.

REFERENCES

1. E. J. BOWEN and A. T. HORTON. *J. Chem. Soc.* 1685 (1936).
2. N. C. YANG and D.-D. H. YANG. *J. Am. Chem. Soc.* **80**, 2913 (1958).
3. E. BERGMAN and S. FUJISE. *Ann.* **483**, 65 (1930).
4. E. PATERNO and G. CHIEFFI. *Gazz. chim. ital.* **39**, 415 (1909).
5. A. SCHÖNBERG and A. MUSTAFA. *J. Chem. Soc.* 551 (1945).
6. E. H. FARMER and S. E. MICHAEL. *J. Chem. Soc.* 513 (1942).
7. E. PATERNO and G. CHIEFFI. *Gazz. chim. ital.* **39**, 341 (1909).
8. (a) G. BÜCHI, C. G. INMAN, and E. S. LIPINSKY. *J. Am. Chem. Soc.* **76**, 4327 (1954). (b) P. DE MAYO. Ultraviolet photochemistry of simple unsaturated systems. *In* *Advances in organic chemistry*. Vol. II. Interscience Pub. 1960. p. 367.
9. H. G. OSWIN, R. REBBERT, and E. W. R. STEACIE. *Can. J. Chem.* **33**, 472 (1955); R. A. HERRMANN and R. M. NOYES. *J. Am. Chem. Soc.* **78**, 5764 (1956).
10. G. FULLER and F. F. RUST. *J. Am. Chem. Soc.* **80**, 6148 (1958).
11. E. C. COYNER and G. A. ROPP. *J. Am. Chem. Soc.* **70**, 2283 (1948).
12. K. WEISS and M. LALANDE. *J. Am. Chem. Soc.* **82**, 3117 (1960).
13. R. L. WEBB and J. P. BAIN. *J. Am. Chem. Soc.* **75**, 4279 (1953).
14. G. CIAMICIAN and P. SILBER. *Ber.* **46**, 3077 (1913); D. ARIGONI, D. H. R. BARTON, R. BERNASCONI, C. DJERASSI, J. S. MILLS, and R. WOLF. *Proc. Chem. Soc.* 306 (1959).
15. M. S. KHARASCH, J. KUDERNA, and W. NUDENBERG. *J. Org. Chem.* **18**, 1225 (1953).
16. M. S. KHARASCH, W. H. URRY, and B. M. KUDERNA. *J. Org. Chem.* **14**, 248 (1949).
17. H. A. SMITH, J. F. FUZEK, and H. T. MERIWETHER. *J. Am. Chem. Soc.* **71**, 3765 (1949).
18. W. HÜCKEL, O. NEUNHOFFER, A. GERCKE, and E. FRANK. *Ann.* **477**, 99 (1930).
19. H. H. MORRIS and M. L. LUSTH. *J. Am. Chem. Soc.* **76**, 1237 (1954).
20. E. J. BOORMAN and R. P. LINSTEAD. *J. Chem. Soc.* 258 (1935).
21. D. L. HUTTORD, D. S. TARBELL, and T. L. KOSZALKA. *J. Am. Chem. Soc.* **74**, 3014 (1952).
22. J. H. BREWSTER and C. J. CIOTTI. *J. Am. Chem. Soc.* **77**, 6214 (1955).
23. H. PINES, A. WEIZMANN, and V. N. IPATIEFF. *J. Am. Chem. Soc.* **70**, 3859 (1948).
24. E. W. R. STEACIE. Atomic and free radical reactions. Vol. I. Reinhold. 1954. pp. 284 *et seq.*; C. R. MASSON, V. BOEKELHEIDE, and W. A. NOYES. *In* *Technique of organic chemistry*. Edited by A. Weissberger. Vol. II. 2nd. ed. Interscience Publishers, Inc., New York. 1956. p. 375.
25. G. V. D. TIERS. *J. Phys. Chem.* **62**, 1151 (1958).
26. P. DE MAYO, J. B. STOTHERS, and W. TEMPLETON. *Proc. Chem. Soc.* 72 (1960).

KINETICS AND THERMODYNAMICS OF THE CRYSTAL STRUCTURE TRANSFORMATION OF SPECTROSCOPICALLY PURE ANATASE TO RUTILE¹

C. N. R. RAO²

ABSTRACT

The transformation of spectroscopically pure anatase to rutile was first investigated by Czanderna, Rao, and Honig. But it was not possible, then, to provide the mechanism on a molecular scale because of the lack of very accurate kinetic data. The kinetics and thermodynamics of the transformation have now been carefully investigated.

EXPERIMENTAL

The preparation of the spectroscopically pure anatase and the procedure adopted in the kinetic studies and in the X-ray analysis of the samples have been described earlier (1). The accuracy of the analytical method is found to be rather poor at anatase concentrations of less than 5% or greater than 95%. In order to obtain reliable kinetic data for fitting them into the order plots, the proportion of anatase was always seen to be within these limits. The temperature fluctuation in a run was within 5°. The purity of the sample is the most important requisite in this study since impurities are known to affect the transformation markedly (2, 3).

The differential thermal analysis of the anatase (preheated to 250° C) was carried out using a high sensitivity (0.25–0.5 cal) apparatus similar to that described by Pask and Warner (4). A sufficiently fast and constant heating rate of 12.5 deg min⁻¹ was employed since the peaks corresponding to crystal structure transformations are usually small.

RESULTS AND DISCUSSION

The kinetic results at different temperatures are shown in Fig. 1(a). In Fig. 1(b), the data are plotted for the first-order equation. The data follow the first-order law fairly well. The first-order rate constants at different temperatures are summarized in Table I.

TABLE I

Temperature, °C	Rate constant, hr ⁻¹ $k \times 10^3$
625	2.9 ₉
643	6.2 ₂
684	36.9 ₆
698	76.7 ₆

The reaction rate constants in Table I follow the Arrhenius equation closely (Fig. 2). The energy of activation is about 80 ± 10 kcal per mole. The frequency factor is about 4 × 10¹⁴ sec⁻¹, which is surprisingly of the same order as expected for the first-order gas or solution reactions. The entropy of activation calculated from Eyring's theory is about 27 e.u. at 643° C.

The kinetic data of this investigation give a value of 610 ± 10° C for the infinite-time

¹Manuscript received September 26, 1960.

²Contribution from the Department of Inorganic and Physical Chemistry, Indian Institute of Science, Bangalore-12, India, and Department of Chemistry, Purdue University, Lafayette, Indiana, U.S.A.

³All the correspondence should be addressed to the Department of Inorganic and Physical Chemistry, Indian Institute of Science, Bangalore-12, India.

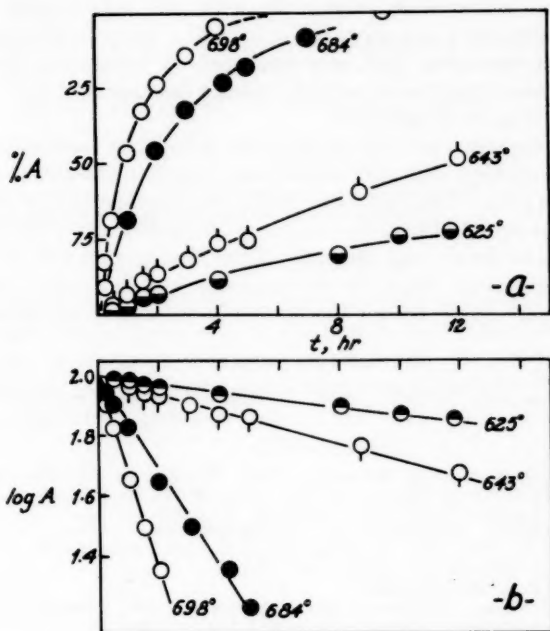


FIG. 1. (a) Plots of % anatase versus time at different temperatures.
(b) First-order plots of the data in (a).

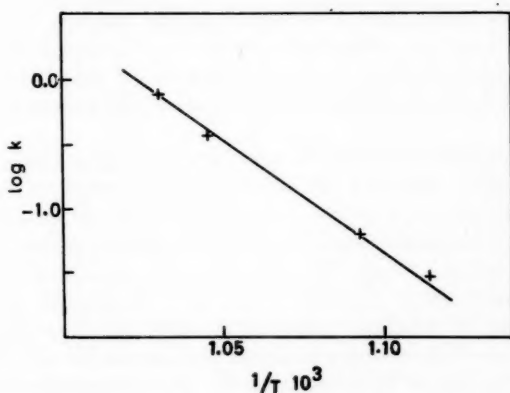


FIG. 2. Arrhenius plot.

temperature. That is, below 610° C, the transformation is immeasurably slow. This is in agreement with the value reported earlier (1).

The differential thermal analysis of the anatase showed a small exothermic peak starting around 630° C corresponding to the transformation to rutile. It was confirmed by X-ray analysis that the transformation was complete after the exothermic peak. This

temperature of 630° C corresponds excellently with the infinite-time temperature mentioned earlier.

The heat of the transformation, ΔH , was estimated by comparing the area of the exothermic peak with the α - β inversion peak of a known amount of quartz. The ΔH thus estimated was only -100 ± 50 cal per mole.

An interpretation of the data on the kinetics of this solid-state transformation may be obtained by drawing an analogy with the thermal decomposition of solids (1, 5). However, a more refined and satisfactory theoretical treatment has been possible, by the application of the order-disorder theory (6). The details of the theory will be discussed elsewhere (7). From the theory it can be shown that the ratio of the propagation rate constant to the nucleation rate constant is small. Also, the observed energy of activation seems to represent mainly the activation energy for the production of the nucleation sites.

ACKNOWLEDGMENT

The author's thanks are due to Prof. M. R. A. Rao for his keen interest.

REFERENCES

1. A. W. CZANDERNA, C. N. R. RAO, and J. M. HONIG. *Trans. Faraday Soc.* **54**, 1069 (1958).
2. C. N. R. RAO, A. TURNER, and J. M. HONIG. *J. Phys. Chem. Solids*, **11**, 173 (1959).
3. C. N. R. RAO and M. P. LEWIS. *Current Sci. (India)*, **29**, 52 (1960).
4. J. A. PASK and M. F. WARNER. *Am. Ceram. Soc. Bull.* **33**, 168 (1954).
5. P. W. M. JACOBS and F. C. TOMPKINS. *In Chemistry of the solid state. Edited by W. E. Garner. Butterworth Scientific Publications, London. 1955. Chap. 7.*
6. J. M. HONIG. *J. Chem. Phys.* **28**, 723 (1958).
7. C. N. R. RAO and J. M. HONIG. Symposium on rate processes. Indian Chemical Society, Bombay, January 1960. To be published in a special volume of *J. Indian Chem. Soc.*

NITRO- AND AMINO-IMIDAZOLESULPHONAMIDES¹

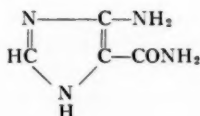
M. H. FISHER, W. H. NICHOLSON, AND R. S. STUART

ABSTRACT

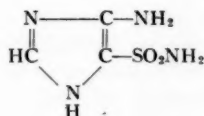
Several 4(5)-nitro- and 4(5)-amino-5(4)-sulphamylimidazoles have been synthesized as potential antagonists to 4(5)-amino-5(4)-carbamylimidazole.

INTRODUCTION

There has recently been considerable interest in the role of 4(5)-amino-5(4)-carbamylimidazole (I) and related compounds in the biosynthesis of purines (1, 2, 3, 4). However, the preparation of imidazole analogues as potential antagonists has not been widely investigated (5). In this work compounds related to 4(5)-amino-5(4)-sulphamylimidazole (II) were synthesized for biological testing.²



(I)



(II)

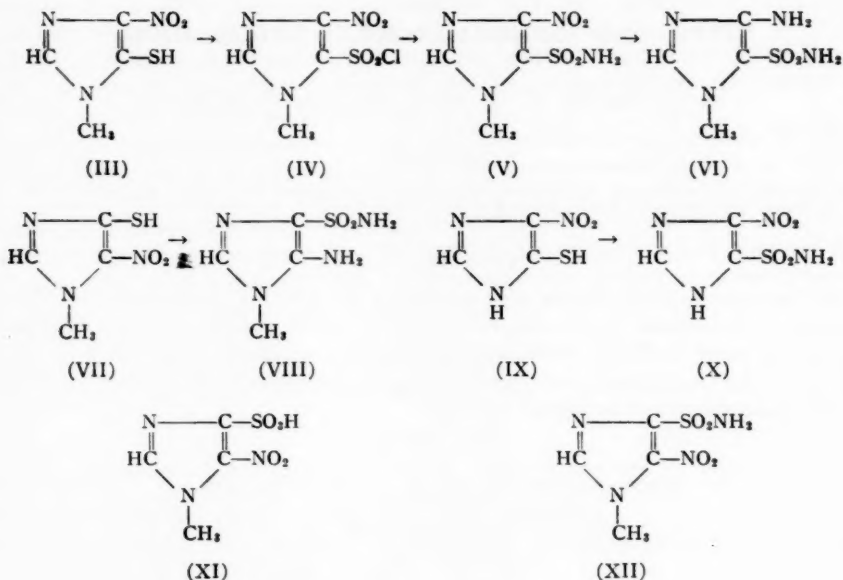
A number of unsuccessful attempts to prepare compounds of this type have been reported, e.g. chlorination of imidazole sulphonic acids, chlorosulphonation of nitro- or acylamino-imidazoles, amination of bromo-imidazoles, and conversion of imidazolethiols to sulphenamides followed by oxidation (5, 6, 7). 4(5)-Bromo-5(4)-sulphamylimidazole was prepared by chlorosulphonation of 4(5)-bromoimidazole (5), but it failed to react with ammonia.

The most attractive approach was the oxidative chlorination of the thiols, a general method described by Sprague and Johnson (8) and later used for the preparation of 2-sulphamylimidazoles (9, 10). 5-Mercapto-1-methyl-4-nitroimidazole (III) (5) was converted to the sulphonyl chloride (IV) by oxidative chlorination in dilute hydrochloric acid. The sulphonyl chloride with concentrated aqueous ammonia yielded 1-methyl-4-nitro-5-sulphamylimidazole (V). Catalytic reduction of this compound gave 4-amino-1-methyl-5-sulphamylimidazole (VI). In a similar manner 5-amino-1-methyl-4-sulphamylimidazole (VIII) was obtained from 1-methyl-4-mercapto-5-nitroimidazole (VII). 4(5)-Mercapto-5(4)-nitroimidazole (IX) (5) was converted to 4(5)-nitro-5(4)-sulphamylimidazole (X) but attempted catalytic reduction caused gross decomposition.

¹Manuscript received November 29, 1960.

²Contribution from the Research Department, Merck and Co. Ltd., Montreal, Que.

³The compounds are being screened for anticancer activity at the Sloan-Kettering Institute for Cancer Research.



The oxidative chlorination of the 4-thiol (VII) yielded variable products. The desired sulphonyl chloride was obtained when the reaction temperature was maintained below 40° and the rate of addition of chlorine carefully controlled. Too rapid addition of chlorine at 20° or above resulted in the formation of 1-methyl-5-nitroimidazole-4-sulphonic acid (XI). Best results were obtained when the chlorine was added rapidly at 0° until the bright yellow starting material became white. The preparation was further complicated because the sulphonamide (XII) was isolated in two forms melting at 149° and 159° . Catalytic reduction of either form yielded the same amine. The oxidative chlorination of the other thiols (III) and (IX) gave good yields of the sulphonyl chlorides at 20° – 30° and 0° respectively.

There was a pronounced difference in stability between the amines. 4(5)-Amino-5(4)-sulphamylimidazole was so unstable that it was neither isolated as the base nor a salt. 4-Amino-1-methyl-5-sulphamylimidazole (VI) was an unstable base and formed a moderately stable hydrochloride. 5-Amino-1-methyl-4-sulphamylimidazole (VIII) was stable either as the base or as the hydrochloride.

EXPERIMENTAL

1-Methyl-4-mercapto-5-nitroimidazole (VII)

4-Chloro-1-methyl-5-nitroimidazole (11) (10 g) was suspended in a warm solution of water (67 ml) and concentrated ammonia (33 ml). Hydrogen sulphide gas was passed into the stirred mixture until a clear, dark red solution was obtained (20 minutes). The ammonium salt of the product crystallized on standing (9 g), m.p. 139° – 140° . Recrystallization by the addition of three volumes of isopropanol to a solution in a minimum volume of water yielded dark orange needles, m.p. 140° – 141° . Found: C, 27.4; H, 4.5; N, 31.1; S, 18.3. Calc. for $C_4H_8N_4O_2S$: C, 27.3; H, 4.5; N, 31.8; S, 18.2%.

4(5)-Nitro-5(4)-sulphamylimidazole (X)

The ammonium salt of 4(5)-mercapto-5(4)-nitroimidazole (5) (1 g) was suspended in 1 *N* hydrochloric acid (10 ml) and cooled in an ice bath. Chlorine gas was passed into the stirred mixture until the suspended solids became buff colored (35 minutes). The sulphonyl chloride produced (m.p. 180°–183°) was collected, washed with a little ice water, and dissolved in concentrated ammonia (10 ml). After 15 minutes the excess of ammonia was evaporated *in vacuo* and the residual solution was acidified with hydrochloric acid. The sulphonamide, which precipitated, was collected and crystallized from water as jagged white needles (0.4 g), m.p. 261°–262°. Found: C, 18.8; H, 2.1; N, 29.3; S, 16.9. Calc. for $C_5H_4N_4O_2S$: C, 18.8; H, 2.1; N, 29.2; S, 16.7%.

1-Methyl-5-nitro-4-sulphamylimidazole (XII)

The ammonium salt of 4-mercapto-1-methyl-5-nitroimidazole (VII) (5.0 g) treated in a similar manner yielded the sulphonyl chloride (m.p. 104°), which was converted into the sulphonamide (3 g), m.p. 158°–159°. Found: C, 23.3; H, 2.9; N, 27.5; S, 15.7. Calc. for $C_5H_6N_4O_2S$: C, 23.3; H, 2.9; N, 27.2; S, 15.5%. The product was also isolated in another form, m.p. 149°–150°. Found: C, 23.4; H, 3.0; N, 26.6; S, 15.5%.

From a similar experiment in which the temperature was allowed to reach 50° there was isolated the ammonium salt of 1-methyl-5-nitroimidazole-4-sulphonic acid (XI) m.p. 260°–265° (decomp.). Found: C, 21.4; H, 3.5; N, 25.0; S, 14.4. Calc. for $C_5H_8N_4O_5S$: C, 21.4; H, 3.6; N, 25.0; S, 14.3%. Acidification of a solution of the ammonium salt in water precipitated the acid m.p. 299°–300°. Found: C, 23.3; H, 2.4; N, 20.0; S, 15.5. Calc. for $C_5H_5N_4O_5S$: C, 23.2; H, 2.4; N, 20.3; S, 15.5%.

1-Methyl-4-nitro-5-sulphamylimidazole (V)

The ammonium salt of 5-mercapto-1-methyl-4-nitroimidazole (5) (22 g) by similar oxidative chlorination at 20°–30° yielded the sulphonyl chloride (m.p. 106°–107°), which was converted into the sulphonamide (16.5 g), m.p. 176°–177°. Found: C, 23.4; H, 3.0; N, 27.0; S, 15.3. Calc. for $C_6H_8N_4O_2S$: C, 23.3; H, 2.9; N, 27.2; S, 15.5%. The acetyl derivative was prepared by refluxing the sulphonamide for 1 hour in an excess of acetic anhydride. Crystallization from water yielded white needles m.p. 219°–220° (decomp.). Found: C, 29.0; H, 3.3; N, 22.7. Calc. for $C_8H_{10}N_4O_2S$: C, 29.0; H, 3.2; N, 22.6%.

4-Amino-1-methyl-5-sulphamylimidazole (VI)

A suspension of 1-methyl-4-nitro-5-sulphamylimidazole (5 g) and Adams' platinum catalyst (0.1 g) in dry ethanol (250 ml) was hydrogenated at room temperature and atmospheric pressure. The theoretical volume of hydrogen was absorbed in 1 hour and a white solid was precipitated. The solid and the catalyst were collected, washed with ether, and suspended in ethanol (125 ml). Concentrated hydrochloric acid (5 ml) was added, the amine was dissolved, and the catalyst was filtered off immediately with the aid of filtercel. The hydrochloride salt of the product crystallized on standing as cream needles (1.9 g), m.p. 180° (decomp.), with sintering at 140°–150°. Found: C, 20.6; H, 4.0; Cl, 15.6; N, 23.9; S, 14.0. Calc. for $C_5H_8N_4O_2S \cdot HCl \cdot H_2O$: C, 20.8; H, 4.8; Cl, 15.4; N, 24.3; S, 13.9%. Attempts to obtain the base were unsuccessful and the hydrochloride salt itself darkened and finally decomposed on long standing.

5-Amino-1-methyl-4-sulphamylimidazole (VIII)

Catalytic reduction of 1-methyl-5-nitro-4-sulphamylimidazole (5 g) in a similar manner yielded the hydrochloride salt of the product as white needles (4.2 g), m.p. 185°–187°

(decomp.). Found: C, 22.6; H, 4.2; N, 26.3; S, 15.4. Calc. for $C_4H_8N_4O_2S$, HCl: C, 22.6; H, 4.2; N, 26.3; S, 15.0%.

An aqueous solution of the hydrochloride salt on addition of an excess of ammonia precipitated the base as white needles m.p. 208°–210° (decomp.).

Reduction of 4(5)-nitro-5(4)-sulphamylimidazole (X)

Catalytic reduction of 4(5)-nitro-5(4)-sulphamylimidazole with Adams' platinum catalyst was attempted in both dry ethanol and in a mixture of glacial acetic acid and acetic anhydride. In each case the solution became dark brown as hydrogen was absorbed. No crystalline products were isolated.

Infrared Spectra

The infrared spectrum of each of the compounds reported was examined. The nitroimidazole sulphonamides showed bands in the regions of 1540 and 1350 cm^{-1} characteristic of the nitro-group and bands in the regions of 1300 and 1175 cm^{-1} characteristic of the sulphonamide group. Reduction of the nitro-compounds caused a disappearance of the bands in the regions of 1540 and 1350 cm^{-1} . The spectra of the aminoimidazole sulphonamides showed two bands in the regions of 3385 and 3315 cm^{-1} characteristic of primary amine stretching absorptions and a band in the region of 1660 cm^{-1} characteristic of primary amine deformation vibrations. The bands in the regions of 1300 and 1175 cm^{-1} characteristic of sulphonamides were still evident.

The determination and interpretation of the infrared spectra was carried out by Professor A. Taurins, Department of Chemistry, McGill University.

REFERENCES

1. M. P. SCHULMAN and J. M. BUCHANAN. *J. Biol. Chem.* **196**, 513 (1952).
2. G. R. GREENBERG. *Federation Proc.* **13**, 745 (1954).
3. B. LEVENBERG and J. M. BUCHANAN. *J. Am. Chem. Soc.* **78**, 504 (1956).
4. H. FRIEDMAN and A. G. MOAT. *Arch. Biochem. Biophys.* **78**, 146 (1958).
5. L. L. BENNETT, JR. and H. T. BAKER. *J. Am. Chem. Soc.* **79**, 2188 (1957).
6. G. R. BARNES and F. L. PYMAN. *J. Chem. Soc.* 2711 (1927).
7. R. FORSYTH, J. A. MOORE, and F. L. PYMAN. *J. Chem. Soc.* **125**, 919 (1924).
8. T. B. JOHNSON and J. M. SPRAGUE. *J. Am. Chem. Soc.* **58**, 1348 (1936).
9. U. S. Patent No. 2,603,649 (1952).
10. R. O. ROBLIN, JR. and J. W. CLAPP. *J. Am. Chem. Soc.* **72**, 4890 (1950).
11. J. SARASIN and E. WEGMANN. *Helv. Chim. Acta*, **7**, 713 (1924).

N.M.R. SPECTRA OF SOME α - β UNSATURATED ESTERS¹

ROBERT R. FRASER AND DONALD E. MCGREER

ABSTRACT

The results of analysis of methyl citraconate and mesaconate, methyl *cis*- and *trans*-crotonate, and methyl *cis*- and *trans*-2-pentenoate are reported. A previously reported analysis of the crotonates by first-order perturbation theory gave significantly different values for the 1,3 coupling constants. The discrepancy in results, which is due to the importance of second-order effects, emphasizes the need for caution in applying the first-order method. From values of 1,3 coupling constants reported here and elsewhere it is concluded that there is no simple relation between the magnitude of 1,3 coupling constants and geometrical configuration of the interacting nuclei.

Much attention has been devoted recently to the N.M.R. spectra of substituted propenes and butenes (1-7). Two aspects of the spectra have received special attention. The first is the magnitude of the 1,3 coupling constants.* Whipple *et al.* have reported 1,3 coupling to be consistently greater in the *trans* 2-substituted propenes ($J_{1,3 \text{ cis}}$) than in the *cis* isomers (2) ($J_{1,3 \text{ trans}}$). In tiglic and angelic acids and their methyl esters the opposite was found (1). Subsequently Jackman and Wiley (4) provided evidence which gave a different assignment to the protons of α -methacrolein from that of Whipple *et al.* and thus provided another case where $J_{1,3 \text{ trans}}$ was greater than $J_{1,3 \text{ cis}}$. The second aspect was the basis of Jackman's studies. He presented compelling evidence for the use of chemical shifts to assign configuration to α - β unsaturated esters. Among the compounds which he has studied were the methyl esters of mesaconic, citraconic, and *cis*- and *trans*-crotonic acids. We have examined these same four esters in addition to the methyl esters of *cis*- and *trans*-2-pentenoic acid. The more exact method of analysis employed in our case has provided some results of particular interest in this field.

Methyl Mesaconate and Methyl Citraconate

The olefinic and C-methyl protons in these esters comprise an AX_3 system. Analysis of such a system can be made by first-order perturbation theory. The complete results are listed in Table I. All coupling constants in this paper are reported with an estimated accuracy of ± 0.05 cycle/sec as the standard deviation of each measurement was ≤ 0.05 cycle/sec. The coupling constants in Table I are in agreement with those of Jackman and Wiley, who found values of 1.60 ± 0.07 for each isomer. All chemical shift measurements are reported as τ values (8).

TABLE I

Compound	Coupling constants		Chemical shifts		
	$J_{1,3 \text{ cis}}$	$J_{1,3 \text{ trans}}$	β -H	β -CH ₃	COOCH ₃
Methyl mesaconate	—	1.56	3.32	7.75	6.22, 6.27
Methyl citraconate	1.64	—	4.23	7.97	6.28, 6.32

¹Manuscript received October 17, 1960.

Joint contribution from the Departments of Chemistry of the University of Ottawa, Ottawa, Ontario, and the University of British Columbia, Vancouver, British Columbia.

*The term 1,3 coupling constant is used to denote the energy of interaction between protons separated by three carbon atoms.

Methyl cis-Crotonate and Methyl trans-Crotonate

The results of analysis by first-order perturbation theory and also by the ABX_3 treatment of Waugh and Fessenden (9) are given in Table II. The relative signs of the coupling constants in these compounds could not be conclusively established from the observed spectra. It was therefore assumed that $J_{1,3}$ has the opposite sign to $J_{1,2}$ and $J_{2,3}$. Both experimental evidence (9, 10, 11, 17) and theoretical calculations (6) on relative signs in olefinic compounds justify this assumption.

The spectrum of the olefinic and β -methyl protons of *cis* methyl crotonate is shown in Fig. 1 and illustrates the nearly first-order appearance of this spectrum. The slight

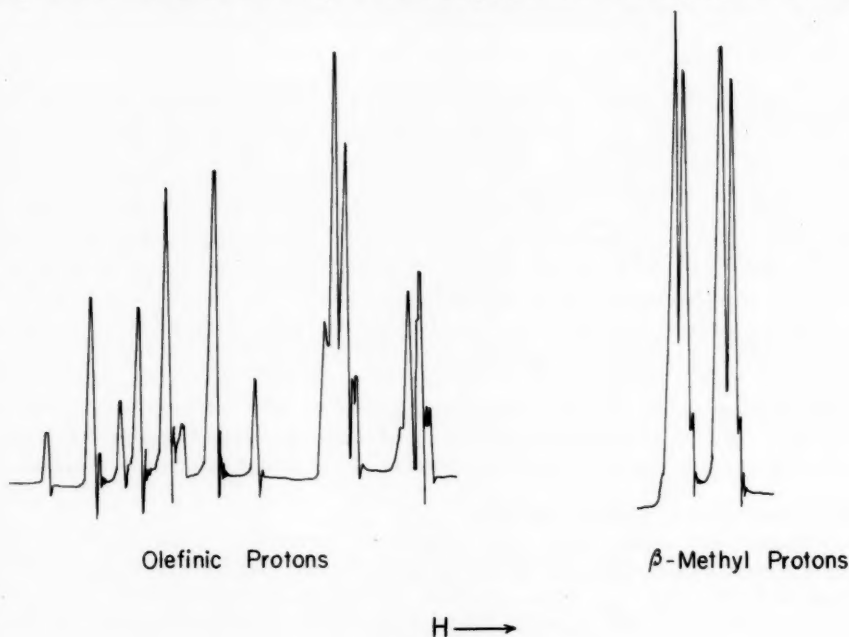


FIG. 1.

skewing of intensities is the only obvious indication of the mixing of proton spin states. Nevertheless, the observed splitting of the methyl group and the average of the three splittings in the weakly split quartets are 0.25 cycle/sec less than the actual interaction energy, $J_{1,3}$. While this error is usually, although not always, small in the determination of large coupling constants, it becomes important when dealing with the weaker long-range interactions. This effect, which was underestimated by one of us (R.R.F.) in the spectra of tiglic and angelic acids (1), emphasizes the need for caution in assuming first-order calculations to be applicable. Unfortunately exact analysis of the tiglic and angelic acids, which are A_3B_3X systems, is too tedious to warrant exact solution. Therefore the previously reported results for the coupling constants in tiglic and angelic acid and their esters must be considered as approximate. The results of first-order analysis of the crotonates agree with those of Jackman and Wiley. However, we found the values for the olefinic protons to be 0.15 p.p.m. to higher field.

TABLE II

Compound	1st order			ABX ₂			Chemical shifts			
	<i>J</i> _{1,3}	<i>J</i> _{1,2}	<i>J</i> _{2,3}	<i>J</i> _{1,3}	<i>J</i> _{1,2}	<i>J</i> _{2,3}	H ₁	H ₂	H ₃	H ₄
$ \begin{array}{c} \text{H(3)} \\ \\ \text{(1)CH}_2\text{---C=C---COOCH}_3\text{(4)} \\ \\ \text{(2)H} \end{array} $	-1.58	6.75	15.5	-1.67	6.85	15.5	8.12	3.10	4.24	6.33
$ \begin{array}{c} \text{COOCH}_3\text{(4)} \\ \\ \text{(1)CH}_2\text{---C=C---H(3)} \\ \\ \text{(2)H} \end{array} $	-1.57	7.03	11.4	-1.82	7.27	11.4	7.86	3.72	4.28	6.36

TABLE III

Compound	1st order			ABX ₂			Chemical shifts			
	<i>J</i> _{1,3}	<i>J</i> _{1,2}	<i>J</i> _{2,3}	<i>J</i> _{1,3}	<i>J</i> _{1,2}	<i>J</i> _{2,3}	H ₁	H ₂	H ₃	H ₄ C-CH ₃
$ \begin{array}{c} \text{CH}_3 \\ \\ \text{(1)CH}_2\text{---C=C---H(3)} \\ \quad \quad \\ \text{(2)H} \quad \text{COOCH}_3\text{(4)} \end{array} $	-1.60	6.26	15.6	-1.69	6.35	15.6	7.78	3.07	4.27	6.33 8.90
$ \begin{array}{c} \text{CH}_3 \\ \\ \text{(1)CH}_2\text{---C=C---COOCH}_3\text{(4)} \\ \quad \quad \\ \text{(2)H} \quad \text{H(3)} \end{array} $	-1.26	7.13	11.5	-1.56	7.43	11.5	7.35	3.83	4.35	6.36 8.95

Methyl cis-2-Pentenoate and Methyl trans-2-Pentenoate

The spectra of the pentenoates are further complicated by the presence of an extra methylene group. Analysis of the olefinic absorption was carried out by treating the olefinic and methylene protons as an ABX₂ system whose solution has been reported in detail by Mortimer (12). Again it was assumed that the sign of $J_{1,3}$ was opposite to that of the other coupling constants. By employing the ABX₂ method we have neglected two factors. First, the effect of the methyl group will be important if it is not sufficiently separated from the methylene protons. In the trans isomer, where this effect is greater, the J/δ ratio for the methyl-methylene interaction is <0.1 and therefore can be neglected. The possibility that the ABC₂ treatment should be employed was eliminated since the calculated second-order perturbation theory corrections (12), which were of the order of 0.02 cycle/sec, were negligible. The results are given in Table III.

DISCUSSION

It has been suggested that geometrical configuration might be the predominant factor in determining the relative magnitudes of $J_{1,3 \text{ cis}}$ and $J_{1,3 \text{ trans}}$ (1). It can be seen that in the three pairs of isomeric esters studied $J_{1,3 \text{ trans}}$ is equal to, greater than, and less than $J_{1,3 \text{ cis}}$. Furthermore Jackman and Wiley have found that in the 2-substituted propenes $J_{1,3 \text{ cis}} > J_{1,3 \text{ trans}}$ in all compounds except methacrolein whereas there was little or no difference in the magnitude of 1,3 couplings in five 1-substituted isobutenes (4). Since Whipple, Goldstein, and Mandell (2) had earlier made an assignment to the olefinic protons of methacrolein in opposition to Jackman and Wiley's rule we examined the effect of changing solvent on the spectrum of methacrolein* in order to confirm one assignment or the other. It was found that both olefinic protons were shifted by 0.88 p.p.m. to higher field in changing from cyclohexane to benzene, whereas the methyl shift was +0.56 p.p.m. Thus this method is not applicable to the assignment of proton structure in α -methacrolein and Jackman's assignment has been accepted.

From the work herein and that of Whipple *et al.* and Jackman and Wiley it is therefore clear that the geometrical configuration about the double bond will not determine the relative magnitude of 1,3 coupling constants. This does not mean that geometry is unimportant. Whipple, Goldstein, and McClure have shown that the coupling constants in 2,3-dihalopropenes vary with solvent composition (3) and have attributed this observation in a reasonable way to changes in geometry which result from a change in the population of conformations with change in solvent polarity.

EXPERIMENTAL

The spectra were obtained with a Varian V-4302 N.M.R. spectrometer at a frequency of 60 Mc/sec. Each measurement reported is the average of at least five determinations. Spectra for determination of coupling constants and chemical shifts were made on 40% (wt.:vol.) solutions in carbon tetrachloride. τ values were obtained from the spectra of 10% solutions in carbon tetrachloride containing 1% tetramethylsilane as internal reference. No difference in chemical shift at the two concentrations was observed.

The preparation of methyl *cis*- and *trans*-crotonate and methyl *cis*- and *trans*-2-pentenoate has been reported elsewhere (13, 14). Methyl citraconate and methyl mesaconate were prepared by conversion of itaconic acid to citraconic and mesaconic acids (15), followed by esterification to the known esters (16).

*Their assignment rested on the assumption that the preferential solvent shift of one olefinic proton and the methyl protons was approximately the same if the two were *cis*. This was applied to 2-chloropropene from which $J_{1,3 \text{ cis}}$ was found to be greater than $J_{1,3 \text{ trans}}$. From this observation assignments in other structures were made on the basis of the relative magnitudes of $J_{1,3 \text{ cis}}$ and $J_{1,3 \text{ trans}}$.

ACKNOWLEDGMENTS

The authors wish to thank the National Research Council for their grants-in-aid of research. The technical assistance of Mrs. V. Nicolson is gratefully acknowledged.

REFERENCES

1. R. R. FRASER. *Can. J. Chem.* **38**, 549 (1960).
2. E. B. WHIPPLE, J. H. GOLDSTEIN, and L. MANDELL. *J. Am. Chem. Soc.* **82**, 3010 (1960).
3. E. B. WHIPPLE, J. H. GOLDSTEIN, and G. R. MCCLURE. *J. Am. Chem. Soc.* **82**, 3812 (1960).
4. L. M. JACKMAN and R. H. WILEY. *J. Chem. Soc.* 2881 (1960).
5. L. M. JACKMAN and R. H. WILEY. *J. Chem. Soc.* 2886 (1960).
6. M. KARPLUS. *J. Am. Chem. Soc.* **82**, 4431 (1960).
7. R. A. HOFFMAN. *Mol. Phys.* **1**, 326 (1958).
8. G. V. D. TIERS. *J. Phys. Chem.* **62**, 1151 (1958).
9. R. W. FESSENDEN and J. S. WAUGH. *J. Chem. Phys.* **30**, 944 (1959).
10. S. ALEXANDER. *J. Chem. Phys.* **28**, 358 (1958).
11. J. A. ELVIDGE and L. M. JACKMAN. *Proc. Chem. Soc.* 89 (1959).
12. J. S. MORTIMER. *J. Mol. Spectroscopy*, **3**, 335 (1959).
13. D. E. MCGREER. *J. Org. Chem.* **25**, 852 (1960).
14. D. E. MCGREER, W. WAI, and G. CARMICHAEL. *Can. J. Chem.* **38**, 2410 (1960).
15. ORGANIC SYNTHESIS. *Coll. Vol. II*, pp. 140, 382.
16. L. VAN DER STRAETE. *Bull. classe sci., Acad. roy. Belg.* **21**, 226 (1935).
17. A. D. COHEN and N. SHEPPARD. *Proc. Roy. Soc. (London), A*, **252**, 488 (1959).

SPECTROPHOTOMETRIC STUDY OF THE REACTION BETWEEN IRON (III) AND KOJIC ACID¹

W. A. E. MCBRYDE² AND G. F. ATKINSON³

ABSTRACT

A method introduced by Vareille enables calculation of formation constants of colored metallic complexes in solution by making appropriate deductions from the presence of isobestic points in the spectra of suitably chosen solutions. The rationale of this method is derived rigorously, and its application extended to include cases where three complexes are present together in certain regions of pH. These principles are applied to derive for the ferric kojates the following formation constants, at 25° C and ionic strength 0.5: $\log K_1 = 10.16$, $\log K_2 = 8.29$, $\log K_3 = 6.90$. The relationship between pH and pL for the experimental conditions is calculated, thereby enabling the estimation of the distribution of the metal among the several species in each solution and the absorption spectrum of each complex.

INTRODUCTION

Vareille (1) has derived and applied a method for obtaining formation constants of metallic complexes which consists in measuring the absorption spectra of solutions of fixed total concentration of metal, $[M]_T$, and ligand, $[L]_T$, and of various pH's; and then in locating, if they are present, isobestic points at which three or more of the spectral curves intersect at a single wavelength. This author interprets the presence of such isobestic points as evidence of the metal being distributed in solution between not more than two species in the ranges of pH in which the isobestic points are found. If the identity of these particular species can be established, it is possible, as Vareille has shown, to deduce the equilibrium constants governing their interconversion. In the first part of this communication we offer a generalized discussion of the principle of the method, showing in particular the conditions necessary or desirable for its application. From this discussion it will be seen that the systems of complexes to which the method may be applied are limited to those which possess a moderately large spread in magnitudes of the successive formation constants. The three systems examined by Vareille are ideal in this respect; but in this paper it is shown that the method may be extended to sets of complexes with less favorable spacing of formation constants.

PRINCIPLE OF THE METHOD

Many of the experimental methods for deriving the formation constants of the successive complexes formed by a metallic ion and a ligand molecule or ion depend on finding corresponding values of \bar{n} , the degree of complex formation, and $[L]$, the molar concentration of free ligand. These are related to the formation constants of the several complexes by Bjerrum's formation function:

$$[1] \quad \bar{n} = \frac{\sum_1^N n\beta_n[L]^n}{1 + \sum_1^N \beta_n[L]^n}$$

¹Manuscript received November 1, 1960.

Contribution from the Department of Chemistry, University of Toronto, Toronto, Ont., and (in part) University of Waterloo, Waterloo, Ont.

²Present address: Department of Chemistry, University of Waterloo, Waterloo, Ontario.

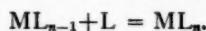
³Present address: Department of Chemistry, University of Western Ontario, London, Ontario.

In this,

β_n is a cumulative formation constant $= K_1 K_2 \dots K_n$

$$= \prod_{i=1}^n K_i$$

K_n is the equilibrium constant for the reaction



Following common practice, charges on individual species are omitted. The so-called equilibrium constants discussed in this paper are, with the exception of hydrogen ion, based on concentrations of the reacting species; they are therefore "formal" or "conditional" constants, applying in theory only to the medium in which they have been determined.

A plot of \bar{n} vs. pL ($= -\log [L]$) yields the formation curve for the system of complexes. From experimentally determined formation curves it is possible to extract the individual formation constants by various numerical methods. The shape of the formation curve depends on the relative magnitudes of the several K 's. Two distinct possibilities occur, and these are illustrated in Fig. 1, showing formation curves calculated by means of equation 1 and the appropriate formation constants for (a) the ferric 5-sulphosalicylates (one of the systems examined by Vareille), and (b) the ferric 5-sulpho-oxinates. The wide spacing in the constants for case (a) results in regions of pL in which each complex, ML , ML_2 , and ML_3 , has exclusive existence; and these correspond to the plateaux in this formation curve. Where the constants are not so widely spaced, as with case (b), the formation curve contains no plateau, and often shows only one point of inflection. For case (b) one may calculate that the quantity

$$[2] \quad \alpha_n = \frac{[ML_n]}{[M]_T} = \frac{\beta_n [L]^n}{1 + \beta_n [L]^n}$$

falls considerably short of the value unity for $n = 1$ or 2 , so that the metal can never exclusively be in the form of ML or ML_2 . This difference is illustrated for the same two sets of complexes in Fig. 2. Examination of these plots shows that, in case (a) only, as pL changes one complex gives way to another in such a way that no more than two species at a time make up practically the entire total concentration of metal.

For any system of metallic complexes with $\bar{n}_{\max} = 3$, such as the foregoing two examples, and such as commonly occurs with many of the bi- and ter-valent transition metals of co-ordination number 6 when coupled with bifunctional ligands to form chelate complexes, the solution may contain, in addition to free and protonated ligand, the following species containing metal: M , ML , ML_2 , and ML_3 . It might also contain protonated metallic species, e.g. MHL , or polynuclear species, e.g. M_2L_2 ; but these will be assumed absent for this description. By introducing the assumption that, at the wavelengths under consideration, the ligand or any protonated form of it absorbs no significant amount of radiation, we may write for the molar extinction coefficient of the solution, ϵ_M , calculated from the total concentration of metal,

$$[3] \quad \epsilon_M = \epsilon_0 \alpha_0 + \epsilon_1 \alpha_1 + \epsilon_2 \alpha_2 + \epsilon_3 \alpha_3$$

$$[4] \quad = \frac{\epsilon_0 + \epsilon_1 \beta_1 [L] + \epsilon_2 \beta_2 [L]^2 + \epsilon_3 \beta_3 [L]^3}{1 + \beta_1 [L] + \beta_2 [L]^2 + \beta_3 [L]^3}$$

in which α is defined by equation 2.

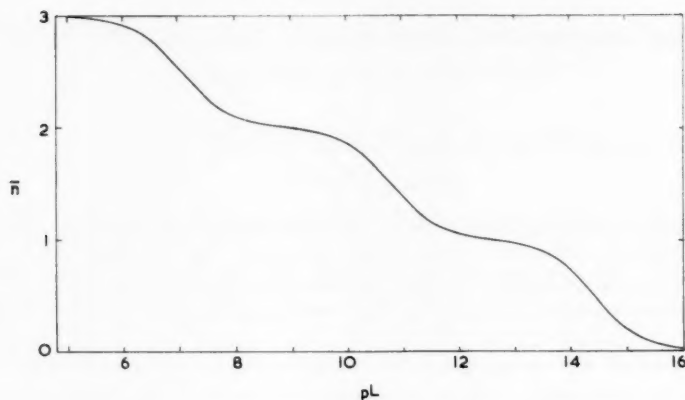


FIG. 1(a). Formation curve for the ferric sulphosalicylates.
 $\log K_1 = 14.42$ $\log K_2 = 10.76$ $\log K_3 = 7.06$

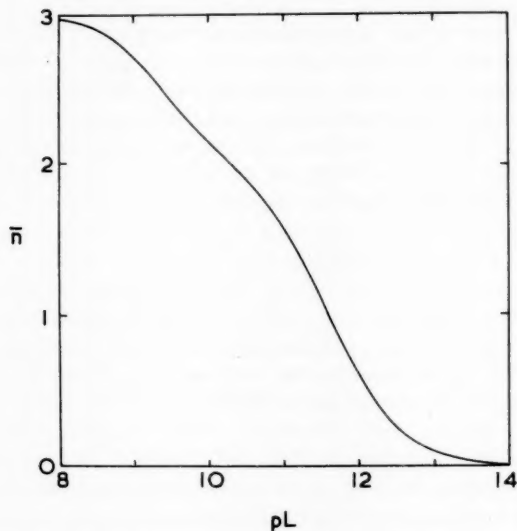


FIG. 1(b). Formation curve for the ferric sulpho-oxinates.
 $\log K_1 = 12.0$ $\log K_2 = 11.2$ $\log K_3 = 9.4$

If the spectra of a series of solutions of these complexes differing only in pL reveal one or more isobestic points, then, at the wavelengths at which these points occur, plots of ϵ_M vs. pL will show horizontal regions which, in the discussion following, we may refer to as isobestic regions. We may derive an expression for the value of $d\epsilon_M/dpL$, and inquire into the conditions that will give this expression the value zero. Differentiating equation 4 with respect to [L], and simplifying, we get:

$$\frac{d\epsilon_M}{d[L]} = \{ (\epsilon_1 - \epsilon_0)\beta_1 + 2(\epsilon_2 - \epsilon_0)\beta_2[L] + 3(\epsilon_3 - \epsilon_0)\beta_3[L]^2 + (\epsilon_2 - \epsilon_1)\beta_1\beta_2[L]^2 \\ + 2(\epsilon_3 - \epsilon_1)\beta_1\beta_3[L]^3 + (\epsilon_3 - \epsilon_2)\beta_2\beta_3[L]^4 \} (1 + \beta_1[L] + \beta_2[L]^2 + \beta_3[L]^3)^{-2}$$

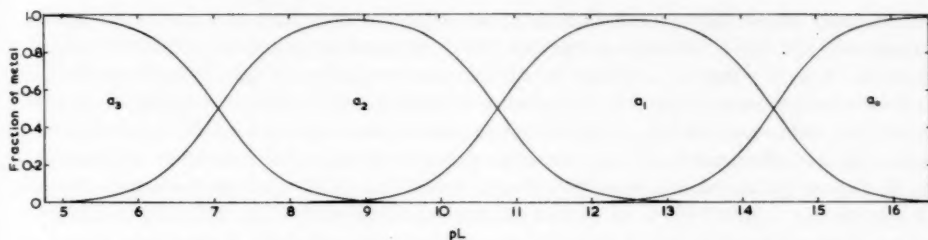


FIG. 2(a). Distribution of metal among simple and complex species: iron (III) + 5-sulphosalicylic acid.

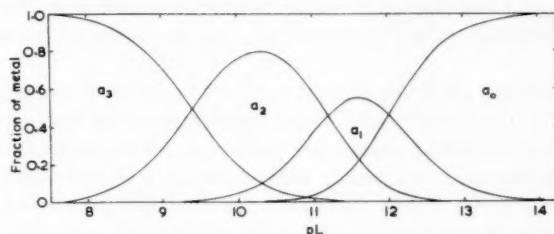


FIG. 2(b). Distribution of metal among simple and complex species: iron (III) + 8-hydroxyquinoline-5-sulphonic acid.

Multiplying both sides by $[L]$, and applying equation 2, this becomes

$$[5] \quad -0.4343 \frac{d\epsilon_M}{dpL} = (\epsilon_1 - \epsilon_0)\alpha_0\alpha_1 + 2(\epsilon_2 - \epsilon_0)\alpha_0\alpha_2 + 3(\epsilon_3 - \epsilon_0)\alpha_0\alpha_3 + (\epsilon_2 - \epsilon_1)\alpha_1\alpha_2 + 2(\epsilon_3 - \epsilon_1)\alpha_1\alpha_3 + (\epsilon_3 - \epsilon_2)\alpha_2\alpha_3.$$

The expression on the right side of this equation will be zero if any one of the values of α becomes unity, since then the other three must be zero. This corresponds to the fact that ϵ_M will not change with pL as long as all the metal is present as a single constituent in solution. The same expression will be zero given the concurrence of any of the following pairs of relationships:

[6a]	$\epsilon_0 = \epsilon_1$	and	$\alpha_0 + \alpha_1 \sim 1$
[6b]	$\epsilon_1 = \epsilon_2$	and	$\alpha_1 + \alpha_2 \sim 1$
[6c]	$\epsilon_2 = \epsilon_3$	and	$\alpha_2 + \alpha_3 \sim 1$
[7a]	$\epsilon_0 = \epsilon_1 = \epsilon_2$	and	$\alpha_0 + \alpha_1 + \alpha_2 \sim 1$
[7b]	$\epsilon_1 = \epsilon_2 = \epsilon_3$	and	$\alpha_1 + \alpha_2 + \alpha_3 \sim 1$

These are the conditions necessary for the generation of isobestic points in a series of absorption spectra of solutions differing only in pL .

The left-hand equations in 6 and 7 depend on wavelength only, and imply that each metallic species must obey Beer's law. The right-hand equations in each pair are independent of wavelength, but do depend on pL . From Fig. 2 it is seen that the relationships given by the right-hand members of the pairs of equations 6a, b, c are actually found for the ferric sulphosalicylates over practically the entire range of pL depicted. However, for the ferric sulpho-oxinates the same conditions are found only within comparatively narrow ranges of pL , especially that corresponding to equation 6b. Instead, for these complexes, the relationships of equations 7a, b are seen to obtain over most of the range of pL shown.

One may reasonably expect that any two adjacent members of a series of metallic complexes will have absorption spectra that intersect at some wavelength (see, for example, Fig. 6); that is, at some particular wavelength $\epsilon_n = \epsilon_{n+1}$. For as many such intersections as occur there will be corresponding isobestic points in a group of spectral curves for solutions differing only in pL, provided that the spacing of formation constants insures adherence to the relationships given by the right-hand members of equations 6a, b, c over moderate ranges of pL. For isobestic points to occur in a system of complexes having a distribution of species such as that shown in Fig. 2(b) is possible only within the narrow regions of pL in which equations 6a, b, c are valid. Where only equations 7a, b apply, the occurrence of isobestic points would require that three ionic species of differing complexity have the same molar extinction coefficient (not zero) at one wavelength; this possibility cannot be ruled out, but it seems to be exceedingly improbable.

In the systems of ferric complexes studied by Vareille, as well as in that considered in this paper, $\epsilon_0 \sim 0$ at the wavelengths under consideration, so that equation 6a does not apply and only two isobestic points are observed. All three sets of complexes in Vareille's work possess formation constants widely enough spaced so that the individual species are distributed as shown in Fig. 2(a). Thus as \bar{n} increases the species ML essentially disappears from the solution before ML_3 forms in appreciable concentration. Also, the isobestic region for $\epsilon_1 = \epsilon_2$ ends at about the same pL (actually pH, but see below) as that for $\epsilon_2 = \epsilon_3$ begins; at this pL the metal is present almost exclusively as ML_2 . At some wavelength (λ_{12}) $\epsilon_1 = \epsilon_2$; and a plot of ϵ_M vs. pL will show a horizontal region in which $\epsilon_M = \epsilon_1 = \epsilon_2$, and also, at lower pL, a horizontal region in which $\epsilon_M = \epsilon_3$. Between these horizontal regions there will be a skew-shaped curve in which $\epsilon_M = \epsilon_2\alpha_2 + \epsilon_3\alpha_3$. For the value of $\epsilon_M = \frac{1}{2}(\epsilon_2 + \epsilon_3)$ the corresponding value of pL = log K_3 . Similarly at another wavelength (λ_{23}) $\epsilon_2 = \epsilon_3$; and when ϵ_M is plotted against pL two horizontal regions are noted, one in which $\epsilon_M = \epsilon_1$ and the other where $\epsilon_M = \epsilon_2 = \epsilon_3$. Between these horizontal regions $\epsilon_M = \epsilon_1\alpha_1 + \epsilon_2\alpha_2$, and the value of pL corresponding to $\epsilon_M = \frac{1}{2}(\epsilon_1 + \epsilon_2)$ is the value of log K_2 . The identity between pL and log K in these two instances is based on the assumption that the logarithmic term in

$$\log K_n = pL + \log \frac{[ML_n]}{[ML_{n-1}]}$$

is zero when $\epsilon_M = \frac{1}{2}(\epsilon_n + \epsilon_{n-1})$. However, this assumption is only valid if $\alpha_n + \alpha_{n-1} \sim 1$, that is, if the solution contains the metal in no more than two complex species in the region of pL in which ϵ_M is changing. It is evident, then, that Vareille's procedure for obtaining K_2 or K_3 cannot be applied without modification to sets of complexes in which the several species are distributed as portrayed in Fig. 2(b). Before introducing a proposal for dealing with such systems of complexes we must comment on the relationship between pL and pH in these solutions.

The majority of the ligands whose attachment to metallic ions is of interest are bases, i.e. proton acceptors, in aqueous solution. Accordingly there is frequently competition between metallic ions and protons for combination with a given ligand. We may derive a relationship between pL and pH in solutions of such complex species, provided we know the relevant equilibrium constants, by the following general equation:

$$[8] \quad [L]_T = [L] \left(1 + \frac{[H]}{K_I} + \frac{[H]^2}{K_I K_{II}} \dots \right) + \bar{n}[M]_T.$$

(The acid dissociation constants, in order of increasing degree of protonation, are K_I , K_{II} , etc.) Corresponding values of pL and pH for a given $[M]_T$ and $[L]_T$ have been

calculated for solutions of the ferric kojates, and are shown graphically in Fig. 5. For purposes of the present discussion it is sufficient to remark that, for fixed total concentrations of metal and ligand, there must be curves similar in shape to those of Fig. 2 showing the relationship between pH and the fractions of metal in the various species. Experimentally pH is usually more readily measured than pL, and any observed shift of absorption spectra then considered as a function of pH. The occurrence of isobestic points among such spectra will result in horizontal regions in a plot of ϵ_M vs. pH. It is in this form that Varelle's data and ours are shown.

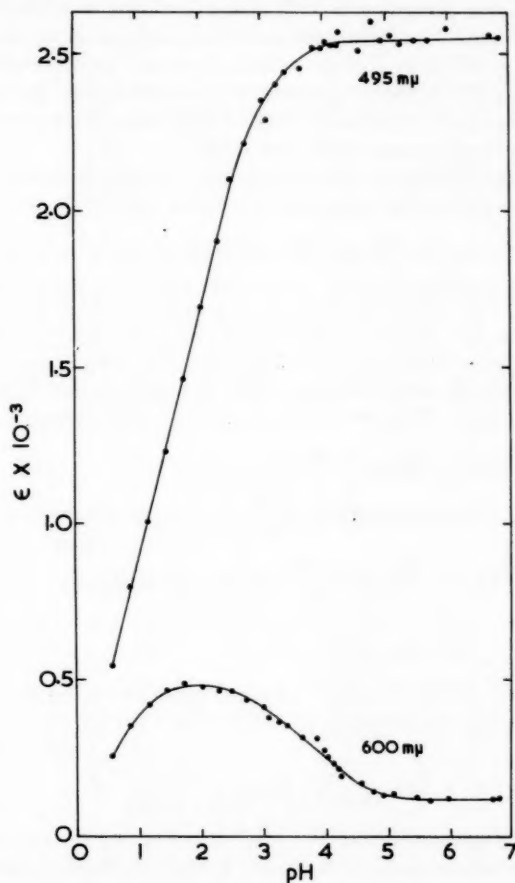


FIG. 3. Varelle curves, showing variation of molar extinction coefficient at isobestic wavelengths with pH.

Considering now the results of our experiments with the ferric kojates, we have confirmed the occurrence of isobestic points, first shown in the spectra published by Moss and Mellon (4), at 495 mμ and at 600 mμ. We have also confirmed, by the method of continuous variations, Moss and Mellon's finding that the complex formed at the highest pH is ML_3 ; we have assumed, by analogy with a great many other sets of ferric complexes, that with decreasing pH the species present are ML_2 and ML . We show in Fig. 3 our values of ϵ_M at the isobestic wavelengths plotted against pH. From the horizontal regions in these curves we may deduce as follows:

(i) above pH 5.2 only one species is present: $[M]_T = [ML_3]$; and at $600 \text{ m}\mu$ $\epsilon_3 = 120 \text{ M}^{-1} \text{ cm}^{-1}$.

(ii) between pH 4.0 and 5.2 $[M]_T = [ML_2] + [ML_3]$; and at $495 \text{ m}\mu$ $\epsilon_2 = \epsilon_3 = 2540$.

(iii) between pH 1.45 and 2.50 $[M]_T = [ML] + [ML_2]$; and at $600 \text{ m}\mu$ $\epsilon_1 = \epsilon_2 = 470$. The absence of any isobestic region between pH 2.50 and 3.85 indicates that in this region $[M]_T = [ML] + [ML_2] + [ML_3]$. This is a difference from the cases investigated by Vareille, and presumably indicates a distribution of species similar to that shown in Fig. 2(b).

The consequence of the foregoing is that, for calculating equilibrium constants, we could not assume as Vareille had done that, at the mid-points of the curved portions of these plots, $[ML_3] = [ML_2]$ or $[ML_2] = [ML]$. Instead, we were obliged to estimate our formation constants by a series of successive approximations; the rapid convergence of the values for the constants with each cycle of approximations encouraged the belief that our extension of Vareille's procedure was valid.

The experimental data permitted calculation, not of the formation constants of the complexes, but of the equilibrium constants for the reaction



and we designate these constants as \mathcal{K}_n . The method of evaluating these is now shown in detail.

Evaluation of \mathcal{K}_3

At pH 3.73 the value of ϵ_M at $600 \text{ m}\mu = 295 = \frac{1}{2}(\epsilon_2 + \epsilon_3)$. At this pH the solution may contain ML, ML_2 , and ML_3 , but since $\epsilon_1 = \epsilon_2$ we may put

$$\begin{aligned} [9] \quad [ML_3] &= [ML_2] + [ML] \\ &= [ML_2] \left(1 + \frac{[H]}{\mathcal{K}_2[HL]} \right) \end{aligned}$$

$$[10] \quad [HL] = \frac{[HL]_T - \bar{n}[M]_T}{1 + K_a/[H]} \sim [HL]_T - \bar{n}[M]_T$$

$$[11] \quad \bar{n} = \frac{5 + \frac{4[H]}{\mathcal{K}_2[HL]}}{2 + \frac{2[H]}{\mathcal{K}_2[HL]}}$$

$$[12] \quad \mathcal{K}_3 = \left(1 + \frac{[H]}{\mathcal{K}_2[HL]} \right) \left(\frac{[H]}{[HL]_T - \bar{n}[M]_T} \right).$$

The value of \mathcal{K}_3 thus depends on the value of \mathcal{K}_2 obtained by the method described below. A cycle of approximations is introduced to find the best values of \bar{n} and $[HL]$. This is begun by putting $\bar{n} = 2.5$ into equation 10, and the consequent value of $[HL]$ into equation 11. When these values became constant, \mathcal{K}_3 was calculated by equation 12.

Evaluation of \mathcal{K}_2

For this purpose Vareille found the pH at which $\epsilon_M = \frac{1}{2}(\epsilon_1 + \epsilon_2)$, and at which $[ML] = [ML_2]$. Our data give no direct indication of ϵ_1 , so that we have had to estimate this quantity in order to calculate \mathcal{K}_2 . Subsequently, with the aid of this value of \mathcal{K}_2 , we were able to refine our estimate of ϵ_1 . This cycle of approximations was repeated until constant values were obtained.

The lower limit of the isobestic region at 600 $m\mu$, corresponding to $\epsilon_1 = \epsilon_2$ and $\alpha_1 + \alpha_2 = 1$, occurs at pH 1.45. If, at this pH, α_1 became nearly unity we should have observed some horizontal region in the plot of ϵ_M vs. pH at 495 $m\mu$; it was, in fact, from just such a horizontal that Vareille took his value of ϵ_1 . We must assume for our solutions that, at and below pH 1.45, some ML_2 remains in solution. For all solutions below pH 2.5 we may write $\epsilon_M = \epsilon_1\alpha_1 + \epsilon_2\alpha_2$, and for 495 $m\mu$ this becomes

$$[13] \quad \epsilon_1 = \frac{\epsilon_M - 2540\alpha_2}{\alpha_1}.$$

The following data apply to the solutions of low pH.

pH	ϵ_M (600 $m\mu$)	ϵ_M (495 $m\mu$)	$\alpha_1 + \alpha_2$
1.45	463	1230	1
0.57	254	545	0.548
0.86	350	794	0.758

Somewhat arbitrarily, in order to make an estimate of \mathcal{K}_2 , we put ϵ_1 at 495 $m\mu = 1100$ as a trial value.

Now, while at pH 1.45 ($\alpha_1 + \alpha_2$) = 1, at any pH below this ($\alpha_1 + \alpha_2$) < 1; and its value is given by the ratio of ϵ_M at this pH to ϵ_M at pH 1.45 measured at 600 $m\mu$. In this way we get the values in the last column of the above table. But $\alpha_1 + \alpha_2 = \alpha_1[1 + (\mathcal{K}_2[HL]/[H])]$, and $[ML] + [ML_2] = (\alpha_1 + \alpha_2)[M]_T = [ML]\{1 + \mathcal{K}_2[HL]/[H]\}$. The conservation equation for L is

$$[14] \quad [HL]_T = [L] + [HL] + [ML] + 2[ML_2] + 3[ML_3]$$

in which, for these solutions, the first and last terms on the right-hand side are relatively negligible. Hence we put

$$[15] \quad \begin{aligned} [HL] &= [HL]_T - [ML] - 2[ML_2] \\ &= [HL]_T - [ML] - 2([M]_T - [M] - [ML]) \\ &= [HL]_T + [ML] - 2[M]_T + 2[M]. \end{aligned}$$

The first estimate of $[HL]$ was made by temporarily assuming $[ML_2] = 0$, and assigning $[ML]$ the value calculated for $([ML] + [ML_2])$. Subsequent estimates were made using trial values of \mathcal{K}_2 , since

$$[16] \quad [ML] = \frac{[ML] + [ML_2]}{1 + \mathcal{K}_2([HL]/[H])}.$$

The calculations quickly showed that the trial value of ϵ_1 had been too high, causing the first estimate of \mathcal{K}_2 to be too low.

The validity of this method of calculating \mathcal{K}_2 rests upon the inference from the isobestic region at 600 $m\mu$ that, at the pH at which $\epsilon_M = \frac{1}{2}(\epsilon_1 + \epsilon_2)$, the metal in solution is present in only the two species, ML and ML_2 .

Evaluation of \mathcal{K}_1

Once a steady value for $[HL]$ in the solutions of pH 0.57 and 0.86 had been obtained from equations 15 and 16, and for $[ML]$ from equation 16, the quantities in the expression for \mathcal{K}_1 could all be evaluated. In this way two estimates of this constant were obtained.

A third estimate, from the solution at pH 1.16, was not considered as reliable since, in this solution, the quantity $[M]$ is obtained as a difference of two similar magnitudes.

The foregoing development of the principles underlying this method of obtaining formation constants of metal complexes does not support Vareille's claim that points of inflection on a plot of λ_{\max} vs. pH will indicate values of pH at which two metallic species are present in equal concentrations.

We may summarize the conditions and assumptions required by this method:

(i) Each metallic complex must have distinctively different absorption spectra, and different also from the simple metallic ion. The spectral curves of each adjacent species must cross at some wavelength in order that an isobestic point may be generated.

(ii) The ligand and its protonated forms must show negligible absorption in the range of wavelengths considered.

(iii) Beer's law must be obeyed by all the metallic species.

(iv) Protonated or polynuclear species must not form to any appreciable extent.

(v) The formation constants sought must be widely enough separated that regions of pH (or pL) shall occur in which the metal is distributed between only two of the possible species at a time. In the method as originally described by Vareille it is a requirement that at some pH practically all of the metal should be present as a single one of the various possible species.

(vi) Since the mass law must be applied, at least in part, to concentrations, measurements should be made in solutions of constant and preferably moderately high ionic strength.

EXPERIMENTAL

Reagents

Kojic acid of purity suitable for this investigation was not found commercially. The available material, consisting of one lot purchased from Matheson, Coleman, and Bell, and a second generously contributed by Charles Pfizer and Co., was purified as follows. The crude acid was recrystallized once from a minimum of hot water. The resulting yellow, crystalline mass was then subjected to two, or in some cases three, extractions with warm ether in a modified Soxhlet apparatus. White needlelike crystals accumulated in the pot, and were from time to time removed by filtration, washed with ether, and air-dried. Product of acceptable purity was dead-white, with m.p. $152-3^{\circ}\text{C}$ (uncorrected), and neutralization equivalent 142. Aqueous solutions of this material retained full potency in reaction with ferric salts for at least a week, and showed no darkening on standing. Off-white crystals obtained after one, or in some cases two, extractions gave drifting pH values when titrated in aqueous solutions with alkali (see below), and the aqueous solutions became yellow on standing.

The following solutions were prepared from analytical reagent grade chemicals (except for chloracetic acid), and standardized as noted:

Ferric nitrate, $2 \times 10^{-3} M + 8 \times 10^{-3} M$ in HNO_3 , standardized gravimetrically as Fe_2O_3 ,

Sodium hydroxide, 0.25 M , carbonate-free, standardized titrimetrically with potassium hydrogen phthalate,

Potassium nitrate, 1.25 M , by direct weighing,

Acetic acid, 0.25 M , standardized titrimetrically with 0.25 M alkali,

Chloracetic acid, 0.25 M , prepared from Eastman White Label reagent, passed through a $\frac{1}{2} \times 24$ in. column of Dowex-50 in the hydrogen form, then standardized titrimetrically with 0.25 M alkali,

Hexamethylenetetramine, 0.25 *M*, by direct weighing,
Nitric acid, 0.50 *M*, standardized titrimetrically with 0.25 *M* alkali,
Potassium tetroxalate, 0.05 *M*, standard for pH 1.67 (25° C),
Potassium hydrogen phthalate, 0.05 *M*, standard for pH 4.00,
Sodium tetraborate decahydrate, 0.05 *M*, standard for pH 9.18,
Radiometer buffer, diluted 1 to 25 from concentrate, standard for pH 6.50.

Apparatus

Optical densities of solutions were measured with a Beckman Model DU spectrophotometer in matched Corex-glass cells of 1-cm path length. The cell compartment was enclosed by thermospacers through which water thermostatted at 25.0° C was circulated.

Measurements of pH were made with commercially available glass and calomel electrodes fitted to either a Beckman Model G or a Radiometer Model 22 meter. The meter assembly was standardized by the buffer solution of pH closest to the range being examined, and the response of the glass electrode was routinely checked by one or two other buffer solutions; this calibration was repeated hourly during periods while pH measurements were being made.

Ionization Constant of Kojic Acid

Aqueous solutions containing accurately weighed portions of purified acid dissolved in known amounts of freshly boiled and cooled doubly distilled water were titrated with standard alkali. The pH was observed throughout the titration, and from 10 points on the titration curve (between 15% and 85% neutralization) values of pK_a calculated by means of the Henderson equation. The end point in the titration was also determined, and a neutralization equivalent for the acid calculated. To examine the influence of ionic strength on the value of pK_a , weighed portions of potassium nitrate were introduced into most of the solutions prior to titration. The ionic strength obviously varies throughout the titration; the value recorded is based on the amount of salts present when the acid is half neutralized.

It was found that substantial drifting toward lower pH values occurred during titration of any sample of the kojic acid that was not pure white, and that in such titrations the solution became somewhat amber as the sample became alkaline. The cause of this observation is not known.

Spectral Curves

A considerable number of solutions were prepared containing fixed amounts of ferric nitrate and kojic acid, various amounts of acid, alkali, or buffers, as noted below, to give a distribution of pH values from 0.57 to 6.82, and a sufficient amount of potassium nitrate to give a final ionic strength of 0.5. These solutions were all made up to known volume and allowed to stand at room temperature (23 to 26° C) for 1 hour. The optical density of each was then measured at intervals of 10 $m\mu$ from 350 $m\mu$ to 700 $m\mu$. Immediately after the spectrum of each solution was obtained, its pH was measured.

Regulation of pH in these solutions was secured by the addition of the following reagents:

- pH 0.57 to 3.01: varying amounts of HNO_3 ,
- 2.03 to 3.40: 0.10 *M* $CH_2ClCOOH$ + varying amounts of NaOH,
- 3.20 to 5.73: 0.10 *M* CH_3COOH + varying amounts of NaOH,
- 3.09 to 3.62: varying small amounts of NaOH,
- 3.85 to 6.82: 0.10 *M* hexamine + varying amounts of HNO_3 .

Continuous Variations

A series of 12 solutions was prepared from a (different) standard iron solution and a kojic acid solution in various proportions adjusted so that the total molarity of these remained constant. In our experiments $[M]_T + [HL]_T = 0.001$, and of this molarity the fraction of iron varied from 0.03 to 0.58. Each solution was buffered by the addition of a fixed amount of sodium acetate and varying amounts of nitric acid to a pH of 5.1 ± 0.2 , and contained sufficient potassium nitrate to make the total ionic strength 0.5. The optical density of each solution was measured, and the values plotted against "mole fraction" of iron in the solution.

RESULTS AND DISCUSSION

Ionization Constant of Kojic Acid

Table I gives the values of pK_a found at the various ionic strengths investigated. Graphical extrapolation to zero ionic strength suggests a value of 7.88 for pK_a and this may provisionally be taken as the thermodynamic constant. The variation in pK_a with ionic strength may be largely accounted for by the variation in activity coefficient of the kojate ion, the magnitude of which, from the above measurements, appears to be comparable to those of other univalent ions. Okáč (5) has reported the value 7.75 for this constant.

As all solutions of the ferric kojates studied absorptiometrically were prepared to be of ionic strength 0.5, the value 7.73 was taken for pK_a when calculating their formation constants.

TABLE I
Ionization constant of kojic acid

Ionic strength	pK_a
0.03	7.83 ± 0.007
0.23	7.77 ± 0.005
0.53	7.73 ± 0.005
1.03	7.81 ± 0.007

Isobestic Points and Vaireille Curves

Moss and Mellon (4) have given spectra for solutions containing fixed concentrations of iron (III) and kojic acid but differing in pH, and these show isobestic points at 495 $m\mu$ and 600 $m\mu$. The spectra of our solutions that do not contain acetate or chloroacetate confirm theirs, including the same isobestic points. In Fig. 3 we show our values of ϵ_M at these two wavelengths for all these solutions. The interpretation of the various regions of these curves has been discussed previously.

Composition of Highest Complex

In the absence of acetate the spectra of the ferric kojate solutions was not altered by increasing the pH above 5. We assume that at and above this pH the maximum co-ordination of kojate ion has occurred. The experiment applying the method of continuous variations (6) showed maximum optical density when the "mole fraction" of iron in the prepared solutions was 0.25. This shows that the complex of maximum co-ordination is ML_3 , as is the case with many other phenolic reagents capable of chelation to the metal. The same observation has been recorded by Moss and Mellon (4).

Formation Constants of Complexes

The method of deriving the equilibrium constants, \mathcal{K}_n , from the data of Fig. 3 has been described previously. For all these solutions $[M]_T = 2.05 \times 10^{-4}$ and $[L]_T = 15.00 \times 10^{-4} M$. The first calculation was that of \mathcal{K}_2 , based on the initial assumption that ϵ_1 (495 m μ) = 1100. The successive estimates were:

ϵ_1 (495 m μ)	Mid-point pH	\mathcal{K}_2
1100 (assumed)	2.18	5.53
964	2.10	6.65
946	2.09	6.82
946	2.09	6.82

The estimation of \mathcal{K}_1 and ϵ_1 was based on the following data:

Points	[H]	[ML] + [ML ₂]	[M]	[HL]
1	2.70×10^{-1}	1.12×10^{-4}	0.93×10^{-4}	$12.76 \times 10^{-4} + [ML]$
2	1.38×10^{-1}	1.55×10^{-4}	0.50×10^{-4}	$11.90 \times 10^{-4} + [ML]$

Refinement in the value of ϵ_1 resulted from changes in the value of [ML], which in turn depended on the value assigned to \mathcal{K}_2 . The successive values obtained in these calculations were:

Point 1				Point 2			
α_1	α_2	ϵ_1	\mathcal{K}_1	α_1	α_2	ϵ_1	\mathcal{K}_1
0.534	0.014	954	229	0.719	0.039	973	304
0.530	0.018	942	227	0.712	0.046	951	301
0.530	0.018	942	227	0.711	0.047	950	301

The average value of \mathcal{K}_1 was taken as 264.

The solution of equations 10 and 11, beginning with the trial value $\bar{n} = 2.5$, led to steady values at pH 3.73 of $[HL] = 9.90 \times 10^{-4}$ and $\bar{n} = 2.49$. Putting these values, and the final value of $\mathcal{K}_2 = 6.82$, into equation 12, gave $\mathcal{K}_1 = 0.191$.

To transform these equilibrium constants into formation constants, as more commonly are reported for metallic complexes we employ the relationship:

$$\log K_n = \log \mathcal{K}_n + pK_a.$$

From this the following values were obtained: $\log K_1 = 10.16$, $\log K_2 = 8.29$, and $\log K_3 = 6.90$. Previous values determined for these constants are assembled in Table II, with the present values for comparison.

TABLE II
Formation constants for ferric kojate complexes

	$\log K_1$	$\log K_2$	$\log K_3$	Ref.
Okáč, Sommer, Rády	3.13	3.99	4.00	(7)
Okáč, Kolařík	9.2	8.0	7.2	(5)
This work	10.16	8.29	6.90	—

The values of Okáč, Sommer, and Rády, which differ signally from the other two, were obtained by the method of continuous variations. Various authors, especially Woldbye (8), have criticized the application of this method to the measurement of formation constants whenever the possibility arises of one complex passing gradually into the next as the ligand concentration is gradually increased. From the formation curve of the ferric kojates, calculated from our constants with equation 1, shown as Fig. 4, it is apparent that such will be the case with these complexes.

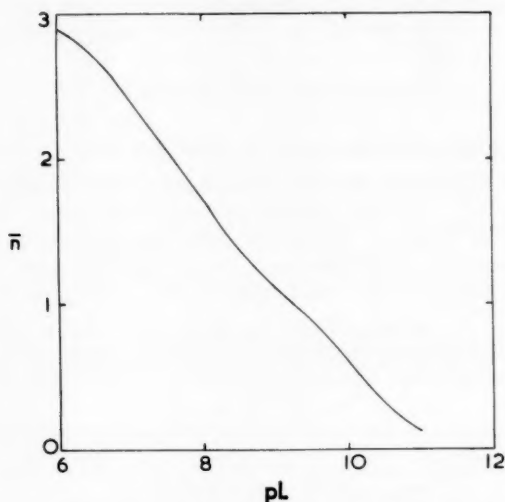


FIG. 4. Formation curve for the ferric kojates calculated from formation constants derived from this investigation.

In order to test the consistency between the conclusions drawn from Fig. 3 and the implications of the formation curve, we have calculated the relationship between pH and pL for our experimental solutions. For each value of pL at which a point on the formation curve was calculated, a value of pH was also obtained by means of equation 17

$$[17] \quad 1 + \frac{[H]}{K_a} = \frac{[L]_T - \bar{n}[M]_T}{[L]}$$

The results of these calculations are summarized in Table III, and shown graphically in Figs. 4 and 5.

Spectra of Single Complex Species

Since the spectra of a number of solutions of the ferric kojate complexes were available, and since the knowledge of the formation constants of these makes possible a calculation of their individual concentrations in the various solutions prepared, we undertook to extract from our data values of the molar extinction coefficients of the individual complexes. For these solutions, whose pH had been measured, a value of pL could be secured from Fig. 5, and with this, values of \bar{n} , α_0 , α_1 , etc. calculated. In the solution of highest pH, $\alpha_3 = 1$, and values of ϵ_3 were immediately available. In the solution of lowest pH the principal absorbing species was ML, but $\alpha_2 \sim 0.01$, so that a small contribution

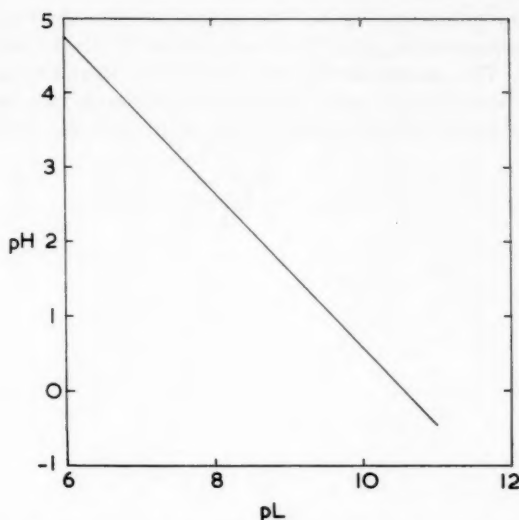


FIG. 5. Relationship between pL and pH for experimental conditions of this investigation

$$[M]_T = 2.05 \times 10^{-4} \text{ molar.}$$

$$[L]_T = 15.00 \times 10^{-4} \text{ molar.}$$

TABLE III
Formation curve for ferric kojates

pL	\bar{n}	α_0	α_1	α_2	α_3	pH
11.0	0.126	0.877	0.123	—	—	-0.44
10.7	0.224	0.776	0.224	—	—	-0.13
10.3	0.420	0.580	0.420	—	—	0.28
10.0	0.607	0.405	0.585	0.010	—	0.59
9.7	0.778	0.250	0.722	0.028	—	0.90
9.3	0.968	0.112	0.808	0.079	—	1.32
9.0	1.10	0.054	0.790	0.154	0.001	1.63
8.7	1.26	0.024	0.700	0.272	0.004	1.94
8.3	1.49	0.007	0.492	0.482	0.019	2.35
8.0	1.72 ₅	0.002	0.322	0.626	0.050	2.67
7.7	1.93	—	0.182	0.707	0.112	2.99
7.3	2.20	—	0.068	0.666	0.266	3.41
7.0	2.38	—	0.028	0.542	0.430	3.73
6.7	2.60	—	0.010	0.384	0.606	4.05
6.3	2.79 ₅	—	0.002	0.200	0.798	4.46
6.0	2.89	—	—	0.112	0.888	4.77

from ML_2 was included in the observed spectrum. A first estimate of ϵ_1 was made from the spectrum of this solution, neglecting the contribution of ϵ_2 . Later, when a value of ϵ_2 had been extracted, a second, modified estimate of ϵ_1 was calculated with equation 3.

The estimate of ϵ_2 was, in this case, based on the spectrum of a solution of pH 2.52, for which we calculate $\alpha_0 = 0.004$, $\alpha_1 = 0.394$, $\alpha_2 = 0.569$, and $\alpha_3 = 0.033$. Values of ϵ_2 were calculated from the expression

$$\epsilon_2 = \frac{\epsilon_M - 0.394\epsilon_1 - 0.033\epsilon_3}{0.569}$$

using in turn the raw and improved estimates of ϵ_1 as described previously.

The results are shown plotted as Fig. 6. It is recognized that the values of ϵ obtained in this way are not very accurate, since their calculation involves taking differences of experimental numbers. The spectra show, with increase in ligand number of the complexes, a hypsochromic shift in λ_{max} , and a roughly proportionate increase in ϵ_{max} , typical of numerous other complexes formed by ferric iron with phenolic chelating agents.

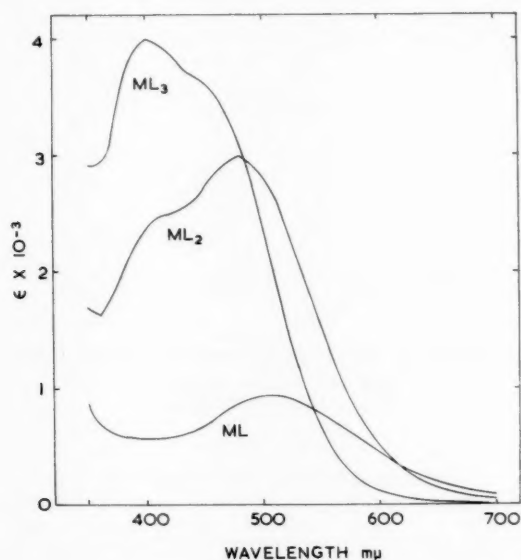


FIG. 6. Spectra of individual species for system iron (III) - kojic acid.

Effect of Acetate and Chloracetate

To prepare solutions of stabilized pH for spectral measurements it was planned to use buffering mixtures of acetic acid or chloracetic acid and sodium hydroxide. The use of acetate buffers is implied in the preparation of the solutions whose spectra had previously been examined by Moss and Mellon. The spectra of our solutions prepared with these buffering agents failed to give sharply defined isobestic points, and plots of ϵ_M vs. pH failed to give the expected horizontal regions. The effect observed is illustrated in Fig. 7, in which our experimental points at 495 mμ are shown together with the Vareille curve ultimately obtained for solutions not containing acetate or chloracetate (cf. Fig. 3). A similar drop in ϵ_M with increasing pH is observed with each set of solutions containing either acetate or chloracetate. This is attributed to a competition between acetate or chloracetate and the kojate ion for co-ordination to the metallic ion. As the concentration of the anion of either buffering acid increases with increase in pH, ferric acetate or chloracetate forms at the expense of the colored kojate. The fact that the experiments for continuous variations indicated a fairly robust 3:1 complex in the presence of a moderate concentration of acetate appears to rule out the likelihood of the formation of stable mixed acetate - kojate complexes.

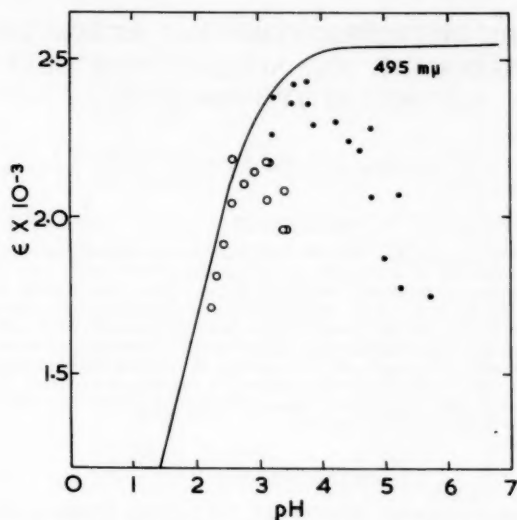


FIG. 7. Influence of acetate and chloracetate on formation of ferric kojates. The solid line shows the Vaireille curve at 495 mμ taken from Fig. 3. Open circles show experimental observations for solutions buffered with chloroacetic acid and alkali; solid circles refer to similar solutions buffered with acetic acid and alkali.

Implications of Results

Apart from any theoretical significance that may be attached to a knowledge of the formation constants and spectra of the three ferric kojate complexes, this study has certain practical consequences in analytical chemistry. Kojic acid has been proposed as a colorimetric reagent and as an indicator for complexometric titrations for iron (III). This work has revealed the superior stability of solutions of the highly purified reagent. It has demonstrated the significance of control of pH and of excess reagent necessary to insure that the solutions prepared for photometric measurement should have the same degree of complex formation. Finally, it has disclosed the deleterious effect of acetate in preventing complete formation of the colored complexes, and demonstrated that hexamine is a preferable buffering agent.

ACKNOWLEDGMENT

The authors gratefully acknowledge financial assistance from the National Research Council for this investigation. One author (G. F. A.) was holder of a Union Carbide Research Fellowship in 1958-59, for which thanks are hereby expressed.

REFERENCES

1. L. VAREILLE. *Bull. Soc. Chim. France*, **870**, 872, 1493, 1496 (1955).
2. L. VAREILLE. *Bull. Soc. Chim. France*, **872** (1955).
3. A. ALBERT. *Biochem. J.* **54**, 646 (1953).
4. M. L. MOSS and M. G. MELLON. *Ind. Eng. Chem., Anal. Ed.* **13**, 612 (1941).
5. A. OKÁČ and Z. KOLAŘÍK. *Chem. listy*, **51**, 2017 (1957); *Collection Czech. Chem. Commun.* **24**, 266 (1959).
6. P. JOB. *Ann. Chim.* **9** (10), 113 (1928).
7. A. OKÁČ, L. SOMMER, and G. RÁDY. *Chem. listy*, **48**, 828 (1954).
8. F. WOLDBYE. *Acta Chem. Scand.* **9**, 299 (1955).

THE COMPLEX DIELECTRIC CONSTANT OF SOLUTIONS OF TRIMETHYLPENTANE AND NITROBENZENE NEAR THE CONSOLUTE TEMPERATURE¹

B. D. RIPLEY² AND R. McINTOSH

ABSTRACT

The complex dielectric constants of three compositions of trimethylpentane and nitrobenzene have been measured as a function of temperature for a range near the consolute temperature. The frequency employed was 3300 Mc/sec. The experimental procedure involved the study of the standing wave established in a coaxial line. The chemical systems showed maxima in both the real and imaginary parts of the complex dielectric constant at temperatures above those at which phase separation occurs. The finding of Semenchenko and Azimov is thus confirmed. A discussion of the validity of applying thermodynamic formulae to dielectrics showing loss is given and some qualitative remarks are offered concerning the change of the systems as they are cooled. These remarks are based upon the effect of the applied field upon the entropy of the solutions.

INTRODUCTION

The properties of one-component systems at the critical temperature and of multi-component systems at the consolute temperature are unusual, and have been frequently studied. Classical thermodynamics suffices to predict much of the behavior, such as the approach of c_p to an infinite value for a one-component system at the critical temperature (1). In the case of such systems the existence of turbidity, the occurrence of marked density gradients due to the extreme value of compressibility (2, 3), and the persistence of liquid-like properties above the temperature of the disappearance of the meniscus have been remarked frequently. Partially miscible liquid systems also show turbidity (4) and other interesting properties near the consolute temperature. Semenchenko and his associates have studied such properties as the viscosity (5), the specific heat (6), and the dielectric constant (7) for systems above the temperature at which phase separation occurs.

In all cases maxima of the physical properties were observed at a temperature between 0.5 and 1.5° C above that of the formation of layers. The magnitudes of the maxima were dependent upon composition and were greatest in each system for the composition corresponding to the consolute temperature. Semenchenko and Azimov (7) investigated the dielectric constant for low frequencies at which the liquids show no loss. Semenchenko (8, 9) has explained the occurrence of the maximum on the basis of the Gibbs' criteria for the existence of critical phases (10). Very briefly, the development follows the course outlined below.

The condition of a system of fixed mass, existing in one phase, is determined by the variables S , entropy, V , volume, and D , the dielectric displacement, which are taken as the independent variables. T , temperature, p , pressure, and E , electric field intensity are taken as dependent variables. The variations of these as a function of the independent variables may be written.

¹Manuscript received November 17, 1960.

Contribution from the Chemistry Department, University of Toronto, based upon a thesis presented for the M.A. degree.

²Graduate Student; present address: c/o International Nickel Co., Port Colborne, Ontario.

$$\begin{aligned}
 dT &= \left(\frac{\partial T}{\partial S} \right)_{m,V,p} dS + \left(\frac{\partial T}{\partial V} \right)_{m,S,p} dV + \left(\frac{\partial T}{\partial D} \right)_{m,S,V} dD, \\
 dp &= \left(\frac{\partial p}{\partial S} \right)_{m,V,D} dS + \left(\frac{\partial p}{\partial V} \right)_{m,S,D} dV + \left(\frac{\partial p}{\partial D} \right)_{m,S,V} dD, \\
 dE &= \left(\frac{\partial E}{\partial S} \right)_{m,V,D} dS + \left(\frac{\partial E}{\partial V} \right)_{m,S,D} dV + \left(\frac{\partial E}{\partial D} \right)_{m,S,V} dD.
 \end{aligned}$$

The restriction of constant mass assures variations of the properties of the phase.

Keeping T and p constant also, the value of $(\partial E / \partial D)_{m,p,T}$ is determined and is given by

$$\begin{vmatrix}
 \left(\frac{\partial T}{\partial S} \right)_{m,V,D} & \left(\frac{\partial T}{\partial V} \right)_{m,S,D} & \left(\frac{\partial T}{\partial D} \right)_{m,V,S} \\
 \left(\frac{\partial p}{\partial S} \right)_{m,V,D} & \left(\frac{\partial p}{\partial V} \right)_{m,S,D} & \left(\frac{\partial p}{\partial D} \right)_{m,V,S} \\
 \left(\frac{\partial E}{\partial S} \right)_{m,V,D} & \left(\frac{\partial E}{\partial V} \right)_{m,S,D} & \left(\frac{\partial E}{\partial D} \right)_{m,V,S}
 \end{vmatrix}$$

divided by

$$\begin{vmatrix}
 \left(\frac{\partial T}{\partial S} \right)_{m,V,D} & \left(\frac{\partial T}{\partial V} \right)_{m,S,D} \\
 \left(\frac{\partial p}{\partial S} \right)_{m,V,D} & \left(\frac{\partial p}{\partial V} \right)_{m,S,D}
 \end{vmatrix}$$

The numerator can be shown by a general argument to become zero at the critical condition, since a system in that condition is at the limit of stability for continuous changes (10). Thus $(\partial E / \partial D)_{m,p,T} = 1/\epsilon = 0$ at the consolute temperature and composition. Since E is neither a maximum nor a minimum, it follows that $(\partial^2 E / \partial D^2)_{m,p,T} = 0$. Since the phase is stable, the necessary condition is that $(\partial E / \partial D)_{m,p,T} > 0$. Semenchko (11) gives the conditions for what he calls false critical points as $(\partial E / \partial D)_{m,p,T} > 0$, $(\partial^2 E / \partial D^2)_{m,p,T} > 0$ and predicts finite values of the maximum.

For time-dependent electrical fields and dielectrics showing power absorption, careful consideration must be given to the validity of applying thermodynamic arguments. It would appear, however, on the basis of the discussion concerning entropy which is given later, that the prediction of a maximum of the real part of the complex dielectric constant can still be made.

The present work is therefore largely a repetition of Semenchko's (7, 11), except that the imaginary part of the dielectric constant has also been measured and the second component is 2,2,4-trimethylpentane instead of octane. A discussion of the validity of thermodynamic treatments for lossy systems is offered, as well as a description of a convenient and precise system of measuring the parts of the complex dielectric constants of such liquid systems.

EXPERIMENTAL

The dielectric cell is shown in Fig. 1. The outer conductor was German silver tubing 13/128 in. thick; the inner conductor was the same metal 6/1000 in. thick down to the region marked E, which had a copper plug 3/8 in. in diameter and 3 1/8 in. in length

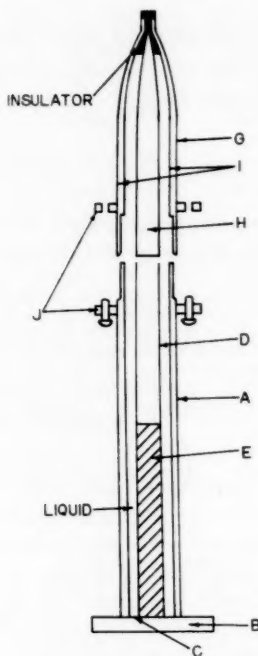


FIG. 1. Schematic representation of the experimental cell.

soldered inside the central conductor. The shorting plate was brass. The cell was designed in this way to provide good thermal conductivity to the fluid of the thermostat, but to reduce heat transfer to the air above the thermostat through the connector at the top of the cell. The cell was $6\frac{3}{8}$ in. long and 1 in. in diameter. A Caro UG-32U adaptor was used to make the connection between the cell and slotted line. The adaptor was designed so that no discontinuity occurred along either the inner or outer conductor surfaces. As indicated in the diagram, the adaptor was held to the cell by screws passing through plates, and these plates formed a tight fit to prevent evaporation of the liquids or absorption of water by them from the air. The oil thermostat was electrically heated and its temperature controlled by means of an adjustable mercury thermoregulator and a relay system. Temperatures were readily controlled to $\pm 0.01^\circ\text{C}$ over a period of several hours, and because of the period of heating and cooling, the temperature of the liquid in the cell was more closely constant than this.

The coaxial line used was a Hewlett Packard model 805A, mounted vertically above the cell. In series with the line was a length of RG-21/U attenuating cable to reduce reflections to the generator. The generators were FXR L771B and S771B oscillators designed to work into a 50-ohm load. The generators were fitted with a series N, UG 107B/U tee adaptor providing connection from one side to the slotted line, and from the other, again through attenuating cable, to an FXR crystal mount. Connectors in both lines were series N, UG-18C/U plugs. Rectification of the r.-f. voltage was achieved by means of 1N21B crystals which were tested and found to provide square-law response in the range of voltages used.

The signal from the crystal of the slotted line was applied to one terminal of a Leeds

and Northrup mirror galvanometer of $0.05 \mu\text{v/mm}$ sensitivity mounted on a vibration-free table. The signal of the crystal in the FXR mount was sent to a voltage-dividing Muirhead resistance box of 10,000 ohms. The output of this box was sent through variable resistors, in series (which served as protective resistances for the galvanometer) to the other terminal of the galvanometer. Very careful shielding of all elements in the circuit was necessary, and an efficient ground connection had to be provided.

The purpose of comparing the rectified signal from the slotted line with a signal from a reference source fed by the same oscillator was to compensate for both long and short term fluctuations of the amplitude of the signal generator. The same technique was used by McCowan and McIntosh (12), but in the present instance no amplification was employed. As the signal is read as a fraction of the oscillator output at the time of measurement, and as both P_x and P_{\min} are so recorded, (where P_x is the output at position x), the ratio between them is immediately given. Power is here considered to be measured because of the square-law response of the detector.

The data obtained were those necessary for the application of the equation given in Von Hippel (13, p. 68)

$$\frac{\tanh \gamma_2 d}{\gamma_2 d} = \frac{-j\lambda_1}{2\pi d} \frac{\frac{E_{\min}}{E_{\max}} - j \tan 2\pi X_0 / \lambda_1}{1 - j \frac{E_{\min}}{E_{\max}} \tan 2\pi X_0 / \lambda_1}$$

where λ_1 is the wavelength of the signal in the guide, d the depth of liquid in the cell, E_{\min} and E_{\max} the magnitudes of the standing wave at a node and at maximum amplitude, and X_0 the distance of the first minimum from the short. The position of the short as experienced by the electric wave had, of course, to be determined initially with no liquid in the cell. This was done relative to the scale readings of the line by determining the distance between successive minima and considering the electrical short position to be at the distance given by the smallest integral number of nodes required to approximate to the geometrical distance of the short from the scale. The average for three frequencies was 39.318 ± 0.004 whereas the corresponding geometrical distance was 33.9 cm. It should be noted also that attenuation along the line proved negligible as the amplitude of the minimum was constant along the line.

Although it would have been feasible to measure the ratio P_{\min}/P_{\max} directly, this was not done because the crystal response departed somewhat from the square-law response near the maximum. The distance $\Delta X/2$ between the position of the minimum and the position for twice the amplitude of the minimum was measured and employed in the formula $E_{\min}/E_{\max} = \pi \Delta X / \lambda_1$ (13, p. 67). The small errors arising from this practice are discussed by Purcell (14) but could not influence the qualitative nature of the results given below. A matter giving rise to some error of unknown and variable extent was the use of the charts in Von Hippel (13, p. 88 *et seq.*) to evaluate $\tanh \gamma_2 d / \gamma_2 d$. This error arose in interpolating, but is again too small to affect the results seriously. Finally, to ensure good performance, the liquid level was changed to give the best depth of liquid for any particular frequency, that is $\lambda_1/4$, where λ_1 is the wavelength. Densities of the liquid compositions at the limits of the temperature range were measured, and the height of liquid at any intermediate temperature computed using the density obtained by linear interpolation between the extreme values.

The 2,2,4-trimethylpentane was British Drug Houses spectroscopic Grade, Laboratory Reagent. The nitrobenzene was B.D.H. Microanalytical Reagent, Organic Standard. Both

substances were stored over "Drierite" and transferred to the cell by the pressure of dry air.

RESULTS

Three experiments using nitrobenzene at 30.0° C were carried out using a variety of frequencies and the frequency of maximum loss established for pure nitrobenzene as 3300 Mc/sec. The average of the values is plotted in Fig. 2.

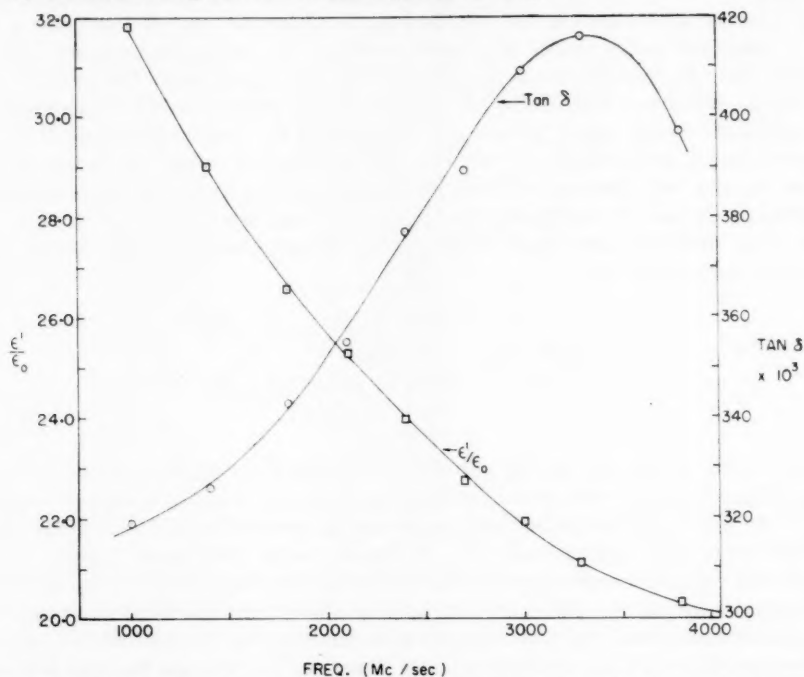


FIG. 2. The values of the real part of the dielectric constant and of $\tan \delta$ of pure nitrobenzene as a function of frequency at 30.0° C.

Three two-component systems were also studied. These were nitrobenzene and trimethylpentane and the concentrations were 25.4%, 48.2%, and 77.1% nitrobenzene, respectively. The frequency used was 3300 Mc/sec. Table I shows the temperatures at

TABLE I
Temperatures of pronounced turbidity and of separation of phases

System	Temperature of turbidity, °C	Temperature of separation of phases, °C
I	22.6-22.7	21.0-21.1
II	29.6-29.7	27.6-27.7
III	23.1-23.2	21.4-21.5

which turbidity became marked and the temperatures at which phase separation occurred. For each of these three systems three series of determinations of complex dielectric constant versus temperature were carried out. The mean deviation never exceeded 0.3% and was usually 0.15% or less for the real part, with error up to 1% in $\tan \delta$. The averages of the real and imaginary parts of the complex dielectric constant are plotted as ϵ'/ϵ (i.e. relative to vacuum) and as $\tan \delta$ in Figs. 3, 4, and 5. It is clear from these plots that

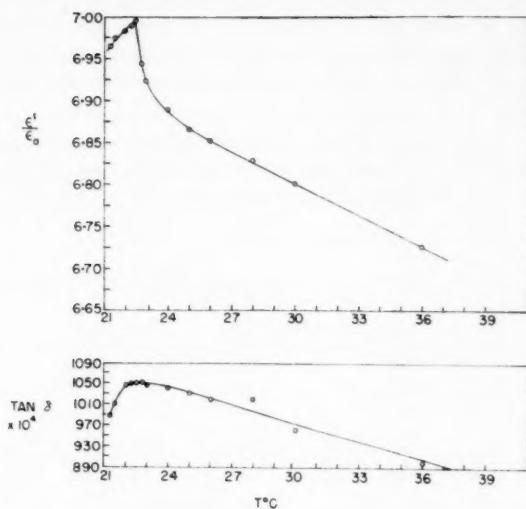


FIG. 3. The values of the real part of the dielectric constant and of $\tan \delta$ of a solution of 25.4% nitrobenzene in trimethyl pentane. Frequency 3300 Mc/sec.

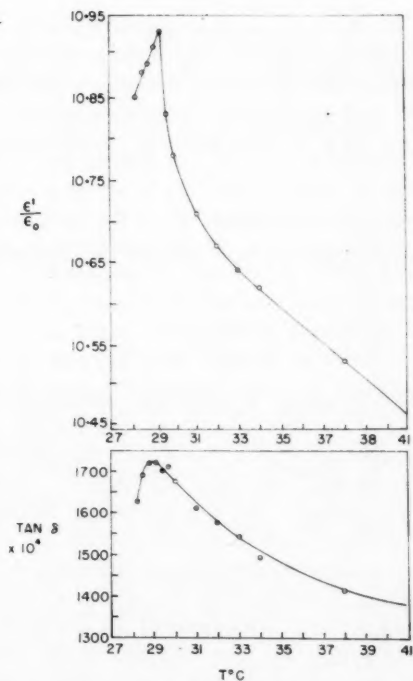


FIG. 4. The values of the real part of the dielectric constant and of $\tan \delta$ of a solution of 48.2% nitrobenzene in trimethyl pentane. Frequency 3300 Mc/sec.

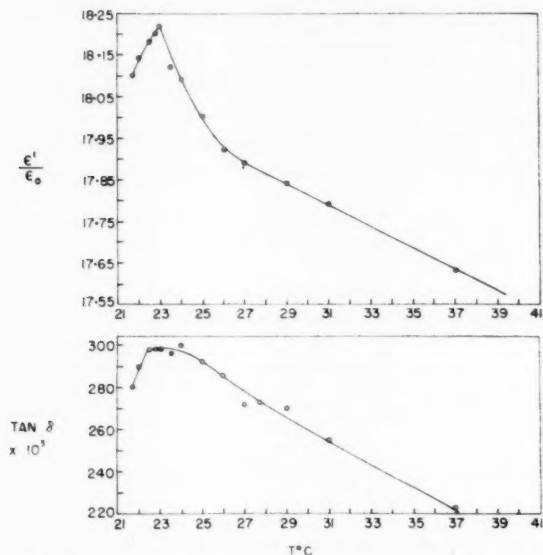


FIG. 5. The values of the real part of the dielectric constant and of $\tan \delta$ of a solution of 77.1% nitrobenzene in trimethyl pentane. Frequency 3300 Mc/sec.

both ϵ' and ϵ'' show maxima at the temperatures where turbidity becomes apparent. The magnitude of the maximum is greatest for the system corresponding most closely to the composition of the system at the consolute condition. The consolute temperature for this system is 30.38° C (15) and the consolute composition was estimated by us as 56% nitrobenzene. The maxima of ϵ confirm findings by Semchenko and Azimov (7, 11).

DISCUSSION

Fröhlich (16) shows that the entropy per unit volume of a dielectric in a static field may be written

$$S = S_0 + \frac{1}{8\pi} \frac{\partial \epsilon}{\partial T} E^2,$$

where S_0 is the entropy of the dielectric at the particular temperature but with no field applied. If $\partial \epsilon / \partial T < 0$, the effect of the field is to reduce the entropy, and if $\partial \epsilon / \partial T > 0$, the effect of the field is to increase it. Fröhlich states that the treatment of the general case of time-dependent fields is complex and does not discuss it further. On the basis of the following considerations it appears that a very similar relation should be valid for time-dependent fields and dielectrics which absorb power.

In the case of lossy dielectrics an irreversible process is occurring due to the absorption of the power, namely the extraction of energy from the field at some temperature $T + \delta T$ and its elimination to the thermostat at T . The value of the energy absorbed per second is given by the imaginary part of $1/t \int_0^t \hat{E} \cdot d\hat{D}$. The real part of the expression represents energy stored by the dielectric and returned to the field twice during each cycle. In spite of the irreversible process and the generation of entropy, the condition of the

dielectric is specified by its temperature, assumed to be T , and by the time-average value of its polarization, which is a function of the value of the applied field at fixed frequency. We may thus consider the dielectric to exchange energy with its surroundings and to be maintained at constant volume, when, analogously with the equation given by Fröhlich (16), one may write $dU = TdS + (1/4\pi) \text{r.p. } \bar{E} \cdot d\bar{D}$, where S is a function of T and the real part of the applied field, and \bar{D} is a function of temperature only at fixed frequency. The bar designates the time-average value and r.p. is the real part of the expression. Since $\bar{D} = \epsilon \bar{E}$ (magnitudes are employed since the vectors are parallel),

$$d\bar{D} = \epsilon d\bar{E} + \bar{E} d\epsilon.$$

On substitution in the differential equation for energy, and using \bar{E}^2 as the variable

$$dU = \left(T \frac{\partial S}{\partial T} + \frac{1}{4\pi} \text{r.p. } \bar{E}^2 \frac{\partial \epsilon}{\partial T} \right) dT + \left(T \frac{\partial S}{\partial \bar{E}^2} + \frac{1}{8\pi} \text{r.p. } \epsilon \right) d\bar{E}^2.$$

Since,

$$\frac{\partial}{\partial \bar{E}^2} \left(T \frac{\partial S}{\partial T} + \frac{1}{4\pi} \text{r.p. } \bar{E}^2 \frac{\partial \epsilon}{\partial T} \right) = \frac{\partial}{\partial T} \left(T \frac{\partial S}{\partial \bar{E}^2} + \frac{1}{8\pi} \text{r.p. } \epsilon \right)$$

on integration, with ϵ independent of \bar{E}^2 , and on evaluation of the time average of the complex field, one obtains

$$S = S_0 + \frac{1}{16\pi} E_0^2 \frac{\partial \epsilon'}{\partial T}$$

where E_0 is the maximum amplitude of the field. As in the static case, the system loses entropy or gains entropy in the presence of the field depending upon the sign of $\partial \epsilon' / \partial T$.

DISCUSSION OF EXPERIMENTAL RESULTS

Semenchenko (8, 9) has pointed out that the prediction of a maximum of the dielectric constant of one-phase systems at the condition of the limit of stability with respect to continuous changes is inherent in the general criteria established by Gibbs (10). He has obtained experimental confirmation of this prediction (7, 11). Using frequencies of measurement from 1000 to 3300 Mc/sec and the system nitrobenzene-trimethylpentane, we have confirmed Semenchenko's finding and have shown also that ϵ'' shows a maximum at the same temperature within the limits of experimental error. Analogous concepts to those of cybotactic groups (17) and regional orientation (18) which have been used to distinguish the liquid from the gaseous state of aggregation may also be employed to permit qualitative descriptions of the transition between single-phase and two-phase systems of several components. In the present instance, if the conclusion is correct that lossy dielectrics in alternating fields are amenable to discussion in terms of the usual thermodynamic treatment, then the maximum of the dielectric constant as a function of temperature permits the following qualitative description of the behavior of the system.

As the temperature is reduced towards the temperature of the maximum, association of the molecules into some type of structure is occurring. That this association is not complete is evident from the fact that the entropy of the system may be further reduced by the application of a field. At temperatures lower than that of the maximum, however, the reaction has occurred to a sufficient extent that application of a field will increase

the entropy, presumably by the destruction of structures which exist when no field permeates the sample. As the value of $\partial\epsilon'/\partial T$ remains constant or increases slightly with diminishing temperature, the application of a field remains effective in destroying order down to the temperature at which separation into phases occurs. As the existence of discrete phases suggests an increasing stability of ordered regions within the fluid as temperature is lowered, and as the effectiveness of the field persists, it is suggested that the amount of ordered matter increases with lowered temperature.

The range of frequency investigated was not sufficiently broad for us to learn much about the nature of the loss in the system. Pure nitrobenzene does not reveal a loss curve of the Debye type. The three solutions of nitrobenzene can only be discussed on the basis of their behavior as a function of temperature. The diminishing values of ϵ'' on both sides of the temperature of maximum ϵ' could be reconciled with the hypothesis of a smaller amount of ordered matter, but the likelihood of this being correct for lower temperatures is small in view of the remarks made earlier. Moreover, a wider distribution of relaxation times or the variation of loss with temperature even for a fixed amount of a single type of molecular aggregate could also explain the experimental facts. The last possibility follows from the knowledge that even for systems of a single relaxation time, the loss curve goes through a maximum for a given frequency as temperature is varied. It therefore seems clear that a much more thorough examination of these systems using a wide range of measuring frequencies would be required to increase the present understanding of their behavior.

ACKNOWLEDGMENTS

We are indebted to the Advisory Committee on Research, University of Toronto, and to the National Research Council, Ottawa, for financial support. It is a pleasure to thank Professors J. M. Anderson and R. H. McKay of the Physics Department, University of Toronto, and Dean A. R. Gordon of this Department for reading the discussion concerning the thermodynamics of lossy dielectrics.

REFERENCES

1. MOLECULAR THEORY OF GASES AND LIQUIDS. J. O. Hirschfelder, C. F. Curtiss, and R. B. Bird. John Wiley & Son, Inc., New York. 1954. p. 369.
2. R. McINTOSH, J. R. DACEY, and O. MAASS. Can. J. Research, B, **17**, 241 (1939).
3. H. B. PALMER. Doctoral Dissertation, University of Wisconsin. 1952. As quoted in Molecular theory of gases. p. 373.
4. F. E. MURRAY and S. G. MASON. Can. J. Chem. **36**, 415 (1958).
5. V. K. SEMENCHENKO and E. L. ZORINA. Doklady Akad. Nauk. S.S.S.R. **80**, 903 (1951); National Research Council Technical Translation TT298.
6. V. K. SEMENCHENKO and V. P. SKRIPOV. Zhur. Fiz. Khim. **25**, 362 (1951); National Research Council Technical Translation TT243.
7. V. K. SEMENCHENKO and M. AZIMOV. Zhur. Fiz. Khim. **30**, 2228 (1956).
8. V. K. SEMENCHENKO. Zhur. Fiz. Khim. **25**, 121 (1951).
9. V. K. SEMENCHENKO. Doklady Akad. Nauk. S.S.S.R. **99**, 1045 (1954).
10. J. A. V. BUTLER. In Commentary of the scientific writings of J. Willard Gibbs. Vol. I. Yale University Press. 1936. p. 146 *et seq.*
11. V. K. SEMENCHENKO and M. AZIMOV. Zhur. Fiz. Khim. **30**, 1821 (1956).
12. J. D. McCOWAN and R. McINTOSH. Can. J. Chem. **39**, 425 (1961).
13. A. VON HIPPEL. Dielectric materials and applications. The Technology Press of M.I.T. and John Wiley & Sons. 1954.
14. E. M. PURCELL. Technique of microwave measurements. M.I.T. Radiation Laboratory Series. McGraw-Hill, 1947. Chap. 8.
15. H. M. WOODBURN, K. SMITH, and H. TETESKY. Ind. Eng. Chem. **36**, 588 (1944).
16. H. FRÖHLICH. Theory of dielectrics. Oxford, Clarendon Press. 1949. p. 9 *et seq.*
17. C. A. BENZ and G. W. STEWART. Phys. Rev. **46**, 703 (1934).
18. O. MAASS and L. A. GEDDES. Phil. Trans. Roy. Soc. London, Ser. A, **236**, 303 (1937).

INFRARED SPECTRA OF GASES CHEMISORBED ON ZINC OXIDE

I. CO AND CO₂

J. H. TAYLOR² AND C. H. AMBERG

ABSTRACT

The infrared spectra of CO and CO₂ adsorbed on zinc oxide have been observed in the region 2-9 μ . The results show that CO does not exist as such on the surface at 155° C, but is immediately oxidized to CO₂. There is no evidence for carbonate formation in the adsorption of CO, the spectra corresponding to structures of the carboxylate type. A band is observed at 2174 cm⁻¹ for CO at 25° C which may correspond to dipole interaction or to an oxidation step.

INTRODUCTION

Previous work (1-5) on the chemisorption of CO on surfaces of zinc oxide has shown that there are two distinct types: one, a weak reversible adsorption occurring at room temperature with a negligible activation energy, the other a stronger adsorption occurring at higher temperature with an activation energy of 5 to 16 kcal/mole (4), in which the CO can be removed only as CO₂. It was thought that the infrared method might give information on the nature of the adsorbed species.

EXPERIMENTAL

The zinc oxide was prepared by the precipitation of either the carbonate from nitrate solution, with subsequent decomposition at 350°, or the oxalate from acetate solution, the oxalate being decomposed by heating at 400° C in air. The oxide was pressed at 40 tons/sq. in. into plates containing about 100 mg/sq. cm, which had a B.E.T. nitrogen area of 25-30 sq. m/g and transmitted approximately 50% of the incident infrared radiation before outgassing. These plates were mounted in a cell similar to that described by Little, Klauser, and Amberg (6). This cell with a path length of 11.0 cm was fitted with a winding device which enabled the sample to be removed from the beam and the background spectrum to be run. A matched cell containing gas at a pressure equal to that in the sample cell was placed in the reference beam. In all experiments the pressure of CO and CO₂ was 20 mm Hg. The instrument was a Beckman IR-4 double beam spectrometer used with sodium chloride optics.

RESULTS

Figure 1 (a, b, c) shows a sequence of spectra taken as the sample was outgassed. It was found that the transmission slowly decreased until after pumping at 320° C for several hours, the sample became completely opaque. The transmission could be entirely restored, as shown in Fig. 1d, by heating for 5 minutes at 350° C under 1 cm oxygen, cooling to room temperature, and pumping to 10⁻³ mm Hg. All the spectra reported here were taken from samples pretreated in this manner.

Figure 2 shows the spectra of CO and CO₂ adsorbed on zinc oxide, with the zinc oxide spectrum subtracted.

The CO at 25° C shows a sharp band at 2174 cm⁻¹ and a weaker one at 1333 cm⁻¹, which were formed immediately upon admission of the gas (Fig. 2a). On standing, the

¹Manuscript received September 26, 1960.

Contribution from the Division of Applied Chemistry, National Research Council, Ottawa, Canada.

Issued as N.R.C. No. 6163.

²National Research Council Postdoctorate Fellow 1959-61.

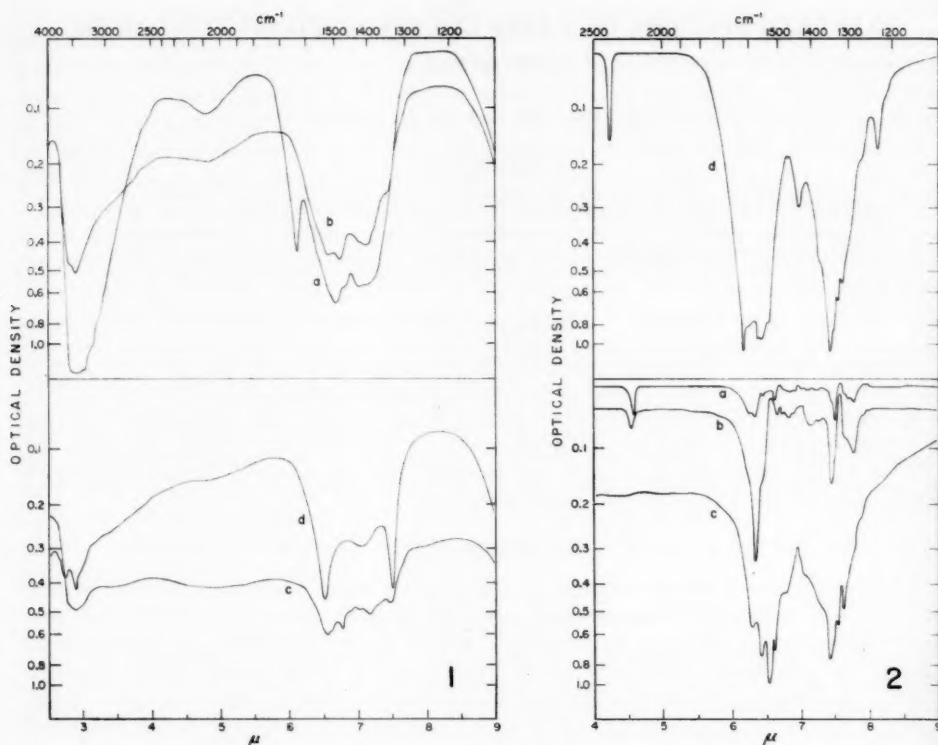


FIG. 1. Spectrum of zinc oxide on outgassing: (a) in air, (b) 3 hours at 150° C, (c) 18 hours at 150° C, (d) 18 hours at 320° C and treatment with 1 cm O₂ at 350° C. Spectra run at 25° C.

FIG. 2. Spectra of adsorbed gases with the zinc oxide spectrum subtracted: (a) CO at 25° C initially, (b) CO at 25° C after 24 hours, (c) CO at 155° C after 3 hours, (d) CO₂ at 25° C after 0.5 hour.

peak at 2174 cm⁻¹ shifted slightly to a higher frequency, usually about 2198 cm⁻¹, and decreased in intensity. At the same time, three strong maxima appeared at 1575, 1342, and 1287 cm⁻¹ and a slow increase in the background absorption was observed (Fig. 2b). The band at 2174 cm⁻¹ disappeared as soon as evacuation was commenced, but those at 1575, 1342, and 1287 cm⁻¹ were removed only by prolonged pumping at 320°.

Figure 2c is the spectrum obtained by admitting CO to zinc oxide at 155° C. In this case there was no peak at 2174 cm⁻¹, but the growth of the spectrum and increase in background absorption was much more rapid than in the cold. After some time at 155° C, a small peak at 2198 cm⁻¹ was observed in some cases.

The adsorption of CO₂ at 25° was very rapid, and as can be seen from Fig. 2d the structure is somewhat complex. On opening of the system to the pumps the band at 2364 cm⁻¹ was immediately removed, and that at 1618 cm⁻¹ shifted to 1600 cm⁻¹. The bands at 1600, 1431, and 1230 cm⁻¹ decreased quite rapidly in intensity and were almost entirely removed after 3 hours pumping at 25° C. The rest of the spectrum was removed only by several hours outgassing at 320° C.

DISCUSSION

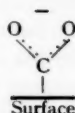
The spectrum shown in Fig. 1a corresponds to those we have obtained from mulls of basic zinc carbonate, and it is thought that in the presence of atmospheric water and CO_2 , a surface carbonate was formed. This was decomposed on outgassing and simultaneously a steady decrease in the transmission of the sample occurred (Fig. 1, b, c). The latter phenomenon has been observed in previous work (7, 8, 9) and is generally ascribed to absorption by electrons in the conduction band. These may be produced by an increase in non-stoichiometry caused by loss of oxygen or the introduction of excess zinc. This readily explains why oxygen treatment restored the transmission since adsorbed oxygen atoms or molecules are known to act as electron traps. As the outgassing proceeded, three bands appeared at 1527, 1389, and 1333 cm^{-1} , those at 1527 and 1333 cm^{-1} in particular being apparently enhanced by the oxygen treatment (Fig. 1d). These peaks are unlikely to be due to nitrate impurity, as has been suggested by Matsushita and Nakata (7), as the same structure was obtained for samples prepared from the carbonate or the oxalate. The spectrum resembles that described by these authors, but a close correlation is not to be expected in view of the very different samples under investigation. The possibility that the two strong bands at 1527 and 1333 cm^{-1} arise from carboxylate residues can probably be discounted on the grounds that a sample outgassed at 570°C for 19 hours, and treated with oxygen as described above, still showed these two bands together with a third which appeared at 1350 cm^{-1} . In the unlikely event that CO_2 surface impurities would remain stable under these conditions one would have to presume that the kinetic experiments which we are attempting to elucidate were similarly performed on samples containing the carboxylate group. We are at present unable to make definite assignments for the bands in question, but since they do not appear in the spectra of single crystals of zinc oxide, we believe that they may be associated with the defect structure of our material. During the adsorption of CO and CO_2 the two bands were apparently unchanged.

In the course of the outgassing treatment the physically adsorbed water was removed, but as can be seen from Fig. 1 a small concentration of hydroxyl groups remained. During the adsorption these bands were unperturbed and apparently took no part in the reaction.

In the spectrum of CO at 25° (Fig. 2a) the peak at 2174 cm^{-1} appears similar to that observed at 2193 cm^{-1} ($4.56\text{ }\mu$) by Eischens and Pliskin (10) in the oxidation of CO over NiO. They attributed this frequency to the asymmetric vibration of a structure of the type $\text{Ni}-\text{O}-\text{C}\equiv\text{O}$ but failed to find any absorption in the 6- or $7\text{-}\mu$ region corresponding to the symmetric vibration. In the present work, a band is observed at 1333 cm^{-1} ($7.5\text{ }\mu$) which would be at the limit of their working range with Cabosil-supported samples and which may be considered a confirmation of their assignment. However, for symmetric and asymmetric vibrations to occur, the two bonds should be of similar order, which is not compatible with the observed fact that the peak at 2174 cm^{-1} is easily removed by pumping at room temperature. It would appear more likely that the interaction is of a weak dipolar nature, rather than a covalent one as suggested by Eischens. Since the small dipole in CO is $-\text{C}\equiv\text{O}^+$, structures in which the oxygen is interacting with the negatively charged surface cannot be neglected. (For a discussion of oxygen chemisorption on zinc oxide surfaces and the resulting negatively charged surface species, see, for instance, Stone (11, 12) and Terenin and Solonitzin (8).) In a separate experiment, the gas desorbed after CO had been adsorbed on zinc

oxide for 10 minutes was examined mass spectrometrically. It was found to contain very little CO_2 (10^{-5} of the gas adsorbed), which favors the second interpretation.

The two principal regions of absorption at 1560 and 1330 cm^{-1} are close to the maxima shown by carboxylate ions such as formate and oxalate, and probably correspond to structures of the type:



The fact that a number of peaks is observed in each of these two regions may be because adsorption is occurring at different sites, giving species of essentially the same geometrical structure, but with a variety of surface-adsorbate bond strengths. Bicarbonates have been shown (13) to have a band between 1610 and 1630 cm^{-1} and another in the 1390 – 1410 cm^{-1} region. Eischens has observed bands at 1640 and 1390 cm^{-1} (6.1 and $7.2\text{ }\mu$) in the adsorption of CO_2 on NiO (10), which he attributes to structures of the type:



Although in our case CO_2 gave a band at 1618 cm^{-1} ($6.18\text{ }\mu$) no absorption was found in the region 1430 – 1350 cm^{-1} (7.0 – $7.4\text{ }\mu$). However, it is difficult to assess how closely the spectra of structures of this type might be expected to resemble that of the bicarbonate ion and our failure to observe a band in the latter region does not necessarily rule out the existence of such structures. Apart from the bands at 2364 , 1618 , 1431 , and 1230 cm^{-1} , all of which are strongly influenced by the removal of the ambient gas, the spectrum of CO_2 at 25°C corresponds very closely to that of CO at 155°C . This indicates that at 155° , CO does not exist on the surface, but is immediately oxidized to CO_2 .

No absorption was observed in the region 1820 – 2080 cm^{-1} , which is normally associated with the $\text{C}=\text{O}$ stretching mode in metallic carbonyls, nor was there any evidence for >C=O which might arise from bridged structures in which the carbon monoxide was adsorbed at dual sites. Carbonates normally give rise to strong absorption in the $7\text{ }\mu$ region. Thus the band at 1431 cm^{-1} in the adsorbed CO_2 spectrum may be due to zinc carbonate, while the absence of bands in this region in either of the CO spectra would indicate that in these cases no carbonate was formed.

In order to assess the validity of a comparison between our results and those reported in the literature, the following facts should be taken into consideration: (a) The general qualitative aspects are the same in all cases, comprising fast room-temperature chemisorption which is reversible, and a slow chemisorption step above about 150° . (b) Kubokawa (5) has shown that oxygen pretreatment has no effect on either of the CO chemisorption steps, and he has concluded that CO chemisorption is independent of the

electronic state of the zinc oxide. However, it should be noted that his initial outgassing temperature (500°) was higher than ours, thus possibly giving rise to a higher Zn:O ratio in the bulk lattice. Also his outgassing temperature after exposure to oxygen (260°) would leave a smaller fraction of adsorbed oxygen on the surface. Our need for high surface areas coupled with infrared transparency has precluded duplication of this author's conditions. Although we do not at present believe the uncertainty arising out of this to be a serious one, it is hoped that work in progress may throw more light on this question.

REFERENCES

1. W. E. GARNER and J. MAGGS. *Trans. Faraday Soc.* **32**, 1744 (1936).
2. T. I. BARRY and F. A. BRIMELOW. United Kingdom Atomic Energy Authority Research Group. Atomic Energy Research Establ. 1/R 2745 (1958).
3. W. E. GARNER and F. J. VEAL. *J. Chem. Soc.* 1487 (1935).
4. Y. KUBOKAWA. *Bull. Chem. Soc. Japan*, **33**, 555 (1960).
5. Y. KUBOKAWA. *Bull. Chem. Soc. Japan*, **33**, 743 (1960).
6. L. H. LITTLE, H. E. KLAUSER, and C. H. AMBERG. *Can. J. Chem.* **39**, 42 (1961).
7. S. MATSUSHITA and T. NAKATA. *J. Chem. Phys.* **32**, 982 (1960).
8. A. TERENCE and YU. SOLONITZIN. *Discussions Faraday Soc.* **28**, 28 (1959).
9. A. REINHOLD. *Naturwiss.* **45**, 282 (1958).
10. R. P. EISCHENS and W. A. PLISKIN. *Advances in Catalysis*, **9**, 662 (1957).
11. F. S. STONE. *Discussions Faraday Soc.* **28**, 72 (1959).
12. T. I. BARRY and F. S. STONE. *Proc. Roy. Soc. A*, **255**, 124 (1960).
13. F. A. MILLER and C. H. WILKINS. *Anal. Chem.* **24**, 1253 (1952).

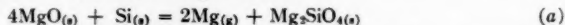
HIGH-TEMPERATURE STUDIES OF METALLURGICAL PROCESSES

PART I. THE THERMAL REDUCTION OF MAGNESIUM OXIDE WITH SILICON¹

J. M. TOGURI² AND L. M. PIDGEON³

ABSTRACT

The rate of reaction (a) has been studied over the temperature range 1140–1460° C, by following the loss in weight of the reactants in high vacuum.



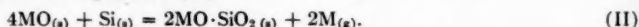
The loss in weight of the reactants was found to be greater than that which can be accounted for by the above reaction. The excess weight loss was found to be due to a brownish, glassy deposit which appeared outside the reaction zone. This material was analyzed by X-ray diffraction and found to be an intimate mixture of Mg_2SiO_4 and Si. Experiments conducted showed that both of these materials are not appreciably volatile at 1350° C. This transfer of silicon and silicate is postulated to occur by the formation of gaseous SiO formed from the reaction mixture. Based on this assumption a possible mechanism for this reaction is postulated.

INTRODUCTION

The reduction of alkaline earth oxides by means of silicon proceeds theoretically according to the equation,



The reaction is reversible and generally proceeds from right to left at low temperatures with emission of heat and from left to right only at high temperatures with the absorption of heat. However, this simple equation is not followed and a secondary reaction always occurs in which the resulting silica combines with a certain amount of unreacted alkaline earth oxide, forming a silicate. Hence, when a theoretical reaction mixture is used according to reaction (I), only 1 mole of oxide is reduced from 2 moles of metal oxide and 1 mole of silicon and 1 mole of metal is formed, and $\frac{1}{2}$ mole silicon remains unused. In order to attain complete utilization of the reducing agent, it is necessary to have twice the amount of oxide as shown in equation (II).



In general, the reaction ceases when a dibasic silicate $2\text{MO} \cdot \text{SiO}_2$ has been formed. Jander (1) has shown that in a system of alkaline earth oxide – silica, the dibasic silicate is preferably formed.

Consequently, in the case of MgO, the reaction follows equation (II) where Mg replaces M.

This method of reduction of alkaline earth oxides by reducing agents producing a volatile metal and non-volatile oxide was known as early as 1878 (2). Schneider and Hesse (3) have studied this particular equilibrium, measuring the equilibrium pressure of magnesium using the transportation method with hydrogen as a carrier gas. From X-ray diffraction studies they identified the solid product as Mg_2SiO_4 .

This reaction, however, has been found to be not as simple as is shown in equation (II). And, in order to have a better understanding of this reaction, it was investigated as a preliminary to the study of the calcined dolomite – silicon reaction.

¹ Manuscript received October 21, 1960.

Contribution from the Metallurgical Engineering Laboratory, based on a thesis submitted by J. M. Toguri in partial fulfillment of the requirements for the degree of Doctor of Philosophy to the School of Graduate Studies, of the University of Toronto, Toronto, Ontario.

² Now at Norges Tekniske Høgskole, Trondheim, Norway.

³ Professor and Head of Department of Metallurgy, University of Toronto.

EXPERIMENTAL PROCEDURES

The experimental method adopted for the determination of the reaction rate was to measure the weight loss of a briquetted mixture of reactants. By holding constant the particle size of the reactants and size and shape of the briquettes, the effect of rate-controlling factors could be determined.

The apparatus used in this investigation was described in detail in a previous paper (4). Briefly, it consists of a high-temperature vacuum furnace incorporating a thermobalance. The thermobalance was constructed from a helical wire spring such that continuous measurements of weight changes could be observed.

Finely powdered magnesium oxide of C.P. grade was used for all experiments. The silicon used was in the form of ferrosilicon, 200 mesh, the analysis of which was 96.7% Si. Briquettes of the reaction mixture were made in a 1-in. diameter mold at a pressure of 1500 p.s.i.

The reaction mixture contained 82% magnesium oxide and 18% ferrosilicon. This corresponds to a $\text{MgO}:\text{Si}$ ratio of 3.33:1 or an excess of Si according to equation (II).

Three briquettes each weighing 10 g were placed in a graphite retort (Fig. 1) which was suspended in the furnace chamber from the helical wire spring. With this spring balance a weight change of 0.020 ± 0.005 g could be observed.

Blank runs using only MgO briquettes, prepared in the same manner as the reaction mixture, showed negligible weight losses due to reactions with the graphite retort over the temperature range 1100–1440° C. Thus, the weight loss of the briquetted reaction mixture was assumed to be due to the reaction between MgO and Si only. It is interesting

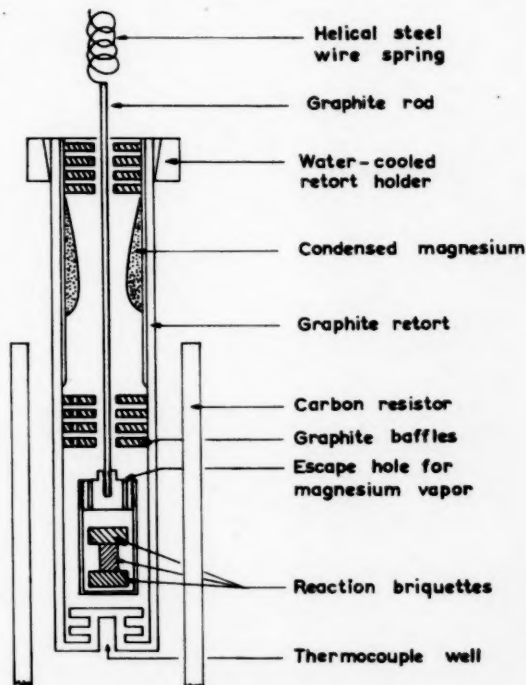


FIG. 1. Diagram of graphite retort.

to note that Kroll and Schlecten (5) found that, under high vacuum, carbon begins to react with MgO at a temperature of 1350°C . This value is lower by approximately 90°C than that determined above. This is to be expected, however, since Kroll and Schlecten used an intimate mixture of MgO and carbon, while in the present investigation a solid briquette of MgO was simply placed on the top of a surface of solid graphite.

The samples were in all cases heated to 750°C for 10 minutes, in order to effect degassing. After degassing, the length of the helical spring was measured by a cathetometer and the temperature of the furnace was increased to the required value. The time for reaching the operating temperature varied from 2 to 5 minutes. Loss in weight of the sample was then measured at constant intervals of time. During the experiments the vacuum of the system was maintained at a pressure of approximately one micron.

The bulk of the magnesium which evolved was successfully condensed as a dense deposit on the water-cooled walls of the condenser. There was no evidence of magnesium condensing on the graphite rod which supports the retort.

RESULTS AND DISCUSSION

The experimental results of this investigation are shown in Fig. 2 and Fig. 3. In Fig. 2

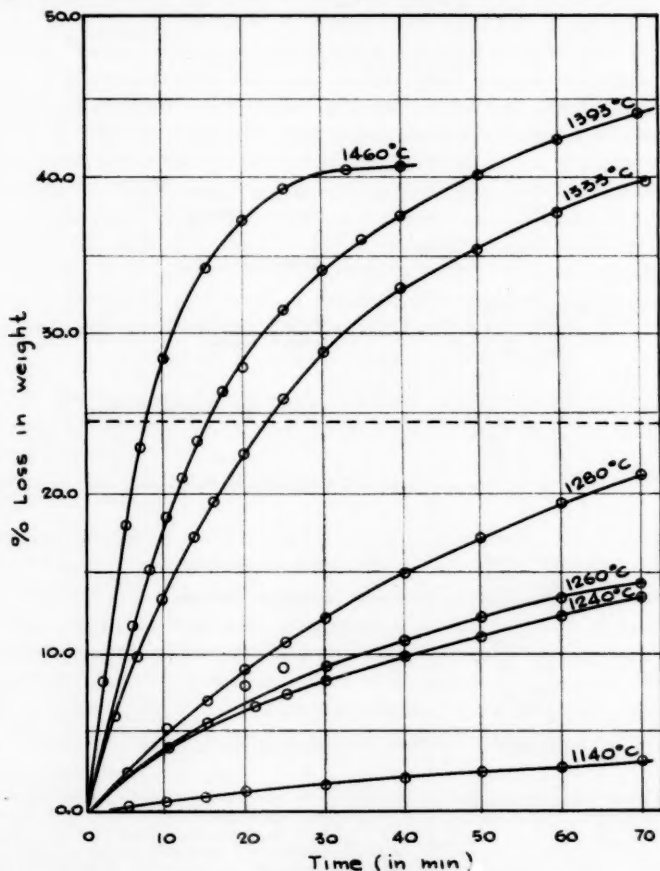


FIG. 2. Rate of reaction.

the percentage loss in weight of the reactant is plotted against time in minutes, while in Fig. 3 the percentage loss in weight of the reactant is plotted against temperature at

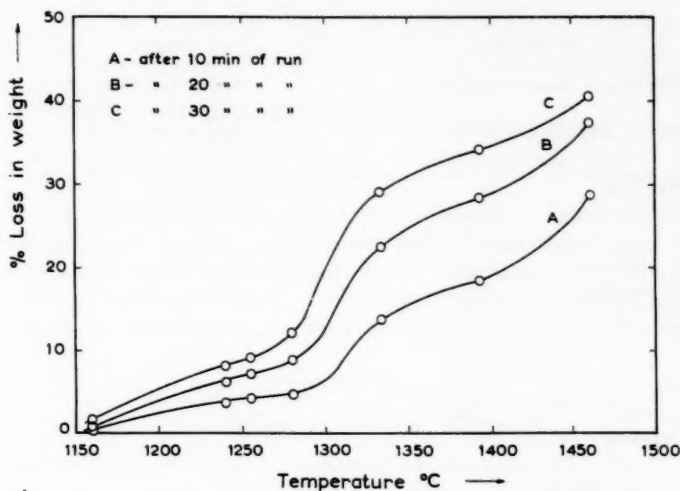


FIG. 3. Effect of temperature at constant time.

various constant times. A horizontal line is drawn through Fig. 2 to represent the maximum theoretical loss in weight, based on the magnesium evolution expected if MgO completely reacted according to equation (II).

The results at 1460°C show a tendency to level off after 25 minutes at temperature. This can be explained by the formation of liquid silicon at 1420°C which tends to agglomerate and thereby decrease the effective reaction surface.

Figure 3 shows a sharp change in the curve at about 1300°C . This suggests that another reaction involving a loss in weight becomes significant at this temperature.

After each experiment, the condenser containing the magnesium was weighed and it was found that the weight loss of the retort was always greater than the magnesium collected. Observation of the reaction retort after all experiments above 1280°C revealed a hard, glassy, brownish condensate on the baffles and condenser, the weight of which corresponded to the excess loss in weight.

On X-ray diffraction analysis, this material was found to be an intimate mixture of Mg_2SiO_4 and Si (compared with the A.S.T.M. Index), as shown in Fig. 4. The volatility of Mg_2SiO_4 and Si was independently investigated by heating each to a temperature of 1350°C . No measurable loss in weight could be observed after 1 hour of heating. The vapor pressure of silicon at 1350°C is approximately 10^{-3} mm of Hg (6). Thus, it was concluded that Mg_2SiO_4 and Si are not volatile at this temperature.

The presence of Mg_2SiO_4 and Si in the regions away from the reactor can be explained by the formation of gaseous silicon monoxide. It is known that when SiO_2 is heated with C, Si, and SiC or by the reduction of various silicates *in vacuo*, a brown distillate corresponding to the composition of SiO is produced. Zintl (7, 8) has suggested using solid SiO as a reducing agent for removing silica from siliceous compounds, or for reducing alkaline earth oxides according to the equation



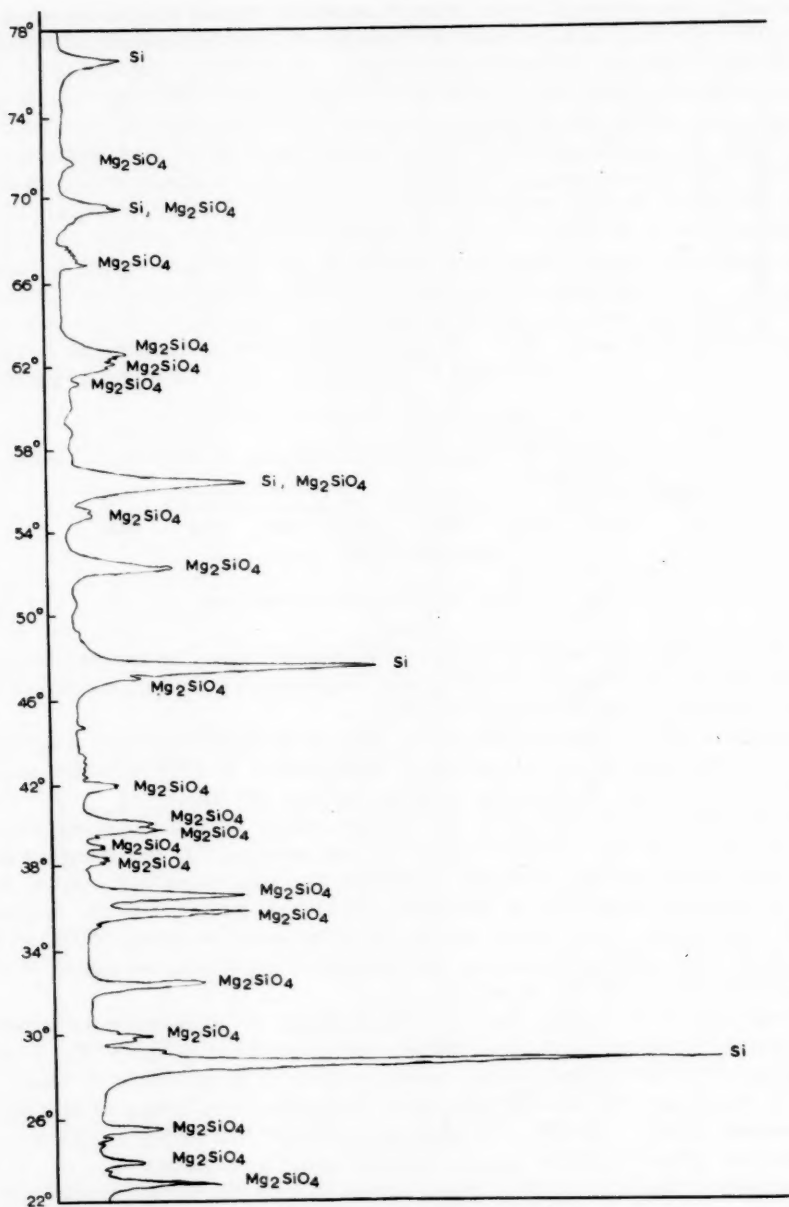


FIG. 4. X-Ray of brown condensate.

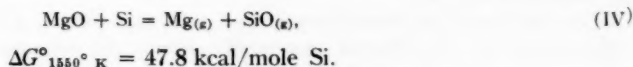
However, Brewer *et al.* (9, 10) reported in their extensive review of the literature on silicon monoxide that SiO solid appeared to be thermodynamically unstable at all temperatures, and that it disproportionated readily to Si and SiO_2 . Spectrographic

TABLE I
The free-energy change for reactions under consideration

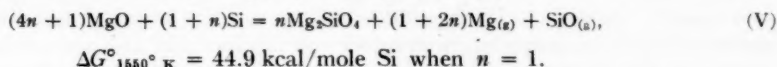
Eq. No.	Reaction	$\Delta G^\circ 1550^\circ \text{ K}$	Equilibrium pressure in mm Hg
IV	$\text{MgO} + \text{Si} = \text{Mg} + \text{SiO}$	47.8 kcal/mole Si	$P_{\text{SiO}} = 3.26 \times 10^{-1}$
V	$(4n+1)\text{MgO} + (1+n)\text{Si} = n\text{Mg}_2\text{SiO}_4 + (1+2n)\text{Mg} + \text{SiO}$	44.9 kcal/mole Si	$P_{\text{SiO}} = 2.27 \times 10^{-1}$
VII	$2\text{SiO} + 2\text{MgO} = \text{Mg}_2\text{SiO}_4 + \text{Si}$	-27.0 kcal/mole MgO	$P_{\text{SiO}} = 1.18 \times 10^{-1}$

investigations have established unequivocally the existence of gaseous SiO. Kubaschewski and Evans (15) have recently summarized the thermodynamic data on gaseous SiO and their suggested value has been used in this discussion.

Of the number of reactions from which SiO can be formed, from a system containing MgO, Si, Mg_2SiO_4 , and Mg gas, the most likely one according to thermodynamic calculations is



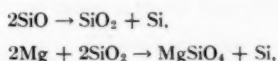
The over-all reaction can then be expressed by equation (V)



The mole ratio of MgO:Si in equation (II) is 4:1, whereas in equation (V), assuming $n = 1$, the ratio is 2.5:1. The experimental ratio was 3.33:1. Therefore, according to equation (II) the reaction mixture should have an excess of silicon while according to equation (V) the reaction mixture should have an excess of magnesium oxide.

That the reaction between MgO and Si proceeds by equation (V) is substantiated by X-ray diffraction analysis of the residue. The diffraction patterns obtained in all experiments below 1280° C showed MgO, Mg_2SiO_4 , and Si, while those above 1280° C showed only MgO and Mg_2SiO_4 even though excess Si was added to the reaction mixture according to equation (II). Since the residue shows in effect excess MgO, the formation of SiO cannot be due to the presence of excess silicon which might have continued its reducing action after most of the magnesium oxide had been removed from the system.

Reaction (V) would also explain the discrepancy in the weight loss of the reactants and the weight of the magnesium collected. The silicon monoxide gas that leaves the reaction zone disproportionates on reaching the cooler sections of the retort. The disproportionated product reacts with the magnesium gas coming from the reaction mixture as follows:



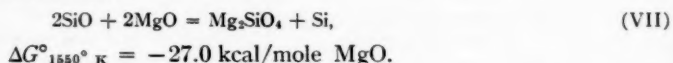
the over-all reaction being represented by equation (VI).



The calculated equilibrium pressure of SiO above reaction (V) is 3.25×10^{-1} mm of Hg at 1300° C . The pressure of the system is of the order of 10^{-2} mm. Therefore one would expect the gaseous SiO to distill readily from the reactor. The discontinuity in the rate curve (Fig. 3) corresponds to the temperature at which the SiO distillation becomes significant.

Possible Reaction Mechanism

Although the present investigation does not permit a complete evaluation of the mechanism, a possible mechanism for the reaction between magnesium oxide and silicon, which accounts for the observed facts, may be expressed by the following equations. The initial reaction that occurs is that represented by equation (IV). The SiO that forms reacts with MgO according to



The calculated P_{SiO} over reactions (IV) and (VII) are 3.26×10^{-1} mm and 1.18×10^{-1} mm of Hg respectively at 1550°K . P_{SiO} must therefore be 1.18×10^{-1} mm of Hg before reaction (VII) will proceed. It is possible that the pressure of SiO is sufficient inside a reacting briquette for reaction (VII) to occur even though the residual pressure of the system is approximately 10^{-2} mm of Hg. At higher temperatures, however, SiO must be evolved faster by reaction (IV) than it can be removed by reaction (VII), thus resulting in distillation of SiO.

The reaction thus proceeds by a solid-solid and solid-gas mechanism. In both reactions (IV) and (VII), the silicons presumably occupy the magnesium sites in the oxide lattice, forming the orthosilicate. As this orthosilicate layer builds up around the silicon, diffusion of the oxygen anion outward to the silicon or diffusion of silicon to the magnesium oxide is necessary. Jander (1, 11) has indicated the rapidity at which alkaline earth oxides diffuse through the orthosilicate structure and this fact may also account for the diffusion process in the present reaction. According to equation (VII) any SiO molecules that react with MgO produce free silicon, which can act as a nucleus for further reaction. This phenomenon would decrease the diffusion path discussed above and may contribute in part to the explanation for the rapidity of this reaction.

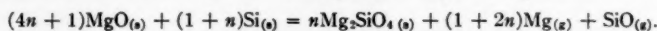
The formation of Mg_2Si has been suggested as an intermediate in the reaction between magnesium oxide and silicon (12, 13). The phase diagram of the Mg-Si system shows only one-compound formation, Mg_2Si , with no solid solubility (14). In the present investigation Mg_2Si was heated to 1100°C in vacuum and complete dissociation according to equation (VIII) was observed on X-ray analysis.



Furthermore when Si was replaced by Mg_2Si in the MgO-Si reaction, no difference in the rate was observed. X-Ray analysis of the residue from the MgO-Si reaction at various stages of the reaction showed no presence of magnesium silicides.

CONCLUSION

In the reaction between magnesium oxide and silicon, gaseous SiO is produced as well as magnesium. The reaction can be expressed by the equation



The pressure of SiO appears to be appreciable above 1300°C .

A solid-solid, and solid-gas mechanism involving SiO is postulated for this reaction. An intermediate formation of Mg_2Si appears to be unlikely.

ACKNOWLEDGMENT

Support of this work through a fellowship (to J. M. T.) from the Steel Company of Canada is gratefully acknowledged.

REFERENCES

1. W. JANDER and E. HOFFMANN. *Z. anorg. Chem.* **218**, 211 (1934).
2. J. W. MALLET. *Liebigs Ann. Chem.* **190**, 62 (1878).
3. A. SCHNEIDER and E. HESSE. *Z. Elektrochem.* **46**, 279 (1940).
4. J. M. TOGURI and D. H. LAING. To be published.
5. W. J. KROLL and A. W. SCHLECTEN. *J. Electrochem. Soc.* **93**, 247 (1948).
6. J. L. MARGRAVE. *Physico-chemical measurements at high temperature. Edited by Bockris, White, and Mackenzie.* Butterworth Scientific Publications, London, 1959.
7. E. ZINTL. *Z. anorg. Chem.* **245**, 1 (1940).
8. E. ZINTL. U.S. Patent No. 2,286,663.
9. L. BREWER and R. K. EDWARDS. *J. Phys. Chem.* **58**, 35 (1954).
10. L. BREWER and F. T. GREENE. *J. Phys. Chem. Solids*, **2**, 286 (1957).
11. W. JANDER and E. WUHRER. *Z. anorg. Chem.* **226**, 225 (1936).
12. W. J. KROLL. U.S. Bureau of Mines I. C. 7327. 1945.
13. W. J. KROLL. *Rev. mét.* **48**, 929 (1951).
14. C. J. SMITHELLS. *Metals reference book.* Butterworth Scientific Publ., London, 1955.
15. O. KUBASCHEWSKI and E. L. L. EVANS. *Metallurgical thermochemistry.* Pergamon Press Ltd., London, 1958.

STEROIDS

1. 12 β -METHYL-12 α -HYDROXYPROGESTERONE¹

GEORGE JUST AND R. NAGARAJAN

ABSTRACT

Lithium aluminum hydride reduction of 3 α ,12 α -diacetoxypregnan-20-one (Ia) gives as the major product pregnane-3 α ,12 α ,20 β -triol (III), whereas the reduction of the corresponding dihydroxypregnanone I affords mainly the epimeric 3 α ,12 α ,20 α -triol II. Triol III was transformed to 12 β -methyl-12 α -hydroxyprogesterone (VIII).

As part of a continuing study of the chemistry of steroids bearing functional groups in ring C, and of the interaction between substituents located at positions 12 and in the side-chain (1, 2), the preparation of 12-methyl-12-hydroxypregnane derivatives such as VI and VII was undertaken.

Engel and Huculak (3) have recently described the preparation of 3 α ,20 β -dihydroxypregnan-12-one bis-methyl succinate (Vb) through the sequence Ia \rightarrow III \rightarrow IIIb \rightarrow Vb. This ketone Vb appeared to us a useful intermediate for the introduction of a 12-methyl substituent.

Lithium aluminum hydride reduction of 3 α ,12 α -diacetoxypregnan-20-one (Ia) gave pregnane-3 α ,12 α ,20 β -triol (III) and a small amount of material which Engel and Huculak (3) had tentatively formulated as pregnane-3 α ,12 α ,20 α -triol (II). Chromic acid oxidation of this material to pregnane-3,12,20-trione (IV) confirmed this assignment of structure. In accordance to the findings of Sarett (4, see also refs. 3 and 5), the difference of increment of molecular rotation due to the acetylation of the 20 β - and the 20 α -hydroxy group was of the order of 200°.

Surprisingly, lithium aluminum hydride reduction of 3 α ,12 α -dihydroxypregnan-20-one (I) gave as the major product pregnane-3 α ,12 α ,20 α -triol (II). A more detailed study of the reduction revealed that the yield of the epimeric triols II and III depended on the solvent and on the nature of the functional group attached at position 12. The results are summarized in Table I.

TABLE I

Starting material	Solvent	%II(20 α -OH)	%III(20 β -OH)
1. Diol I	Tetrahydrofuran	58.5	27.0
2. Diol I	Diethyl ether	65.8	10.2
3. Diacetate Ia	Tetrahydrofuran	9.2	69.7*
4. Diacetate Ia	Tetrahydrofuran	5.8	81 (3)
5. Diacetate Ia	Diethyl ether	37	46.8

*No attempt was made in this case to obtain the maximum yield.

The reduction of the 20-keto diacetate Ia to the 20 β -triol III proceeds according to Cram's rule of steric control of asymmetric induction (6). The stereochemistry of the reduction of the 20-keto diol I to the 20 α -triol II can be readily explained, if one assumes

¹Manuscript received November 7, 1960.

Contribution from the Department of Chemistry, McGill University, Montreal, Que. This paper forms a part of the Ph.D. thesis of R. Nagarajan, to be presented to the Faculty of Graduate Studies, McGill University.

the formation of an intermediate complex of the type $\begin{array}{c} | \\ -C_{12}-O-Al \cdots O=C_{20} \\ | \end{array}$. The

carbonyl group is then reduced by another hydride molecule. Sicher *et al.* (7) have postulated a similar complex to explain why dehydrochloramphenicol and its *O*-acetate form threo- and erythro-chloramphenicol, respectively, upon Meerwein-Ponndorf reduction.

The co-ordination of the aluminum hydride alcoholate by the carbonyl group is competing with solvation by ether and tetrahydrofuran (8). As tetrahydrofuran is more basic than ether (9), one would expect less co-ordination of the 20-carbonyl oxygen in the lithium aluminum hydride reduction in tetrahydrofuran, and hence more 20 β -alcohol III would be formed in that solvent. This hypothesis is confirmed by experimental evidence (Table I, columns 1 and 2).

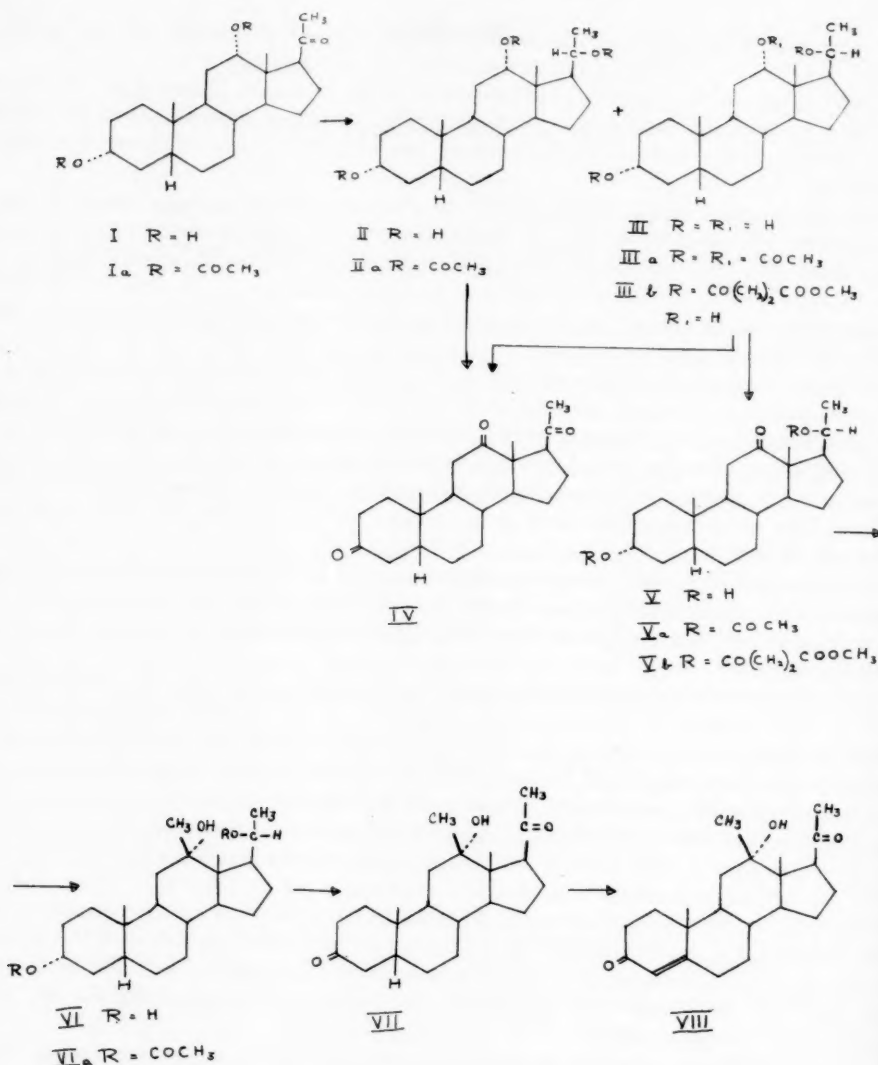
An explanation of the solvent effect in the reduction of the diacetoxo ketone Ia would follow similar lines. The only assumption which would have to be made is that the 20-keto group is reduced at a similar rate as the 12-acetate group. Reduction of keto diol I with a fivefold excess of sodium borohydride indicated the hindered nature of the 20-carbonyl group, since even after 20 hours it was not complete, as evident from infrared measurements. This experiment does lend some weight to the assumption made, without, however, proving it.

A co-ordination complex involving aluminum hydride would also account for the conversion of 17 α -hydroxypregnane-20-ones by the action of lithium aluminum hydride to a mixture of 20 β - and 20 α -dihydroxypregnane derivatives, in which the latter predominated (5).

Succinylation of triol III to the succinate IIIb (3), followed by oxidation, afforded the 12-keto disuccinate Vb (3). Prolonged treatment of the ketone Vb with methyl magnesium iodide in diethyl ether led to a reaction mixture containing sizable amounts of starting material. The keto disuccinate Vb was therefore hydrolyzed with methanolic potassium hydroxide to the dihydroxy ketone V, which was converted to the corresponding diacetate Va. Treatment of the 12-keto diacetate Va with excess ethereal methyl magnesium iodide for 20 hours gave a 73% yield of the desired 12 β -methylpregnane-3 α ,12 α ,20 β -triol VI. Triol VI formed a diacetate VIa, and was easily oxidized to 12 β -methyl-12 α -hydroxypregnane-3,20-dione (VII), thus establishing the tertiary nature of the 12-hydroxy group. The assignment of configuration of the 12-methyl group will be substantiated in a following paper. It is in disagreement with the assignment of configuration made by Levine and Wall (10) and Bladon and McMeekin (11), who transformed hecogenin to "12 α -methyl-12 β -hydroxy tigogenin".

Because of the considerable interest in steroid hormone analogues containing alkyl and other substituents in the steroid nucleus (see, e.g. 10, 11, 12), we decided to transform 12 β -methyl-12 α -hydroxypregnane-3,20-dione (VII) into the closely related 12 β -methyl-12 α -hydroxyprogesterone (VIII). This was readily achieved by bromination in position 4, followed by dehydrobromination (13). The progesterone analogue thus obtained did not exhibit any notable progestational, androgenic, diuretic, hypotensive, or anabolic properties.²

²Biological tests were carried out by Dr. C. I. Chappel and Dr. Clara Revesz, Ayerst, McKenna and Harrison, Montreal.

EXPERIMENTAL^{3, 4, 5, 6}*Reduction of 3α,12α-Diacetoxypregnan-20-one (Ia) in Ether*

A solution of the diacetate Ia (14) (30.0 g, 0.0717 mole, m.p. 122–123°) in absolute ether (500 ml) was added with stirring to a solution of lithium aluminum hydride (33 g) in absolute ether (1500 ml). The reaction mixture was heated under reflux for 1 hour and

³All the melting points were corrected.

⁴Only the best yields were reported.

⁵The commercially available aluminum oxide (Woelm) was used.

⁶The microanalyses were carried out by Dr. Alfred Bernhardt, Germany.

left at room temperature overnight. The excess lithium aluminum hydride was destroyed by adding ethyl acetate (175 ml) and then 2 *N* sulphuric acid (450 ml). The solvents were removed by distillation and the reaction mixture extracted with chloroform. The chloroform layer was washed with 5% sodium bicarbonate solution, water, saturated sodium chloride solution, and dried over magnesium sulphate.

Repeated crystallizations from chloroform gave the 20 α -alcohol II (8.902 g, 37.0%), m.p. 225–226°, [α]_D²⁵ 46° (*c* 0.59 in CHCl₃). The substance was slightly hygroscopic. Crystallization from acetone did not change the melting point. Calcd. for C₂₁H₃₆O₃: C 74.98%, H 10.78%. Found: C 74.94%, H 10.66%.

Crystallization of the mother liquors from acetone gave the 20 β -alcohol III (3) (11.260 g, 46.8%), m.p. 236–238°, [α]_D²⁵ 34° (*c* 0.78 in CHCl₃).

Calcd. for C₂₁H₃₆O₃: C 74.98, H 10.78%. Found: C 74.84, H 10.61%.

Reduction of 3 α ,12 α -Dihydroxypregnan-20-one (I) in Ether

A solution of the diol I (14) (1.414 g, 0.00423 mole, m.p. 168–172°; crude product obtained by alkaline hydrolysis of the diacetate Ia) in absolute ether (200 ml) was added with stirring to a solution of lithium aluminum hydride (1.5 g) in absolute ether (100 ml). The reaction mixture was worked up as described above. The yields of 20 α -alcohol II, m.p. 225–226°, and of 20 β -alcohol III, m.p. 236–238°, were 65.5% and 10.5% respectively. The alcohols were identified by mixed melting point and comparison of I.R. spectra.

Reduction of 3 α ,12 α -Dihydroxypregnan-20-one (I) in Tetrahydrofuran

A solution of the diol I (2.635 g, 0.00789 mole, m.p. 168–172°, crude product obtained by alkaline hydrolysis of the diacetate Ia) in absolute tetrahydrofuran (200 ml) was added dropwise, with stirring, to a solution of lithium aluminum hydride (3.0 g) in absolute tetrahydrofuran (250 ml). The reaction mixture was worked up as described above. The yields of the 20 α -alcohol II, m.p. 225–226°, and of 20 β -alcohol III, m.p. 236–238°, were 58.5% and 27.2% respectively. The identity of the alcohols was confirmed by mixed melting point and superimposability of I.R. spectra.

Reduction of 3 α ,12 α -Diacetoxypregnan-20-one (Ia) in Tetrahydrofuran (3)

A solution of the diacetate Ia (30.9 g, 0.0739 mole, m.p. 122–123°) in absolute tetrahydrofuran (200 ml) was reduced with lithium aluminum hydride (36 g) in 1500 ml of absolute tetrahydrofuran (3). Chloroform extraction afforded 21.1 g (85% yield) of the crude product. Separation of the triols, as described above, afforded 2.40 g of the 20 α -triol II (m.p. 221–224°, 9.5% yield), and 17.3 g of the 20 β -triol III (m.p. 231–233°, 69.7% yield).

3 α ,12 α ,20 α -Triacetoxypregnane (IIa)

Triol II (130 mg, m.p. 225–226°) was heated under reflux for 1 hour in pyridine (3 ml) and acetic anhydride (1 ml). The reaction mixture was worked up as usual and afforded, on crystallization from ether–hexane, the triacetate IIa, m.p. 147–148°, [α]_D²⁵ 95° (*c* 0.73 in CHCl₃).

Calcd. for C₂₇H₄₂O₆: C 70.09%, H 9.15%. Found: C 70.27%, H 9.20%.

3 α ,12 α ,20 β -Triacetoxypregnane (IIIa)

Triol III (130 mg, m.p. 236–38°) was treated as described above. Crystallization of the crude product from ether–hexane yielded the triacetate IIIa (3), m.p. 201–202°, [α]_D²⁵ 127° (*c* 0.81 in CHCl₃). The melting point was not depressed upon admixture with an authentic sample⁷ and the I.R. spectra were identical.

⁷Kindly supplied by Dr. C. R. Engel, Department of Chemistry, Laval University, Quebec.

Pregnane-3,12,20-trione (IV)

In parallel runs, a solution of triol II and of triol III (300 mg) in acetic acid (15 ml) was treated with a solution of chromium trioxide (300 mg) in 3 ml of 90% acetic acid at room temperature for 20 hours. Extraction and crystallization gave in each case an 80–90% yield of IV (15), m.p. 203–205°. The identity of the samples in both cases was confirmed by mixed melting point and superimposability of I.R. spectra.

3 α ,12 α ,20 β -Trihydroxypregnane 3 α ,20 β -bis-Methyl Succinate (IIIb)

To a solution of the triol III (4.38 g) in pyridine (40 ml), succinic anhydride (10.2 g) was added. The reaction mixture was heated at 90° on a water bath for 4 hours, and left overnight at room temperature. It was diluted with ice-cold water (1500 ml) and left for 1 hour. The solution was extracted with ether, washed with 2 *N* sulphuric acid, and twice with water. The ethereal extract was dried over magnesium sulphate. Upon evaporation of the solvent to 250 ml, 4.054 g of the bis-hemisuccinate, m.p. 188–189°, crystallized.

Crystallization of mother liquors from acetone–hexane afforded 2.192 g, m.p. 188–189°.

Recrystallization for analysis raised the m.p. to 190–191° (m.p. 182–184° (3)).

Calcd. for C₂₉H₄₄O₉: C 64.91%, H 8.26%. Found: C 64.79%, H 8.35%.

A solution of the bis-hemisuccinate (6.152 g) in ether (1500 ml) was methylated with an excess of diazomethane in ether. One crystallization from ether–hexane afforded 5.855 g of IIIb (3), m.p. 96–97°, [α]_D²⁹ 67° (*c* 0.97 in CHCl₃). Crystallization of the mother liquors gave 0.257 g of IIIb, m.p. 94–95° (yield 84%).

3 α ,20 β -Dihydroxypregnan-12-one bis-Methyl Succinate (Vb)

Oxidation with chromium trioxide in acetic acid of the bis-methyl succinate IIIb (6.025 g) afforded 5.971 g of the keto bis-methyl succinate Vb (3), m.p. 112–113°, [α]_D²⁹ 110° (*c* 0.91 in CHCl₃).

3 α ,20 β -Dihydroxypregnan-12-one (V)

To a solution of the keto bis-methyl succinate Vb (10.0 g) in methanol (700 ml) and water (100 ml) was added potassium carbonate (12.5 g) and the mixture was refluxed for 17 hours. The major part of the methanol was distilled off *in vacuo*. The reaction mixture was worked up as usual and on crystallization from acetone–hexane, 2.868 g of the hydroxy ketone V, m.p. 221–222°, was obtained. The I.R. spectrum of the mother liquors showed that the hydrolysis was not complete. The mother liquors were further hydrolyzed with 5% methanolic potassium hydroxide for 8 hours at reflux temperature and worked up as usual. Crystallization from acetone–hexane afforded 3.044 g of the hydroxy ketone V, m.p. 220–222° (yield 96%).

A portion of the hydroxy ketone V was crystallized twice from acetone–hexane for analysis, m.p. 222–223°, [α]_D²⁹ 131° (*c* 0.95 in CHCl₃).

Calcd. for C₂₁H₃₄O₃: C 75.41, H 10.24. Found: C 75.20, H 10.06.

3 α ,20 β -Diacetoxypregnan-12-one (Va)

A solution of the hydroxy ketone V (400 mg) in pyridine (10 ml) and acetic anhydride (10 ml) was kept in a water bath at 90° overnight. Ether extraction gave 511 mg of crude product. One crystallization from ether–hexane yielded 416 mg of the ketone Va, m.p. 136–137°. Crystallization of mother liquors afforded 53 mg of Va, m.p. 135–136° (yield 93%).

A portion of ketone *Va* was crystallized twice from ether-hexane for analysis, m.p. 136–137°, $[\alpha]_D^{29}$ 179° (c 1.09 in CHCl_3).

Calcd. for $\text{C}_{30}\text{H}_{48}\text{O}_5$: C 71.73, H 9.15. Found: C 71.91, H 9.25.

12 β -Methyl-3 α ,12 α ,20 β -trihydroxypregnane (VI)

To 200 ml of an ethereal solution of methyl magnesium iodide (from 270 mg of magnesium and 0.7 ml of methyl iodide) was added with stirring 575 mg of the ketone *Va*, dissolved in 200 ml of absolute ether. The reaction mixture was refluxed for 20 hours. A solution of ammonium chloride (10 g) in water (200 ml) was added to the reaction mixture. It was then extracted with ether and the organic solution washed with water until neutral. The ethereal extract was dried over magnesium sulphate. On evaporating the major part of the ether, crystals of the triol *VI* (110 mg, m.p. 213–214°) were obtained. Crystallization of mother liquors afforded 98 mg of the triol *VI*, m.p. 210–213°.

Recrystallizations from aqueous methanol and methanol raised the m.p. to 213–215°, $[\alpha]_D^{29}$ 39° (c 0.88 in CHCl_3).

Calcd. for $\text{C}_{22}\text{H}_{38}\text{O}_3$: C, 75.37, H 10.92. Found: C 75.21, H 10.92.

The mother liquors were acetylated and the resulting oil (435 mg) chromatographed on alumina (4.5% water). The hexane-benzene (4:1) fractions consisted mainly of the unreacted ketone. Hexane-benzene (1:1) fractions were collected and on crystallization from hexane gave 73 mg of the diacetate *VIa*, m.p. 119–121°. The mother liquors on crystallization from hexane afforded 15 mg of the diacetate *VIa*, m.p. 119–121°.

A portion of the diacetate *VIa* was crystallized twice from hexane for analysis, m.p. 122–124°, $[\alpha]_D^{29}$ 78° (c 1.01 in CHCl_3).

Calcd. for $\text{C}_{26}\text{H}_{42}\text{O}_5$: C 71.86, H 9.74. Found: C 71.66, H 9.99.

The mother liquors of the hexane-benzene (1:1) fractions and the remainder of the fractions of the chromatogram afforded upon alkaline hydrolysis and crystallization from ether-hexane 71 mg of the triol *VI*, m.p. 208–210° (yield 73%).

12 β -Methyl-12 α -hydroxypregnane-3,20-dione (VII)

Chromium trioxide (490 mg) in 90% acetic acid (5 ml) was added with stirring to a solution of the triol *VI* (750 mg) in acetic acid (50 ml) and left at room temperature overnight. Ether extraction afforded 723 mg of the crude hydroxy ketone *VII*, m.p. 184–186°. One crystallization from acetone-hexane gave 663 mg of the hydroxy ketone *VII*, m.p. 187–188°. Crystallization of mother liquors afforded 15 mg of *VII*, m.p. 186–187° (yield 92%).

A portion of the hydroxy ketone *VII* was crystallized twice from acetone-hexane for analysis, m.p. 187–188°, $[\alpha]_D^{29}$ 102°, (c 1.05 in CHCl_3).

Calcd. for $\text{C}_{22}\text{H}_{34}\text{O}_3$: C 76.25, H 9.89. Found: C 76.10, H 9.87.

12 β -Methyl-12 α -hydroxypregesterone (VIII)

A solution of bromine (141 mg) in acetic acid (9.4 ml) was added to a solution of the hydroxy ketone *VII* (300 mg) in acetic acid (10 ml) with stirring. After 5 minutes, the reaction mixture was poured into ice-water (500 ml), and extracted with ether. The organic layer was washed with water and dried. There was obtained 395 mg of an oil which resisted crystallization.

The crude bromo ketone was dehydrobrominated according to the method of McGuckin and Kendall (13). The crude product (240 mg of oil) on crystallization from ether-hexane afforded 125 mg of the progesterone derivative *VIII*, m.p. 140–150°. Repeated

crystallizations gave 97 mg of analytically pure VIII, m.p. 152–153°, $[\alpha]_D^{20}$ 182° (*c* 1.01 in CHCl_3), $\lambda_{\text{max}}^{\text{EtOH}}$ 239 m μ , (ϵ 17500), $\nu_{\text{max}}^{\text{CCl}_4}$ 1710 cm^{-1} (20-ketone), 1680 cm^{-1} , 1620 cm^{-1} (Δ^4 -3-ketone).

Calcd. for $\text{C}_{22}\text{H}_{32}\text{O}_3$: C 76.68, H 9.37. Found: C 76.40, H 9.40.

ACKNOWLEDGMENTS

We wish to thank the National Research Council, Messrs. Ayerst, McKenna and Harrison, and the Department of Chemistry, McGill University, for generous financial support.

REFERENCES

1. CH. R. ENGEL, K. F. JENNINGS, and G. JUST. *J. Am. Chem. Soc.* **78**, 6153 (1956).
2. G. JUST and CH. R. ENGEL. *J. Org. Chem.* **23**, 12 (1958).
3. CH. R. ENGEL and W. HUCULAK. *Can. J. Chem.* **37**, 2031 (1959).
4. L. H. SARETT. *J. Am. Chem. Soc.* **71**, 1175 (1949).
5. D. K. FUKUSHIMA and E. D. MEYER. *J. Org. Chem.* **23**, 174 (1958), and references cited therein.
6. D. J. CRAM and F. A. ABD ELHAFAZ. *J. Am. Chem. Soc.* **74**, 5828 (1952).
7. J. SICHER, M. SYOBODA, M. HRDÁ, J. RUDINGER, and F. ŠORM. *Collection Czechoslov. Chem. Commun.* **4**, 487 (1953).
8. N. L. PADDOCK. *Chem. & Ind. (London)*, 63 (1953).
9. H. C. BROWN and R. M. ADAMS. *J. Am. Chem. Soc.* **64**, 2557 (1942).
10. S. G. LEVINE and M. E. WALL. *J. Am. Chem. Soc.* **82**, 3391 (1960).
11. P. BLADON and W. McMEEKIN. *J. Chem. Soc.* 2191 (1960).
12. B. G. CHRISTENSEN, R. G. STRACHAN, N. R. TRENNER, B. H. ARISON, R. HIRSCHMANN, and J. M. CHEMERDA. *J. Am. Chem. Soc.* **82**, 3995 (1960).
13. W. F. MCGUCKIN and E. C. KENDALL. *J. Am. Chem. Soc.* **74**, 5811 (1952).
14. W. H. HOEHN and H. L. MASON. *J. Am. Chem. Soc.* **60**, 1493 (1938).
15. T. REICHSTEIN and E. v. ARX. *Helv. Chim. Acta*, **23**, 747 (1940).

THE DEMETHYLATION OF SUGARS WITH HYDROGEN PEROXIDE¹

B. FRASER-REID, J. K. N. JONES, AND M. B. PERRY

ABSTRACT

Demethylation of methylated sugars can be achieved using hydrogen peroxide and ferrous iron (Fenton's reagent). The reaction is not specific and further oxidation of the sugar also occurs. The preparation of 3,4-di-*O*-methyl-D-mannose from the corresponding mannitol derivative is described. Mono-*O*-methyl derivatives of D-mannose and of D-mannitol as well as D-mannose and D-mannitol were also produced. The course of the demethylation of 2,3,4,6-tetra-*O*-methyl methyl α -D-glucoside by Fenton's reagent has been examined.

Hydrolysis of methylated yeast mannan yields 3,4-di-*O*-methyl-D-mannose as a major component of the methylated sugars (1, 2). No simple method is available for the synthesis of this sugar but Aspinall and Zweifel (3) have shown how it may be obtained from D-mannose by a rather long and involved route.

As early as 1894, Fenton (4) showed that ferrous iron had a specific influence on the oxidation of hydroxyl-containing compounds by hydrogen peroxide and other oxidizing agents. He showed, for example, that it was possible to convert various polyhydric alcohols into the corresponding aldoses (5). This method suggested itself to us as convenient for the conversion of 3,4-di-*O*-methyl-D-mannitol to 3,4-di-*O*-methyl-D-mannose, the starting material being readily available from 1,2-5,6-di-*O*-isopropylidene-D-mannitol. An attraction of this scheme is the symmetry of the dimethyl mannitol, which ensures that only one aldohexose would be produced regardless of which end of the molecule was oxidized.

It was surprising, therefore, to find that, when 3,4-di-*O*-methyl-D-mannitol was oxidized by Fenton's reagent in ice-cold solution and the resulting solution analyzed chromatographically, sugars corresponding to mannitol, mannose, and their mono-*O*-methyl and di-*O*-methyl derivatives were detected, as well as methylated pentoses and uronic acids. Repetition of this experiment under a variety of conditions confirmed these observations.

Because of the strangeness of these findings we investigated the action of the reagent on a fully methylated sugar. It was observed that 2,3,4,6-tetra-*O*-methyl methyl α -D-glucoside was demethylated to yield among other products D-glucose and the possible mono-, di-, tri-, and tetra-*O*-methyl-D-glucoses. Our analyses of the mixture of monomethyl glucoses so obtained indicate that the methoxyl groups on carbons 2 and 4 are most strongly attacked, those on carbon 6 next strongly, and those on carbon 3 least strongly attacked.

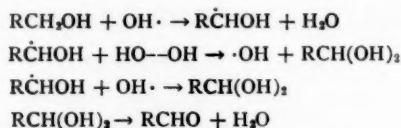
Saunders (6) has shown that, under the catalytic influence of the enzyme ferriperoxidase, hydrogen peroxide will oxidize *p*-anisidine to 2-amino-5-*p*-anisidino benzoquinone di-*p*-methoxyphenylimine with elimination of one methoxyl group. But as far as we are aware the observations described above are the first in which the elimination of methoxyl groups by oxidation from sugar residues has been described.

It is well established that the ferrous-peroxide system produces hydroxyl radicals and the reaction sequence first formulated by the Haber-Weiss theory (7) was later confirmed and expanded by Evans (8). Waters *et al.* (9, 10) have shown that the kinetics of the system is consistent with the thesis that the oxidizing species is the free radical. Grinstead

¹Manuscript received November 23, 1960.

Contribution from the Department of Chemistry, Queen's University, Kingston, Ontario.

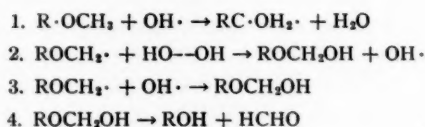
(11, 12) has suggested how they may attack various substrates and Waters (9, 10) has postulated that the radical attacks primary hydroxyl groups as follows (scheme A).



SCHEME A

This scheme explains the oxidation of hexitol to hexose. The latter may then be further oxidized to a hexonic acid, and if oxidized further a pentose may arise by oxidative decarboxylation, a well-known reaction in carbohydrate chemistry.

We suggest that the hydroxyl free radical is also the demethylating species and that the scheme operates as follows (scheme B).



SCHEME B

Cleavage of the $\text{R}-\text{OCH}_3$ bond seems unlikely because (a) this would involve the more complex radical abstraction of $-\text{OCH}_3$ and (b) some inversion of configuration at the reaction center might be expected, especially in view of the absence of steric hindrance in the zigzag form of the hexitol in solution. No products resulting from such an inversion have been detected. The electronegativity of the hydroxyl radical should render it capable of such hydrogen abstraction (cf. ref. 13). Quantitative experiments with 2,3,4,6-tetra-*O*-methyl methyl- α -D-glucoside indicated that the reducing power of the reaction mixture, after acidic hydrolysis, was increased only by 27% of the theoretical value. This indicated that the glucosidic methoxyl group was attacked to the extent of 73%. In neutral solution demethylation proceeds only to a limited extent.

If the hydroxyl radical is engaged in both oxidation and demethylation then some competition for the radical to be involved in either of the processes (schemes A and B) is to be expected. Tables I and II record the conditions and results of experiments. In these tables the relative order of intensity of sugars as detected chromatographically is given in the form $1 > 2 > 3$, etc. The reaction was initially exothermic and was accompanied by a considerable evolution of carbon dioxide. The solution rapidly became acidic

TABLE I

Experiment	Dimethyl mannitol (g)	Ferrous sulphate (g)	15% H_2O_2 (ml)	Temp. ($^{\circ}\text{C}$)
A	1.0	—	5	23-25
B	1.0	1.0	5	"
C	1.0	0.1	5	"
D	1.0	0.1	5	0-5
E	1.0	0.1	10	0-5
F	1.0	0.1	2.5	0-5

TABLE II

Experiment	Mannose	Monomethyl mannose	Dimethyl mannose	Pentose*	Unreacted dimethyl mannitol	Reducing group†
A	None	None	None	None	1	<1
B	1	2	3	Trace	4	40
C	3	3	3	2	1	20
D	4	3	2	Trace	1	36
E	2	Trace	None	1	None	13
F	2	2	2	Trace	1	54

*Free, mono-, and di-methyl.

†As percentage from available primary alcohol.

(pH 6 \rightarrow pH 1) (cf. ref. 14). From the percentage of reducing groups produced it is clear that much of the hexitol is converted into reducing sugars and then further oxidized to aldonic acids. Osones were not detected, nor was formaldehyde. The latter was presumably further oxidized to carbon dioxide. After completion of the reaction, the solution in certain cases (see Experimental Section) was neutralized and deionized and the products separated chromatographically. It is clear that in the absence of ferrous sulphate no demethylation occurs and that a decrease in the concentration of ferrous sulphate or in the temperature of the reaction mixture results in less demethylation. High concentration of hydrogen peroxide and high temperatures favor the formation of pentoses and non-reducing acidic materials.

We have also investigated the fate of anisole when subjected to Fenton's reagent at 0–3° C. The reaction is only very slightly exothermic and an immediate dirty-green color is produced on the addition of peroxide. At least four phenolic products have been obtained, one being identified (by paper chromatography) as guaiacol. Infrared analyses indicate that very little of the methoxyl group is removed. Thus it appears that the aromatic nucleus is much more readily attacked than is the methoxyl group.

The removal of the methyl group from a methoxyl group by hydroxyl radicals is of biochemical interest because a similar mechanism may be operative in some organisms.

EXPERIMENTAL

The following solvent systems were used to separate sugars on paper chromatograms: (i) butan-1-ol, ethanol, water (3:1:1) and (ii) butan-1-ol, pyridine, water (10:3:3) (all vol/vol). Reducing sugars were detected with (a) the *p*-anisidine hydrochloride spray (15) and components with adjacent hydroxyls (reducing and non-reducing) were detected with (b) 0.1 *M* sodium periodate followed after about 5 minutes with the *p*-anisidine spray (cf. ref. 16).

Phenols were separated by reverse phase chromatography on paper (Whatman No. 1) previously impregnated with 10% tetrahydro naphthalene in methanol and allowed to dry in air. The irrigant was water:methanol (8:2) and the phenols on the air-dried chromatogram were sprayed with a solution of sulphanilic acid followed immediately after with 20% sodium bicarbonate solution (17).

Paper electrophoresis was performed on Whatman 3mm paper saturated with borate buffer pH 10 at ca. 1500 volts for 1–1½ hours (18, 19).

Deionizations were effected by passing the solution down columns of Amberlite IR120 (H⁺ form) followed by passage through Duolite A4 (OH⁻ form). All solutions were concentrated under diminished pressure below 50° C.

Melting points and mixed melting points were determined simultaneously on a standard Fischer-Johns block and the values quoted are uncorrected. Optical rotations were determined in water ($C = 1$).

Chromatographic fractionations were effected by placing the syrup on a cellulose column in the usual manner (20). The columns were irrigated with butan-1-ol, light petroleum mixture (4:1) to remove tri- and higher methylated sugars; butan-1-ol - water mixture (95:5) was used to remove the lower methylated and free sugars. In every case the combined fractions were concentrated to a syrup which was purified by deionization and by refluxing their solutions in methanol with decolorizing charcoal.

PART I

Preparation of 3,4-Di-O-methyl-D-mannitol

3,4-Di-O-methyl-D-mannitol (m.p. 145-147° C) was prepared by methylation (Kuhn's method (21,22)) of 1,2-5,6-di-O-isopropylidene-D-mannitol, the latter being prepared from D-mannitol (23).

Oxidation of 3,4-Di-O-methyl-D-mannitol

To a solution of dimethyl mannitol (15 g) in water (100 ml) ferrous sulphate (45 g) was added with stirring. When solution was complete hydrogen peroxide (75 ml, 15%) was added gradually during 1½ hours and the temperature of the solution was maintained between 20-25° C by use of an ice-water bath. After the addition the reaction mixture was kept with stirring at room temperature for an additional 2 hours. The solution was neutralized and the precipitate was removed by filtration and the light-green-colored filtrate deionized. The solution was concentrated to give a syrup (9.5 g) which was fractionated on a cellulose column.

Fraction I gave a syrup which chromatographed as a single spot corresponding to authentic 3,4-di-O-methyl-D-mannose. This was crystallized from ethanol-ether. The crystals so deposited melted between 90-95° C and were possibly a mixture of the hydrated and anhydrous forms. The mixture was redissolved in dry acetone-ether and after about 6 weeks spherically shaped crystals had deposited, m.p. 77-79° C, mixed m.p. 78-81° C, $[\alpha]_D^{20} = 16.6^\circ$ (initial) $\rightarrow 8^\circ$ (after 24 hours, constant value) (cf. Aspinall and Zwielfel (3)).

Fraction II was identified as unchanged 3,4-di-O-methyl-D-mannitol.

Fraction III was identified chromatographically as a mixture of mono-O-methyl-D-mannoses. The purified syrup was dissolved in water (100 ml) (solution A) and the solution was used for further experiments.

Preparation and Analysis of Monomethyl Mannosides

The above solution (20 ml corresponding to 65 mg of syrup) was removed and evaporated to a syrup which was converted to the glycosides in the usual manner (see glycosidation of monomethyl glucoses below). The syrupy glycosides were purified by twice extracting them under reflux with ethanol, and once with water in the presence of decolorizing charcoal. The product was dried at 50° C (P_2O_5) to a constant weight (40.9 mg). This syrup was dissolved in water, diluted to 50 ml and periodate oxidation studies were conducted on 40 ml ($\equiv 32.7$ mg) of the solution so prepared (31, 32). (See experimental on monomethyl glucose below.) After 35 hours the periodate uptake had a constant value of 0.41 mole, and the formic acid liberation was negligible (0.01 mole). These results indicate that approximately 40% of the monomethyl mannose is present as the 4-O-methyl isomer.

The oxidized solution was deionized and the deionized solution hydrolyzed with 2 *N* sulphuric acid. The hydrolyzate was neutralized with barium carbonate, filtered, deionized, and analyzed qualitatively by paper electrophoresis using authentic 3-*O*-methyl-D-mannose as standard. The presence of this isomer was clearly indicated.

Reduction of Monomethyl Mannose

Potassium borohydride (0.2 g) was added to solution A (30 ml) and the mixture was left at room temperature overnight, after which it gave a negative reaction to Fehling's solution. The solution was neutralized by adding Amberlite resin IR120 (H^+ form), filtered, and the filtrate was evaporated to dryness. The boric acid was removed by repeated codistillation with methanol. The resulting product was twice crystallized from ethanol, and then dried at 65° C to give white crystals; m.p. 133–134° C; $[\alpha]_D^{25} = +18^\circ$, in good agreement with Hudson's constants for 3(4)-*O*-methyl-D-mannitol (24). Thus both sugars give one product upon reduction and this indicates conclusively that the two components are 3-*O*-, and 4-*O*-monomethyl-D-mannoses.

Fraction IV was monomethyl mannitol. The clear syrup was crystallized from ethanol. The dried crystals melted at 131–133° C and when mixed with the reduced monomethyl mannose above melted at 131–133° C. This fraction therefore contains only one component, which was identified as 3-*O*-monomethyl-D-mannitol (equivalent to the 4-*O*-methyl isomer).

Fraction V was identified as D-mannose. To the syrup obtained after purification 0.23 g phenylhydrazine reagent (6 ml) (1 g phenylhydrazine hydrochloride, 2.4 g sodium acetate, 0.6 ml acetic acid, and 25 ml water) was added. An almost immediate precipitate of D-mannose phenylhydrazone formed. The crystals were removed and recrystallized from ethanol. They had m.p. 190–191° C, mixed m.p. 191–192° C.

Fraction VI was identified as D-mannitol. The purified syrup was crystallized from methanol; m.p. 166–168° C, mixed m.p. 165–168° C.

PART II

Preparation of 2,3,4,6-Tetra-O-methyl Methyl- α -D-glucoside

Tetramethyl methyl glucoside was prepared by a Kuhn (21, 22) type methylation of reagent grade methyl- α -D-glucoside. The product had a refractive index of 1.4449 at 20° C [the accepted value is 1.4454 (25)].

Oxidation of 2,3,4,6-Tetra-O-methyl Methyl- α -D-glucoside

The glucoside (6 g) was dissolved in water (30 ml) and ferrous sulphate (36.6 g) was added with stirring. Hydrogen peroxide (50 ml, 15%) was added cautiously with stirring and the temperature was maintained between 20–25° C. After 18 hours at room temperature the mixture was neutralized with barium carbonate. The solution was filtered and the pale green filtrate was made 2 *N* with respect to sulphuric acid and the solution was boiled under reflux for 3½ hours. The cooled solution was neutralized (barium carbonate), filtered, and deionized and the solution evaporated to a syrup (0.992 g). A second oxidation was carried out using the same quantities of reagents but a smaller quantity of hydrogen peroxide.

The combined syrups (2.55 g) were fractionated on a cellulose column.

Fraction I was identified by paper chromatography as 2,3,4,6-tetra-*O*-methyl-D-glucose (260 mg). A partial crystallization occurred overnight. The crystals were removed and converted to the *N*-phenyl glucosylamine by the method of Wolfrom (26). The product had m.p. 133–135° C; mixed m.p. 132–135° C.

Fraction II (tri-*O*-methyl-D-glucoses) yielded a syrup (274 mg) which was a mixture. It was made up to a known volume (solution A) in water.

Detection of 2,3,4-Tri-O-methyl-D-glucose

A portion of solution A equivalent to ca. 20 mg of sugars was evaporated to a syrup which was then dissolved in phosphate buffer (10 ml, pH 7.4). The solution was then saturated with sodium periodate and left overnight at room temperature (solution B). To the oxidized solution (5 ml) excess inositol was added to destroy excess of periodate and acetyl acetone (3 ml) added. Within 1 minute a strong fluorescence developed indicative of the presence of formaldehyde (27). A blank of water treated similarly failed to show any fluorescence even when viewed under ultraviolet light.

Bell has shown (28) that 2,3,4-tri-*O*-methyl-D-glucose is attacked by periodate with non-quantitative liberation of formaldehyde. The presence of 2,3,4-tri-*O*-methyl-D-glucose is therefore established.

Detection of 3,4,6-Tri-O-methyl-D-glucose

The remainder of solution B (5 ml) was deionized and studied by paper chromatography in solvent systems (i) and (ii). A spot running evenly with 2,3,5-tri-*O*-methyl-D-arabinose indicated the presence of the latter in the periodate-oxidized material. This therefore confirms the presence of 3,4,6-tri-*O*-methyl-D-glucose as one of the components in the mixture.

The residue of tri-*O*-methyl-D-glucoses which had not been attacked by periodate was examined on the chromatogram and presumably contained the 2,3,6- and the 2,4,6-isomers since no color developed when the oxidized sample was treated with the triphenyl tetrazolium chloride spray (29, 30) (see Experimental Section on 3,4-di-*O*-methyl-D-glucose).

Fraction III contained di-*O*-methyl-D-glucoses.

Detection of 2,3- and 4,6-Di-O-methyl-D-glucoses

The syrup obtained (340 mg) was compared with authentic specimens of dimethyl glucose isomers by means of chromatograms run in solvent systems (i) and (ii) for 65 hours (*p*-anisidine spray). A major spot was revealed; but immediately ahead of it and immediately behind it, two distinct components were identifiable as 2,3- and 4,6-di-*O*-methyl-D-glucose respectively. The syrup (ca. 100 mg) was separated on paper in solvent system (i) and strips corresponding to the "major spot" removed and extracted with water, the extract now being evaporated to give a syrup (syrup B). Attempts to induce crystallization from ethanol, ethyl acetate, isopropyl acetate, and methanol were all unavailing.

Detection of 3,4- and 3,6-Di-O-methyl-D-glucoses

An electrophoretic analysis on a portion of syrup B against authentic samples of 3,4- and 4,6-di-*O*-methyl-D-glucoses revealed four components:

- (i) a trace of a sugar which moved at the speed of the 4,6-isomer;
- (ii) a large percentage of a sugar which corresponded with the 3,4-isomer;
- (iii) a fast-moving constituent;
- (iv) material which had remained on the base line.

A second electrophoretogram similarly prepared but developed with triphenyl tetrazolium chloride showed characteristic red coloration indicating free adjacent hydroxyls at carbons 1 and 2 (29, 30) and corresponding to (i), (ii), and (iii) above. Component (iii) was therefore probably the 3,6-di-*O*-methyl isomer.

Detection of 2,4-Di-O-methyl-D-glucose

A portion of syrup B was oxidized overnight at room temperature with sodium periodate solution. It was then deionized and the solution was chromatographed and showed residual sugar to be present. 2,4-Di-O-methyl-D-glucose is the only isomer in syrup B which is not oxidized by periodate and is therefore probably present in the mixture. The 2,6-di-O-methyl isomer was the only one not positively identified.

Fraction IV contained mono-O-methyl glucoses.

Preparation of Glucosides

A portion of the syrup obtained (250 mg) was converted to the glucosides by refluxing it with 5% methanolic hydrogen chloride for 18 hours. After neutralization with dry silver carbonate and removal of the precipitate by filtration, the methanolic solution was saturated with hydrogen sulphide, and the precipitated silver sulphide was filtered off through Celite. The filtrate, after decolorizing with charcoal, was evaporated to give a semicrystalline mass which was dried *in vacuo* over phosphorus pentoxide to a constant weight of 78 mg. It had a negative reaction to Fehling's solution.

The syrupy glucosides were made up to a volume of 25 ml with water. Of this, 10 ml (equivalent to 31.2 mg) was removed and 10 ml 0.1 M sodium periodate was added and the whole diluted to 100 ml. A blank of water was similarly prepared. Aliquots (5 ml) were removed at various time intervals and analyzed for periodate uptake by the method of Neumuller and Vasseur (31) and for formic acid liberation by that of Andrews *et al.* (32). The 3-O-methyl isomer is the only one which will survive attack (if all are pyranosides). (See Table III and Fig. 1.)

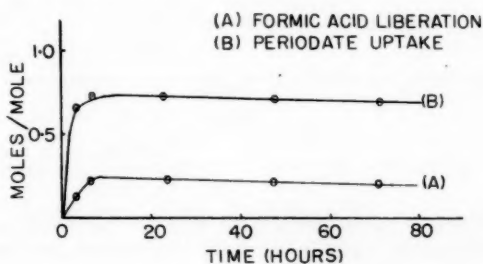


FIG. 1.

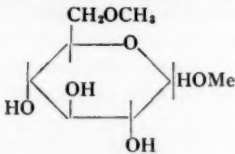
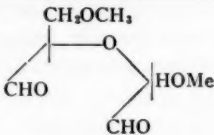
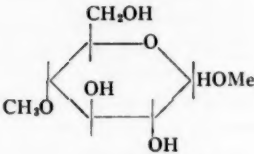
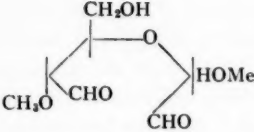
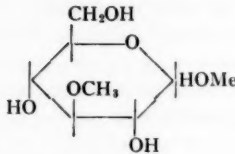
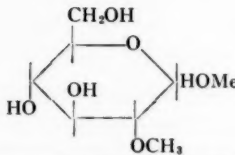
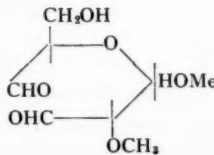
6-O-Monomethyl-D-glucose.—The molar production of formic acid is equivalent to the molar concentration of this isomer. This value is seen to be 0.23 mole, i.e. 23% of the mixture is present as 6-O-methyl-D-glucose.

4- and 2-O-Methyl-D-glucose.—The total periodate consumption (0.68 mole) minus the molar concentration of the 6-O-methyl isomer (0.23 mole) gives the molar concentrations of both the 4- and 2-O-methyl isomers. Hence these two are present to the extent of 45% in the mixture.

3-Mono-O-methyl-D-mannose.—The remaining 32% of the mixture must be the 3-mono-O-methyl isomer.

Fraction V was identified as free glucose. The semicrystalline syrup (20 mg) obtained was dissolved in methanol (1 ml) and *p*-nitroaniline (20 mg) was added. The mixture was

TABLE III

Possible constituents	Oxidation products	IO ₄ ' uptake (moles)	HCOOH liberation (moles)
		2	1
		1	0
	No reaction	0	0
		1	0

transferred to a bulb blown in glass tubing (3 mm in diameter), one drop of 13% methanolic hydrogen chloride was added, the tube was sealed and heated at 70° C for 20 minutes. After the mixture had been allowed to stand in the cold overnight, crystals of D-glucose-*N*-*p*-nitrophenylglucosylamine separated, m.p. 179–181° C, mixed m.p. 179–182° C.

Oxidation of Anisole.—Ferrous sulphate (2 g) was dissolved in water (15 ml) and reagent grade anisole (5 ml) added and the mixture was cooled to 0° C. Hydrogen peroxide (15 ml, 15%) was then added during 45 minutes and the whole was allowed to stand for 1½ hours (at 0° C), after which excess sodium arsenite was added to reduce excess peroxide. A copious green precipitate was removed by centrifugation during 1 hour at 0° C, and the green supernatant liquid was saturated with sodium chloride and repeatedly extracted with chloroform. The orange-colored chloroform phase was washed with (a) 5% sodium bicarbonate solution, then (b) with 5% sodium hydroxide solution, and finally evaporated to dryness, to give a residue (i) smelling strongly of anisole. Both the sodium bicarbonate and sodium hydroxide washings were then neutralized with dilute hydrochloric acid, and each extracted with chloroform, and the extracts were evaporated to dryness to give two residues (ii) and (iii) respectively. When chromatographed, (i)

and (ii) showed only traces of phenols which had escaped extraction, but at least four components were recognized in (iii), one being identifiable as guaiacol, and another as hydroquinone.

ACKNOWLEDGMENTS

The authors wish to thank Mr. C. R. Willis for undertaking the experimental work leading to the results shown in Tables I and II. One of us (B.F.-R.) is grateful to Queen's University for a Reuben Wells Leonard Foundation Fellowship and to the National Research Council for a grant, which made this work possible.

REFERENCES

1. W. N. HAWORTH, E. L. HIRST, and F. A. ISHERWOOD. *J. Chem. Soc.* 784 (1937).
2. W. N. HAWORTH, R. L. HEATH, and S. PEAT. *J. Chem. Soc.* 833 (1941).
3. G. O. ASPINALL and G. ZWIEFEL. *J. Chem. Soc.* 2271 (1957).
4. H. J. H. FENTON. *J. Chem. Soc.* 65, 899 (1894).
5. H. J. H. FENTON and H. JACKSON. *J. Chem. Soc.* 75, 1 (1899).
6. D. G. DANIELS and B. F. SAUNDERS. *J. Chem. Soc.* 2112 (1951).
7. F. HABER and J. WEISS. *J. Proc. Roy. Soc. A*, 147, 332 (1934).
8. M. G. EVANS. *J. Chem. Soc.* 266 (1947).
9. J. H. MERZ and W. A. WATERS. *J. Chem. Soc.* 2427 (1949).
10. J. H. MERZ and W. A. WATERS. *J. Chem. Soc.* 515 (1949).
11. R. GRINSTEAD. *J. Am. Chem. Soc.* 82, 3472 (1960).
12. R. GRINSTEAD. *J. Am. Chem. Soc.* 82, 3464 (1960).
13. A. F. TROTMAN-DICKENSON. *Free radicals*. Methuen & Co. Ltd., London. 1959. p. 90.
14. N. URI. *Chem. Revs.* 50, 375 (1952).
15. L. HOUGH, J. K. N. JONES, and W. H. WADMAN. *J. Chem. Soc.* 1702 (1950).
16. J. A. CIFONELLI and F. SMITH. *Anal. Chem.* 26, 1132 (1954).
17. B. N. AMES and N. K. MITCHELL. *J. Am. Chem. Soc.* 74, 252 (1952).
18. D. R. BRIGGS *et al.* *Anal. Chem.* 28, 1333 (1956).
19. A. B. FOSTER. *Chem. & Ind. (London)*, 1050 (1952).
20. J. K. N. JONES and H. SEPTON. *Can. J. Chem.* 38, 753 (1960).
21. R. KUHN. *Angew. Chem.* 67, 32 (1955).
22. R. KUHN. *Ber.* 88, 1540 (1955).
23. *BIOCHEMICAL PREPARATIONS*. Vol. 2. John Wiley & Sons, Inc., New York. 1952. p. 33.
24. C. HUDSON *et al.* *J. Am. Chem. Soc.* 65, 70 (1943).
25. W. N. HAWORTH. *J. Chem. Soc.* 107, 8 (1915).
26. M. L. WOLFROM. *J. Am. Chem. Soc.* 50, 2822 (1928).
27. T. NASH. *Biochem. J.* 55, 416 (1953).
28. D. J. BELL. *J. Chem. Soc.* 992 (1948).
29. K. WALLENFELS. *Naturwiss.* 37, 491 (1950).
30. D. J. BELL and R. DEDONDER. *J. Chem. Soc.* 2866 (1954).
31. G. NEUMULLER and E. VASSEUR. *Arkiv Kemi*, 2, 235 (1953).
32. P. ANDREWS, L. HOUGH, and J. K. N. JONES. *J. Chem. Soc.* 806 (1954).

CHEMISTRY OF THE TRIFLUOROMETHYL GROUP

PART III. PHENYLBISTRIFLUOROMETHYLPHOSPHINE AND RELATED COMPOUNDS¹

M. A. A. BEG AND H. C. CLARK

ABSTRACT

The reaction of trifluoroiodomethane with tetraphenylcyclotetraphosphine leads to the formation of phenylbistrifluoromethylphosphine and phenyltrifluoromethyliodophosphine. The mechanism of the reaction is discussed and the physical and chemical properties of these compounds are reported. Bromine reacts with phenylbistrifluoromethylphosphine to form phenylbistrifluoromethyldibromophosphorane which is hydrolyzed to phenyltrifluoromethylphosphinic acid, $C_6H_5(CF_3)_2P(O)OH$.

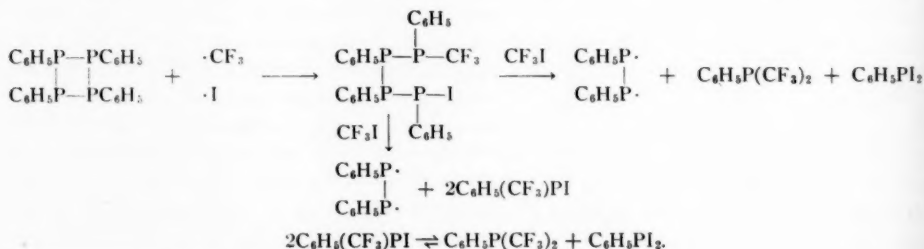
INTRODUCTION

In previous papers in this series, the donor properties of methyl-trifluoromethylphosphines were studied by the investigation of their ability to form complexes with boron trifluoride and platinum (II) chloride (1), and with a series of nickel (II) salts (2). Since much is known of the corresponding complexes of aryl phosphines, it seemed worthwhile to study the donor properties of aryl-trifluoromethyl-phosphines. Unlike the methyl-trifluoromethyl-phosphines which have been known for some time (3, 4, 5), the phenyl-trifluoromethyl-phosphines had not been previously reported, although their arsine analogues had been prepared (6). We now report the preparation of phenylbistrifluoromethylphosphine.

DISCUSSION AND RESULTS

Phenylbistrifluoromethylphosphine has been prepared by the reaction of trifluoroiodomethane with tetraphenylcyclotetraphosphine, the properties of which have been reported by other workers (7, 8, 9). The reaction was performed at 185°, above the melting point of the tetraphosphine, and the other reaction products, besides phenylbistrifluoromethylphosphine, are phenyltrifluoromethyliodophosphine, which is a very involatile reddish brown liquid, and small amounts of fluoroform and hexafluoroethane.

The mechanism of this reaction, involving the interaction of a perfluoroiodoalkane with a four-membered phosphorus ring is of some interest. A free-radical mechanism involving fission of phosphorus-phosphorus bonds by the attack of CF_3 radicals seems probable. This is supported by the fact that the reaction will occur thermally or on ultraviolet irradiation of the tetraphosphine with trifluoroiodomethane. Since the simultaneous breaking of four P—P bonds is unlikely, the following reaction scheme may be suggested.



¹Manuscript received December 5, 1960.

Contribution from the Department of Chemistry, University of British Columbia, Vancouver, B.C. From part of the thesis presented by M.A.A.B. in partial fulfillment of the requirements for the Ph.D. degree.

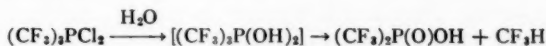
This scheme is supported by the observation that the reaction products contain phenylbistrifluoromethylphosphine and phenyltrifluoromethyliodophosphine in an approximately 2:1 ratio, and also by the results of a separate experiment which indicated extensive disproportionation of the iodophosphine at 200° as indicated above.

Phenylbistrifluoromethylphosphine is a colorless liquid boiling at 148–150°; it is stable at 200° and prolonged heating to 300° causes only partial decomposition. It is not hydrolyzed by acids, but reacts very slowly with water at 100° and much more rapidly with aqueous sodium hydroxide at 80°. The hydrolysis products are fluoroform and either phenylphosphonous acid $C_6H_5PO_2H_{27}$, or its sodium salt.

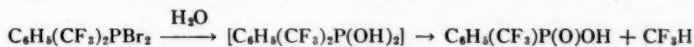
Phenylbistrifluoromethylphosphine does not react with iodine at room temperature, but at 185° the trifluoromethyl groups are cleaved as trifluoroiodomethane. There is no evidence of the formation of the diiodophosphorane, $C_6H_5(CF_3)_2PI_2$. However, the phosphine reacted vigorously with bromine at room temperature to form phenylbistrifluoromethyl dibromophosphorane. This is in agreement with the usual decrease in stability for dichloro-, dibromo-, and diiodo-phosphoranes. Phenylbistrifluoromethyl dibromophosphorane is readily hydrolyzed by water losing only one of the two trifluoromethyl groups per molecule as fluoroform and producing phenyltrifluoromethylphosphinic acid, $C_6H_5(CF_3)P(O)OH$.

Phenyltrifluoromethyl iodophosphine is a reactive liquid which is readily hydrolyzed. Whereas alkaline hydrolysis produced fluoroform and the sodium phenylphosphonate, treatment with water gives phenyltrifluoromethylphosphine and phenyltrifluoromethylphosphinic acid, $C_6H_5(CF_3)P(O)OH$.

The production of phenyltrifluoromethylphosphinic acid from the aqueous hydrolysis of phenylbistrifluoromethyl dibromophosphorane provides an interesting link between the trifluoromethyl- and aryl-phosphorus compounds. Whereas hydrolysis of triaryl dichlorophosphoranes yields phosphine oxides (10), hydrolysis of tris(trifluoromethyl) dichlorophosphorane (11) gives bistrifluoromethylphosphinic acid and one equivalent of fluoroform.

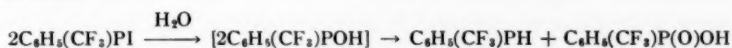


The hydrolysis of phenylbistrifluoromethyl dibromophosphorane shows that the intermediate compound $C_6H_5(CF_3)_2P(OH)_2$ is unstable.



The trifluoromethyl groups behave in the same way as in the hydrolysis of tris(trifluoromethyl) dichlorophosphorane and the phenyl group shows its customary resistance to hydrolytic attack.

The formation of phenyltrifluoromethylphosphinic acid from the hydrolysis of phenyltrifluoromethyl iodophosphine is consistent with the general reactions of halophosphines (12). The spontaneous oxidation-reduction of the apparently unstable hydrolysis product leads to the production of phenyltrifluoromethylphosphine and phenyltrifluoromethylphosphinic acid.



The infrared spectra of these phenyl-trifluoromethylphosphorus compounds show the expected features. Absorption associated with the strong carbon-fluorine stretching vibrations occurred in the 1100–1200 cm^{-1} region. However, it is of interest to notice

that the spectrum of silver phenyltrifluoromethylphosphinate, $C_6H_5(CF_3)P(O)OAg$, showed absorption at 1225 cm^{-1} corresponding to the P:O vibration. This absorption occurs in the same region for the aryl and alkyl phosphinic acids $R_2P(O)OH$, which are weak acids. For the strong acid, trifluoromethylphosphonic acid, this vibration is shifted to the higher frequency of 1300 cm^{-1} (13, 14). This might suggest that phenyltrifluoromethylphosphinic acid is a fairly weak acid.

EXPERIMENTAL

The preparations of the starting materials were carried out in a nitrogen atmosphere. Reactions with trifluoroiodomethane were carried out in sealed evacuated Pyrex tubes and the products and reactants were manipulated by standard vacuum techniques, out of contact with air and moisture.

Preparation of Tetraphenylcyclotetraphosphine

Phenyldichlorophosphine was obtained by the method of Buchner and Lockhart (15). The preparation of phenylphosphine by the Michaelis method (16, 17) is very cumbersome and gives a low yield. A much easier method (9, 18) is by reduction of phenyldichlorophosphine with lithium aluminum hydride. Phenyldichlorophosphine (18.8 g) dissolved in 100 ml diethyl ether was added cautiously to a well-stirred suspension of lithium aluminum hydride (3 g) in 100 ml ether. The reaction was vigorous and cooling was necessary. After the addition of phenyldichlorophosphine had been completed, the mixture was refluxed for 30 minutes and 5 ml of water were added dropwise. After being refluxed for an hour, the mixture was distilled and the resulting phenylphosphine, distilling at 160° , was dried over calcium chloride (yield 55%).

The preparation of tetraphenylcyclotetraphosphine by the Michaelis' method (19) is not convenient and the compound was prepared by adding phenylphosphine (11 g) in 50 ml ether to a well-stirred solution of phenyldichlorophosphine (18 g) in 50 ml ether. The solution gradually turned yellow but solid was not immediately deposited. After the addition was complete, the solution was refluxed for 3 hours during which time a white solid was deposited. The ether solution was decanted and the remaining solid was washed and dried. The yield of tetraphenylcyclotetraphosphine (m.p. $149-50^\circ$) was 90%.

Reaction of Tetraphenylcyclotetraphosphine with Trifluoroiodomethane

Tetraphenylcyclotetraphosphine (1.0 g) was sealed with trifluoroiodomethane (2.025 g) and left at room temperature for 24 hours. The solid phosphine was insoluble in trifluoroiodomethane. No reaction occurred at 70°C over 24 hours, nor at 150°C for 12 hours, but on heating at 185°C for 12 hours a dark-red involatile liquid was obtained and 0.558 g of unreacted trifluoroiodomethane was recovered. The dark-red liquid was shaken with mercury and the remaining liquid extracted with ether. After removal of the ether, a liquid (0.45 g) of low volatility was obtained and identified as phenylbistrifluoromethylphosphine (Found: C, 39.35%; H, 2.10%; F, 45.40%; P, 12.30%. Calculated for $C_6H_5F_3P$: C, 39.03%; H, 2.03%; F, 46.36%; P, 12.60%).

Phenylbistrifluoromethylphosphine is a colorless oily liquid whose odor is not as obnoxious as those of other phosphines. It boils at $148-150^\circ$ and its vapor pressure is given by the equation $\log p_{\text{mm}} = 7.5606 - (1985/T)$, whence the latent heat of vaporization is $9054\text{ cal mole}^{-1}$ and the Trouton's constant is 21.37. It is stable in air and does not react with water up to 100°C . It does not react with silver iodide, a solution of silver iodide in potassium iodide, or with carbon disulphide.

Two separate experiments were performed to investigate the mechanism of the above reaction and to characterize the other reaction products.

(1) Tetraphenylcyclotetraphosphine (2 g) was sealed with trifluoroiodomethane (5 g) in a Pyrex tube and was irradiated with ultraviolet radiation from a 200-watt U.V. lamp. The reaction was slow (possibly because of the heterogeneous phases), but after 15 days phenylbistrifluoromethylphosphine (0.899 g) and unreacted trifluoroiodomethane (2.192 g) were obtained. The rest of the product was a thick reddish syrup which showed strong absorption in the I.R. between 8–9 μ , characteristic of C—F stretching frequencies. This was not identified.

(2) Tetraphenylcyclotetraphosphine (7.5 g) was sealed with 18 g trifluoroiodomethane and heated at 185° C for 12 hours. A volatile mixture of hexafluoroethane and fluoroform (0.022 g), and 5.5 g of unreacted trifluoroiodomethane were recovered. The remaining liquid was subjected to fractional distillation under 20 mm pressure. Two fractions were obtained, one boiling at 62–65° (4.9 g) and the other boiling at 112–116° (3.8 g). A thick liquid which solidified on standing remained in the distillation flask. This showed strong absorption in the I.R., corresponding to the C—F stretching frequencies. Another experiment to identify this completely involatile liquid showed that it contained some iodides, including phosphorus triiodide. When treated with a large excess of trifluoroiodomethane and mercury, some pure phenylbistrifluoromethyl phosphine was obtained, but the main product was a very viscous pale-yellow liquid, presumably polymeric.

The liquid distilling at 62–65° was identified as phenylbistrifluoromethylphosphine and the fraction distilling at 112–114° was identified as phenyltrifluoromethyliodophosphine. (Found: I, 41.2%. Calculated for $C_6H_5F_3PI$: I, 41.78%.)

Reactions of Phenylbistrifluoromethylphosphine

(a) Hydrolysis

Phenylbistrifluoromethylphosphine (0.277 g) was sealed with water (1.28 g). There was no reaction at room temperature and the reactants formed two separate layers. After heating at 80° for 24 hours, only a trace of fluoroform was obtained, while after 36 hours at 110°, 0.038 g fluoroform was evolved. Traces of benzene were also identified spectroscopically. There remained a white crystalline solid which melted at 69° and was identified as phenylphosphonous acid.

Phenylbistrifluoromethylphosphine (0.273 g) was sealed with 5 ml of 20% aqueous sodium hydroxide solution. The reaction was slow at room temperature with the evolution of fluoroform. The tube was heated to 80° for 24 hours. The production of 0.149 g fluoroform (mol. wt. obtained 70.0, calculated 70.0) showed that the hydrolysis was 96.4% complete (CF_3 obtained as CF_3H : 54.8%; calculated for $C_6H_5P(CF_3)_2$: 56.1%). The solid obtained on evaporation of the solution was identified spectroscopically as the sodium salt of phenylphosphonous acid.

Phenylbistrifluoromethylphosphine (0.372 g) and 36 *N* hydrochloric acid (2 g) were sealed. There was no reaction at room temperature and the reactants formed separate layers. There was no reaction at 80° for 24 hours and at 110° for 48 hours. The tube was finally heated to 185° for 120 hours. At the end of this period the amount of fluoroform evolved was only 0.0022 g and the phosphine was recovered almost quantitatively.

(b) Reaction with Halogens

(1) *Iodine*.—Phenylbistrifluoromethylphosphine (0.389 g) and iodine (1.163 g) did not react at room temperature, nor after heating at 150° for 24 hours. The mixture was finally heated to 185° for 48 hours. The products obtained, were fluoroform (0.032 g),

trifluoroiodomethane (0.481 g), (mol. wt. 194, calculated 196), benzene (0.055 g), and traces of unreacted phosphine. The conversion into fluoroform and trifluoroiodomethane accounted for 91.5% of the trifluoromethyl group. The formation of fluoroform and benzene may be due to the presence of small traces of moisture on the iodine which is not removed even on extensive drying. The solid left in the tube, after pumping off the volatiles, contained phosphorus triiodide and no phenyltrifluoromethylidophosphine.

(2) *Bromine*.—Phenylbistrifluoromethylphosphine (0.6965 g) and bromine (0.450 g) were combined. The ensuing vigorous reaction was controlled by performing the experiment in carbon tetrachloride solution and pumping off the volatiles after the reaction was complete. This was marked by the persistence of the bromine color. The reaction gave an orange-yellow solid which was very reactive towards moisture and was identified as phenylbistrifluoromethyldibromophosphorane (Found: Br, 38.93%. Calculated for $C_6H_5F_6PBr_2$: Br, 39.41%). On reacting the dibromophosphorane with water, one equivalent of CF_3 was lost and a white solid was left. The dibromophosphorane (0.324 g) was sealed with water (1.0 g) and left at room temperature overnight. Fluoroform (0.060 g) was evolved corresponding to a loss of one equivalent of CF_3 per mole (Found: CF_3 , 18.4%. Calculated for $C_6H_5F_6PBr_2:CF_3$, 34.5%). A white solid was obtained by pumping off the liquids, recrystallizing the residue from water, and finally drying over phosphorus pentoxide. The solid was identified spectroscopically as phenyltrifluoromethylphosphinic acid, $C_6H_5(CF_3)P(O)OH$. The acid melted at 84–86°. The silver salt of the acid was obtained as needle-shaped crystals by treating the aqueous solution of the acid with silver oxide. The same salt could also be obtained from the reaction mixture of phenylbistrifluoromethyldibromophosphorane and water which had stood overnight and had lost one equivalent of CF_3 . The silver salt $C_6H_5(CF_3)P(O)OAg$ (Found: Ag, 33.81%. Calculated for $C_7H_5F_3PO_2Ag$: Ag, 34.06%) melted at 294–96° and was very sensitive to light.

(c) *Pyrolysis of the Phosphine*

Phenylbistrifluoromethylphosphine (1.058 g) was heated to 210° for 48 hours; 1.004 g of the phosphine and traces of fluoroform and silicon tetrafluoride (identified spectroscopically) were obtained. Phosphine (0.639 g) was heated to 300° for 48 hours. The tube walls were etched but the phosphine was not all pyrolyzed: 0.48 g was recovered unchanged. The other volatile materials were fluoroform, silicon tetrafluoride, and some benzene trifluoride.

Reactions of Phenyltrifluoromethylidophosphine

Phenyltrifluoromethylidophosphine is a reddish-brown liquid which boils at 112–114° at 20 mm. It fumes in air and reacts slowly with water. The solution obtained by absorption of water is highly acidic. It disproportionates on heating.

(a) *Hydrolysis*

Phenyltrifluoromethylidophosphine (0.334 g) was treated with 5 ml of 20% sodium hydroxide. There was immediate reaction at room temperature. The tube was heated to 100° for 15 hours. Fluoroform (0.0694 g) (mol. wt. found 69.8, calculated 70.0) was evolved (CF_3 found, 20.75%; calculated for $C_7H_5F_3PI$, 23.03%). The hydrolysis was only 90% complete. The residue contained a hygroscopic sodium salt whose I.R. spectrum corresponded with that of sodium phenylphosphonate.

Phenyltrifluoromethylidophosphine (0.334 g) was treated with 0.125 g water and left in a sealed tube overnight. When water and other liquids were removed, a white solid was left. The melting point was 84–86° and in all respects the compound was similar to

that obtained from the hydrolysis of phenylbistrifluoromethyldibromophosphorane. The silver salt was also prepared by reacting more of the iodophosphine with water and precipitating the iodide as silver iodide. The solution was concentrated *in vacuo* and the solid dried over P_2O_5 . The silver salt was identified analytically (Found: Ag, 33.80%. Calculated: Ag, 34.06%) by its melting point of 294–96°, and also spectroscopically.

The above treatment of the iodophosphine also gave a small amount of a liquid whose I.R. spectrum showed the presence of P—H, P—C₆H₅, and P—CF₃ bonds. The hydrolysis with water therefore appears to give some phenyltrifluoromethylphosphine.

(b) *Reaction with Trifluoroiodomethane*

The iodophosphine (2.347 g) was heated with trifluoroiodomethane (2.299 g) at 200° for 12 hours. Trifluoroiodomethane (2.210 g, 96.1%) was recovered and the main products of reaction, presumably from the disproportionation of the iodophosphine, were phenylbistrifluoromethylphosphine (0.617 g), phosphorus triiodide, and benzene. Some of the unreacted iodophosphine was also identified among the products.

(c) *Reactions with Trifluoroiodomethane and Mercury*

The iodophosphine (2.8 g) and trifluoroiodomethane (10 g), with 54 g mercury, were sealed in a tube and shaken for 24 hours. Trifluoroiodomethane (8.9 g) was recovered and phenylbistrifluoromethylphosphine (1.5 g) was obtained. The loss of 1.1 g of trifluoroiodomethane indicated that the reaction $C_6H_5PCF_3I + CF_3I \xrightarrow{Hg} C_6H_5(CF_3)_2P$ had occurred. Besides the phosphine, some polymers were also obtained as mentioned earlier.

Pyrolysis of phenyltrifluoromethylphosphine iodide: The iodophosphine (2.003 g) was heated in a sealed tube to 220° for 12 hours. Fluoroform (0.02 g) and trifluoroiodomethane (0.06 g) were obtained as the volatile products and there remained phenylbistrifluoromethylphosphine, benzene, phosphorus triiodide, and some unreacted phenyltrifluoromethyl iodophosphine.

The I.R. spectra were taken on a Perkin-Elmer model 21 double-beam instrument with rock salt optics. Liquid films were used for liquids and KBr pellets for solids. The following absorption bands were noted for the compounds mentioned.

Phenylbistrifluoromethylphosphine					
3080 (w)	2920 (w)	2320 (w)	1980 (w)		
1870 (w)	1835 (w)	1810 (w)	1770 (w)	1745 (w)	
1730 (w)	1670 (w)	1645 (w)	1590 (w)	1490 (w)	
1445 (m)	1330 (w)	1265 (w)	1190 (s)	1140 (s)	
1100 (s)	1070 (m)	1030 (w)	1000 (m)	875 (w)	
805 (w)	750 (m)	745 (m)	690 (m)		
Phenyltrifluoromethyliodophosphine					
3060 (w)	2900 (w)	2340 (w)	1880 (w)	1800 (w)	
1725 (w)	1710 (w)	1690 (w)	1675 (w)	1660 (w)	
1585 (w)	1490 (w)	1440 (m)	1385 (w)	1335 (w)	
1310 (w)	1270 (w)	1210 (m)	1150 (s)	1115 (s)	
1070 (m)	1025 (m)	1000 (m)	830 (w)	745 (s)	
715 (w)	690 (m)				
Silver phenyltrifluoromethyl phosphinate					
3080 (w)	2900 (w)	2300 (w)	1860 (w)		
1815 (w)	1725 (w)	1710 (w)	1690 (w)	1756 (w)	
1640 (w)	1630 (w)	1590 (w)	1555 (w)	1485 (w)	
1440 (m)	1335 (w)	1225 (s)	1200 (m)		
1140 (s)	1110 (s)	1045 (m)	1015 (m)	995 (m)	
970 (m)	870 (w)	760 (w)	740 (m)	715 (m)	695 (m)

ACKNOWLEDGMENTS

We gratefully acknowledge the support of the National Research Council, and one of us (M.A.A.B) expresses thanks for a scholarship received from C.S.I.R. (Pakistan) under the auspices of the Colombo Plan.

REFERENCES

1. M. A. A. BEG and H. C. CLARK. *Can. J. Chem.* **38**, 119 (1960).
2. M. A. A. BEG and H. C. CLARK. *Can. J. Chem.* This issue.
3. R. N. HASZELDINE and B. O. WEST. *J. Chem. Soc.* 3631 (1956).
4. R. N. HASZELDINE and B. O. WEST. *J. Chem. Soc.* 3880 (1957).
5. A. B. BURG and G. BRENDLE. *J. Am. Chem. Soc.* **80**, 3198 (1958).
6. W. R. CULLEN. *Can. J. Chem.* **38**, 445 (1960).
7. J. W. B. REESOR and G. F. WRIGHT. *J. Org. Chem.* **22**, 385 (1957).
8. W. KUCHEN and H. BUCHWALD. *Chem. Ber.* **91**, 2296 (1958).
9. P. R. BLOOMFIELD and K. PARVIN. *Chem. & Ind.* 541 (1959).
10. G. M. KOSOLAPOFF. *Organophosphorus compounds*. John Wiley & Sons, Inc., New York. 1950. p. 70.
11. H. J. EMELEUS, R. N. HASZELDINE, and R. C. PAUL. *J. Chem. Soc.* 563 (1955).
12. G. M. KOSOLAPOFF. *Organophosphorus compounds*. John Wiley & Sons, Inc., New York. 1950. p. 137.
13. L. W. DAASCH and D. C. SMITH. *Anal. Chem.* **23**, 853 (1957).
14. F. W. BENNETT, H. J. EMELEUS, and R. N. HASZELDINE. *J. Chem. Soc.* 3598 (1954).
15. B. BUCHNER and L. B. LOCKHART. *J. Am. Chem. Soc.* **73**, 755 (1951).
16. A. MICHAELIS. *Chem. Ber.* **7**, 6 (1874).
17. A. MICHAELIS. *Ann.* **265**, 181 (1876).
18. T. WEIL, B. PRIJS, and H. ERLMEYER. *Helv. Chim. Acta*, **35**, 616 (1952).
19. A. MICHAELIS and H. KOHLER. *Chem. Ber.* **10**, 807 (1877).

DIELECTRIC RELAXATION IN LIQUIDS

I. THE REPRESENTATION OF RELAXATION BEHAVIOR¹

D. W. DAVIDSON

ABSTRACT

Methods are described for the determination from experimental data of the parameters used in the skewed-arc representation in the complex dielectric constant plane of dielectric relaxation in liquids. Graphs give the frequency dependence of the real and imaginary parts of the dielectric constant predicted by the skewed-arc equation. Evidence, which includes an analysis of published data and of some new data, is presented for the frequent occurrence of this type of relaxation behavior in liquids. The resolution of the effects of different relaxation processes is discussed.

The recent defect-diffusion model of Glarum is found to lead, under some conditions, to complex dielectric constant loci which are practically indistinguishable from skewed-arc loci over much of the frequency range of dispersion. It predicts departures from skewed-arc behavior at relatively high frequencies which are possibly related to experimentally observed departures.

It is concluded that skewed-arc characteristics arise from the presence of co-operative relaxation processes, possibly aided by the diffusion of disordered regions, in which the individual mechanisms of relaxation cannot be resolved by application of the superposition principle.

I. INTRODUCTION

The question of the accuracy with which empirical representations fit the experimental dielectric relaxation data is of considerable importance in the development of adequate models of liquid relaxation. In a recent publication of the National Bureau of Standards (1), Buckley and Maryott have collected dielectric dispersion and absorption data for some 193 compounds in the liquid state, as found in the literature to the end of 1956. The dielectric behavior of many of these compounds has been represented analytically, either in terms of the simple Debye equation involving only a single relaxation time and a semicircular locus in the complex dielectric constant plane, or in terms of the equation due to Cole and Cole which is an arc of a circle in the complex plane and involves a logarithmically symmetrical distribution of relaxation times about a most probable value. Among the liquids whose relaxation parameters are tabulated by Buckley and Maryott, two (glycerol and 1,2-propanediol) were described by a third representation, the skewed-arc locus proposed by Cole and Davidson which corresponds to an asymmetrical distribution of relaxation times.

More recently, however, comparatively accurate data for a considerable number of other liquids have been fitted to this third representation. These include most of the liquids originally cited by Cole and Cole (2) as evidence for their symmetrical circular arc description in the complex dielectric constant plane. Moreover, many other liquids have been characterized by Cole-Cole parameters (1) on the basis of rather inaccurate and incomplete relaxation data. This is particularly true for measurements in the experimentally difficult frequency range above 100 Mc/sec. In fact, unlike many solids, no liquid seems to have a principal dispersion region appreciably broader than that given by the Debye equation for which the adequacy of the Cole-Cole representation has been established.

It is the purpose of the present paper to consider the application of the Cole-Davidson equation in some detail. Methods of analyzing experimental results are discussed and

¹Manuscript received October 11, 1960.

Contribution from the Division of Applied Chemistry, National Research Council, Ottawa, Canada.

Issued as N.R.C. No. 6128.

applied to data in the literature as well as to some new data. In subsequent papers the results of studies of other liquids will be presented.

II. THE DEBYE EQUATION

According to the classical Debye equation (3) the complex dielectric constant $\epsilon(i\omega) = \epsilon' - i\epsilon''$ is given by

$$[1] \quad \epsilon(i\omega) - \epsilon_1 = (\epsilon_0 - \epsilon_1)/(1 + i\omega\tau)$$

in which ϵ_0 and ϵ_1 are the values of the dielectric constant on the low- and high-frequency sides of the dispersion region, ω is the angular frequency, and τ the (single) relaxation time. This equation appears to be applicable (4) to the cases of relaxation of polar molecules in dilute solution in non-polar solvents, at least when the solute molecules are large in comparison with those of the solvent. Individual polar molecules are then in similar environments and a single relaxation time for rotation is adequate.

The Debye equation also describes the principal dielectric dispersion of water, at least to a high level of approximation (5), and of a large number of undiluted mono-hydroxy alcohols, within the accuracy of the measurements (6). In these liquids hydrogen bonding between molecules leads to a regularity of environment which may again account for the presence of only one relaxation time, although there is evidence (see VI(b) below) that here relaxation occurs by a co-operative process involving a large number of molecules.

Between these two extremes, a large number—probably the majority—of polar liquids show broader dielectric dispersion and absorption than can be attributed to a single relaxation time. There has been tendency to treat such departures from Debye behavior in terms of the symmetrical Cole-Cole locus (1), a procedure which has been reasonably successful in some cases. However, the data generally seem inadequate to show preference for this representation over other possible representations, in particular over that to be discussed in subsequent paragraphs.

III. THE SKEWED-ARC REPRESENTATION

The equation of the skewed-arc locus

$$[2] \quad \epsilon(i\omega) - \epsilon_1 = (\epsilon_0 - \epsilon_1)/(1 + i\omega\tau_0)^\beta$$

in which β is a positive parameter no greater than unity, was originally used (7) to represent, within the experimental accuracy, the relaxation behavior of glycerol and 1,2-propanediol and, subsequently, 1,3-propanediol (8). More recently, it has been successfully applied to accurate bridge data obtained for a variety of chemically dissimilar liquids (see IV below).

Methods of Applying the Equation to Extensive Data

The complex locus given by equation [2] is illustrated in Fig. 1. The imaginary part of the complex dielectric constant is plotted against the real part. It is an asymmetrical locus which resembles a semicircle on the low-frequency side and approaches asymptotically a line making an angle of $\beta\pi/2$ with the real axis on the high-frequency side. This behavior is apparent from an examination of the real and imaginary parts of equation [2]:

$$[3] \quad \frac{\epsilon' - \epsilon_1}{\epsilon_0 - \epsilon_1} = (\cos \phi)^\beta \cos \beta\phi$$

and

$$[4] \quad \frac{\epsilon''}{\epsilon_0 - \epsilon_1} = (\cos \phi)^\beta \sin \beta \phi,$$

where ϕ is the principal value of $\tan^{-1} \omega \tau_0$. The ratio of these is

$$[5] \quad \frac{\epsilon''}{\epsilon' - \epsilon_1} = \tan \beta \phi.$$

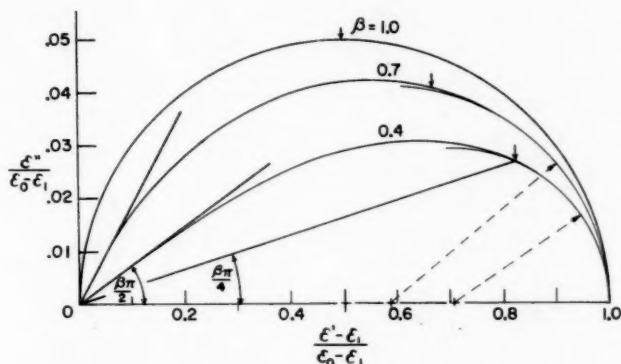


FIG. 1. Skewed-arc loci on the complex dielectric constant plane. Arrows indicate frequencies at which $\omega = 1/\tau_0$, broken lines the radii of circular arcs which coincide with the loci at low frequencies.

When an experimental locus has the characteristic shape of Fig. 1 the appropriate value of β may be obtained from the limiting slope at high frequencies. Since, for $\omega = 1/\tau_0$, $\epsilon''/(\epsilon' - \epsilon_1) = \tan \beta\pi/4$, τ_0 may be obtained as the reciprocal of the estimated radian frequency at which the bisector of the limiting angle cuts the locus. A more accurate method of evaluating the relaxation time τ_0 , which is not dependent merely upon a few experimental points at values of ω in the vicinity of $1/\tau_0$, is to plot $\tan\{\tan^{-1}[\epsilon''/(\epsilon' - \epsilon_1)]/\beta\} = \omega\tau_0$ versus frequency, whence τ_0 may be evaluated from the frequency for which this function is unity. This also serves as a check of how well the data fit the predicted straight-line relationship. The plot is best made logarithmic in view of the large frequency range over which dispersion takes place. However, the validity of equation [5] is not a sufficient condition for the validity of equations [3] and [4]. Moreover, in many cases only one of ϵ' or ϵ'' (often only ϵ'') is accurately measured. Figures 2 and 3 show the individual variation of ϵ' and ϵ'' with frequency for a number of values of β and may be used to facilitate direct comparison with experiment.

Analysis of Less Extensive Data

The above methods for checking the agreement between experiment and the skewed-arc locus are applicable only when data are available for a considerable range of frequencies which includes the dispersion region. In cases where the data are less complete it is sometimes possible to use less straightforward methods. This may sometimes be done for data available at only a limited number of fixed frequencies provided that they are obtained over a considerable interval of temperature.

An aggregate complex locus may be drawn by plotting $\epsilon''/(\epsilon_0 - \epsilon_1)$ versus $(\epsilon' - \epsilon_1)/(\epsilon_0 - \epsilon_1)$ for data obtained at different temperatures. This method requires evaluation of ϵ_0 at the required temperatures by extrapolation of high temperature values and of ϵ_1 by extrapolation from low temperatures. Provided that β is not strongly temperature dependent (the evidence is that it increases slightly with increasing temperature), equation [2] requires that the points fall on a common skewed locus, from which β may

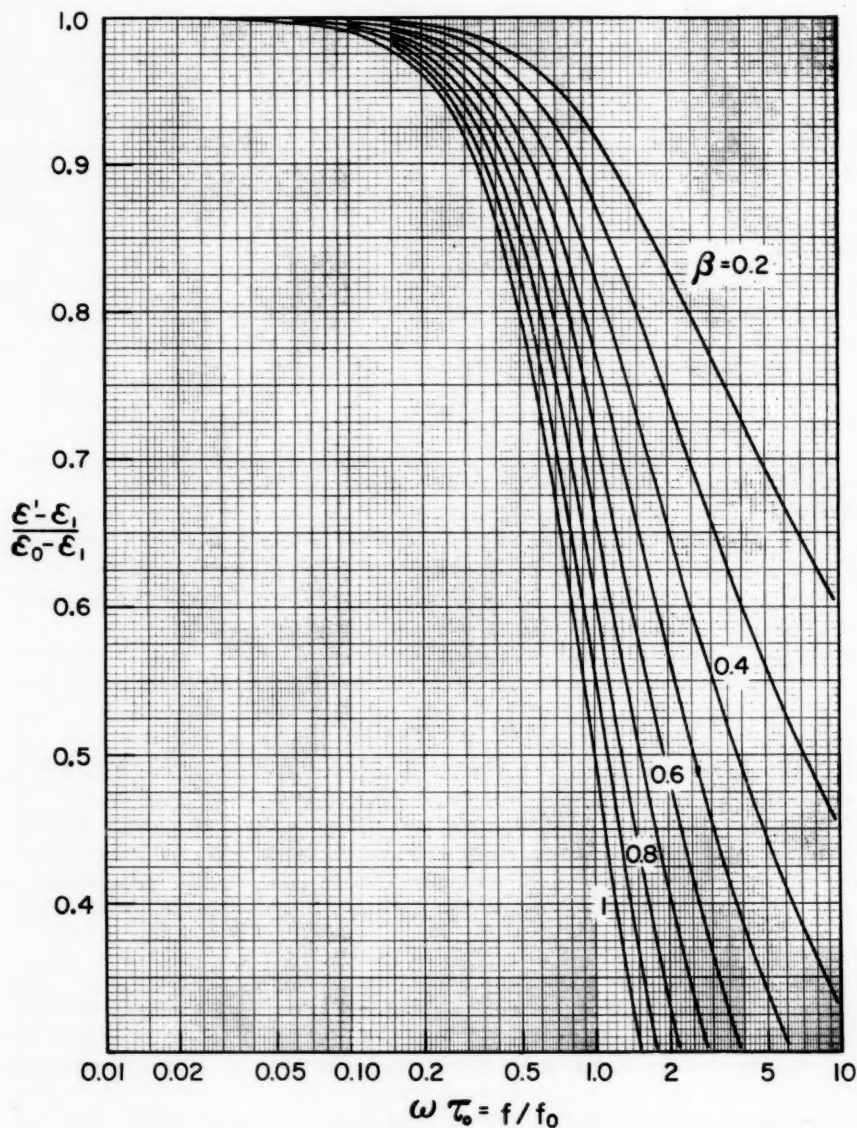


FIG. 2(a). Variation of ϵ' with frequency for skewed-arc behavior.

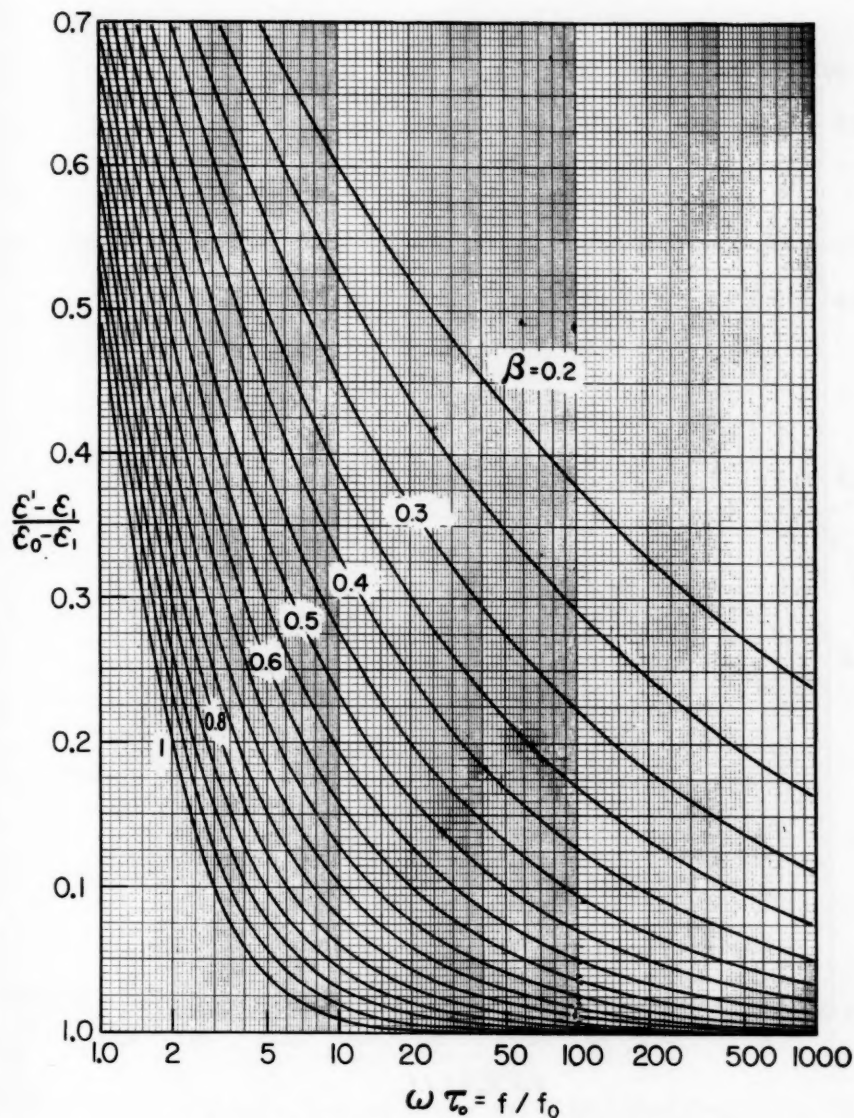


FIG. 2(b). Variation of ϵ' with frequency for skewed-arc behavior.

be determined. A value of τ_0 may then be obtained for each frequency of measurement at the estimated temperature at which the locus for that frequency is intercepted by the bisector of the limiting angle. A more complete analysis is possible if some reasonable assumption may be made about the variation of τ_0 with temperature. For example, τ_0 is sometimes proportional to the viscosity η , especially for viscous liquids (7, 9, 10), or, with more justification (11), to η/T .

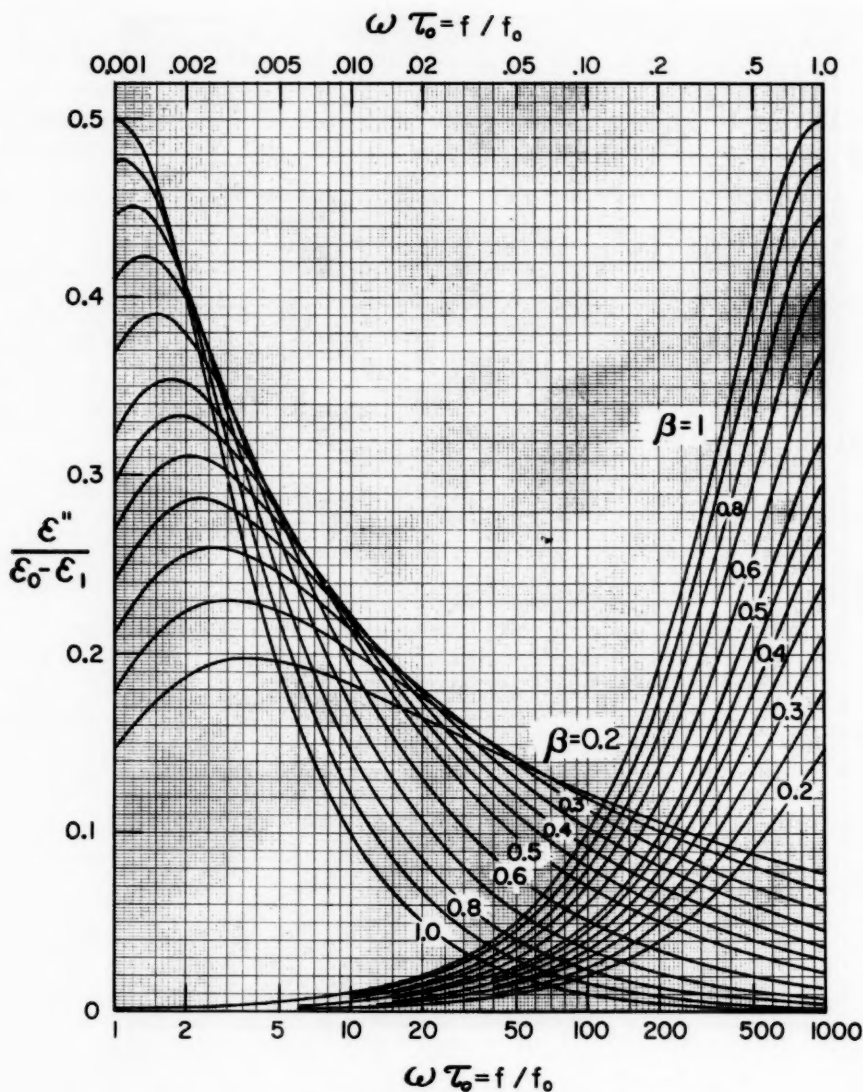


FIG. 3. Variation of ϵ'' with frequency for skewed-arc behavior.

An alternative method may be applied to data obtained at a fixed frequency over an adequate temperature range. The maximum in a plot of $\epsilon''/(\epsilon_0 - \epsilon_1)$ versus temperature occurs at a temperature (T_0) such that the value of τ_0 is related to the fixed frequency of measurement $\omega_t/2\pi$ by

$$[6] \quad \omega_t \tau_0 = \tan \frac{\pi}{2(1+\beta)} \quad (\text{at } T_0).$$

At the same temperature (T_0) equations [3] and [4] become

$$[7] \quad \frac{\epsilon' - \epsilon_1}{\epsilon_0 - \epsilon_1} = \left[\cos \frac{\pi}{2(1+\beta)} \right]^{1+\beta} \tan \frac{\pi}{2(1+\beta)} \quad (\text{at } T_0),$$

and

$$[8] \quad \frac{\epsilon''}{\epsilon_0 - \epsilon_1} = \left[\cos \frac{\pi}{2(1+\beta)} \right]^{1+\beta} \quad (\text{at } T_0).$$

The variations of these functions with β are shown in Fig. 4. The simplest method of

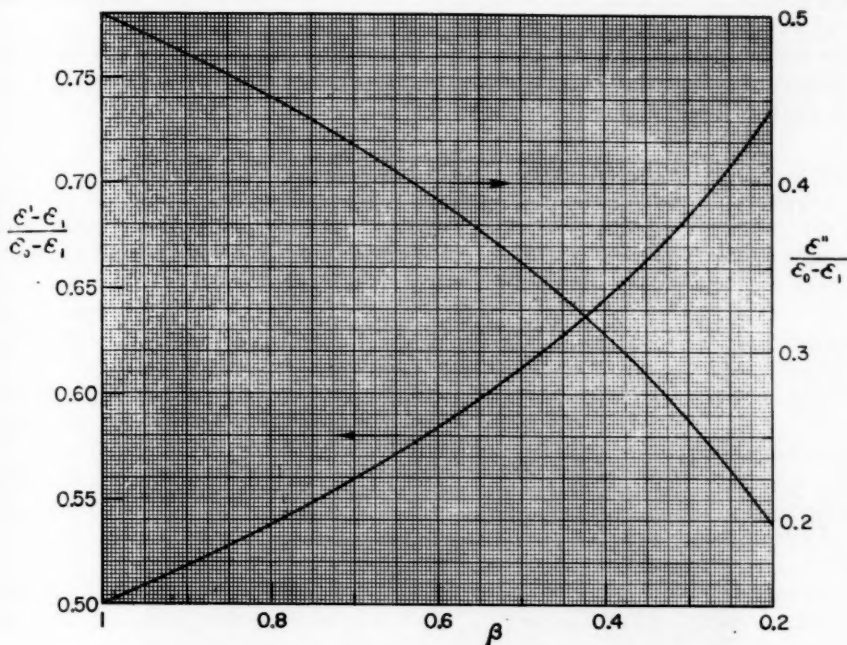


FIG. 4. Variation of reduced ϵ' and ϵ'' with β under conditions of maximum loss.

estimating β and τ_0 is from

$$[9] \quad \frac{\epsilon' - \epsilon_1}{\epsilon''} = \omega \tau_0 = \tan \frac{\pi}{2(1+\beta)} \quad (\text{at } T_0).$$

Determination of β and τ_0 from values of ϵ' and ϵ'' for a fixed frequency at the temperature of maximum loss, however, is meaningful only if there is some reason to believe that the behavior is of the skewed-arc type. This may be tested by considering the data at other temperatures. In one approach that has proved useful, the temperature dependence of the relaxation time τ_0 is assumed to be given by

$$[10] \quad \tau_0 = A e^{B/T}$$

over a narrow temperature range about T_0 and β is considered constant over this same temperature range. Suppose that two temperatures T_1 and T_2 are defined by $1/T_1$

$= 1/T_0 - \Delta$ and $1/T_2 = 1/T_0 + \Delta$. Δ may be chosen, for example, to make ϵ'' of the order of $\epsilon_{\max}''/2$. The values of $\epsilon''/(\epsilon' - \epsilon_1)$ at T_1 and T_2 , according to equation [5], are then

$$\tan \beta [\tan^{-1}(\omega \tau_0^0 e^{-B\Delta})] \quad \text{and} \quad \tan \beta [\tan^{-1}(\omega \tau_0^0 e^{B\Delta})],$$

respectively, in which τ_0^0 is the value of τ_0 at T_0 . τ_0^0 and β are assumed to have been determined by the method of the previous paragraph. A necessary condition for the skewed-arc locus is that for some value of $B\Delta$ a pair of $\epsilon''/(\epsilon' - \epsilon_1)$ values can be computed which agree, within the experimental uncertainty, with the measured values at T_1 and T_2 . Such pairs of values are given, for different values of β and $B\Delta$, in Fig. 5. If the data warrant it, the value of B so obtained may be used to calculate the dependence of ϵ' and ϵ'' on temperature, with the help of Figs. 2 and 3.

Under similar assumptions, the Cole-Cole symmetrical-arc locus gives rise to values of ϵ'' which are symmetrical in $1/T$ about the temperature of maximum loss and $\epsilon' - \epsilon_1$ at T_1 is equal to $\epsilon_0 - \epsilon'$ at T_2 .

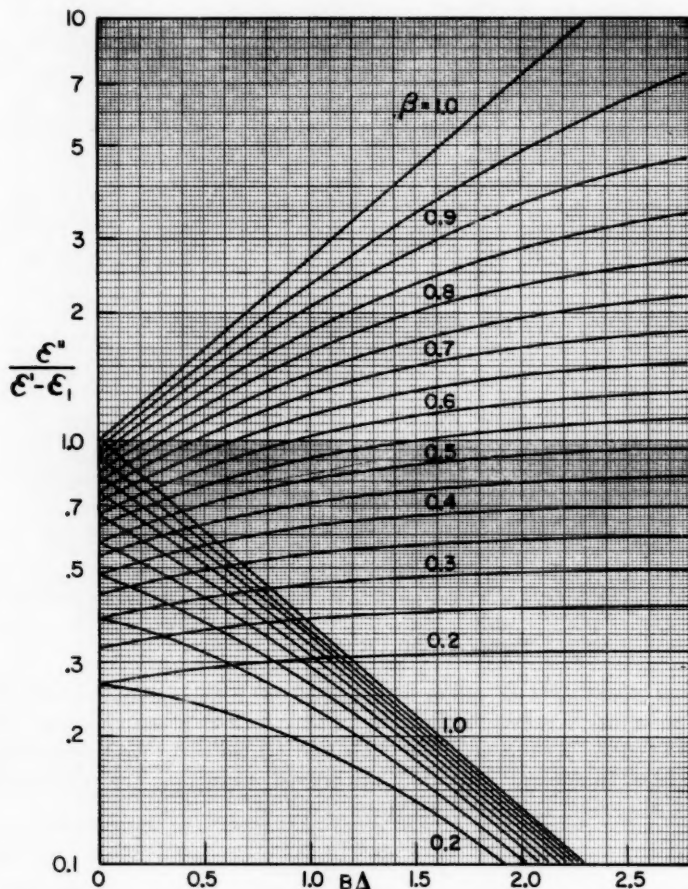


FIG. 5. Compatibility relationships for skewed-arc behavior at temperatures other than those of maximum loss.

Transient Measurements

At temperatures sufficiently low that polarization takes place too slowly to follow the changing phase of a low-frequency voltage, transient methods may be substituted for bridge methods. In these the charging or discharging current is measured as a function of time following application or removal of a suitable voltage.

TABLE I

Transient current $I(t)$, $t \geq 0$, for:		
Applied voltage	Debye locus	Skewed-arc locus
$V(t) = 0, \quad t < 0$ $= V_0, \quad t \geq 0$	(1) $V_0 C_0 \left[\epsilon_1 \delta_0 + \frac{\epsilon_0 - \epsilon_1}{\tau} e^{-t/\tau} \right]$	(2) $V_0 C_0 \left[\epsilon_1 \delta_0 + \frac{\epsilon_0 - \epsilon_1}{\tau_0 \Gamma(\beta)} \left(\frac{t}{\tau_0} \right)^{\beta-1} e^{-t/\tau_0} \right]$
$V(t) = 0, \quad t < 0$ $= at, \quad t \geq 0$	(3) $a C_0 \left[\epsilon_1 + (\epsilon_0 - \epsilon_1)(1 - e^{-t/\tau}) \right]$	(4) $a C_0 \left[\epsilon_1 + (\epsilon_0 - \epsilon_1) \frac{\Gamma t / \tau_0 (\beta)}{\Gamma(\beta)} \right]$

Table I summarizes the transient currents which follow the application of step and ramp voltage pulses to dielectrics having the Debye and skewed-arc characteristics. These equations result from application of the method of Fourier transforms (12, 13) to the equations for the frequency-dependent loci. The time variation of charge on the sample for a step voltage has the same form as the variation of current through the sample for a ramp voltage.

In Table I C_0 is the capacitance of the empty cell, δ_0 the delta function or unit impulse at $t = 0$, $\Gamma_{1/\tau_0}(\beta)$ and $\Gamma(\beta)$ the incomplete and complete gamma-function, respectively. The ratio of the two gamma-functions has been tabulated by Pearson (14), whose parameters are related to the present ones by $u = t/(\tau_0 \sqrt{\beta})$ and $p = \beta - 1$.

The ramp pulse is the more convenient since it does not give rise to the initial current surge which accompanies application of the step voltage and since it is somewhat simpler to evaluate the required parameters from the experimental transient behavior. However, it is easier to generate a constant voltage than a linearly rising one and the former may be used to advantage in the investigation of comparatively slow relaxation (as has been done, for example, with *n*-propanol at low temperatures (15)). An approximate method has been given by Hamon (16) for converting the results of time-dependent direct-current measurements to the equivalent frequency-dependent dielectric loss form.

In general transient methods do not seem capable of the same accuracy as bridge methods. They are, however, useful for extending the range of temperatures over which measurements of relaxation can be made by some 10 or 20°.

IV. EXPERIMENTAL EVIDENCE FOR THE SKEWED-ARC LOCUS

Hydroxyl Compounds

Practically all monohydroxyl alcohols that have been so far investigated are satisfactorily represented by the Debye semicircle in the complex plane (6), except for secondary dispersion regions (to be discussed below) at comparatively high frequencies which usually make a minor contribution to the value of the static dielectric constant. This semicircular behavior may be regarded as a limiting case of either the circular-arc locus of Cole and Cole (with $\alpha = 0$) or of the skewed-arc locus (with $\beta = 1$). At least one monohydroxyl alcohol, tetrahydrofurfuryl alcohol, exhibits an asymmetric dispersion locus of the skewed type. This is illustrated by Fig. 6 for which the data were obtained by L. Kuhi in this laboratory.

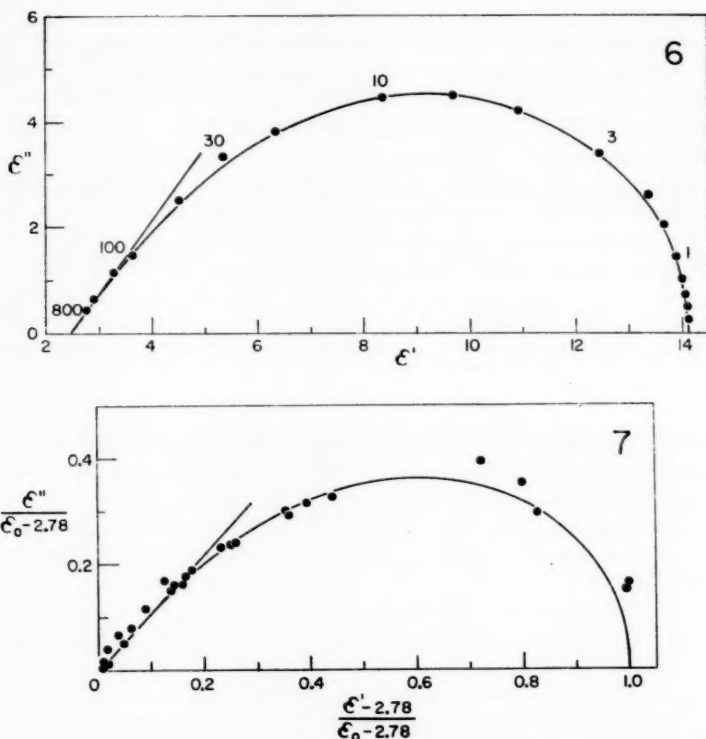


FIG. 6. Tetrahydrofurfuryl alcohol at -105.9°C . Skewed-arc locus is drawn for $\beta = 0.592$. Numbers beside points are frequencies in kc/sec.

FIG. 7. Aggregate plot for 2-methyl-2,4-pentanediol at temperatures between -45 and -79°C and frequencies of 1, 10, 30, and 100 kc/sec. Locus is drawn with $\beta = 0.525$.

The skewed-arc locus was originally used to describe the dispersion-absorption behavior of the polyhydroxyl liquids glycerol (7), 1,2-propanediol (7), and 1,3-propanediol (8). Data for the first two of these liquids are included in Fig. 11. The predicted form of transient current for systems giving skewed-arc loci (formula (4) of Table I) has been shown (12) to fit the transient behavior of glycerol at temperatures at which τ_0 is of the order of milliseconds. Koizumi and Hanai (17) expressed the results of a study of supercooled tetraethylene glycol by the skewed arc.

The dispersion of five isomeric pentanediols is accurately represented by equation [2] (18). 2-Methyl-2,4-pentanediol was examined by White and Morgan (19) whose data for four frequencies and a number of temperatures are shown in the aggregate plot of Fig. 7. The skewed-arc locus drawn represents the results in a satisfactory manner when it is considered that the variation of β with temperature is ignored. Data are not reported at sufficiently small temperature intervals to make analysis by the maximum loss method possible.

Halogen Compounds

Denney (20) has used the skewed-arc locus to describe the dielectric behavior of isobutyl bromide, isoamyl bromide, and isobutyl chloride at low temperatures. Winslow,

Good, and Berghausen (21) found it fitted the behavior of pentachlorobiphenyl (a mixture of isomers bearing the trade name Arochlor 1254) and hexachlorobiphenyl (Arochlor 1260), at temperatures below room temperature. Examination of the Massachusetts Institute of Technology data at 25° C (22), though reported only at frequencies which differ, for the most part, by a factor of 10, shows that in all probability the same behavior extends to higher temperatures. The M.I.T. tables indicate that the other polychlorodiphenyls probably exhibit skewed-arc-locus behavior. This is true also for Arochlor 4465 (a mixture of chlorinated bi- and ter-phenyls) and Arochlor 5460 (non-chloroterphenyls) for which β appears to be of the order of 0.2 and lower frequency measurements show the presence of d-c. conductance.

The skewed-arc behavior of 1,2-dibromopentane is illustrated in Fig. 8(a), which gives the results of bridge measurements at -112° where τ_0 is of the order of a millisecond, and in Fig. 8(b), which presents transient results at -127° where τ_0 is of the order of 10 seconds.

The method based on the temperature of maximum loss (see III) may be applied to the data of Turkevich and Smyth (23) for 2-methyl-1,2-dichloropropane, shown for low

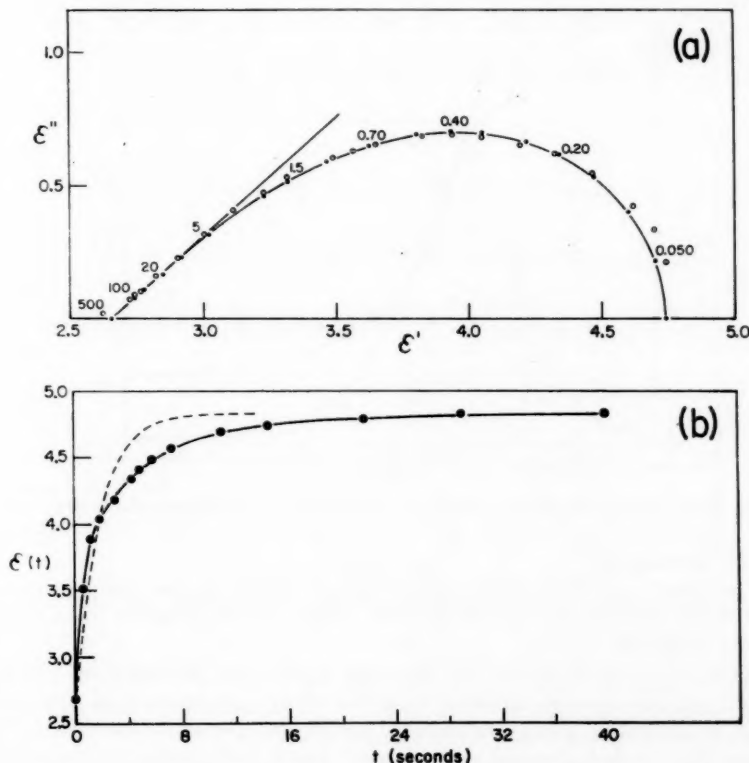


FIG. 8(a). ○ Data for 1,2-dibromopentane at -112.0° C, ● calculated points for $\beta = 0.463$, $\tau_0 = 7.58 \times 10^{-4}$ sec.

FIG. 8(b). Transient data for 1,2-dibromopentane at -127.2° C. Solid curve is the incomplete Γ -function with $\beta = 0.35$, $\tau_0 = 8.6$ sec, broken curve the exponential which rises to $(1 - e^{-1})(\epsilon_0 - \epsilon_1)$ in the same time.

temperatures in Fig. 9. The 50-kc points show a loss maximum of about 5.45 at -137.9°C . At this temperature and frequency $\epsilon' = 12.65$ and, taking $\epsilon_1 = 2.30$ (a reasonable value since ϵ' approaches 2.36 at -188°C), one finds $(\epsilon' - \epsilon_1)/\epsilon'' = 1.901$. The relaxation time τ_0 (at -137.9°C) is then $1.90/(2\pi \times 50,000)$ or 6.1×10^{-6} seconds and $\beta = 0.446$ (equation [9]). For $\Delta = 2 \times 10^{-4}$, T_1 is -141.5°C and T_2 is -134.1°C , which correspond to $\epsilon''/(\epsilon' - \epsilon_1)$ values of about 0.756 and 0.177, respectively. Inspection of Fig. 5, for $\beta = 0.45$ shows a value of $B\Delta$ at T_1 of about 1.37 and at T_2 of about 1.51. This is satisfactory agreement, which may be improved by allowing β to assume values slightly smaller than 0.45. B is then 7.2×10^3 and the "energy of activation" (BR) some 14 kcal/mole. Application of the same technique to the 5-kc points leads to a similar value of β . The loss maximum at 500 c, however, of the order of $(\epsilon_0 - \epsilon_1)/2$, is anomalously high. A similar anomaly for isobutyl chloride at the same frequency (23) is not confirmed by the results of Denney (20).

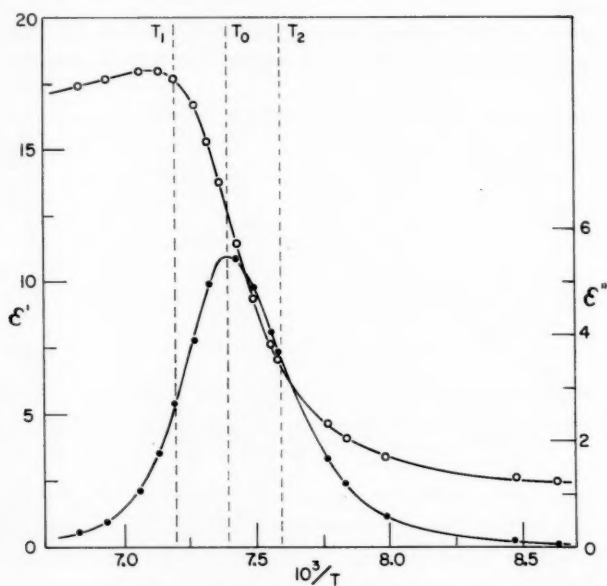


FIG. 9. Low-temperature dielectric behavior of 2-methyl-1,2-dichloropropane at 50 kc/sec.

Miscellaneous Compounds

Grant, Davidson, and Gray (24) found *n*-propyl nitrite at low temperatures to fit the skewed locus (see Fig. 11) as did Winslow, Good, and Berghausen (21) in the case of tolyl xylyl sulphone.

Schallamach's data at 9 Mc for the aldehyde citral (25), analyzed by the method of maximum loss, give results consistent with the skewed-arc locus, with β of the order of 0.75 and an activation energy of some 11 kcal/mole. The same author's results for the corresponding alcohol, geraniol, on the other hand, are adequately described by a single relaxation time ($\beta = 1$).

Polymers

Polar polymers in general exhibit very broad loss spectra (see, for example, the M.I.T.

tables (22)) which, although they may resemble the skewed-arc behavior in some respects, do not accurately conform to it. Dielectric relaxation in polymers proceeds by orientation of chain segments (26) and therefore differs from that in simple liquids.

The case of the poly(vinyl acetates) has been investigated by the author in some detail. Seven Gelvas (Shawinigan Chemicals Limited) ranging in Gelva number from 1.5 to 134 and in number-average molecular weight from 5,000 to ca. 200,000 were studied. The locus shown in Fig. 10, in which the ordinates are in arbitrary capacitance units, is

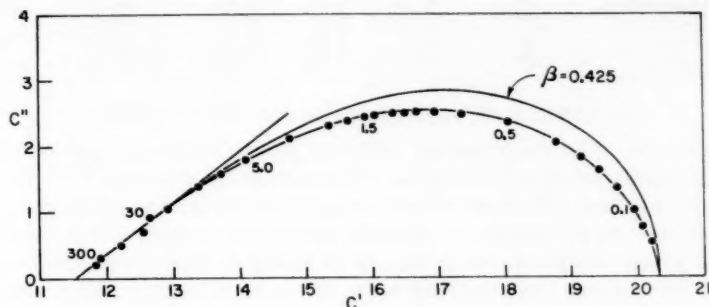


FIG. 10. Poly(vinyl acetate) (Gelva 134) at 68°C.

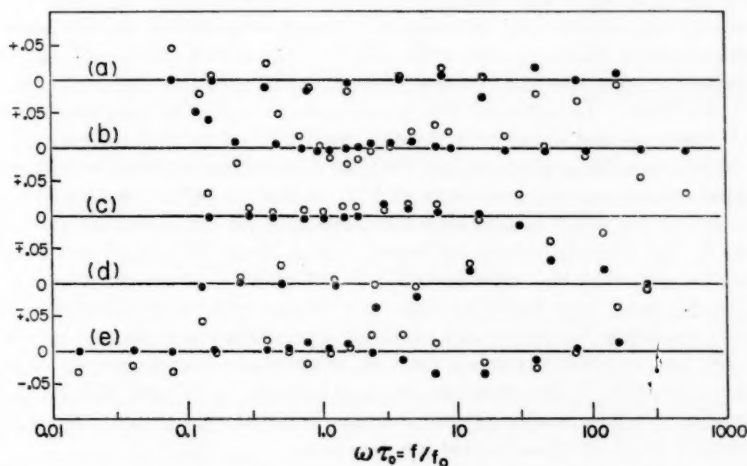


FIG. 11. $(\epsilon'_{\text{obs}} - \epsilon'_{\text{calc}})/\epsilon'_{\text{obs}}$ (●) and $(\epsilon''_{\text{obs}} - \epsilon''_{\text{calc}})/\epsilon''_{\text{obs}}$ (○) vs. frequency, for the liquids and parameters listed in Table II.

typical. The loss in the vicinity of the maximum and at lower frequencies is less than would be predicted by equation [2] for a β determined by the high frequency behavior, generally between 0.40 and 0.45. There appears to be no consistent dependence of this high frequency β on molecular weight. There is evidence that the presence of traces of benzene may broaden the loss spectrum.

Figure 11 illustrates the extent of the agreement for five liquids between the experimental values of ϵ' and ϵ'' and those computed from equation [2] with the parameters

shown in Table II. There appears to be no systematic disagreement. Periodic variations seem to be due to temperature fluctuations of the sample.

TABLE II
Parameters used to calculate $\epsilon''(\omega)$ in Fig. 11

	Liquid	T ($^{\circ}$ K)	ϵ_0	ϵ_1	β	τ_0 (sec)	Reference
(a)	Glycerol	223.2	64.1	4.10	0.603	1.26×10^{-4}	42
(b)	1,2-Dibromopentane	161.2	4.73 ₉	2.65 ₄	0.463	7.58×10^{-4}	This work
(c)	Isoamyl bromide	133.8	13.16	2.84	0.60	2.36×10^{-6}	20
(d)	<i>n</i> -Propyl nitrite	95.9	40.13	3.58	0.705	3.93×10^{-4}	This work
(e)	1,2-Propanediol	209.0	53.71	3.68	0.693	1.24×10^{-4}	8

V. THE EFFECT OF TEMPERATURE ON THE DISPERSION

There is therefore good experimental evidence for the rather general occurrence in liquids of a relaxation behavior that can be characterized by the skewed-arc locus. Most of this evidence has been obtained at low temperatures where the relaxation processes are sufficiently slow to be studied by accurate techniques. Whether these observations are valid only at low temperatures or may be extended to higher temperatures as well remains to be determined. Unfortunately many of the experimental results presented in the literature are not sufficiently complete to enable the shape of the dispersion-absorption locus to be adequately defined.

An interesting example of what might be a change in the shape of the dispersion locus with temperature is provided by the case of tetraethylene glycol. In the supercooled state, at temperatures between -44 and -71° C, this glycol shows (17) a dielectric relaxation behavior very near that represented by the skewed arc with a β value of the order of 0.4. Koizumi (27) extended the measurements to higher temperatures and to microwave frequencies and found that the new results could be best represented by the symmetrical-arc locus. The parameter α of the Cole-Cole representation for tetraethylene glycol assumed values ranging from 0.23 at 5° C to 0.14 at 50° C (see Fig. 12(a)). An attempt is made to represent Koizumi's microwave data for tetraethylene glycol by the skewed locus in Fig. 12(b) by assuming values of β of about 0.60 at 5° and about 0.70 at 50° . It can be seen that this representation is not quite as successful as the circular-arc one, although there is not sufficient data near the top and on the low-frequency side of the locus to establish the preference of either representation with any certainty.

Glarum (28) has recently extended the low temperature measurements of Denney (20) on isoamyl bromide to the temperature range between -75° and 25° and to microwave frequencies. He has concluded that for this liquid the skewed-arc representation probably remains valid at these higher temperatures.

VI. THE RESOLUTION OF RELAXATION PROCESSES

The separation of the effects of different relaxation processes is of obvious importance if the individual mechanisms of relaxation are to be studied. It is necessary to distinguish between (a) the case in which each relaxation process is independent of the others and the principle of superposition may be applied to the polarization or the complex dielectric constant and (b) the case in which two or more relaxation mechanisms occur either as successive stages or alternate routes in the relaxation process and superposition may not be used to separate the individual components of relaxation. Examples of case (a) include orientation of a polar group within the molecule by a different mechanism from

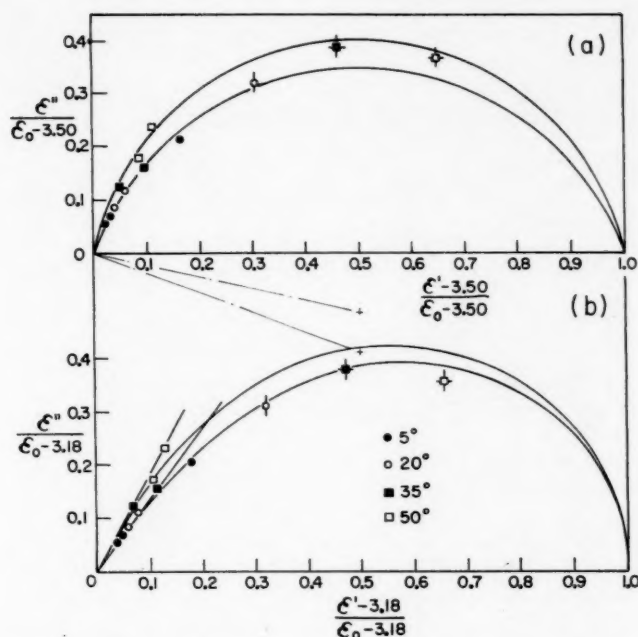


FIG. 12. Comparison of symmetric-arc (a) and skewed-arc (b) representations of microwave data for tetraethylene glycol.

orientation of the molecule as a whole, and orientation of different molecules in different fixed environments by different mechanisms. For each of these examples, assuming only two modes of relaxation, the total polarization decays as

$$P(t) = P_1 e^{-t/\tau_1} + (P_0 - P_1) e^{-t/\tau_2},$$

in which P_0 is the initial polarization, P_1 the polarization contributed by the first process, and τ_1 and τ_2 are the relaxation times of the two processes, each assumed to decay exponentially. An example of case (b) is provided by the orientation of molecules whose environments are subject to change during the period of relaxation and whose relaxation rates change with the environment. If there are only two types of environment, the simplest form of the polarization is

$$P(t) = P_0 e^{-t/\tau_1} e^{-t/\tau_2},$$

which is indistinguishable from a simple exponential decay function. Brot has proposed a model to account for the failure of superposition when the resolved dispersion regions apparently overlap (29).

(a) Independent Polarization Processes

Discontinuous Relaxation

Even in this case, the nature of relaxation spectra is such that resolution of different processes is difficult unless the corresponding relaxation times are widely different. This is illustrated in Fig. 13 for the most favorable case possible, that of two independent

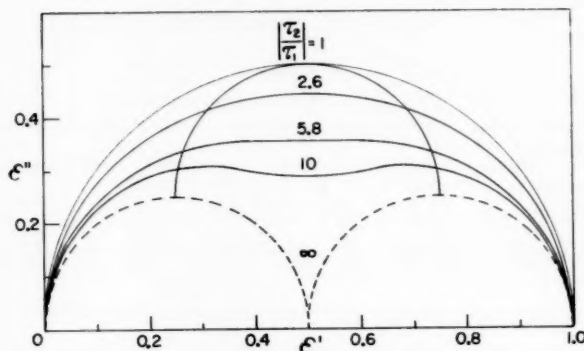


FIG. 13. Dependence of locus of $\epsilon' - i\epsilon'' = 0.5(1 + i\omega\tau_1)^{-1} + 0.5(1 + i\omega\tau_2)^{-1}$ on τ_2/τ_1 . Upper semicircle is locus of points at which $\omega = 1/\tau_1$ and $1/\tau_2$.

polarization processes each characterized by a single relaxation time and by the same amplitude of dispersion. Separate loss maxima occur only for relaxation times which differ by more than a factor of 5.8 (strictly, $3 + 2\sqrt{2}$). If the individual dispersion regions are considerably broader than this and are considerably different in amplitude, separate loss peaks may appear only when the appropriate relaxation times or critical frequencies differ by a factor of 100 or more. It is not surprising that the results may sometimes be analyzed in more than one way.

Examples of solutions for which the relaxation spectra are readily resolvable have been given (30, 31, 32), but most of the liquids that have been extensively studied exhibit broad dispersion-absorption behavior in which separate loss peaks do not occur.

The monohydroxyl alcohols, in addition to the principal (semicircular) dispersion region, show at considerably higher frequencies one or more additional dispersion regions of relatively small amplitude. Although in general not showing separate ϵ'' peaks, the high-frequency data for some alcohols have been reduced to a Cole-Cole arc by subtracting the contributions of the Debye relaxation region. A second dispersion region has been defined in this way for the alcohols from ethanol through the butanols (except for *t*-butanol) (33, 34, 35), for *n*-hexanol (36), cyclohexanol (37), *n*-heptanol (36), and four isomeric octanols (36, 38, 39, 40) and for *n*-propanol-*d* (15) and *n*-octanol-*d* (36). Most of these results also show signs of further dispersion at still higher frequencies which, by a further subtraction of the effects of the second dispersion, has been shown to be representable, within rather large experimental uncertainties, by an additional arc in the cases of *n*-propanol, *n*-propanol-*d*, and the octanols.

The question naturally arises as to whether behavior such as has been described by the asymmetric locus of equation [2] can be represented by the superposition of several discrete relaxation processes. Poley (41) first suggested that the main relaxation properties of glycerol could be attributed to the combined effects of a low-frequency semicircle and a high-frequency symmetric arc. Cole (42) has indicated that a detailed examination of the experimental data for glycerol does not support this suggestion. A number of glycols (1,2-ethanediol, 1,2-propanediol, 1,3-butanediol, and 1,5-pentanediol), which exhibit asymmetric loci have recently been analyzed (43, 44) in terms of one or more high-frequency arcs and a low-frequency semicircle or arc. The relaxation behavior of 1,2-propanediol, for example, over the range of frequencies between 0.1 and 25,000 Mc/sec,

has been expressed by the superposition of a symmetric arc and a semicircle. The reported (43) parameters at -40°C have been used to construct the locus shown in Fig. 14(a).

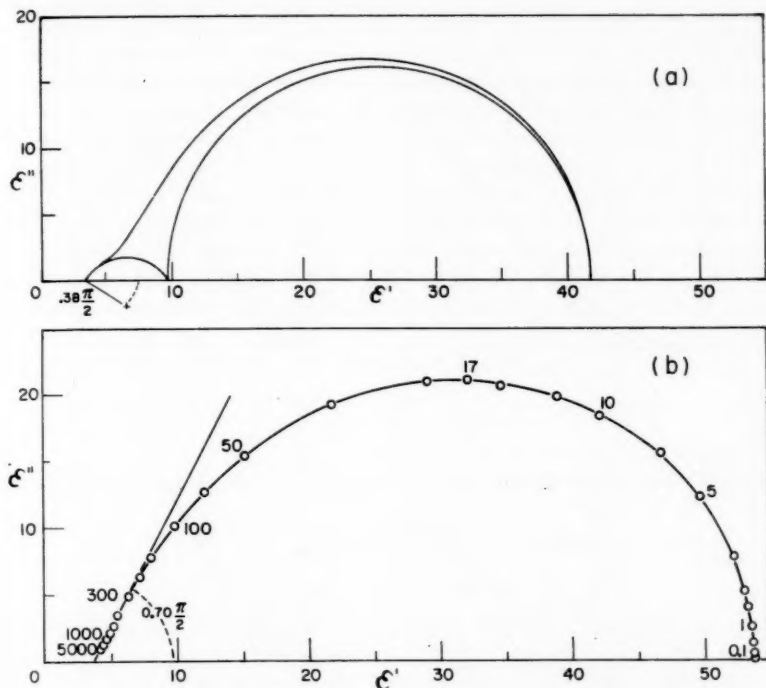


FIG. 14. Comparison for 1,2-propanediol of (a) the representation of the behavior at -40° suggested in reference 43 with (b) experimental data at -64.2° (●) and skewed-arc locus with $\beta = 0.70$.

From comparison with the locus shown in Fig. 14(b), from measurements at -64°C , it must be concluded that either the experimental behavior changes markedly with temperature or that the type of resolution proposed is not justified by the data for this liquid.

In some cases the proposed resolution has led to an overlapping of the resolved regions (29, 38, 44, 45). For example, the low-frequency limiting value of the dielectric constant for the second dispersion region may be appreciably greater than the limiting high-frequency value for the first (low-frequency) dispersion region. Brot (29, 38) has proposed on this basis that the superposition principle, in the form that assumes direct additivity of contributions to the complex dielectric constant from the individual relaxation processes, is violated. Although limitations of space have usually prevented publication of the full experimental data, it appears possible that in at least some cases the data may be adequately described by equation [2] or some other asymmetric representation. It is evident from inspection of Fig. 14(a) that a better approximation to the behavior of Fig. 14(b) may be realized by allowing the low-frequency side of the arc to overlap the high-frequency side of the semicircle, but it is doubtful whether this will lead to as good a fit of the data as equation [2].

In most liquids to which the skewed-arc behavior has been attributed there is a slight "tailing-off" of the high-frequency end of the experimental locus which is not described by equation [2] (Fig. 15). Although this behavior may correspond to a separate, very broad relaxation process, it is at least qualitatively predicted by the Glarum model to be considered below.

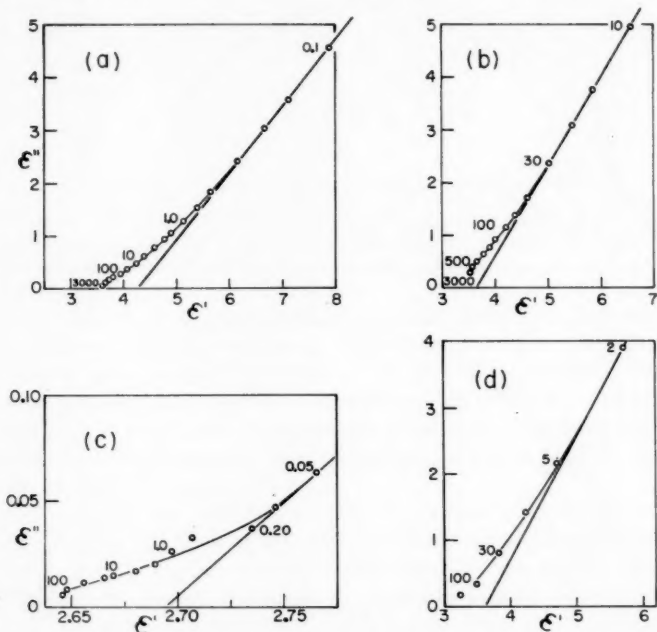


FIG. 15. Departures of dispersion behavior from skewed-arc type (straight lines) at relatively high frequencies for (a) glycerol at -70.0° , (b) 1,2-propanediol at -77.9° , (c) 1,2-dibromopentane at -127.1° , and (d) *n*-propyl nitrite at -179° .

Continuous Relaxation

The previous section has mentioned examples of the resolution of dispersion effects into different dispersion regions, some of which are much broader than predicted by the Debye equation. The principle of superposition may be applied to such a dispersion region, assumed to arise from a continuum of simple exponential decay functions, in the form

$$[11] \quad \epsilon(i\omega) = \epsilon_1 + (\epsilon_0 - \epsilon_1) \int_{-\infty}^{\infty} \frac{G(\tau) d \ln \tau}{1 + i\omega\tau},$$

which defines, along with $\int_{-\infty}^{\infty} G(\tau) d \ln \tau = 1$, a distribution function $G(\tau)$ such that $G(\tau) d \ln \tau$ represents the fractional contribution to $\epsilon_0 - \epsilon_1$ arising from that part of the relaxation process having relaxation times whose logarithms lie between $\ln \tau$ and $\ln \tau + d \ln \tau$.

For the $\epsilon(i\omega)$ of equation [2], $G(\tau)$ becomes (7)

$$[12] \quad G(\tau) = \frac{\sin \beta \pi}{\pi} \left(\frac{\tau}{\tau_0 - \tau} \right)^\beta, \quad \tau \leq \tau_0 \\ = 0, \quad \tau > \tau_0,$$

a function with a singularity at $\tau = \tau_0$. This form of $G(\tau)$ has been criticized (41) as being physically unrealistic. Such a criticism may be applied with equal relevance to the classical Debye behavior, for which $G(\tau) = \delta[\ln(\tau/\tau_0)]$, the delta function. This is an improper function, with discontinuities on both sides of $\tau = \tau_0$. It is nevertheless of use in quantum mechanics where, as in the present case, it occurs as an integrand (46).

It may be argued that the presence of either a unique relaxation time or of a distribution of relaxation times which ends abruptly at its most probable value is inconsistent with the variations in molecular environment that occur in liquids. They do, however, lead formally to expressions for $\epsilon(i\omega)$ which are capable for many liquids of describing the experimental results within the accuracy of the measurements. It may be that additional accuracy will lead to modifications of these distribution functions. The results of Grant, Buchanan, and Cook (6) suggest that a finite distribution of relaxation times is present in water, although the departure from Debye dispersion is barely detectable. It would be possible to modify equation [12] by replacing the abrupt cutoff at $\tau = \tau_0$ by a rapid but monotonic decline to zero for $\tau > \tau_0$ without producing much change in the resulting form of $\epsilon(i\omega)$.

Figure 16 illustrates the integral distribution function

$$F(\tau) = \int_0^\tau G(\tau) d \ln \tau$$

for $G(\tau)$ defined by equation [12]. $F(\tau)$ is a special case of the incomplete β -function (7):

$$[13] \quad F(\tau) = \frac{\sin \beta \pi}{\pi} \int_0^{\tau/\tau_0} (\tau/\tau_0)^{\beta-1} (1-\tau/\tau_0)^{-\beta} d(\tau/\tau_0), \quad \tau \leq \tau_0, \\ = 1, \quad \tau > \tau_0,$$

which may be evaluated by graphical integration. Pearson (47) has tabulated the incomplete β -function for parameters related to those of equation [13] by $p = \beta$, $q = 1 - \beta$, and $x = \tau/\tau_0$, but the large intervals between successive entries make these tables of little use for the range of parameters of interest here.

In Fig. 17 the integrated distribution function for $\beta = 0.70$ is compared with the sum of the integrated functions for the Cole-Cole arc and Debye semicircle suggested (see above) for 1,2-propanediol.

The picture of relaxation which results from the assumption of the physical reality of the distribution function of equation [12] is one of molecular rotation which takes place at rates which differ widely and continuously with the molecular environment by mechanisms each of which makes an additive contribution to the dielectric constant and shows a simple exponential dependence on time. The maximum relaxation time in the distribution may then be the orientation time of molecules in surroundings of greatest order. It is not easy to reconcile this picture with the evidence that liquid relaxation is a co-operative process (see next paragraph) nor with the observation that relaxation in many different liquids may be represented by the same simple analytic expression.

(b) Relaxation Processes not Resolvable by Superposition

It is likely that the behavior characterized by the skewed-arc locus arises from the presence of co-operative processes in which individual molecules in general do not rotate independently of one another.

The evidence for co-operative effects involving many molecules in the relaxation process may be summarized as follows:

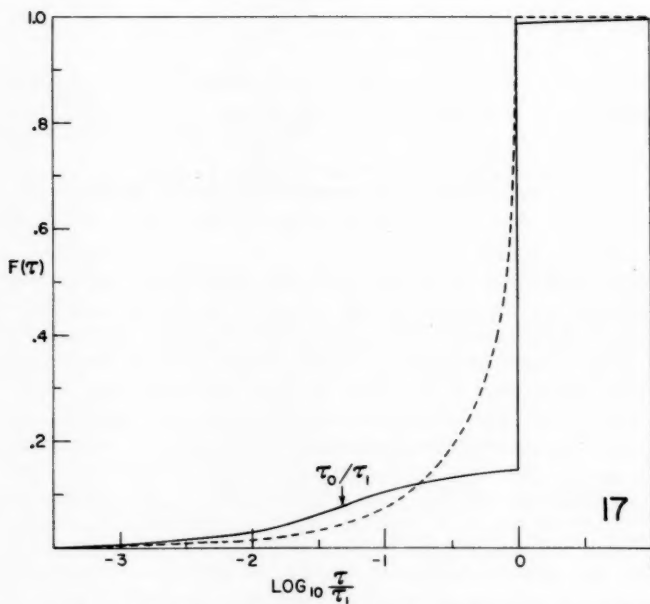
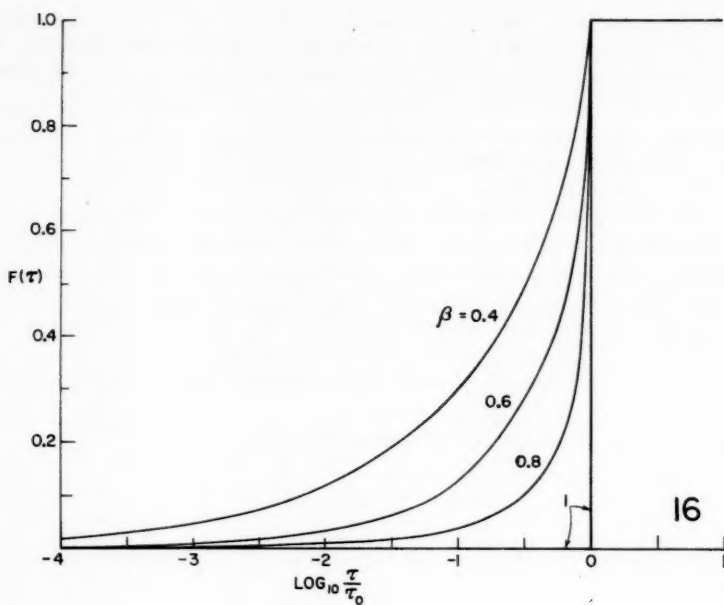


FIG. 16. The integral distribution function of relaxation times for various values of β .

FIG. 17. Comparison of integral distribution function arising from superposition of a semicircle (relaxation time τ_0) and a circular arc ($\alpha = 0.38$, $\tau_1 = 20.9\tau_0$) (solid curve) with that for a skewed arc ($\beta = 0.70$, broken curve).

(a) The temperature dependence of the relaxation times of many liquids leads to very large positive entropies of activation (48).

(b) Solutions of similar liquids in one another (e.g., alcohols (49) or halides (31)) lead to only one principal dispersion process, with little or no change in the shape of the dispersion. This suggests that the relaxing unit is large enough to contain the different molecules in the same proportion as in bulk solution.

(c) A similar inference may be drawn from the effect of electrolytes in changing the relaxation times of water and alcohols (50) without appreciably changing the width of the dispersion region.

(d) The similarity between the temperature dependence of such properties as dielectric relaxation time, macroscopic shear viscosity, and d-c. conductance in many liquids at low temperatures (see, for example, references 7 and 9) suggests that a common rate-determining process is involved. Such a process which involves only single molecules is difficult to envisage.

An interesting model which, under some conditions, leads approximately to a skewed-arc locus, has been recently proposed by Glarum (28). The polarization equation is

$$P(t) = P_0 e^{-t/\tau_0} [1 - x(t)]$$

where τ_0 is the relaxation time of molecular orientation when there are no defects in the vicinity and $x(t)$ is the mole fraction of molecules which have relaxed completely as a result of the diffusion of defects. For the one-dimensional diffusion of randomly distributed defects in which only the defect initially nearest the molecule is permitted to reach it, the theory (28) leads to

$$\frac{\epsilon(i\omega) - \epsilon_1}{\epsilon_0 - \epsilon_1} = \frac{1}{1 + i\omega\tau_0} + \frac{i\omega\tau_0}{(1 + i\omega\tau_0)[1 + \sqrt{a_0(1 + i\omega\tau_0)}]}$$

with $a_0 = l_0^2/D\tau_0$, where l_0 is the average distance over which the nearest defect must diffuse to reach the molecule when the diffusion coefficient is D . Since l_0^2/D represents an average diffusion time, a_0 may be considered to be the ratio of a relaxation time arising from the diffusion of defects to a relaxation time in the absence of defects. The locus changes gradually with increasing a_0 from a skewed-arc locus with $\beta = 0.5$ for $a_0 = 1$ to a simple Debye semicircle for $a_0 \gg 1$. The behavior at some intermediate values of a_0 is illustrated in Fig. 18. It is apparent that there is significant departure from a skewed arc only at high frequencies.

As plotted in Fig. 18 the Glarum locus approaches the origin at an angle of 45° with the real axis at high frequencies, a feature which gives the appearance of a small additional dispersion region for values of a_0 greater than unity. Since experimental results frequently show effects of roughly this type (compare Fig. 15), the value of ϵ_1 for "best fit" of the Glarum locus to experimental data is somewhat lower than that which is used for the skewed-arc representation (by an amount $\Delta\epsilon_1$). A more realistic comparison of the two representations than is shown in Fig. 18 is possible if the Glarum locus is expanded by a factor $1 + \Delta\epsilon_1/(\epsilon_0 - \epsilon_1)$ and the high-frequency intercept shifted a distance of $-\Delta\epsilon_1/(\epsilon_0 - \epsilon_1)$ from the origin. The Glarum locus for $a_0 = 8$ has been modified in this way for $\Delta\epsilon_1 = 0.0175(\epsilon_0 - \epsilon_1)$, and the results compared with the skewed-arc representation for $\beta = 0.756$ in Table III. For values of $\omega\tau_0$ up to about 30 the differences are well within the likely error of any comparable experimental data.

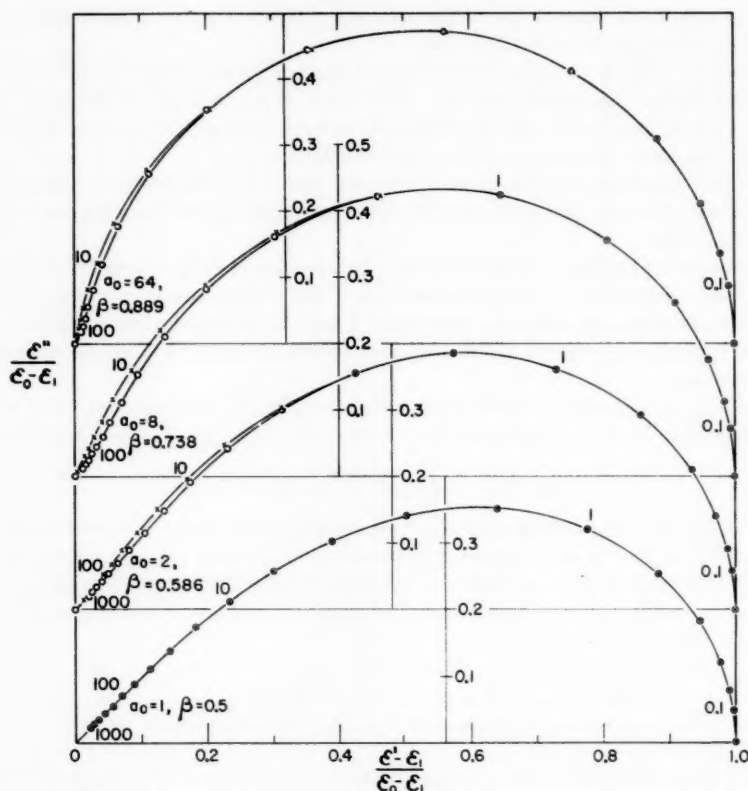


FIG. 18. Comparison of Glarum plots (O) for various values of a_0 with skewed-arc plots (X) for values of $\beta = \sqrt{a_0}/(1 + \sqrt{a_0})$. Successive frequencies increase by a factor of 1.585.

As may be inferred from Fig. 18, $\Delta\epsilon_1$ becomes very small as a_0 either gets very large or approaches 1. The Glarum model therefore cannot account for the high-frequency dispersion effects appearing in the spectra of the alcohols (VI(a)) nor for some of the effects illustrated in Fig. 15. It is apparent, however, that a more critical experimental examination of the frequency range above $\omega\tau_0 = 100$ is required.

The Glarum theory shows, for the first time, that relaxation (which may be relatively slow) by an alternative mechanism to simple molecular orientation in a fixed environment may lead to a broadening of the Debye locus in the sense of increased dispersion and absorption on the high-frequency side, that is, in the sense required for skewed-arc behavior. The theory also predicts the Cole-Cole arc behavior in the case in which a_0 is very small (that is, relaxation proceeds by a defect diffusion mechanism only) and has possible application to relaxation in solids, for which symmetric-arc behavior is common.

It is formally possible for the Glarum model to take into account such co-operative effects as are mentioned above. Thus, τ_0 may be identified with the (macroscopic) relaxation time for co-operative molecular orientation in highly ordered regions of the liquid, a concept which requires further elaboration by a statistical approach.

TABLE III
Comparison of Glarum and skewed-arc representations

$\omega\tau_0$	Modified Glarum locus ($a_0 = 8$)		Skewed-arc locus ($\beta = 0.756$)	
	Reduced ϵ'	Reduced ϵ''	Reduced ϵ'	Reduced ϵ''
1.000×10^{-2}	0.9999	0.0075	0.9999	0.0076
1.000×10^{-1}	.9936	.0746	.9934	.0750
2.512	.9608	.1799	.9604	.1808
6.310	.8042	.3638	.8024	.3638
1.000×10^0	.6394	.4313	.6377	.4306
1.585	.4502	.4303	.4498	.4294
2.512	.2922	.3694	.2925	.3696
3.981	.1858	.2881	.1853	.2895
6.310	.1205	.2144	.1184	.2156
1.000×10^1	.0803	.1566	.0773	.1566
1.585	.0546	.1140	.0516	.1123
2.512	.0371	.0833	.0351	.0800
3.981	.0247	.0612	.0242	.0568
6.310	.0154	.0454	.0168	.0402
1.000×10^2	.0084	.0340	.0117	.0284
1.585	.0029	.0257	.0082	.0201
2.512	-0.0014	.0195	.0058	.0142
3.981	-0.0047	.0149	.0041	.0103
6.310	-0.0074	.0115	.0029	.0071
1.000×10^3	-0.0095	.0089	.0020	.0050
∞	-0.0175	0	0	0

VII. OTHER RELAXATION PHENOMENA

Distributions of relaxation times have long been used in the interpretation of relatively slow viscoelastic or mechanical relaxation processes. More recently (51, p. 454) the need for distributions of relaxation times has been demonstrated by the results of measurements of the dispersion of sound velocity and the absorption of ultrasonic energy in liquids. Although the measurements are not of sufficient accuracy to preclude other possible distributions, and the distribution function is not defined in quite the same way, it is interesting to find that the application of the distribution function of equation [12] to the complex compressional modulus leads to an adequate description of the main aspects of ultrasonic relaxation in a number of polyhydroxyl compounds (51, p. 479).

The classical theory of the nuclear magnetic resonance correlation time has been modified (52) to provide better agreement with experiment by the introduction of a distribution of correlation times. For two of the liquids showing the skewed-arc-locus type of dielectric behavior (glycerol (53) and isobutyl bromide (54)), the "most probable" correlation times are in surprisingly good agreement with dielectric relaxation times derived from the maxima of the dielectric loss curves. A rectangular distribution function is assumed for the correlation times although other distribution functions are equally possible.

It is likely that such a comparison of dielectric, ultrasonic, and n.m.r. relaxation behavior as has been initiated by Powles (53, 54), will facilitate attempts to devise an adequate mechanism of structural relaxation in liquids.

ACKNOWLEDGMENTS

The author is greatly indebted to Dr. S. D. Baxter for computations on which Figs. 1 to 5 and 18 are based and to Professor R. H. Cole for the opportunity to examine the manuscript of reference 28 in advance of publication.

REFERENCES

1. F. BUCKLEY and A. A. MARYOTT. Tables of dielectric dispersion data for pure liquids and dilute solutions. Natl. Bur. Standards Circular 589. 1958.
2. K. S. COLE and R. H. COLE. *J. Chem. Phys.* **9**, 341 (1941).
3. C. P. SMYTH. Dielectric behavior and structure. McGraw-Hill Book Co., Inc., New York. 1955. p. 56.
4. F. BUCKLEY and A. A. MARYOTT. Tables of dielectric dispersion data for pure liquids and dilute solutions. Natl. Bur. Standards Circular 589. 1958. Table 5.
5. E. H. GRANT, T. J. BUCHANAN, and H. F. COOK. *J. Chem. Phys.* **26**, 157 (1957).
6. F. BUCKLEY and A. A. MARYOTT. Tables of dielectric dispersion data for pure liquids and dilute solutions. Natl. Bur. Standards Circular 589. 1958. Table 2 (see entries to individual alcohols).
7. D. W. DAVIDSON and R. H. COLE. *J. Chem. Phys.* **19**, 1484 (1951).
8. D. W. DAVIDSON. Unpublished results. R. H. COLE. *J. Chem. Phys.* **23**, 493 (1955).
9. D. J. DENNEY. *J. Chem. Phys.* **30**, 159 (1959).
10. C. P. SMYTH. Dielectric behavior and structure. McGraw-Hill Book Co., Inc., New York. 1955. p. 103.
11. J. A. SAXTON. *Proc. Roy. Soc. (London)*, A, **213**, 473 (1952).
12. D. W. DAVIDSON, R. P. AUTY, and R. H. COLE. *Rev. Sci. Instr.* **22**, 678 (1951).
13. G. A. CAMPBELL and R. M. FOSTER. Fourier integrals for practical application. Bell Telephone System Tech. Publs. Monograph B 584. 1931.
14. K. PEARSON. Tables of the incomplete gamma-function. H.M. Stationery Office, London. 1922.
15. D. W. DAVIDSON and J. WHEELER. *J. Chem. Phys.* **30**, 1357 (1959).
16. B. V. HAMON. *Proc. Inst. Elec. Engrs. (London)*, Pt. IV, **99**, 1 (1952).
17. N. KOIZUMI and T. HANAI. *J. Phys. Chem.* **60**, 1496 (1956).
18. D. W. DAVIDSON. To be published.
19. A. H. WHITE and S. O. MORGAN. *Physics*, **2**, 313 (1932).
20. D. J. DENNEY. *J. Chem. Phys.* **27**, 259 (1957).
21. J. WINSLOW, JR., R. J. GOOD, and P. E. BERGHAUSEN. *J. Chem. Phys.* **27**, 309 (1957).
22. A. R. VON HIPPLE. Dielectric materials and applications. The Technology Press of M.I.T., and John Wiley & Sons, Inc., New York, 1954. pp. 363, 364, 315.
23. A. TURKEVICH and C. P. SMYTH. *J. Am. Chem. Soc.* **64**, 737 (1942).
24. R. F. GRANT, D. W. DAVIDSON, and P. GRAY. *J. Chem. Phys.* **33**, 1713 (1960).
25. A. SCHALLAMACH. *Trans. Faraday Soc. A*, **42**, 180 (1946).
26. J. G. KIRKWOOD and R. M. FUOSS. *J. Chem. Phys.* **9**, 329 (1941).
27. N. KOIZUMI. *J. Chem. Phys.* **27**, 625 (1957).
28. S. H. GLARUM. *J. Chem. Phys.* **33**, 639 (1960).
29. C. BROU. *J. chim. phys.* **55**, 451 (1956).
30. M. DAVIES and R. J. MEAKINS. *J. Chem. Phys.* **26**, 1584 (1957).
31. D. J. DENNEY. *J. Chem. Phys.* **30**, 1019 (1959).
32. C. P. SMYTH. Dielectric behavior and structure. McGraw-Hill Book Co., Inc., New York. 1955. p. 129.
33. F. X. HASSION and R. H. COLE. *J. Chem. Phys.* **23**, 1756 (1955).
34. R. H. COLE and D. W. DAVIDSON. *J. Chem. Phys.* **20**, 1389 (1952).
35. W. DANNHAUSER and R. H. COLE. *J. Chem. Phys.* **23**, 1762 (1955).
36. M. BRUMA. Thesis, Paris. 1952.
37. R. ARNOULT, A. LEBRUN, and C. BOULLET. *Arch. sci. (Geneva)*, (spec. no.), **9**, 44 (1956).
38. C. BROU. Thesis, Paris. 1956.
39. R. ARNOULT, A. LEBRUN, C. MORIAEZ, M. MORIAEZ, and R. WEMELLE. *Arch. sci. (Geneva)*, (spec. no.) **10**, 48 (1957).
40. R. WEMELLE. *Compt. rend.* **246**, 3232 (1958).
41. J. PH. POLEY. *Physica*, **19**, 301 (1953).
42. R. H. COLE. *J. Chem. Phys.* **23**, 493 (1955).
43. C. MORIAEZ-BOULLET. *Compt. rend.* **246**, 2364 (1958).
44. C. MORIAEZ. *Arch. sci. (Geneva)*, (spec. no.) **11**, 77 (1958).
45. R. WEMELLE. *Compt. rend.* **244**, 775 (1957).
46. P. A. M. DIRAC. Quantum mechanics. 3rd ed. Clarendon Press, Oxford. 1947. p. 58.
47. K. PEARSON. Tables of the incomplete beta-function. University Press, Cambridge, 1934.
48. W. KAUZMANN. *Revs. Modern Phys.* **14**, 12 (1942).
49. D. J. DENNEY and R. H. COLE. *J. Chem. Phys.* **23**, 1767 (1955).
50. J. B. HASTED and G. W. RODERICK. *J. Chem. Phys.* **29**, 17 (1958).
51. K. F. HERZFELD and T. A. LITOVITZ. Absorption and dispersion of ultrasonic waves. Academic Press, New York. 1959.
52. H. S. GUTOWSKY, A. SAIKA, M. TAKEDA, and D. E. WOESSNER. *J. Chem. Phys.* **27**, 534 (1957).
53. K. LUSZCZYNSKI, J. A. E. KAIL, and J. G. POWLES. *Proc. Phys. Soc. (London)*, **75**, 243 (1960).
54. K. LUSZCZYNSKI and J. G. POWLES. *Proc. Phys. Soc. (London)*, **74**, 408 (1959).

NOTES

CHEMISTRY OF THE TRIFLUOROMETHYL GROUP PART II. NICKEL (II) COMPLEXES OF TRIFLUOROMETHYL PHOSPHINES*

M. A. A. BEG AND H. C. CLARK

The ability of tri-alkyl and -aryl phosphines to form co-ordination compounds with transition metal salts is well established. However, this ability is considerably modified when the phosphine contains the highly electronegative trifluoromethyl group. This has been shown in the reactions of methyl-trifluoromethyl-phosphines with boron trifluoride and platinum (II) chloride (1), where the results have been interpreted in terms of the effect of the electron-withdrawing power of the trifluoromethyl group on the donor properties of the phosphines, and of the large steric requirements of the trifluoromethyl group.

These two factors of the perturbing power or ligand field strength of the phosphines, and their steric requirements are just those that have been considered important in producing tetrahedral nickel (II) complexes (2). The first example of an apparently tetrahedral complex was $(\text{PEt}_3)_2\text{Ni}(\text{NO}_3)_2$ (3), although the lack of a full structure determination left room for alternative configurations. For the triphenylphosphine complexes $(\text{PPh}_3)_2\text{NiX}_2$ where $\text{X} = \text{NO}_3^-$, Cl^- , Br^- , I^- , detailed studies (4) leave no doubt that they possess tetrahedral structures. Other examples of tetrahedral nickel (II) complexes are now known (5). It therefore seemed of interest to examine the nickel (II) complexes of $(\text{CH}_3)_3\text{P}$, $(\text{CH}_3)_2\text{PCF}_3$, $\text{CH}_3\text{P}(\text{CF}_3)_2$, and $\text{P}(\text{CF}_3)_3$ wherever stable compounds could be isolated. Only the first two of these phosphines gave stable complexes and there were no indications of reaction between nickel (II) salts and either methyl-bis(trifluoromethyl)phosphine or tris(trifluoromethyl)phosphine. The complexes of dimethyl-trifluoromethylphosphine were considerably less stable than those of trimethylphosphine. The properties of the newly prepared compounds are shown in the table.

Compound	Magnetic moment (B.M.)	Color	Absorption maxima
$(\text{Me}_2\text{P})_2\text{Ni}(\text{NO}_3)_2$	3.17	Dark red	4850(m), 3950(s), 3325(s)
$(\text{Me}_2\text{P})_2\text{NiCl}_2$	Diamagnetic	Crimson	5320(s), 3880(m), 3650(m), 2650(s)
$(\text{Me}_2\text{P})_2\text{NiBr}_2$	"	Crimson	5400(m), 3800(m), 2700(s), 2425(w)
$(\text{Me}_2\text{P})_2\text{NiI}_2$	"	Dark brown	5175(m), 3875(w), 2850(vs), 2600(s)
$(\text{Me}_2\text{P})_2\text{Ni}(\text{SCN})_2$	"	Orange-yellow	4600(sh), 3550(vs), 2975(s), 2600(s)
$(\text{Me}_2\text{PCF}_3)_2\text{Ni}(\text{NO}_3)_2$	2.93	Dark red	5550(w), 4850(s), 4150(s), 3270(s)
$(\text{Me}_2\text{PCF}_3)_2\text{NiCl}_2$	Diamagnetic	Pink	4800(w), 4050(m), 3450(s), 2550(s)
$(\text{Me}_2\text{PCF}_3)_2\text{NiBr}_2$	"	Black	4875(s), 3950(s), 2625(s), 2400(s)
$(\text{Me}_2\text{PCF}_3)_2\text{NiI}_2$	"	Dark brown	3750(m), 3550(m), 3140(m), 2280(s)
$(\text{Me}_2\text{PCF}_3)_2\text{Ni}(\text{SCN})_2$	"	Yellow	4600(m), 3675(vs), 2550(s)

The trimethylphosphine complexes have not been reported previously and it is not surprising that the nitrate is paramagnetic and like its triethylphosphine analogue may be considered to be tetrahedral. The halogen and thiocyanate complexes are diamagnetic in accordance with the greater ligand strengths of these anions. The complexes of dimethyltrifluoromethyl phosphine are very similar to the trimethylphosphine compounds, only the nitrate is paramagnetic and possibly tetrahedral.

*From part of a thesis submitted by M.A.A.B. in partial fulfillment of the requirements for the Ph.D. degree.

The intensity of the colors of the solid compounds and of the observed absorption bands suggest that charge-transfer transitions are involved.

The fact that a nickel (II) complex of tristrifluoromethyl phosphine could not be obtained is consistent with its inability to give a platinum (II) compound (1). The smaller size of the nickel atom compared with platinum may explain why the latter but not the former can give a complex with methylbistrifluoromethyl phosphine.

EXPERIMENTAL

The methyl-trifluoromethyl-phosphines were prepared as described previously (1). All nickel salts were prepared in the anhydrous state, except the nitrate which was used as the hexahydrate. The trimethylphosphine complexes were prepared by direct reaction of the phosphines with the nickel salts in 2:1 ratio in sealed evacuated tubes, and were purified by refluxing with butanol for about 30 minutes when crystals of the complexes separated. In the case of nickel nitrate, the product could not be crystallized satisfactorily and solutions of the complex were used where necessary. For the dimethyltrifluoromethyl-phosphine complexes, crystallization was not possible owing to their instability. The preparations in these cases were therefore performed in the presence of excess phosphine which acted as a solvent and gave reasonably pure products. The analyses of the compounds are given in the table.

Compound	% Ni		% X	
	Found	Calc. for $\text{NiX}_2(\text{PR}_3)_2$	Found	Calc. for $\text{NiX}_2(\text{PR}_3)_2$
$(\text{PMe}_3)_2\text{Ni}(\text{NO}_3)_2$	17.33	17.37	—	—
$(\text{PMe}_3)_2\text{NiCl}_2$	20.05	20.56	25.14	25.27
$(\text{PMe}_3)_2\text{NiBr}_2$	16.01	15.68	42.70	43.24
$(\text{PMe}_3)_2\text{NiI}_2$	11.85	12.50	54.30	54.72
$(\text{PMe}_3)_2\text{Ni}(\text{SCN})_2$	17.27	17.79	34.45	34.60
$(\text{Me}_2\text{PCF}_3)_2\text{Ni}(\text{NO}_3)_2$	13.22	13.12	—	—
$(\text{Me}_2\text{PCF}_3)_2\text{NiCl}_2$	14.72	14.91	18.15	18.25
$(\text{Me}_2\text{PCF}_3)_2\text{NiBr}_2$	11.84	12.14	34.10	33.47
$(\text{Me}_2\text{PCF}_3)_2\text{NiI}_2$	9.76	10.14	43.80	44.40
$(\text{Me}_2\text{PCF}_3)_2\text{Ni}(\text{SCN})_2$	13.42	13.36	26.25	26.73

All the complexes except the iodides and thiocyanates decomposed in the presence of moisture. Although stable in dry solvents, wet polar solvents caused decomposition. Magnetic measurements were made on a Gouy magnetic balance, using powdered samples except for the nitrates for which solutions were used. Spectra were determined in carbon tetrachloride or methanol solutions using a Cary model 14 spectrophotometer.

ACKNOWLEDGMENTS

The financial support of the National Research Council is gratefully acknowledged as is the award of a Colombo Plan scholarship to M.A.A.B.

1. M. A. A. BEG and H. C. CLARK. *Can. J. Chem.* **38**, 119 (1960).
2. L. M. VENANZI. *J. Inorg. & Nuclear Chem.* **8**, 137 (1958).
3. K. A. JENSEN. *Z. anorg. u. allgem. Chem.* **229**, 225 (1936).
4. L. M. VENANZI and H. M. POWELL. *Proc. Chem. Soc.* **6** (1956).
5. N. S. GILL and R. S. NYHOLM. *J. Chem. Soc.* 3997 (1959).

RECEIVED DECEMBER 5, 1960.
CHEMISTRY DEPARTMENT,
UNIVERSITY OF BRITISH COLUMBIA,
VANCOUVER, B.C.

PRESSURE EFFECT AND MECHANISM IN ACID CATALYSIS

VI. HYDROLYSIS OF α -D-GLUCOSE-1-PHOSPHATE¹A. R. OSBORN² AND E. WHALLEY

INTRODUCTION

α -D-Glucose-1-phosphate hydrolyzes by acid catalysis (1) with carbon-oxygen fission (2, 3). It is usually assumed that there is a pre-equilibrium proton transfer to the ester, and that the slow step is either a unimolecular decomposition of the protonated form or a bimolecular attack of water. The conclusion (3) on the basis of the Zucker-Hammett hypothesis that the slow step is unimolecular is invalid because the Zucker-Hammett hypothesis is invalid (4-6). We have measured the effect of pressure on the rate of hydrolysis in order to determine the mechanism. The effect of temperature was also measured.

EXPERIMENTAL METHODS AND RESULTS

Dipotassium α -D-glucopyranose-1-phosphate was obtained from General Biochemicals, Inc. It was about 96% pure according to both optical rotation (7) and hydrolyzable organic phosphate determined by Fiske's method (8). The hydrolyses were carried out at 25°C in at least 2-M perchloric acid to suppress the ionization of α -D-glucose-1-phosphate, which has a pK_a of 1.10 (9). The initial concentration of the ester was about 0.1 M and so potassium perchlorate was precipitated if the potassium salt was used. Potassium ions were therefore removed by passing a solution of the salt through an ion-exchange column of Dowex 50W-X-8 in the acid form.

The hydrolysis was followed by the change of optical rotation. The rate constants are accurate to about 5%. The high-pressure technique has been described elsewhere (10, 11).

The first-order rate constants are summarized in Table I. At normal pressure the

TABLE I
Acid-catalyzed hydrolysis of α -D-glucose-1-phosphate

p /bar	Temp.	$c^{\circ}\text{HClO}_4$ /mole l. ⁻¹ *	$10^4 k_1/\text{sec}^{-1}$
1	25.00°C	2.00	126
1	25.00°	3.00	328
1	30.00°	2.00	290
1	35.00°	2.00	580
500	25.00°	2.00	126
1000	25.00°	2.00	118
1500	25.00°	2.00	105

* $c^{\circ}\text{HClO}_4$ is the concentration of perchloric acid at room pressure and temperature.

ratio of the rates in 3-M and 2-M perchloric acid is much greater than 1.5,² and is² near the ratio of the acidity function h_0 of the two solutions, so confirming Barnard *et al.*'s observation (3) that the rate is approximately proportional to h_0 . The second-order

¹Issued as N.R.C. No. 6164.

²National Research Council Postdoctorate Fellow 1958-60.

constants in 2-*M* perchloric acid at normal pressure and 25, 30, and 35° C followed the Arrhenius law and yielded

$$E_A = 27.8 \text{ kcal mole}^{-1},$$

$$\log_{10} A/\text{sec}^{-1} = 16.5, \quad \Delta S^\ddagger = 14.8 \text{ cal deg}^{-1} \text{ mole}^{-1}.$$

From the effect of pressure up to 1500 bar at 25.00° C we find graphically

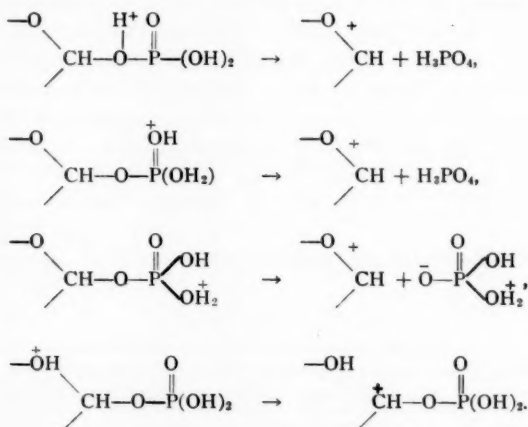
$$\partial \ln k_1 / \partial p = 3.2 \pm \sim 1.2 \text{ cm}^3 \text{ mole}^{-1},$$

and assuming the compressibility χ of 2-*M* perchloric acid to be the same as that of water, remembering that $RT \partial \ln k_1 / \partial p = -\Delta V^\ddagger + \chi RT$,

$$\Delta V^\ddagger = 4.3 \pm \sim 1.6 \text{ cm}^3 \text{ mole}^{-1}.$$

DISCUSSION

There are many protonated α -D-glucose-1-phosphates and it is not known which of them undergo hydrolysis. The following reactions and their bimolecular counterparts, in which a molecule of water attacks the carbon atom of the pyranose ring, seem to be the most likely. For clarity only the oxygen and one carbon atom of the pyranose ring are shown, and each reaction is presumed to be followed by the usual rapid steps.



The first and last of these were mentioned by Barnard *et al.* (3).

The first, second, and last mechanisms do not result in major changes of polarity and so the volumes of activation should depend mainly on the volume changes of the reactants. According to arguments and experiments in earlier papers in this series they should therefore have small positive volumes of activation if unimolecular, and negative volumes, about $-10 \text{ cm}^3 \text{ mole}^{-1}$, if bimolecular. The measured volume of activation of $4.3 \pm \sim 1.6 \text{ cm}^3 \text{ mole}^{-1}$ eliminates the bimolecular reactions. In the third mechanism there is a great increase in polarity and so the volume of activation of either the unimolecular or the bimolecular mechanism would be negative because of electrostriction of solvent. Both these can therefore be eliminated. Thus the unimolecular first, second, or last mechanisms are consistent with the measured pressure effect.

The entropy of activation is $14.8 \text{ cal deg}^{-1} \text{ mole}^{-1}$. Although all or nearly all entropies

of activation of unimolecular acid-catalyzed reactions are positive, it is not easy to understand why they should be (12), and so while the entropy is certainly consistent with the proposed mechanisms, it does not confirm them strongly.

REFERENCES

1. C. P. CORI, S. P. COLOWICK, and G. T. CORI. *J. Biol. Chem.* **121**, 465 (1937).
2. M. COHN. *J. Biol. Chem.* **180**, 771 (1949).
3. P. W. C. BARNARD, C. A. BUNTON, D. R. LLEWELLYN, K. G. OLDHAM, L. B. SILVER, and C. A. VERNON. *Chem. & Ind. (London)*, 760 (1955).
4. J. KOSKIKALLIO and E. WHALLEY. *Trans. Faraday Soc.* **55**, 815 (1959).
5. J. KOSKIKALLIO and E. WHALLEY. *Can. J. Chem.* **37**, 788 (1959).
6. G. ARCHER and R. P. BELL. *J. Chem. Soc.* 3228 (1959).
7. M. L. WOLFRAM and D. E. PLETCHER. *J. Am. Chem. Soc.* **63**, 1050 (1941).
8. C. H. FISKE. *J. Biol. Chem.* **46**, 285 (1921).
9. W. D. KUMLER and J. J. EILER. *J. Am. Chem. Soc.* **65**, 2355 (1943).
10. J. KOSKIKALLIO and E. WHALLEY. *Trans. Faraday Soc.* **55**, 809 (1955).
11. A. R. OSBORN and E. WHALLEY. To be published.
12. E. WHALLEY. *Trans. Faraday Soc.* **55**, 798 (1959).

RECEIVED DECEMBER 12, 1960.
DIVISION OF APPLIED CHEMISTRY,
NATIONAL RESEARCH COUNCIL,
OTTAWA, CANADA.

OXIDATION OF CHOLEST-4-EN-3-ONE WITH PERIODATE-PERMANGANATE

J. T. EDWARD, D. HOLDER, W. H. LUNN,¹ AND I. PUSKAS¹

For stereochemical studies (1) we required large quantities of the keto acid, 5-oxo-3,5-seco-A-norcholestan-3-oic acid, first prepared by Windaus (2) by oxidizing cholest-4-en-3-one with alkaline permanganate. Later workers (3, 4) had obtained better yields (60–85%) by oxidizing 2–3 g of the unsaturated ketone with ozone, but we found yields low and capricious when oxidation with this reagent was carried out on a larger scale. However, 50 g of the ketone could be oxidized to the acid in 79–81% yield with the permanganate-periodate reagent of Lemieux and von Rudloff (5, 6), while with 5 g of the ketone the yield rose to 88%.

EXPERIMENTAL

Potassium carbonate (28 g) in water (800 ml) was added with vigorous stirring to a solution of cholest-4-en-3-one (50 g) in *t*-butanol–water azeotrope (3 l.), followed by 500 ml of a solution prepared from sodium metaperiodate (200 g) and water (2.5 l.), and then 50 ml of 0.8% aqueous potassium permanganate. The remainder of the periodate was added at the rate of 110 ml/minute for 10 minutes, and then at 30 ml/minute for the next 30 minutes. Permanganate solution was added when necessary to maintain the permanganate color, 50 ml being usually required after the first 5 minutes and a further 75 ml at intervals over the next 30 minutes.

After 2 hours, the excess permanganate was destroyed with sodium bisulphite. The resultant iodine-colored solution was concentrated at reduced pressure to a volume of about 4 l., cooled to 4° C, acidified with ice-cold 50% sulphuric acid, and extracted with ether (2.5 l., 1.5 l., and 1.5 l.). The ethereal extract was washed with sodium bisulphite solution until free from iodine, with water until neutral, and dried (magnesium

¹Holder of National Research Council of Canada Studentships, 1958–60.

sulphate). It was then concentrated to 700 ml, diluted with hexane, and further concentrated to 250 ml. After standing for 8 hours at room temperature and 8 hours at 4° C, the solution yielded white needles (36.6–38.3 g) of the keto acid, m.p. 153–154° C (lit. m.p. 154–155.5° C (4)). The mother liquors, on being concentrated to about 60 ml and chilled, gave after several days a second crop of impure acid, from which pure acid (4.2–4.9 g), m.p. 153–154° C, was obtained by recrystallization from ether–hexane.

1. J. T. EDWARD and P. F. MORAND. *Can. J. Chem.* **38**, 1316, 1325 (1960).
2. A. WINDAUS. *Ber.* **39**, 2008 (1906).
3. C. C. BOLT. *Rec. trav. chim.* **57**, 905 (1938).
4. R. B. TURNER. *J. Am. Chem. Soc.* **72**, 579 (1950).
5. R. U. LEMIEUX and E. VON RUDLOFF. *Can. J. Chem.* **33**, 1701, 1710 (1955).
6. E. VON RUDLOFF. *Can. J. Chem.* **33**, 1714 (1955); **34**, 1413 (1956).

RECEIVED NOVEMBER 23, 1960.
DEPARTMENT OF CHEMISTRY,
MCGILL UNIVERSITY,
MONTREAL 2, QUE.

Symposium on Nuclear Chemistry and Radiochemistry

The papers that follow were presented at a symposium held at Atomic Energy of Canada Limited, Chalk River, Ontario, on September 6, 7, and 8, 1960, under the joint auspices of the Inorganic Chemistry Subject Division of the Chemical Institute of Canada, and Atomic Energy of Canada Limited. The meeting was organized by Dr. R. H. Betts of A.E.C.L. Some of the papers presented are not published here because of prior commitments.

The symposium committee wishes to express its appreciation to the sponsoring organizations for their generous support and co-operation, and to the Editor-in-Chief and staff of the Canadian Journal of Chemistry for their valuable assistance.

THE RANGE OF Na^{24} IONS OF KILOELECTRON VOLT ENERGIES IN ALUMINUM¹

J. A. DAVIES AND G. A. SIMS

ABSTRACT

Detailed studies are reported for the depth of penetration in aluminum of monoenergetic Na^{24} ions over the energy region 0.7–60 kev. Below 20 kev the median range (R_M) increases linearly with energy as predicted by the Bohr-Nielsen equation. As was observed in a previous study with Cs^{137} ions in aluminum, the experimental distribution curves are not Gaussian in shape, but consist of a markedly asymmetric peak followed by a pronounced exponential "tail". The results of a Monte Carlo calculation show that the observed distribution curves correspond quite closely to those predicted by an isotropic elastic-scattering model.

Above 20 kev, a slight deviation from the linear range-energy relationship is observed; also, the distribution curves become narrower and more symmetrical, suggesting that electronic interactions are starting to play a significant role in the stopping process. Some preliminary results for the range of accelerated ions of Rb^{86} and K^{42} in aluminum are also included for comparison. Median ranges for each of the alkali metal ions are compared with those predicted by the Bohr-Nielsen treatment.

INTRODUCTION

A program of research on the penetration depth and range straggling of heavy ions in solids at bombardment energies up to 100 kev has been under way in this laboratory for the past three years. Previous papers (1, 2) have described the development of a sufficiently sensitive technique for measuring the extremely small depths of penetration involved, and its application to the study of Cs^{137} ions in aluminum. The present paper extends these measurements in aluminum to other alkali metal ions, particularly Na^{24} , in an attempt to further our understanding of the mechanism of the elastic-scattering process and its dependence on the energy, mass, and atomic number of the bombarding ion. One important advantage of this technique is that it provides detailed information not only on the range but also on the extent of range straggling.

Until recently, there had been almost no reliable experimental results reported for heavy particles below 100 kev. The situation has now improved considerably, particularly as a result of papers being presented at this conference (see footnote 1). Powers (3) has used proton scattering to study accurately the range of several rare-gas ions in carbon, beryllium, boron, and aluminum targets; Schmitt and co-workers (4, 5), by a recoil-atom technique, have determined the average range of the radioactive atoms produced by (γ, n) processes in various solids. However, neither of these methods was sufficiently sensitive to give detailed information on the shape of the range-distribution curve.

¹Manuscript received November 3, 1960.

Contribution from Research Chemistry Branch, Atomic Energy of Canada Limited, Chalk River, Ontario. Presented at the Third Symposium on Nuclear Chemistry and Radiochemistry held at Atomic Energy of Canada Limited, Chalk River, Ontario, September 6–8, 1960.

Issued as A.E.C.L. No. 1150.

EXPERIMENTAL PROCEDURE

Our experimental approach consists simply in bombarding an optically flat aluminum target with a monoenergetic beam of radioactive ions, and then measuring the depth of penetration of the incident beam by dissolving successive uniform layers of aluminum from the target surface and measuring the amount of radioactivity in each layer. The ion bombardments were carried out using an electrostatic accelerator specially designed for the purpose (2). The development of a sufficiently sensitive technique for dissolving extremely thin layers of known thickness from the surface of an aluminum foil has already been described in detail (1). The technique consists essentially of two steps: electrochemical oxidation at constant voltage in aqueous ammonium citrate, followed by chemical removal of the anodic oxide film in a phosphoric acid chromium trioxide solution. Due to the highly protective nature of the anodic oxide film, this process permits highly reproducible surface layers of metal as thin as 37 Å to be removed, the thickness of the layer increasing linearly with the anodic voltage. Furthermore, the process may be repeated as often as desired, so that it is possible to obtain the complete range-distribution curve from a single bombardment.

RESULTS

The results for a typical run, illustrating the determination of the Na^{24} distribution in a bombarded target, are shown in Table I. The thickness W per layer (column 3)

TABLE I
Distribution of 10-kev Na^{24} ions in an aluminum target

Layer No.	Anodic voltage	Amount of Al removed		Residual target activity (c.p.m.)	Na ²⁴ activity per layer (calculated from col. 5)	
		Per layer ($\mu\text{g}/\text{cm}^2$)	Total ($\mu\text{g}/\text{cm}^2$)		(c.p.m.)	(c.p.m./ μg Al)
(1)	(2)	(3)	(4)	(5)	(6)	(7)
0				20,174		
1	4.2	1.8+0.5*	2.3	16,817	3,357	1,460
2	4.2	1.8	4.1	13,726	3,091	1,717
3	4.2	1.8	5.9	10,484	3,242	1,801
4	4.1	1.8	7.7	7,924	2,560	1,422
5	8.0	2.9	10.6	4,407	3,517	1,213
6	10.2	3.6	14.2	2,461	1,946	541
7	25.0	8.0	22.2	966	1,495	187
8	25.0	8.0	30.2	417	549	68.6
9	51.5	16.0	46.2	108	309	19.3
10	50.5	15.7	61.9	30	78	5.0

*An extra 0.5 $\mu\text{g}/\text{cm}^2$ is added to the first layer in each run to take account of the oxygen that was present during the bombardment as an oxide layer on the target surface.

was calculated from the anodic voltage V by using the previously established relationship (1) $W = 0.30 (V+1.8)$.

As was observed in the earlier study with Cs^{137} (2), the distribution of Na^{24} ions in the target is markedly asymmetric. This may be seen more clearly in Fig. 1, in which the Na^{24} content in each layer is plotted against the total depth beneath the original surface. The distribution curves show a characteristic highly penetrating "tail"; as a result, the most probable range R_p is somewhat less than the median value R_M . It will

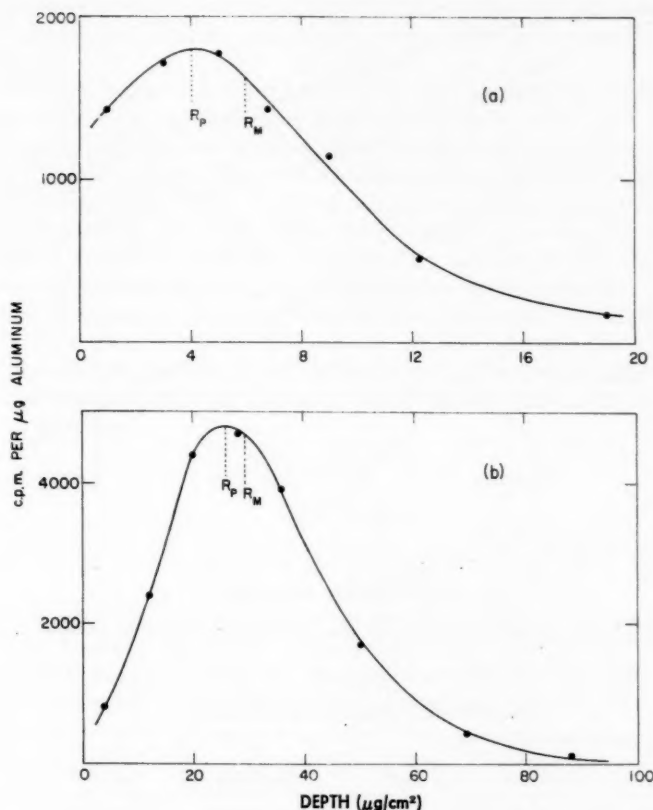


FIG. 1. Depth of penetration of Na^{24} ions in aluminum: (a) 10-kev Na^{24} ions, (b) 60-kev Na^{24} ions.

be noted, however, that with Na^{24} the asymmetry becomes less pronounced at high energy (Fig. 1b), and the peak becomes much sharper. The possible significance of this will be discussed in the next section; it suggests strongly that some process other than elastic scattering is starting to contribute to the rate of energy loss.

Typical distribution curves for the residual target activity (column 5, Table I) at various energies are shown in Fig. 2. In each case, the activity eventually falls off exponentially with depth.

Values of R_P , R_M , and the half-thickness ($X_{1/2}$) of the exponential region are shown as a function of energy in Table II, together with previous results for Cs^{137} (2). It will be noted that, over the energy region studied, the range increases approximately linearly with energy. However, a careful analysis of the data shows that at higher energies, a slight deviation from linearity occurs, and R_P and R_M gradually approach one another (see Table III). Some preliminary data for K^{42} and Rb^{86} have been included for comparison.

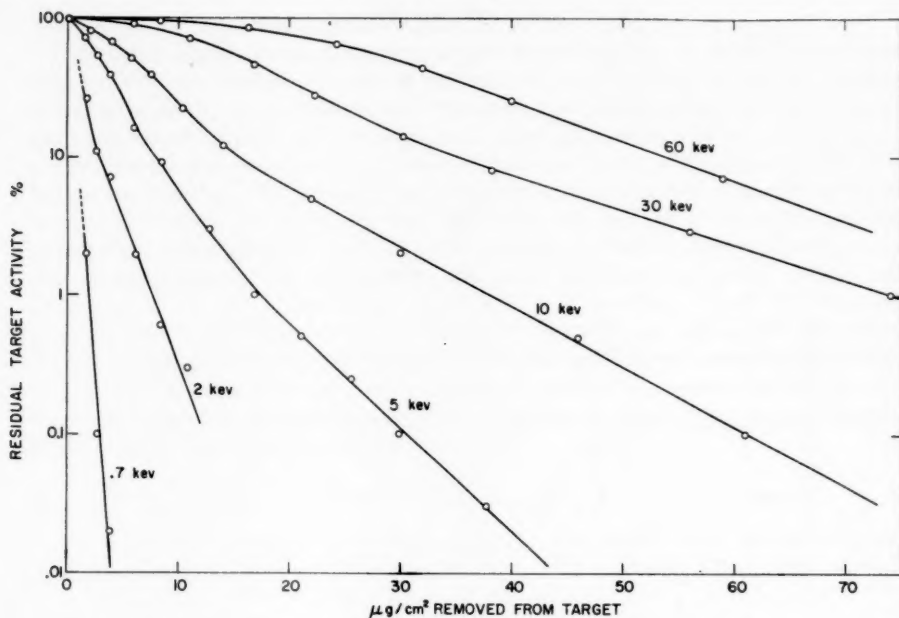


FIG. 2. Distribution curves of residual target activities for Na^{24} ions of various energies in aluminum.

TABLE II
Range of alkali metal ions in aluminum

Ion	Energy (kev)	R_p ($\mu\text{g}/\text{cm}^2$)	R_M ($\mu\text{g}/\text{cm}^2$)	$X_{1/2}$ ($\mu\text{g}/\text{cm}^2$)
Na^{24}	0.7	—	$0.4 \pm .2$	$0.4 \pm .1$
	1.0	—	$0.5 \pm .2$	$0.7 \pm .1$
	2.0	$0.7 \pm .3$	$1.1 \pm .2$	1.6
	5.0	$1.6 \pm .4$	3.0	3.6
	10.5	$3.9 \pm .4$	6.2	8.3
	15.0	—	7.8	9.0
	24	9.8	12.0	—
	30	13.1	15.0	15.5
	60	26	29.5	16
K^{42}	2	—	$0.6 \pm .2$	$0.6 \pm .1$
	30	6.8	9.0	9.2
Rb^{86}	30	6.6	8.1	5.4
Cs^{137}	2	—	$0.6 \pm .3$	$0.4 \pm .1$
	5	—	$0.9 \pm .3$	$0.6 \pm .1$
	20	$4.0 \pm .4$	4.8	2.9
	30	$5.7 \pm .4$	7.4	4.0
	50	9.5	11.3	6.5

NOTE: The estimated experimental error is $\pm 6\%$ except where otherwise noted.

DISCUSSION OF RESULTS

The most striking feature about these results—the marked asymmetry in the distribution curves—can be explained quite readily. Nielsen (6) has pointed out that scattering in a screened Coulomb field should be approximately isotropic in the center-of-mass

system. This means that, even with Cs¹³⁷ in aluminum, the average energy loss per collision is almost 30%; hence, only the first few collisions contribute significantly to the total range.

Under such conditions, it has been shown (2), by a somewhat oversimplified mathematical approach, that the predicted distribution curve would in fact consist of an asymmetric peak, followed eventually by an exponential region of half-thickness identical with that for the first collision. The problem was treated analytically in a manner analogous to that used by Bateman (7) for resolving growth and decay curves of successive radioactive transformations, only with distance replacing time as the independent variable. This analytical treatment provides a qualitative explanation for the experimentally observed distribution curves, but is not suitable for quantitative comparison: it makes no allowance for variations in energy transfer from one collision to another (all collisions were assumed to transfer exactly the average energy), nor for the difference between the total path length and the depth of penetration. The latter difference may quite easily be taken into account by replacing the mean free path λ by its projection $\lambda \cos \bar{\psi}$ in the forward direction,

i.e.

$$\lambda_0 = \lambda_0,$$

$$\lambda_1 = \lambda_1 \cos \bar{\psi},$$

and

$$\lambda_n = \lambda_n \cos^n \bar{\psi},$$

where the subscript refers to the number of collisions which the incident ion has undergone and $\bar{\psi}$ is the scattering angle in laboratory co-ordinates for an "average collision". When this relationship is inserted into the Bateman equation (see appendix to reference 2), the following series of exponential terms is obtained:

$$\sum_{n=1}^{n=\infty} \frac{1}{a_n} \left\{ \exp - [(1 - \bar{T}) \cos \bar{\psi}]^n \cdot \frac{r}{\lambda_0} \right\}.$$

This series is rapidly convergent and leads to the distribution curves shown as (a) in Fig. 3. It has been assumed that the mean free path λ decreases linearly with the ion energy, and that the average energy transfer per collision (\bar{T}) is equal to $0.5T_{\max}$. The dotted line represents the distribution of incident particles which have not yet had a single collision.

A much more satisfactory method of calculating the shape of the distribution curve has recently been developed (8), viz. a Monte Carlo type of calculation, which permits both the angular scattering and the fractional energy transfer to be varied at random from one collision to another. The resulting distribution curves (b) are shown in Fig. 3. In order to test the validity of Nielsen's prediction (6), the scattering process was assumed to be isotropic in center-of-mass co-ordinates. The close agreement between curves (a) and (b), particularly at the higher mass ratio, suggests that one may use the much simpler "average collision" method to predict the approximate shape of range-distribution curves. Experimental results for two runs (10-kev Na²⁴, and 30-kev Cs¹³⁷) have been included for comparison; the abscissa scales were normalized by letting $\lambda_0 = 3.9 \mu\text{g}/\text{cm}^2$ and $5.7 \mu\text{g}/\text{cm}^2$ for the Na²⁴ and Cs¹³⁷ runs, respectively. It will be noted that the isotropic scattering model predicts both the height and the shape of the experimental peaks extremely well, even in the extreme case of Na²⁴ in aluminum, where the masses of the incident ion and the target atom are approximately equal. In such a case, T_{\max} is

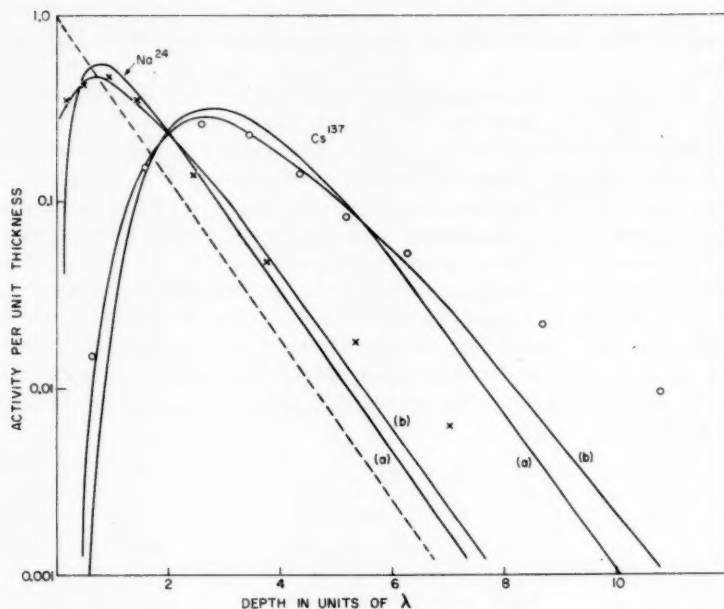


FIG. 3. Calculated distribution curves for Na^{24} and for Cs^{137} in aluminum using: (a) "average" collision method, (b) Monte Carlo method. Experimental results: X, 10.5-kev Na^{24} ; O, 30-kev Cs^{137} .

equal to 0.997, and hence the incident ion may lose almost all its energy in a single collision.

For both Na^{24} and Cs^{137} ions, a significant deviation between the predicted and observed distribution curves occurs at large depths of penetration. At about twice the median range, the experimental curve exhibits a point of inflection (see Fig. 2) which is not predicted by either the Monte Carlo or the "average collision" calculations. The half thickness ($X_{1/2}$) of the subsequent exponential "tail" is almost exactly a factor of two larger than the predicted value. A satisfactory explanation for this deviation has not yet been found. However, it involves less than 5% of the incident particles and hence should not appreciably affect the determination of R_P and R_M .

One very sensitive test of the agreement between the observed distribution and that predicted by the isotropic scattering model is to determine, for different mass ratios, how rapidly the curve falls off on either side of the maximum. The usual criterion for making such a comparison is the straggling parameter; however, with a markedly asymmetric peak, the normal definition of a straggling parameter has little theoretical significance.

Instead, let us consider the relative height (N/N_{\max}) of the distribution curve at two selected abscissa values: at $x = \frac{1}{4}R_P$ and at $x = 2R_P$. In Fig. 4, the two solid lines represent the variation of N/N_{\max} with the mass ratio, as determined by the Monte Carlo calculations. Typical experimental values for each of the alkali metal ions have been plotted, together with an estimate of the experimental error. With the exception of the higher-energy Na^{24} runs, the isotropic scattering model fits the observed straggling.

Furthermore, the discrepancy with Na^{24} at higher energies may quite reasonably be

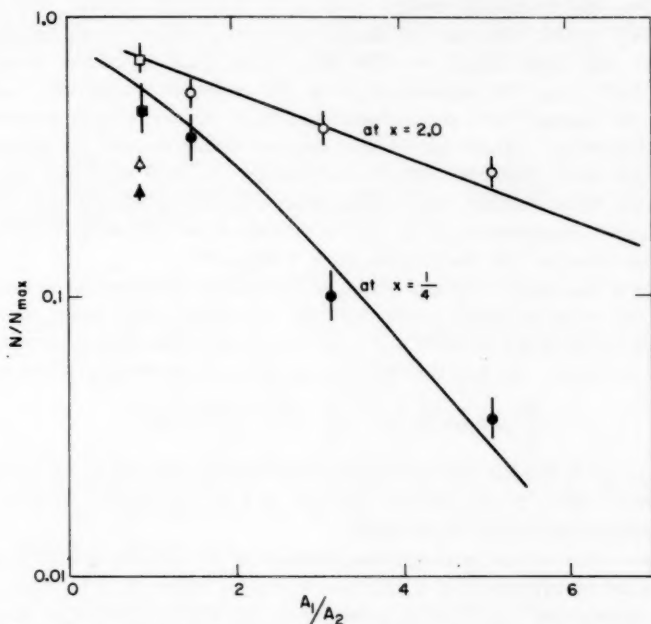


FIG. 4. Relative activity (N/N_{\max}) vs. mass ratio. Solid lines are calculated from Monte Carlo distribution curves. Experimental points: \blacksquare , 10.5 keV; \bullet , 30 keV; \blacktriangle , 60 keV; solid points at $x = \frac{1}{4}R_F$; open points at $x = 2R_F$.

attributed to a gradual increase in the significance of electronic interactions as a slowing-down process at higher velocities. It has been shown (9, 10) that heavy recoil atoms from α -decay undergo significant electronic interactions along their path, dissipating perhaps 20% of their energy in this manner. Yet these atoms have an initial velocity less than that of a 60-keV Na^{24} atom. Electronic stopping involves extremely small energy transfers per "collision", and so would tend to produce a narrower, more symmetrical peak. Such a trend was in fact observed (Fig. 1), and would account, at least qualitatively, for the low relative activity of 60-keV Na^{24} in Fig. 4.

Another convenient parameter for describing the degree of asymmetry is the ratio (R_F/R_M) of the most probable range to the median range (Table III). For electronic

TABLE III
Ratio (R_F/R_M) for alkali metal ions in aluminum

Energy (keV)	Na^{24}	K^{42}	Rb^{86}	Cs^{137}
2	.6			
5	.5			
10	.6 ₃			
20	.81			.83
30	.87	.75	.81	.77
60	.88			.85
Predicted value (isotropic scattering)	.57	.68	.79	.87

scattering (where the fractional energy transfer is extremely small), the ratio should be almost exactly unity, whereas for elastic scattering (where large fractional energy transfers occur), the ratio would be much less. Once again, with the exception of the higher-energy Na^{24} runs, the agreement with the isotropic scattering model is quite reasonable. In the case of Na^{24} , the measured ratio at 30 keV is approximately halfway between the theoretical values for elastic nuclear collision and for electronic interactions. It would seem therefore that at this energy the two processes are of roughly equal importance. Since velocity rather than energy is the significant criterion for determining the relative importance of the two processes, it is not surprising that no such discrepancy was observed in the earlier work with Cs^{137} .

So far, we have discussed only the shape of the range-distribution curve; the actual magnitude of the range is much more difficult to predict. The most commonly used theoretical approach is based on Bohr's (11) treatment of collisions in a screened Coulomb field, from which Nielsen (6) has derived the familiar range-energy relationship,

$$[1] \quad \frac{R}{E} = 0.60 \frac{A_1 + A_2}{A_1} \cdot \frac{A_2}{Z_2} \cdot \frac{(Z_1^{2/3} + Z_2^{2/3})^{1/2}}{Z_1},$$

where R is the range in micrograms per square centimeter, E is the energy of the incident ion in kiloelectron volts, A_1 , A_2 are the masses, and Z_1 , Z_2 are the atomic numbers of the incident and target atoms respectively.

One necessary criterion for screened-field scattering is that the collision diameter, or minimum distance of approach in a head-on collision, must be somewhat larger than the screening parameter. Otherwise, unscreened or Rutherford-type scattering can occur. Using Bohr's value for the screening parameter, viz. $0.528 \times 10^{-8} / (Z_1^{2/3} + Z_2^{2/3})^{1/2}$, it can be shown that this criterion is fulfilled at the energies used in the present work, except for some of the Na^{24} runs where the critical energy is only 25 keV. For Cs^{137} , on the other hand, the critical energy is over 500 keV. Since, as noted above, the runs with Na^{24} at higher energies also involve a significant contribution from electronic stopping, their interpretation is obviously much more complicated and will not be discussed further at this time.

Unfortunately, in testing the validity of Bohr's screened-field model, it is not possible to use the above range-energy relationship for a direct comparison with our experimental data; this is because the equation may be applied only when $A_1 \gg A_2$. This restriction arises because equation [1] was obtained by integrating an expression for the stopping power ($\Delta E / \Delta R$). Such an integration assumes that the energy decrease per collision is small enough that the stepwise slowing-down process may be replaced by a smooth curve. Secondly, the expression predicts the total path length travelled rather than the actual depth of penetration. Neither of these assumptions holds true when using an aluminum target. Even with Cs^{137} ions, where $A_1 = 5.1 A_2$, the energy transfer per collision can be as large as 55%; with Na^{24} , up to 99.7% of the energy may be lost in a single collision and the average angular deflection in laboratory co-ordinates is approximately 45° .

However, by a somewhat modified theoretical treatment combined with the results of the Monte Carlo calculations (Fig. 3), it is possible to develop a completely general expression for the depth of penetration, one which is applicable for any value of A_1 / A_2 . Nielsen's expression for the stopping power may be written as follows:

$$[2] \quad -\frac{\Delta E}{\Delta R} = 1.68 \frac{A_1}{(A_1 + A_2) A_2} \cdot \frac{Z_1 Z_2}{(Z_1^{2/3} + Z_2^{2/3})^{1/2}}$$

where $(\Delta E/\Delta R)$ is expressed in kev cm² μg⁻¹. Instead of integrating, we may write an alternative expression for the stopping power in terms of the average fractional energy transfer \bar{T} per collision and the mean free path λ of the particle,

$$[3] \quad -\frac{\Delta E}{\Delta R} = \frac{\bar{T}E}{\lambda}.$$

λ must be expressed in the same units as R , viz. micrograms per square centimeter. If the scattering process is approximately isotropic, then \bar{T} may be expressed as $2A_1A_2/(A_1+A_2)^2$ and hence

$$[4] \quad -\frac{\Delta E}{\Delta R} = \frac{2A_1A_2}{(A_1+A_2)^2} \cdot \frac{E}{\lambda}.$$

Combining equations [2] and [4], we obtain the following expression for the mean free path of the incident ion:

$$[5] \quad \lambda = 1.19 \frac{A_2^2}{A_1+A_2} \cdot \frac{(Z_1^{2/3} + Z_2^{2/3})^{1/2}}{Z_1 Z_2} \cdot E.$$

It should be recognized that λ is only an "effective" mean free path: it applies to the approximately isotropic scattering process, but does not include the increased frequency of very small angular deflections which, according to Nielsen, have a negligible influence on the over-all rate of energy loss.

To calculate R_p , R_M , or the mean range \bar{R} from equation [5], one simply multiplies λ by a numerical factor (k_p , k_M , or \bar{k}) for each mass ratio. These factors are computed from Monte Carlo distribution curves such as those in Fig. 3. Appropriate values for various mass ratios are given in Table IV.

In Table V, these factors are used to compare the predicted and experimental ranges

TABLE IV
 k -Factors for various mass ratios

Mass ratio	Ion	k_p	k_M	\bar{k}
0.889	Na ²⁴ in Al ²⁷	0.70	1.23	1.50
1.556	K ⁴² in Al ²⁷	1.00	1.49	1.79
3.185	Rb ⁸⁶ in Al ²⁷	1.75	2.21	2.55
5.074	Cs ¹³⁷ in Al ²⁷	2.70	3.10	3.46

TABLE V
Experimental and predicted values of R/E
(μg cm⁻² kev⁻¹)

Ion	Energy region (kev)	R_p/E		R_M/E	
		Exptl.	Calc.	Exptl.	Calc.
Na ²⁴	0.7-10	.36	.27	.59	.47
K ⁴²	30	.23	.18	.30	.27
Rb ⁸⁶	30	.22	.11 _s	.27	.14 _s
Cs ¹³⁷	2.0-30	.19	.09	.25	.10

for each of the alkali metal ions. Clearly, although the theoretical values do have the correct order of magnitude, the observed variation from Na²⁴ to Cs¹³⁷ is much less than that predicted by the Bohr-Nielsen screened-field treatment. Holmes and Leibfried (12)

have recently criticized Nielsen's replacement of the Bohr screened-field potential by an $(1/r^2)$ potential. They also point out that the predicted range is extremely sensitive to the choice of screening parameter " a ", since " a " occurs in the exponential term determining the interaction potential.

However, while it is interesting to speculate on possible causes for the discrepancy between experiment and theory, it is felt that further discussion should be postponed until more data become available.

ACKNOWLEDGMENTS

It is a pleasure to acknowledge our gratitude to Dr. R. H. Betts for his advice and encouragement throughout this work. We are also particularly indebted to Dr. J. M. Kennedy and B. Miles for suggesting and programing the Monte Carlo calculations used in interpreting the experimental results.

REFERENCES

1. J. A. DAVIES, J. FRIESEN, and J. D. McINTYRE. *Can. J. Chem.* **38**, 1526 (1960).
2. J. A. DAVIES, J. D. McINTYRE, R. L. CUSHING, and M. LOUNSBURY. *Can. J. Chem.* **38**, 1535 (1960).
3. D. POWERS. Unpublished. Paper presented at Third Symposium on Nuclear and Radiochemistry, held at A.E.C.L., Chalk River, Ontario, Sept. 6-8, 1960.
4. R. A. SCHMITT, V. A. J. VANLINT, and C. S. SUFFREDINI. Unpublished. Paper presented at Third Symposium on Nuclear and Radiochemistry, held at A.E.C.L., Chalk River, Ontario, Sept. 6-8, 1960.
5. R. A. SCHMITT and R. A. SHARP. *Phys. Rev. Letters*, **1**, 445, (1958).
6. K. O. NIELSEN. *In* Electromagnetically enriched isotopes and mass spectrometry. Academic Press, Inc., New York. 1956. pp. 68-81.
7. H. BATEMAN. *Proc. Cambridge Phil. Soc.* **15**, 423 (1910).
8. J. A. DAVIES, J. KENNEDY, and B. Miles. To be published.
9. W. G. STONE and L. W. COCHRAN. *Phys. Rev.* **107**, 702 (1957).
10. W. P. JESSE and J. SADAUSKIS. *Phys. Rev.* **102**, 389 (1956).
11. N. BOHR. *Kgl. Danske Videnskab. Selskab, Mat-fys. Medd.* **18** (8) (1948).
12. D. K. HOLMES and G. LEIBFRIED. *J. Appl. Phys.* **31**, 1046 (1960).

ISOTOPE EFFECT IN HEAVY ION RANGE STUDIES¹

J. A. DAVIES, J. D. McINTYRE,² AND G. A. SIMS

ABSTRACT

From measurements of the isotope ratio ($\text{Na}^{22}/\text{Na}^{24}$) at various depths of penetration, it has been possible to determine at 24 kev the small difference in the median ranges of the sodium isotopes. Na^{22} has the slightly larger median range, as is predicted by the Nielsen equation. Monte Carlo calculations show that an isotropic elastic-scattering model provides a reasonable explanation for the magnitude of the range difference and for the observed variation in the isotope ratio as a function of depth.

INTRODUCTION

The preceding paper on the range of alkali metal ions of kiloelectron volt energies in aluminum (1) showed that although the mean depth of penetration increases linearly with ion energy as predicted by Bohr (2), the variation with mass and atomic number of the incident ion was considerably smaller than would be expected on theoretical grounds.

In order to determine the relative contribution of each term to the observed depths of penetration, it was decided to investigate the possible existence and magnitude of an isotope effect, i.e. to study the effect of a variation in mass without varying the atomic number.

The sodium isotopes, Na^{22} and Na^{24} , were selected for this experiment for three reasons: (a) the fractional mass difference is large; (b) the mass ratio between the incident ion and the target atoms (Al^{27}) is close to unity, a situation where one might expect to observe the maximum effect; (c) both isotopes are radioactive and can be readily detected and measured.

According to the Nielsen equation (3), the ratio of the mean ranges for two isotopes of the same ion is given by

$$\frac{R_1}{R_2} = \frac{A_2}{A_1} \cdot \frac{A_1 + A_T}{A_2 + A_T}$$

where A_T is the mass of the target atoms. For the case of sodium ion in aluminum, R_{22}/R_{24} would be 1.048. However, the Nielsen equation is applicable only as a limiting case, i.e. when A_1 (and A_2) $\gg A_T$. If the more general treatment outlined in the preceding paper (1) is used, then the predicted ratio is even smaller.

Since the reproducibility between duplicate runs in our previous range studies was no better than $\pm 5\%$, it was obviously not feasible to study such a small isotope effect by measuring R_{22} and R_{24} independently in separate runs. However, by bombarding the target simultaneously with a mixture of Na^{22} and Na^{24} ions, and then measuring the $\text{Na}^{22}/\text{Na}^{24}$ activity ratio at various depths beneath the surface, it is possible to obtain R_{22}/R_{24} directly from a single run. In this way, most of the sources of error are eliminated, except those involved in the actual counting process.

¹Manuscript received, November 3, 1960.

Contribution from the Research Chemistry Branch, Atomic Energy of Canada Limited, Chalk River, Ontario. Presented at the Third Symposium on Nuclear Chemistry and Radiochemistry held at Atomic Energy of Canada Limited, Chalk River, Ontario, September 6-8, 1960.

Issued as A.E.C.L. No. 1149.

²Present address: Frick Chemical Laboratory, Princeton University, Princeton, N.J., U.S.A.

EXPERIMENTAL PROCEDURE

The method used for bombarding aluminum targets with monoenergetic radioactive ions, and for subsequently removing thin, uniform layers of aluminum of accurately known thickness has been described in detail elsewhere (4, 5).

The ion source for each run was prepared by evaporating a small volume of aqueous Na_2SO_4 containing appropriate amounts of the radiochemical isotopes Na^{22} and Na^{24} . For maximum statistical accuracy during the subsequent counting operations, the initial relative activity was chosen to be approximately 20% Na^{22} and 80% Na^{24} . Immediately after the bombardment, a series of thin layers were removed successively from the target; the thickness of each layer was chosen so that approximately equal amounts of radioactivity were present in each one. The anodizing and film-stripping solutions from each layer were combined and γ -counted in a 5-ml volumetric flask using a 3×3 in. NaI well-type scintillation counter.

The total activity ($\text{Na}^{22} + \text{Na}^{24}$) in each flask was measured immediately after the bombardment. The samples were then set aside for 2 weeks to allow the Na^{24} to decay completely, and carefully recounted to obtain the Na^{22} activity. The original Na^{24} activity was determined by difference.

On each occasion the sample was counted at least three times, for a total period sufficient to reduce the standard deviation to less than 0.5%. The Na^{24} counts were corrected for decay to a standard time, using a value of 15.0 hours for the half-life. The maximum decay time involved in such corrections never exceeded 6 hours; furthermore, the samples were counted in random sequence in order to reduce the contribution from any subjective counting errors.

Sets of 5-ml counting flasks were carefully selected from a much larger number on the basis of uniformity of weight, bulb diameter, and position of graduation mark. To test their reproducibility, several flasks from each set were used to measure the isotopic composition of the Na_2SO_4 stock solution. The ratios of $\text{Na}^{22}/\text{Na}^{24}$ activity obtained with different flasks from any one set agreed within the statistical counting error. A different set was used for each complete run.

RESULTS

Results for a typical run, illustrating the variation of isotope ratio with depth of penetration, are shown in Table I. The estimated standard deviation for the normalized isotope ratios is ± 0.005 . Three runs have been carried out, all using 24-keV sodium ions in aluminum. In each case, an abnormally high Na^{22} content was observed in the first

TABLE I
Distribution of 24-keV sodium ions in aluminum

Depth beneath surface ($\mu\text{g}/\text{cm}^2$)	c.p.m. per μg aluminum		Isotope ratio $\text{Na}^{22}/\text{Na}^{24}$	
	Na^{22}	Na^{24}	Observed	Normalized
0.6	371	1160	.320	1.12 ₀
2.9	348	1233	.282	0.98 ₆
6.4	586	2095	.279	0.97 ₅
9.9	664	2340	.284	0.99 ₃
13.4	520	1810	.287	1.00 ₃
18.1	312	1070	.292	1.02 ₁
36.0	47.8	164	.292	1.02 ₁
Total target	11,720	40,840	.286	1.000

layer; the subsequent variation with depth agrees at least qualitatively with the prediction that Na^{22} has a slightly longer mean range.

By plotting the distribution curves on an expanded scale and interpolating, it is possible to obtain the ratio of the median ranges quite accurately. The results of this interpolation are shown in Table II. The absolute value of each median range has a

TABLE II
Median range (R) of 24-kev sodium ions in
aluminum

Run No.	R_{22}	R_{24}	R_{22}/R_{24}
1	13.6 ₈	13.4 ₁	1.018
2	13.0 ₂	12.7 ₃	1.023
3	13.0 ₈	12.8 ₈	1.014
			1.018 \pm .004

probable error of at least $\pm 5\%$, but, as noted above, most of this error cancels out in determining the isotope ratio R_{22}/R_{24} .

DISCUSSION OF RESULTS

In order to obtain a theoretical estimate for the magnitude of the isotope effect, let us apply the generalized treatment of the elastic-scattering process outlined in the preceding paper (1), viz.

$$R_M = k_M \lambda,$$

where λ is the mean free path of the incident ion and k_M , a numerical factor, is a function only of the mass ratio of the incident ion to the target atom. Appropriate values of k_M for each of the sodium isotopes in aluminum have been evaluated by using a Monte Carlo calculation based on an isotropic scattering model (details of this calculation will be described in a later paper). The resulting values are 1.204 for Na^{22} and 1.230 for Na^{24} .

Hence, the isotope effect may be expressed as

$$\frac{R_{22}}{R_{24}} = \frac{1.204\lambda_{22}}{1.230\lambda_{24}} = 0.979 \left(\frac{\lambda_{22}}{\lambda_{24}} \right).$$

But, from equation 5 in the preceding paper

$$\lambda \propto \frac{A_T^2}{A_{\text{ion}} + A_T}.$$

Therefore,

$$\frac{\lambda_{22}}{\lambda_{24}} = \frac{24+27}{22+27} = 1.041$$

and

$$R_{22}/R_{24} = 0.979 \times 1.041 = 1.019.$$

It will be noted that this predicted ratio agrees with the measured values of 1.018, 1.023, and 1.014 within the estimated experimental error of $\pm 0.5\%$.

In the preceding paper, the Na^{24} range studies indicated that, above 10 kev, elastic scattering is not the only significant process contributing to the slowing down of the incident ion, but that electronic interactions become increasingly important at higher energies. Unfortunately, the existence of significant electronic interactions at such low energies was not fully realized when these isotope effect measurements were undertaken; as a result, the energy selected for the present study is somewhat higher than would now seem desirable. However, it is probably safe to conclude that, even at 24 kev, elastic scattering is still the more significant mechanism.

A qualitative explanation for the observed variation in isotope ratio as a function of depth (Table I) can quite readily be found: Na^{22} has the larger velocity, and hence the longer mean free path; this produces a normalized $\text{Na}^{22}/\text{Na}^{24}$ ratio slightly less than unity at depths less than the median range, and slightly greater than unity at depths greater than the median range. The only abnormal result is the very large Na^{22} content in the surface layer. This may be attributed to the fact that Na^{22} , being the lighter ion, suffers larger angular deflections per collision. It can be shown that, if the scattering process is approximately isotropic in center-of-mass co-ordinates, then in the laboratory co-ordinate system approximately 20% of the Na^{22} ions are deflected through 90° or more in a single collision, whereas the corresponding figure for Na^{24} is only 15%. This considerable difference in the frequency of large-angle deflections is sufficient to produce the enhanced Na^{22} content observed in the first layer. The sodium content in the first layer is caused almost entirely by those ions that undergo large angular deflections in their *first* collision, and that have this collision near the surface. In such a collision, more than 95% of the energy is lost, and hence these ions do not travel much further.

A modification of the Monte Carlo method for calculating the shape of distribution curves (1) may be used to put the above explanation on a more quantitative basis. The statistical accuracy obtainable in Monte Carlo calculations is determined by the number of individual particle tracks followed; and it would require a prohibitive amount of computer time to reduce the statistical error to $\pm 0.5\%$ for the Na^{22} and Na^{24} abundances in each of the seven layers in Table I. However, the random numbers used to characterize each collision in the calculation are not truly random in that they are generated by some arithmetical device: in other words, they are only "pseudo-random", and it is possible to regenerate exactly the same sequence if desired.

Therefore, in order to compute the isotope ratio theoretically, a reasonable number of particles ($\sim 10^4$) were followed through a random sequence of collisions (six collisions per particle) with the mass ratio set at 0.81, i.e. the Na^{22} ion case; then, with the mass ratio set at 0.89 (the Na^{24} case), the same number of particles were followed through exactly the same "random" sequence. Since we are interested only in the *ratio* of the Na^{22} activity to the Na^{24} activity at various depths, most of the statistical fluctuations cancel out.

These Monte Carlo calculations give the isotopic distribution ($\text{Na}^{22}/\text{Na}^{24}$) at various multiples of the mean free path (λ) of the incident ion. In order to compare the calculated and experimentally measured ratios at various depths, it is necessary to introduce the ratio of the mean free paths ($\lambda_{22}/\lambda_{24}$). The value of 1.041 obtained above in computing the ratio of median ranges was used for this purpose. The resulting values for the predicted variation of isotope ratio with depth are compared with experiment in Table III. Considering the errors involved both in the calculation and in the experimental measurement, the agreement between the observed and calculated ratios is quite satisfactory, and provides further support for the approximate validity of the isotropic

TABLE III
Variation in isotope ratio with depth of penetration

Depth ($\mu\text{g}/\text{cm}^2$)	Na ²³ /Na ²⁴ activity ratio	
	Observed	Calculated
0.6	1.120	1.080
2.9	0.986	0.972
6.4	0.975	0.960
9.9	0.993	0.964
13.4	1.003	0.998
18.1	1.021	1.009
36.0	1.021	1.048

scattering assumption. In particular, the theoretical treatment accounts for the anomalously high Na²³ content in the surface layer.

ACKNOWLEDGMENTS

It is a pleasure to acknowledge the invaluable assistance of Dr. J. M. Kennedy and B. Miles in the development and programing of the special Monte Carlo calculations used in this work.

REFERENCES

1. J. A. DAVIES and G. A. SIMS. *Can. J. Chem.* **39**, 601 (1961).
2. N. BOHR. *Kgl. Danske Videnskab. Selskab, Mat-fys. Medd.* **18** (8) (1948).
3. K. O. NIELSEN. In *Electromagnetically enriched isotopes and mass spectrometry*. Edited by M. L. SMITH. Academic Press, New York, 1956. p. 73.
4. J. A. DAVIES, J. D. MCINTYRE, R. L. CUSHING, and M. LOUNSBURY. *Can. J. Chem.* **38**, 1535 (1960).
5. J. A. DAVIES, J. FRIESEN, and J. D. MCINTYRE. *Can. J. Chem.* **38**, 1526 (1960).

THE KINETIC ENERGY OF Cs^{136} PRIMARY FRAGMENTS FROM FISSION OF U^{235} ¹

F. BROWN AND B. H. OLIVER

ABSTRACT

The ranges of Cs^{136} , Cs^{137} , and Ba^{140} fission fragments in aluminum have been measured using an anodizing technique to strip layers from the aluminum together with radiochemical methods to determine the fission products. The mean ranges are, in milligrams per square centimeter: Cs^{136} , 2.64; Cs^{137} , 2.91; and Ba^{140} , 2.82. The range distributions were of near-Gaussian form with the following percentage full widths at half height: Cs^{136} , 17.7; Cs^{137} , 17.0; and Ba^{140} , 17.5. The range-energy relationship of Bohr, $R = \text{const. } A^{1/2} E^{1/2} Z^{-2/3}$, was tested using the range data of Katcoff (7) and of Niday (2) together with the kinetic energy data of Milton and Fraser (15) and found to be accurate, within experimental error, over any limited range of fragment masses. Using this formula it then appears that the total kinetic energy in the fission mode leading to Cs^{136} is ~ 21 Mev less than normal.

INTRODUCTION

The general features of the distribution of nuclear charge in low-energy fission are well known. The situation is usually described in terms of the distribution in primary charge of fragments having a fixed mass. It is then found that the charge distribution is, at least approximately, independent of the particular mass chosen and can be represented by a Gaussian-like distribution around a most probable charge Z_p . The value of Z_p for any mass can be found using the empirical rule due to Glendenin (1) known as the "equal chain length hypothesis". An alternative, but equivalent, description is obtained by considering the distribution in mass of fragments having a fixed primary charge.

This latter distribution emphasizes the fact that the observed charge distribution can be modified by neutron emission from the fragments (a phenomenon which is well known in high-energy fission). The number of neutrons emitted in fission is not constant, and one can therefore ask whether those primary fragments found relatively close to stability (i.e. having less than the most probable mass for a fixed primary charge) have emitted more than the average number of neutrons. One associates a more than average neutron emission with fragments which possess more than average internal excitation and, if the total energy release for the formation of these fragments is normal, one then expects them to have less than normal kinetic energy.

Ideally one would like to have measurements of the total energy release, the kinetic energy, the γ -ray energy, and the neutron emission for fragments formed close to stability (and likewise for those formed exceptionally far from stability) but such fragments are rare and the present techniques for such measurements, by time of flight and so on, are not applicable. This suggests the use of radiochemical methods, which are highly specific. In particular it is possible, in principle, to measure the range of any fission fragment and given the range-energy relationship to obtain its kinetic energy. The paper presents the results of experiments to measure the kinetic energy of the fragment Cs^{136} which, being a shielded nuclide, is a primary fragment.

A collimated beam of fission fragments was directed into an aluminum catcher foil.

¹Manuscript received November 3, 1960.

Contribution from the Research Chemistry Branch, Atomic Energy of Canada Limited, Chalk River, Ontario. Presented at the Third Symposium on Nuclear Chemistry and Radiochemistry held at Atomic Energy of Canada Limited, Chalk River, Ontario, September 6-8, 1960.

Issued as A.E.C.L. No. 1151.

Successive layers of the foil were dissolved by an anodizing technique and analyzed for Cs^{136} , Cs^{137} , and Ba^{140} . The relationship between range and energy was derived from theory and confirmed by the Cs^{137} and Ba^{140} data together with other data from the literature.

The results of these experiments show that, as anticipated, the range of Cs^{136} fragments is abnormally low. During the preparation of this work for publication a new set of range measurements, for U^{235} fragments in uranium, has become available (Niday (2)). These measurements also show that Cs^{136} and Rb^{86} (another shielded nuclide) have abnormally low ranges. The significance of these observations on shielded nuclides is discussed at the end of this paper.

EXPERIMENTAL

Apparatus

An electropolished aluminum plate approximately 1.5×4.0 cm was covered with a layer of U^{235} as oxide deposited using the lacquer technique and of thickness $\sim 100 \mu\text{g}$ $\text{U}^{235}/\text{cm}^2$. This plate was covered with an aluminum collimating plate 3/16 in. thick drilled with 1/16 in. diameter holes. Against this was placed the catcher foil, a plate of electropolished, high-purity aluminum. The assembly was placed in an irradiation container, filled with hydrogen at atmospheric pressure, and hermetically sealed. The hydrogen was introduced to provide some cooling to the container walls. An irradiation of 1 week was made in a vacant fuel rod position of the NRX reactor at a neutron flux of $\sim 5 \times 10^{13}$ neutrons/cm² sec.

Sampling

After removal from the reactor and disassembly by remote handling the catcher foil was "stripped" using the anodizing technique developed by Davies (3). In this technique the specimen is anodized by applying a known voltage in a citrate buffer solution which causes an oxide layer to form whose thickness is proportional to the voltage and essentially independent of time after the first 5 minutes. The specimen is then removed, washed, and placed in a hot (95° C) stripping solution of chromic oxide and phosphoric acid which rapidly dissolves the oxide (2 minutes) but does not attack the metal. The process is then repeated as required. In the present case the anodizing voltage was 100 volts, which results in the stripping of $\sim 25 \mu\text{g}/\text{cm}^2$ of aluminum in each cycle. Since this is an unnecessarily small layer two oxide layers were dissolved in each sample of stripping solution so that each sample contained $\sim 50 \mu\text{g}/\text{cm}^2$ of the specimen. The actual amount stripped was determined by weighing the specimen after every seven samples and was found to be $54.3 \mu\text{g}/\text{cm}^2$ per sample (in agreement with the data obtained by Davies). This figure could be in error by about 3% due to a possible error in measuring the area of the foil; the electropolishing process caused the edges of the foil to be somewhat rounded. This error would affect only the absolute values of the ranges measured.

The consistency in sampling was indicated by comparing the weights removed in each group of seven samples. The standard deviation from the mean was 1.4%. The weight loss for seven samples was ~ 5.0 mg, the error in the weighings ~ 0.05 mg, so that within the accuracy of measurement there were no significant variations between the groups of seven samples.

Purification

Each sample of stripping solution contained measured quantities of cesium and barium carriers. The barium was precipitated as carbonate, purified by the hydrochloric acid-ether method of Glendenin (4), collected on weighed filter papers, weighed as $\text{BaCl}_2 \cdot 2\text{H}_2\text{O}$,

and finally mounted for γ -ray counting. The cesium was purified by the sodium tetraphenyl boron method of Handley and Burros (5). It was found necessary to apply this procedure twice in order to obtain sufficient radiochemical purity. Thus the precipitate of cesium tetraphenyl boron obtained from the first purification cycle was destroyed by fuming nitric acid and the whole cycle was repeated. The final precipitate was collected, weighed, and mounted for γ -ray counting as in the barium case.

Counting

The samples were counted by a 3 \times 3 in. sodium iodide crystal mounted as recommended by Heath (6). For the cesium counting this was connected to a 100-channel kicksorter equipped with typewriter readout. The stability of both counting rate and energy scale was checked using Cs^{137} and Co^{60} standards and no corrections were found to be necessary. The spectra, corrected for background, showed the 661-keV peak from Cs^{137} and peaks from Cs^{136} at 822 keV, 1.04 MeV, and higher energies. The Cs^{136} counting rate was taken as the total rate in the 822-keV and 1.04-MeV peaks corrected for the high-energy tail from the 661-keV Cs^{137} peak. This correction was actually negligible except in the few samples which contained a very high $\text{Cs}^{137}/\text{Cs}^{136}$ ratio when it amounted to $\sim 3\%$. The Cs^{137} counting rate was taken as the rate in the 661-keV peak corrected for the Compton contribution from the higher-energy Cs^{136} γ -rays. This contribution was estimated by comparing spectra of pure Cs^{137} with those from various Cs^{136} - Cs^{137} mixtures. The correction varied from $\sim 1\%$ to $\sim 25\%$ depending on the $\text{Cs}^{136}/\text{Cs}^{137}$ ratio. In the samples of greatest interest it was $\sim 5\%$. These data were then corrected for the chemical yield and for decay of the Cs^{136} to obtain the results shown in Fig. 1.

For the Ba^{140} counting the crystal was connected to a discriminator and the total γ -ray count above 700 keV was recorded. All samples had been allowed to decay sufficiently before counting so that the La^{140} had reached secular equilibrium. The rates were corrected for background and chemical yield and are shown in Fig. 1. No corrections for decay were required since all the samples were counted within a short space of time and only relative rates were required.

RESULTS

The experimental data are shown in Fig. 1 where the activity for each nuclide, in arbitrary units, is plotted against the sample number. In each case the distribution shows the expected Gaussian-type distribution plus a tail of approximately constant level on the low-range side. This tail could arise from U^{235} lost from the source during irradiation and deposited on the surface of the catcher foil. The experiment was repeated with the uranium covered by $\sim 700 \mu\text{g}/\text{cm}^2$ of aluminum in order to prevent transfer of uranium. The intensity of the tail was reduced to about one half. The remaining tail is presumably caused by scattering but it would seem desirable to perform experiments specifically designed to study this effect before attempting to draw any firm conclusions. Corrections for these tails were made by assuming they consisted of a square distribution smeared by a Gaussian of the same width as the main peak. The data so corrected are shown on Fig. 2. Typical errors are shown by the vertical bars. In the case of Ba^{140} and Cs^{137} they arise mainly from the chemical yield determinations, but in the Cs^{136} case the uncertainty in background correction is also involved and thus the errors are relatively larger for the low-activity points.

In order to test the shape of the distributions the data were integrated and plotted on probability paper; it was found that the mean range was, in all cases, slightly less

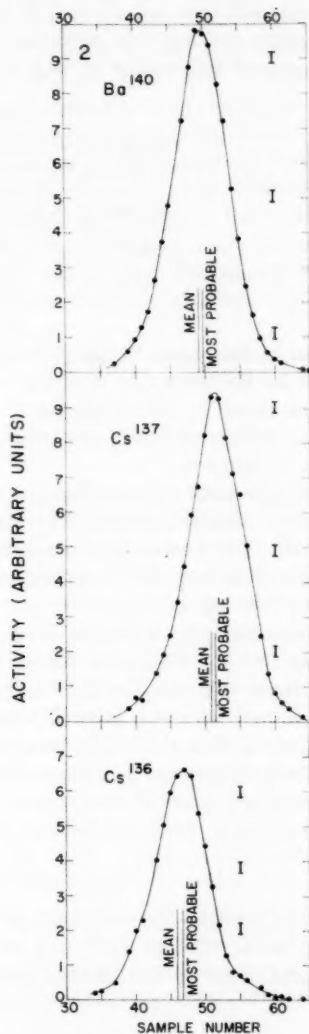
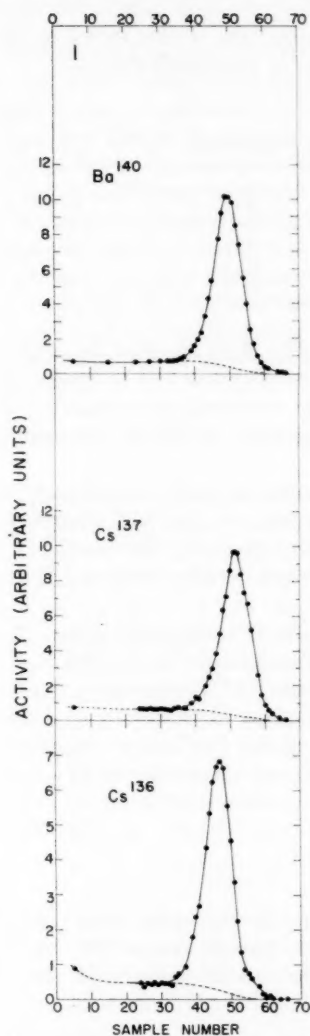


FIG. 1. Range distributions, uncorrected.

FIG. 2. Range distributions, corrected.

than the most probable, the difference being between 1 and 2%. This agrees qualitatively with the results of Katcoff *et al.* (7), who found, for Pu^{239} fission fragments in air, that the distributions were slightly steeper on the high-range side. As in the case of the Katcoff experiment it is not clear whether this small effect is fundamental or is caused by the experimental setup.

To convert sample number to range in aluminum it is necessary to multiply by $54.3 \mu\text{g}/\text{cm}^2$ and to add a small correction for the weight of hydrogen in the collimator holes and for the source thickness. This correction amounts to the equivalent of ~ 2.3

samples and although it is not accurately established it has no significant effect on the final analysis. After making this correction one obtains the results shown in Table I for the mean ranges and full widths at half maximum of the distributions.

TABLE I
Ranges and range dispersions in aluminum

Nuclide	Range (mg/cm ²)	Width (%)
Ba ¹⁴⁰	2.82	17.5
Cs ¹³⁷	2.91	17.0
Cs ¹³⁶	2.64	17.7

The precision of the mean range values is $\sim 0.4\%$; their absolute accuracy is about 4% . This is set by the error in correcting for source thickness and hydrogen absorption ($\sim 2\%$) and the error in the value for the weight removed per sample ($\sim 3\%$). The precision of the widths is $\sim 3\%$ and thus the variation in widths between the three nuclides is not significant.

The present experiments were designed primarily to detect differences in ranges rather than to set absolute values. The absolute range of the Ba¹⁴⁰ fragments can be compared directly with the value obtained by Finkle *et al.* (8) for Ba¹⁴⁰ from U²³⁵ stopping in aluminum, viz. 2.75 mg/cm². A recent measurement by Alexander and Gallagher (9) gives a value of 2.98 mg/cm².

The widths obtained by Good and Wollan (10) for I¹³⁷ fragments from U²³⁵ stopping in various gases are: H₂, 4.3%; D₂, 8.0%; He, 6.3%; air, 15.7%; A, 18.2%. The width obtained by Katcoff *et al.* for the Ba¹⁴⁰ fragments from Pu²³⁹ stopping in air was 12.6%. The widths obtained with the present technique appear therefore to be reasonable.

It should be noted that the range dispersion in all but the lightest stopping media is due almost entirely to straggling; the contributions from the variations in kinetic energy and nuclear charge are small in comparison. In the present experiment the contributions from source thickness ($\sim 1\%$) and finite collimator angle ($\sim 2.5\%$) are also very small.

DISCUSSION

The following discussion is presented in three parts: (a) range-energy relationships for fission fragments, (b) calculation of the kinetic energy released in forming Cs¹³⁶, and (c) the significance of the kinetic energy deficit which is found in the formation of Cs¹³⁶.

(a) Range-Energy Relationships for Fission Fragments

It is clear from the present experiment and from the results of Niday (2) that the Cs¹³⁶ fragments have abnormally low ranges. Before discussing the significance of this fact it is necessary to know what this amounts to in terms of the kinetic energy of the fragment and it is in this question that the greatest difficulty arises. The only range data for particles of fission product masses and initial energies are those obtained on fission products themselves. Whilst, in principle, these range data can be combined with fragment energy data obtained by time-of-flight techniques in order to establish some relationship between fragment mass A , nuclear charge Z , and initial energy E , in practice it is difficult to draw any unambiguous conclusions. The difficulty is that, for normal fission fragments, A , Z , and E are correlated, viz. Z is approximately proportional

to A and E is very approximately inversely proportional to A . Another set of potentially useful data are those concerning the rate of energy loss dE/dx or rate of velocity loss dV/dx obtained by Lassen (11), Leachman and Schmitt (12), and Fulmer (13). Apart from the fact these studies involve only the "median light" and "median heavy" fragments there is also a fundamental difficulty in using them to establish a range-energy relationship, viz. the range-energy relationship changes as the fission fragments slow down. This is due to the change in effective charge as the fragment slows down, which means that the mechanism of energy loss changes from being predominantly ionization at high velocities to predominantly screened field scattering at low velocities. For the present purpose we are interested in the effect on the range when the initial energy is changed by only a rather small amount from the normal. We should also pay special attention to the effect of nuclear charge because the nuclear charge of a Cs^{136} fragment is abnormally high in relationship to its mass.

An approximate formula for the range, R , can be obtained from Bohr's theoretical discussions (14),

$$[1] \quad R = k \frac{A^{1/2} E^{1/2}}{Z^{2/3}}$$

where k is a constant depending on the stopping material. This can be approximated to $R = E^{1/2} A^{-1/6}$ (see reference 7) by assuming Z proportional to A ; however, for the present, it is preferable to retain the Z dependence. The validity of the expression can be checked to some extent by using the range data of Katcoff *et al.* (7) for fragments from Pu^{239} stopping in air and the range data of Niday (2) for U^{235} fission fragments stopping in uranium together with the fragment kinetic energy data obtained by time-of-flight techniques. We have used here the energy data obtained by Milton and Fraser (15), corrected for neutron emission as follows. Let E_p be the total prompt kinetic energy measured at prompt mass ratio A_H/A_L . The prompt kinetic energies of the separate fragments are given as usual by $E_p/(1+A_L/A_H)$ and $E_p/(1+A_H/A_L)$ but the kinetic energies of interest in range studies are those after neutron emission, which are given by

$$\left[\frac{E_p}{(1+A_L/A_H)} \right] \frac{A_L - \nu_L}{A_L} \quad \text{and} \quad \left[\frac{E_p}{(1+A_H/A_L)} \right] \frac{A_H - \nu_H}{A_H}$$

where ν_L and ν_H are the numbers of neutrons emitted by the light and heavy fragments respectively. The corresponding masses, as observed in range studies are of course $A_L - \nu_L$ and $A_H - \nu_H$. In the case of U^{235} the value of ν_L and ν_H was obtained from the data of Apalin *et al.* (16); in the Pu^{239} case the following relationships, due to Milton (17), were employed:

$$\nu_L = \frac{2.89}{2} + (A_L - 100) 0.045 \quad \text{and} \quad \nu_H = \frac{2.89}{2} + (A_H - 140) 0.067.$$

The appropriate values of Z are the most probable charges Z_p and were obtained from the empirical Z_p function of Wahl (18). We have then calculated the values of the constant k for each fragment measured and we have plotted the results in Fig. 3 (Katcoff's data (7) for fragments stopping in air) and Fig. 4 (Niday's data (2) for fragments stopping in uranium). Both figures show small but significant trends in the "constant" k , but for fragments whose masses differ by only a few units the formula is as good as the data used to check it. (The lines in Figs. 3 and 4, which have been drawn only for illustration,

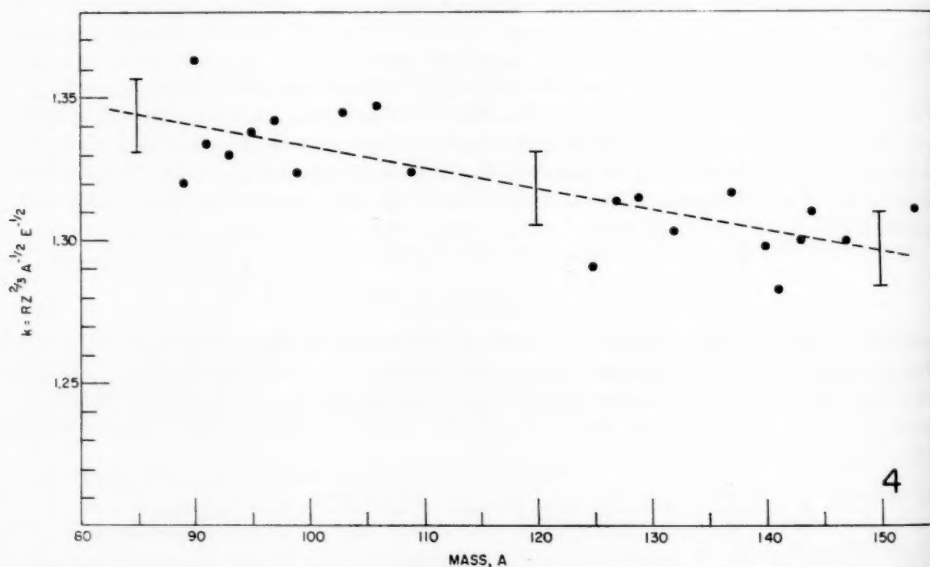
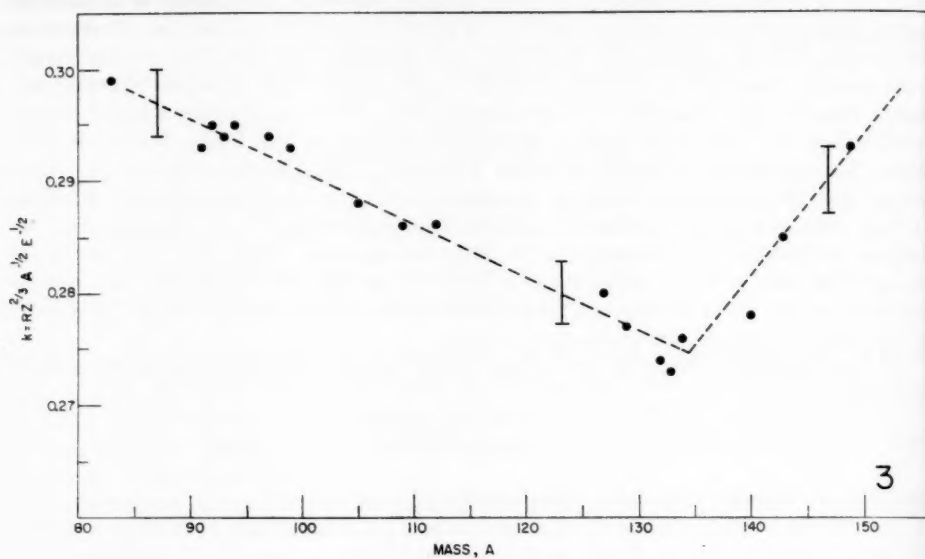


FIG. 3. Values of $k = RZ^{2/3} A^{-1/2} E^{-1/2}$; data of Katcoff *et al.* (7) for Pu^{239} fragments in air.
 FIG. 4. Values of $k = RZ^{2/3} A^{-1/2} E^{-1/2}$; data of Niday (2) for U^{238} fragments in uranium.

have slopes of 0.12 and 0.06% per mass unit respectively. The vertical bars show deviations of $\pm 1.0\%$ in k .)

Niday (2) in the interpretation of his data for fission fragment ranges in uranium has

discussed Bohr's treatment of ranges and used the theoretical expressions as a basis for a semiempirical range formula as follows:

$$[2] \quad R = \frac{A(V_1 - V_e)}{2.411(K + 4.762K^{5/3})}$$

where V_1 is the initial fragment velocity, V_e the velocity at which the collision diameter becomes greater than the screening parameter (see reference 2 for definition of these quantities), and $K = 1.077Z^{1/3}$. This formula was fitted to the range data and the velocity data of Stein (19). With the numerical constants given it applies to ranges in uranium. It may be noted that this expression, equation [2], approximates to the simpler expression, equation [1]. Thus V_e is small compared with V_1 , the term K is small compared with the term $4.762K^{5/3}$, and since $V_1 = (2E/A)^{1/2}$ we then have

$$R = \text{const.} \frac{A^{1/2}E^{1/2}}{Z^{5/6}}.$$

Alexander and Gallagher (9) have considered the range-energy relationship for "median heavy" and "median light" fragments. Leachman and Schmitt's data (12) give the velocity (V) of these "average" fragments after passing through aluminum foils of known thickness, whilst Fulmer's data (13) give their energies (E), measured by a cesium iodide crystal, after passing through known thicknesses of various materials including aluminum. Alexander and Gallagher found that for these "average" fragments whose mass and charge, although not precisely defined, are constant, the range-energy data are fitted by either of two relationships,

$$[3] \quad R = kV - \Delta$$

or

$$[4] \quad R = KE^{2/3},$$

where k , K , and Δ are constants. Both these expressions fit the available data reasonably well over a rather *wide range* of energies. However, if we consider data for fragments slowed down only *slightly* we find that the range is more nearly proportional to $E^{1/2}$. This is of course implied by equation [3] since for fragments having their normal initial velocities or thereabouts the term Δ is small compared to kV ; compare also equation [2]. This point is demonstrated by the data in Table III. To obtain this we have proceeded as follows. Let R_1 be the range of the unslowed fragment in aluminum and let E_1 be its initial energy. After passing through a given thickness of aluminum, t , its energy is E_2 (as given by Leachman and Schmitt (12) or by Fulmer (13)) and its range R_2 is just $R_1 - t$. We used our value for the Ba^{140} range as representative of the median heavy fragment to which Table III applies. The table lists (R_1/R_2) , $(E_1/E_2)^{1/2}$, and $(E_1/E_2)^{2/3}$ and although the $E^{2/3}$ dependence gives the best over-all fit the $E^{1/2}$ dependence is better when E_2 is close to E_1 . This test is of course of poor sensitivity when E_2 is close to E_1 and we present the table to illustrate the trend.

When equations [3] and [4] are applied to the ranges of fragments of different masses it is found that the "constants" Δ and K vary with mass. This is to be expected since the equations have no allowance for the effect of A and Z , but provided the variation is smooth and can be established, as was done by Alexander and Gallagher, it is possible to interpolate for K or Δ . It is interesting to note that equation [1] becomes equation [4] if we make the approximation that Z is proportional to A and A is inversely proportional to E .

TABLE III
Range-energy relationship for "median heavy"
fragment

$(E_1/E_2)^{1/3}$	R_1/R_2	$(E_1/E_2)^{2/3}$
1.12	1.10	1.17*
1.22	1.22	1.30*
1.44	1.55	1.60*
1.50	1.60	1.67†
1.72	2.14	2.06*
1.96	2.82	2.46†

*Using reference 13 (Fulmer).

†Using reference 12 (Leachman and Schmitt).

(b) *The Kinetic Energy Released in the Formation of Cs¹³⁶*

We have used equation [1] to obtain the kinetic energy of the Cs¹³⁶ fragments because (a) it contains terms for the Z and A dependence and (b) the constant of proportionality k is established by our own data on Cs¹³⁷ and Ba¹⁴⁰. The Z dependence is important because the change from $Z = 52.6$ (Z_p for mass 136) to $Z = 55.0$ (Z for Cs¹³⁶) accounts for a change in range of some 2.8% (for a $1/Z^{2/3}$ dependence) out of an observed range anomaly of some 10%.

Z_p values were taken from Wahl (18). Kinetic energies were obtained from the data of Milton and Fraser (15) corrected for neutron emission as before. From the measured Cs¹³⁷ and Ba¹⁴⁰ ranges the constant k in equation [1] was obtained: the values were 0.418 and 0.419, respectively, in excellent agreement. The kinetic energy of the Cs¹³⁶ fragment was then calculated using $k = 0.418$ and found to be 61.0 Mev. Assuming that two neutrons were emitted in the formation of this fragment, the kinetic energy of the prompt fragment (Cs¹³⁸) was 61.9 Mev and by conservation of momentum the total kinetic energy (for the two fragments) was 149.0 Mev. The total kinetic energy for a normal fission into prompt masses 138 and 98 is, according to Milton and Fraser, 169.8 Mev; by normal we mean having the normal charge distribution appropriate to the masses involved. The fission to produce Cs¹³⁶, whose Z is 55 compared with a Z_p of 52.6 for mass 136, has therefore about 21 Mev less kinetic energy than the normal fission to mass 136.

This conclusion relies on the range formula and although we have data (12, 13) to show that the energy dependence of the range is not likely to be in *serious* error we do not have any direct evidence for the relationship between range and charge or between range and mass. It is, however, encouraging to note that Niday (2), using his own range data and equation [2], calculated the kinetic energy of the Cs¹³⁶ fragment to be 61.6 Mev, compared with our value of 61.0 Mev. It is also interesting to find that using energies from Milton and Fraser, range data from the present work and Alexander's range-energy relationship (equation [4], above) we find the kinetic energy of the Cs¹³⁶ to be 60.5 Mev. If Niday's range data are used with this equation the result is again 60.5 Mev.

It is clear, therefore, that if we trust our present ideas on fission fragment ranges and energies we must conclude that the production of Cs¹³⁶ involves some 21 Mev less total kinetic energy than is normal for this mass ratio. Niday's results show that the situation is similar in the production of Rb⁸⁶, another shielded nuclide; the deficit in total kinetic energy is again ~20 Mev. The following sections of this paper are an attempt to discuss the significance of these facts.

(c) *The Kinetic Energy Deficit in the Formation of Cs¹³⁶*

We expect the fissions which produce Cs¹³⁶ as a primary fragment to produce less kinetic energy than normal for two reasons. (a) Because Cs¹³⁶ is neutron deficient (for a fission fragment) it will be associated with events which involve greater than average neutron emission, which means greater than average internal excitation of the fragments and hence less kinetic energy for any given total energy release. (b) Because the charge division required to produce Cs¹³⁶ is a long way from the most probable charge division there will be less total energy release.

We shall next attempt to make quantitative estimates of these two effects beginning with the question of neutron emission in the formation of Cs¹³⁶. Ideally we wish to know the distribution of neutron emission probabilities for heavy fragments in the mass range 136 to about 140. The distribution of neutron emission probabilities averaged over all pairs of fragments is known; Terrell (20) has shown that this distribution can be represented by a Gaussian with standard deviation $\sigma_{H+L} = 1.08$. We also know from the work of Apalin *et al.* (16) that the average numbers of neutrons from the heavy and light fragments are approximately the same at the mass ratio corresponding to Cs¹³⁶. To obtain the distribution for the heavy fragment alone we shall make two alternative assumptions. (a) Assume that the distributions for the light and heavy fragments are not correlated to each other. In this case the standard deviation for the heavy fragment is $\sigma_H = \sigma_{H+L}/\sqrt{2} = 1.08/\sqrt{2}$. (b) Assume that the distributions for heavy and light fragments are correlated in a positive sense, i.e. if the heavy fragment emits more than the average number of neutrons the light fragment also does; this implies that the two fragments share the available excitation energy in a constant proportion. In this case $\sigma_H = \sigma_{H+L}/2 = 1.08/2$. Using these distributions we can now calculate the probabilities, P_n , that a fragment of mass 136 is formed from fragments of prompt mass 136, 137, 138, etc. by emission of 0, 1, 2, etc. neutrons.

In order to say how many of these mass 136 fragments so formed will actually be Cs¹³⁶ we must know the probability P_{55} that each of the prompt mass precursors will have a nuclear charge 55. We thus need the charge distribution before neutron emission. The charge distribution after neutron emission is known; Nethaway and Wahl (21) have shown that it can be presented by a Gaussian with standard deviation σ_{obs} where $2\sigma_{obs}^2 = 1.0$. We can correct the charge distribution for neutron emission as follows. The fluctuations in the mass of the heavy fragment due to neutron emission have a standard deviation σ_H (defined above) and since for the heavy fragments $\Delta Z/\Delta A = 0.49$ this corresponds to a fluctuation in charge of $\sigma_Z = \sigma_H \times 0.49$. The corrected charge distribution will thus have a standard deviation σ_{cor} given by $\sigma_{cor}^2 = \sigma_{obs}^2 - \sigma_Z^2$ where $2\sigma_{obs}^2 = 1.0$, $\sigma_Z = \sigma_H \times 0.49$, and σ_H is either $1.08/\sqrt{2}$ or $1.08/2$ according to the alternative assumptions discussed above. It is interesting to see that the effect of neutron emission in broadening the observed charge distribution is not negligible.

From the corrected charge distribution we now obtain the probabilities P_{55} that each prompt mass, 136, 137, 138, etc., will have $Z = 55$. We have previously calculated the probabilities P_n that each of these precursors will yield a fragment of mass 136 by emission of ν neutrons. The product $P_n P_{55}$ is the probability that Cs¹³⁶ will be formed by emission of ν neutrons. The number of neutrons emitted in forming Cs¹³⁶ is thus $\sum \nu P_n P_{55}$, the number of Cs¹³⁶ fragments formed is $\sum P_n P_{55}$, and the average number of neutrons $\bar{\nu}_{Cs^{136}}$ emitted in forming Cs¹³⁶ is given by

$$\bar{\nu}_{Cs^{136}} = \frac{\sum \nu P_n P_{55}}{\sum P_n P_{55}}.$$

These calculations show that for assumption (a) (uncorrelated neutron emissions from light and heavy fragments) $\bar{\nu}_{Cs^{136}}$ is 2.52. The normal neutron emission from the heavy fragment at this mass ratio is 1.21 neutrons (16) and thus the *extra* neutron emission in forming Cs^{136} is $\Delta\nu_{Cs^{136}} = 2.52 - 1.21 = 1.31$ neutrons. If we assume that the emission of each neutron involves the expenditure of 6.7 Mev (Terrell (22)) this requires an extra 8.8 Mev of excitation and leaves, correspondingly, 8.8 Mev less kinetic energy. For assumption (b) (correlated neutron emission from light and heavy fragments) the value of $\bar{\nu}_{Cs^{136}}$ is 2.01 and thus $\Delta\nu_{Cs^{136}}$ is $2.01 - 1.21 = 0.80$. Since we have assumed correlated neutron emissions the light fragment will also emit an equal number of extra neutrons so that the extra neutron emission involved is $2 \times 0.80 = 1.60$ neutrons. This involves 10.7 Mev extra excitation and thus 10.7 Mev less kinetic energy.

Having estimated the deficit in kinetic energy due to extra neutron emission we must add to it the deficit in total energy release caused by unfavorable charge division in order to obtain the total deficit in kinetic energy. The deficit in total energy release can be obtained using the mass tables of Cameron (23) provided we know the prompt masses involved. We have assumed $\bar{\nu}_{Cs^{136}} = 2.0$, i.e. a prompt mass ratio of 138:98. The most probable charge division for this mass ratio is almost exactly 53:39 and gives a total energy release of 183.9 Mev. The production of cesium by a charge division of 55:37 releases 176.2 Mev, i.e. 7.7 Mev less.

Thus our estimates for the deficit in kinetic energy involved in forming Cs^{136} are, for assumption (a), $8.8 + 7.7 = 16.5$ Mev and, for assumption (b), $10.7 + 7.7 = 18.4$ Mev. The measured deficit is 21 Mev.

Both estimates are low, but the agreement is reasonable considering the assumptions involved. We derived the number of neutrons emitted in forming Cs^{136} from the average distribution of neutron emission probabilities measured for all fissions. This could be a mistake, due, for example, to the existence of the 82-neutron shell in the precursor Cs^{137} . We have also assumed that the emission of each neutron requires an energy of 6.7 Mev; again this figure is an average for all fissions and could be quite inappropriate for the particular fragments we are discussing. Finally, in estimating the deficit in total energy release by means of Cameron's mass formula we have taken a unique prompt mass ratio, 138:98 and compared two unique charge divisions 53:39 and 55:37. We should have considered suitably weighted averages over several mass ratios and charge divisions but the uncertainty regarding neutron emissions makes it impossible to do this rigorously. We could also account for the difference between our estimates and measurement if we assumed that the internal excitation of the fragments is greater when the charge division is unfavorable.

In summary, considering the uncertainties in the estimates and the reliance we have placed on the range formula, we can say that the results of this experiment are in general agreement with expectations based on our present knowledge of the fission process.

ACKNOWLEDGMENTS

The authors wish to thank Dr. J. A. Davies of A.E.C.L., for advice concerning the anodizing technique and for helpful discussions on the ranges of heavy ions. They are also very grateful to Mr. G. C. Hanna, of A.E.C.L., who has contributed much to the interpretation and discussion of the experimental results.

REFERENCES

1. L. E. GLENDENIN. M.I.T. Tech. Rept. No. 35. 1949.
2. G. B. NIDAY. University of California Radiation Laboratory, UCRL-5816. 1960.
3. J. A. DAVIES. Can. J. Chem. 38, 1526 (1960).

4. L. E. GLENDENIN. National Nuclear Energy Series. Vol. 9, Paper 288. McGraw-Hill. 1951.
5. T. H. HANDLEY and C. L. BURROS. Anal. Chem. **31**, 332 (1959).
6. R. L. HEATH. IDO-16408. 1957.
7. S. KATCOFF, J. A. MISKEL, and C. W. STANLEY. Phys. Rev. **74**, 631 (1948).
8. B. FINKLE, E. J. HOAGLAND, S. KATCOFF, and N. SUGARMAN. National Nuclear Energy Series. Vol. 9, Paper 46. McGraw-Hill. 1951.
9. J. M. ALEXANDER and M. F. GALLAGHER. University of California Radiation Laboratory, UCRL-8978. 1960.
10. W. M. GOOD and E. O. WOLLAN. Phys. Rev. **101**, 249 (1956).
11. N. O. LASSEN. Kgl. Danske Videnskab. Selskab, Mat-fys. Medd. **25**, No. 11 (1949).
12. R. B. LEACHMAN and H. W. SCHMITT. Phys. Rev. **96**, 1366 (1954).
13. C. B. FULMER. Phys. Rev. **108**, 1113 (1957).
14. N. BOHR. Phys. Rev. **59**, 270 (1941); Kgl. Danske Videnskab. Selskab, Mat-fys. Medd. **18**, No. 8 (1948).
15. J. C. D. MILTON and J. S. FRASER. Private communication.
16. V. F. APALIN, U. P. DOBRININ, V. P. ZAHAROVA, I. E. KUTIKOV, and L. A. MIKHAYLAN. Atomic Energy U.S.S.R. **8**, 15 (1960).
17. J. C. D. MILTON. Private communication.
18. A. C. WAHL. J. Inorg. & Nuclear Chem. **6**, 263 (1958).
19. W. E. STEIN. Phys. Rev. **108**, 94 (1957).
20. J. TERRELL. Phys. Rev. **108**, 783 (1957).
21. D. R. NETHAWAY and A. C. WAHL. Quoted by E. K. HYDE. University of California Radiation Laboratory, UCRL-9036. 1960.
22. J. TERRELL. Phys. Rev. **113**, 527 (1959).
23. A. G. W. CAMERON. Can. J. Phys. **35**, 1021 (1957).

THE THERMAL NEUTRON FISSION YIELDS OF U^{233} ¹

D. R. BIDINOSTI, D. E. IRISH, AND R. H. TOMLINSON

ABSTRACT

Using the mass spectrometer and isotope dilution technique, 27 cumulative fission yields from the thermal neutron fission of U^{233} along with 13 other fission product chains relative to each other have been determined. After normalization of the latter, values are obtained for all but seven fission decay chains whose yields are in excess of 0.5%.

INTRODUCTION

Numerous studies have been made of the thermal neutron fission yields of U^{233} . Katcoff (1) has summarized the work preceding 1958, but since this time further mass spectrometric studies by Ivanov *et al.* (2) and radiochemical studies by Santry and Yaffe (3) and Bartholomew *et al.* (4) have been published.

In the present work, fission yields have been determined for isotopes of the elements rubidium, strontium, zirconium, molybdenum, ruthenium, cesium, cerium, neodymium, and samarium. These yields, together with the relative yields of the isotopes of krypton and xenon previously published from this laboratory (5), make the most complete study of the fission yields of U^{233} that have been made up to this time.

EXPERIMENTAL

Samples of U^{233} diluted with U^{238} were irradiated as U_2O_8 in quartz capsules along with cobalt flux monitors in the NRX Chalk River reactor. The U^{238} was added as a diluant to minimize flux depression in the samples. Since the U^{238} was a separated isotope obtained from the Oak Ridge National Laboratories, the U^{235} present in the samples was found to be less than 1% of the U^{233} .

The cobalt flux monitors, weighing approximately 1.14 mg, were made of 0.13 mm diameter cobalt wire which was sealed in aluminum tubing. After irradiation the activity of the cobalt monitors was measured with a well-type ionization chamber (Harwell type T.P.A. Mk II) relative to standards provided by R. C. Hawkins of Chalk River. The evaluation of the neutron flux by this method has been previously described (6). Sample 3 was not monitored in this manner, an approximate flux value being obtained from the extent of depletion of Cs^{135} which results from neutron absorption during the irradiation. Sample 4 was irradiated in a thermal column at a flux less than 10^{11} neutron/cm² sec. This sample was used to obtain the relative yield of the mass 135 and 137 chains, since at this flux Xe^{135} removal is small. The irradiation data for the various samples is shown in Table I.

The number of fissions (F) in samples 1 and 2 were computed from the relation

$$F = N^{233} \frac{\hat{\sigma}_f}{\hat{\sigma}_a} (1 - e^{-\hat{\sigma}_a \phi t})$$

where N^{233} is the number of U^{233} atoms in each sample, $\hat{\sigma}_f$ and $\hat{\sigma}_a$ are the effective fission and absorption cross sections of uranium as defined by Westcott (7), and ϕt the integrated flux. The effective cross sections for samples 1 and 2 have been obtained from the tables of Westcott (7) assuming the thermal neutron cross section values of $\sigma_f = 534$ barns and $\sigma_a = 589$ barns (8), and Westcott's r values of 0.026 and 0.018 which were appropriate to the irradiation positions in the reactor. Values of 6.91×10^{17} and 1.036×10^{17} have been estimated for the number of fissions in samples 1 and 2.

¹Manuscript received November 3, 1960.

Contribution from the Chemistry Department, McMaster University, Hamilton, Ontario. Presented at the Third Symposium on Nuclear Chemistry and Radiochemistry held at Atomic Energy of Canada Limited, Chalk River, Ontario, September 6-8, 1960.

TABLE I
Irradiation data for U²³⁵ samples

Sample	U ²³⁵ /U ²³⁸	Weight of U ₃ O ₈ sample (grams)	Time in reactor (days)	ϕt , neutrons/cm ² $\times 10^{-19}$
1	13.30 \pm 0.05	0.04085	55.9	2.16
2	18.54 \pm 0.10	0.03641	30.4	4.77
3	18.54 \pm 0.10	0.02938	30.4	2
4	13.30 \pm 0.05	0.07335	309	0.23

The analysis of the fission products in the samples were carried out by means of the mass spectrometer and isotope dilution techniques as has been previously described (9). Essentially complete recovery of the fission products was obtained by dissolution of the end of the quartz ampoule, which contained the sample, with hydrogen fluoride. After most of the contents had fallen from the ampoule, the remainder was obtained by rinsing the quartz until all radioactivity had been recovered.

Relative yields of masses 85 and 87 have been obtained from rubidium fission products; 88, 89, and 90 from strontium; 91, 92, 93, 94, 95, and 96 from zirconium; 95, 97, 98, and 100 from molybdenum; and 101, 102, 104, and 106 from ruthenium. The relative yields of the six zirconium isotopes were normalized to the four molybdenum isotopes by means of the common measurement at mass 95. Two samples of zirconium fission products were analyzed at less than the Zr⁹⁵ half-life from the time of their formation. The yield of the mass 95 chain relative to other zirconium chains was therefore obtained after decay corrections were applied to the observed mass spectrometric ratios. The molybdenum 95 was observed from the samples after the Zr⁹⁵ had decayed. The ruthenium yields have been normalized to the molybdenum and zirconium yields by the radiochemical normalization given by Katcoff (1). The rubidium yields were normalized to the previously published yields (5) of the krypton isotopes through the mass 85 fission chain, which is common to both elements. The absolute yields of these isotopes were obtained from the previously published (5) ratio of Kr⁸⁶ to Cs¹³³ = 0.567 and the absolute yield of Cs¹³³ = 5.77%, which is obtained below. The absolute yields of the three strontium isotopes were obtained by isotope dilutions.

The present work together with the previously reported mass spectrometric work from this laboratory therefore gives absolute yields of mass chains 83-90 constituting 32.04% of the light mass fission products. Yields of chains below mass 83 have been obtained by extrapolation and when added to the measured yields give a total of 32.94% yield for fragments of mass 90 or less. The yields of masses 91-117 must therefore total 67.06%. The yields of the zirconium, molybdenum, and ruthenium isotopes which had been normalized to each other along with interpolated yields at 99, 103, 105 and extrapolated yields between 107 and 117 have been forced to total 67.06%. Although there are many assumed yields in this grouping their total is only 6.94% of which the assumed yield of 4.84% for mass 99 is the major contribution. The fission yields of the light mass fragments obtained in this manner together with some of the recent literature values are given in Table II. Graphical representation of the present data is given in Fig. 1.

For the heavy mass fragments yields the following procedures were followed. The relative yields of the cesium isotopes 133 and 137 to those of the xenon isotopes 131, 132, and 134 have been previously measured in this laboratory (5). The fission products used in this previous study were formed at high fluxes and the observed Cs¹³⁵ was highly depleted and the observed Xe¹³⁶ equally enhanced by Xe¹³⁵ burning. It was therefore only possible in this work to obtain the sum of the 135 and 136 yields. From sample 4

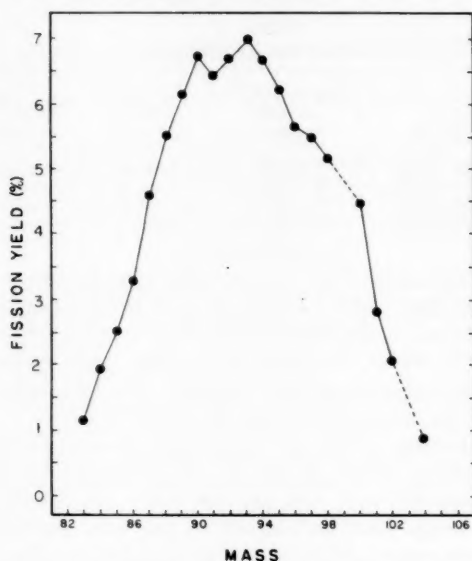
FIG. 1. Light mass yields in thermal neutron fission of U^{235} .

TABLE II
The cumulative yields of the light mass fragments formed in the thermal neutron fission of U^{235}

Mass chain	Cumulative fission yield	Literature values		
		Katcoff (1)	Yaffe (3)	Bartholomew <i>et al.</i> (4)
<80	0.15*			
81	0.25*			
82	0.50*			
83	1.18	1.14		
84	1.97	1.90		
85	2.54	2.45		
86	3.30	3.18		
87	4.61			
88	5.54			
89	6.15	6.5	5.56	5.87
90	6.75		6.19	
91	6.45†	6.53	{ 4.82 (Sr^{91}) 3.55 (Y^{91}) }	5.61
92	6.72†	6.70		
93	7.01†	7.10		
94	6.68†	6.82		
95	6.23†	6.10	{ 5.01 (Zr^{95}) 5.16 (Nb^{95}) }	
96	5.67†	5.60		
97	5.51†	5.35		
98	5.22†	5.18		
99	4.84*	4.8		
100	4.49†	4.40		
101	2.87†	3.00		
102	2.10†	2.37		
103	1.56*	1.6	2.02	
104	0.94†	0.96		
105	0.43*			
106	0.22†	0.28	0.264	
107-117	0.11*			

*Assumed yields; obtained by interpolation or extrapolation of observed data.

†Relative yield normalized to measured yield in such a manner that total of all yields is 100%.

it was possible to obtain the relative yields of the 133, 135, and 137 chains since the correction for Xe^{135} burning was only 1.4%. With the relative yield of the 135 chain it was possible to correct the previously published Xe^{136} yields. The relative yields of Cs^{133} and Cs^{137} found in the fission products of the present samples were essentially the same as those previously published.

Relative yields of the 140, 142, and 144 chains were obtained from cerium isotopes and these were normalized to the relative neodymium yields of isotopes 143, 144, 145, 146, 148, and 150 by means of the isobaric 144 nuclides. The values for the relative yields of the samarium isotopes 149, 151, 152, and 154 have been taken from previously published work from this laboratory (10) since the high neutron cross sections of Sm^{149} and Sm^{151} together with the large integrated fluxes severely altered the measured yields. The sum of Sm^{149} and Sm^{150} relative to the sum of Sm^{151} and Sm^{152} did correspond to the same ratio obtained in the earlier work.

Isotope dilution of the samarium made possible the determination of the number of atoms of Sm^{149} and Sm^{150} , which, together, are the cumulative number of atoms of the mass 149 fission chain. This made possible the normalization of the relative samarium yields to those of neodymium and cesium since both of the latter elements were also isotope diluted. The yields of isotopes of xenon, cesium, cerium, neodymium, and samarium were therefore all normalized to each other.

The atom yields of mass chains 138, 139, 141, 147, and 153 were obtained by interpolation and the yields between 117 and 131 as well as those above 154 were obtained by extrapolation. The atom yields obtained in this manner for the samples 1, 2, and 3 have normalized to total 100%. The average yields obtained from these three determinations are shown in Table III along with some of the recent literature values. The maximum difference between the three values obtained for any yield in the mass region 131-150 was less than 2.0% of the average value for that yield. The yields given in Table I are shown graphically in Fig. 2.

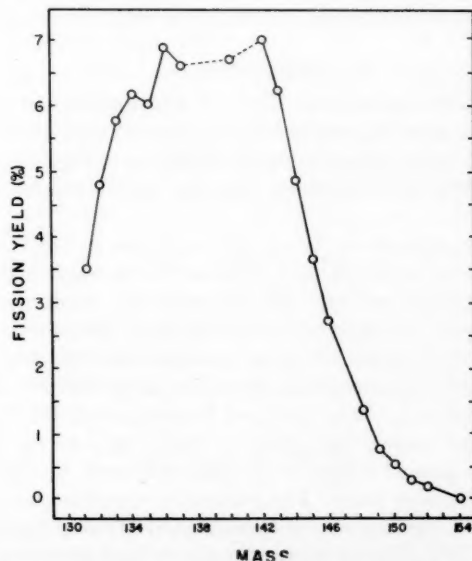


FIG. 2. Heavy mass yields in the thermal neutron fission of U^{235} .

TABLE III
The cumulative yields of the heavy mass fragments formed in the
thermal neutron fission of U^{235}

Mass chain	Cumulative fission yield	Literature values			
		Katcoff (1)	Ivanov (2)	Yaffe (3)	Bartholomew <i>et al.</i> (4)
117-130	3.02†				
131	3.52	3.74		2.84	
132	4.82	5.10		4.64	
133	5.77	6.18	5.5	3.40	
134	6.18	6.54			
135	6.02	>4.9			
136	6.89	<8.9			
137	6.58	7.16	6.16	5.39	
138	6.73†				
139	6.71†				5.59
140	6.72	5.6	6.16	5.48	5.60
141	6.92†			5.30	6.17
142	7.00	5.6	6.06		
143	6.22	5.2	5.19	6.99	
144	4.87	4.0	3.84	3.69	
145	3.66	3.0	2.88		
146	2.74	2.3	2.24		
147	2.08†	1.71			
148	1.40	1.15	1.07		
149	0.790	0.61	0.70		
150	0.567	0.48	0.49		
151	0.334	0.26	0.54		
152	0.222	0.17			
153	0.122†	0.095			
154	0.048	0.037			
155--	0.033†				
	99.97%				

*Average of three independent determinations of which greatest difference in individual yields was about 2%.

†Assumed yields; obtained by interpolation or extrapolation of observed data.

DISCUSSION

It is difficult to assess the absolute accuracy of the yields of the light mass fragments shown in Table II. Only those values between masses 82 and 90 may be considered as absolute, the remainder being relative yields whose normalization has been chosen so that all yields total 100%. It is believed that the values should be within 4% error at each mass.

In general, the yields obtained in the present work are in very good agreement with those listed by Katcoff (1). With the exception of the ruthenium normalization, which involves about 8 fission yield per cent, the yields in this work are independently normalized from those given by Katcoff. The absolute zirconium, molybdenum, and ruthenium yields given by Katcoff are mass spectrometric relative yields by Steinberg *et al.* (11) normalized to the Steinberg radiochemical values for Sr^{89} , Zr^{95} , and Ru^{103} . With these yields and the relative krypton yields of Fleming *et al.* (5), Katcoff has drawn a smooth curve so that the total of the yields is 100%. It is to be noted that Katcoff's zirconium yields are in general higher than those reported in this work, whereas his molybdenum yields are slightly lower. The zirconium-molybdenum normalization given in the present work, through mass spectrometric relative yields determined for mass 95, should be more reliable. The absolute strontium yields, as determined by isotope dilution,

along with the relative rubidium yields, normalized to the krypton yields, give a more complete picture of the left side of the light mass curve than was given by Katcoff.

The data as plotted in Fig. 1 indicates fine structure in the mass 90 region. Since the break from a smooth curve occurs at the mass where the zirconium yields are normalized to the strontium yields, this fine structure may not be real. It is worth noting, however, that the yield of the complementary fragment (approximately mass 142) is also high. A similar fine structure at masses 90 and 144 are observed in U^{235} fission (12) which may lend some weight to the reality of that found in this work. Bartholomew *et al.* (4) have given the ratio of Sr^{89} to Zr^{91} as 1.05:1.00. This is considerably greater than the ratio of 0.95:1.00 found in this work. Had the Bartholomew value been used to normalize the strontium and zirconium yields, the yield of mass 90 would be 15% greater than that of mass 91 and the total of the fission yields would be only 94%.

The yields of the heavy mass fragments given in Table III are considered accurate to within 3%. There are various reasons for considering this to be the case. Firstly, there was excellent correspondence between the yields obtained from the three independent measurements, no yield being as much as 2.0% different from the mean. Secondly, the methods used to normalize the yields of the isotopes of the various elements to each other were direct. Isobaric yield determinations were used to normalize the isotopes of xenon to those of cesium as well as the cerium to the neodymium. Isotope dilution was used to normalize the cesium, neodymium, and samarium element yields. Thirdly, in the cases of samples 1 and 2, whose flux had been monitored, it was possible to estimate the number of fissions and compare these values to the total number of atoms found in all heavy mass fission chains. In samples 1 and 2 the number of fissions estimated were lower than the sum of the atoms found by 4% and 2% respectively. With the possible errors in monitoring the flux and the uncertainty of the fission cross section for the neutron spectra of the irradiation positions, these differences are considered slight. The importance of estimating the number of fissions from the flux and cross section is that this serves as a check against gross errors in normalizing by isotope dilution procedures. Had the differences been greater than were found, considerably less faith would have been given to the yields in Table III.

The yields of the heavy mass fragments found in this work are smaller for the 131-139 mass region and larger for the chains of mass greater than 140 than estimated by Katcoff (1). Since the Katcoff values are largely relative mass spectrometric yields from this laboratory that have been normalized by arbitrary means, there is no inconsistency with the present data. On the other hand the values reported more recently by Yaffe (3) are much lower at every mass with significant yield as are those of Bartholomew *et al.* (4) and Ivanov (2).

There are several criteria for concluding that the present values are approximately correct. Firstly the values measured, together with a relatively small percentage of interpolated values, total 100%. It is difficult to see how this condition can be met by any of the other recent measurements. A critical test of any fission yield curve is the estimation of the total number of neutrons liberated per fission. For U^{235} this may be obtained from the relation

$$\nu = 234 - \frac{\sum \text{mass} \times \text{yield}}{\text{yield}}$$

where ν is the average number of neutrons, including delayed neutrons, liberated per fission. This relation should be valid provided that insignificant amounts of light particles

and ternary fission products are formed. Since ν obtained from this relation is the difference between two comparable numbers it is very sensitive to small errors in the values of the yields used. With the yields given in Tables II and III a value of 2.32 is obtained which may be considered in fair agreement with the accepted value of 2.51 given by Hughes and Harvey (8).

Careful normalization of the xenon and cesium yields, and cesium ratios obtained from a thermal column irradiation, ensure the reality of the fine structure appearing at mass 134 (Fig. 2). Although it is much smaller in magnitude, it is similar to that found in the thermal neutron fission of U^{235} and other nuclides. The apparently high yield at mass 136 can in part be smoothed out by correction for delayed neutron emission.

Keepin *et al.* (13) attribute a 0.197% chain transfer to delayed neutron emission by I^{137} . Together with delayed neutron emission in the mass 138 and 139 chains (13) most of the mass 136 fine structure would be removed.

ACKNOWLEDGMENTS

We wish to thank the Atomic Energy of Canada Limited for the neutron irradiations and the National Research Council of Canada for financial assistance.

REFERENCES

1. S. KATCOFF. *Nucleonics*, **16**, 78 (1958).
2. R. N. IVANOV, V. K. GORSHKOV, M. P. ANIKINA, G. M. KUKAVADZE, and B. V. ERSHLER. *J. Nuclear Energy*, **9**, 46 (1959).
3. D. C. SANTRY and L. YAFFE. *Can. J. Chem.* **38**, 421 (1960).
4. R. M. BARTHOLOMEW, J. S. MARTIN, and A. P. BAERG. *Can. J. Chem.* **37**, 660 (1959).
5. W. FLEMING, R. H. TOMLINSON, and H. G. THODE. *Can. J. Phys.* **32**, 522 (1954).
6. H. R. FICKEL and R. H. TOMLINSON. *Can. J. Phys.* **37**, 926 (1959).
7. C. H. WESTCOTT. Atomic Energy of Canada Limited, CRRP-787. 1958.
8. D. J. HUGHES and J. A. HARVEY. Brookhaven National Laboratory, BNL-325. 1958.
9. J. A. PETRUSKA, E. A. MELAIKA, and R. H. TOMLINSON. *Can. J. Phys.* **33**, 640 (1955).
10. E. A. MELAIKA, M. J. PARKER, J. A. PETRUSKA, and R. H. TOMLINSON. *Can. J. Chem.* **33**, 830 (1955).
11. E. P. STEINBERG, L. E. GLENDENIN, M. G. INGRAM, and R. J. HAYDEN. *Phys. Rev.* **95**, 867 (1954).
12. J. A. PETRUSKA, H. G. THODE, and R. H. TOMLINSON. *Can. J. Phys.* **33**, 693 (1955).
13. G. R. KEEPIN, T. F. WIMETT, and R. K. ZEIGLER. *J. Nuclear Energy*, **6**, 1 (1957).

DISTRIBUTION OF NUCLEAR CHARGE IN THE PROTON-INDUCED FISSION OF Th^{232}

PART II¹

A. KJELBERG,² H. TANIGUCHI,³ AND L. YAFFE

ABSTRACT

The fractional chain yields of Ga^{72} , Br^{82} , Ag^{112} , and La^{140} , formed in the proton-induced fission of Th^{232} , have been measured at proton energies ranging between 12.8 and 82.4 Mev. The yields are compared with data previously obtained by others from uranium and thorium fission, and with predictions made by Coryell.

During the course of this investigation, the half-life of Zn^{72} was checked and found to be 46.5 ± 0.1 hours, rather than 49 hours as previously reported.

INTRODUCTION

A great deal of data has been amassed dealing with the distribution of nuclear mass in fission. Nevertheless, studies in this aspect are still going on since many of the data published are in disagreement, especially those obtained by mass spectrometry as compared with those obtained radiochemically. While the above state of affairs is semisatisfactory, that of the charge distribution in fission is as yet highly unsatisfactory. A small amount of data has been accumulated for thermal fission and very much less for higher-energy fission.

One attempts to obtain a value for the most probable charge, Z_p , by reference to various postulates regarding the mechanism in which the fission act takes place. These postulates are summarized below:

(1) *Unchanged Charge Distribution (UCD)*

This suggests that, by analogy to the simplest form of the liquid drop model, the charge divides in the same manner as it was present in the fissioning nucleus, i.e. the neutron-to-proton ratio is the same in the fragments as in the parent nucleus.

(2) *Minimum Potential Energy (MPE)*

This proposes that the fission act is preceded by a nucleonic rearrangement such that the fission will take place in a manner to minimize the sum of the binding energies, the decay energies, and the electrostatic energy of mutual repulsion (calculated from two spheres in contact).

The thermal fission data collected did not support either hypothesis, although some evidence purported to show that the former held true for higher-energy fission.

(3) *The Postulate of Equal Charge Distribution (ECD)*

This suggestion was empirically derived by Glendenin, Coryell, and Edwards (1). In effect, mathematically, it tells us that

$$Z_{pL} - Z_{AL} = Z_{pH} - Z_{AH}$$

where L and H refer to the heavy and light fragments, Z_p again is the most probable charge, and Z_A is the non-integral value of the most stable charge for nuclides of mass A .

¹Manuscript received November 7, 1960.

Contribution from the Radiochemistry Laboratory, Department of Chemistry, McGill University, Montreal, Que., with financial assistance from the National Research Council of Canada, Ottawa, Canada. Presented at the Third Symposium on Nuclear Chemistry and Radiochemistry held at Atomic Energy of Canada Limited, Chalk River, Ontario, September 6-8, 1960.

²Present address: Nuclear Chemistry Division, Department of Chemistry, Oslo University, Blindern, Norway.

³Present address: Department of National Health and Welfare, Ottawa, Ontario.

(4) *The Postulate of Non-Uniform Charge Distribution (NUCD)*

This theory, proposed originally by Present (2), proposes a division of charge calculated on the basis of two spherical nuclei in contact. The charge distribution in such a system is expected to be non-uniform radially due to the tendency of the charge to collect at the surface of a body and will result in the smaller fraction of an asymmetric division having a greater charge-to-mass ratio than the larger.

The latter two postulates give predictions which, at thermal energies, are reasonably concordant with the data. Inherent in the third postulate is the assumption that the same symmetrical charge distribution curve can be used to describe all fission-product chains. Indeed it has been used for all heavy fissioning nuclei.

A great deal of discussion has taken place regarding the proper value of Z_A to be used. Glendenin *et al.* (1) used a continuous Z_A function while Pappas (3) and others have suggested a Z_A function that was discontinuous at shell edges. This controversy is still raging.

Wahl (4) suggested the use of an empirical Z_p curve obtained directly from independent and cumulative yield values and the universal charge distribution curve. This showed a good degree of success for thermal fission as most data were found to lie on the empirical Z_p curve.

Unfortunately very little of the above-mentioned reasoning applies in the case of higher-energy fission. No satisfactory postulate for determining Z_p has as yet appeared. No universal charge distribution curve is known. Neutron emission soon begins to compete favorably with fission so that a variety of fissioning nuclei have to be taken into account.

The problem is made more difficult because of the paucity of high-energy independent yield data available. The paper by Pate, Foster, and Yaffe (5) summarizes those up to the beginning of 1958. Other papers of interest are those of Alexander and Coryell (6) and Stevenson *et al.* (7), which give some later references. It rapidly becomes apparent that one cannot use a single-charge distribution curve to fit all the data. Thus it is of some interest then to accumulate independent yield data to determine the best method of finding Z_p .

The paper by Pate, Foster, and Yaffe gave values for independent yields of isotopes of iodine and tellurium in the mass range 130 to 135. A study of this mass range permitted conclusions to be drawn regarding the variation with energy of the charge distribution, neglecting possible effects of mass number.

The previous work has been extended to give information about the range of mass numbers 72 to 140. Similar results at higher energies are now available for the proton-induced fission of uranium. These enable one to study the variation of charge distribution with atomic number of target and mass number of the products.

For the study of charge distribution the relatively few shielded nuclides are best suited. There are, however, also some semishielded nuclides, with a precursor of a long half-life compared with that of the daughter, and these can, under specific conditions, give valuable information. A study of the shielded nuclide Br^{82} , and the semishielded nuclides Ga^{72} , Ag^{112} , and La^{140} , in the energy interval of 15 to 85 Mev, is reported here.

EXPERIMENTAL TECHNIQUES

(a) *Target and Irradiation*

The target and irradiation details were essentially as reported by Pate *et al.* (5). Three thorium metal foils of about 200 mg/cm² superficial density were carefully aligned and

bombarded in the internal proton beam of the McGill 82-in. synchrocyclotron. The outer foils, serving as guard foils correcting for recoil losses, were discarded and the central foil was used for chemical processing. As the calculations of fractional yields were independent of absolute yield determinations, no monitoring of the proton beam was necessary.

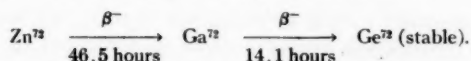
The energy of the bombarding protons was obtained from a known radius-energy relation (8). Corrections for energy loss for the protons in the target itself were calculated using data from Aron *et al.* (9). Bombardments were of $\frac{1}{2}$ - to 1-hour duration.

(b) *Chemical Processing and Measurement*

In the case of the semishielded isotopes, two separations of the nuclide in question were performed from the same master solution. The first sample contained the activity formed independently and that produced by decay during bombardment and in the short time interval before the separation from the precursor in the chain. The second sample contained activity formed by decay of the precursor only and gave information on the chain yield. Complete separation of the nuclide from its precursor and accurate timing of the separations were essential.

(i) Ga⁷²

This nuclide occurs in the following fission product chain:

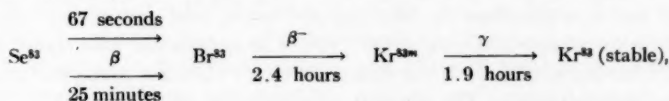


The thorium target foil was dissolved in concentrated hydrochloric acid (with SiF₆⁻ catalyst present) shortly after bombardment. The separation occurred essentially as described by Siegel and Glendenin (10), except for the elimination of Ga₄[Fe(CN)₆]₃ precipitation, which had been found to be unsatisfactory (11). Briefly, gallium and zinc carriers were added and gallium was separated from zinc and most fission products by twice extracting with ethyl ether from 6 *N* hydrochloric acid. The time of the second ether extraction was used as the time of separation of Ga⁷² from Zn⁷². Gallium was further purified by a number of scavenging precipitations and repeated extractions. Care was taken in all operations to avoid any loss of Zn⁷². Gallium carrier was added to the master solution containing the zinc, and after about 1 day a second separation was performed using the same procedure. The two samples obtained, Ga-I and Ga-II, were made to equal volume in counting vials and the activity determined using a well-type gamma scintillation counter. Since all measurements were relative, absolute disintegration rates did not have to be determined.

By tracer experiments it was found that the loss of zinc by coextraction with gallium, and the retention of gallium with zinc, were 1% or less under the experimental conditions used. Chemical yields were determined by EDTA titrations (12).

(ii) Br⁸²

This nuclide (35.9 hours) is shielded. Br⁸², which occurs in the chain,



was used as an internal monitor for Br⁸² (see section "Treatment of Data"). After dissolution of the target (ice-cooled), bromine was separated about 4 hours after bombardment. This allowed complete decay of Se⁸² to Br⁸². The chemical method used was,

with minor modifications, that of Glendenin *et al.* (13), and is based on cyclic extractions of bromine into and out of carbon tetrachloride by successive oxidation and reduction steps.

Two points were specifically checked, namely possible loss of bromine during dissolution of the target, and completeness of exchange between carrier and active bromine. In one experiment, during dissolution, air was slowly bubbled through the ice-cooled solution and any bromine possibly escaping was trapped in sulphurous acid. No evidence of bromine activity was found in the trap, as determined by measurement of the activity of the chemically separated bromine. Also in one case the initial separation was carried out in duplicate using bromine and bromate carriers, respectively, to check the exchange. The bromate portion was reduced with hydrogen sulphide and the separation was continued in a manner identical with that used with the bromide carrier. No detectable difference attributable to the different carriers was found in the resultant samples. This is similar to results obtained for iodine when the irradiated material is a metallic matrix. Therefore the direct use of bromide carrier was chosen for subsequent separations.

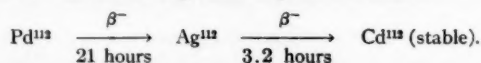
The final solution was slightly acidic with the activity in the form of bromide. To prevent losses due to volatilization, the solution was neutralized with a measured amount of lithium hydroxide. The chemical yields were determined by titration according to Volhard's method.

The activity was measured with a 4π β -counter (14-18). To prevent loss of bromine during preparation of the samples (heating under an infrared lamp), about 100% excess silver nitrate was added. This is the same technique used by Pate *et al.* (5). It was found that the $\text{Kr}^{83\text{m}}$ formed by decay of Br^{83} contributed significantly to the count rate of the sample through the conversion electrons from its 0.033-Mev gamma transition.

This krypton activity could not be removed by reheating the sample. Fresh samples therefore were periodically prepared to construct the decay curve of Br^{83} . This introduced a slight uncertainty in the time for the last separation from krypton, as the drying of the sample required about 30 minutes. It was later found that the addition of silver nitrate to the bromide solution was unnecessary, provided a slight excess of lithium hydroxide was present. The lithium bromide sources were much thinner and more uniform and permitted the krypton to diffuse out of the sample completely. No loss of bromine activity was detected using this technique. The thinner sources were also better suited for accurate self-absorption corrections. Incidentally, a similar technique was found to work well for iodine samples in so far as lithium iodide continually released xenon formed by decay of iodine activity, in contrast to what was found for silver iodide (5). No measurable loss of iodine activity was found.

(iii) Ag^{112}

This nuclide occurs in the following fission product chain:



The target foil was dissolved in concentrated nitric acid containing silver carrier to prevent adsorption losses of active silver (19). The separation essentially followed the procedure of Glendenin (20) and was based on silver chloride precipitations alternated by scavenging precipitations. The time of separation of Ag^{112} from Pd^{112} was taken as the time of centrifugation of the silver chloride first precipitated, about 2 minutes after precipitation. This should therefore take care of exchange between silver chloride and active silver after precipitation.

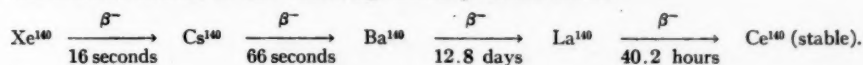
The second sample was separated by adding silver carrier to the hot master solution. After 2 minutes of vigorous stirring, the silver chloride was centrifuged and further purified. The time for separation of Ag¹¹² from Pd¹¹² was again taken as the time at the start of centrifugation.

Tracer experiments showed that less than 2% of Pd¹¹² was lost from the collected master solution by the silver chloride precipitations. Another point of concern was whether complete exchange was obtained between Ag¹¹² and silver carrier added for the second silver sample, Ag-II. As this carrier was added to a solution containing some hydrochloric acid (less than 1 *N*), one inevitably had precipitation of silver chloride before complete mixing took place. Sunderman and Meinke (21) have found that the exchange between freshly precipitated inactive silver chloride and active silver tracer is very rapid at high temperatures. Their data indicate that, under the conditions used, well above 95% exchange was obtained. The reproducibility of the experiments was quite good, confirming a rapid exchange. The chemical yields were determined by titration according to Volhard's method. In a few ammoniacal samples, EDTA titrations (22) were used.

The two samples Ag-I and Ag-II were made up of equal volume and the activity determined by gamma-ray measurement. Ag¹¹² and Ag¹¹³ have half-lives which are fairly close, 3.2 and 5.3 hours respectively. Since Ag¹¹³ was reputed to have no gamma ray with energy greater than 0.3 Mev, an attempt was made to measure only the high-energy gamma rays of Ag¹¹². It was soon found that a considerable portion of the Ag¹¹³ decay took place via high-energy gamma transitions (23). Subsequent measurements were performed using a 3 in. X 3 in. NaI (Tl) crystal coupled to a 100-channel pulse-height analyzer. Gamma rays of 1.3 Mev and higher gave a pure 3.2-hour decay curve for Ag¹¹².

(iv) La¹⁴⁰

This nuclide occurs in the following fission product chain:



The target foil was dissolved in nitric acid in the presence of lanthanum and barium carriers. Barium chloride was then separated from the ice-cooled solution by addition of hydrochloric acid - ether mixture. Twice again barium carrier was added to complete the removal of Ba¹⁴⁰. The combined barium chloride precipitates were dissolved and a small precipitate formed by the addition of ammonia (caused by traces of thorium and lanthanum). This precipitate was further purified to remove barium and combined with the master solution for later separation of La-I. To the combined solutions containing barium was added lanthanum carrier, and this was stored for subsequent separation of La-II. According to Sunderman and Meinke (21) the above procedure should separate barium from lanthanum without loss.

The La-I was further purified by removal of thorium by precipitation as iodate. The solution was allowed to stand for 2 days so that short-lived activities could die away, cerium carrier was added, oxidized with bromate, and removed by precipitation as iodate. Ruthenium sulphide was next precipitated, and the final purification performed by passing a solution in 9 *N* hydrochloric acid through a Dowex-1 anion exchange column. The time of the first precipitation with ammonia in the barium solution was taken as the time of separation of La¹⁴⁰ from Ba¹⁴⁰ in La-I.

The samples were made to equal volume. It was found, despite the fact that no attempt had been made to effect a separation of lanthanum from the rest of the rare

earth elements, that a measurement of the 1.6-Mev gamma peak gave a decay curve with a 40.2-hour half-life (less than 1% long-lived contamination).

RESULTS AND DISCUSSION

(a) Decay Curves

The gallium samples Ga-I showed a very high proportion of the 4.87-hour Ga^{72} . When this was allowed to decay, the 14.1-hour Ga^{72} could be quite easily measured, although at the very lowest bombardment energies the activity of Ga^{72} was very low. A few samples showed long-lived contaminating activities, for which corrections were made. The Ga-II samples generally showed a pure 14.1-hour decay curve.

The half-life of Zn^{72} was checked and was found to be 46.5 ± 0.1 hours rather than 49.0 ± 1 hours as reported (24).

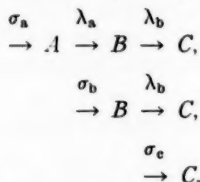
The bromine samples showed only the 35.9-hour Br^{82} and 2.4-hour Br^{83} activities, with 1.9-hour Kr^{83m} contributing in some samples, as discussed previously.

In the silver samples which were measured on the gamma spectrometer, only the 3.2-hour Ag^{112} was observed, with a trace of a long-lived tail in the Ag-I samples, presumably the 270-day Ag^{110m} .

The lanthanum samples showed a decay of 40.2 hours, the half-life of La^{140} , with the La-I samples containing less than 1% of longer-lived activities.

(b) Treatment of the Data

Using the same symbols as Pate *et al.* (5), the general case under consideration is



The fractional chain yield of B is then given by

$$[1] \quad f = \frac{\sigma_b}{\sigma_a + \sigma_b + \sigma_c}$$

where it is assumed that σ_a represents the total yield of A formed independently and by decay of the short-lived precursors in the chain. These are assumed to have disintegration constants very much larger than A and will not be present at the time of chemical separation.

The rate of formation of any nuclide n is given by

$$[2] \quad r_n = Nf\sigma_n$$

where N and f are the number of target nuclei and bombarding particle flux, respectively, and σ_n is the appropriate cross section.

The bombardment time is T , the time between the end of bombardment and the first separation of the nuclide B from its precursor A is t_1 , the time between the first and second separation t_2 . Generally, the disintegration rate $D_b(T, t_1)$ of B at time t_1 is

$$[3] \quad D_b(T, t_1) = Nf \left[\sigma_a \left[\frac{\lambda_b}{\lambda_b - \lambda_a} (1 - e^{-\lambda_a T}) e^{-\lambda_a t_1} - \frac{\lambda_a}{\lambda_b - \lambda_a} (1 - e^{-\lambda_b T}) e^{-\lambda_b t_1} \right] + \sigma_b [(1 - e^{-\lambda_b T}) e^{-\lambda_b t_1}] \right].$$

For a shielded nuclide, where A is stable, this reduces to

$$[4] \quad D_b(T, t_1) = Nf\sigma_b(1 - e^{-\lambda_b T})e^{-\lambda_b t_1}.$$

If $\lambda_a > \lambda_b$, and $t_1 \gg \ln 2/\lambda_a$, equation [3] can be transformed into

$$[5] \quad D_b(T, t_1) = Nf(\sigma_a + \sigma_b)(1 - e^{-\lambda_b T})e^{-\lambda_b t_1} \times P$$

where

$$[6] \quad P = \frac{\lambda_a}{\lambda_a - \lambda_b} \left(1 - \frac{\lambda_b}{\lambda_a} \frac{\sigma_b}{\sigma_a + \sigma_b} \right).$$

The factor P is always larger than unity and less than $\lambda_a/(\lambda_a - \lambda_b)$.

If $\lambda_a < \lambda_b$ and $t_1 < (\ln 2/\lambda_a)$, equation [3] applies and gives the amount of B formed independently and by decay from A .

A second separation of B from A at the time t_2 after the first separation will give B formed by decay from A only and will be given by

$$[7] \quad D_b(t_2) = Nf\sigma_a(1 - e^{-\lambda_a T})e^{-\lambda_a t_1} \frac{\lambda_b}{\lambda_b - \lambda_a} (e^{-\lambda_a t_2} - e^{-\lambda_b t_2}).$$

In the experiments with Ga^{72} , Ag^{112} , and La^{140} , the appropriate equations are [3] and [7]. Here, N , f , σ_a , and σ_b are unknown, the rest are experimentally determinable terms. If therefore for these determinable terms one inserts 'constants' k_i as follows, equations [3] and [7] become

$$[8] \quad k_1 = Nf(\sigma_a k_2 + \sigma_b k_3),$$

$$[9] \quad k_4 = Nf\sigma_a k_5.$$

If equation [8] is divided by equation [9] and terms are rearranged, then

$$[10] \quad \frac{\sigma_b}{\sigma_a} = \frac{1}{k_3} \left(\frac{k_1 k_5}{k_4} - k_2 \right) = k_6.$$

Substitution in equation [10] to solve for k_6 gives

$$[11] \quad k_6 = \frac{1}{\lambda_b - \lambda_a} \left\{ \lambda_b \frac{1 - e^{-\lambda_a T}}{1 - e^{-\lambda_b T}} e^{(\lambda_b - \lambda_a) t_1} \left[\frac{D_b(T, t_1)}{D_b(t_2)} (e^{-\lambda_a t_2} - e^{-\lambda_b t_2}) - 1 \right] + \lambda_a \right\}.$$

The fractional chain yield as defined in equation [1] becomes

$$[12] \quad f = \frac{\sigma_b}{\sigma_a + \sigma_b + \sigma_c} \simeq \frac{\sigma_b}{\sigma_a + \sigma_b} = \frac{k_6}{1 + k_6}$$

provided $\sigma_c \ll \sigma_a + \sigma_b$, which generally is the case in these experiments. For the worst possible case, La^{140} at the highest energy, this would give a yield about 4% too high.

It is seen that only the ratio between the disintegration rates for two samples is required, thus facilitating the simple sample preparation and counting method used.

In the case of the shielded nuclide Br^{82} , the Br^{83} was used as an internal monitor for the beam. In equations [4] and [5] the factors N and f are the same for Br^{82} and Br^{83} , but the cross sections refer to different chains. Provided a relation between the yields for the chains 82 and 83 were known, such as

$$[13] \quad (\sigma_a + \sigma_b)_{82} = R(E)(\sigma_a + \sigma_b)_{83}$$

where $R(E)$ is an energy-dependent function, equations [4] and [5] can be used directly.

With the previous notation, if $x = \text{Br}^{82}$, $y = \text{Br}^{83}$, and $z = \text{Se}^{83}$, then

$$[14] \quad \frac{D_x(T, t_1)}{D_y(T, t^1)} = \frac{\sigma_z(1 - e^{-\lambda_z T})e^{-\lambda_z t}}{P(\sigma_x + \sigma_y)(1 - e^{-\lambda_y T})e^{-\lambda_y t^1}}$$

or

$$[15] \quad f = \frac{\sigma_z}{R(E)(\sigma_x + \sigma_y)} = \frac{PD_x(T, t_1)(1 - e^{-\lambda_y T})e^{-\lambda_y t^1}}{R(E)D_y(T, t^1)(1 - e^{-\lambda_z T})e^{-\lambda_z t}}$$

where t and t^1 are times after bombardment when the activities of Br^{82} and Br^{83} were measured. According to equation [6], for this specific chain

$$[16] \quad P = \frac{\lambda_{\text{Se}^{83}}}{\lambda_{\text{Se}^{83}} - \lambda_{\text{Br}^{83}}} \left[1 - \frac{\lambda_{\text{Br}^{83}} \sigma_{\text{Br}^{83}}}{\lambda_{\text{Se}^{83}} (\sigma_{\text{Se}^{83}} + \sigma_{\text{Br}^{83}})} \right].$$

An estimate of the function $R(E)$ as defined in equation [13] can be made using the rather limited chain yield data available for thorium and uranium proton-induced fission at higher energies. For thorium, data are available only for the energy interval 8 to 21 Mev (25), except for one value at 450 Mev (26). Therefore data for uranium have been used to establish a trend, and a somewhat idealized curve for the function $R(E)$ for uranium has been established. The same curve shape has been assumed valid for thorium, with a shift in ordinate as shown in Fig. 1. The equation for $R(E)$ for

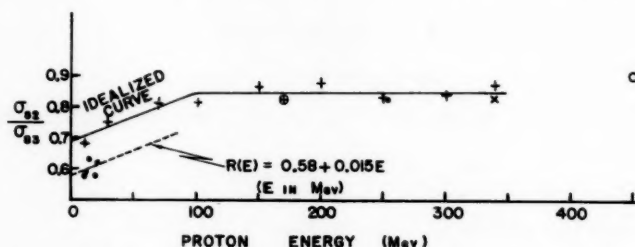


FIG. 1. Variation of the ratio of yields of Br^{82} to Br^{83} with proton-bombarding energy: ● Th fission (25), ○ Th fission (26), + U fission (7), × U fission (30), ⊕ U fission (27).

thorium deduced on this basis is

$$[15] \quad R(E) = 0.58 + 0.015E$$

where E is in Mev. The energy interval of interest was 15 to 85 Mev, and here $R(E)$ varies between 0.60 and 0.71, and the absolute uncertainty in these values is probably not more than about 10%.

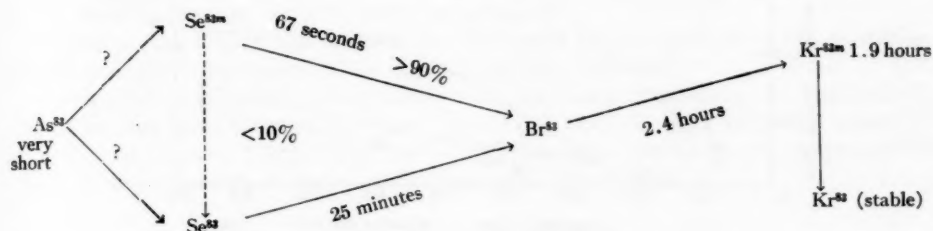
The factor P in equation [14] has also been estimated. Inserting values for the disintegration constants one gets

$$[16] \quad P = 1.21 \left(1 - 0.174 \frac{\sigma_{\text{Br}^{83}}}{\sigma_{\text{Se}^{83}} + \sigma_{\text{Br}^{83}}} \right).$$

The ratio of the independent cross section of Br^{83} to that of the chain up to and including that nuclide can be estimated from Fig. 8 in reference 5 to be about 0 to 0.19 for the energy interval of concern. (Allowance has been made for the finding in the present

work that the abscissa scale should be shifted about 1.0 unit to the left for the mass number 83, i.e. to indicate a longer chain.) P therefore varies from 1.17 to 1.21 for the energy interval 15 to 85 Mev.

A more difficult factor to evaluate is the effect of the short-lived isomer Se^{83m} . The decay scheme for the 83-chain is



The factor P as already calculated is a maximum value, as it is assumed that all of Br^{83} is produced via Se^{83} . Any Se^{83m} in the chain produced by decay or by independent formation will make P approach 1.00.

No general conclusion as to the variation of the yields of isomers with energy can presently be drawn from the limited amount of experimental data available (26). In addition, the chain contribution from As^{83} is unknown. Therefore, a mean value for P of 1.10 for the whole energy interval was used, a factor which at most can have an error of 10%.

The fractional yields for Ga^{72} , Br^{82} , Ag^{112} , and La^{140} are given in Table I. Figure 2 gives these results together with similar data taken from reference 5. Also given are the values of $Z_A - Z$, the distance of the nuclide from the most stable charge for the mass number A (27, 28). For comparison, Fig. 3 gives similar data for uranium fission (7, 29).

TABLE I
Fractional chain yields, in per cent

Energy in Mev	12.8	17.2	18.6	25.8	36.1	39.5	40.7	55.5	82.4
Ga^{72}					2.1		3.3	6.8	13.2
Br^{82}	0.43		0.67			3.5		6.2	10.9
									12.5
Ag^{112}		1.8		3.5			5.8	7.7	15.4
								8.9	15.8
La^{140}				4.3				22	22

The errors associated with the fractional yield data are due mainly to (a) uncertainty in the exact proton energy at which the bombardments were made due to the radial distribution of the proton beam and (b) energy losses in the target itself as calculated (9). Nevertheless the beam energy was probably known to 2-5 Mev. The disintegration rates were measured relatively so that errors associated with these are small ($\sim 1\%$). The graphical decay curve analyses, associated extrapolation data and chemical analyses, present no difficulties and these errors are certainly less than 5%. It is believed that an uncertainty of $\pm 10\text{--}15\%$ on an over-all basis would cover the above and include systematic errors.

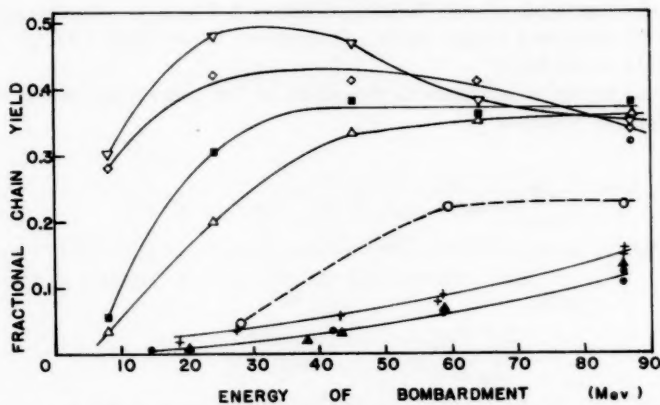


FIG. 2. Fractional chain yield in Th^{232} proton fission. (Values of $Z_A - Z$ in parentheses.) This work: \blacktriangle Ga^{72} (1.0), \bullet Br^{82} (0.8), $+$ Ag^{112} (1.4), \circ La^{140} (1.0). Pate *et al.* (5): \odot I^{130} (0.8), \triangle I^{131} (1.1), ∇ Te^{131} (2.1), \blacksquare I^{132} (1.5), \diamond I^{134} (2.2).

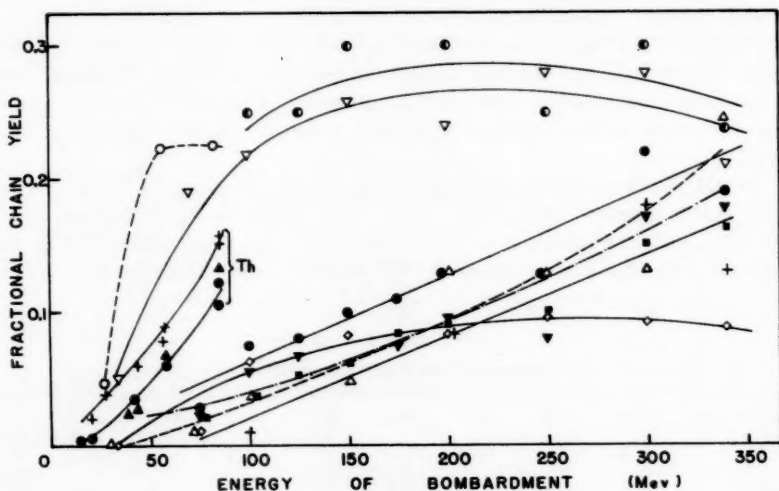


FIG. 3. Fractional chain yields in the proton-induced fission of thorium and uranium. (Values of $Z_A - Z$ in parentheses.) This work: \blacktriangle Ga^{72} (1.0), \bullet Br^{82} (0.8), $+$ Ag^{112} (1.4), \circ La^{140} (1.0). Hicks and Gilbert (29): U^{238} (p, f): \blacktriangledown Br^{80} (0.0), \bullet Br^{82} (0.8), \blacksquare Nb^{98} (1.2), $+$ Ag^{112} (1.4), \bullet Cs^{138} (0.9). Stevenson *et al.* (7): U^{238} (p, f): \triangle Y^{90} (0.6), ∇ La^{140} (1.0), \diamond Pr^{143} (0.9).

It is very difficult at this point, with the scarcity of data available in this energy range, to discuss the results theoretically. One cannot draw reasonable charge distribution curves to obtain a Z_p value at each energy as Pate, Foster, and Yaffe (5) did since the range of $Z_A - Z$ values covered here is so small.

Coryell (31) has devised an elegant method for deriving Z_p values for any nuclide formed in fission at the energies with which we are concerned. Essentially he assumes that the excited nucleus, after bombardment, will de-excite by neutron emission and,

after neutron boil-off, fission then occurs. He then used the Z_p values obtained from U^{235} thermal fission and derives the appropriate Z_p value for another mode of fission by the following equation:

$$Z_{p_{\text{corr}}} = Z_p - \frac{1}{2}(Z_e - 92) + 0.21(A_e - 236) - 0.19 \times 0.12(E^* - 6.5)$$

where $Z_{p_{\text{corr}}}$ and Z_p are the most probable charges for that mass for the mode of fission being investigated and for U^{235} fission respectively.

Z_e and A_e are charge and mass of the compound nucleus, and E^* is the excitation energy calculated by means of an appropriate mass formula.

No complete application of this equation has been made to our data, but qualitatively the fit on this basis between the Pate, Foster, and Yaffe (5) data and those presented in this paper is good. Further data are now being accumulated to enable an appropriate check of this equation at these medium energies.

REFERENCES

1. L. E. GLENDENIN, C. D. CORYELL, and R. R. EDWARDS. *Phys. Rev.* **75**, 337 (1949).
2. R. D. PRESENT. *Phys. Rev.* **72**, 7 (1947).
3. A. C. PAPPAS. U.S. Atomic Energy Commission Report AECU-2806. 1953.
4. A. C. WAHL. *J. Inorg. & Nuclear Chem.* **6**, 263 (1958).
5. B. D. PATE, J. S. FOSTER, and L. YAFFE. *Can. J. Chem.* **36**, 1691 (1958).
6. J. M. ALEXANDER and C. D. CORYELL. *Phys. Rev.* **108**, 1274 (1957).
7. P. C. STEVENSON, H. G. HICKS, W. E. NERVIK, and D. R. NETHAWAY. *Phys. Rev.* **111**, 886 (1958).
8. R. E. BELL. Private communication.
9. W. A. ARON, B. G. HOFFMAN, and F. C. WILLIAMS. U.S. Atomic Energy Commission Report AECU-663. 1951.
10. J. M. SIEGEL and L. E. GLENDENIN. *National Nuclear Energy Series. Div. IV, Vol. 9, Paper 227, Book 3.* McGraw-Hill Book Co., Inc., New York. 1951.
11. W. W. MEINKE. U.S. Atomic Energy Commission Report AECD-2738. 1949.
12. H. FLASCHKA and H. ABDINE. *Mikrochim. Acta*, 657 (1954).
13. L. E. GLENDENIN, R. R. EDWARDS, and H. GEST. *National Nuclear Energy Series, Div. IV, Vol. 9, Paper 232, Book 3.* McGraw-Hill Book Co., Inc., New York. 1951.
14. B. D. PATE and L. YAFFE. *Can. J. Chem.* **33**, 15 (1955).
15. B. D. PATE and L. YAFFE. *Can. J. Chem.* **33**, 610 (1955).
16. B. D. PATE and L. YAFFE. *Can. J. Chem.* **33**, 929 (1955).
17. B. D. PATE and L. YAFFE. *Can. J. Chem.* **33**, 1656 (1955).
18. B. D. PATE and L. YAFFE. *Can. J. Chem.* **34**, 265 (1956).
19. R. L. FOLGER and H. G. HICKS. U.S. Atomic Energy Commission Report UCRL-432. 1949.
20. L. E. GLENDENIN. *National Nuclear Energy Series. Div. IV, Vol. 9, Paper 267, Book 3.* McGraw-Hill Book Co., Inc., New York. 1951.
21. D. N. SUNDERMAN and W. W. MEINKE. *Anal. Chem.* **29**, 1578 (1957).
22. H. FLASCHKA. *Mikrochim. Acta*, 38 (1952).
23. A. KJELBERG, H. TANIGUCHI, and L. YAFFE. *Can. J. Phys.* **38**, 866 (1960).
24. J. W. SIEGEL and L. E. GLENDENIN. *National Nuclear Energy Series, Div. IV, Vol. 9, Paper 53, Book 2.* McGraw-Hill Book Co., Inc., New York. 1951.
25. H. A. TEWES and R. A. JAMES. *Phys. Rev.* **88**, 860 (1952).
26. P. KRUGER and N. SUGARMAN. *Phys. Rev.* **99**, 1459 (1955).
27. A. KJELBERG and A. C. PAPPAS. *Nuclear Phys.* **1**, 322 (1956).
28. C. D. CORYELL. *Ann. Rev. Nuclear Sci.* **2**, 305 (1953).
29. H. G. HICKS and R. S. GILBERT. *Phys. Rev.* **100**, 1286 (1955).
30. R. L. FOLGER, P. C. STEVENSON, and G. T. SEABORG. *Phys. Rev.* **98**, 107 (1955).
31. C. D. CORYELL. *Can. J. Chem.* **39**, 000 (1961).

SEARCH FOR CORRELATIONS OF MOST PROBABLE NUCLEAR CHARGE Z_P OF PRIMARY FISSION FRAGMENTS WITH COMPOSITION AND EXCITATION ENERGY¹

CHARLES D. CORYELL, MORTON KAPLAN,² AND RICHARD D. FINK³

ABSTRACT

The repartition of nuclear charge in fission has a narrower dispersion than almost any other property connected with the fission process. To a crude approximation, the distribution of nuclear charge between light and heavy partners L and H leads to the most probable charges $(Z_P)_L$ and $(Z_P)_H$ displaced from the respective charges Z_A of β -stability by the same amount for the two fragments (Glendenin rule of equal charge displacement ECD, 1946). The existence of shell offsets in the Z_A vs. A function for different neutron- and proton-shell regions must be considered. All available data for thermal fission $U^{235}(n_{th},F)$ are examined critically. The data show sudden offset-like drifts (fine structure) that may well be associated with shell properties of the products before the "neck" has dissolved. It is shown that these data eliminate naive equal charge displacement ECD, also an older competitive prescription of constant charge ratio CCR for the products, and an empirical Russian prescription (Apalin *et al.*, 1960). The data are also examined in the light of the postulate that fission gives minimum nuclear plus coulombic potential energy (Present 1947, Fong 1955, Swiatecki-Blann 1960), and it is shown that the present mass formulas give too much uncertainty three to four β -decays from stability to give a useful test, but that shell effects in masses must be retained. Data from charged-particle fission with energy deposit up to 40–50 Mev are in reasonable accord with the low-energy data on correcting for composition and neutron boil-off. It is concluded from experiment that Z_P is a single-valued function of A , known to about ± 0.15 unit for low-energy fission and ± 0.25 unit for medium-energy fission, and that the fine structure very probably present is an indication of intrinsic nuclear chemistry.

The early thinking on the wartime Manhattan Project about nuclear charge distribution in low-energy fission, before any yield data were available, was based on the concept (1, 2) of constant charge ratio CCR. Professor Wheeler had suggested (4) a search for positron emitters to see how wide the charge dispersion might be: the results of crude searches in the products of $U^{235}(n_{th},F)$ were, of course, negative (5). Way and Wigner (7) postulated that the charge would distribute to give a minimum nuclear potential energy, and Present (8) postulated a minimum for the sum of nuclear potential energy plus coulombic energy (equal to final kinetic energy). Present took considerable pains to handle the coulombic term for polarizable spheres with non-uniform proton density.

The identification of shielded nuclides⁴ 36-hour Br^{82} , 19-day Rb^{86} , and 13-day Cs^{136} among the fission products gave the first experimental leverage on charge distribution. The first detailed treatment of the problem (5) established the classical rule, or prescription (3, 6) of equal charge displacement ECD; namely that the nuclear charge distribution between light and heavy partners L and H leads to most probable charges Z_P displaced from stability Z_A by about the same amount for the two fragments,

$$[1] \quad (Z_A - Z_P)_L = (Z_A - Z_P)_H.$$

¹Manuscript received November 3, 1960.

Contribution of the Department of Chemistry and Laboratory for Nuclear Science of the Massachusetts Institute of Technology, Cambridge 39, Mass., with financial support from the U.S. Atomic Energy Commission. Presented at the Third Symposium on Nuclear Chemistry and Radiochemistry held at Atomic Energy of Canada Limited, Chalk River, Ontario, September 8–8, 1960.

²Present address: Ernest Orlando Lawrence Radiation Laboratory, University of California, Berkeley 4, California.

³With partial support as National Science Foundation Summer Fellow, 1960, and Eastman Kodak Fellow 1960–61.

⁴A shielded nuclide is one unlikely to be formed by negatron decay since the isobar of $Z-1$ is stable, with little prospect of having a β -unstable isomer.

There is often ambiguity about whether the prescription is meant for usage before or after prompt neutron emission. Equation [1] may be sharpened to give the most probable charge Z_P of a fission product of final mass number A_1 after the emission of ν_1 neutrons,

$$[2] \quad Z_P(A_1) = Z_{(A_1+\nu_1)} - \frac{1}{2}[Z_{(A_1+\nu_1)} + Z_{(A_C-A_1-\nu_1)} - Z_C],$$

where Z_C and A_C denote the charge and mass of the compound nucleus formed by the target plus bombarding particle, and Z_A is the most stable charge associated with mass number A .

This first treatment was based on the fractional chain yields of the three species mentioned above and 9.2-hour Xe^{135} , a quasi-shielded nuclide⁵ in $\text{U}^{235}(n_{th},F)$, together with the roughly 10-fold higher fractional chain yield of Cs^{136} in $\text{Pu}^{239}(n_{th},F)$. It was postulated that the charge dispersion curve, f_1 vs. $Z - Z_P^j$ would be an A -independent curve, symmetric about zero abscissa, if a reasonable j -th prescription Z_P^j were found. The area under the curve must be unity. The very low yields found for Br^{82} and Rb^{86} showed that f_1 falls very rapidly with $|Z - Z_P|$ when this is more than 2.0. The analytical method usually employed was to invoke a rule for some Z_P^j , and test the experimental f_1 values against $Z - Z_P^j$ for coherence, continuity, and reasonable shape. The charge-dispersion curve for correlation of $\log f_1$ with $Z - Z_P$ seems to be approximately Gaussian when $\log f_1 > -2.0$, and linear when $\log f_1$ is < -2.0 .

The CCR rule for products after the emission of ν_T total prompt neutrons (both fragments) is

$$[3] \quad Z_P = \frac{Z_C A_1}{A_C - \nu_T}.$$

Low-energy fission data do not agree with this rule (5, 18, 19, 20), but evidence has been cited for high-energy data, beginning with the Goeckermann and Perlman study (9) of bismuth fission with 190-Mev deuterons, $\text{Bi}^{209}(d_{190},F)$. A number of papers (10-16), mostly at Berkeley, examine this rule in the intermediate energy region (~ 50 Mev), and give it partial support. Pate (17) has, however, established a strong case against CCR and for ECD even up to very high-energy deposition before fission.

The postulate of minimal nuclear potential energy (7) seemed to have been eliminated by the first test (5), but question should be raised as to the validity of the mass equation⁶ used in the calculations of Z_P . These were based on Bohr and Wheeler data (21). The related postulate of Present (8) was later tested by Glendenin (22); this was found to be in fair accord with the apparent empirical observation (5) of ECD except for very light or very heavy fragments, where data still are few.⁷

The ECD rule (eq. [1]) received substantial support in 1955 in two major reviews (19, 22). Pappas and Coryell (18) had raised the question of how discontinuities in Z_A

⁵A quasi-shielded nuclide is one formed by the negatron decay of a moderately long-lived precursor of charge $Z-1$, whose half-life is long enough that daughter growth during irradiation and separation does not prevent estimation of the activity independently formed in fission. It may be shown that the ratio of the activity A_s^d formed in decay to that A_s^i formed independently is λ_1/f_2 , where λ_1 is the disintegration constant of the precursor, t is the time to chemical separation after a very short burst of fission, and f_2 is the fractional chain yield of the quasi-shielded nuclide (Z, A).

⁶All available data indicate that nuclear potential energy is essentially parabolic with Z at constant A , with pairing terms $p.t.$ for oddness or evenness of Z and N , namely,

$$M(Z, A) = M(Z_A, A) + (B_A/2)(Z_A - Z)^2 + p.t.$$

Numerous evaluations of B_A and $p.t.$ are available; see especially Coryell (23, 24), Fix (25), Green (26), Levy (27), and Cameron (28).

⁷The senior author has weighted the ECD (equal charge displacement) postulate more heavily than that of minimum potential energy MPE, although both were given similar weight in an earlier review (22).

caused by the crossing of neutron- and proton-shell edges⁸ should effect Z_F . If ECD (eq. [1]) holds strictly, then Z_F is set solely by properties of the primary products. One would expect by eq. [1] frequent discontinuities in Z_F as A increases, whenever the composition of the fragment crosses a neutron- or proton-shell number, the discontinuities being half of those given in footnote 8. Correspondingly, discontinuities should occur when the complementary fragment crosses any shell number. Dispersion in neutron emission should change the discontinuities from breaks to sudden steep drifts in the Z_F vs. composition curve. Note, however, that the point in Z_F vs. composition diagrams where steep drifts occur for shell crossings in the complementary fragment are dependent on Z_C and A_C of the fissioning nucleus.

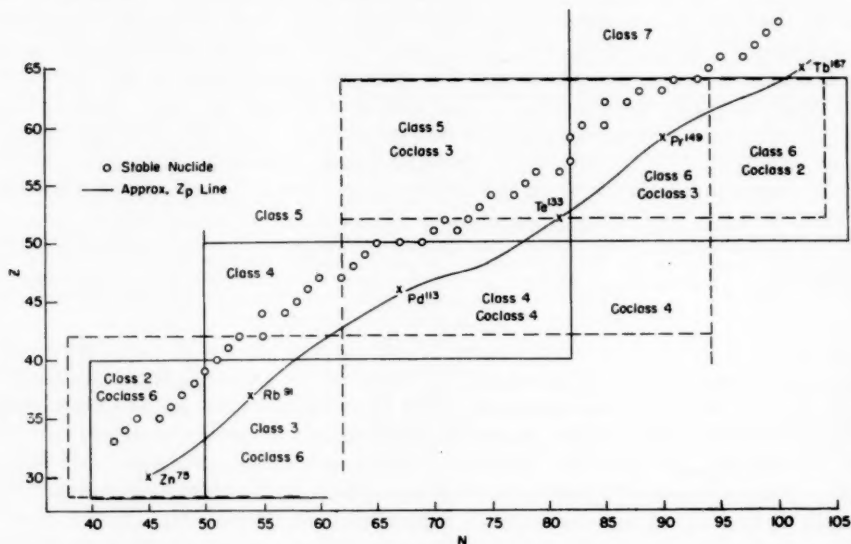


FIG. 1. Designation for $U^{236}(n,F)$ of shell classes for fragment and complement.

Figure 1 is a graphical breakdown of the shell classes of the pairs of fragments in the products of fission of U^{236} (as from thermal neutron fission of U^{235} at excitation energy $E^* = 6.5$ Mev) before neutron emission. The various rectangles designate classes: solid lines for the nucleus in question, broken lines for the complement (coclasses). The shell crossings designated are from the successive lines in Levy's master tables (27),⁹ but the chart covers principally regions of interest in fission chemistry. Going to larger Z_C raises the ordinates of the Z -coclass lines; similarly going to larger $N_C = A_C - Z_C$ raises the abscissas of the N -coclass lines.

For reference, the stable odd- A nuclides ($Z_{stable} = Z_A \pm 0.5$) are shown, together with a rough idea of Z_F given as the sinuous curve. This Z_F line is taken from Glendenin (5) to avoid shell-edge prejudice.

⁸It is well established (18, 23) that Z_A is essentially linear with A in a given nucleon-shell region, with slope ~ 0.4 , but that Z_A undergoes upward discontinuity on crossing a neutron-shell edge, and downward discontinuity on crossing a proton-shell edge, the discontinuities ΔZ for $N = 50$, $N = 82$, and $Z = 50$ being (23) $+0.9$, $+1.4$, and -1.3 charge units, respectively.

⁹Levy's shell class distinctions (27) can be represented in the array: cl.1 ($N = 40$) cl.2 ($N = 50$) cl.3 ($Z = 40$) cl.4 ($Z = 50$) cl.5 ($N = 82$) cl.6 ($Z = 64$) cl.7 ($Z = 82$, $N = 126$) cl.8 ($N = 140$) cl.9. The numbers in parentheses are the shell crossings dividing the classes.

Pappas (18) tried to determine how shell-crossings affect Z_P with few data to guide him (see Coryell (29) for criticism of paucity of data). He made the *ad hoc* decision, now not considered necessary, that the shell class and coclass that are to be used are those at the end of the decay chains. Steinberg and Glendenin (20) assumed that ECD was valid with a drift over three to four units of A in going from one shell-class set to the next.

It was established fairly well (18, 19, 20) that the data from thermal neutron fission of U^{235} , U^{233} , and Pu^{239} were compatible on a plot of $\log f_1$ vs. $Z - Z_P$ when Z_P is computed by eq. [1], assuming ECD. Similar analyses of the fission of U^{238} and Th^{232} with 14-Mev deuterons (30) and of U^{235} with 14-Mev deuterons and 24-Mev alpha particles (31) showed that fission with excitation energy near 20 Mev gave compatible results on the assumption of reasonable values for neutron emission ν_1 .

In 1958 Wahl (32) made a very significant contribution. He used data for 28 fission products in the reaction $U^{235}(n_{th}, F)$ to show that one can reverse the conventional procedure of using consistency in the dispersion of f_1 with $Z - Z_P$ to check Z_P values. He proposed using the Glendenin (5) charge-dispersion curve to obtain $Z - Z_P$ values from experimental f_1 values. This method established empirical Z_P values. He found a continuous but somewhat winding curve in a plot of Z_P vs. A and that the $(Z_P)_L$ values and the $(Z_P)_H$ values intercompare well using average neutron emission $\bar{\nu} = 2.5$. Until Wahl's paper, no firm values existed for cumulative fractional chain yields f_c for very early members of chains, obtained for example by gas sweeping of krypton and xenon (2), or by rapid quantitative precipitation of short-lived halogens, with yields determined by radiochemical assay of long-lived descendants. Yield values for such species, which will be called "swept-out" nuclides, would give the first measurements¹⁰ on the left side of the curve for $\log f_1$ vs. $Z - Z_P$. Wahl (32) obtained results for krypton isotopes up to 3-second Kr^{92} and xenon isotopes up to 1-second Xe^{143} and ~ 1 -second Xe^{144} . This study provided the first examples of even- Z species except for Xe^{135} , and the first even- Z - even- N species. It failed to show evidence for the odd-even sawtooth in observed fission yields that Herrington (33) predicted by simple evaporation theory from an assumed primordial yield-mass curve smooth in A . Further data have been obtained by Wahl and co-workers on other krypton and xenon isotopes (34), strontium, barium, and cerium isotopes (35, 36), and other species of odd Z , including (37) the three niobium isotopes¹¹ of mass number 96, 97, and 98.

This new body of data (32, 34-37) has led to a reanalysis of the charge dispersion curve (38). Figure 2 shows the Glendenin curve (5), labelled GCE, together with three Gaussian curves

$$[4] \quad y_1 = \frac{1}{\sqrt{\pi C}} e^{-(Z-Z_P)^2/C}$$

with the parameter C for variance as 0.8, 1.0, and 1.43. It is seen that the Glendenin curve is very close to the Gaussian of $C = 1.43$ for $|Z - Z_P| < 1.8$. At high values of $|Z - Z_P|$ it is found that the curve is exponential,

$$[5] \quad \frac{d \log_{10} f_1}{d(Z - Z_P)} \cong \pm 3.2 \quad \text{for } (|Z - Z_P| > 2.2),$$

as far as experimental calibrations exist.¹² Wahl reports (38) that most data for chains

¹⁰The change from observed f_c to computed f_1 is obvious (32).

¹¹Considerations of isomerism indicate that in niobium only the yields of high-spin isomers of even A are being measured.

¹²The curve is calibrated at present out to about $Z - Z_P = 3.2$, and extrapolations to ~ 4 are made.

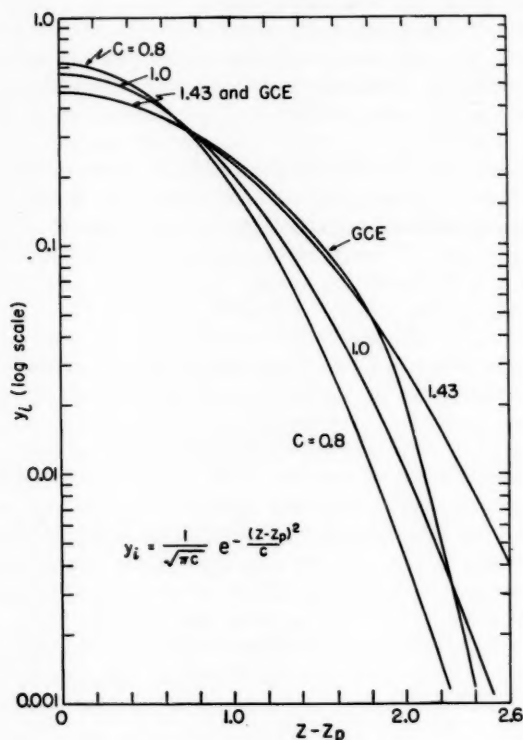


FIG. 2. Charge dispersion.

with several f_i points at different Z values follow Gaussians with $0.8 < C < 1.0$. He now uses this type of curve (38) to measure Z_P by the 1958 method (32); the present paper is based on this method (32) but we still use the Glendenin curve (5, 32), one which gives a somewhat larger scatter in Z_P values.

It will be of interest to search for correlation of Z_P with Z_A , particularly with reference to fine structure (breaks or sudden drifts) in the former data, which are treated as a continuous curve in Z_P vs. A co-ordinates for a given type of fission. The type of fission chosen is $U^{235}(n_{th}, F)$, the one best studied and most accessible. It may be noted that in the fission-product region, the average slope dZ_A/dA in a given shell region is 0.37, (23, 24, 25). It is clear that dZ_P/dA must be about the same. It is therefore useful to present all Z_A and Z_P data as $Z_A - 0.4A$ and $Z_P - 0.4A$ when plotting against A as abscissa as this function removes most of the drift present. This procedure will be used throughout this paper.

It is useful to check various prescriptions against the fairly comprehensive body of data for f_i values for shielded, quasi-shielded, and swept-out nuclides formed in the reaction $U^{235}(n_{th}, F)$. A summary of these data is presented in Table I; half-lives are from Katcoff (39) and most of the yield data are given in the Croall review (40), except that values obtained by difference (35, 36) are not included.

In Fig. 3 is a test by which eq. [3] for CCR fails for $U^{235}(n_{th}, F)$. The ordinate is

TABLE I
 Independent fractional chain yields, f_i , for the thermal neutron fission of U^{235}

Species	f_i	or	f_o	$Z-Z_P$	Z_P	$Z_P-0.4A$	References
$^{87}As^{78}$	$(8.5 \pm 2.5) \times 10^{-3}$			2.12	30.88	-0.32	41a
$^{81}Br^{82}$	3×10^{-4}			2.64	32.3	-0.50	32
$^{87}Rb^{86}$	1.5×10^{-3}			3.08	33.92	-0.48	32
$^{86}Kr^{89}$		0.960 ± 0.009		0.82	35.18	-0.42	32
$^{86}Kr^{90}$		0.86		0.35	35.65	-0.35	32
$^{84}Kr^{91}$		0.59 ± 0.01		-0.32	36.32	-0.08	32
$^{86}Sr^{91}$	$0.06 \pm .04$			1.70	36.30	-0.10	36
$^{86}Kr^{92}$		0.31		-0.90	36.90	0.10	32
$^{86}Kr^{93}$		0.075		-1.65	37.65	0.45	34
$^{86}Kr^{94}$		0.015		-2.02	38.02	0.42	34
$^{86}Kr^{95}$		1.12×10^{-3}		-2.40	38.40	0.40	34
$^{41}Nb^{96}$	$(1.0 \pm 0.2) \times 10^{-4}$			2.80	38.20	-0.20	37
$^{41}Nb^{97}$	$(1.7 \pm 1.3) \times 10^{-3}$			2.35	38.65	-0.15	37
$^{41}Nb^{98}$	$0.011 \pm 0.004^*$			2.00	39.00	-0.20	37
$^{53}I^{99}$	$(9.8 \pm 1.0) \times 10^{-3}$			2.78	50.22	-0.98	32
$^{53}I^{100}$	2.8×10^{-4}			2.62	50.38	-1.62	32
$^{55}Te^{101}$	0.11			1.4	50.6	-1.8	32
$^{55}Te^{102}$	0.36 ± 0.017			0.0 to 1.2	50.9	-1.9	32
$^{55}I^{103}$	< 0.05			> 1.8	< 51.2	< -2.0	32
$^{55}I^{104}$	0.12			1.44	51.56	-2.04	32
$^{54}Xe^{105}$	0.037			1.88	52.1	-1.9	32
$^{54}Cs^{106}$	9.5×10^{-4}			2.43	52.67	-1.83	32
$^{54}Cs^{107}$	0.045 ± 0.005			1.84	53.16	-2.04	34
$^{54}Xe^{109}$		0.82		0.20	53.80	-1.80	32
$^{54}Ba^{109}$	0.011 ± 0.005			2.08	53.92	-1.68	36
$^{54}Xe^{140}$		0.59		-0.32	54.32	-1.68	32
$^{57}La^{140}$	$(7.0 \pm 0.4) \times 10^{-4}$			2.68	54.32	-1.68	35
$^{54}Xe^{141}$		0.205		-1.1	55.1	-1.3	34
$^{57}La^{141}$	$(4 \pm 2) \times 10^{-3}$			2.23	54.77	-1.63	35
$^{54}Ba^{141}$	0.27 ± 0.06			0.92	55.08	-1.32	35
$^{54}Xe^{142}$		0.059		-1.73	55.73	-1.07	34
$^{57}La^{142}$	0.018 ± 0.006			2.00	55.00	-1.80	35
$^{54}Xe^{143}$		8.5×10^{-3}		-2.13	56.13	-1.07	32
$^{54}Ce^{143}$	0.010 ± 0.004			2.10	55.90	-1.30	35
$^{54}Xe^{144}$		1.1×10^{-3}		-2.40	56.40	-1.20	32
$^{61}Pm^{150}$	0.0022			2.32	58.68	-1.32	41b

*Cumulative yield (37).

$Z-0.4A$, the upper set of tilted lines corresponding to different shell regions of Z_A , with N - and Z -shell numbers indicated. The lower line is the prediction of eq. [3], the crosses marking computed points for products after neutron emission.¹³ The double circle at $Z_P = 46.0$, $A = 116.75$ represents the requirement in exactly symmetric fission that $Z_P = Z_C/2$.

We prefer to treat the experimental data in three categories:

(i) Early members of chains (here only krypton and xenon isotopes) where $Z-Z_P$ is negative: these come from fissions where the fragment of interest has had very low neutron boil-off.

(ii) Low-yield species ($f_i < 0.1$ or $Z-Z_P > 1.5$): these come from fissions of rather high neutron boil-off.

(iii) High-yield species ($f_i > 0.1$), where the Glendenin curve is less precise in setting $Z-Z_P$.

There is no evidence, however, in Fig. 3 that the data from any of these three classes diverge from the others.

¹³The average value of 1.25 is taken for ν_1 throughout this paper for $U^{235}(n_{th},F)$, ignoring for the present the Whelstone-Vladimirskii effect (42, 43, 44), namely that ν_A is a double sawtooth function of A . Incorporation of this effect would make little difference.

The remarkable part of Fig. 3 is that it reveals that the large body of data on $Z_P - 0.4A$ from Table I represents a coherent body, in that checks agree well except at $A \cong 141$. There is a sharp drift up in Z_P (or $Z_P - 0.4A$) between $A = 90$ and 93 , and a sudden drop between Kr^{95} and Nb^{96} , Kr^{97} , and Nb^{97} , the latter two species not being affected by isomerism (see footnote 11). Another sharp fall is apparent between the Kennett and Thode data (45) for I^{128} and I^{130} (reflected also in $U^{233}(n_{th}, F)$ and $Pu^{239}(n_{th}, F)$). The blurred rise near $A = 141$ has been mentioned, and problems with $A = 141$ are discussed elsewhere (35).

The present authors consider that the data, as presented here, show that

- (i) Z_P is a single-valued function of A .
- (ii) Z_P is known to about ± 0.15 unit.¹⁴
- (iii) Z_P shows fine structure (an indication of nuclear chemistry).

In Fig. 4 there is provided a test for a recent Russian prescription, given casually by Apalin *et al.* (44). This prescription is based on eq. [3] for CCR after neutron boil-off with a correction term vanishing for symmetric fission; it is

$$[6] \quad (Z_P)_L = \frac{A_L}{A_H} Z_{PH} + 5.90 - 0.05A_L$$

This can be expressed in explicit form as

$$[7a] \quad (Z_P)_L = 5.90 + 0.319A_L + 0.000214A_L^2,$$

$$[7b] \quad (Z_P)_H = 0.419A_H - 0.000214A_H^2.$$

It is seen that the curve in the lower part of Fig. 4 for $Z_P - 0.4A$ (Russian Z_P), based on crosses for computed points, fits the experimental data better than does CCR (Fig. 3). The prescription carries no provision for the fine structure which we admire. The average deviation would be lower if the coefficient of A_L in the last term of eq. [6] were taken near 0.033.

Figure 5 presents a test of an unpublished empirical (essentially graphical) prescription of Wahl (38). This prescription is based on a composite of data (32, 38, 40) for thermal neutron fission (U^{235} , U^{233} , Pu^{239}) and a few points (38) for spontaneous fission (Cm^{244} , Cf^{252}). The fit to the data is excellent; it is even better if the improved Wahl Z_P values (see footnote 14) are taken. It would seem, however, that the Wahl prescription is characteristic of the fission process, not of the composition of the products, as is indicated in Fig. 6, where there is given a schematic representation of the prescription as applied to $U^{235}(n_{th}, F)$, $U^{235}(\alpha_{40}, F)$, and $Cf^{252}(\text{spont. } F)$, characterized by their compound nuclei and excitation energy E^* .

Figure 7 represents a treatment of the same data in the framework of the classical ECD approach of eqs. [1] and [2], with full recognition of shell effects (18, 19, 23, 24). Near-vertical broken lines represent the divisions between different shell regions for the Z and A values of the nucleus in question and its complement, denoted as "comp." The plot refers to $U^{235}(n_{th}, F)$ with (see footnote 13) $\nu_T = 2.5$, so the sum of the charges is 92 and the sum of the A values is 233.5. Going to compound nuclides of higher Z_C or $N_C - \nu_T$ for the fission source leads to a rightward motion of the proton complementary lines or a rightward motion of the neutron complementary lines.

The Pappas prescription (18, 19) that the shell structure at the end of decay chain

¹⁴Professor Wahl reports (38) that the new empirical Z_P curve is within 0.1 charge unit of the sums of the uncertainties (in the calculated Z_P values) due to experimental error and to the charge distribution curve ($C=0.8$ to 1.0) for greater than 80% of the points (Wahl 1960 method of determining Z_P).

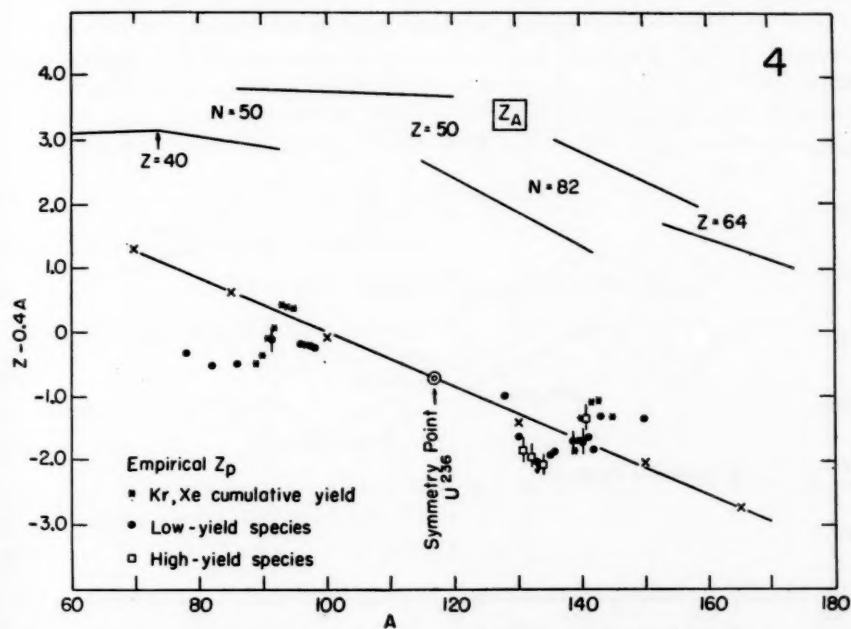
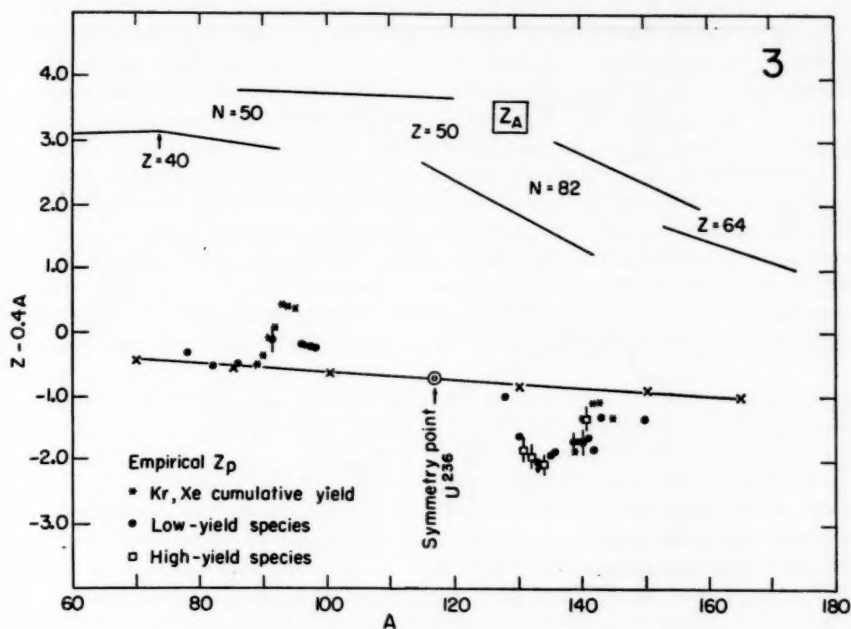


FIG. 3. Most probable charge Z_P in fission: constant charge ratio (CCR) for U^{235} (n, F).

FIG. 4. Most probable charge Z_P in fission: Russkaya formula (Apalin-Dobrynin-Zakharova-Kutikov-Mikaelyan (1960) for U^{235} (n, F)).

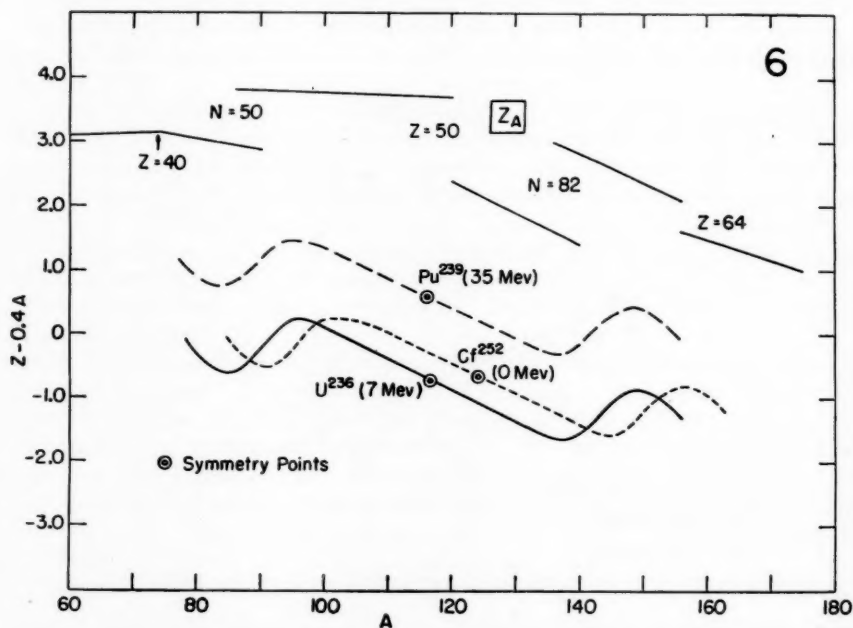
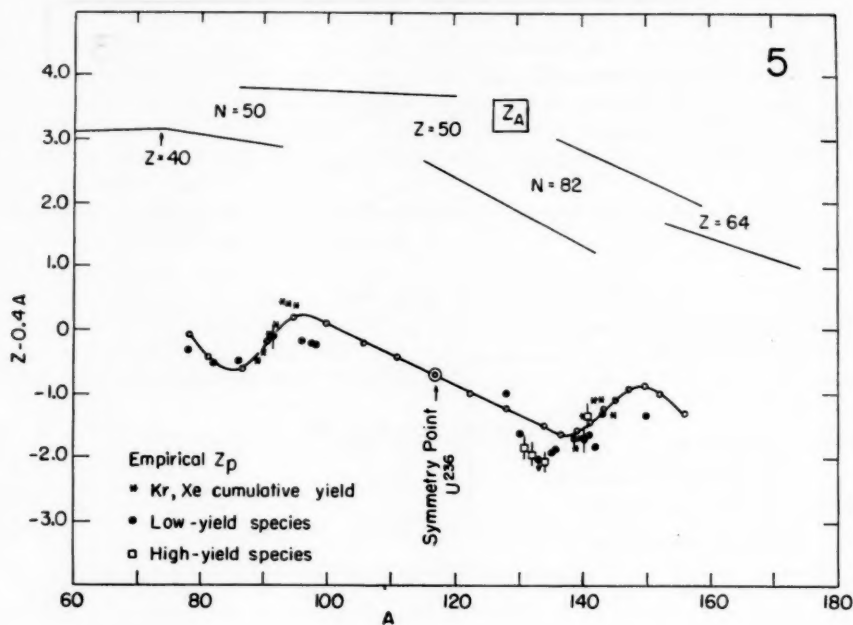


FIG. 5. Most probable charge Z_p in fission: Wahl prescription (1960) for $U^{235}(n, F)$.

FIG. 6. Wahl prescriptions for most probable charge Z_p in fission of various types: $U^{235}(n, F)$, $U^{235}(\alpha_{40}, F)$, $Cf^{252}(\text{spont. } F)$.

sets the Z_A from which Z_P is calculated by ECD from eq. [1] or [2] would require that neutron-shell breaks in the data occur to the right of the offsets shown in the Z_P lines, not inconsistent with the observations. It also requires neutron breaks for shell in the complement to occur to the left. Opposite effects are required for proton shell-breaks in species and complement. Difficulties are seen at $A = 96$, ~ 129 , and 150. If on the other hand it be considered, as del Marmol and Coryell suggest (31), that occurrence of neutron or proton shells is "sensed" by the two nascent nuclei before contact is lost, underestimation of neutrons and protons should occur by the number of each coming from the neck. Thus breaks should be expected to occur to the right of the offsets shown in the Z_P lines for both neutron and proton shells and to the left for the complements. This new prescription is not inconsistent with the breaks at 91, 95, and 141, but has trouble with I^{128} and probably Pm^{150} . The identification of "breaks" is considered more important than the verification of eq. [1] or [2] (ECD) for predicting absolute values of Z_P .

Regarding the broken Z_P lines in the lower part of Fig. 7 (related to the breaks in the Z_A lines in the upper part), it should be noted that the breaks for the different shell crossings are comparable in magnitude to the sudden drifts in the experimental Z_P values shown as points. The approach of Fig. 7 differs greatly from that of Fig. 5, in that it presumes that all of the fine structure comes from composition of the fission products. Little change in the breaks would come from considering the effects of the sawtooth ν_1 function (see footnote 13, Whetstone-Vladimirovskii effect (42, 43, 44)).

It should be pointed out also that the general closeness of the experimental Z_P points to the various segments of Z_P lines predicted by ECD, as shown in Fig. 7, is an empirical justification for the Glendenin ECD rule.¹⁵ The rule is totally *ad hoc*, however, with no theoretical justification, as Halperin (6) also decides.

Until recently there has been no convenient and attractive way to intercompare $Z_P(A)$ among various types of fission differing in Z_C , A_C , and E^* or ν_T . The regularities in Z_A , and the approximate parallel relation between Z_P and Z_A (Fig. 7), show an easy way to handle changes in Z_C and A_C . Recalling (23, 24, 25) that

$$[8] \quad \frac{dZ_A}{dA} = \frac{dZ_P}{d\nu} \cong 0.38$$

it can be shown that eq. [2] transforms to

$$[9] \quad Z_P(A) = \frac{1}{2}[Z_A + 0.38\nu_1 - Z_{(A_0-A-\nu_T)} - 0.38\nu_2 + Z_C].$$

Using the approximation (see footnote 13)

$$[10] \quad \nu_1 = \nu_T - \nu_2 \cong \nu_2$$

we find that

$$[11] \quad Z_P(A) = \frac{1}{2}[Z_C + Z_A - Z_{(A_0-A-\nu_T)}].$$

Consider as a reference type of fission that of $U^{235}(n_{th}, F)$, for which $A_C = 236$, $Z_C = 92$, and $\nu_T = 2.5$, for which eq. [11] is

$$[12] \quad Z_P(A)^{ref} = \frac{1}{2}[92 + Z_A - Z_{(233.5-A)}].$$

By subtracting eq. [12] from eq. [11], it is seen that the difference $\Delta Z_P(A)$ is

$$[13a] \quad \Delta Z_P(A) = Z_P(A) - Z_P(A)^{ref} = \frac{1}{2}(Z_C - 92) - \frac{1}{2}[Z_{(A_0-A-\nu_T)} - Z_{(233.5-A)}].$$

¹⁵This means that the drifts are not very far from the breaks in predicted Z_P lines.

The effect of increasing energy deposit on the type of fission is assumed to be only that of increasing the total neutron boil-off, in the amount

$$[14] \quad \frac{d\nu_T}{dE} = 0.12 \text{ Mev}^{-1},$$

as shown by Leachman (46, 53) for spontaneous fission and for neutron-induced fission in the energy region 0 to 14 Mev. Thus the last term on the right of eq. [13] can be expressed as

$$[15] \quad [Z_{(A_C-A-\nu_T)} - Z_{(233.5-A)}] = 0.38(A_C - 236) - 0.38(\nu_T - 2.5).$$

Thus eq. [13] for the shift $\Delta Z_P(A)$ for a given chain A by changing A_C , Z_C , and ν_T from that for the reference state of $U^{235}(n_{th}, F)$ becomes¹⁶

$$[16] \quad \Delta Z_P(A) = \frac{1}{2}(Z_C - 92) - 0.19(A_C - 236) + 0.19(\nu_T - 2.5).$$

Equation [16] can be used to correct a $Z_P(A)$ value for a given type of fission (determined by the Wahl 1958 method (see footnote 14) (32)) to the reference state $U^{235}(n_{th}, F)$:

$$[13b] \quad Z_P^{corr} = Z_P(A) - \Delta Z_P(A).$$

The ΔZ_P values are independent of A and can be computed at once for a given Z_C , A_C , and E^* (or given target and projectile energy).

In Fig. 8 are shown Z_P^{corr} values for various shielded and quasi-shielded nuclides from typical studies of medium-energy fission: del Marmol (31), $U^{235}(d_{14}, F)$ and $U^{235}(\alpha_{26}, F)$; Chu (14), $U^{235}(\alpha_{46}, F)$; and Yellin (47), $U^{235}(d_{14}, F)$ for 3.2-hour Ag^{112} . In our experience, most other recent data with energy deposit of 20 to 60 Mev fall in the same general region. These data are presented in a framework like that of Fig. 7, and the general course of the $U^{235}(n_{th}, F)$ data are presented as a cross-hatched background.

It is concluded from Fig. 8 that Z_P^{corr} values for medium-energy fission (with E^* up to about 50 Mev) show a somewhat greater scatter than for low-energy fission (E^* up to 7 Mev), but that they lie near the low-energy fission Z_P^{corr} curve. It seems that there is a filling in of the Z_P hollow near $A = 135$. For further specific results on 13-day Cs^{136} , see Appendix I.

It has been proposed by Swiatecki (48, 49) that earlier theories of Way and Wigner (7), Present (8), and Fong (50) hold considerable promise, i.e., that the most probable division of charge in fission is that which leads to a minimum in the sum of nuclear potential energy and coulombic energy. This corresponds to maximizing the excitation energy and, in a rough way, the level density (50). The contribution of the coulombic term is less important than that of the nuclear potential energy.

Blann (49) has shown the comparison between Z_P data for $U^{235}(n_{th}, F)$ and predictions of CCR by eq. [3], ECD by eq. [1], and the Swiatecki (48) prescription, a simplification of that of Present (8). The energy to be minimized for each mass split can be visualized roughly as the sum of the two steep concave-up energy parabolas (see footnote 6) for the light and heavy fragments, the first centered on $(Z_A)_L$, the second on $(Z_A)_H$, plus an inverted flat parabola for the coulombic term centered on $Z_C/2$. The net result, except for small pairing terms p.t. and shell offsets (23-29), is essentially a parabola, whose

¹⁶Dr. J. P. Butler has pointed out that there is a fairly steady rise in ν_T for various fissioning species with A (46), so that the coefficient of the second term on the right should be raised to about 0.21 with ν_T as the nominal value of 0.12 ($E^* - 6.5$).

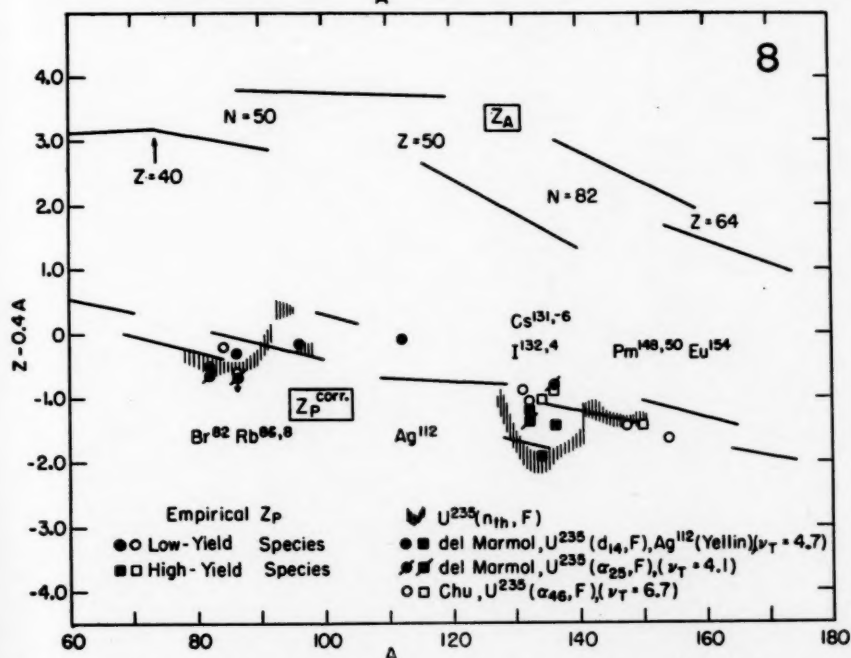
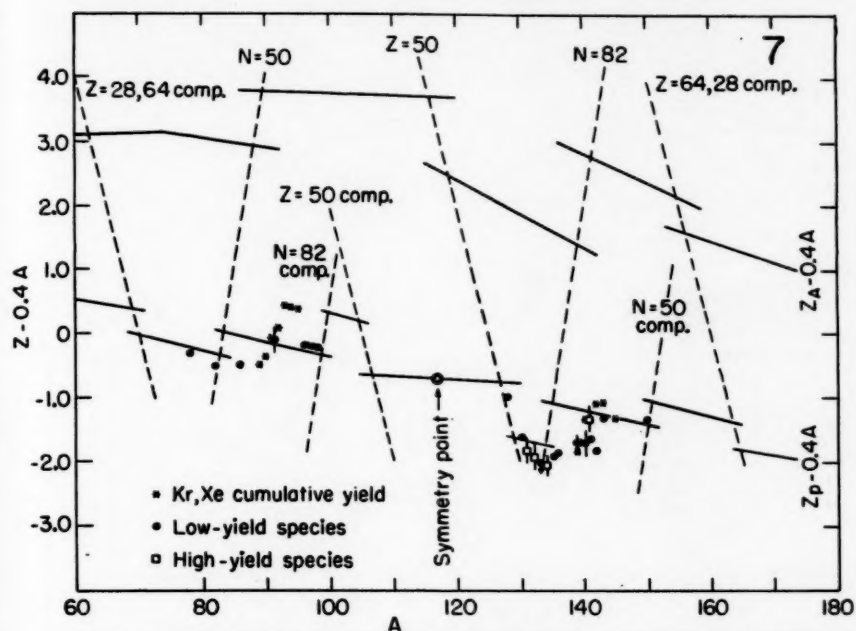

 FIG. 7. The function $Z_A - 0.4A$ vs. A and its application to thermal neutron fission of U^{235} .

 FIG. 8. Most probable charge Z_P in fission: change with fissile nuclide. Medium energy; $Z_P^{corr} = Z_P - 0.5(Z_C - 92) + 0.19(A_C - 236) - 0.19(\nu_T - 2.5)$.

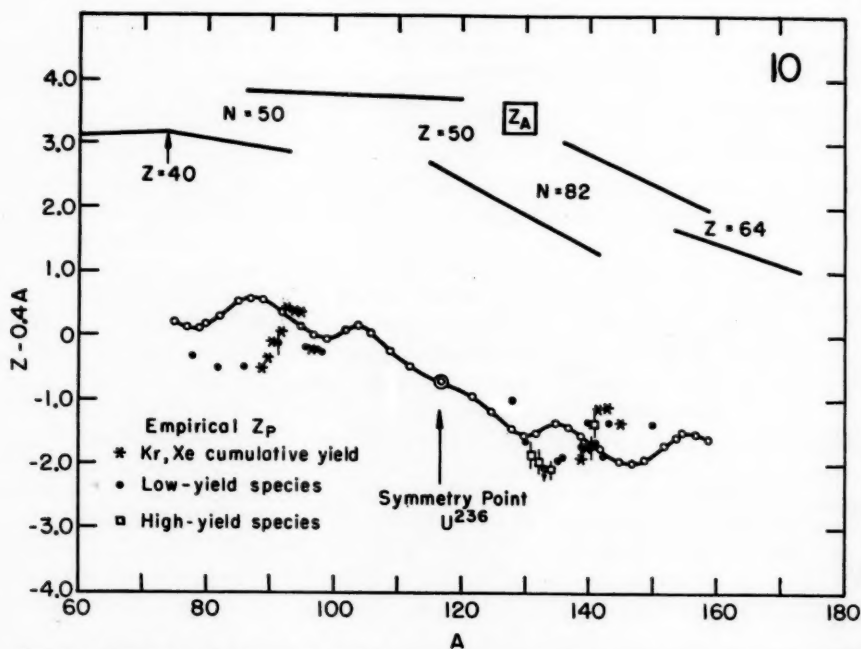
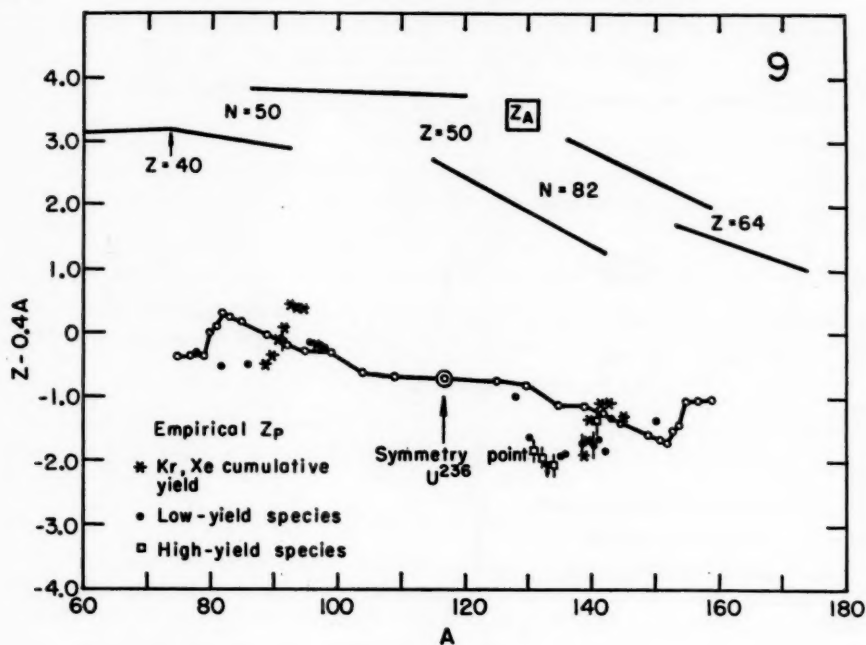


FIG. 9. Most probable charge Z_P in fission: minimum potential energy and Levy mass equation for $U^{236}(n, F)$.

FIG. 10. Most probable charge Z_P in fission: minimum potential energy and Cameron mass equation for $U^{236}(n, F)$.

minimum (called Z_0) is hopefully to be identified as Z_P . Swiatecki and Blann (49) computed Z_P by this prescription for maximum excitation energy. They selected the Grummitt and Milton (51) continuous Z_A values and basic B_A values of Green (26) before shell corrections were evaluated (a so-called liquid-drop formula). This odd prescription for Z_P (on graphical correlation with experiment) fits the low-energy data fairly well and agrees rather well with ECD. Part of its promise lies in the fact that it represents fairly well the Z_P function for the high-energy fission of gold with 112-Mev C^{12} ions, $Au^{197}(C_{112}^{12}, F)$.

The dropping of shell terms from the mass equation (nuclear potential energy) removes all chance of representing fine structure in the Z_P vs. A correlation in low-energy fission. The apparent filling in Fig. 8 of the hollow at $A = 135$ with medium-energy fission (E^* of 20 to 40 Mev) may reflect the decrease in shell effects with increasing excitation, culminating in the Blann success (49) in the 110-Mev region.

The basic idea, however, of maximum excitation computed with shell terms included would seem to be an attractive one for further study. We have explored this in Fig. 9 using the tabulated Levy (27) mass data. Fine structure is present to some degree, principally in the region of highly asymmetric fission, in the opposite direction from the Present prediction (8). In Fig. 10 is given the same type of calculation using the tabulations of the Cameron mass equation (28). The fine structure is quite different. This shows that randomly chosen mass equations differ greatly in predictions of nuclear mass in regions about three to four β -decays from stability.

The parabolas in Fig. 11 emphasize differences between two popular, readily accessible

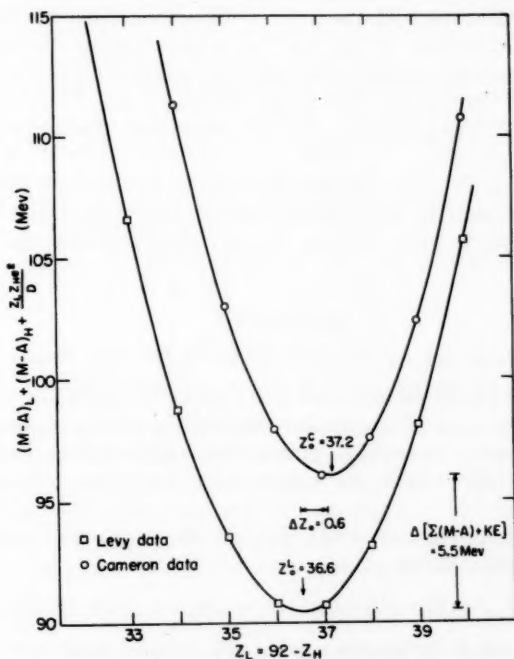


FIG. 11. Swiatecki prescription. Nuclear P.E. + (coulombic P.E. = K.E.) is at minimum for $Z = Z_P$, called Z_0 . Prescription largely dependent on mass formula used. Total energy for split $A_L = 93$, $A_H = 143$ (no shell crossing).

mass tabulations for the mass split $A_L = 93$, $A_H = 143$, as from $U^{235}(n_{th}, F)$ before prompt neutron emission. This split was chosen to avoid shell effects in the Z_L region near known Z_P . The energy function we wish to minimize is plotted in Fig. 11 against the charge Z_L of the light fragment,

$$[17] \quad F(P.E. + K.E.) = (M - A)_L + (M - A)_H + \frac{Z_L(92 - Z_L)e^2}{D}$$

where value of D is an internuclear distance (53) parameter, larger than $r_0(A_L^{1/3} + A_H^{1/3})$ by about 15% to account for the experimental kinetic energy of 167 Mev (46, 53).

The upper parabolic curve in Fig. 11 is the curve for the Cameron masses (28), with a minimum for eq. [17] at $Z_0 = 37.2$ at about 96 Mev. The lower parabola is that for the Levy masses (27), with a minimum at $Z_0 = 36.6$ at about 90.5 Mev. These two modern mass formulas give results for Z_0 (which we would like to call Z_P) differing by 0.6 charge unit, far beyond the uncertainty of the experimental data. The energy difference between the minima (5.5 Mev) is equally surprising.

It may not be too much to hope that the experimental course of Z_P as a function of A may be used to derive a more reliable mass formula. It will be interesting to see how firm the evidence is for fine structure, and how this relates to mass and nuclear shells, if the principle of maximum excitation (48) is established as a good approximation. These prospects make fission radiochemistry exciting.

ACKNOWLEDGMENTS

We are indeed grateful to Professor Arthur C. Wahl of the Washington University of St. Louis for providing us with the latest information from his group, for advance information on his correlation of Z_P , and for many fruitful discussions. The senior author wishes to express his gratification with the sessions on fission at the very constructive Chalk River Conference on Nuclear Chemistry and Radiochemistry. It was a great help that Atomic Energy of Canada, Ltd., furnished photo-offset preprints of the figures for this paper.

Many other people have given substantial help, especially Drs. John M. Alexander, Glen E. Gordon, Lawrence E. Glendenin, Ellis P. Steinberg, Leo Yaffe, and Nathan Sugarman. We also thank Mrs. Virginia Ekman, Grace Rowe, and Norma Osborne for indispensable aid.

APPENDIX I

INTERCOMPARISON OF $Z_P(A)$ VALUES: Z_P^{corr} FOR 13-DAY Cs^{136}

Reference to Fig. 8 shows considerable drift in Z_P^{corr} , filling in the hollow around $A = 135$ on moving the type of fission into the medium-energy region. It is interesting to explore this effect, and it is useful to provide the reader with explicit examples of the method of calculating Z_P^{corr} from Z_P values derived either by Wahl's 1958 or 1960 formulas, (32) or (38).

We anticipate the improvement of eq. [16] by the suggestion (see footnote 16) of Butler, and offer the prescription

$$[18] \quad Z_P^{corr} = Z_P - \frac{1}{2}(Z_C - 92) + 0.21(A_C - 236) - 0.19 \times 0.12(E^* - 6.5).$$

We choose $A = 136$, where coherence among the data is poor, but where numerous data on f_1 for Cs^{136} are to be found. Typical values are given in Table II.

TABLE II
Data for fractional chain yield and Z_F for Cs^{136} in various fission types

Type	$E^*(\text{Mev})$	Fractional chain yield	$Z - Z_F$	Z_F^{corr}	$Z_F^{\text{corr}} - 0.4A$	Reference
$U^{235}(n_{\text{th}}, F)$	6.5	$1. \times 10^{-3}$	2.42	52.58	-1.82	32
$U^{235}(n_{\text{th}}, F)$	6.76	0.0181	2.02	52.55	-1.85	39
$Cm^{240}(sp, F)$	0	0.123	1.50	52.80	-1.60	20
$Pu^{239}(n_{\text{th}}, F)$	6.38	0.0166	2.03	52.81	-1.59	39
$Cf^{250}(sp, F)$	0	5.69×10^{-3}	2.18	52.92	-1.48	55
$U^{235}(n_{14}, F)$	20.5	0.040	1.87	52.97	-1.43	54
$Th^{232}(d_{12,6}, F)$	21.93	0.033	1.91	52.99	-1.41	30
$U^{235}(\alpha_{24}, F)$	19.00	0.0292	1.93	53.03	-1.37	14
$U^{235}(\alpha_{24}, F)$	18.76	0.2847	0.86	53.48	-0.98	14
$U^{235}(\alpha_{24}, F)$	18.76	0.084	1.60	52.74	-1.66	31
$U^{235}(d_{14}, F)$	22.10	0.037	1.88	53.09	-1.31	30
$U^{235}(\alpha_{45,7}, F)$	40.50	0.4435	0.28	53.55	-0.85	14

The first column gives the type of fission; subscripts for the projectiles denote the projectile energy in million electron volts. The second column gives the excitation energy based on the nuclear masses of Everling *et al.* (52). The third column gives values of the fractional chain yield found by workers cited in the last column. The $Z - Z_F$ values of the fourth column were found by using the Glendenin curve given in Fig. 2, or taken from the literature (5, 19, 20, 32), reading the $Z - Z_F$ abscissa corresponding to the observed $\log f_1$ ordinate. (The Wahl 1960 method (38) should be better (see footnote 14).) The fifth column gives Z_F^{corr} , using the revised eq. [18], which differs but slightly from the eq. [16] used for Fig. 8. The sixth column is $Z_F^{\text{corr}} - 0.4A$, column five diminished by 54.4, giving values like those plotted in Figs. 3-10.

The data in Table II have been presented in order of increasing Z_F or $Z_F - 0.4A$. The low-energy fission data are in fair agreement, although the values seem to rise about 0.3 unit with A going up 16 units to Cf^{252} (spont. F). There is a discrepancy of factor 3.4 between f_1 data of Chu (14) and del Marmol (31) for Cs^{136} in $U^{235}(\alpha_{24}, F)$ leading to a difference in Z_F of 0.7. It is hard to see a dependence of A in the medium-energy region, but there may be a dependence on E^* .

As is noted in Fig. 8, the Z_F^{corr} values for say Br^{82} scatter far less than the values around $A = 136$.

APPENDIX II

AN ALTERNATIVE E^* TREATMENT OF ΔZ_F

An alternative to eq. [16] was outlined by Kaplan (56), using an empirical calibration for the effect of excitation energy E^* rather than using eq. [14] to estimate ν_T . He used the energy dependence of Z_F established by Pate, Foster, and Yaffe (57) based on f_1 values of tellurium and iodine isotopes for the reaction $Th^{232}(p, F)$. This gave a term $\delta_2 Z_F(E^*)$ to replace the ν_T term in eq. [16]. This new term is thought to be valid up to $E^* \sim 40$ Mev, since the charge dispersion seems to be independent of E^* for this energy region.

When all available data in the energy region $0 < E^* < 40$ are so treated, average deviations of Z_F^{corr} from a median curve are about ± 0.2 charge unit, slightly larger than that from the treatment based on eq. [16] as given above.

REFERENCES

1. N. SUGARMAN and A. TURKEVICH. Private communication, 1944.
2. W. RUBINSON. Chicago Report CC-3146. September, 1945; National Nuclear Energy Series. Div. IV, Vol. 9, Paper 314. McGraw-Hill Book Co., New York. 1951.
3. C. D. CORYELL and N. SUGARMAN (*Editors*). Radiochemical studies: the fission products. National Nuclear Energy Series. Div. IV, Vol. 9. McGraw-Hill Book Co., New York. 1951.
4. J. A. WHEELER. Private communication, 1943.
5. L. E. GLENDENIN, R. R. EDWARDS, and C. D. CORYELL. Clinton Laboratory Report CL-LEG-1. July, 1946. L. E. GLENDENIN, C. D. CORYELL, and R. R. EDWARDS. National Nuclear Energy Series. Div. IV, Vol. 9, Paper 52. McGraw-Hill Book Co., New York. 1951.
6. I. HALPERIN. *Ann. Rev. Nuclear Sci.* **9**, 321 (1959).
7. K. WAY and E. P. WIGNER. Private communication, 1944; Chicago Report CC-3032. June, 1945; *Phys. Rev.* **73**, 1318 (1948); National Nuclear Energy Series. Div. IV, Vol. 9, Paper 43. McGraw-Hill Book Co., New York. 1951.
8. R. D. PRESENT. Private communication, 1946; *Phys. Rev.* **72**, 7 (1947).
9. R. H. GOECKERMANN and I. PERLMAN. *Phys. Rev.* **76**, 628 (1949).
10. W. M. GIBSON. University of California Radiation Laboratory, UCRL-3493. 1956.
11. B. M. FOREMAN. University of California Radiation Laboratory, UCRL-8223. 1958.
12. R. VANDENBOSCH. University of California Radiation Laboratory, UCRL-3858. 1957. R. VANDENBOSCH, T. D. THOMAS, S. E. VANDENBOSCH, R. A. GLASS, and G. T. SEABORG. University of California Radiation Laboratory, UCRL-8032. Revised 1958.
13. R. M. LESSLER. University of California Radiation Laboratory, UCRL-8439. 1958.
14. Y. Y. CHU. University of California Radiation Laboratory, UCRL-8926. 1958.
15. L. J. COLBY. Ph.D. Thesis in Chemistry, Purdue University, Lafayette, Ind. 1960.
16. H. M. BLANN. University of California Radiation Laboratory, UCRL-9190. 1960.
17. B. D. PATE. *Can. J. Chem.* **36**, 1707 (1958).
18. A. C. PAPPAS. Ph.D. Thesis in Chemistry, University of Oslo, Oslo, Norway. Given as Technical Report No. 63, Massachusetts Institute of Technology Laboratory for Nuclear Science. 1953; also United States Atomic Energy Commission, AECU-2806. 1953.
19. A. C. PAPPAS. Proceedings of the International Conference on the Peaceful Uses of Atomic Energy, 1955. Vol. 7. United Nations, New York. 1956. p. 19.
20. E. P. STEINBERG and L. E. GLENDENIN. Proceedings of the International Conference on the Peaceful Uses of Atomic Energy, 1955. Vol. 7. United Nations, New York. 1956. pp. 3-14, 31-35.
21. N. BOHR and J. A. WHEELER. *Phys. Rev.* **56**, 426 (1939).
22. L. E. GLENDENIN. Ph.D. Thesis in Chemistry, Massachusetts Institute of Technology, Cambridge, Mass. August, 1949.
23. C. D. CORYELL. *Ann. Rev. Nuclear Sci.* **2**, 305 (1953).
24. C. D. CORYELL. Lecture Notes for Massachusetts Institute of Technology Course 5.09. October, 1956.
25. R. C. FIX. Ph.D. Thesis in Chemistry, Massachusetts Institute of Technology, Cambridge, Mass. September, 1956.
26. A. E. S. GREEN and N. A. ENGLER. *Phys. Rev.* **91**, 40 (1953). A. E. S. GREEN and D. F. EDWARDS. *Phys. Rev.* **91**, 46 (1953). A. E. S. GREEN. Nuclear physics. McGraw-Hill Book Co., New York. 1955. pp. 244-270; *Revs. Modern Phys.* **30**, 569 (1958).
27. H. B. LEVY. University of California Radiation Laboratory, UCRL-4588 and UCRL-4713 Livermore Laboratory. 1955; *Phys. Rev.* **106**, 1265 (1957); J. RIDDELL. Numerical tables. Atomic Energy of Canada Ltd. Report AECL-339. 1956.
28. A. G. W. CAMERON. *Can. J. Phys.* **35**, 1021 (1957); Numerical tables. Atomic Energy of Canada Ltd. Report AECL-433. 1957.
29. C. D. CORYELL. Dedication U.S. Naval Radiological Defense Laboratory, San Francisco, Calif. August, 1957.
30. J. M. ALEXANDER and C. D. CORYELL. *Phys. Rev.* **108**, 1274 (1957).
31. P. DEL MARMOL. Ph.D. Thesis in Chemistry, Massachusetts Institute of Technology, Cambridge, Mass. January, 1959.
32. A. C. WAHL. *J. Inorg. & Nuclear Chem.* **6**, 263 (1958).
33. A. C. HERRINGTON. D.Sc. Thesis in Chemical Engineering, Massachusetts Institute of Technology, Cambridge, Mass. 1957.
34. K. WOLFSBERG. Ph.D. Thesis in Chemistry, Washington University, St. Louis, Mo. 1959.
35. D. R. NETHAWAY. Ph.D. Thesis in Chemistry, Washington University, St. Louis, Mo. 1959.
36. R. L. FERGUSON. Ph.D. Thesis in Chemistry, Washington University, St. Louis, Mo. 1959.
37. D. E. TROUTNER. Ph.D. Thesis in Chemistry, Washington University, St. Louis, Mo. 1959.
38. A. C. WAHL. Private communication.
39. S. KATCOFF. Brookhaven National Laboratory Report BNL-4977. 1960; *Nucleonics*, **16**, No. 4, 78 (1958).
40. I. F. CROALL. Harwell Report AERE-R3209. 1960.
- 41a. A. KJELBERG and A. C. PAPPAS. *J. Inorg. & Nuclear Chem.* **11**, 173 (1959).
- 41b. Y. Y. CHU. Private communication.
42. S. L. WHETSTONE. *Phys. Rev.* **114**, 581 (1959).
43. V. V. VLADIMIRSKIL. *J. Exptl. Theoret. Phys. (U.S.S.R.)* **32**, 822 (1957); *Soviet Phys. JETP*, **5**, 673 (1957).
44. V. F. APALIN, U. P. DOBRYNIN, V. P. ZAKHAROVA, I. E. KUTIKOV, and L. A. MIKAEVYAN. *Atomnaya Energ.* **8**, 15 (1960).

45. T. J. KENNETT and H. G. THODE. *Phys. Rev.* **103**, 323 (1956).
46. R. B. LEACHMAN. *Proceedings of the International Conference on the Peaceful Uses of Atomic Energy*, Geneva. Vol. 15. United Nations, Geneva, 1958. p. 229. (cf. Fig. 17); *Phys. Rev.* **101**, 1005 (1956).
47. E. YELLIN. Ph.D. Thesis in Chemistry, Massachusetts Institute of Technology, Cambridge, Mass. June, 1960.
48. W. SWIATECKI. Private communication.
49. H. M. BLANN. University of California Radiation Laboratory, UCRL-9190. 1960.
50. P. FONG. *Phys. Rev.* **102**, 434 (1956).
51. W. E. GRUMMITT and G. M. MILTON. *J. Inorg. & Nuclear Chem.* **5**, 93 (1957).
52. F. EVERLING, L. A. KÖNIG, J. H. E. MATTAUCH, and H. A. WAPSTRA. *Nuclear Phys.* **18**, 529 (1960).
53. E. K. HYDE. University of California Radiation Laboratory, UCRL-9036. 1960.
54. G. P. FORD. Report AEC-D-3597. 1952.
55. W. E. NERVIK and P. C. STEVENSON. *Quoted in ref. 53*, p. 169.
56. M. KAPLAN. Ph.D. Thesis in Chemistry, Massachusetts Institute of Technology, Cambridge, Mass. January, 1960.
57. B. D. PATE, J. S. FOSTER, and L. YAFFE. *Can. J. Chem.* **36**, 1691 (1958).
58. A. C. WAHL. *Phys. Rev.* **99**, 730 (1955).

THE ATTACHMENT OF INERT GASES TO POWDERS FOLLOWING (n,γ) EVENTS¹

ROGER KELLY

ABSTRACT

It has been found that, when argon, krypton, and xenon are irradiated with neutrons in the presence of various powders, a portion of the inert-gas activity becomes "attached" to the powder. The attached activity was shown to be highly enriched, and to be distinguishable from adsorbed activity. Expressing the attachment in terms of the *attachment efficiency*, $A = (\text{inert-gas activity attached to target})/(\text{total inert-gas activity})$, it was found that A was independent of irradiation time and neutron flux, and for fine powders was also independent of pressure between 0.7 and 700 mm. The use of a very coarse powder or no powder at all led to a decrease in A , on the basis of which it was estimated that the maximum distance from a surface that attached activity can originate is about 200 mean free paths. The following miscellaneous relations were observed to hold: (i) $A \ll 1$, (ii) $A_{Ar} > A_{Kr} > A_{Xe}$, (iii) $A_{\text{oxide}} > A_{\text{metal}}$ (approximate). The results were in general consistent with a mechanism of attachment based on electrical attraction: inert-gas atoms first acquire a high charge due to vacancy cascades initiated by the conversion of capture gamma rays; they then wander about, and, upon approaching a solid surface, are accelerated electrically into it.

In accordance with I.U.P.A.C. recommendations (1), the symbol "Ar" has been used for argon. In addition, left superscripts are used for mass numbers, thus leaving the right superscript position free for indicating ionic charge (cf. equations [4]).

The chemical effects of beta and gamma emission from radioactive atoms have been studied from several points of view. Most of the work has been done on the breaking of chemical bonds due either to the recoil of the emitting atom or to the state of charge acquired by the emitting atom (2). A limited amount of work on "release"² effects has also been described; for example, Yosim and Davies (4) have considered the release of ¹¹⁶In and ¹⁹⁸Au from the surfaces of the metal lattices following (n,γ) events, while, in a related study, Baulch and Duncan (5) observed the release of ²¹²Bi from PbO and Pb₃O₄ following the beta decay of adsorbed ²¹²Pb. Complementary to the release work is that in which the "attachment"² of the products of beta or gamma emission to a target is studied. Species with which attachment studies have been made include: (i) metal atoms released from a metal film which is being irradiated with neutrons (4, 6), (ii) atomic bromine and iodine formed in neutron-irradiated ethyl bromide and iodide (7), and (iii) atomic tellurium formed in the decay of gaseous ^{127m}Te(C₂H₅)₂ and ^{129m}Te(C₂H₅)₂ (8).

The present work was concerned with attachment, in particular attachment following (n,γ) events in the inert gases. It was anticipated that the use of inert gases would yield information not obtainable with more reactive substances, such as were used in references 4, 6, 7, and 8. The reason is the difference in exchangeability. Material which becomes attached to a target in connection with (n,γ) events (e.g. ¹⁹⁸Au) will at first contain a smaller proportion of the parent isotopes (e.g. ¹⁹⁷Au) than does the unattached material; i.e. it will be *isotopically enriched* in the products of the (n,γ) event. With a reactive substance, the enrichment will tend to persist regardless of whether the attachment is

¹Manuscript received November 3, 1960.

Contribution from the Development Chemistry Branch, Atomic Energy of Canada Limited, Chalk River, Ontario. Presented at the Third Symposium on Nuclear Chemistry and Radiochemistry, held at Atomic Energy of Canada Limited, Chalk River, Ontario, September 6-8, 1960.

Issued as A.E.C.L. No. 1165.

²The terms "release" and "attachment" are used in preference to "emanation" and "penetration" since they are more general. For example, "emanation" is usually applied strictly to the release of inert gases (3).

due to penetration into the lattice of the target or simply to surficial adsorption or reaction, for the chemical or physical differences between the attached and unattached material will inhibit exchange. In other words, the details of the attachment will be obscured. With substances which are simultaneously *unreactive*, *monatomic*, and *gaseous*, on the other hand, it is likely that enrichment will persist only under conditions of penetrative attachment. A distinction between penetrative and surficial attachment is then possible, and the mechanism of the attachment can be developed in detail.

The method used was quite simple. Inert gases were irradiated with neutrons in the presence of fine powders, and the distribution of inert-gas activity between the gas phase and the powder was then determined.

EXPERIMENTAL

For each experiment, a capsule was made from thin-walled quartz tubing having an I.D. of about 0.47 cm. The capsule was filled to a depth of between 2.5 and 3 cm with a given powder, drawn down close above the surface of the powder, and attached to a vacuum system with black wax. The inert gas (argon, krypton, or xenon) was now added, and the capsule was sealed off by applying a flame to the drawn portion.

After irradiation in a thermal neutron flux of between 2 and 27×10^{12} neutrons $\text{cm}^{-2} \text{sec}^{-1}$ for a period of about 12 hours, the capsule was loaded into the "sample holder" as shown in Fig. 1A, and the sample holder was evacuated to about 40 mm. The capsule was cracked open by lifting a nail magnetically and dropping it, the residual air helping to prevent dispersal of the powder. The gases in the sample holder, including that portion of the inert-gas activity still remaining in the gas phase, were led to a trap containing activated charcoal and cooled with liquid nitrogen, henceforth called the "counting trap" (Fig. 1B). The unattached activity was now measured with a single-channel gamma counter. (The presence of activated charcoal was found to be essential for a quantitative collection of inert-gas activities. Thus, without charcoal, xenon activity was lost at the rate of 18% per hour when the counting trap was pumped upon, and the other activities were lost even more rapidly.)

After no further activity could be drawn from the sample holder, the counting trap was freed from activity. With argon and krypton this was accomplished simply by heating the trap with a carbonizing flame, though the charcoal generally had to be changed to eliminate the last traces of xenon activity. A furnace (F in Fig. 1A) was now drawn up over the bottom of the sample holder and the latter was heated, first to about 200°C to confirm that the powder was truly free of *unattached* activity, and then to about 1000°C to remove *the attached* activity. The adequacy of a temperature of 1000°C in removing attached activity was demonstrated by the fact that there was no appreciable release of activity when powder, previously heated to 700°C , was (i) heated to 1000°C (cf. Fig. 2) or (ii) dissolved in a suitable acid or flux.

Several points concerning the counting techniques require comment. With the irradiation and decay times used, the only readily countable isotopes were ^{41}Ar (1.83 hours), $^{85\text{m}}\text{Kr}$ (4.4 hours), and ^{126}Xe (18 hours), though ^{133}Xe (5.27 days) was easily distinguished after the shorter-lived ^{126}Xe had decayed for several days. While ^{135}Xe (9.2 hours) was presumably also present, the photopeak could not be resolved from the larger ^{126}Xe photopeak. Activities were expressed in terms of the integrated count, less background, in the region of the photopeak. It was not necessary to consider absolute counting rates, since ratios of activities were used. Resolving-time errors in high activities and background errors in low activities were minimized by the appropriate positioning of the

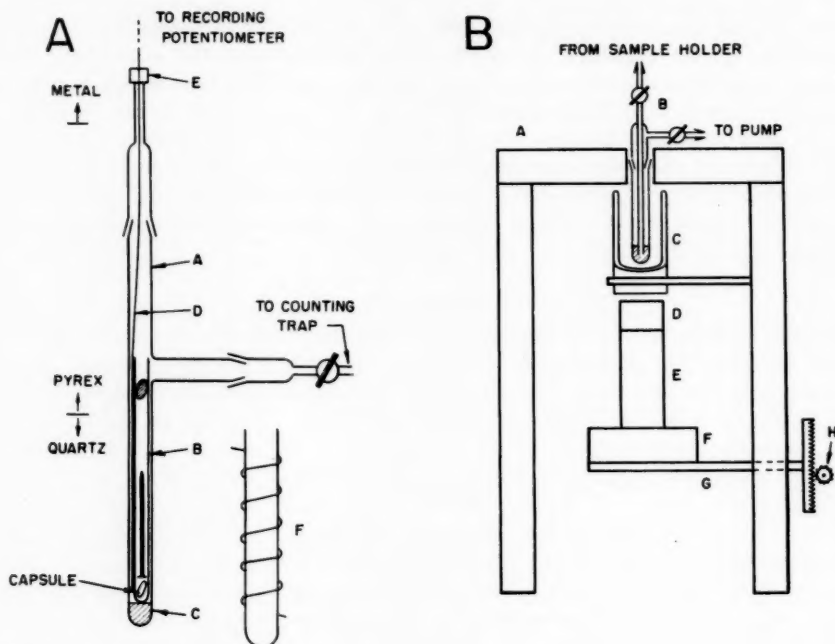


FIG. 1.

(A) The "sample holder". A = body of sample holder. B = disposable quartz tube. The tube is shown loaded with a capsule, a nail, and a wad of Pyrex wool. C = powdered SiO_2 to protect the bottom of A. D = thermocouple wires. E = assembly for admitting the thermocouple wires. The assembly consists of a perforated Teflon plug which can be shrunk around the wires by means of a suitably shaped brass fitting, the latter being soldered to the copper portion of a tubular "Housekeeper" seal. F = furnace. The temperature of the furnace was regulated by feeding the output of a thermocouple (not D) located outside A into a Minneapolis-Honeywell "Pulse Pyrovane" controller.

(B) System for trapping and counting (drawn to 2/3 the scale used in (A)). A = lead castle with lid split into two parts such that one part can be slid aside. The inside of the castle, including the lid, is lined with 0.15 cm of cadmium and 0.051 cm of copper. B = counting trap containing activated charcoal. C = Dewar for liquid nitrogen. D = 2-in. NaI(Tl) scintillation crystal. E = photomultiplier. F = pre-amplifier. G = supporting piece which extends through a vertical slit in the castle wall and bears a 14-cm rack at the end. H = pinion to move rack and thence scintillation crystal. The counting rate could be varied by a factor of 7.7 according to the position of the crystal.

scintillation crystal using the elevating mechanism shown in Fig. 1B (G and H). Errors due to the unreproducible dispersion of activity throughout the charcoal of the counting trap amounted to about $\pm 10\%$ for high crystal positions. Occasional experiments were ruined due to the attached activity being increased by krypton and xenon activities formed by the fission of uranium impurities. (The possible presence of fission activities was indicated whenever the integrated count *above* the photopeak was excessive.)

RESULTS

It soon became apparent in the course of the experiments that when the inert gases argon, krypton, and xenon were irradiated with neutrons in the presence of a powder, a portion of the inert-gas activity became attached to the powder.

Enrichment

The activities attached to the powders were shown to be highly enriched in the products of the (n, γ) reactions. A Xe-TiO₂ mixture was irradiated with neutrons, the xenon activity attached to the TiO₂ was released at 1000° C, and the ¹²⁹Xe was counted. The activity was then transferred to a quartz capsule containing a small amount of charcoal, allowed to decay for several weeks, and finally reirradiated under conditions similar to those of the original irradiation. It was found that the amount of gaseous activity with gamma energies in the region of the ¹²⁹Xe photopeak was now only 2 to 3% of the original attached activity. The experiment was done in duplicate.

Release of Attached Activity

Attached activity was shown to be released much less readily than adsorbed activity. Thus, activity which had become attached to a powder did not come off at a measurable rate until the powder was heated, a temperature of between 600 and 700° C being necessary to drive off 95% of the activity (Fig. 2). By contrast, activity which had been frozen down with liquid nitrogen to a glass or charcoal surface, i.e. to either an empty trap or a trap filled with activated charcoal, was 95% released within a few minutes after the coolant was removed (Fig. 3). Note how the rate of release was independent of whether or not the activity was enriched. The 8-minute induction period observed in the release of activity from charcoal presumably represents the time required for the charcoal to warm up.

The characteristic plateaus observed in the release of attached activity (Fig. 2) are evidently not an idiosyncrasy of the system Xe-TiO₂, for similar plateaus were observed in the release of argon from TiO₂ and xenon from silver.

Time and Flux Variation

Before considering further results, it is convenient to define the *attachment efficiency*,

$$[1] \quad A = \frac{(\text{inert-gas activity attached to target})}{(\text{total inert-gas activity})}$$

The results given in Tables I and II show that A is independent of irradiation time

TABLE I
Effect on A of variation in irradiation time

System*	Time (hours)	A (equation [1])
Ar-Al	2	.019
Ar-Al	6	.014
Ar-Al	110	.021
Xe-Al	2	.010
Xe-Al	27	.0088
Xe-Al	110	.0095

*Inert gas at about 700 mm.

and neutron flux, at least for the times and fluxes used. In addition, A is unaffected by an increase in the proportion of fast neutrons (Table II, fifth line).

Variation in Pressure and Particle Size

The attachment efficiency, A , was found to be independent of pressure using a fine powder, but to vary in an inverse manner with pressure when a very coarse powder or no powder at all was used. Thus, referring to Table III, it is seen that the values of A

TABLE II
Effect on A of variation in neutron flux

System*	Position†	Approximate neutron flux (neutrons cm ⁻² sec ⁻¹ × 10 ⁻¹²)	A (equation [1])
Ar-TiO ₂	S-15-1	2	.16, .16
Ar-TiO ₂	S-15-3	6	.16
Ar-TiO ₂	S-3-5	13	.10, .12, .12
Ar-TiO ₂	NRU-J	27	.13
Xe-TiO ₂	S-15-3 + Cd	0.7	.020, .025
Xe-TiO ₂	S-15-3	6	.016, .017
Xe-TiO ₂	S-9-5	17	.016, .016, .017 .019, .025

*Inert gas at about 700 mm.

†Positions with designations such as "S-15-1" refer to the "self-serve" facility of the Chalk River NRX reactor. The position "NRU-J" refers to the "self-serve J-rod" of the Chalk River NRU reactor. The designation "+Cd" means that the sample was wrapped in 0.038 cm of cadmium to reduce the thermal neutron flux.

TABLE III
Effect on A of variation in pressure and particle size

Solid	Dimensions of solid (microns)	Pressure (mm)	A^* (using Ar)	A (using Kr)	A^* (using Xe)
TiO ₂	<10	700	.14†	{.026, .031 .036, .043	.019†
TiO ₂	<10	70	.18, .18		.014, .019, .025
TiO ₂	<10	7	.1 ₅		
TiO ₂	<10	0.7	.1 ₃		
Al	590-840 (i.e. 20-30 mesh)	700	.0035, .0037		
Al	590-840	70	.014, .021, .02 ₅		
Al	<10	700	.018†		
Empty quartz capsule	4700 (I.D.)	700	.0002 ₉ , .0005 ₃		{.0001 ₃ , .0001 ₇ .0003 ₁
Empty quartz capsule	4700 (I.D.)	72			.0006 ₁ , .0008 ₃
Empty quartz capsule	4700 (I.D.)	11			.008 ₃
Empty quartz capsule	4700 (I.D.)	7.6			.01 ₁
SiO ₂ powder	<75	700	.055, .057		.014, .023, .026
Crushed quartz tubing	Indefinite	7			.02 ₆

*Whenever the attached activity was very low (<2000 counts min⁻¹), and the value of A therefore uncertain, the second figure of A is written as a subscript.

†Mean value based on data given in Tables I and II.

for systems involving <10 μ TiO₂ were essentially the same whether the inert gas was at 700 or 70 mm (or even at a lower pressure in the case of the system Ar-TiO₂). On the other hand, with 590-840 μ aluminum, A increased by a factor of 5 when the pressure was lowered from 700 to 70 mm. The value of A observed at the lower pressure was evidently the limiting value, since it agrees with the value obtained with <10 μ aluminum. To further demonstrate the effect of using a coarse powder, inert gases were irradiated in the usual quartz capsules *but without any powder present*. A was now exceedingly low at 700 mm, though it increased rapidly as pressure was decreased. The values of A obtained with powdered SiO₂ or crushed quartz tubing presumably represent the limits

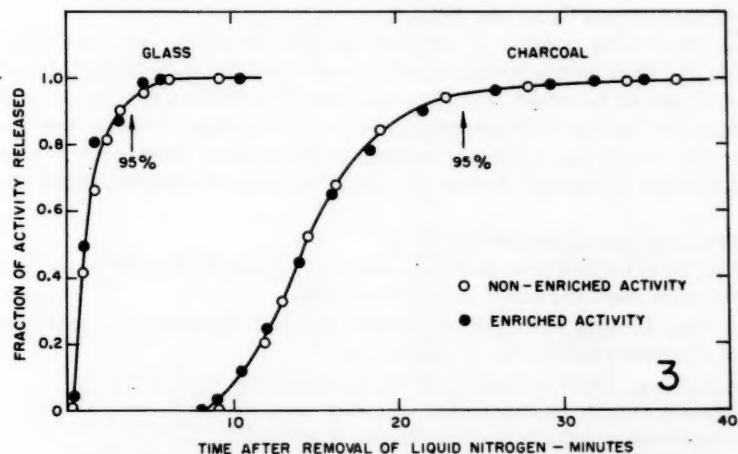
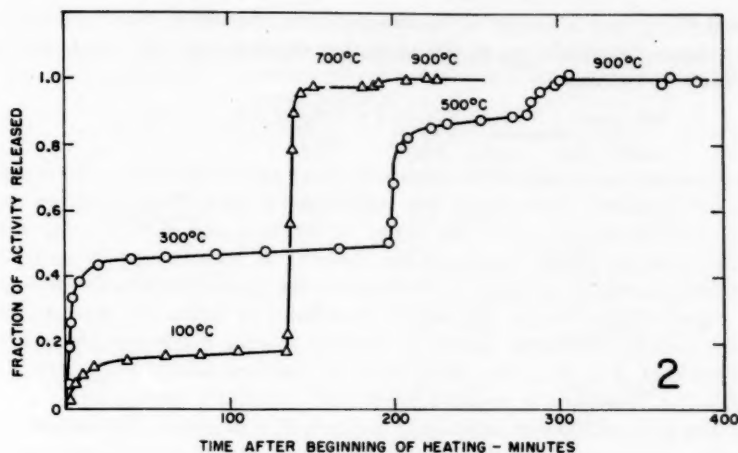


FIG. 2. Release of ^{135}Xe activity which has become attached to TiO_2 . Two typical experiments out of a total of 11 are shown. In each experiment the temperature was raised rapidly (i.e. within 2 to 3 minutes) to a given value, was held constant until a well-defined plateau was reached, and was then raised to the next value indicated.

FIG. 3. Release of ^{135}Xe activity from glass and charcoal surfaces. The activity was frozen down to the surfaces at liquid-nitrogen temperature, and at zero time the liquid nitrogen was removed. The enriched activity was obtained by driving attached activity out of silicon.

of the increase. (The possibility that the small activities attached to the quartz capsules were due to ^{135}Xe formed by the fission of uranium impurities was tentatively eliminated in blank experiments, i.e. by irradiating evacuated quartz capsules.)

The "Collection Distance"

The results of the experiments on pressure and particle-size variation will be more suited for subsequent discussion if they are expressed in terms of the "collection distance", i.e. the apparent maximum distance from which attached activity can originate. Consider the empty-quartz-capsule experiments. The capsules were cylinders with an

I.D. ($2r$) of 0.47 cm and a length (l) of about 2.5 cm. Assuming that one half of the activity in a layer the thickness of the collection distance (d) will reach the capsule in an attachable state, then

$$[2] \quad A_{\text{observed}} = \left(\frac{A_0}{2}\right) \left(\frac{2\pi r l d + 2\pi r^2 d}{\pi r^2 l}\right),$$

where A_0 is the attachment efficiency under conditions when the limiting value is observed, i.e. using a fine powder. Interpreting the experimental data (Table III) in terms of equation [2], one obtains $d = 16 \mu$ for argon at 700 mm and $d = 15 \mu$ for xenon at 700 mm. (The figure for xenon represents the mean of all relevant experiments, with A corrected to 700 mm where necessary.) A collection distance is less readily derived from the powder experiments in Table III, since it is difficult to define the pore spacing in a loosely packed powder. However, assuming that the spacing is comparable to the grain size, it follows that $d > 10 \mu$ (i.e. there was no pressure effect with $< 10 \mu$ TiO_2), $d < 590\text{--}840 \mu$ (i.e. there was a pressure effect with $590\text{--}840 \mu$ aluminum).

The mean free path at 700 mm is 0.11μ in argon, 0.07μ in xenon. The values obtained for the collection distance are therefore about 200 times larger than the mean free paths.

Trends among the Different Gases and Powders

The values of A for a number of different systems involving argon and xenon are given in Table IV; data for the system Kr- TiO_2 were included in Table III. In assessing these results, it should be noted that the experimental variables had values such that A will be largely unaffected (i) by differences in irradiation time, neutron flux, pressure, and particle size, or (ii) by activity attached to the quartz capsule or formed from uranium impurities in the quartz. Any trends among the different systems should therefore be real.

The most obvious trends are the following:

(i) $A \ll 1$. Thus for systems involving argon, A generally lies between 0.011 and 0.14; when xenon is used, the range is 0.0025 to 0.026.

(ii) $A_{\text{Ar}} > A_{\text{Xe}}$. Judging from the one system in which krypton was used, this relation can likely be extended to $A_{\text{Ar}} > A_{\text{Kr}} > A_{\text{Xe}}$.

(iii) $A_{\text{oxide}} > A_{\text{metal}}$. There is a fair number of exceptions to this trend.

(iv) Considering just the systems involving elemental solids, it appears that A does not vary systematically with the atomic weight of the solid.

DISCUSSION

It has been found that, when the inert gases argon, krypton, and xenon are irradiated with neutrons in the presence of various powders, a portion of the inert-gas activity becomes attached to the powder. A number of empirical characteristics of the attachment has already been considered, and it remains only to discuss certain general matters.

Mechanism of Attachment

It was pointed out in the introductory section that material which becomes attached to a target in connection with (n, γ) events will, at the moment of attachment, be isotopically enriched in the products of the (n, γ) event. However, if the attached material is an inert gas, the enrichment will persist only if the attachment is penetrative, as distinct from surficial. The high degree of enrichment observed in the present work therefore points to attachment which (i) is due to (n, γ) events, and (ii) is penetrative. Penetrative attachment is also suggested by the fact that the attached activity was released much less readily than adsorbed activity.

TABLE IV
Values of A for various systems involving argon and xenon*

Solid	Atomic weight of solid	A (using Ar)	A (using Xe)
B	11	{ .002 ₄ , .0024 = .0043, .0089 .002 ₄ , .0045	
C (diamond)	12	.012	
C (graphite)	12	.054, .063	
Al	27	.018†	.0095†
Al ₂ O ₃		.037, .041	.0033, .0039
Al ₂ O ₃ (hydrated)		.032	
Si	28	.032, .033	.012, .018
SiO ₂		.055, .057	.014, .023, .026
CaF ₂		.052	
Ti	48	.022, .034	.0027, .0044
TiO ₂		.14†	.019†
V ₂ O ₅		.050, .069	
Fe	56	.045, .076	
Fe ₂ O ₃		.036	
Co	59	.027	
Ni	59	.011, .012	
Ni ₂ O ₃		.064	
Zn	65	.027	
Se	79	.0035, .009 ₁	
Nb	93	.014	.0080
Nb ₂ O ₅		.14	.018
Rh	103	.019	
Ag	108	.003 ₄ , .0053	.0025, .0033
Ag ₂ O		.001 ₁	.0004, .0007
Sn	119	.021	.0026
Ta	181	.029	
Pb	207	.018	.0028
PbO		.079	.0031
PbF ₂		.014	

NOTE: Pairs of systems which are exceptions to the trends $A_{Ar} > A_{Xe}$ and $A_{oxide} > A_{metal}$ are indicated with double lines.

*The inert gas was always at about 700 mm. The powders generally had assorted grain sizes ranging up to about 75 μ , though in certain cases the grains were consistently smaller than 10 μ (C-graphite, Al, TiO₂, Co, Se, and Rh). In one case (Al₂O₃), the grains were consistently coarse. See also footnote * of Table III.

†Mean value based on data given in Tables I and II.

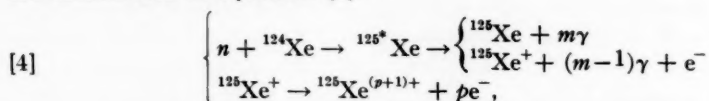
At least two mechanisms can be envisaged by which penetrative attachment could come about following (n, γ) events. According to what may be called the "recoil mechanism", the emission of the capture gamma rays might cause the capturing atoms to recoil directly into the target. Gamma-recoil energies are given by

$$[3] \quad E_{\text{recoil}} = 536 E_{\gamma}^2 / M,$$

where E_{recoil} is in electron volts, E_{γ} in million electron volts, and M in atomic mass units. The recoil energies thus vary in the right direction to explain the trend $A_{Ar} > A_{Kr} > A_{Xe}$. Consider, however, the actual values of E_{recoil} . Assuming capture gamma energies of 4 Mev (there is nothing published on the capture spectra of the inert gases), E_{recoil} works out to about 210 ev for argon and 70 ev for xenon. Energies this low would probably

be degraded below the level at which penetration is possible within a few collisions.³ Accordingly, it appears that a recoil mechanism would *by itself* be quite incompatible with the experiments on pressure and particle-size variation, for, as has been shown, these experiments require that attached activity be able to originate from a distance about 200 times larger than the mean free path.

An alternative mechanism of penetration is the "attraction mechanism", which is based on the electrical attraction between charged inert-gas atoms and solid surfaces. Atoms undergoing (n, γ) reactions not only gain recoil energy (equation [3]), but may also become highly charged. The charge is acquired due to the twofold effect of inner electrons being expelled by the conversion of capture gamma rays (7, 10), plus the vacancy-cascade process which occurs whenever there is an inner electron vacancy and in which still further electrons are expelled ("Auger electrons"). Thus, the conversion of a single inner electron has been observed to lead to mean charges of +4.3 for argon (11)⁴ and +8 for krypton and xenon (12, 13). The steps leading to the build-up of charge are summarized in equations [4]:



where m is a number between 1 and 6 (14), and p is a number between 0 and about 20 (13). Suppose that the charged atoms escaped neutralization in the gas phase for a sufficient number of collisions that they finally found themselves in the vicinity of a solid surface. Then, *regardless of whether or not recoil energy was still present*, they would be accelerated electrically towards the surface. The acceleration might come about in several ways: (i) electric-image attraction, (ii) attraction between the charged atoms and their separated electrons (the latter would presumably accumulate on surfaces), or (iii) attraction between the charged atoms and electrons formed as a result of the passage of pile gamma rays through the sample. The acceleration would continue until, at a distance of a few angstroms from the surface, the atoms would probably lose their charge due to electron transitions (15). The neutral atoms would then coast the remaining distance to the surface, and, provided sufficient energy had been gained, might penetrate.

The main requirement of the attraction mechanism is seen to be that the charged atoms formed in the (n, γ) events must escape neutralization in the gas phase; in other words, the charge-exchange cross sections must be small. While the cross sections for charge exchange between ions and the corresponding neutral species have, unfortunately, not been studied beyond charges of +3 (16), there is reason to believe that they become exceedingly small with increasing charge.⁵ The attraction mechanism is therefore more nearly compatible than the recoil mechanism with the large values observed for the collection distance.

On the other hand, the attraction mechanism has several weaknesses. The extent to which the capture gamma rays are converted may be very low in the nuclides with which the present work is concerned. Also, the trend $A_{\text{Ar}} > A_{\text{Kr}} > A_{\text{Xe}}$ is the reverse to what might be expected: (i) the nuclear-level density increases with mass (17, p.

³The minimum energy at which penetration can occur is perhaps to be identified with the displacement energy, E_d . The value of E_d is about 25 ev (9).

⁴It was shown in the work of reference 11 that the ${}^{36}\text{Cl}$ atoms formed by electron capture in ${}^{36}\text{Ar}$ have a mean charge of 3.3. Other things being equal, conversion in argon would accordingly lead to a mean charge of 4.3.

⁵This view was expressed by Dr. J. B. Hasted (University College, London, England) in a private communication. Further discussion of charge exchange will be postponed for a subsequent paper.

406), so that heavy atoms should have a greater number of low-energy capture gamma rays than light atoms (conversion coefficients vary inversely with gamma energy (17, p. 222)); (ii) the conversion coefficients at a given gamma energy increase with atomic number (17, p. 223); (iii) the charge produced in vacancy cascades is greater for krypton and xenon than for argon (11, 12, 13). A more detailed discussion of the attraction mechanism will be possible when work currently underway at this laboratory on the capture spectra of the inert gases is completed.

The observation that A is independent of time and flux is compatible with either of the mechanisms that has been considered, for it implies simply that the rate of attachment is independent of time and directly dependent on flux. It is conceivable, however, that for very large values of (time) \times (flux) the rate of attachment, and thence A , will decrease to zero due to the surfaces of the powder becoming saturated.

Sample Heating

If a powder became heated to much over 200° C while under irradiation, the penetrated inert gas would be partially released (cf. Fig. 2). That sample heating is not ordinarily important is shown both by the fact that A is independent of neutron flux when TiO_2 is used, and the fact that the selenium and tin did not melt. On the other hand, sample heating might well account for the unusually low values of A in systems involving boron, silver, and Ag_2O . Boron will heat up owing to the prominent (n, α) reaction in ^{10}B , and silver and Ag_2O owing to the high cross sections with which the short-lived beta emitters ^{108}Ag and ^{110}Ag are formed. Similarly, the fact that three of the six exceptions to the trends $A_{\text{Ar}} > A_{\text{Xe}}$ and $A_{\text{oxide}} > A_{\text{metal}}$ are associated with boron, silver, and Ag_2O may be due to non-uniformity in the effects of sample heating among different systems. (Rhodium should also heat up, though the value of A for the system Ar-Rh appears to be normal.)

Enrichment and Storage of Activity

It is difficult to see how bond-breaking or release effects could be applied to enriching inert-gas activities. The present work indicates that *attachment*, on the other hand, is quite effective in bringing about enrichment with the inert gases. An attachment technique has the added advantage that the enriched activity is in a form convenient for handling or storing. (Compare the method of introducing ^{85}Kr into clathrate compounds (18).)

The possibility of using attachment for enriching activities with substances other than the inert gases was previously suggested by Magnusson (6), who succeeded in applying an attachment technique to gold.

ACKNOWLEDGMENTS

The writer wishes to acknowledge the contributions to the present work made by Drs. J. A. Davies and W. H. Stevens, who assisted in the interpretation of the results. The method of sealing thermocouple wires shown in Fig. 1A (E) was devised by Mr. V. T. Buckley, and the latter also helped design the castle and elevating mechanism.

REFERENCES

1. INTERNATIONAL UNION OF PURE AND APPLIED CHEMISTRY. Nomenclature of inorganic compounds. Butterworths Publications Ltd., London. 1959.
2. J. W. BARNES, W. H. BURGUS, and J. A. MISKEL. In *Radioactivity applied to chemistry*. Edited by A. C. WAHL and N. A. BONNER. John Wiley & Sons, Inc., New York. 1951.
3. A. C. WAHL. In *Radioactivity applied to chemistry*. Edited by A. C. WAHL and N. A. BONNER. John Wiley & Sons, Inc., New York. 1951.
4. S. YOSIM and T. H. DAVIES. *J. Phys. Chem.* **56**, 599 (1952).

5. D. L. BAULCH and J. F. DUNCAN. Proceedings of the Second United Nations International Conference on the Peaceful Uses of Atomic Energy. Vol. 29. United Nations, Geneva, 1958. p. 400.
6. L. B. MAGNUSSON. Phys. Rev. **81**, 285 (1951).
7. S. WEXLER and T. H. DAVIES. J. Chem. Phys. **20**, 1688 (1952).
8. G. T. SEABORG, G. FRIEDLAENDER, and J. W. KENNEDY. J. Am. Chem. Soc. **62**, 1309 (1940).
9. G. J. DIENES. Proceedings of the First United Nations International Conference on the Peaceful Uses of Atomic Energy. Vol. 7. United Nations, New York, 1956. p. 634.
10. C. T. HIBDON and C. O. MUEHLHAUSE. Phys. Rev. **88**, 943 (1952).
11. A. H. SNELL and F. PLEASANTON. Phys. Rev. **100**, 1396 (1955).
12. S. WEXLER. Phys. Rev. **93**, 182 (1954).
13. F. PLEASANTON and A. H. SNELL. Proc. Roy. Soc. (London), A, **241**, 141 (1957).
14. C. O. MUEHLHAUSE. Phys. Rev. **79**, 277 (1950).
15. L. J. VARNERIN. Phys. Rev. **91**, 859 (1953).
16. I. P. FLAKS and L. G. FILIPPENKO. Soviet Phys.—Tech. Phys. **4**, 1005 (1960).
17. R. D. EVANS. The atomic nucleus. McGraw-Hill Book Co., Inc., New York. 1955.
18. D. J. CHLECK and C. A. ZIEGLER. Intern. J. Appl. Radiation and Isotopes, **7**, 141 (1959).

HALF-LIVES OF Rb^{94} , Sr^{94} , Y^{94} , Rb^{95} , Sr^{95} , Y^{95} ¹

K. FRITZE, T. J. KENNETT, AND W. V. PRESTWICH²

ABSTRACT

The existence of a new rubidium isotope, Rb^{94} , has been established and its half-life measured. The half-life of this fission product was determined using the technique of timed precipitations. The value obtained for Rb^{94} was 2.9 ± 0.3 seconds. With this same technique only an upper limit of 2.5 seconds could be assigned to Rb^{95} . The half-lives of the strontium and yttrium daughters were also determined. The strontium isotopes were studied both by timed precipitations and direct measurements. The half-lives of Sr^{94} and Sr^{95} were found to be 1.36 ± 0.06 minutes and 0.8 ± 0.15 minute, respectively. Direct measurements lead to half-lives of 20.35 ± 0.20 minutes for Y^{94} and 10.9 ± 0.2 minutes for Y^{95} .

Experiments, carried out by Hahn and Strassmann (1, 2) and Dillard *et al.* (3, 4), showed the existence of krypton ancestors of Y^{94} and Zr^{95} . Since essentially all fission products decay by β -emission, these experiments also proved the existence of all the intermediate members of the two decay chains (Rb^{94} , Sr^{94} and Rb^{95} , Sr^{95} , Y^{95} , respectively). More direct measurements of some of these nuclides were done by Hahn and Strassmann (1, 2) and Knight *et al.* (5) for Sr^{94} , by Hoffman *et al.* (6) for Sr^{95} , and by Knight *et al.* for Y^{95} (7). This paper reports the first measurement of the Rb^{94} half-life as well as remeasurements of the half-lives of Sr^{94} , Sr^{95} , Y^{94} , and Y^{95} . In addition an estimate for the upper limit of the Rb^{95} half-life is given.

(A) Rubidium 94

The timed precipitation technique as described previously (8) was used to determine the half-life of Rb^{94} . Briefly, this method proceeds as follows: U^{235} is irradiated in a solution which is divided into two portions after the end of the irradiation and rubidium precipitated as perchlorate in both samples at two different times. The two precipitates are later (after almost complete decay of the 1.36-minute Sr^{94}) analyzed radiochemically for Y^{94} . From the amount of Y^{94} in each precipitate, the time interval between the two precipitations and the chemical yields, the half-life of Rb^{94} can be calculated. The experimental details as far as the chemistry is concerned were essentially the same as in the determination of the half-lives of Rb^{92} and Rb^{93} (8). However, the whole procedure had to be accelerated because of the relatively short 20-minute half-life of Y^{94} . Furthermore, the rubidium carrier was added to the uranium solution before the start of the irradiation in order to save time. Counting was usually started approximately 30 minutes after the end of the irradiation.

A gross β -decay curve of yttrium isolated from quickly precipitated rubidium perchlorate clearly shows the following components: 20.35-minute Y^{94} , 3.53-hour Y^{92} , 10.1-hour Y^{93} , and some long-lived Y^{91} . These decay curves, however, are not particularly suitable to determine the relative quantities of Y^{94} in two different samples since these amounts are rather small in comparison with the Y^{92} and Y^{93} present. This arises from the low independent yield and the short half-life of Rb^{94} compared with both the Rb^{92} and Rb^{93} half-lives. For this reason the Y^{94} was counted in a way which would discriminate against the other yttrium isotopes. In the first run this was done by com-

¹Manuscript received November 3, 1960.

Contribution from McMaster University, Hamilton, Ontario. Presented in part at the Third Symposium on Nuclear Chemistry and Radiochemistry held at Atomic Energy of Canada Limited, Chalk River, Ontario, September 6-8, 1960.

²Holder of an Ontario Research Foundation Scholarship 1960-61.

paring the intensities of the 920-kev γ -ray associated with the decay of Y^{94} (5) in the two yttrium samples. A 3×3 in. NaI(Tl) crystal and a 256-channel analyzer was employed. The two samples were counted for a total time of 20 minutes. The samples were alternated in such a way as to cancel the half-life effects. The events of sample No. 1 were stored in the first 128 channels and those of sample No. 2 in channels 129–256. Each group of 128 channels covered the energy region from 0.2 to 1.5 Mev. In run No. 2 the counting was done similarly. However, the selected energy range was from 0.5 to 4.0 Mev and the samples were directly attached to the aluminum can of the NaI(Tl) crystal. Consequently a large number of high-energy β -rays were counted in addition to any γ -rays of this energy range. The decay of the yttrium samples was followed for several half-lives. The high-energy end of this type of spectrum contained only a 20-minute component. This was to be expected since Y^{94} emits β -rays of up to 5.0 Mev and γ -rays of up to 3.5 Mev (5) whereas the β - and γ -energies of the other three yttrium isotopes are considerably lower (5, 9). The counting rates of all channels which contained only events due to the decay of Y^{94} were added and used as a measure of the relative content of Y^{94} in the two rubidium perchlorate precipitates. This second method was also used for runs Nos. 3 and 4. The results of the four half-life measurements for Rb^{94} are given in Table I.

TABLE I
Summary of Rb^{94} half-life data

Run	U^{235} (μ g)	Flux (neutrons $cm^{-2} sec^{-1}$)	Duration of irradiation (seconds)	RbClO ₄ precipitation times (seconds)		Rb^{94} half-life (seconds)
				1st ppt.	2nd ppt.	
1	200	3×10^{12}	10	9.0	11.7	2.8 ₁
2	400	3×10^{12}	10	7.6	11.1	2.6 ₂
3	400	3×10^{12}	10	8.9	12.9	3.1 ₃
4	300	3×10^{12}	10	6.1	9.1	2.8 ₃

The half-life values given in Table I are seen to have good internal consistency. The suggested value is 2.9 ± 0.3 seconds. The sources of error which may not effect this consistency have been discussed previously (8).

In order to check the reliability of the method, the yttrium samples can be analyzed for both Y^{93} and Y^{94} from which one can obtain the ratios of the Rb^{93} and Rb^{94} half-lives. This ratio is, of course, independent of the precipitation times provided that the half-lives and independent yields of the precursors are similar. This ratio $T_{1/2}(Rb^{94})/T_{1/2}(Rb^{93})$ was determined for runs No. 2, 3, and 4, and yielded a value of 0.48 ± 0.05 . Using 5.6 seconds (8) for the half-life of Rb^{93} one obtains 2.7 ± 0.3 seconds for Rb^{94} . This value is expected to be somewhat low because of precursor effects.

(B) Strontium 94

Hahn and Strassmann (1) showed the existence of a decay period of approximately 2 minutes among the strontium isotopes produced in fission. They also were able to establish the genetic relationship to the 20-minute Y^{94} (1). Knight *et al.* (5) measured the half-life of Sr^{94} by milking yttrium from a purified fission product strontium sample and obtained 1.3 ± 0.2 minutes. Two methods were used in this work; the timed precipitation technique and direct counting. Strontium can be precipitated quickly and in sufficient purity as the nitrate. The coprecipitation of yttrium was found to be around 0.1%. The procedure employed is completely analogous to the one used for the half-life

determination of Rb^{94} with one exception; the strontium nitrate precipitate was separated from the supernatant solution of 80% nitric acid by means of glass filter crucibles having medium porosity and selected for fast filtration speed. A separation in approximately 15 seconds was achieved when a precipitating volume of 10 ml was used. The strontium nitrate was analyzed for its Y^{94} content starting approximately 8 minutes after the end of the irradiation. The amounts of Y^{94} were either obtained by unravelling gross β -decay curves using a least-squares method (runs No. 1 and No. 2) or by comparing the intensities of the 920-keV γ -ray (5) associated with the decay of Y^{94} (run No. 3). The results of these measurements are:

- (1) 1.37 minutes,
 - (2) 1.31 minutes,
 - (3) 1.45 minutes,
- average 1.38 ± 0.07 minutes.

This half-life, although short, makes feasible the observation of the γ -rays associated with the decay of Sr^{94} . To do this the following procedure was used. Immediately after the irradiation of U^{235} , strontium and barium were precipitated as nitrates. The barium was removed as the chromate and the filtrate was counted using a 3×3 in. NaI(Tl) crystal and a 256-channel pulse-height analyzer. The counting began about 1.7 minutes after the end of the irradiation. The spectrum, which was rather complex, extended to about 3.5 MeV. The two major periods associated with the spectrum were about 1 minute ($\text{Sr}^{94} + \text{Sr}^{95}$) and 7.5 minutes (Sr^{93}). A prominent γ -ray of 1.42 MeV was assigned to Sr^{94} on the basis of apparent half-life. Consequently this transition was used to determine the half-life of Sr^{94} by direct measurement. A series of measurements was carried out in which the spectra were recorded as a function of time, using the four 64-channel subgroups of the analyzer. Three such runs were done and the area of the 1.42-MeV photopeak was determined for each spectrum.

The half-lives determined from these runs are:

- (1) 1.34 minutes,
 - (2) 1.33 minutes,
 - (3) 1.36 minutes,
- average 1.34 ± 0.04 minutes.

The direct measurement agrees very well with the results of the timed precipitation experiment. The combined values give a half-life of 1.35 ± 0.05 minutes, which is entirely consistent with the results of Knight (5).

(C) *Yttrium 94*

Most authors agree that the half-life of this nuclide is 20 minutes (1, 5, 10) with the exception of Brown and Katcoff, who report 16.5 minutes (11). The decay of Y^{94} was measured by observing the rate of disappearance of the 920-keV line in the γ -spectrum of Y^{94} (5). The counting system for this purpose has been described previously (8). This method has the obvious advantage of discriminating strongly against other yttrium isotopes. The yttrium was isolated from fission product strontium which had been precipitated as a nitrate. Since the half-life of Sr^{96} is about half that of Sr^{94} one can by proper choice of the separation time discriminate against ingrowing Y^{95} . The radio-strontium was allowed to decay for a few minutes and then the yttrium was separated as the hydroxide. In this way the Y^{92} and Y^{93} content of the final sample was kept as

low as possible. The yttrium was then purified using standard procedures (12). A decay curve is shown in Fig. 1 and the results of two such measurements obtained from a least-squares analysis of the data were:

- (1) 20.4 minutes,
- (2) 20.3 minutes,
- average 20.35 ± 0.2 minutes.

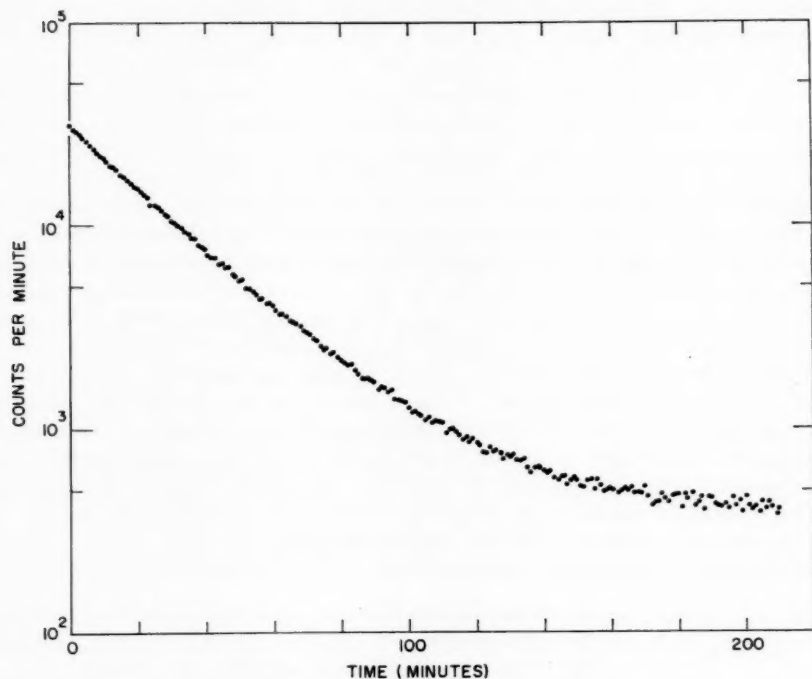


FIG. 1. A decay curve obtained for Y^{94} . The only events recorded were those whose pulse height fell within a 6% window centered about the 920-kev γ -ray line.

This value is in very good agreement with most of the previously reported measurements. An explanation for the lower value of 16.5 minutes is the undetected presence of 10.9-minute Y^{95} .

(D) Rubidium 95

An attempt was made to prove the existence of Rb^{95} directly. Rubidium perchlorate was precipitated 8 seconds after the end of a 10-second irradiation of 400 μ g of U^{235} at a flux of 3×10^{12} neutrons/cm² sec. The rubidium isotopes and their respective strontium daughters were then allowed to decay for 10 minutes after which the sample was analyzed for radioyttrium. The sample was directly mounted on the face of a 3 \times 3 in. NaI(Tl) crystal. A single-channel analyzer was set to accept γ -rays in the interval 2.0 to 3.7 Mev. The thin aluminum can of the crystal also permits β -counting. The decay of the combined radiations was followed for 220 minutes and the decay curve is shown in Fig. 2. It can be seen from Fig. 2 that there is no indication of a 10.9-minute Y^{95} .

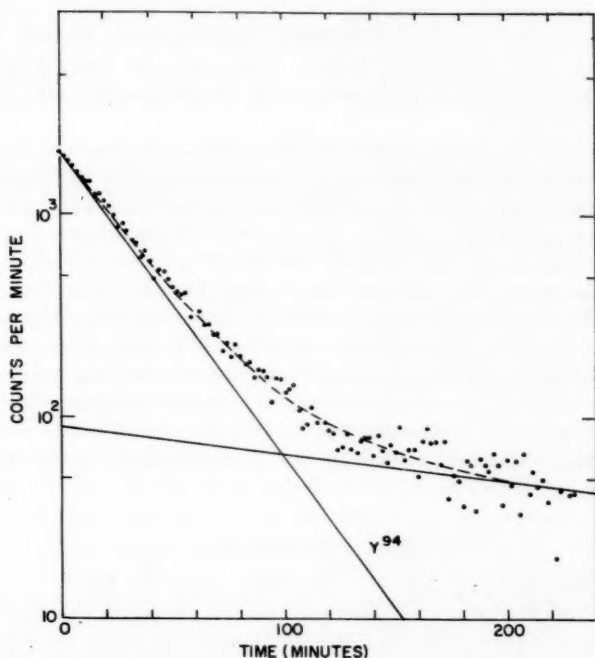


FIG. 2. This decay curve was used to infer that the half-life of Rb^{86} is less than 2.5 seconds. If Rb^{86} had a half-life greater than or equal to 2.5 seconds, the decay curve shown would have had a 10.9-minute Y^{86} component with an initial counting rate of 500 c.p.m. Since the curve is represented quite well by 20-minute Y^{84} and 3.5-hour Y^{82} components, the Y^{86} component must be small.

component, although its decay characteristics do satisfy the imposed counting conditions. From the time schedule of the whole experiment and the independent yields of Rb^{84} and Rb^{85} (13) an upper limit of 2.5 seconds for the Rb^{85} half-life can be estimated. This is based on the assumption that a 25% contribution of Y^{86} to the original counting rate would have been found.

(E) Strontium 95

So far the only half-life measurement of Sr^{95} was done by Hoffman *et al.* (6), who obtained approximately 0.7 minute. It can be assumed that their method was the same as the one used by Knight *et al.* (5) for Sr^{94} .

Two values for the half-life of Sr^{95} were obtained from the relative quantities of Y^{95} in the yttrium samples of runs No. 1 and No. 2 which are mentioned in Section (B). The values obtained were:

- (1) 0.6₈ minute,
 - (2) 0.8₈ minute,
- average 0.8 ± 0.15 minute.

An attempt was made to measure the half-life directly by observing the high-energy β -rays emitted from rapidly separated strontium. The results were consistent with the value quoted above. However, the technical difficulties encountered restricted the usefulness of the method.

(F) Yttrium 95

Only two values for the half-life of Y^{95} have been reported. Knight, Burgus, and Prestwood (7) quote 10.5 minutes in private communication and Knight *et al.* (5) mention a 9.5 minute Y^{95} activity as a low-intensity component in gross β -decay curves of fission product yttrium.

In order to remeasure the decay period of Y^{95} a sample was prepared in the following way. Immediately after the irradiation of U^{235} and the addition of strontium carrier, strontium nitrate was precipitated, centrifuged, and washed with 80% nitric acid. The strontium nitrate was dissolved in water, reprecipitated as the nitrate, and centrifuged. The supernate was directly used for a tributylphosphate extraction (12) of the yttrium which had grown in during the 3-minute interval between the two strontium nitrate precipitations. In this way the Y^{95} was enriched as much as chemically possible. The yttrium was further purified and finally β -counted as the oxalate long enough to allow a correction to be made for the small contribution due to the long-lived components. The data were then subjected to a least-squares analysis for two components. Half-lives of 10.9 ± 0.2 minutes and 20.4 ± 0.3 minutes were obtained for Y^{95} and Y^{94} respectively. The value of 20.4 ± 0.3 minutes agrees very well with the results given in Section (C) for Y^{94} .

ACKNOWLEDGMENTS

We wish to acknowledge the financial assistance given by the National Research Council and one of us (W.V.P.), that from the Ontario Research Foundation. We also appreciate the co-operation received from the McMaster University Reactor staff.

REFERENCES

1. O. HAHN and F. STRASSMANN. *Naturwiss.* **31**, 249 (1943).
2. O. HAHN and F. STRASSMANN. *Z. Physik*, **121**, 729 (1943).
3. C. R. DILLARD, R. M. ADAMS, H. FINSTON, and A. TURKEVICH. *National Nuclear Energy Series-PPR. Vol. 9.* McGraw-Hill Book Co., Inc., New York. 1951. p. 616.
4. C. R. DILLARD, R. M. ADAMS, H. FINSTON, and A. TURKEVICH. *National Nuclear Energy Series-PPR. Vol. 9.* McGraw-Hill Book Co., Inc., New York. 1951. p. 624.
5. J. D. KNIGHT, D. C. HOFFMAN, B. J. DROPESKY, and D. L. FRASCO. *J. Inorg. & Nuclear Chem.* **10**, 193 (1959).
6. D. C. HOFFMAN, J. D. KNIGHT, D. L. FRASCO, and B. J. DROPESKY. Unpublished data quoted in D. Strominger, J. M. Hollander, and G. T. Seaborg. *Revs. Modern Phys.* **30**, 866 (1958).
7. J. D. KNIGHT, W. H. BURGUS, and R. J. PRESTWOOD. Private communication listed in *National Nuclear Energy Series-PPR. Vol. 9.* McGraw-Hill Book Co., Inc., New York. 1951. p. 2063.
8. K. FRITZE and T. J. KENNETT. *Can. J. Phys.* **38**, 1614 (1960).
9. W. A. CASSATT and W. V. MEINKE. *Phys. Rev.* **99**, 760 (1955).
10. C. R. DILLARD, R. M. ADAMS, H. FINSTON, and A. TURKEVICH. *National Nuclear Energy Series-PPR. Vol. 9.* McGraw-Hill Book Co., Inc., New York. 1951. p. 692.
11. L. J. BROWN and S. KATCOFF. *J. Chem. Phys.* **17**, 497 (1949).
12. C. H. STANLEY. *Atomic Energy Commission Report L.A.-1721.* p. 104.
13. A. C. WAHL. *J. Inorg. & Nuclear Chem.* **6**, 263 (1958).

HALF-LIFE OF Cs^{137} ¹

H. FARRAR, A. K. DASGUPTA, AND R. H. TOMLINSON

ABSTRACT

The half-life of Cs^{137} was found to be 30.4 ± 0.4 years by determining the amount of Ba^{137} produced in various times from a known number of Cs^{137} atoms. The numbers of barium and cesium atoms were determined from isotope dilution data obtained with a mass spectrometer.

INTRODUCTION

In recent years there have been numerous measurements of the half-life of Cs^{137} . The original estimate by Glendenin and Metcalf (1) was 33 ± 3 years. Wiles and Thode (2) later published a value 33 ± 2 years which was obtained with a mass spectrometer by observing, over a period of years, the decrease in the relative amount of Cs^{137} with respect to Cs^{133} in fission product cesium.

Later experiments used the isotope dilution technique with a mass spectrometer to determine the number of Cs^{137} atoms in a given sample, and 4π absolute β -counting to determine the activity. In this way, values of 26.6 ± 0.4 years (3), 30.0 ± 0.4 years (4), 28.6 ± 2 years (5), and 32.6 ± 1.6 years (6) were obtained. Owing to the considerable disagreement in these values, a new method was desirable.

Rather than determine the rate of decay of Cs^{137} by counting the radiation released, the present work reports on the determination of the half-life by measuring the rate of formation of the daughter nuclide, Ba^{137} , from a known amount of Cs^{137} . Both measurements use isotope dilution technique with a mass spectrometer, and do not require any absolute counting procedures. It is also important that the present method is independent of the decay scheme and of radioactive contaminants.

EXPERIMENTAL

About 0.5 mg of fission product cesium was used for this experiment, amounting to about 20 mc of activity and generating about 1×10^{-8} grams of Ba^{137} per day.

Preliminary experiments with a 0.4-ml column of Dowex 50 cation exchange resin (100–200 mesh) in the acid form were made to determine conditions for the separation of barium from cesium. Using 0.5 mg of Cs^{133} with tracer Cs^{137} , and also the radioisotope Ba^{139} , it was found that when the column was eluted with 1 M HCl, virtually all the cesium was removed within the first 15 ml, the maximum coming off in the 9th ml, whereas the barium remained adsorbed until after the 90th ml. It was found that after the 22nd ml, an increase in concentration to 3 M HCl removed the barium tracer within a further 30 ml of eluate.

The fission product cesium was adsorbed on a new column and eluted as previously described. The eluate was set aside to allow the accumulation of Ba^{137} . While this was taking place, a weighed aliquot of isotope-enriched Ba^{134} solution was added. At the end of a measured period, the cesium plus the mixture of Ba^{137} and Ba^{134} were adsorbed on a new column. The cesium was eluted as before with 1 M HCl and was retained for a further period. The concentration of the elutriant was increased after the 22nd ml to 3 M, and the Ba^{137} plus the Ba^{134} were collected. Complete elution of the barium was

¹Manuscript received November 3, 1960.

Contribution from Hamilton College, McMaster University, Hamilton, Ontario. Presented at the Third Symposium on Nuclear Chemistry and Radiochemistry held at Atomic Energy of Canada Limited, Chalk River, Ontario, September 6–8, 1960.

unnecessary since only the ratio of the Ba^{134} and Ba^{137} isotopes was needed to determine the number of Ba^{137} formed in the period. The barium solution was evaporated first in a pyrex beaker and then on a teflon sheet to one drop, which was placed on the filament of a 90° solid source mass spectrometer, for isotopic analysis.

RESULTS

Small amounts of natural barium were evident in the mass spectrograms. Since the isotopic content of natural barium is principally Ba^{138} , which is very different from the enriched Ba^{134} solution, a measurement of the ratio of Ba^{134} to Ba^{138} in any sample gives a precise knowledge of the amount of Ba^{137} contamination present. This correction varied almost linearly from 20% for the shortest period of growth to 0.8% for the longest.

Measurements of the amount of Ba^{137} formed in eight different periods have been made. The period in each case was the time between similar parts of consecutive cesium elutions. In case the rate of elution were to vary from one separation to the next, these parts were chosen when the 9th ml of eluate, which included most of the cesium, left the column.

Apart from the correction to the Ba^{137} for natural barium contamination, which already has been mentioned, the only correction made was that due to the loss and decay of Cs^{137} during the series of separations. To obtain this correction, the relative activity of the total sample was counted between each separation with a 4π ionization chamber.

The original number of Cs^{137} atoms, found by three independent isotope dilutions with natural cesium, had an average value of 7.592×10^{17} atoms. The maximum deviation from this was 0.4%. To prevent excessive increases of Cs^{138} in the sample, the first two isotope dilutions were performed with a small known fraction of the total. In the third case, the total sample was used.

The concentration of the barium isotopes in the Ba^{134} enriched isotope dilution solution was found by three independent isotope dilutions using natural barium. The average concentration was found to be 5.861×10^{14} atoms of Ba^{134} per gram of solution, the maximum deviation from this being 0.7%.

One cesium and one barium isotope dilution were performed without the use of the electron multiplier in the mass spectrometer. These results showed no difference from those obtained with the electron multiplier. Furthermore, a careful determination of the relative abundances of natural barium isotopes has been made both with and without the electron multiplier. Since both sets of results were identical and also in agreement with the values obtained by Nier (7), it can be concluded that no significant mass discrimination occurred at the electron multiplier.

The results of the data obtained for each separation are shown in Table I.

TABLE I
Accumulation of Ba^{137} for various periods

Period, days	Number of Ba^{137} formed
0.924	$0.459 \pm 0.008 \times 10^{14}$
2.975	$1.415 \pm 0.005 \times 10^{14}$
5.046	$2.338 \pm 0.014 \times 10^{14}$
6.074	$2.968 \pm 0.021 \times 10^{14}$
8.215	$3.948 \pm 0.043 \times 10^{14}$
10.085	$4.794 \pm 0.044 \times 10^{14}$
16.715	$7.91 \pm 0.10 \times 10^{14}$
48.960	$23.25 \pm 0.13 \times 10^{14}$

Column 2 gives the numbers of Ba^{137} formed from the initial amount of Cs^{137} , which are corrected to allow for loss and decay of the Cs^{137} . This correction accumulated to 5.00% for the final period. Of this, approximately 1% was due to decay and almost all the rest was lost in the separation between the fifth and sixth periods. A linear least-squares plot of the data in Table I is shown in Fig. 1. The slope for points obtained before

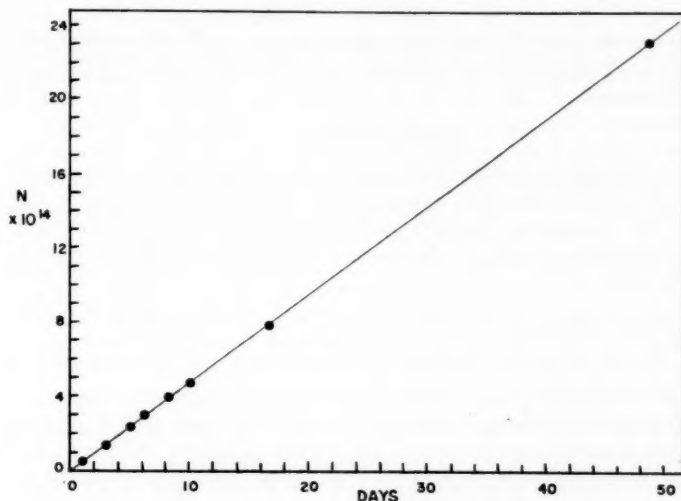


FIG. 1. Rate of growth of Ba^{137} .

the loss of cesium is the same as the slope for points obtained after, the appropriate corrections having been made. The slope thus obtained was found to be 4.746×10^{13} Ba^{137} per day. An error of $\pm 1.2\%$ has been arbitrarily assigned to this slope noting that six of the nine points, including (0,0), lie within these limits. The least-squares plot passes close to the origin, giving, at $t = 0$, 33 minutes of growth of Ba^{137} , which is small compared with the time intervals.

From these data, the half-life was calculated to be 30.4 ± 0.4 years. The error in the half-life has been estimated from the assigned errors in each of the measured quantities.

ACKNOWLEDGMENTS

This research was supported by the National Research Council of Canada. One of us (H. F.) is indebted to the Eldorado Mining and Refining Limited for the award of the Charles G. Williams Fellowship.

REFERENCES

1. L. E. GLENDENIN and R. P. METCALF. National Nuclear Energy Series. Vol. 9, Paper 152. McGraw-Hill Book Co., Inc., New York. 1951.
2. D. R. WILES, B. W. SMITH, R. HORSLEY, and H. G. THODE. Can. J. Phys. **31**, 419 (1953).
3. D. M. WILES and R. H. TOMLINSON. Phys. Rev. **99**, 188 (1955).
4. F. BROWN, G. R. HALL, and A. J. WALTER. J. Inorg. & Nuclear Chem. **1**, 241 (1955).
5. A. J. MOSES and H. D. COOK. United States Atomic Energy Commission, TID-7568, 1958.
6. L. E. GLENDENIN and E. P. STEINBERG. Private communication.
7. A. O. NIER. Phys. Rev. **54**, 275 (1938).

SEARCH FOR THE (n,t) REACTION AT 14 MEV IN SOME MEDIUM WEIGHT NUCLEI¹

A. P. BAERG AND G. C. BOWES

ABSTRACT

The (n,t) reaction at 14.6 Mev has been observed to occur in S^{32} with a cross section of 4 ± 1 microbarns. Upper limits for the cross section of this reaction are also given for Ca^{40} , Cr^{50} , Fe^{54} , and Zn^{64} and the results are discussed qualitatively in the light of recently reported $(10) (n, He^3)$ reactions.

INTRODUCTION

Among various types of nuclear reactions which are energetically possible with 14-Mev neutrons, the (n,t) reaction has been studied only in very light nuclei (1, 2, 3, 4). In accordance with the reciprocity theorem such reactions should be important in some cases since reactions of the type (t,n) are known to occur at 2.65 Mev in medium weight nuclei (5, 6).

Intuitively the emission of a complex loosely bound structure such as a triton seems much less probable than that of single-particle emission. In early work on (p,t) reactions, however, Cohen and Handley (7) already concluded that the inherent probability for triton emission, in the breakup of a compound nucleus at least, was little, if any, less than that for protons or neutrons. Reactions of the type (n,t) are in general characterized by large negative Q values and on the statistical theory the cross sections are expected to be generally very small. In lighter elements, however, a strong component of direct interaction is evident in Li^6 and Li^7 (1) as well as in Be^9 (3). More recent work by Cohen and others (8, 9) on the (p,t) reaction at 23 Mev shows strong evidence for a pickup mechanism for this reaction in heavier elements.

Recently Kumabe *et al.* (10) have reported the occurrence of (n, He^3) reactions at 14.8 Mev in Mn^{55} , Co^{59} , As^{75} , and Rh^{103} . The cross sections observed range in value from 1 to 6 millibarns and the authors have suggested several possible direct interaction mechanisms to account for the cross-section magnitudes.

In view of the accumulating evidence of significant contributions from direct interaction in 14-Mev neutron reactions, we have made a cursory search for the (n,t) reaction in medium weight elements. Several isotopes were selected for study by the activation method, from a consideration of reaction Q values and unambiguous identification of the product nucleus with the (n,t) reaction. This has restricted us to stable even-even target nuclei of low neutron number, to avoid interference from (n,p) or (n,d) reactions on other isotopes.

EXPERIMENTAL

The various targets were bombarded with neutrons of average energy 14.6 Mev (11) from the $T(d,n)He^4$ reaction using about 1 ma of 120-kev deuterons incident on a thick tritium-loaded titanium target.* Cross sections were measured by comparison of the positron activity induced in the sample with that induced in a fluorine "flux monitor"

¹Manuscript received November 3, 1960.

Contribution from the Division of Applied Physics, National Research Council, Ottawa, Ontario. Presented at the Third Symposium on Nuclear Chemistry and Radiochemistry held at Atomic Energy of Canada Limited, Chalk River, Ontario, September 6-8, 1960.

Issued as N.R.C. No. 6140.

*A 160-kilovolt Texas Nuclear Corporation neutron generator was used.

from the $(n,2n)$ reaction on F^{19} giving 112-minute F^{18} . The cross section for the latter reaction was taken to be 53 millibarns (cf. 61 millibarns ref. 12), as measured in separate experiments relative to 556 millibarns for the $(n,2n)$ reaction on Cu^{63} (13). The fluorine monitors were used in the form of sheets of "teflon", $(C_2F_4)_n$, placed on either side of the samples for the irradiation. During the irradiation the neutron flux was maintained constant within 5% as determined by continuous monitoring with a BF_3 -filled ionization chamber and a $B^{10}F_3$ "long counter".

The positron activities were detected by scintillation counting of the annihilation radiation and identified by half-life measurements. Chemical separations were not made. The radiations from samples and fluorine monitors were measured under conditions identical, as nearly as possible, with respect to geometry and absorber material. (For the type of detector used see reference 14.) It is estimated that a maximum systematic error of 15% may be applicable to the relative activity measurements.

The samples were prepared from the elements or from suitable compounds such as hydrides, oxides, or organic salts which do not produce interfering activities. In several cases atmospheric nitrogen adsorbed in the sample produced interfering 10-minute N^{13} from the $(n,2n)$ reaction on N^{14} . This was reduced to tolerable levels by evacuation of the samples and irradiation in an atmosphere of pure methane or helium.

RESULTS AND DISCUSSION

Among the five isotopes studied (S^{32} , Ca^{40} , Cr^{50} , Fe^{54} , and Zn^{64}) the (n,t) reaction was observed to occur only in S^{32} , producing the 2.5-minute P^{30} positron emitter with, however, a very small cross section. The gamma-ray spectrum of the irradiated sulphur is shown in Fig. 1 in which only the 0.511-Mev photopeak ascribed to P^{30} is present. In

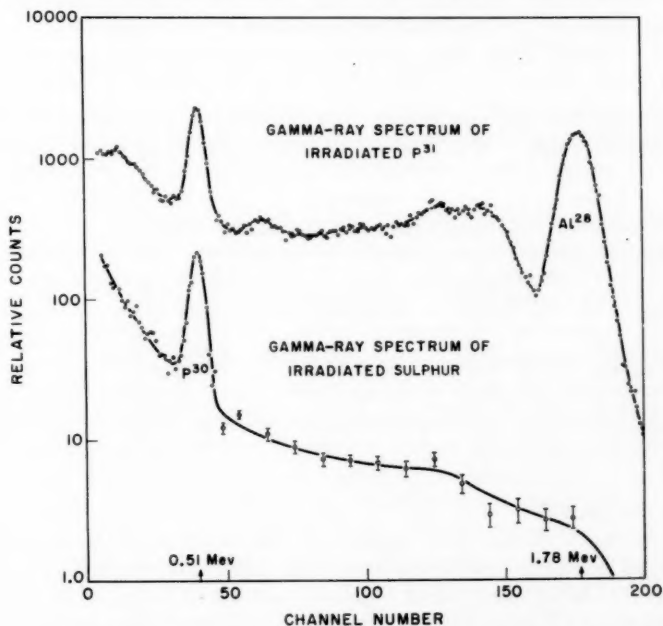


FIG. 1. Gamma-ray spectra of irradiated sulphur and phosphorus.

order to demonstrate that this activity did not arise from an $(n,2n)$ reaction on possible phosphorous impurity, the gamma-ray spectrum of irradiated P^{31} is given as well in this figure. This shows, in addition to the 0.511-Mev line, a strong peak at 1.78 Mev due to Al^{28} from the (n,α) reaction, which, however, is absent in the irradiated sulphur spectrum.

The decay of the 0.511-Mev photopeak showed a half-life of about 2.5 minutes with a smaller 10-minute component. This longer-lived component is ascribed to N^{13} resulting from an $(n,2n)$ reaction on a small amount of residual nitrogen in the samples. A typical decay curve is shown in Fig. 2.

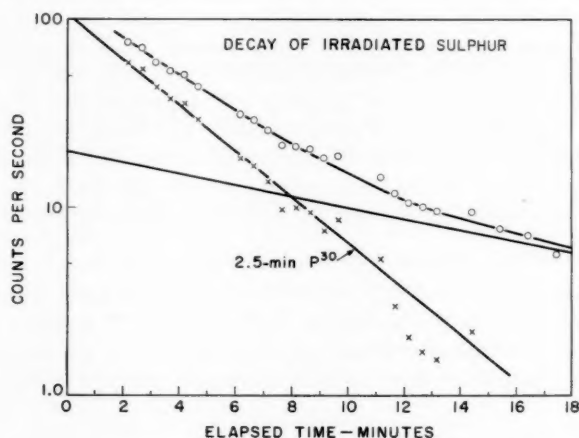


FIG. 2. Decay of 0.511-Mev photopeak in irradiated sulphur.

The experimental data and calculated cross sections for six irradiations of different samples are given in Table I. The cross sections are given relative to 53 millibarns for

TABLE I
Experimental results for (n,t) reaction on S^{32}

Sample	Duration of irradiation, minutes	P^{30} activity, c.p.m./g S^{32}	F^{18} activity, c.p.m./g F^{19}	Cross section, barns $\times 10^6$
Elemental sulphur	2.5	80.1	55.5×10^3	4.0
Elemental sulphur	2.5	73.4	54.3×10^3	3.7
Carbon disulphide	3.0	23.3	21.1×10^3	3.2
Carbon disulphide	3.0	60.1	37.8×10^3	4.6
Carbon disulphide	3.0	43.6	34.1×10^3	3.7
Carbon disulphide	2.5	56.0	35.5×10^3	4.3

the $(n,2n)$ reaction on F^{19} .

Activities resulting from the (n,t) reaction on the other nuclides studied were not definitely observed and upper limits only have been assigned for the cross sections. These assignments were made on the basis of a careful analysis of counting data and gamma spectra, taking into account isotopic abundances and positron branching ratios (15). The results for the various reactions sought are given in Table II together with the reaction

TABLE II
Cross sections for (n,t) reactions

Reaction	Q , Mev	t_1 of residual nucleus	$\sigma(n,t)$ observed, barns $\times 10^6$	Estimated theoretical $\sigma(n,t)$, barns $\times 10^6$
$S^{32}(n,t)P^{30}$	-12.56	2.5 minutes	4 ± 1	5
$Ca^{40}(n,t)K^{39}g.s.$	-12.59	7.7 minutes	<20	0.002
$Cr^{50}(n,t)V^{48}$	-13.00	16.0 days	<200	0.06
$Fe^{54}(n,t)Mn^{52}g.s.$	-13.16	5.6 days	<75	0.001
$Zn^{64}(n,t)Cu^{62}$	-9.72	9.7 minutes	<100	2

Q values taken from the nuclear mass and binding energy tabulation given by Cameron (16). The sulphur experiments yield an average cross-section value of 4 ± 1 microbarns with the error based on a standard deviation of 10% and a possible systematic error of 15% in the relative activity measurements.

The last column in Table II gives approximate theoretical cross sections calculated on the compound nucleus formalism (17, 18). Since there are rather large uncertainties (~ 200 kev) associated with the reaction Q values, approximate solutions only have been given but these are believed reliable to within a factor of 5. These calculated values are thus intended as a guide to the order of magnitude expected on the compound nucleus model. Since cross-section upper limits only were obtained experimentally for most of the reactions, the comparison with calculated values has some significance only in the case of S^{32} where the agreement is very satisfactory.

Perhaps a more instructive comparison is that with the (n,He^3) cross sections recently reported by Kumabe *et al.* (10) in Mn^{55} , Co^{59} , As^{75} , and Rh^{103} . The cross sections lie in the range 1 to 6 millibarns while the reaction Q values are comparable with those for the (n,t) reactions in the present study (e.g. for $Mn^{55}(n,He^3)V^{53}$, $Q = -12.65$ Mev). Thus the (n,He^3) cross sections given by Kumabe *et al.* are at least one or two orders of magnitude greater than the (n,t) cross sections for the nuclides studied here. This result seems surprising in view of the generally higher coulomb barriers for the nuclides studied by Kumabe *et al.* and the lower barrier penetrability to be expected for He^3 particles relative to that for tritons.

On the basis of evidence given by Wilkinson (19) for nucleon clustering in the nuclear surface, Kumabe *et al.* have suggested a direct interaction mechanism for the (n,He^3) reactions in which the incident neutron knocks out a preformed He^3 cluster. In this concept, the results on (n,t) reactions would imply a much lower probability for triton clusters relative to He^3 clusters.

As a further possibility these authors suggest a double-proton pickup mechanism. McManus (20) notes that the two protons would, in the usual case, be picked up from a given shell model state, i.e. from the last shell being filled. In deuteron pickup, however, i.e. in the (n,t) reaction, the neutron and proton picked up would normally occupy states of quite different energy in the target nucleus. On these grounds, since rather little energy is available for the reactions under consideration, the deuteron pickup might be expected to be a much less probable event. In this connection it is interesting to note that in N^{14} , with an odd proton and an odd neutron outside of the stable C^{12} core, a large (n,t) cross section is observed at 7 to 8.2 Mev (4). It is perhaps also noteworthy that the analogous (p,t) reactions are well-known while (p,He^3) reactions, involving deuteron pickup, appear generally to be inhibited (21).

In order to decide on the mechanism involved in the (n, He^3) reactions and to arrive at the explanation for the apparent difference with (n, t) reactions, further information such as angular and energy distributions of outgoing particles is obviously required. Unfortunately this is difficult to obtain with presently available neutron sources and measuring techniques.

ACKNOWLEDGMENTS

The authors wish to thank Dr. H. McManus and Dr. E. Vogt for valuable discussions in connection with this work.

REFERENCES

1. G. M. FRYE. *Phys. Rev.* **93**, 1086 (1954).
2. J. BENVENISTE, A. C. MITCHELL, C. D. SCHRADER, and J. H. ZENGER. U.S. Atomic Energy Commission Report UCRL-5596.
3. S. S. VASELEV, V. V. KOMAROV, and A. M. POPOVA. *Soviet Phys. "Doklady"*, **3**, 354 (1958).
4. F. GABBARD, H. BICHSEL, and T. W. BONNER. *Proceedings of the International Congress of Nuclear Physics*, Paris, July, 1958, p. 406.
5. J. D. KNIGHT, T. B. NOVEY, C. V. CANNON, and A. TURKEVITCH. *National Nuclear Energy Series*, Div. IV, Vol. 9, Paper 326. McGraw-Hill Book Company, Inc., New York, 1951.
6. T. A. EASTWOOD. Atomic Energy of Canada Limited. Private communication.
7. B. L. COHEN and T. H. HANDLEY. *Phys. Rev.* **93**, 514 (1954).
8. B. L. COHEN and A. G. RUBIN. *Phys. Rev.* **114**, 1143 (1959).
9. J. B. BALL and C. D. GOODMAN. *Phys. Rev.* To be published.
10. I. KUMABE, A. D. POULARIKAS, I. L. PREISS, D. G. GARDNER, and R. W. FINK. *Phys. Rev.* **117**, 1568 (1960).
11. J. D. SEAGRAVE. Los Alamos Scientific Laboratory Report LAMS-2162.
12. E. B. PAUL and R. L. CLARK. *Can. J. Phys.* **31**, 267 (1953).
13. SHINJIRO YASUMI. *J. Phys. Soc. Japan*, **12**, 443 (1957).
14. R. L. HEATH. U.S. Atomic Energy Commission Report IDO-16408.
15. D. STROMBERGER, J. M. HOLLANDER, and G. T. SEABORG. *Revs. Modern Phys.* **30**, 585 (1958).
16. A. G. W. CAMERON. Atomic Energy of Canada Limited Report CRP-690.
17. L. M. BLATT and V. F. WEISSKOPF. *Theoretical nuclear physics*. John Wiley & Sons, New York, 1952.
18. A. M. LANE and R. G. THOMAS. *Revs. Modern Phys.* **30**, 257 (1958).
19. D. H. WILKINSON. *Phil. Mag.* **4**, 215 (1959).
20. H. McMANUS. Atomic Energy of Canada Limited. Private communication.
21. B. L. COHEN, A. G. RUBIN, and C. B. FULMER. *Proceedings of the International Congress of Nuclear Physics*, Paris, July, 1958, p. 392.

$\text{Th}^{232}(n,2n)\text{Th}^{231}$ CROSS SECTION FROM THRESHOLD TO 20.4 MEV¹

J. P. BUTLER AND D. C. SANTRY

ABSTRACT

The excitation curve for the reaction $\text{Th}^{232}(n,2n)\text{Th}^{231}$ has been measured by the activation method from the threshold energy, 6.34 Mev, to 20.4 Mev, relative to the known cross section for the $\text{S}^{32}(n,p)\text{P}^{32}$ reaction. Monoenergetic neutrons were obtained from the $\text{D}(d,n)\text{He}^3$ and $\text{T}(d,n)\text{He}^4$ reactions employing a Tandem Van de Graaff accelerator. From threshold to 9.0 Mev, the $(n,2n)$ cross section rises rapidly, reaching its maximum value of 1.88 ± 0.09 barns in the region of 9.5 to 11.0 Mev. Above 11.5 Mev the $(n,2n)$ cross section decreases due to competition of the $(n,3n)$ and $(n,2nf)$ reactions and at 20.4 Mev it has a value of 0.22 ± 0.01 barns.

INTRODUCTION

Although many measurements of fast neutron cross sections $(n,2n)$, (n,p) , and (n,α) have been made with 14-Mev neutrons, relatively few data have been published over a range of neutron energies for which these reactions have appreciable cross sections. Due to the scarcity of data on neutron cross sections as a function of energy and the lack of agreement among existing results, a program has been initiated to measure fast neutron cross sections from threshold energies to about 21 Mev. These cross sections will be determined whenever possible with an accuracy of $\pm 5\%$.

The recent development of the Tandem Van de Graaff accelerator now makes it possible to obtain measurements of fast neutron cross sections over a greater energy range. By accelerating deuterons to a precise energy, the reactions $\text{D}(d,n)\text{He}^3$ and $\text{T}(d,n)\text{He}^4$ can be used to produce monoenergetic neutrons at any energy from about 5 to 21 Mev.

Results have been published on the cross section for absorption reactions of fast neutrons with Th^{232} . The (n,γ) reaction has been measured up to 14 Mev (1) and the fission cross section has been measured by several investigators from threshold energies up to 11 Mev (1, 2) and at 14.5 Mev (1, 3). However, data on the significant $(n,2n)$ cross section are only available at a few energies (4, 5). The present investigation was undertaken to determine the cross section for the reaction $\text{Th}^{232}(n,2n)\text{Th}^{231}$ from threshold, 6.34 Mev, to 20.4 Mev. The reaction $\text{S}^{32}(n,p)\text{P}^{32}$ was used to monitor the fast neutron flux. After the irradiation, thorium was purified radiochemically, and the Th^{231} as well as the P^{32} produced were determined by absolute beta counting. The $(n,2n)$ cross section at a particular neutron energy was then calculated from the Th^{231} - and P^{32} -activity measurements and the known cross section for the sulphur (n,p) reaction (6).

EXPERIMENTAL METHOD

A. Neutron Sources

Neutrons with energies from 6 to 11.6 Mev were obtained from the reaction $\text{D}(d,n)\text{He}^3$ employing the Chalk River Tandem Van de Graaff accelerator. A gas target cell similar to that described by Johnson and Banta (7) and illustrated in the lower part of Fig. 1 was used to contain the deuterium. The bombarding deuteron beam was magnetically analyzed, focused with a set of quadrupole magnets, and collimated by a 0.125-in. gold aperture. Deuterons scattered off the edge of the collimating aperture were

¹Manuscript received November 3, 1960.

Contribution from the Research Chemistry Branch, Atomic Energy of Canada Limited, Chalk River, Ontario. Presented at the Third Symposium on Nuclear Chemistry and Radiochemistry held at Atomic Energy of Canada Limited, Chalk River, Ontario, September 6-8, 1960.

Issued as A.E.C.L. No. 1180.

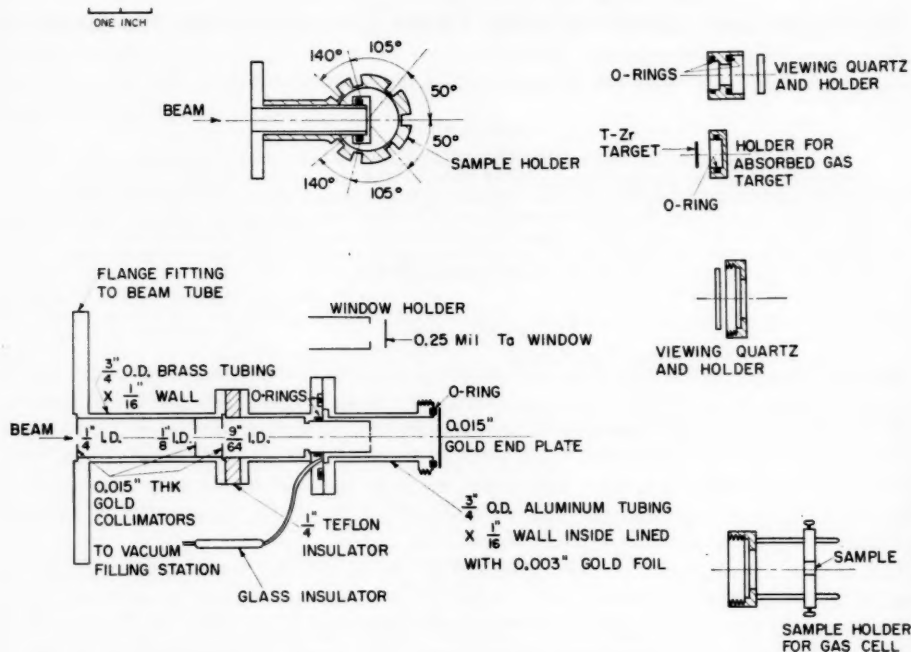


FIG. 1. Irradiation assemblies. The lower section of the diagram shows the deuterium gas target cell with the beam collimators and sample holder; the upper section shows the tritium-zirconium target and the arrangement of the samples.

prevented from entering the gas cell by a second gold aperture of slightly larger diameter, 0.140 in. The target cell was insulated from the beam tube by a 1/4 in. thick teflon ring. This enabled the cell to be used as a Faraday cup to measure the beam current during an irradiation. The cell consisted of three parts: a brass connecting section which is attached to the rest of the assembly with bolts passing through nylon insulating bushings, a brass window holder, and the outer aluminum chamber with a gold end plate. The deuteron beam enters the gas target cell through a 0.00025-in. tantalum foil which is cemented with Araldite to the brass window holder. Tantalum was found to be very suitable as a window material because of its high tensile strength. It has the added advantage that its high atomic number reduces the number of extraneous neutrons formed from (d,n) reactions. The window holder, which is held as a push fit, is aligned by a flange and makes a vacuum seal with the inner O-ring. The holder can readily be replaced if the tantalum foil ruptures. The gas chamber slips over the window holder and forms a vacuum seal with the outer O-ring. Deuterium gas enters the cell through a small hole between the O-rings and through the annular region between the chamber and the window holder. The gas target cell, which is 1.6 cm in diameter and 2.7 cm in length, was filled with deuterium to a pressure of 225 cm of Hg. The cell is made of aluminum to minimize neutron scatter and it was lined with 0.003-in. gold foil to prevent deuterons scattered in the entrance foil from striking the aluminum side walls and producing extraneous neutrons. The deuteron beam

was stopped in a 0.015-in. gold end plate which is held in position with the sample holder. For aligning and focusing the deuteron beam the gold end plate could be replaced by a piece of optical quartz.

Neutrons with energies from 12.5 to 20.4 Mev were produced by the $\text{T}(d,n)\text{He}^4$ reaction using a zirconium-tritium target with the Tandem accelerator providing a beam of 4.0-Mev deuterons. The target consisted of a 0.020 in. thick tungsten foil onto which was melted a thin layer of zirconium metal, 8 mg/cm². Tritium containing about 2% normal hydrogen was absorbed in the zirconium layer, the tritium content being about 1.2 cm³/cm² at N.T.P. or 3.1 curies/cm².^{*} The deuteron energy loss in passing through the zirconium layer was about 600 kev and this was taken into account in determining the average deuteron energy. The irradiation assembly is illustrated in the upper part of Fig. 1. The neutron energy was varied by selecting the angular position of the sample relative to the deuteron beam. Data were obtained for the various energies in a single irradiation with the samples placed on a circular arc at a distance of 1.4 cm from the center of the Zr-T target. The samples were irradiated at angles of 50°, 105°, and 140° on both sides of the axis of the deuteron beam and at 0°. Any slight misalignment of the deuteron beam was corrected by averaging the activities produced in the samples at duplicate angles.

Neutrons of 14.5 Mev were also obtained from a 100-kev accelerator using the $\text{T}(d,n)\text{He}^4$ reaction. For these irradiations a Zr-T target as described above was used.

B. Irradiations

The Th^{232} was irradiated as metal disks of 3/16-in. diameter and 0.040-in. thickness. For irradiations employing the deuterium gas target, two thorium disks were stacked together in the sample holder at 0° to the deuteron beam and at a distance of 1.4 cm from the end of the gas target cell. To obtain the required neutron fluxes without excessive energy spread, the samples were only exposed at this position and a separate run was carried out for each neutron energy. At this position the half-angle subtended by the thorium disks from the average point of origin of the neutrons was about 6°. For irradiations using Zr-T targets the corresponding angle was about 9°. Irradiation times varied from 3 to 6 hours and the deuteron beam current from 0.4 to 1.0 μa .

In the irradiations performed with the 100-kev accelerator the thorium and sulphur samples were irradiated at 45° to the beam and at deuteron beam current of 10 to 30 μa .

The neutron beam was monitored with the reaction $\text{S}^{32}(n,p)\text{P}^{32}$. The sulphur monitors were prepared by compressing sulphur at 25 tons per square inch into pellets of the same dimensions as the thorium disks. In the irradiations the thorium samples were sandwiched between two sulphur monitors. The neutron beam was also monitored with a neutron long counter identical with that described by McTaggart (8). Besides obtaining a total neutron count for each irradiation, the output of the counter went to a counting rate meter which was connected to a chart recorder. This gave a continuous record of the neutron intensity throughout the irradiation. Normally, the neutron intensity was constant within 10%. Since the half-life of the product nuclide Th^{231} is longer than the irradiation times, it could be assumed that the neutron flux was constant during the irradiation. However, in several irradiations the neutron intensity varied more markedly and in these irradiations the chart record was divided into time increments and each

^{*}The zirconium-tritium targets were obtained from the Radiochemical Centre, United Kingdom Atomic Energy Authority, Amersham, Bucks, England.

portion was weighted by the neutron intensity and the exponential decay factor. The fraction of the radioactive nuclei which survived to the end of the irradiation calculated in this manner did not differ by more than 2% from that calculated assuming a constant neutron flux.

C. Radiochemical Analysis

After the irradiation, the thorium samples were dissolved and the thorium was radiochemically purified from fission products and the decay products of natural thorium by a modification of the procedure given by Prestwood (9). The method involved the precipitation of thorium as the iodate, oxalate, and the hydroxide as well as a mesityl oxide solvent extraction. The purified thorium was mounted as ThO_2 and beta counted in a methane flow beta proportional counter of about 2π geometry. The actual counting was done by an automatic sample changer coupled with automatic scaling, timing, and print-out devices.

After the samples of thorium had decayed about a day there was considerable radioactivity due to the decay products of Th^{232} - Th^{228} . To correct for this activity, unirradiated thorium was separated from daughter activities and counted as a function of time to determine the growth in activity. The activity of Th^{231} in the irradiated samples was obtained by subtracting the activity due to the growth of the natural decay products of Th^{232} - Th^{228} . The Th^{231} decayed with an accepted value of 25.52 hours (10). The counter was calibrated for Th^{231} , by separating Th^{231} from a weighed amount of its parent U^{235} by means of an anion exchange resin (Dowex A1 100-200 mesh). The separation was performed with a known weight of natural thorium and the counter was calibrated for various weights of ThO_2 .

The irradiated sulphur pellets were placed on counting trays and ignited. By measuring the activity ratio of unburnt to burnt sulphur pellets for pellets irradiated in a uniform neutron flux as a function of the pellet thickness, it was determined that $93.0 \pm 0.5\%$ of the P^{32} activity is left behind on the counting tray as essentially a weightless source. The efficiency of the counter for P^{32} was determined from aliquots of a solution of P^{32} standardized by 4π counting. The P^{32} samples were found to decay with the accepted half-life of 14.22 days (11).

RESULTS AND DISCUSSION

Values of the $\text{Th}^{232}(n,2n)\text{Th}^{231}$ cross sections were calculated from the observed activities of Th^{231} and P^{32} corrected to the end of the irradiation and the measured cross section for the reaction $\text{S}^{32}(n,p)\text{P}^{32}$, as reported by Allen *et al.* (6). Separate analyses were performed on the two thorium disks so that in each irradiation two measurements of the $(n,2n)$ cross section were obtained. Before the measured P^{32} activity could be used to calculate the neutron flux at the position of the thorium samples several corrections were necessary. These corrections took into account: (1) the difference in distance from the neutron source to the thorium and to the sulphur pellets, (2) neutron losses due to absorption and scattering in the pellets, (3) background neutrons which arise from neutrons generated in the beam plumbing, collimators, target window, and the gold end plate, (4) breakup neutrons produced by the reaction $\text{D}(d,np)\text{D}$, which has a threshold in the laboratory system of 4.45 Mev. The first two corrections were both calculated and measured experimentally by performing irradiations in which the thorium disks were replaced by sulphur pellets.

Typical corrections that were applied for the extraneous neutrons (corrections 3 and 4) in the neutron beam at various neutron energies are listed in Table I. The effect of

TABLE I
Typical corrections for extraneous neutrons

Deuteron energy (Mev)	Neutron energy (Mev)	% Various types of neutrons at 0° to deuteron beam			% Correction applied to P^{32} activity for	
		Monoenergetic $\text{D}(d,n)\text{He}^3$	Background	Breakup $\text{D}(d,np)\text{D}$	Background neutrons (obs.)	Breakup neutrons (calc.)
3.25	6.50	99.0	1.0	0	-0.5	0.0
5.30	8.50	95.4	2.6	2.0	-1.7	0.0
7.50	10.62	67.2	4.5	28.3	-4.0	-10.0

background neutrons was determined by performing irradiations with the gas cell evacuated. For $\text{T} + \text{D}$ neutrons, zirconium targets without absorbed tritium were used. The percentage of breakup neutrons in the beam was calculated from the measurements of Cranberg *et al.* (12). From the table it is seen that their number increases rapidly as the deuteron energy is increased over the threshold for the reaction. The correction applied to the observed P^{32} activity due to the presence of breakup neutrons is listed in the last column of the table. It was calculated by graphical integration from the known spectrum of breakup neutrons (12) and the sulphur cross section. At the highest deuteron energy (8.55 Mev) this correction was 20%. It was not necessary to correct the observed Th^{231} activity for background and breakup neutrons since these neutrons have energies below the threshold for the $(n,2n)$ reaction.

For the angle irradiations, relative cross sections were obtained at various energies (12.5 to 20.4 Mev) by employing the differential cross section data of Bame and Perry (13) for the $\text{T}(d,n)\text{He}^4$ reaction to account for the variation in the neutron yield with angle. The values were normalized at a neutron energy of 14.45 Mev (sample at 105° to the deuteron beam) with the $\text{Th}^{232}(n,2n)$ cross section measured at this energy with sulphur monitors using the 100-kev accelerator.

The $(n,2n)$ cross section data are tabulated in Table II and displayed in Fig. 2. The cross sections are the average of at least two determinations. The errors quoted refer to the counting data, plus a 4% uncertainty in the absolute counting of Th^{231} and a 2% uncertainty in the counting of P^{32} . The errors do not include any error in the sulphur cross section. The sulphur (n,p) cross sections used in the calculations are also listed in the table and it is seen that the cross section is nearly constant in the energy range in which it was used.

For each irradiation an average neutron energy was calculated using the tables of Fowler and Brolley (14). The neutron energy is a direct function of the deuteron energy and the angle between the incident deuteron beam and the emitted neutron. To obtain the neutron energy, the following factors were considered: the deuteron energy loss in passing through the tantalum window or zirconium layer (15), the energy degradation in the deuterium gas, and the angular spread of the neutrons irradiating the thorium disks, as defined by the finite dimensions of both the disks and the deuteron beam. For each irradiation the effective neutron spectrum at the thorium disks was estimated. For irradiations employing the deuterium gas target, the spectrum was approximately

TABLE II
Summary of $\text{Th}^{232}(n,2n)\text{Th}^{231}$ cross section data

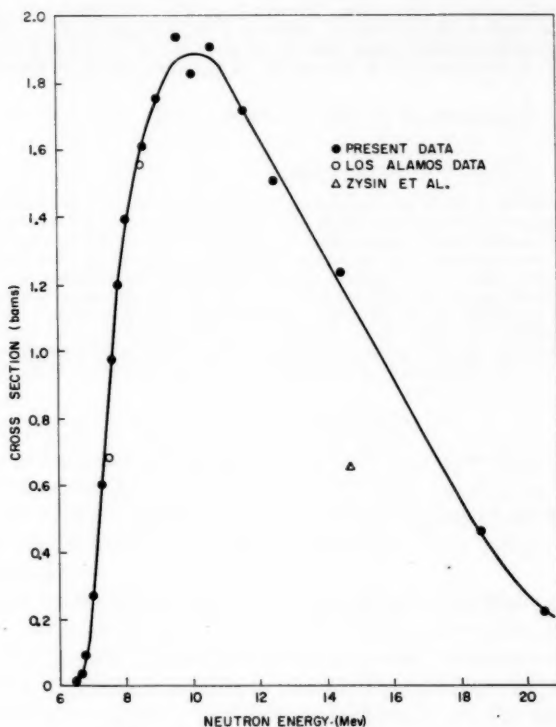
Neutron energy (Mev) average spread	Sulphur (n,p) cross section (barns)*	$\text{Th}^{232}(n,2n)$ cross section (barns)
6.51 ^{+1.10} _{-0.14}	0.338	0.015 \pm 0.007
6.68 ^{+0.10} _{-0.13}	0.336	0.036 \pm 0.003
6.79 ^{+0.09} _{-0.13}	0.336	0.094 \pm 0.008
7.01 ^{+0.09} _{-0.13}	0.338	0.271 \pm 0.013
7.28 ^{+0.08} _{-0.12}	0.340	0.603 \pm 0.028
7.59 ^{+0.08} _{-0.12}	0.342	0.976 \pm 0.045
7.84 ^{+0.32} _{-0.32}	0.344	1.20 \pm 0.07
8.01 ^{+0.07} _{-0.11}	0.346	1.39 \pm 0.07
8.61 ^{+0.05} _{-0.11}	0.350	1.61 \pm 0.07
9.02 ^{+0.05} _{-0.11}	0.353	1.75 \pm 0.08
9.63 ^{+0.05} _{-0.11}	0.357	1.94 \pm 0.09
10.03 ^{+0.05} _{-0.11}	0.359	1.83 \pm 0.08
10.62 ^{+0.05} _{-0.11}	0.356	1.91 \pm 0.09
11.61 ^{+0.05} _{-0.11}	0.345	1.72 \pm 0.08
12.53 \pm 0.26	—	1.51 \pm 0.08
14.45 \pm 0.20	0.229	1.23 \pm 0.06
18.52 \pm 0.5	—	0.459 \pm 0.027
20.40 \pm 0.20	—	0.225 \pm 0.015

*Allen *et al.* Phys. Rev. **107**, 1363 (1957).

trapezoidal with a greater number of lower-energy neutrons. An average energy was obtained by graphical analysis. The neutron energies given in Table II are average values and the spread quoted represents the standard deviation in the energy as seen by the thorium pellets.

In the graph of the data, Fig. 2, results from Los Alamos (4) at 7.5 and 8.5 Mev are also plotted. They appear to be consistent with the present measurements. However, the Russian value report by Zysin *et al.* (5) at 14.7 Mev lies outside the experimental errors quoted.

From the graph it is seen that the threshold for the reaction is 6.4 ± 0.1 Mev in agreement with the value of 6.34 ± 0.4 Mev (16) determined for the reaction $\text{Th}^{232}(\gamma,n)\text{Th}^{231}$. The decrease in cross section at about 12 Mev is attributed to competition with ($n,3n$) and ($n,2nf$) processes which have thresholds at 11.43 and 11.6 Mev respectively.

FIG. 2. $\text{Th}^{232}(n,2n)\text{Th}^{231}$ cross section versus neutron energy.

ACKNOWLEDGMENTS

We wish to express our appreciation to Mr. P. G. Ashbaugh and his staff for the operation of the Tandem Van de Graaff accelerator and to Drs. R. J. Clarke and W. G. Cross for the many helpful discussions and for the use of their 100-kev accelerator.

REFERENCES

1. D. J. HUGHES and R. B. SCHWARTZ. Neutron cross sections. 2nd ed. Brookhaven National Laboratory Report, BNL-325. 1958.
2. S. P. KALININ and V. M. PANKRATOV. Proceedings of the International Conference on the Peaceful Uses of Atomic Energy, Geneva. Vol. 16. 1958. p. 136.
3. A. A. BEREZIN, G. A. STOLIAROV, I. V. NIKOL'SHII, and I. E. CHELNOKOV. J. Nuclear Energy, **11**, 175 (1960).
4. R. J. HOWERTON. Tabulated neutron cross sections. Part 1, Vol. III. University of California Radiation Laboratory, UCRL-5226. 1958.
5. I. A. ZYSIN, A. A. KOVRIZHNYKH, A. A. LBOV, and L. I. SEL'CHENKOV. Atomnaya Energ. **8**, 360 (1960).
6. L. ALLEN, JR., W. A. BIGGERS, R. J. PRESTWOOD, and R. K. SMITH. Phys. Rev. **107**, 1363 (1957).
7. C. H. JOHNSON and H. E. BANTA. Rev. Sci. Instr. **27**, 132 (1956).
8. M. H. McTAGGART. AWRE Report NR/A-1. 1959.
9. R. J. PRESTWOOD. Los Alamos Report LA-1721. 1958.
10. M. J. CABELL. Can. J. Phys. **36**, 989 (1958).
11. O. U. ANDERS and W. W. MEINKE. Nucleonics, **15** (12), 68 (1957).
12. L. CRANBERG, A. H. ARMSTRONG, and R. L. HENKEL. Phys. Rev. **104**, 1639 (1956); and private communications with Dr. L. Cranberg.

13. S. J. BAME, JR. and J. E. PERRY, JR. *Phys. Rev.* **107**, 1616 (1957).
14. J. L. FOWLER and J. E. BROLLEY, JR. *Revs. Modern Phys.* **28**, 103 (1956).
15. J. H. COON. *In Fast neutron physics. Part I. Edited by J. B. MARION and J. L. FOWLER.* Interscience Publishers Inc., New York. 1960. Chap. IV.D.
16. L. B. MAGNUSSON, J. R. HUIZENGA, P. R. FIELDS, M. H. STUDIER, and R. B. DUFFIELD. *Phys. Rev.* **84**, 166 (1951).

EVIDENCE FOR LOW-MOMENTUM-TRANSFER PROCESS IN $K^{41}(\alpha, n)Sc^{44m,g}$ REACTIONS FROM RANGE MEASUREMENTS OF PRODUCTS¹

TAKU MATSUO AND T. T. SUGIHARA

ABSTRACT

Average forward ranges have been measured for the product nuclides Sc^{43} , Sc^{44m} , and Sc^{44g} as produced in the reactions $K^{41}(\alpha, xn)$ with alpha particles in the energy region 23 to 39 Mev. These ranges, which are determined by a thick target - thick catcher technique, indicate that the (α, n) -produced isomers are formed in part by a low-momentum-transfer process above 30 Mev, its contribution being larger for the ground-state nuclide Sc^{44g} . From a thick target - thin catcher experiment at 40 Mev, it is found that the range distribution for Sc^{43} is that expected for a compound-nucleus reaction. Normalizing the Sc^{44m} and Sc^{44g} activity distributions to that of Sc^{43} for the catchers farthest from the target, we estimate the lower limits for the contribution of a direct-reaction low-momentum-transfer process to the formation of Sc^{44m} and Sc^{44g} at 40 Mev to be about 30% and 46% respectively.

A. INTRODUCTION

The ratio of formation cross sections of Sc^{44m} and Sc^{44g} (the "isomeric ratio") as produced in the reaction $K^{41}(\alpha, n)$ has previously been reported for the alpha energy region 6-30 Mev (1). These experiments have been extended to 40 Mev, and the excitation function for the reaction $K^{41}(\alpha, 2n)Sc^{43}$ has also been measured (2). The results are summarized in Fig. 1.

The increase in the isomeric ratio from threshold to 26 Mev can be accounted for by a compound-nucleus mechanism, and the decrease in the region above 26 Mev was interpreted as resulting from the contribution of a non-compound-nucleus reaction (2). The latter reaction is expected to impart less linear momentum to the target nucleus than a compound-nucleus reaction. The linear momentum of the target nucleus is directly related to the recoil range of the product nucleus (3). Thus, a study of the recoil ranges of the Sc^{44} isomers should be useful in understanding the mechanisms by which these nuclides are produced. In this work, we report the average forward ranges in potassium chloride and aluminum of Sc^{43} , Sc^{44m} , and Sc^{44g} as produced by (α, xn) reactions on K^{41} in the alpha energy region 23-40 Mev.

In work by others, the recoil technique has recently been used by Winsberg and Alexander (3) in heavy-ion reactions, by Valyocsik (4) and by Harvey and co-workers (5) in deuteron and alpha reactions of heavy elements.

B. EXPERIMENTAL

Potassium chloride targets were prepared by evaporation on aluminum foil, and their thicknesses measured by weighing a target of known area. Fluctuations in thickness from point to point on the target were estimated to be less than 10%. Aluminum foils of high purity were used as recoil catchers. Stacks made up of target, catchers, and energy-degrading aluminum foils were bombarded in the deflected alpha beam of the 60-in. cyclotron at Brookhaven National Laboratory. The alpha-particle energy at each target foil was calculated from the range-energy curves of Aron (6). Schematic views of the

¹Manuscript received November 3, 1960.

Contribution from Jeppson Laboratory of Chemistry, Clark University, Worcester, Massachusetts, with financial assistance from U.S. Atomic Energy Commission under contract AT(30-1)-1930. Presented at the Third Symposium on Nuclear Chemistry and Radiochemistry held at Atomic Energy of Canada Limited, Chalk River, Ontario, September 6-8, 1960.

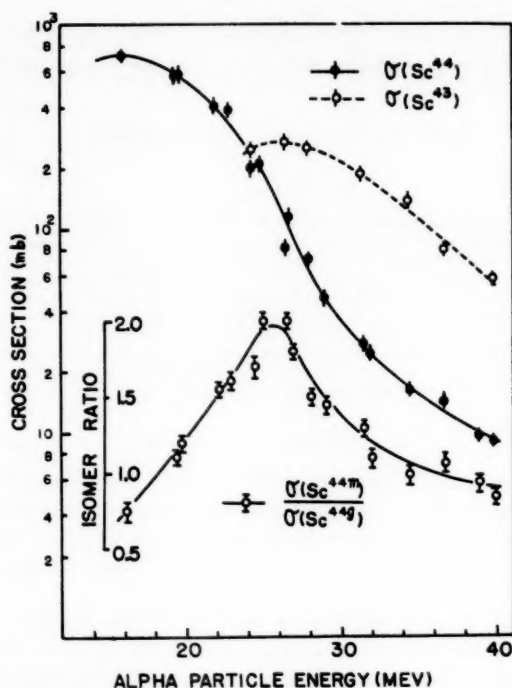


FIG. 1. Excitation functions for the $K^{41}(\alpha, n)$ (solid circles) and $K^{41}(\alpha, 2n)$ (open circles) reactions. The (α, n) points include the contribution of both Sc^{44} isomers. The inset curve gives the isomeric ratio $\sigma(Sc^{44m})/\sigma(Sc^{44g})$.

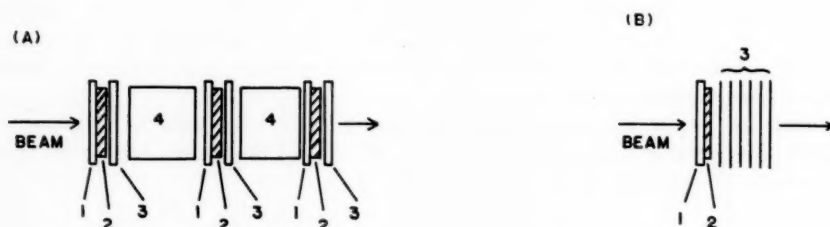


FIG. 2. Schematic diagram of target and catcher arrangement for (A) the thick-target-thick-catcher experiment and (B) the thick-target-thin-catcher experiment. 1 refers to an aluminum backing on which the KCl target 2 had been evaporated. The aluminum recoil catchers 3 are thick with respect to the range (A), or thin (B), where several such thin catchers are used. In (A) 4 refers to aluminum absorbers that were used to degrade the alpha-particle energy.

target and catcher arrangement are shown in Figs. 2a and 2b, and the details are discussed below.

After irradiation, target foils (on their aluminum backing) and catcher foils were separately dissolved in 8 M hydrochloric acid. Scandium carrier was added and extracted into tributyl phosphate, back extracted into 0.1 M hydrochloric acid, and precipitated as the hydroxide. The hydroxide was dissolved in minimum dilute hydrochloric acid.

Excess sodium carbonate was added, and lanthanum carbonate was precipitated. Scandium remains in solution as a carbonato complex. The supernate was acidified, and carbon dioxide was removed by boiling. Scandium hydroxide was precipitated again, dissolved in dilute hydrochloric acid, and finally precipitated as the salt of hypophosphorous acid (7).

Counting was done on a 3 in. \times 3 in. sodium iodide crystal, Sc^{43} being detected by its 0.38-Mev γ ray and Sc^{44g} by its 1.16-Mev γ ray. Since Sc^{44m} decays to Sc^{44g} , measurements of the 1.16-Mev γ ray as a function of time lead to a determination of both isomers. The γ -ray spectra of Sc^{43} and Sc^{44g} in equilibrium with Sc^{44m} are shown in Fig. 3. The Sc^{43} spectrum was obtained from a pure sample made by the reaction $Ca^{40}(\alpha, n)Ti^{43} \xrightarrow{\beta^+} Sc^{43}$. From Fig. 3 it is clear that even when the Sc^{43} activity is 10 times that of Sc^{44g} , the 1.05-Mev γ ray of Sc^{43} does not appreciably contribute to the 1.16-Mev photopeak of Sc^{44g} .

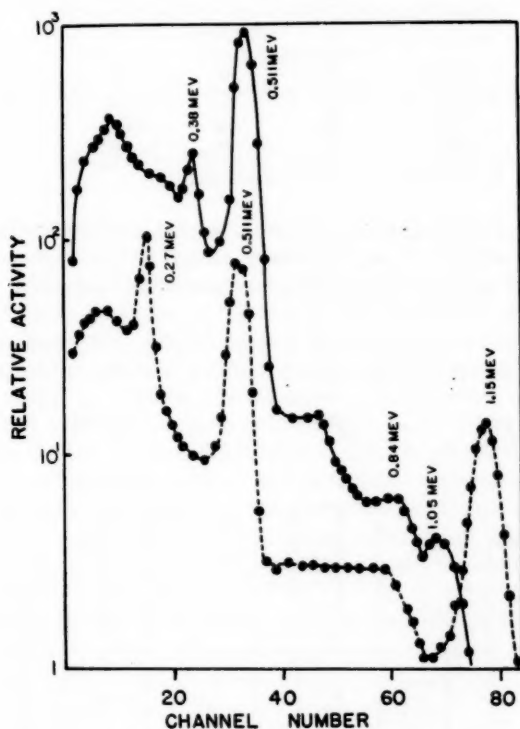


FIG. 3. Gamma-ray spectra of 4.0-hr Sc^{44g} in equilibrium with 2.4-day Sc^{44m} (dashed line) and of 3.9-hr Sc^{43} (solid line), as taken on a 3 in. \times 3 in. NaI crystal using a 100-channel analyzer. The Sc^{43} source was prepared by the reaction $Ca^{40}(\alpha, n)Ti^{43} \xrightarrow{\beta^+} Sc^{43}$ and was free of Sc^{44} . Sc^{43} does not interfere with the determination of Sc^{44g} (and hence Sc^{44m}) at 1.16 Mev even if Sc^{43} has a 10-fold higher abundance. Sc^{43} was followed by its 0.38-Mev γ ray.

C. RESULTS

The average range (in the target material) of a nuclide can be measured in a thick target - thick catcher experiment such as that shown schematically in Fig. 2a. If the target

thickness is T and the fraction of the activity found in forward catcher is F , the average range R_0 is given (3) by

$$[1] \quad R_0 = FT.$$

"Thick" in this context means considerably greater than R_0 .

The results obtained for R_0 with a target thickness of 2.47 mg/cm² potassium chloride and an aluminum catcher of 7.3 mg/cm² are shown in Table I for alpha energies 23, 32, and 39 Mev. The estimated error in the determination of F is less than 5%; combined with possible fluctuations in the target thickness T , we estimate the over-all error in R_0 to be about 10%.

TABLE I
Thick-target ranges in KCl ($\mu\text{g}/\text{cm}^2$)*

Nuclide	E_α (Mev)		
	23	32	39
Sc ⁴³	380	423	575
Sc ^{44m}	408	396	495
Sc ^{44g}	413	361	430

*The errors are estimated to be about 10%.

The recoil behavior of the scandium nuclides was also studied in a thick target - thin catcher experiment at 40 Mev. A stack of foils similar to that shown schematically in Fig. 2b was irradiated. The target was 1.23 mg/cm² potassium chloride and each aluminum catcher 0.17 mg/cm².

The amount of the three nuclides found in each catcher, corrected for chemical yield, is shown in Table II and Fig. 4. The data in Table II and Fig. 4 are in arbitrary units,

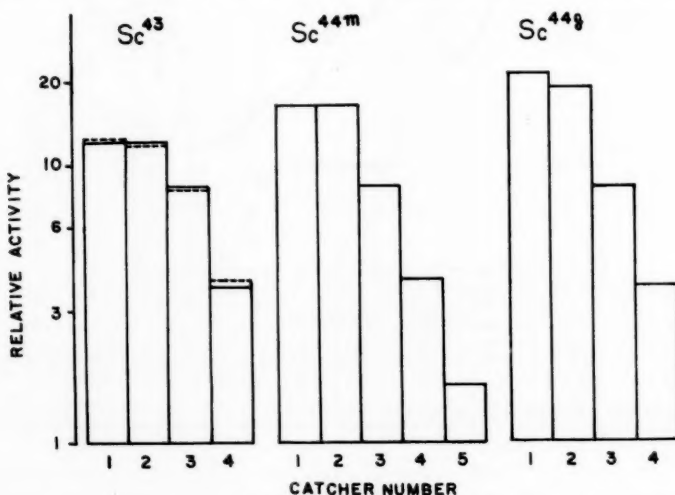


FIG. 4. The activity distribution of Sc⁴³, Sc^{44m}, and Sc^{44g} in thin forward catchers at 40 Mev. The dotted lines in the Sc⁴³ distribution are the values expected from equation [7] for $n = 2.1$, $R_0 = 580 \mu\text{g}/\text{cm}^2$, and $\bar{p} = 0.45$.

TABLE II
Normalized differential distribution of products at $E_\alpha = 40$ Mev*

Nuclide	Catcher number (each 0.17 mg/cm ² Al)				
	1	2	3	4	5
Sc ⁴³	12.2	12.1	8.30	3.62	—
Sc ^{44m}	16.3	16.3	8.30	3.87	1.6
Sc ^{44g}	21.0	18.6	8.30	3.60	—

*The errors are estimated to be about 5%.

normalized to give the same activity of all three nuclides in catcher number 3. The reason for this normalization procedure is discussed below.

D. DISCUSSION

The distribution in the forward range R of a product nucleus can be expressed (3) as

$$[2] \quad P(R)dR = \frac{dR}{\sqrt{2\pi\rho R_0}} \exp \left[-\frac{(R - R_0)^2}{2\rho^2 R_0^2} \right]$$

where R_0 is the average range and ρ the straggling parameter. R_0 contains contributions from the momentum imparted by the incident particle, in this case an alpha particle, and from that resulting from emission of nucleons leading to the product nucleus. In reactions such as (α, n) or $(\alpha, 2n)$ at relatively low energies, the latter contribution is small and is neglected here. The straggling parameter also consists of two terms (3), one characteristic of the stopping process and the other dependent on the angular distribution of the outgoing particles. The first term predominates over the latter (3).

The thick catcher experiment can give only R_0 as indicated in equation [1]. The data in Table I indicate that the ranges of Sc⁴³, Sc^{44m}, and Sc^{44g} differ from each other at energies above 30 Mev. It will be assumed that Sc⁴³ is formed in a compound-nucleus reaction. Evidence to support this assumption is presented below. Lower R_0 values for Sc^{44m} and Sc^{44g} as compared to that for Sc⁴³ indicate the contribution of a low-momentum-transfer or non-compound-nucleus reaction. This result is consistent with the interpretation for the decrease in isomeric ratio (2).

It has been shown (8) that R_0 is related to the kinetic energy E (in Mev) of a recoiling atom in a stopping material of atomic weight m and atomic number z in the following way:

$$[3] \quad \frac{R_0}{E} = 0.600 \frac{m(m+M)}{M} \frac{(z^{2/3} + Z^{2/3})^{1/2}}{zZ} \text{ mg/cm}^2$$

where M and Z are the atomic weight and atomic number of the recoiling atom. R_0 values have been calculated from equation [3] for the compound nucleus formed by complete transfer of alpha-particle momentum to the K^{41} nucleus. These values as well as the observed Sc⁴³ ranges are summarized in Table III. The ratio of the values calculated to those observed is about 2.5 and constant within experimental error at the three energies. Other workers (3, 4) have found also that observed ranges are substantially less than those

TABLE III
Comparison of calculated and observed ranges

	Ranges in KCl (mg/cm ²)		
	<i>E_α</i> (Mev)		
	23	32	39
<i>R₀</i> calculated for compound nucleus (eq. [3])	0.847	1.18	1.44
<i>R₀</i> observed for Sc ⁴³	0.380	0.423	0.575
Ratio calculated/observed	2.2	2.8	2.5

calculated by equation [3], particularly when the recoiling atom and stopping material are of nearly the same atomic weight and number, as is the case here. The constancy in the ratio implies that the range of Sc⁴³ nuclei is increasing with energy in a manner consistent with equation [3]. Since the calculated *R₀* assumes compound-nucleus formation, we consider the data of Table III to be evidence that Sc⁴³ is formed chiefly by a compound-nucleus mechanism at all three energies. The fluctuations in the ratio are attributed primarily to variations in thickness of the target.

The differential-catcher method gives the straggling parameter ρ as well as *R₀*. If the recoiling atom traverses both target material and catcher, the probability that the atom will be found at some point *x* in the catcher is given by

$$[4] \quad P(x)dx = \frac{dx}{\sqrt{2\pi\bar{p}R_0}} \int_0^T \exp \left[-\frac{(cx+t-R_0)^2}{2\bar{p}^2R_0^2} \right] dt$$

where *x* and *t* are the path lengths in catcher and target respectively as measured in the beam direction, \bar{p} is the straggling parameter averaged over the target and catcher material, *T* is the target thickness, and *c* is a factor that converts range in catcher to that in the target material as follows:

$$[5] \quad c = \frac{m_1(m_1+M)}{m_2(m_2+M)} \left(\frac{z_1^{2/3} + Z^{2/3}}{z_2^{2/3} + Z^{2/3}} \right)^{1/2} \frac{z_2}{z_1}$$

The subscripts 1 and 2 refer to target and catcher respectively; the other symbols are as in equation [3].

The straggling parameter is given by (8)

$$[6] \quad \rho = [2mM/3(m+M)^2]^{1/2}$$

In our case both the target material and catcher material affect ρ ; their relative importance depends on the ratio of *t* to *x*. However, since ρ_{KCl} and ρ_{Al} are 0.405 and 0.396 from equation [6], it is permissible to use an average value \bar{p} without introducing appreciable error.

The integrand of equation [4] can be transformed into that of a normal distribution by making the substitution $u = (cx + t - R_0)/R_0$.

$$[7] \quad P(x)dx = \frac{dx}{\sqrt{2\pi\bar{p}}} \int_{(cx-R_0)/R_0}^{[cx+R_0(n-1)]/R_0} \exp \left(-\frac{u^2}{2\bar{p}^2} \right) du$$

where $n = T/R_0$. The function $P(x)$ of equation [7] is shown in Fig. 5* for several values

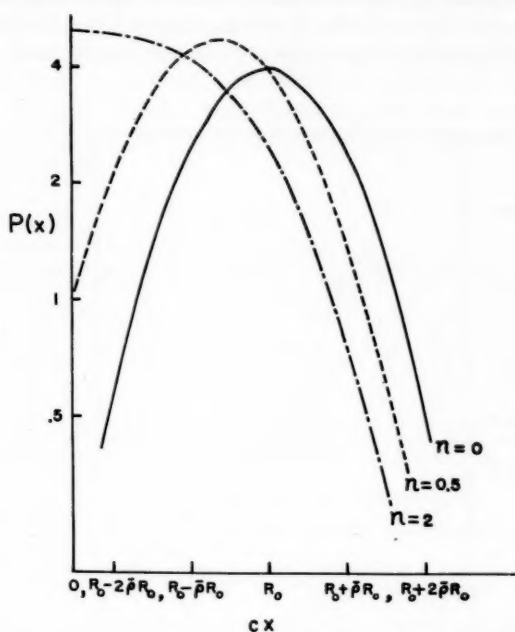


FIG. 5. The distribution function $P(x)$, equation [7], plotted as a function of cx . The various curves indicate the change in shape with reduced target thickness $n = T/R_0$. \bar{p} has been taken to be 0.4.*

of n , indicating the shape of the distribution for various target thicknesses. For a given n value, if a nuclide is produced by several mechanisms of different momentum transfer and different R_0 , a range distribution different in shape from those of Fig. 5 is expected.

When $n > 2$ and $\bar{p} \leq 0.45$,

$$[8] \quad \frac{1}{\sqrt{2\pi\bar{p}}} \int_{(n-1)}^{\infty} \exp\left(-\frac{u^2}{2\bar{p}}\right) du \leq 0.013.$$

That is, the range distribution given by equation [7] is represented to a good approximation by

$$[9] \quad P(x)dx = \frac{dx}{\sqrt{2\pi\bar{p}}} \int_{(cx-R_0)/R_0}^{\infty} \exp\left(-\frac{u^2}{2\bar{p}}\right) du.$$

The change in the upper limit of the integral does not appreciably affect the value of $P(x)$.

Thus it is apparent that probability paper should be used to determine \bar{p} from the data of the thin-catcher experiment. The relative activity of a given nuclide found in catcher 1 (Table II) is plotted at $x_1 = 1/2$ thickness of catcher 1. That in catcher 2 is plotted at $x_2 =$ thickness of catcher 1 + $1/2$ thickness of catcher 2 and so on. The relative activity for $x = R_0/c$ is estimated by interpolation. The R_0 value is taken from the thick-catcher

*NOTE ADDED IN PROOF: The ordinate scale is in arbitrary units.

experiment (Table I). If this activity is taken to be 50%, then the range distribution is suitably normalized. This process was followed for each of the nuclides, and the resulting plot on probability paper is shown in Fig. 6. We see that $\bar{p} = 0.45 \pm 0.02$ is a reasonable value for all three nuclides, and in fair agreement with the calculated values of \bar{p} from equation [6].

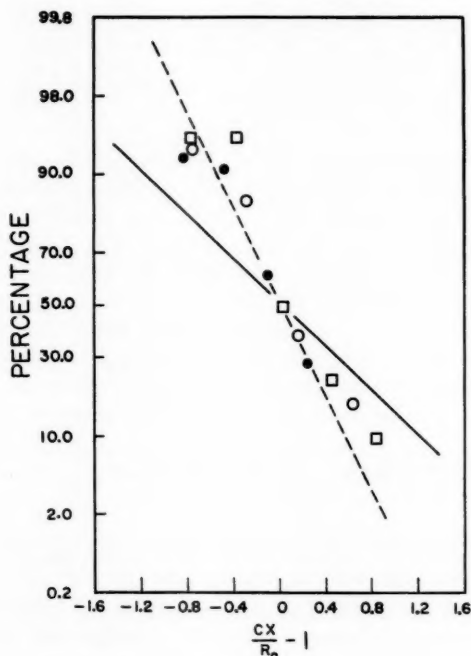


FIG. 6. Probability-paper plot of activity distribution in catchers as a function of $(cx/R_0) - 1$. The open circles refer to Sc^{44g} , the solid circles to Sc^{43} , and the squares to Sc^{44m} . The dashed line corresponds to $\bar{p} = 0.45$ and the solid line to $\bar{p} = 1.0$.

The activity distribution of Sc^{43} (Fig. 4) corresponds to that expected from equation [7] for $n = 2.1$. Other evidence (isomeric ratio and R_0 values) suggests that above 26 Mev a low-momentum-transfer process contributes to the formation of Sc^{44m} and Sc^{44g} . If we assume that at 40 Mev all of the Sc^{43} nuclei and some of the Sc^{44m} and Sc^{44g} nuclei are formed by a compound-nucleus mechanism, the observed range distributions should be the same for large values of x . Differences in range distribution should appear only for small values of x since a low-momentum-transfer contribution of smaller R_0 value is postulated. Thus the observed yields of the three nuclides in the various catcher foils have been normalized in Table II such that the distributions coincide for large values of x .

These data can now be used to estimate the amount of contribution of non-compound-nucleus reactions. The quantities used in this calculation are summarized in Table IV. The fraction found in the catcher, column (2), is obtained for each nuclide from measured R_0 values (Table I) and the target thickness T (1.23 mg/cm² KCl). Column (3) lists the sum of the activity found in the catchers, and column (4) is the calculated amount left in the target. In columns (3) through (8), the activity units are the normalized units of

Table II. Column (5) is simply the sum of (3) and (4), the total activity produced. In column (6) the activity in the catchers attributed to a direct reaction is calculated, assuming that this is obtained by subtracting the Sc^{43} activity in the catchers from that of Sc^{44m} and Sc^{44g} . The direct-reaction contributions to Sc^{44m} and Sc^{44g} are similarly calculated for the activity remaining in the target in column (7). Column (8), which is the sum of (6) and (7), represents the total contribution of direct reactions. The fractions of Sc^{44m} and Sc^{44g} activity that can be attributed to a direct reaction (column (8)/column (5)) are listed in column (9).

TABLE IV
Direct-reaction contribution to formation of Sc^{44m} and Sc^{44g} at 40 Mev

Nuclide	Fraction out*	Activity†						Fraction by direct reaction
		A	B	C	D	E	F	
Sc^{43}	0.467	37.8‡	43.2	81	—§	—§	—§	—§
Sc^{44m}	0.402	46.4	69.0	115	9	26	35	0.30
Sc^{44g}	0.350	53.1‡	98.6	152	15	55	70	0.46

NOTE: A = Activity in catchers. B = Activity in target. C = Total activity, target and catchers. D = Direct-reaction activity, catchers. E = Direct-reaction activity, target. F = Direct-reaction activity, total.

*Calculated from R_0 values of Table I at 39 Mev and $T = 1.23$ mg/cm² KCl.

†Normalized activity units used in Table II.

‡Assumed that 1.6 activity units of Sc^{43} and Sc^{44g} would have been found in catcher 5 (as in the case of Sc^{44m}) if detection sensitivity had been higher.

§ Sc^{43} assumed to be formed only by compound-nucleus mechanism.

The calculated direct-reaction contributions, 30% for Sc^{44m} and 46% for Sc^{44g} , are only lower limits. It is conceivable that a direct reaction producing products of intermediate or long range could have contributed to the Sc^{44m} and Sc^{44g} activity found in catcher 3 and beyond. In this calculation, it has been assumed that all activity in these catchers could be attributed to a compound-nucleus reaction. If Sc^{43} is formed partially by a direct reaction at 40 Mev, the calculated direct-reaction contributions to Sc^{44m} and Sc^{44g} would also be low.

ACKNOWLEDGMENTS

We are greatly indebted to Dr. R. W. Dodson and Dr. G. Friedlander for their generous hospitality in making available to us many of the facilities of Brookhaven National Laboratory and to Dr. C. P. Baker and members of the cyclotron operating crew for their assistance in irradiations. We gratefully acknowledge some illuminating discussions with Dr. J. M. Alexander.

REFERENCES

1. T. MATSUO and T. T. SUGIHARA. Bull. Am. Phys. Soc. II, **4**, 141 (1959).
2. T. MATSUO. Annual Progress Report, Clark University, Worcester, Mass. Contract AT(30-1)-1930. 1960.
3. L. WINSBERG and J. M. ALEXANDER. Lawrence Radiation Laboratory Reports UCRL-8618 (1959) and UCRL-8997 (1960).
4. E. W. VALYOCSEK. Lawrence Radiation Laboratory Report UCRL-8855. 1960.
5. B. G. HARVEY, W. H. WADE, and P. F. DONOVAN. Phys. Rev. **119**, 225 (1960).
6. W. A. ARON, B. G. HOFFMAN, and F. C. WILLIAMS. U.S. Atomic Energy Commission Report AECU-663. 1949.
7. D. R. BOMBERGER. Anal. Chem. **30**, 1907 (1958).
8. J. LINDHARD and M. SCHARFF. Private communication quoted in R. B. LEACHMAN and H. ATTERLING. Arkiv Fysik, **13**, 101 (1959).

A GAS-CHROMATOGRAPHIC APPARATUS FOR THE STUDY OF THE HOT-ATOM CHEMISTRY OF ORGANIC HALIDES¹

M. D. SILBERT AND R. H. TOMLINSON

ABSTRACT

The construction of an easily assembled and inexpensive gas-chromatographic apparatus is described. This system has been designed to determine β -active materials. The operation of this instrument involves the use of a temperature program in order to resolve materials boiling over a wide range of temperature.

INTRODUCTION

Libby (1, 2) made the first attempts to isolate and identify the individual organic products from neutron-irradiated alkyl halides. From the reaction, $\text{Br}^{81}(n,\gamma)\text{Br}^{82}$, in *n*-propyl bromide he separated some eight active organic products using the technique of fractional distillation. Willard (3) using the same compound and separational method later increased the number of products to 11.

The technique of fractional distillation suffers from one great disadvantage. It cannot operate at the tracer level; carriers must be added for all components present. If carriers are not added the tracers will tend to contaminate each other or any carriers that are present.

Willard and Evans (4, 5) were the first to adapt gas-chromatographic methods to the study of hot-atom reactions of alkyl halides. From neutron-irradiated *n*-propyl bromide they obtained more than 20 active organic products without prior addition of macro amounts of inactive carrier. They had thus shown that gas chromatography was a method of analysis that was suitable not only for operation at the macro level, but also at a tracer level.

EXPERIMENTAL

In Fig. 1 is shown a schematic diagram of the gas-chromatographic apparatus constructed for determination of the β -active products from the hot-atom reactions of alkyl halides. The detection system employed was one designed for detection of active products; it is conceivable, however, that it could be substituted by or complemented with a conventional type of gas-chromatographic detection system for detection of inactive materials or added carriers.

The gas entered through a fine capillary (A) whose resistance to flow was greater than that of the column; thus it determined the flow rate of carrier through the entire system. With this device it was possible to program the column temperature with a minimum variation in flow rate.

The sample introduction system (D) shown in Fig. 2 had been designed to make use of the micropipettes commonly used in gas-chromatographic analysis. The pipette, filled by capillary action, was inserted through the rubber seal up to the stopcock. The stopcock was then opened and the pipette inserted until its tip plugged the hole in the silicone rubber disk. This blocked the normal carrier gas flow and thus forced the carrier gas to flow through the pipette, blowing the measured volume of liquid into the system. The pipette could then be withdrawn.

¹Manuscript received November 3, 1960.

Contribution from the Department of Chemistry, Hamilton College, McMaster University, Hamilton, Ontario. This paper was presented at the Third Symposium on Nuclear Chemistry and Radiochemistry held at Atomic Energy of Canada Limited, Chalk River, Ontario, September 6-8, 1960.

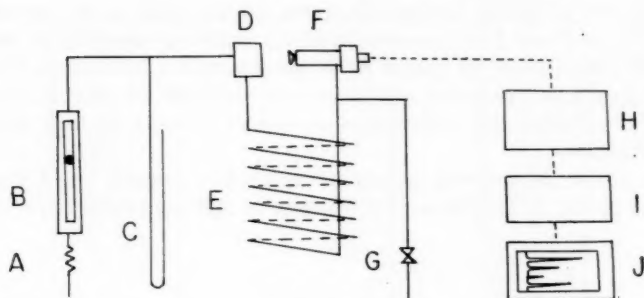


FIG. 1. Schematic diagram of gas-chromatographic apparatus.

A. Capillary flow restriction. B. Flowmeter. C. Mercury manometer. D. Sample introduction system. E. Column. F. Flow counter. G. Methane inlet. H. High-voltage supply and linear pulse amplifier. I. Rate meter. J. Recorder.

Solid lines indicate gas flow. Broken lines indicate electrical connections.

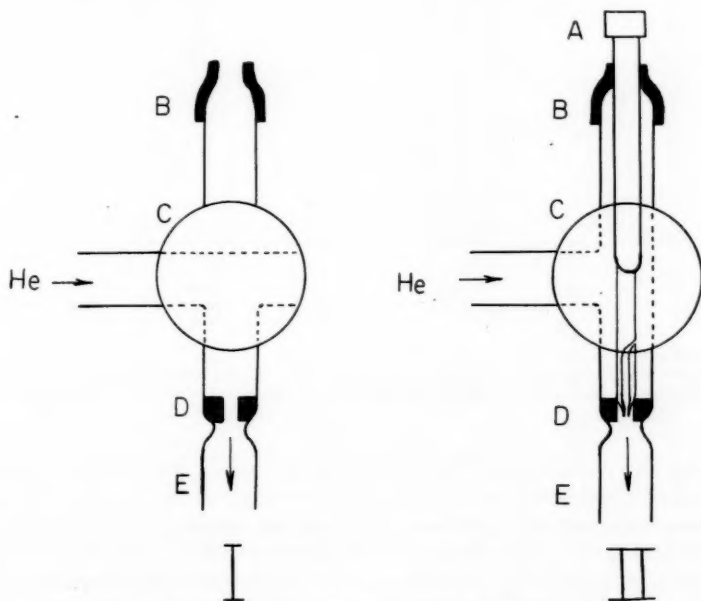


FIG. 2. Sample introduction system. I. Normal flow. II. Sample introduced.

A. Micropipette. B. Rubber seal. C. Large stopcock. D. Silicone rubber disk. E. Column.

A second sample-introduction system made use of a microsyringe and a puncture seal. The sample volume could be increased as a function of time thereby correcting for radioactive decay and normalizing all chromatograms to the same starting time after irradiation.

The column (E in Fig. 1) was heated by an air oven. This consisted of a metal can 30 cm high and 13 cm in diameter. It was wrapped with asbestos, nichrome wire, and aluminum foil. Temperature programming was achieved by increasing the voltage to the nichrome wire heater at preset time intervals.

The column was a helix of 6-mm O.D. pyrex tubing coiled to an outside diameter of 6.5 cm. Lengths of 2 and 4 meters were used. The packing was 30% by weight General Electric SF-96 (40) silicone oil coated on Johns-Manville Chromosorb P (30-60 mesh). This packing gave good resolution and short analysis times for alkyl halides. It also had the property of allowing the components to emerge in order of their boiling points, a help in identification.

The outlet of the column was connected to the flow counter (F in Fig. 1) which is shown in detail in Fig. 3. The connection was kept at 200° C in order to prevent condensa-

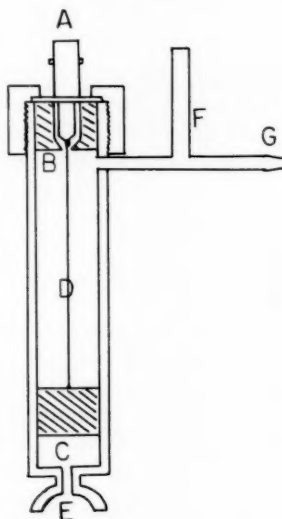


FIG. 3. Cross section of flow counter.

A. UG 931/U high-voltage connector. B. Teflon plug. C. Teflon plug grooved to permit flow of gas. D. 0.05-mm tungsten wire. E. Ball joint. F. Methane inlet. G. Connection to column, 7/25 standard taper joint.

tion of the high-boiling components. The carrier gas was mixed with methane (natural gas was also found suitable) before entering the active volume of the counter. The active components present in the carrier gas were then counted as part of the counting gas, inside the counter with a very high efficiency. This system was the most sensitive of all present day systems of monitoring gas streams. The relative sensitivity and resolution could be varied by adjusting the flow of the methane relative to the carrier gas as this determined the length of time the active fraction remains in the counter. A trap was connected to the exit of the counter using a spherical ground joint; this was necessary to dispose of the active waste.

The output of the flow counter was fed into a linear pulse amplifier and rate meter. The rate meter ran a standard 10-mv potentiometer recorder which plotted the radiochromatogram.

RESULTS

Figure 4 shows chromatograms of the products from the reaction $\text{Br}^{79} (n, \gamma) \text{Br}^{80}$ in pure *n*-propyl bromide. Results are shown for irradiation at liquid air temperature

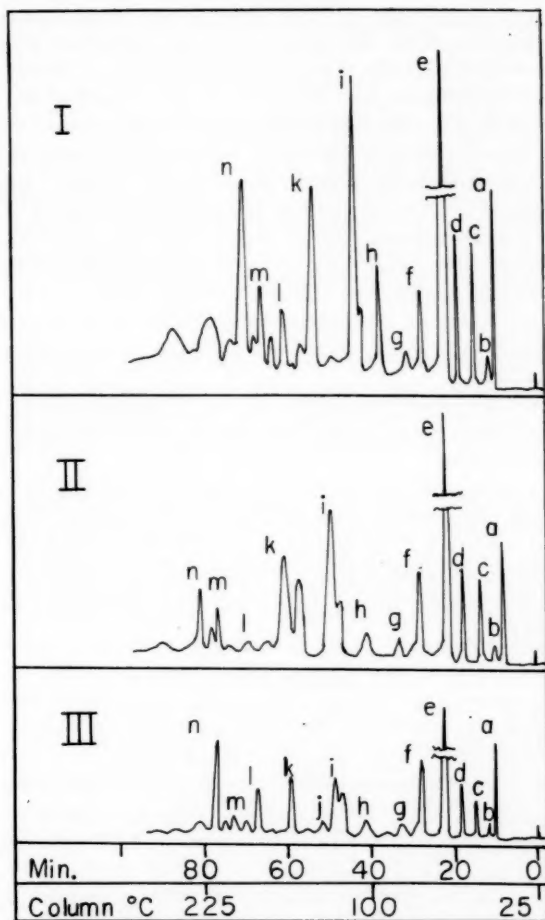


FIG. 4. Radiochromatograms of the products of the $\text{Br}^{79}(n,\gamma)\text{Br}^{80}$ reaction in *n*-propyl bromide. I, at liquid N_2 temperature (-196°C). II, at core temperature (30°C). III, elemental bromine scavenger (30°C).

IDENTIFICATION OF PRODUCTS:

- | | |
|------------------------------|---------------------------|
| (a) Methyl bromide | (h) 1,2-Dibromoethane |
| (b) Vinyl bromide | (i) 1,2-Dibromopropane |
| (c) Ethyl bromide | (j) Bromoform |
| (d) <i>i</i> -Propyl bromide | (k) 1,3-Dibromopropane |
| (e) <i>n</i> -Propyl bromide | (l) 1,1,2-Tribromoethane |
| (f) Methylene bromide | (m) Carbon tetrabromide |
| (g) 1,1-Dibromoethane | (n) 1,2,3-Tribromopropane |

Vertical axis represents relative response of the recorder.

(-196°C) and at the reactor temperature (30°C). At the reactor temperature the effects of elemental bromine scavenger are also shown.

The samples sealed in quartz were irradiated in the Rabbit System of the McMaster Nuclear Reactor for 30 seconds at a flux of 5×10^{12} n/cm² sec. The background γ field, as determined by cobalt glass, was 10^6 r integrated over this 30-second irradiation period.

DISCUSSION

The detection system used in this apparatus was a gas-flow proportional counter designed to operate with a mixture of helium and methane. It was of similar design to the counter described by Wolfgang and Rowland (6) for studies of tritiated compounds.

The great advantage of this detection method was its great sensitivity. As the counting was done internally the counter was essentially 100% efficient for β radiation.

Both Willard (4, 5) and Herr (7) passed the carrier gas through external tubing close to scintillation crystals, thereby incurring loss due to both geometry and crystal efficiency. The literature also described several other systems which externally monitor the gas stream; these, however, lose sensitivity by geometrical losses. These included both Geiger-Müller (7, 9) and scintillation (10) detection systems.

Harris (8) collected fractions in charcoal traps which were counted in a well-type crystal. Although this method is very sensitive it does not give continuous chromatograms and is not as convenient.

Ionization chambers have been described (11, 12) using continuous flow systems. The geometrical losses have thus been reduced but the sensitivity remains less than that of a proportional counting system.

The proportional counter suffers from the big disadvantage that it can not be used at elevated temperatures. In general, Geiger-Müller and proportional counters do not perform satisfactorily above 75° C. Wolfgang and Rowland (6) have found, however, that their design performed satisfactorily up to 200° C, the only change having been a shortening in the length of the plateau. This result was confirmed with the flow counter used in this laboratory.

REFERENCES

1. L. W. FRIEDMAN and W. F. LIBBY. *J. Chem. Phys.* **17**, 647 (1949).
2. M. S. FOX and W. F. LIBBY. *J. Chem. Phys.* **20**, 487 (1952).
3. J. C. W. CHIEN and J. E. WILLARD. *J. Am. Chem. Soc.* **79**, 4872 (1957).
4. J. B. EVANS and J. E. WILLARD. *J. Am. Chem. Soc.* **78**, 2908 (1956).
5. J. B. EVANS. Ph.D. Thesis, University of Wisconsin. 1957. University Microfilms, Ann Arbor, Mich.
6. R. WOLFGANG and F. S. ROWLAND. *Anal. Chem.* **30**, 903 (1958).
7. W. HERR, F. SCHMIDT, and G. STÖCKLIN. *Z. Anal. Chem.* **170**, 301 (1959).
8. W. E. HARRIS. Paper presented at the Third Symposium on Nuclear and Radiochemistry, Chalk River, Ontario. Sept. 6-8, 1960. *Can. J. Chem.* **39**, 121 (1961).
9. G. BLYHOLDER. *Anal. Chem.* **32**, 572 (1960).
10. G. L. GRANDY and R. C. KOCH. *Rev. Sci. Instr.* **31**, 786 (1960).
11. L. H. MASON, H. J. DULTON, and L. R. BAIR. *J. Chromatog.* **2**, 322 (1959).
12. NUCLEAR CHICAGO CORPORATION. Model DCF gas flow ion chambers.

SCINTILLATION COUNTING WITH ORGANIC PHOSPHORS¹

B. LIONEL FUNT

ABSTRACT

Current techniques employed in scintillation detection of beta emitters are reviewed. Internal liquid scintillation counting, with a number of homogeneous mixed solvent systems, is described. Heterogeneous counting systems containing radioactive material in the dispersed phase include scintillating gels, thickened scintillators, and emulsions, and a number of methods embodying direct counting of active deposits on filter paper. Heterogeneous systems with the radioactive material in the continuous phase are described and include plastic capillary counters, plastic filaments, or organic crystals wetted with aqueous solutions.

INTRODUCTION

Internal sample scintillation counting provides inherent advantages of high sensitivity, energy discrimination, 4π geometry, and lower background for a given sample size.

Comparisons between different counting methods are often misleading, but it is nevertheless instructive to try to assess the potentialities and merits of different counting techniques.

Guinn (1), for example, compared Geiger and liquid scintillation counting of beta emitters. He drew the distinction between "absolute sensitivity" i.e. the minimum amount of an isotope detectable to a given standard deviation in a reasonable counting time, and "concentration sensitivity", which represents the minimum concentration detectable under the same conditions. Gas counting methods furnished superior or equal absolute sensitivities to those attainable with liquid scintillation counting. The merits of liquid scintillation counting were evident when the concentration sensitivities were compared. Here results that were superior by orders of magnitude to those attainable with gas counting methods were obtained for isotopes of low energy. The superiority of liquid scintillation counting in this comparison is primarily a reflection of the much larger quantity of isotope which can be introduced into the counting volumes with this method.

The technical problems encountered in the application of internal scintillation counting methods stem primarily from two sources: (1) sample insolubility and (2) quenching effects. The potentialities of the counting technique cannot, in general, be realized if the sample cannot be incorporated effectively into the counting volume. Since the choice of liquid scintillator solvent is limited to relatively non-polar compounds, the assay of many samples is hindered by the relative insolubility of the material in the scintillator solution. The use of mixed solvents may in many instances partially overcome these difficulties, but generally, this is at the expense of a decreased luminescent output with accompanying losses in counting efficiency (2, 3, 4, 5).

Even when the sample is directly soluble in the scintillator solution the quenching effects of various polar groups may result in a serious reduction in luminescent efficiency and of detection sensitivity (6). Furthermore, light absorption, particularly by colored compounds, will reduce the effectiveness of the counting methods (7).

Many of these difficulties have been overcome successfully by a variety of ingenious methods. Although an ideal counting technique cannot be said to exist, an intelligent

¹Manuscript received November 3, 1960.

Contribution from the Chemistry Dept. University of Manitoba, Winnipeg, Manitoba. Paper presented at the Third Symposium on Nuclear Chemistry and Radiochemistry held at Atomic Energy of Canada Limited, Chalk River, Ontario, September 6-8, 1960.

choice of a counting method from those recently described can provide a simple, reproducible, and sensitive solution to most counting problems.

Homogeneous Liquid Scintillation Counting

This method provides the greatest inherent sensitivity and is most adaptable to samples of any size. Frequently the sample is directly soluble in the scintillator solution. For example, in our work on C-14-labelled polystyrene it was sufficient to dissolve the sample directly in the scintillator solution (8). For non-polar hydrocarbons surprisingly little quenching of the scintillations is found. Where quenching is suspected, compensating corrections may be applied. Frequently this is accomplished by the addition of an internal standard (9, 10) of known activity to the sample volume after the completion of the sample count. The counting efficiency of the sample plus standard is assumed to be equal to that for the standard alone.

Dilution of the sample solution with additional liquid scintillator will also serve to determine quenching effects and allow correction by extrapolation to zero concentration of quencher (10). Recently a novel suggestion for correction for quenching in H-3 counting has been made (11). A source of Co-60 on a platinum needle is inserted into the liquid scintillator where the 14-kev beta energy is detected. This procedure eliminated the contamination of the sample inherent in the use of an internal standard.

Where ultimate sensitivity is of the utmost importance, as in archaeological dating of natural radiocarbon, simplicity may be sacrificed to elaborate sample preparation. In such work the sample may be burned and the CO₂ synthesized to an aromatic hydrocarbon, or more simply to a soluble compound of moderate quenching action. The preparation of toluene (12), paraldehyde (13), methyl borate (14), and *p*-cymene (15) for such purposes has been reported.

In the more usual analysis, particularly of inorganic substances, such syntheses cannot be employed. There the expedient of using multicomponent homogeneous solvents is often practiced and solutions containing water-ethanol-toluene (16) or water-dioxane (2, 17, 18) have been described. The addition of naphthalene, as a secondary solvent, greatly reduces quenching effects in such systems (18, 19, 20). A composition employed frequently is that due to Kinard (21) which utilizes xylene-dioxane-ethanol and naphthalene. For inorganic salts, tributylphosphate can be employed in scintillator systems (22). Since this compound is a common extracting agent in various liquid-liquid extractions, its direct use appears to offer potentialities which do not appear to have been fully explored.

The use of the metal salts of 2-ethyl-hexanoic acid offers another method of incorporating many metallic substances into solution at concentrations ranging up to 10% of the metal by weight (23, 24). This procedure, although more elaborate than direct counting of aqueous solutions, will accommodate much greater amounts of the desired isotope, with a lower quenching effect. The weak natural activities of Sm-147, for example, have been studied by this method (25).

Several new solvents, including monoisopropylbiphenyl (26) and silicones (27) have recently been reported, and these deserve special consideration because of their lower quenching behavior and different solvent properties.

Heterogeneous Counting Systems

For routine counting of numerous samples some new methods offer an effective compromise between maximum sensitivity and minimum sample preparation. The use of heterogeneous counting systems circumvents the problems of quenching action and

sample insolubility but introduces new difficulties in the forms of light collection and self-absorption of energy.

Suspensions of solids in aluminum stearate gel scintillators were described by Funt and Hetherington (28) and their method can be applied to the assay of a wide variety of colorless salts or insoluble inorganic materials. The aluminum stearate gel scintillators were modified by White and Helf to suspensions in Thixcin (29), a castor oil derivative, and to liquid scintillators thickened with polymers, by Fleishman and Shadkidzhanyan (30). Another suspending agent, Cab-O-Sil, a finely divided form of silica was suggested by Ott *et al.* (31) and Gordon (32). In addition we have found that the original aluminum stearate gels can be replaced by aluminum-2-ethyl hexanoate which gels immediately without heating in the liquid scintillation medium (23). Alternatively the aluminum stearate suspensions may be gelled by the addition of phenols or cresols without the application of heat (23).

Scintillating emulsions have been described recently by Shapira and Perkins (33). As with suspensions in gels and thickened systems, the opacity of the scintillator does not greatly reduce the counting efficiency, and counting has been performed with 10% efficiency for H^3 and 52% for C^{14} .

We have considered the use of transparent emulsions in order to overcome the opalescence associated with the usual emulsion systems. Bowcott and Schulman (34) have described the preparation of such systems, and their possible application to scintillation detection is obvious.

Another interesting and effective method of scintillation counting in heterogeneous systems employs direct counting on filter paper. In many instances the active material is collected on filter paper or separated on a filter paper chromatogram. Roucayrol (35) reported that wetting the filter paper with a liquid scintillator solution rendered it transparent and made direct counting of the collected material possible. Funt and Hetherington (36) modified this technique by employing monoisopropylbiphenyl as the scintillator solvent thus reducing air quenching effects and overcoming variations in detection sensitivity due to solvent evaporation. Wang and Jones (37) found that the suspension of filter paper strips in counting vials containing liquid scintillator gave good counting efficiencies and reproducibilities and was eminently suitable for the counting of numerous samples in a commercial liquid scintillation spectrometer. The question of the best orientation of the strips was raised by Loftfield (38), who claimed differences in counting efficiency dependent upon orientation which are, however, disputed by other workers (39). Davidson (40) recently reported excellent results with this technique when circles of filter paper were arranged parallel to the phototube surface and this is very similar to the filter paper counting methods described above (36).

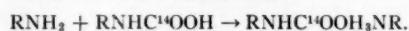
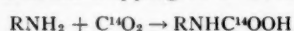
An alternative method of heterogeneous counting employs the organic phosphor in the dispersed phase with the active material in the continuous phase. Naphthalene and anthracene crystals were first suggested for the gaseous counting of tritium in 1950, (41, 42, 43) but an adaptation of these methods has only recently gained favor. Steinberg (44) described the use of packed broken filaments of plastic scintillator wetted with active material in aqueous solution. Powdered anthracene crystals were later reported for the same purpose (45). Best reproducibility is achieved when the counting vial is packed with the powdered phosphor and filled above the level of the phosphor with excess active solution.

A device for the counting of active aqueous solutions or gases in flow or static systems was described by Funt and Hetherington (46), who employed a spiral capillary of plastic

scintillator. The wall thickness and bore diameter were designed to provide maximum interaction with the betas and minimum self absorption in the aqueous medium. This device is now available commercially* and has found application in monitoring effluents from chromatographic columns. Its use in the detection of Ca^{45} (47) has recently been described.

Some particularly effective techniques limited to C^{14}O_2 counting employ liquid scintillator solutions containing long chain quaternary amines. Passmann, Radin, and Cooper introduced this technique (48) and valuable modifications have since appeared (49, 50, 51). Oppermann, Nystrom, Nelson, and Brown (52) and Radin and Fried (53) described the use of Primene 81-R (a mixture of tertiary alkyl primary C^{12} - C^{14} amines) obtained commercially from Rohm and Haas Co.

The reactions involved in the trapping of C^{14}O_2 in such systems are:



The complexes formed are stable, particularly at low temperatures, and only moderate quenching action, which is attributed to the methanol employed as solvent, is observed.

Sheets of plastic scintillator have obvious applications for direct counting of beta emitters. Evaporation of an aqueous solution and the resultant deposition of radioactive material may be employed, or a flow system may be utilized (54). Special plastic well units for beta-ray spectroscopy have also been devised (55).

CONCLUSIONS

A comparison of the various counting systems is presented in Table I. It is evident that

TABLE I
Comparisons of counting systems

Method	Advantages	Disadvantages	Typical application	Sample size
Internal liquid scintillation counting	Highest ultimate sensitivity	Limited sample solubility; quenching	C^{14} , H^3 isotopes of low specific activity	Unlimited
Suspension of radioactive substance in gel or thickened liquid scintillator	Little sample preparation; no quenching	Reduced optical transmission	Inorganic salts and organic substances insoluble in aromatic solvents	Sample thickness limited by opacity; 1 g
Filter paper counting	Little sample preparation; no quenching	Self-absorption	Inorganic salts and organic substances insoluble in aromatic solvents	Milligram quantities
Anthracene or plastic scintillator filaments in aqueous medium	Direct analysis of aqueous sample	Self-absorption in aqueous phase. Low efficiency	Aqueous solutions of energetic beta emitters	Three milliliters of aqueous solution
Quaternary ammonium salts or amines in liquid scintillator	Direct absorption of C^{14}O_2	C^{14}O_2 only	Direct analysis of combustion products	Milligram quantities of C^{14}O_2
Plastic scintillator capillary	Continuous analysis of flow systems	Self-absorption in aqueous phase	Chromatographic effluents	<1 ml volume

*Nuclear Enterprises, Winnipeg, Manitoba.

each of the counting methods has its particular merits and that the choice of the most suitable counting system must represent a delicate balance between maximum convenience and efficiency. Nevertheless it is obvious that the development of new alternative methods has hastened the adoption of scintillation detectors for many applications dependent upon the routine analysis of numerous samples. While the homogeneous liquid scintillator still represents the method of choice for extreme sensitivity, filter paper strips, or suspensions can be effectively employed in commercially available scintillation counters capable of automatically measuring many dozens of samples per day. For very small amounts of substance of high specific activity the heterogeneous detector systems also possess advantages in lower gamma backgrounds due to small scintillator size, and the elimination of quenching effects.

REFERENCES

1. V. P. GUINN. Liquid scintillation counting. C. G. Bell and F. N. Hayes (Editors). Pergamon Press, New York. 1958. p. 179.
2. E. C. FARMER and I. A. BERSTEIN. *Science*, **115**, 460 (1952).
3. B. N. AUDRIC and J. V. P. LONG. *Research* (London), **5**, 46 (1952).
4. J. C. ROUCAYROL and E. OBERHAUSEN. *Naturwissenschaften*, **42**, 411 (1955).
5. E. MATSUKAWA and E. EABORN. *Research* (London), *Research Correspondence Suppl.* **9**, 537 (1956).
6. F. N. HAYES, B. S. ROGERS, and P. C. SANDERS. *Nucleonics*, **13** (1), 46 (1955).
7. J. HERBERG. *Anal. Chem.* **32**, 42 (1960).
8. B. L. FUNT and W. M. PASIKA. *Can. J. Chem.* **38**, 1865 (1960).
9. F. N. HAYES, B. S. ROGERS, and W. H. LANGHAM. *Nucleonics*, **14** (3), 48 (1956).
10. J. D. DAVIDSON and P. FEIGELSON. *Intern. J. Appl. Radiation and Isotopes*, **2**, 1 (1957).
11. J. KAUFMAN, A. NIR, G. PARKS, and R. M. HOURS. Studies of low level liquid scintillation counting of tritium. University of New Mexico Conference on Organic Scintillation Detectors, Albuquerque, New Mexico. August, 1960.
12. R. W. PRINGLE, W. TURCHINETZ, and B. L. FUNT. *Rev. Sci. Instr.* **26**, 859 (1955).
13. C. LEGER and L. PICHAT. *Compt. rend.* **244**, 190 (1957).
14. R. W. PRINGLE, W. TURCHINETZ, B. L. FUNT, and S. DANYLUK. *Science*, **125**, 69 (1957).
15. F. N. HAYES, D. L. WILLIAMS, and B. ROGERS. *Phys. Rev.* **92**, 512 (1953).
16. G. T. OKITA, J. SPRATT, and G. V. LEROY. *Nucleonics*, **14** (3), 76 (1956).
17. F. N. HAYES and R. G. GOULD. *Science*, **117**, 480 (1953).
18. F. N. HAYES, W. J. EVERSOLE, W. H. LANGHAM, and T. T. TRUJILLO. *J. Lab. Clin. Med.* **47**, 819 (1956).
19. M. FURST, H. KALLMANN, and F. H. BROWN. *Nucleonics*, **13** (4), 58 (1955).
20. M. FURST and H. KALLMANN. *Phys. Rev.* **97**, 583 (1955).
21. F. E. KINARD. *Rev. Sci. Instr.* **28**, 293 (1957).
22. R. C. AXTMANN and L. CATHEY. *Intern. J. Appl. Radiation and Isotopes*, **4**, 26, 261 (1959).
23. B. L. FUNT and R. W. PRINGLE. Defence Research Board of Canada Report Contract P69-5-276. 1955.
24. A. R. RONZIO. *Intern. J. Appl. Radiation and Isotopes*, **4**, 196 (1959).
25. G. B. BEARD and W. H. KELLY. Contract AF 49(638)-AD-158307 Michigan State University AFOSR-TN-58-497. June 18, 1958.
26. W. L. BUCK and R. K. SWANK. *Rev. Sci. Instr.* **29**, 252 (1958).
27. H. A. MIRANDA, JR. and H. SCHIMMEL. *Rev. Sci. Instr.* **30**, 1128 (1959).
28. B. L. FUNT and A. HETHERINGTON. *Science*, **125**, 986 (1957).
29. C. G. WHITE, S. HELF, and R. N. SHELLY. *Anal. Chem.* **32**, 238 (1960).
30. D. G. FLEISHMAN and L. G. SHADKIDZHANYAN. *Atomnaya Energ.* **6**, 669 (1959).
31. D. G. OTT, C. R. RICHMOND, T. T. TRUJILLO, and H. FOREMAN. *Nucleonics*, **17** (9), 106 (1959).
32. C. F. GORDON and A. L. WOLFE. *Anal. Chem.* **32**, 574 (1960).
33. J. SHAPIRA and W. H. PERKINS. *Science*, **131**, 414 (1960).
34. J. E. BOWCOTT and J. H. SCHULMAN. *Z. Elektrochem.* **59**, 283 (1955).
35. J. C. ROUCAYROL, E. OBERHAUSEN, and R. SCHULER. Radioisotopes in scientific research. Proceedings of the First UNESCO International Conference. Vol. 1. Pergamon, New York. 1958. p. 648.
36. B. L. FUNT and A. HETHERINGTON. *Science*, **131**, 1608 (1960).
37. C. H. WANG and D. E. JONES. *Biochem. Biophys. Research Commun.* **1**, 203 (1959).
38. R. B. LOFTFIELD. *Atomlight*, No. 13, 1, June (1960).
39. J. W. GEIGER and L. D. WRIGHT. *Biochem. Biophys. Research Commun.* **2**, 282 (1960).
40. J. D. DAVIDSON. Some recent developments in liquid scintillation counting of biochemical samples. University of New Mexico Conference on Organic Scintillation Detectors, Albuquerque, New Mexico. August 16-17, 1960.
41. R. F. TASCHER and H. T. GITTINGS. *Phys. Rev.* **74**, 1553 (1948).
42. D. K. BUTT. *Physica*, **18**, 1142 (1952).
43. W. J. RAMLER and M. S. FREEDMAN. *Rev. Sci. Instr.* **21**, 784 (1950).

44. D. STEINBERG. *Nature*, **182**, 740 (1958).
45. D. STEINBERG. *Nature*, **183**, 1253 (1959).
46. B. L. FUNT and A. HETHERINGTON. *Science*, **129**, 1429 (1959).
47. E. D. PICKERING, H. L. REED, and R. L. MORRIS. *Anal. Chem.* **32**, 1214 (1960).
48. J. M. PASSMANN, N. S. RADIN, and J. A. D. COOPER. *Anal. Chem.* **28**, 484 (1956).
49. M. VAUGHAN, D. STEINBERG, and J. LOGAN. *Science*, **126**, 446 (1951).
50. D. STEINBERG, M. VAUGHAN, C. B. ANFENSEN, J. D. GORRY, and J. LOGAN. *Liquid scintillation counting*. C. G. Bell and F.N. Hayes (*Editors*). Pergamon Press, New York. 1958. pp. 230-236.
51. R. J. HERBERG. *Anal. Chem.* **32**, 42 (1960).
52. R. A. OPPERMAN, R. F. NYSTROM, W. O. NELSON, and R. E. BROWN. *Intern. J. Appl. Radiation and Isotopes*, **7**, 38 (1959).
53. N. S. RADIN and R. FRIED. *Anal. Chem.* **30**, 1926 (1958).
54. E. SCHRAM and R. LOMBAERT. *Anal. Chim. Acta*, **17**, 417 (1957).
55. D. G. GARDNER and W. W. MEINKE. *Intern. J. Appl. Radiation and Isotopes*, **3**, 232 (1958).

DETERMINATION OF THE DISINTEGRATION RATE OF NUCLIDES DECAYING BY ELECTRON CAPTURE¹

J. R. S. DROUIN² AND L. YAFFE

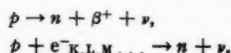
ABSTRACT

In an attempt to determine disintegration rates of nuclides decaying by electron capture, various properties of a 2π proportional counter spectrometer were studied. These included gas multiplication, energy resolution, and energy linearity. The result of varying anode size, gas pressure, and nature of the gas was also investigated. An experimentally determined average path length for characteristic X-ray energies between 4 and 24 kev was found.

INTRODUCTION

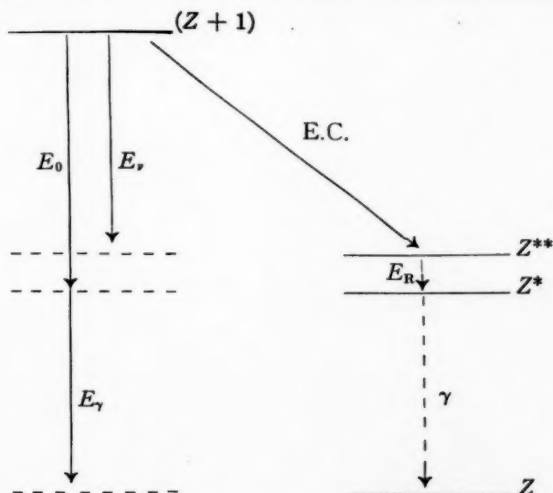
Charged-particle irradiations normally lead to the formation of a new nucleus where the proton-to-neutron ratio is greater than that required for stability. In turn, the proton in excess will decay by one or two different modes, namely positron emission and (or) capture of one of the orbital electrons.

The two transformations can be represented as a nuclear transition from a proton state to a neutron state with accompanying neutrino emission (ν) in the following schematic picture:



The first transformation can be ascertained by measuring the radiation due to the annihilation of the positron or by measuring the positrons themselves.

The second transformation can be described by the following energy diagram wherein a parent nucleus with atomic number ($Z + 1$) captures one of its own orbital electrons and emits a neutrino transforming itself to the nucleus with atomic number Z .



¹Manuscript received November 3, 1960.

Contribution from the Radiochemistry Laboratory, Department of Chemistry, McGill University, Montreal, Que., with financial assistance from the National Research Council of Canada. Presented at the Third Symposium on Nuclear Chemistry and Radiochemistry held at Atomic Energy of Canada Limited, Chalk River, Ontario, September 6-8, 1960.

²Holder of National Research Council Bursary 1956-57, and National Research Council Studentships 1957-58, 1958-59, and 1959-60.

Subsequent de-excitation by γ -ray emission may occur with energy E_γ . Thus the total energy for the transition equals $E_0 + E_\gamma$, where E_γ may be zero. Further,

$$E_0 = E_\nu + E_R$$

where E_ν is the energy available for the neutrino and E_R is the energy of the radiation characteristic of an atomic shell rearrangement, i.e. a characteristic X-ray or Auger electron.

In a small fraction of the cases, a continuous spectrum of internal bremsstrahlung results from the sudden change of nuclear charge. In this case the energy is shared between the bremsstrahlung and the neutrino.

One can attempt to standardize electron-capture transitions in three ways. The first relies on the absolute measurement of the primary radiations due to the internal bremsstrahlung. The second and third methods are based on the absolute measurement of the secondary radiations due to characteristic Auger electrons or characteristic X-rays.

In 1955, Rasmussen (1) suggested an elegant method which involved direct coincidence counting of the internal bremsstrahlung and the shell rearrangement radiation. However, Hayward demonstrated in 1958 (2) that the method was not entirely reliable, especially for low-energy transitions and for high atomic number elements, where the apportioning of the radiations due to capture of K-electrons becomes very difficult. Also, interference by radioactive impurities, background, and gamma de-excitation radiation, and the low probability ($\sim 0.001\%$) (3) of internal bremsstrahlung do not militate in favor of such a method.

A more convenient way would be the absolute measurement of the Auger electrons or the characteristic X-rays. For low atomic number elements (< 30) the Auger electrons give a major contribution but their energies are very low (few kiloelectron volts). With normal source preparation methods, absolute measurement is rendered very difficult due to source absorption problems. The situation is much less difficult if one tries to measure the characteristic X-rays emerging after shell rearrangement. We have attempted to investigate the variables concerned with the operation of a 2π -proportional counter spectrometer. This would then enable the standardization of nuclides, decaying by electron capture, by measure of the characteristic X-rays.

EXPERIMENTAL TECHNIQUE AND RESULTS

The design of the counter is, with minor modifications, similar to that used by others, and is shown in Fig. 1. Curran, Angus, and Cockcroft in 1948 (4) and simultaneously Kirkwood, Pontecorvo, and Hanna (5) used gaseous sources with counters of this type and were the first to apply the spectrometric properties of such counters in the study of low energy β^- - and X-ray spectra. Our instrument is a windowless counter, of 2π -geometrical efficiency, which can be operated at elevated pressures. The experimental data reported here deal only with solid sources.

Various fundamental properties of proportional counters were investigated. These important criteria for performance were checked with a mixture of argon-methane (9:1) as counter gas, although some work was done with krypton-methane (9:1).

First of all the voltage plateaux were studied. Their respective shapes are critically dependent on the counter gas (pressure and nature), the anode to cathode ratio, and the electronic circuit. A block diagram of the electronic arrangement is shown in Fig. 2. It was found necessary to incorporate a White cathode follower (6) with the proper

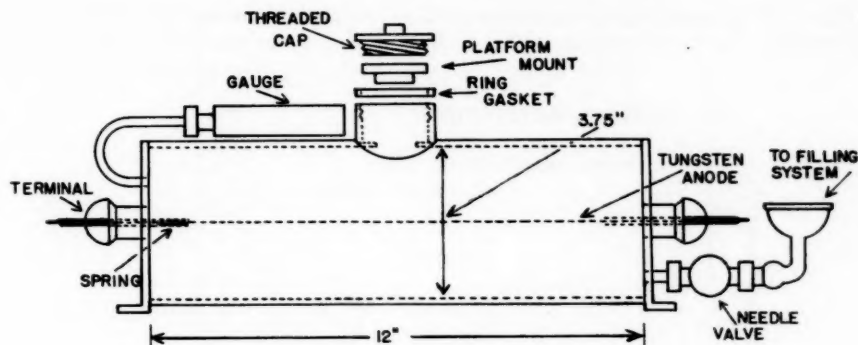
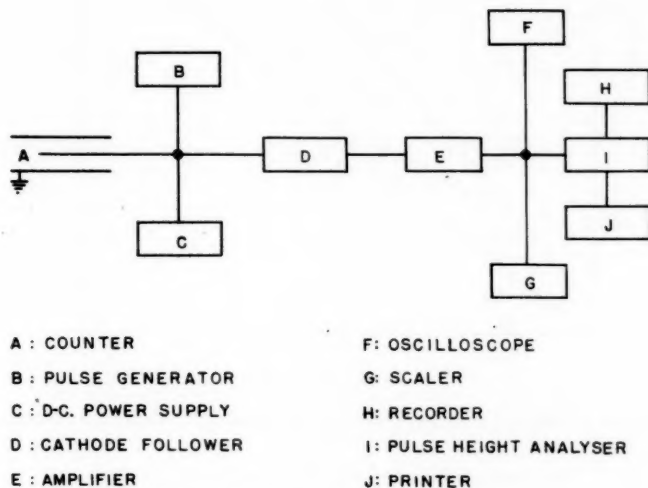
FIG. 1. 2π -Proportional counter.

FIG. 2. Block arrangement of electronic equipment.

coupling constant for adequate performance. Figure 3 shows the plateau lengths obtained for different gas pressures and anode sizes. At a pressure of one atmosphere, for example, plateau lengths of about 600 volts with negligible slope were attainable when the anode diameters were 0.002 in., 0.003 in., 0.004 in., and 0.005 in. An anode diameter of 0.002 in. was used in the course of our work, unless otherwise mentioned.

Another intrinsic property of a proportional counter is the gas multiplication factor which is governed by the voltage across the chamber, the pressure and type of gas, and the anode-to-cathode ratio. In 1941, Rose and Korff (7) developed a theoretical treatment of this factor assuming an ionization cross section linear with electron energy up to 40 volts above the ionization threshold. They obtained experimental verification of the following equation, for amplification factors between 10^2 and 10^3 over a small voltage range (~ 150 volts).

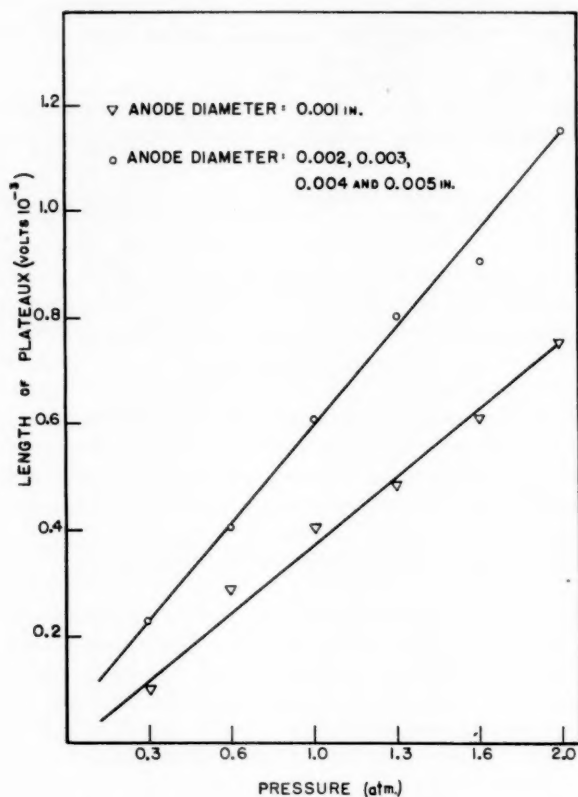


FIG. 3. Variation of length of voltage plateaux with counter gas pressure for various anode sizes.

$$A = \exp 2[a \cdot N \cdot c \cdot r_1 V_o]^{\frac{1}{2}} \cdot \left[\left(\frac{V_o}{V_p} \right)^{\frac{1}{2}} - 1 \right]$$

where a = rate of increase of the ionization cross section with incident energy,

N = number of atoms or molecules inside the sensitive volume,

$$c = \frac{1}{\log_e \frac{r_2}{r_1}}$$

where r_2 is radius of the cathode and r_1 is radius of the anode,

V_o = operating voltage, and

V_p = proportional threshold voltage.

For amplification factors greater than those used by Korff, it was found necessary to modify this equation by introducing another variable $f(0)$ into the exponential factor as follows:

$$A = \exp 2[a \cdot N \cdot c \cdot r_1 \cdot f(0) \cdot V_o]^{\frac{1}{2}} \cdot \left[\left(\frac{V_o}{V_p} \right)^{\frac{1}{2}} - 1 \right]$$

Fig. 4 shows the variation of $f(0)$ when the anode size and gas pressure are varied over a wide range. From these data one can now calculate amplification factors between 10^4 and 10^6 for voltage ranges up to 1000 volts.

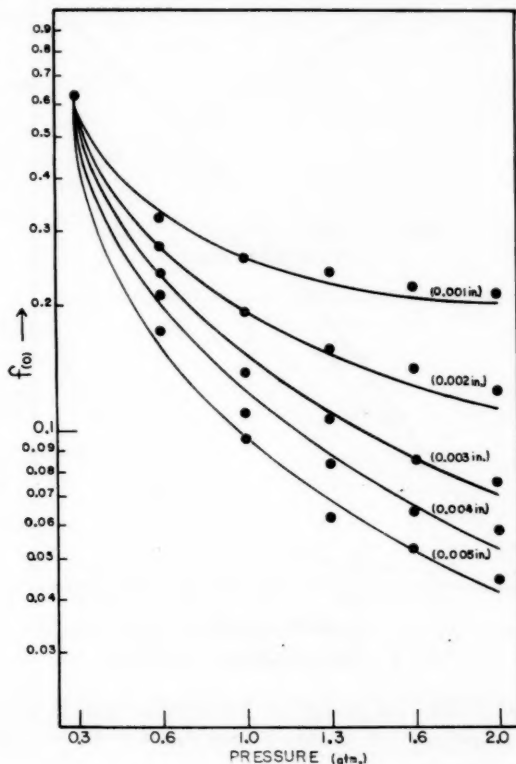


FIG. 4. Variation of $f(0)$ with pressure and anode size.

The energy linearity of the system was investigated for energy pulses between 3 and 24 kev as shown in Fig. 5. Only a very small departure from linearity at high energies was found.

Another important criterion for the operation of the device is the energy resolution. This was checked for anode wires of varying radii at different gas pressures. A standard source of Fe^{55} (5.9-kev X-rays) was used. The results in Fig. 6(a) show the variation of the energy resolution when five different anode sizes were employed.

If the anode size is kept constant and the pressure is varied, the mean free path of the electrons producing secondary ionizations will invariably be altered. According to calculations made by Korff (8), the mean free path should approximately be inversely proportional to the pressure. Then, as the pressure is decreased, statistical fluctuations in the pulse formations will increase. The energy resolution of the spectrometer was found to vary with pressure in the manner described in Fig. 6(b).

The pulse-size distribution from monoenergetic radiations in the energy range between 4 and 24 kev was analyzed. The size of every output pulse of a proportional counter,

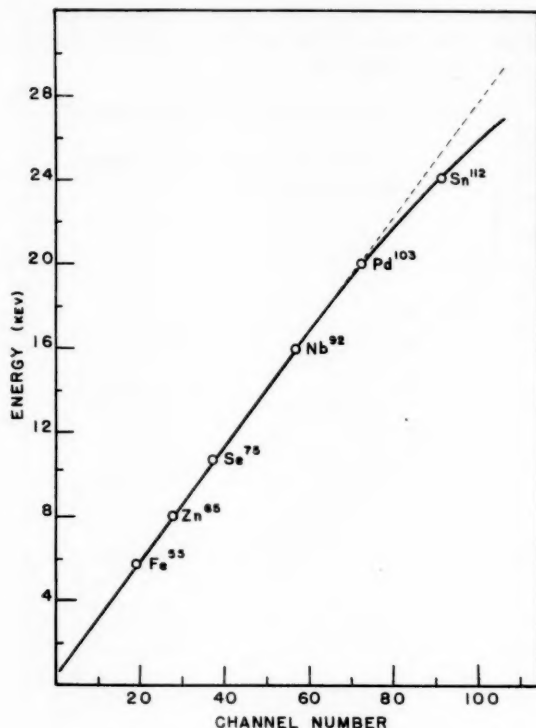


FIG. 5. Energy calibration of system.

arising from absorption of the full energy in the counter gas, is subject to statistical fluctuations. These fluctuations are mainly introduced by the statistics of the multiplication process in the counter.

A theoretical treatment by Frisch (9) and experimental results by Hanna *et al.* (10) have demonstrated that the relative variance (mean square relative standard deviation) of the output pulse size is practically independent of the multiplication factor. The pulse-size distributions produced by the radiations under investigation were studied. They could be fitted with Gaussian curves, at least in an interval of about ± 3 standard deviations.

The standard deviation (σ_P) can therefore be obtained by measuring the width (ΔE) of the peak at half maximum. This leads to $\Delta E = 2.36 \sigma_P$, where $(\sigma_P/P)^2$ is the relative variance of the output pulse.

As may be seen from Fig. 7, (σ_P/P) , the root mean square of the relative variance of the output pulse size, is plotted against the energy (E) of the radiations. The distribution was found to be slightly smaller than would be expected from a Poisson distribution.

The relationship derived from these experimental data can be described by

$$(\sigma_P/P) = 0.17 E^{-1/2}.$$

Thus, resolving power = $0.42 E^{-1/2}$.

Now that the criteria for performance of the counter are ascertained, one needs to define the geometrical properties.

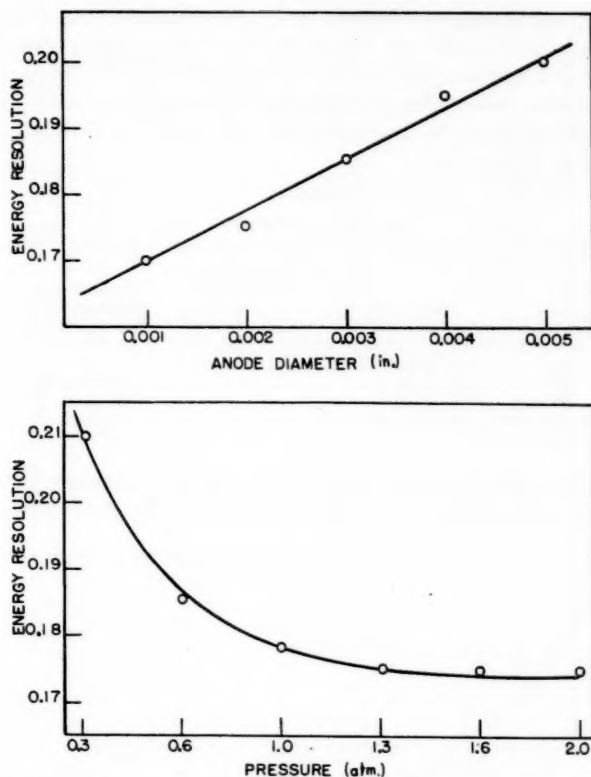


FIG. 6. (a) Variation of energy resolution with anode diameter (pressure = 1 atm). (b) Variation of energy resolution with pressure.

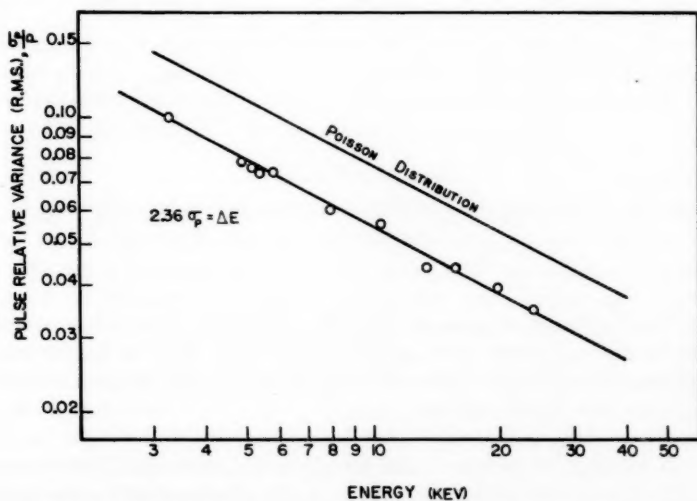


FIG. 7. Relation between the relative variance of the pulse and the X-ray energy.

The first factor is the geometrical efficiency. This was evaluated as 2π steradians when intercomparison was made with two other counters, (a) a high pressure proportional counter calibrated by Campion (11) and (b) a 4π β -counter calibrated by Pate and Yaffe (12). For this purpose, two different types of radiations were used, namely 5.9-keV X-rays from Fe^{55} and β^- particles emitted by H^3 , Ni^{63} , and C^{14} . The values obtained are summarized in Table I.

TABLE I
Geometrical efficiency

Nuclides	This work (c.p.m. $\times 10^{-3}$)	High-pressure proportional counter (c.p.m. $\times 10^{-3}$)	4π β -counter (bottom half) (c.p.m. $\times 10^{-3}$)
Fe^{55}	34.00 ± 0.05	34.07 ± 0.07	—
H^3	41.2 ± 0.2	—	41.5 ± 0.2
Ni^{63}	47.3 ± 0.2	—	47.5 ± 0.2
C^{14}	46.2 ± 0.2	—	46.7 ± 0.2

A second correction which has to be introduced is that for the escape peak. For energies between 3 and 20 keV, Fig. 8 shows the ratio of the area under the escape peak to that of

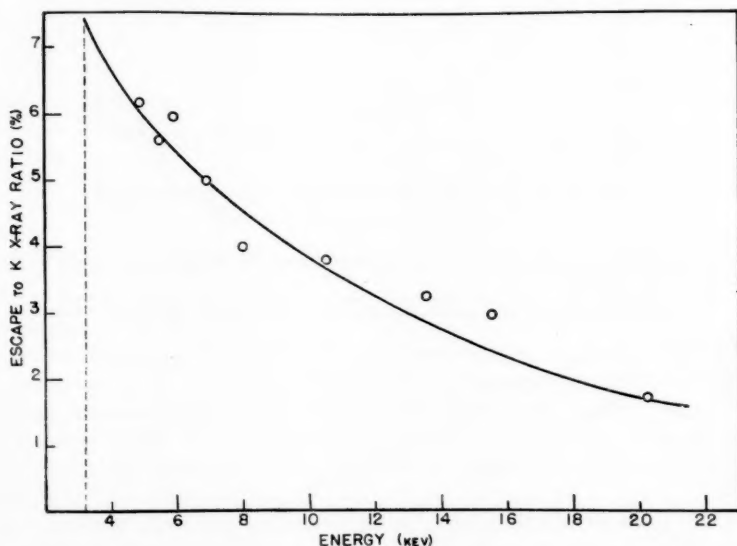


FIG. 8. Relation between the ratio of the escape peak to K X-ray and energy of the X-ray emitter.

the area under the K X-ray photopeak when the counter is operated at 1 atmosphere.

The third correction which has to be made resides in the absolute transmission of the X-rays through the finite sensitive volume of the counter. An average path length for these radiations in the counter was measured.

This was experimentally determined when four different radionuclides, namely Mn^{54} (5.4 keV), Fe^{55} (5.9 keV), Co^{57} (6.4 keV), and Zn^{65} (8.0 keV) were used. The pressure of the counter gas was increased up to a value where, if the relative count rates were plotted

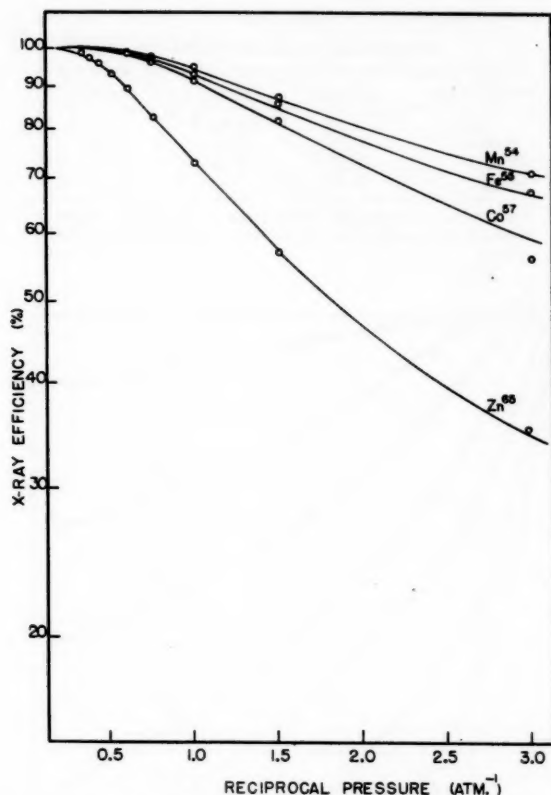


FIG. 9. Relation between X-ray counter efficiency and reciprocal pressure.

against the reciprocal pressures, as shown in Fig. 9, a plateau occurred. This was taken as total absorption in the counter. Such plots were originally investigated by Allen in 1957 (13). From these experimental data, an average path length can be derived from the equation for the absorption of photons passing through matter:

$$I = I_0 \exp -\mu t.$$

I and I_0 are the transmitted and incident radiation respectively, and t is the path length. The values for the linear absorption coefficient μ were obtained from Hagedoorn and Wapstra (14).

The results are summarized in Table II and give an average path length of 6.8 cm. Four of them were obtained from the plateau counting rates, while the other four were derived from integrating the counting rate beneath the K X-ray photopeaks.

With the above experimental path length, the efficiency of the 2π -proportional counter spectrometer was derived for K X-ray energies between 5 and 25 keV when the counter is operated at one atmosphere, argon-methane (9:1). Experimental relative efficiencies are shown in Fig. 10 when the pressure of the counter gas is varied. The contribution due to the escape peak has been included.

TABLE II
Average-path-length determination

Nuclides	t_p (cm)	t_s (cm)	\bar{t} (cm)
Mn ⁵⁴	6.18	6.05	6.8
Fe ⁵⁴	6.75	6.95	
Co ⁵⁷	7.35	7.10	
Zn ⁶⁵	6.90	7.05	

NOTE: t_p = average path length based on calculations on the plateaux. t_s = average path length based on calculations on the spectra.

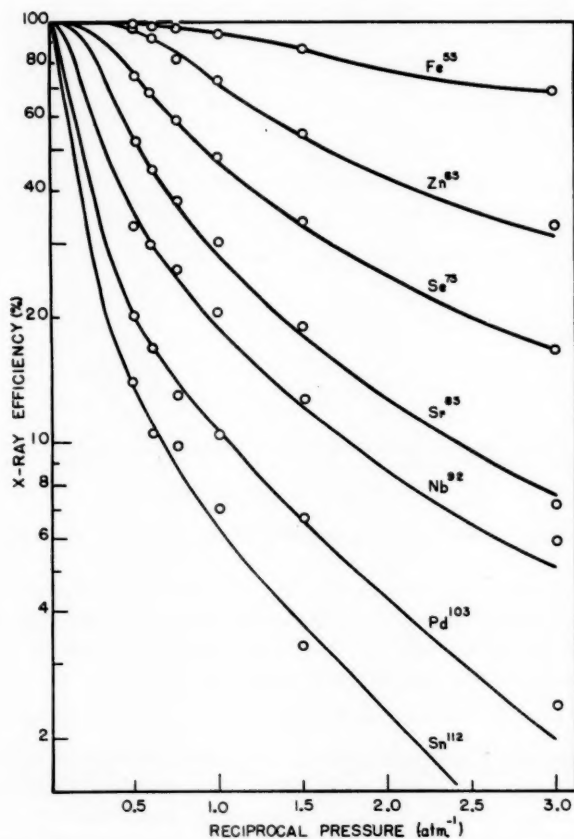


FIG. 10. Relation between X-ray counter efficiency and reciprocal pressure for argon-methane (9:1) (escape peak included).

For higher energy X-ray emitters, it is desirable to use a krypton-methane (9:1) mixture in order to take advantage of the enhanced absorption. These data are shown in Fig. 11 and again include the escape peak contribution.

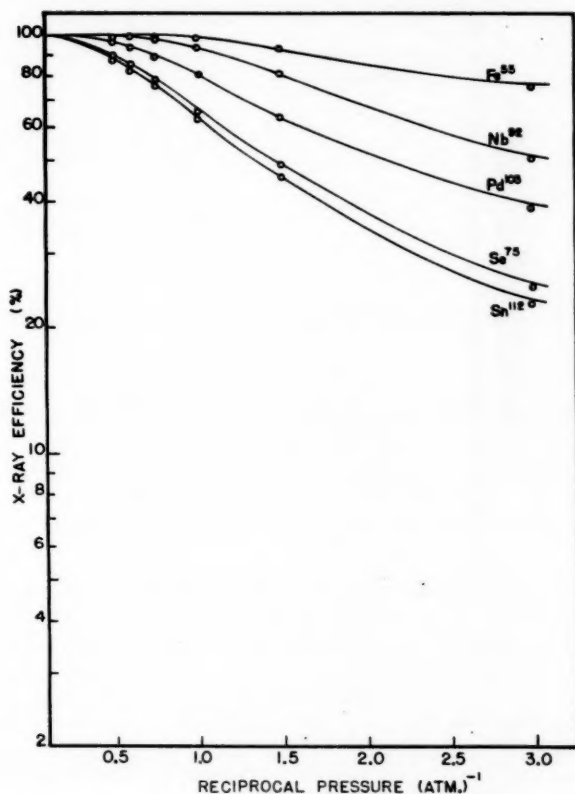


FIG. 11. Relation between X-ray counter efficiency and reciprocal pressure for krypton-methane (9:1) (escape peak included).

Figure 12 gives the ratio of the X-ray efficiencies for the two counter gases as a function of energy.

With a solid source, screened by sufficient aluminum to cut out the Auger electrons, a knowledge of the operational characteristics of the instrument and the evaluation of the correction factors necessary as described, one can now establish an equation for the disintegration rate N_0 of radionuclides decaying by electron capture when the counting rate R has been measured. The following equation applies:

$$R = N_0 \cdot G \cdot f_a \cdot f_t \cdot f_{w_k} \cdot f_r$$

where

G = defined source-to-counter geometrical efficiency (Table I).

f_a = factor correcting for total absorption inside the counter (Figs. 10 and 11).

f_t = factor for the transmission of K X-rays through the Auger electron absorber (11).

f_{w_k} = factor due to the K -fluorescence yield (15).

f_r = factor due to L -capture events (16, 17).

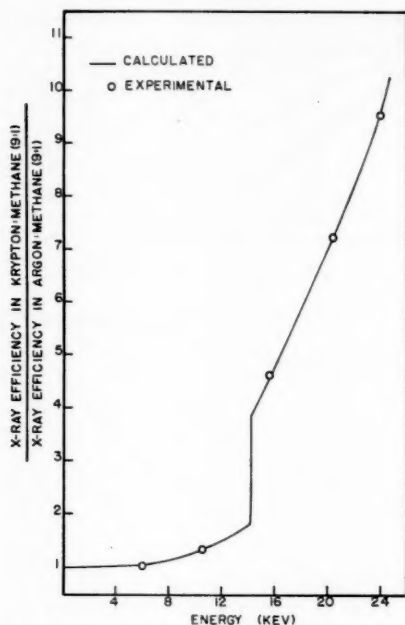


FIG. 12. Ratio between the X-ray efficiencies for the two counter gases at various energies.

REFERENCES

1. N. C. RASMUSSEN. Circular to National Research Council of U.S.A. Subcommittee on Beta and Gamma-Ray Measurement and Standards. April, 1955.
2. R. H. HAYWARD. Measurements and standards of radioactivity. Nuclear Science Series Report No. 24. National Academy of Sciences, National Research Council of U.S.A. Publication 573. 1958.
3. P. MORRISON and L. I. SCHIFF. *Phys. Rev.* **58**, 24 (1949).
4. S. C. CURRAN, J. ANGUS, and A. L. COCKCROFT. *Nature*, **162**, 302 (1948).
5. D. H. W. KIRKWOOD, B. PONTECORVO, and G. C. HANNA. *Phys. Rev.* **74**, 497 (1948).
6. E. L. C. WHITE. U.S. Patent No. 2,358,428 (September 19, 1944).
7. M. E. ROSE and S. A. KORFF. *Phys. Rev.* **59**, 850 (1941).
8. S. A. KORFF. *Handbuch der Physik*. Vol. XLV, 1958. p. 52.
9. O. R. FRISCH. *Progr. in Nuclear Phys.* **30**, 18 (1953); Statistics of multiplicative processes. Unpublished lectures. 1948.
10. G. C. HANNA, D. H. W. KIRKWOOD, and B. PONTECORVO. *Phys. Rev.* **75**, 985 (1949).
11. P. J. CAMPION and W. F. MERRITT. Atomic Energy of Canada Limited Report No. 532. 1957.
12. B. D. PATE and L. YAFFE. *Can. J. Chem.* **33**, 610 (1955).
13. R. A. ALLEN. *Intern. J. Appl. Radiation and Isotopes*, **1**, 289 (1957).
14. H. L. HAGEDOORN and A. H. WAPSTRA. *Nuclear Phys.* **15**, 146 (1960).
15. C. D. BROYLES, D. A. THOMAS, and S. K. HAYNES. *Phys. Rev.* **89**, 715 (1953).
16. H. BRYSK and M. E. ROSE. *Revs. Modern Phys.* **30**, 1169 (1958).
17. B. L. ROBINSON and R. W. FINK. *Revs. Modern Phys.* **32**, 117 (1960).

Recueil des travaux chimiques des Pays-Bas

FONDÉ EN 1882 PAR

W. A. VAN DORP, A. P. N. FRANCHIMONT, S. HOOGEWERFF,
E. MULDER ET A. C. OUDEMANS

EDITED BY THE ROYAL NETHERLANDS CHEMICAL SOCIETY

Generally the "Recueil des travaux chimiques des Pays-Bas" only accepts papers for publication from members of the Royal Netherlands Chemical Society who are also subscribers to the Recueil. Applications for membership of this society should be sent to The Secretariate, Lange Voorhout 5 The Hague.

The Recueil contains papers written in English, French or German and appears if possible monthly except in August and September, in issues of varying size. It is obtainable from D. B. Centen's Uitgeversmaatschappij, P.O.B. 507, Hilversum (the Netherlands), or through any bookseller in Holland or abroad. The subscription is 50.— guilders for Holland and 52.50 guilders abroad. Authors receive 75 reprints of their papers free of charge.

Editorial Office: Lange Voorhout 5, The Hague.

SYMPOSIUM ON NUCLEAR CHEMISTRY AND RADIOCHEMISTRY

<i>J. A. Davies and G. A. Sims</i> —The range of Na^{24} ions of kiloelectron volt energies in aluminum	601
<i>J. A. Davies, J. D. McIntyre, and G. A. Sims</i> —Isotope effect in heavy ion range studies	611
<i>F. Brown and B. H. Oliver</i> —The kinetic energy of Cs^{131} primary fragments from fission of U^{235}	616
<i>D. R. Bidinosti, D. E. Irish, and R. H. Tomlinson</i> —The thermal neutron fission yields of U^{235}	628
<i>A. Kjelberg, H. Taniguchi, and L. Yaffe</i> —Distribution of nuclear charge in the proton-induced fission of Th^{232} . Part II	635
<i>Charles D. Coryell, Morton Kaplan, and Richard D. Fink</i> —Search for correlations of most probable nuclear charge Z_p of primary fission fragments with composition and excitation energy	646
<i>Roger Kelly</i> —Th attachment of inert gases to powders following (n, γ) events	664
<i>K. Fritze, T. J. Kennett, and W. V. Prestwich</i> —Half-lives of Rb^{84} , Sr^{84} , Y^{84} , Rb^{86} , Sr^{86} , Y^{86}	675
<i>H. Farrar, A. K. Dasgupta, and R. H. Tomlinson</i> —Half-life of Cs^{137}	681
<i>A. P. Boerg and G. C. Bowes</i> —Search for the (n, t) reaction at 14 Mev in some medium weight nuclei	684
<i>J. P. Butler and D. C. Santry</i> — $\text{Th}^{232}(n, 2n)\text{Th}^{231}$ cross section from threshold to 20.4 Mev	689
<i>Taku Matsuo and T. T. Sugihara</i> —Evidence for low-momentum-transfer process in $\text{K}^{41}(\alpha, n)\text{Sc}^{44m-4s}$ reactions from range measurements of products	697
<i>M. D. Silbert and R. H. Tomlinson</i> —A gas-chromatographic apparatus for the study of the hot-atom chemistry of organic halides	706
<i>B. Lionel Funt</i> —Scintillation counting with organic phosphors	711
<i>J. R. S. Drouin and L. Yaffe</i> —Determination of the disintegration rate of nuclides decaying by electron capture	717

Contents

Corrections	i
J. E. Sador—Exchange reactions between zinc and its ions	393
Ross Stewart and L. J. Muenster—Protonation of the amide group. II. Dicyclohexylurea-O ¹⁴	401
G. Frangatos and A. Taurins—Steroids. V. Pyridinium betaines of 2- α -bromocholestan-3-one	410
John C. Grivas and Alfred Taurins—Infrared spectra - structure correlations of N-substituted trifluoroacetamides	414
M. M. Baig and W. R. Cullen—The reaction of alkyl iodides with iodo-arsines in the presence of mercury	420
J. D. McCowan and R. McIntosh—The complex dielectric constant at low microwave frequencies of ethyl chloride adsorbed on porous Vycor glass	425
K. Grjotheim, O. Herstad, and J. M. Toguri—The aluminum reduction of magnesium oxide. I. The vapor pressure of magnesium over the system Al-MgO	443
Robin M. Hochstrasser—The crystal spectrum of perylene	451
Robin M. Hochstrasser—The effect of intramolecular twisting on the emission spectra of hindered aromatic molecules. Part I. 1,1'-Binaphthyl	459
K. U. Ingold and D. R. Taylor—The infrared frequencies and intensities of the hydroxyl band in ortho-substituted phenols	471
K. U. Ingold and D. R. Taylor—The effect of solvent and temperature on the cis-trans isomerism of ortho- <i>tert</i> -alkyl phenols	481
P. de Mayo, J. B. Stothers, and W. Templeton—Photochemical syntheses. I. The reaction of aldehydes and ketones with cycloalkenes	488
C. N. R. Rao—Kinetics and thermodynamics of the crystal structure transformation of spectroscopically pure anatase to rutile	498
M. H. Fisher, W. H. Nicholson, and R. S. Stuart—Nitro- and amino-imidazole-sulphonamides	501
Robert R. Fraser and Donald E. McGreer—N.M.R. spectra of some α - β unsaturated esters	505
W. A. E. McBryde and G. F. Atkinson—Spectrophotometric study of the reaction between iron (III) and kojic acid	510
B. D. Ripley and R. McIntosh—The complex dielectric constant of solutions of trimethylpentane and nitrobenzene near the consolute temperature	526
J. H. Taylor and C. H. Amberg—Infrared spectra of gases chemisorbed on zinc oxide. I. CO and CO ₂	535
J. M. Toguri and L. M. Pidgeon—High-temperature studies of metallurgical processes. Part I. The thermal reduction of magnesium oxide with silicon	540
George Just and R. Nagarajan—Steroids. I. 12 β -methyl-12 α -hydroxyprogesterone	548
B. Fraser-Reid, J. K. N. Jones, and M. B. Perry—The demethylation of sugars with hydrogen peroxide	555
M. A. A. Beg and H. C. Clark—Chemistry of the trifluoromethyl group. Part III. Phenylbis(trifluoromethyl)phosphine and related compounds	564
D. W. Davidson—Dielectric relaxation in liquids. I. The representation of relaxation behavior	571
Notes:	
M. A. A. Beg and H. C. Clark—Chemistry of the trifluoromethyl group. Part II. Nickel (II) complexes of trifluoromethyl phosphines	595
A. R. Osborn and E. Whalley—Pressure effect and mechanism in acid catalysis. VI. Hydrolysis of α -D-glucose-1-phosphate	597
J. T. Edward, D. Holder, W. H. Lunn, and I. Puskas—Oxidation of cholest-4-en-3-one with periodate-permanganate	599

(Continued on inside)

